INTERNATIONAL COUNCIL FOR RESEARCH AND INNOVATION
IN BUILDING AND CONSTRUCTION

WORKING COMMISSION W18 - TIMBER STRUCTURES

CIB - W18

MEETING FORTY-TWO

DÜBENDORF

SWITZERLAND

AUGUST 2009

INTERNATIONAL COUNCIL FOR RESEARCH AND INNOVATION
IN BUILDING AND CONSTRUCTION

WORKING COMMISSION W18 - TIMBER STRUCTURES

CIB - W18

MEETING FORTY-TWO

DÜBENDORF

SWITZERLAND

AUGUST 2009

Lehrstuhl für Ingenieurholzbau und Baukonstruktionen
Universität Karlsruhe
Germany
Compiled by Rainer Görlacher
2009

ISSN 1864-1784

CONTENTS

0 List of Participants

INTERNATIONAL COUNCIL FOR RESEARCH AND INNOVATION IN BUILDING AND CONSTRUCTION
WORKING COMMISSION W18 - TIMBER STRUCTURES

MEETING FORTY-TWO
Duebendorf, Switzerland, 23 - 27 August 2009

LIST OF PARTICIPANTS

AUSTRIA

J K Denzler	Holzforschung Austria, Viennna
H Krenn	Graz University of Technology
G Pirnbacher	Graz University of Technology
G Schickhofer	Graz University of Technology

AUSTRALIA

K Crews	UTS,Dural

CANADA

F Lam	University of British Columbia
Chun Ni	FPInnovations - Forintek Division, Vancouver
M Popovski	FP Innovations Forintek, Vancouver
I Smith	University of New Brunswick, Fredericton

DENMARK

H J Larsen	Copenhagen
J Munch-Andersen	Danish Timber Information Council, Lyngby

FINLAND

A Ranta-Maunus	VTT Technical Research Centre of Finland, Espoo
T Poutanen	Tampere University of Technology

GERMANY

S Aicher	MPA University Stuttgart
P Aldi	Universität Stuttgart
H J Blaß	Universität Karlsruhe
P Dietsch	TU München
M Frese	Universität Karlsruhe
G Gebhardt	Universität Karlsruhe
R Görlacher	Universität Karlsruhe
U Kuhlmann	Universität Stuttgart
J W van de Kuilen	TU München / TU Delft
P Mestek	TU München
W Meyn	Berlin
S Schmid	TU München
M Sieder	TU München
S Winter	TU München
H Zeitter	Ingenieurbüro Wagner Zeitter, Wiesbaden

ITALY

A Ceccotti	IVALSA-CNR
M Fragiacomo	University of Sassari, Alghero

JAPAN

M Yasumura	Shizuoka University

NEW ZEALAND

A Buchanan	University of Canterbury, Christchurch
D Carradine	University of Canterbury, Christchurch
J Jensen	University of Auckland
P Quenneville	University of Auckland

SLOVENIA

B Dujic	University of Ljubljana

SWEDEN

C Bengtsson	SP, Boras
R Crocetti	SP-Trätek, Borås
U A Girhammar	Umeå University
K Karlsson	Chalmers University of Technology, Gothenburg
B Källsner	SP Trätek, Stockholm
J König	SP Trätek, Stockholm
J Schmid	SP Trätek, Stockholm
G Tlustochowicz	Luleå University of Technology

SWITZERLAND

G Fink	ETH Zürich
A Frangi	ETH Zürich
E Gehri	Rüschlikon
S Gerber	Purbond AG, Sempach-Station
R Jockwer	EMPA Wood Laboratory, Dübendorf
M Klippel	ETH Zürich
J Köhler	ETH Zürich
M Sandomeer	ETH Zürich
C Sigrist	Berner Fachhochschule, Biel
R Steiger	EMPA Wood Laboratory, Dübendorf
T Tannert	Berner Fachhochschule, Biel
M Theiler	ETH Zürich
R Widmann	EMPA Wood Laboratory, Dübendorf

THE NETHERLANDS

A Jorissen	TU Eindhoven
C Sandhaas	TU Delft

USA

T Williamson	American Plywood Association, Tacoma
B Yeh	American Plywood Association, Tacoma

1. Chairman's Introduction

2. General Topics

3. Limit State Design Structural Design Codes

4. Stress Grading Test Methods

5. Stresses for Solid Timber

6. Timber Joints and Fasteners

7. Timber Beams

8. Laminated Members

9. Structural Stability

10. Fire

11. Any Other Business

12. Venue and Program for Next Meeting

13. Close

14. Peer Review of Papers for the CIB-W18 Proceedings

INTERNATIONAL COUNCIL FOR RESEARCH AND INNOVATION IN BUILDING AND CONSTRUCTION

WORKING COMMISSION W18 - TIMBER STRUCTURES

MEETING FORTY-TWO

DÜBENDORF, SWITZERLAND 24 TO 27 AUGUST 2009

M I N U T E S
(F Lam)

1 CHAIRMAN'S INTRODUCTION

Prof. Hans Blass welcomed the delegates to the 42nd CIB W18 Meeting in Zurich, Switzerland. He thanked René Steiger and Jochen Köhler for hosting the meeting. Twenty seven papers will be presented this year. The presentations are limited to 20 minutes each, allowing time for meaningful discussions after each paper. The Chair asked the presenters to conclude the presentation with a general proposal or statements concerning impact of the research results on existing or future potential application and development in codes and standards. R. Görlacher will deal with questions regarding the meeting proceedings.

Papers brought directly to the meeting would not be accepted for presentation, discussions, or publication. Papers presented by non-authors or non-coauthors are not recommended except in exceptional situations because the discussion process might be compromised.

There are 11 topics covered in this meeting: Limit State Design Codes (1), Stress Grading (1), Stresses for Solid Timber (3), Timber Joints and Fasteners (9), Timber Beams (1), Laminated Members (5), Structural Stability (4), and Fire (3).

René Steiger discussed organizational matters for the meeting.

2 GENERAL TOPICS

Ario Cecotti provided information on WCTE 2010. Over 700 abstracts have been received, most of which are from Japan (over 400). Other notable countries contributing abstracts are Italy (70), Germany (53) and USA (50).

3 LIMIT STATE DESIGN

42 - 1 - 1 Calculation of Partial Safety Factors 41 - 102- 1 – **T Poutanen**

Presented by T Poutanen

H.J. Larsen stated that if the paper is correct, then it points out that there is something wrong with the Eurocode. What the author will do about it, as the partial saftety factors issue is outside the scope of CIB W18. T. Poutanen answered that this issue is indeed difficult. He added that the variability in timber is high compared to other building materials. Eurocode is good for steel and penalizes timber; therefore, there is excessive safety in timber.

J. Munch-Andersen said that he is not convinced whether the results are right because there would have been more failures in steel structures. T. Poutanen said that since the safety margin in codes is so high, steel failures are not observed even if the factors were wrong.

J. Köhler commented that the approach is conceptually wrong because it uncoupled the design with the load combination process. For example a given beam designed to carry gravity load will have to be sized differently if additional live load is applied in combination. He suggested that the paper needs to explain how this work relates to how other people's work is done.

A. Ranta-Maunus stated that he does not understand why loads are considered as dependent and why material is dependent on the load. There are no references to scientific literature as this is something the author has created. T. Poutanen answered that this is mathematics and that loads become dependent when applied to the member simultaneously.

H.J. Blass concluded that there are critical questions related to this work.

H.J. Blass announced the formation of a small subgroup to consider the suitability of papers for publication in the CIB W18 proceedings. Not all papers accepted for presentation will necessarily be published in the proceedings.

(Remark: the paper was not accepted for publication in the proceedings according to the peer review procedure given in chapter 14 of the proceedings)

4 STRESS GRADING

42 - 5 - 1 *Machine Strength Grading – a New Method for Derivation of Settings* - **R Ziethén, C Bengtsson**

Presented by C Bengtsson

H.J. Blass stated that very conservative settings could result if different settings were not available for a single grade. In the case where different settings for one grade are currently set if the number of grades produced in a mill is different is an important issue.

C. Bengtsson answered that it is not good to have a complicated system where people do not understand how it works. She agrees that the proposed process could be conservative and it is possible to consider the issues in question.

M. Sandomeer states that output control or monitor process is also possible to be considered to improve grading process.

A. Jorissen asked whether not having different settings for the same grade is practically wrong. C. Bengtsson answered that it is not practically wrong but we currently have a large combination and it is too complicated.

A. Ranta-Maunus said that when considering only the 5th percentile value this is not wrong but when considering the lower tail, it may be incorrect. He agrees with H.J. Blass that it is not fully economical and work should be done.

J. Köhler stated that it is important to rethink the issue of grading with output control system. It may be an issue for the code writing body. It is also important to look into lower tails rather than just 5th percentile.

C. Bengtsson answered that it is possible to consider the issues as additional work.

5 STRESSES FOR SOLID TIMBER

42 - 6 - 1 *Variability of Strength of European Spruce* - **A Ranta-Maunus, J K Denzler**

Presented by A Ranta-Maunus

S. Aicher stated that when looking at the strong decrease in strength and stiffness when comparing 175 mm to 225 mm width, it may be related to sawing pattern of the logs; otherwise, this information may also concern the timber resources in central Europe. A. Ranta-Maunus answered that sawing pattern may be a problem but forest management practice is also an important issue where other countries may have different approach compared to Scandinavia. H.J. Blass stated that the forest management practice is different in central Europe as they do not harvest trees from the same age group therefore large sizes timber from Central Europe should still be okay in terms of strength properties.

J.W.G. van de Kuilen received clarification of the procedures by checking subsamples with large specimens.

G. Schickhofer and R. Steiger received confirmation that k_v (EN 384) was used. A. Ranta-Maunus commented that he did not like the factor.

42 - 6 - 2 *Impact Loaded Structural Timber Elements Made from Swiss Grown Norway Spruce* **- R Widmann, R Steiger**

Presented by R Widmann

F. Lam commented that the shape and size of the loading tub/head will influence results. Also the influence of the inertia load of the beam was not considered without mounting an accelerometer on the specimen. R. Widmann agreed that the shape of the loading head has an influence. Although the influence of the inertia loads were not considered, the results seem reasonable.

H.J. Larsen stated in the case of impact loading on scaffolding planks where the plank may break from a person jumping on it. The interaction of the human body is very important and in this study, the loading head is very stiff. R. Widmann agreed the specific case of a man jumping on a board will influence the response. Successive drops at increasing heights are also tests specified in test standards; it is a good method for specific cases but will not address the general problem of impact strength of material.

J.W.G. van de Kuilen stated that the impact speed k_{mod} factor of 1.3 is reasonable. R. Widmann stated that without considering the comments from F. Lam, his results indicated ~ 1.27 so the k_{mod} of 1.3 seems reasonable.

A. Jorissen received confirmation about the integrals of force versus deformation and force versus time and the relationship between them.

The possibility of needing to develop individual test methods for different applications is discussed.

42 - 6 - 3 *Modelling the Bending Strength of Timber Components –Implications to Test Standards*- **J Köhler, M Sandomeer, T Isaksson, B Källsner**

Presented by J Köhler

F. Lam commented that the factors developed from Isaksson's data are applicable to high quality timber. Lower quality material with more variability will behave differently; H.J. Larsen and J. Köhler discussed the issue of bias being prescribed in the standard and the issue of whether there is a need to change the test standard to remove the bias. They also discussed the fact that limited data is available when testing more than one section within a piece and the majority of the data in Europe were obtained based on the existing test standard.

J. Munch-Anderson stated that if ones test the specimen with randomly placed weak point, it would be difficult to account for different load conditions.

J Köhler commented that the "bias" needs to be specified. J.W.G van de Kuilen stated that in many wood species in the world the weak section cannot be determined.

6 TIMBER JOINTS AND FASTENERS

42 - 7 - 1 Base Parameters of self-tapping Screws - **G Pirnbacher, R Brandner, G Schickhofer**

Presented by G Pirnbacher

H.J. Blass commented that changing definition of f_{ax} or f_1 in Eurocode would make things difficult.

A. Jorissen questioned whether r^2=0.3 is enough. He also asked about the safety of the realized connection. G. Pirnbacher answered that the low r^2 values are inherent to the material properties.

H.J. Blass received confirmation that the tests were performed with the screw direction parallel to grain and the long term strength effect was not considered.

J.W. G. van de Kuilen discussed the fact that in machine grading, the overall density of the board is considered rather than the density of the individual specimen and asked what would be the influence of this effect. G. Pirnbacher answered that r^2 values would decrease because of the variability of density.

42 - 7 - 2 Joints with Inclined Screws and Steel Plates as Outer Members - **H Krenn, G Schickhofer**

Presented by H Krenn

S. Aicher received confirmation of how the overlap distance of 4d was measured. He commented that the moment caused by the misalignment of the shear forces of the screws and the reaction would only level out if there are a large number of rows and the 4d overlap might not be appropriate if there are few screws. H. Krenn responded that there are different provisions in the paper for cases with few screws.

R. Crocetti commented that the splitting problem can be resolved by installing reinforcement perpendicular to grain. H. Krenn agrees.

P. Quenneville questioned why there is a split and H. Krenn explained via free body diagram.

42 - 7 - 3 Models for the Calculation of the Withdrawal Capacity of Self-tapping Screws - **M Frese, H J Blaß**

Presented by M Frese

J.W. G. van de Kuilen received confirmation that the pitch was not included because it did not have significant effect.

G Schickhofer questioned whether there is a difference in performance between different producers. M. Frese responded that the main aim of the paper is to create a model to explain the behaviour independently of the producer. H.J. Blass stated that 15 to 20 producers were considered in Universität Karlsruhe and it seems there are no major differences between producers.

G Schickhofer commented that the model indicates that the code values are too conservative. He asked whether the model will be used. H.J. Blass agreed that the model can be used. In some cases there is a 100% increase in characteristic values.

42 - 7 - 4 Embedding Strength of New Zealand Timber and Recommendation for the NZ Standard - **S Franke, P Quenneville**

Presented by P Quenneville

J.W. G. van de Kuilen received confirmation that the diameter can be ignored in one of the cases.

H.J. Larsen stated that he has no doubt that it is useful to get the data but he questioned the distinction between acquiring data and knowledge; where knowledge acquisition needs research. He asked what the research content of the paper is. P. Quenneville agreed that the paper does not have a high level of new research content. However the new data is needed to address code changes issues in New Zealand therefore it is valuable. It is also important to confirm applicability of EC5 provisions for New Zealand engineers.

A. Buchanan stated since LVL and lumber are the same radiata pine material in New Zealand, he questioned why there is a difference. P. Quenneville stated that they are different materials because of density difference.

H.J. Blass commented that density of individual specimens was used in the development of the equation and there are other significant factors which can be masked by this approach. For the final proposal in the code equation additional procedures are needed. P. Quenneville agreed.

42 - 7 - 5 Load Carrying Capacity of Timber-Wood Fiber Insulation Board – Joints with Dowel Type Fasteners – **G Gebhardt, H J Blaß**

Presented by G Gebhardt

B. Dujic asked whether one can add the contribution of WFIB with respect to adding different normal sheathing. He said the normal sheathing may have higher stiffness so its contribution in roof application will be minimal. He received clarification of the shear flow in plane and asked about the shear modulus of WFIB. G. Gebhardt said that the shear modulus of WFIB ranges from 50 N/mm^2 to 250 N/mm^2. H.J. Blass said that the thickness of WFIB in roof application is high so that it can contribute to the overall stiffness and confirmed that thick plate connections will fail first but thinner plates may have different mode of failure. H.J. Blass added that shear wall and diaphragm tests will be conducted.

T. Poutanen asked what would happen if one add adhesive. G. Gebhardt answered that initial stiffness would increase. H.J. Blass added that this was tried already and failure will be in the panels.

S. Winter commented that this panel is used commonly in roof applications and doubt the stiffness will be enough for roof construction because there are usually many smaller sub-plates which means that you do not have a continuous plate. H.J. Blass said that they are trying WF/WF connections to make it into one big sheet with mechanical fasteners.

42 - 7 - 6 Prediction of the Fatigue Resistance of Timber-Concrete-Composite Connections – **U Kuhlmann, P Aldi**

Presented by P Aldi

H.J. Blass received confirmation that the groove joints failed in shear. He asked how you would design such a case. P. Aldi said that code values would be used and uniform distribution of shear stress would be considered which is higher than values in the standard. A simplified model will be used as there is not much literature available.

They discussed the fact that results are dependent on the geometry and the static resistance of the timber uses kfatigue info from the code. H.J. Blass stated that this still needs shear strength information of the material; the approach needs more work.

J. Köhler asked whether the temperature was measured. P. Aldi gave a positive response in which the temperature was measured and there was small difference especially with low frequency. J. Köhler asked about the issue of accumulative time to loading and DOL effect in timber.

P. Aldi said that there are load duration models in timber but these are not the main points of the thesis.

P. Crocetti asked whether a modified shape of the groove would give better results. P. Aldi agreed that one can have the benefit. Some references however show the case with different angles and there seemed to be little impact. He said that in this case there are some compression forces in the notch. Also the theory under predicted the test results which shows there must be some compression.

M. Fragiacomo stated that the inclined surface with shrinkage of timber may create a gap so it may not be reliable. P. Aldi said that they have been trying to develop a model. H.J. Blass questions whether there will be a separating layer between the concrete and timber. There may be a gluing effect between timber and concrete. This means that the influence of inclination will not be strong.

42 - 7 - 7 Using Screws for Structural Applications in Laminated Veneer Lumber – **D M Carradine, M P Newcombe, A H Buchanan**

Presented by D M Carradine

H.J. Blass discussed about the EC5 values and the model assumptions at the pivot point. He asked whether there is compression stresses perpendicular to grain there. Given the pivoting deformation the other screws may have minor impact. He also asked how the thickness of the steel plate was chosen. D.M. Carradine answered that the design of the steel plate was based on bending for all different types of specimens.

E Gehri discussed shearing out failure of the timber and commented that the behaviour of the timber is important because of group action as this is part of the failure.

A. Ceccotti stated that the self centering idea is a good one and asked whether there are plans to study other cases such as wall system. D.M. Carradine responded that this will be considered.

Tuomo Poutanen stated that this technique looks expensive and asked whether a study on the cost of these joints will be carried out. D.M. Carradine agreed that this could be expensive.

F. Lam commented that average values should not be compared against characteristic values.

K. Crews stated that there are also interests in cost of repair after an earthquake and the speed of construction is okay.

42 - 7 - 8 Influence of Fastener Spacings on Joint Performance - Experimental Results and Codification – **E Gehri**

Presented by E Gehri

H.J. Blass asked on what basis was the influence of edge distance considered and will one consider the reduction of edge distance? E. Gehri stated yes. The screws can be long and if they are not installed correctly they can go through to the outside of the beam,

A. Jorissen discussed the accumulation of stresses perpendicular to grain and shear; if the spacing is reduced, their influence can increase. The friction between dowel/timber glued-in-rods/timber and screw/timber is different which can influence the stresses. He commented that he can't see why the screws would react the same way as glue-in rod. Finally laterally loaded fastener versus withdrawal behavior was discussed.

P. Quenneville asked how one can say that the measured values are statistically different for the 4th group of a/H. E. Gehri said that it is based on engineered judgment. G. Schickhofer also added that there are recognized group and system effects which support the engineered judgment.

J. Jensen said that the glue effect factor for glued in rods is failing in yielding and not rod in withdrawal and group effect in yielding will not occur. He said that in Eurocode 1st failure is in yielding mode then wood failure mode. In practice you can't get glued in length long enough for yielding to occur; therefore, wood withdrawal failure is occurring. H.J. Blass asked whether there were withdrawal failures or yielding failure of the rods. E. Gehri answered only withdrawal failures were noted.

*42 - 7 - 9 Connections with Glued-in Harwood Rods Subjected to Combined Bending and Shear Actions – **J L Jensen, P Quenneville***

Presented by J L Jensen

H.J. Blass commented that there is information from Karlsruhe on steel rod under pure shear mode where shear failures were observed. He received explanation of one of the test configuration where almost the entire section has dowels covering it. Here he/h would be close to one as k approaches infinity where dowel load bearing capacity would be in terms of bending and embedment.

E. Gehri asked how would one control the gluing of the rods. J.L. Jensen said that in testing the rod were pulled.

R. Crocetti asked what would be the advantage of using hard wood rod and whether the placement of the rod has been optimized for shear capacity. J.L. Jensen said that the steel rods can corrode and the connection is intended to take large moment.

R. Steiger commented that since the paper only deals with hardwood dowel the title should be adjusted (Remark: done by the author).

S. Aicher stated that tension perpendicular to grain stress can be expected in bending in location near the tension rods close to the bending tension edge. This behaviour is commonly seen in steel rods. The bending stiffness of the hardwood dowel is more compatible with the timber member hence you did not get such a failure mode. He asked what would the efficiency of a joint with lots of dowels be. In design you have to make reduction according to the hole created by the rods. Therefore the efficiency would be low. H.J. Blass said that this is a wrong engineering assumption which explains the good observed efficiency in the connector.

A. Buchanan asked whether the equation would be applicable to glulam to steel connections. He stated that glued-in rod with crosswise reinforcement was used in Sydney. J.L. Jensen said that this was thought of but was not done. A. Buchanan also stated that B. Madsen did similar work in UBC with 45 degree steel rods and this work should be considered. J.L. Jensen said that wood-steel situation would give different solutions.

U. Kuhlmann said that it would be nice to have such joints in the code for timber to timber as well as timber to other materials. In this work material values were assumed and were specific to the tested material (eg G); therefore, more work is needed to get a general solution. The glued-in-rod perpendicular as reinforcement is effective. J.L. Jensen agrees.

7 TIMBER BEAMS

42 - 10 -1 Relationships Between Local, Global and Dynamic Modulus of Elasticity for Soft- and Hardwoods – **G J P Ravenshorst, J W G van de Kuilen**

Presented by JWG van de Kuilen

R. Steiger asked why EN384 adjustment equations were not used. He commented that MOE_{local} versus MOE_{global} ratio of 1.15 was found in EMPA study and there is no point of having an equation with a non zero offset. Specimens with low MOE are too much on the safe side. J.W.G. van de Kuilen replied that the current study ratio of 1.13 agrees with the 1.15 factor of EMPA study and agrees with the other comments.

A. Ranta-Maunus stated the results are in-line with Finnish experience and he doesn't believe in the adjustment equation in EN384.

R Steiger asked whether there is any dependency on the frequency of wave propagation such that ultrasonic devices need to be excluded because the results may be wave speed/ equipment dependent. He asked would there be rules to exclude some devices. J.W.G. van de Kuilen replied that damping issues of ultrasonic wave would influence results; therefore, only stress wave results were focused and they have confidence in the data.

8 LAMINATED MEMBERS

42 - 12 - 1 Glulam Beams with Holes Reinforced by Steel Bars – **S Aicher L Höfflin, M Jung**

Presented by S Aicher

H.J. Blass asked how to explain the difference between screw in and glue in rods. S. Aicher replied that the difference in results should not be over-interpreted. There is a moment in the rod which makes the design complicated. This can contribute to the differences as there is higher deformability due to the moment.

H.J. Larsen commented that he is impressed with the size of the test program and asked about the shear strength of the cross section. S. Aicher replied that they have tested for the shear strength of the cross section.

H.J. Larsen commented that rather stating that the design method should be improved, reinforcement should be used. S. Aicher said that both issues are important. Even with reinforcement one does not reach capacity which indicates it does not depend on design method. H.J. Blass said that in cases of rectangular hole you would not reach capacity even with reinforcement.

T. Poutanen asked what would happen in the reinforcement situation if the timber dries out. S. Aicher said that the overall failure mechanism will stay the same but initial crack load could be reduced.

J.W.G. van de Kuilen received clarification on the detail of the FEM where the rods were modeled by discretely connected beam elements.

42 - 12 - 2 Analysis of X-lam Panel-to-Panel Connections under Monotonic and Cyclic Loading – **C Sandhaas, L Boukes, J W G van de Kuilen, A Ceccotti**

Presented by C. Sandhaas

H.J. Blass received clarification that the 30 mm deformation was related to 2 connections; therefore, 15 mm per shear connection.

H Zeitter asked and received explanation on why one of the four sets of results was used and whether the specimens were identical. He also asked and received information about the gaps in the wall elements and the results are symmetrical.

B. Dujic stated that he has tested a similar system and the ductility was more than 6. He asked whether one could get 7 or 8 for ductility if the loading was continued. C. Sandhaas said that the expected capacity was almost reached and they discussed why the damping ratio was higher with increasing cycles.

F. Lam commented on the test configuration where the gap closure during testing might lead to friction which can influence the test result.

A. Buchanan initiated discussions about the building system, the rocking mechanisms, the screw quality, storey height, and energy dissipation mechanism.

H. Zeitter further questioned about the gaps between main wall elements and stated that the gap in the test set up should be maintained.

M. Yasumura stated that if the connection is too rigid energy dissipation may not be achieved.

M. Popovski asked about the influence of the floor slab which could prevent rocking movement. C. Sandhaas replied that the floor slab may not be continuous and compression perpendicular to grain stresses and deformations also occur. B. Dujic stated that there are screw connections between the floor and the wall which are quite a lot weaker; therefore, one will have rocking.

I. Smith discussed the concept of ductility.

T. Williamson stated that this type of work is very much needed if the CLT products were to make its way to the US.

42 - 12 - 3 Laminating Lumber and End Joint Properties for FRP-Reinforced Glulam Beams – **T G Williamson, B Yeh**

Presented by TG Williamson

H.J. Blass asked whether a flat line can be used to represent the stress strain relationship in compression. T.G. Williamson replied yes.

A. Buchanan asked whether the approval involves getting a calculation model approved and a design method approved. T.G. Williamson replied that one can use the APA/University of Maine model and calibrate it with one's data. The University of Maine model is proprietary.

I. Smith and T.G. Williamson discussed the approach to size effect and what can be done as follow up.

J.W.G. van de Kuilen asked how one will handle gluing of the fiber in practice and fire issue. T.G. Williamson answered the gluing of fiber is not as complex as previous cases. Here sanding technique is no longer needed. Fire behaviour was reported in a previous CIBW18 meeting.

S. Aicher stated that in Europe gain of using FR beam was not attractive and design model was not appealing. T.G. Williamson answered that in the past the process and design model for FR beam in US was convoluted. The current system is much simpler and very attractive to manufacturers.

A. Jorissen stated that the gain in stiffness is not that high. T.G. Williamson answered stiffness control 5% of the time especially with camber.

R. Crocetti suggested that the price of carbon fiber must be too high and asked if steel plate was considered. He also asked about γ_m and γ_{dol} values. T.G. Williamson said hat fiber has the advantage of coming in spool and glass fiber has much lower cost. University of Maine results show DOL and moisture factors have not changed.

42 - 12 - 4 Validity of Bending Tests on Strip-Shaped Specimens to Derive Bending Strength and Stiffness Properties of Cross-Laminated Solid Timber (CLT) **– R Steiger, A Gülzow**

Presented by R. Steiger

H.J. Blass stated that the difference between shear and rolling shear failure is not apparent. R. Steiger agreed.

J. Köhler stated that multiple parameters can have several optima. R. Steiger said that he took more Eigen frequencies than needed to derive the nine elastic constants.

H.J. Blass and R. Steiger discussed the failure mode of the four-side supported panel with restraint against lifting. H.J. Blass asked whether the rolling shear in the panel compared to strip was compared. R. Steiger said not yet.

42 - 12 - 5 Mechanical Properties of Stress Laminated Timber Decks - Experimental Study **– K Karlsson, R Crocetti, R Kliger**

Presented by K Karlsson

M. Frese wondered why the drawing shows an unsymmetrical response. K. Karlsson said that the drawing exaggerates the unsymmetrical behaviour.

R. Widmann received clarification that the deflections are relative deflections.

9 STRUCTURAL STABILITY

42 - 15 - 1 Design Aspects on Anchoring the Bottom Rail in Partially Anchored Wood-Framed Shear Walls **– U A Girhammar, B Källsner**

Presented by U A Girhammer

S. Aicher questioned from a practical point of view why a stiff steel plate was not used instead of washer as a cheap effective solution. U.A. Girhammar replied that the stiff steel plate is a safe option. S. Aicher asked why this was not calculated. U.A. Girhammar replied that an analytical study is underway and results will be available soon.

H.J. Larsen commented about the statement that design rules are needed and more research is also needed. He asked why you don’t come up with design rules so that more research is not needed. U.A. Girhammar agreed that they will aim to achieve this.

B. Källsner stated that the use of a stiff steel plate is an economic question. S. Aicher stated that may be use of a small washer with a small stiff wood plate can also be done. B. Källsner said that this would not be common practice.

I. Smith commented that foundation is also important because the rigidity of the foundation will influence the performance such that a mechanistic based approach would be more difficult. U.A. Girhammar stated they have not yet addressed this issue.

B. Dujic stated that this failure mode is unrealistic because the influence of vertical stud acting as a restraint has been ignored. B. Källsner stated that in this situation the vertical stud will follow the sheathing material and there will be separation between the stud and the plate; therefore, its influence will be minimal.

B. Dujic and U.A. Girhammar also discussed the issue of the influence of the aspect ratio of the wall.

S. Winter commented that bolts are doweled to concrete with small edge distances; therefore, brittle failure mode in the concrete may occur. Also multi story building would need hold-downs to carry uplift and anchor bolts would carry racking forces. The subject of this paper is more suited for small simple building. B. Källsner said that concentrated forces can be more distributed without the hold-down devices which could be desirable.

H.J. Blass commented that we need a unified design method that can cover all cases and the plastic design is such a method.

C. Ni said that this issue has been identified in the Northridge Earthquake. In N. America we specify the use of large washer to achieve the desired safety. Minimum splitting strength is difficult to estimate and unreliable as annual ring orientation can come into play also. U.A. Girhammar agrees that annual ring orientation is important.

B.J. Yeh asked about the anchor bolt spacing as this is a two dimensional issue. In US no more than 40 mm o/c and washer size is 75 mm diameter minimum. U.A. Girhammar agrees and will study it.

S. Aicher stated that the spacing and diameter of nails are unrealistic. This will be problematic because it is not practical to convert results to reality. U.A. Girhammar stated that the experiment was designed to force the desire mode of failure so that we can measure the splitting strength.

B. Källsner provided a comment towards H.J. Larsen's question that a simple solution is not apparent because the situation is more complex.

42 - 15 - 2 New Seismic Design Provisions for Shearwalls and Diaphragms in the Canadian Standard for Engineering Design in Wood – **M Popovski, E Karacabeyli, Chun Ni, G Doudak, P Lepper**

Presented by M Popovski

A. Buchanan asked about the basis to come up with this process. M. Popovski answered that the work is a little bit of everything with past Nonlinear time step analysis, test results from the past and consultation with design community. A. Buchanan stated that he does not understand the concept of non-yielding diaphragm. M. Popovski said that it came from National Building Code of Canada provisions. I. Smith added reinforced concrete diaphragm is non-yielding and the NBCC committee is dominated by concrete experts. He also commented that there are many uncertainties on the load side. C. Ni said that this is an issue for hybrid construction with concrete or masonry walls and wood diaphragm.

R. Steiger discussed the over-strength factor of 1.2 to modify the load versus the resistance. M. Popovski said that there are plans to do this.

M. Fragiacomo stated that in EC5 there is no over-strength design factor and asked why this factor was applied to the 1st floor. M. Popovski explained that the provisions tried to address the issue of soft story failure in the 1st two stories.

A. Buchanan commented that one can't tell the building to have yielding at every point simultaneously. The key is to make sure we don't have yielding in undesirable places. You try to do this but it is not apparent that it has been achieved.

42 - 15 - 3 Stability Capacity and Lateral Bracing Force of Metal Plate Connected Wood Truss Assemblies – **Xiaobin Song, F Lam, Hao Huang, Minjuan He**

Presented by F. Lam

H.J. Blass asked about the use of battens versus sheathing. F. Lam replied that testing is expensive therefore we used a combined testing/modeling approach and only addressed a limited number of cases to verify the model. With a verified model we can apply it to battens as well.

H.J. Blass asked why only one set of webs were tied to a support. F. Lam responded that it is intended to push and test the model as much as possible by introducing complication condition in the testing. H.J. Blass commented that in the 2D analogy bending moment will be introduced into the web when diagonal braces are not tied to the web nodal point. F. Lam agreed.

T. Poutanen asked about the load –deformation curve of the truss system as he suspects the load would not decrease much due to buckling. F. Lam said the load-deformation information would be available in Dr. Song's thesis. The load was sustained for a long time after buckling occurred. K. Crews asked whether loading was kept up after the failure. F. Lam replied no.

P. Quenneville asked what factor one would recommend instead of the 2% rule. F. Lam said that for the system studied the 2% rule is too conservative by a factor of 2 or more. Since only one system was studied, more work should be done with a variety of system and cases to come up with sound recommendation.

J. Köhler found the work interesting to tie probability of failure to system behaviour. He asked whether sensitivity analysis of model uncertainties were studied, F. Lam replied this was not yet done. The reliability work is a framework within which more study and analysis should be and can be done.

42 - 15 - 4 Improved Method for Determining Braced Wall Requirements for Conventional Wood-Frame Buildings – **Chun Ni, H Rainer, E Karacabeyli**

Presented by C Ni

B.J. Yeh asked whether the analysis shown in Tables 1 and 2 take gypsum in to consideration. He asked in the case of baseline braced wall line how can one conclude that it is inadequate. C. Ni explained that there is no need for partition or interior wall because of the geometry in one direction and in the other direction gypsum wall board was considered as an interior wall with gypsum on both sides. B.J. Yeh commented that wind and seismic being different in US code. Gypsum is good in wind but not good in seismic. N. Chun said it makes a lot of sense to separate the two cases.

A. Ceccotti asked whether the Canadian prescriptive code requires buildings to be symmetrical. N. Chun responded yes it is a requirement in the Canadian prescriptive code. A. Ceccotti then asked how one would define symmetry as for example in cases of a garage.

S. Aicher received definition of braced wall panel and the bottom plate only anchored to foundation; no requirement of hold-down.

I. Smith commented that light frame construction can be susceptible to moisture so the case of wind with or without rain needs to be considered. T.G. Williamson responded that the buildings are assumed water tight so issue of rain and moisture does not come into play. In US there is a 100 plus page document prepared to explain the 10 page prescriptive code. H.J. Blass commented that it would be easier to just design shear wall and braced wall. C. Ni stated Part 9 of the Canadian code is a prescriptive code so we need this information. The philosophy is that these buildings tend to perform well so they don't need engineering design.

10 FIRE

42 - 16 - 1 Advanced Calculation Method for the Fire Resistance of Timber Framed Walls **– S Winter, W Meyn**

Presented by W Meyn

J. König stated his concern about the title of the paper as the paper deals with material properties and commented that one could verify the EC model with the calculations. S. Winter responded that the FEM based calculation model is intended to take into account the influence of cracks and find the phenomenon of the influence of mass transfer on fire performance including the heating effect due to the cracks. EC 5 is far on the safe side as shown in the experiments.

S. Aicher stated that there are no new cracks considered with existing cracks in the model. In reality new cracks can evolve between existing cracks. S. Winter replied that no new crack is an assumption.

A. Frangi commented on the differences between calculated and test results up to 20 minutes. The formation of cracks is very complex regarding material properties which can contribute to the added complication of these modeling processes. S. Winter responded that we have to start somewhere.

A. Buchanan received confirmation of how the thermal properties of the wall mass transfer are modeled and the specific heat capacity is calculated, not measured. A. Buchanan stated that moisture wave is an important issue. Lund University has done good work in this area with modeling.

42 - 16 - 2 Fire Design Model for Multiple Shear Steel-to-Timber Dowelled Connections **– C Erchinger, A Frangi, M Fontana**

Presented by A Frangi

H.J. Blass commented that in some dowels the edge distance after the fire duration is very low and asked if the model takes this into consideration. A. Frangi responded that the model considers this.

H.J. Blass asked how the designer knows. A. Frangi replied the designer only needs charring depth and needs to respect minimum requirement according EC5.

R. Crocetti asked how manufacturing tolerance of the gap between steel plate and wood alter the results. A. Frangi replied the influence may not be too much.

A. Buchanan stated that the design method involves design at room temperature and allow for charring rate. The design method doesn't check the embedment strength of each dowel. Difference in the embedment strength for each dowel and along the length of the dowel would lead to more of a plastic deformation. He asked when FEM was done, was the dowel considered stationary or moving. A. Frangi replied that the dowel movement was not considered. He said there are two parameters (embedment strength and temperature) but one equation. Therefore one can make the adjustments to make it work.

T. Poutanen discussed rule of thumb to determine the volume of wood after charring.

S. Aicher asked in the 3D calculation was the temperature progression according to end grain face considered. A. Frangi replied yes.

S. Winter commented that the paper is excellent. Most discussions look for complicated issues however the final design proposal is actually very simple which is based on the cross section after charring.

42 - 16 - 3 Comparison between the Conductive Model of Eurocode 5 and the Temperature Distribution within a Timber Cross-section Exposed to Fire **– M Fragiacomo, A Menis, P Moss, A Buchanan, I Clemente**

Presented by M Fragiacomo

H.J. Blass and M. Fragiacomo discussed how the model parameters were determined and confirmed fire test results were used to fit the model.

S. Winter discussed the charring rate of LVL in two different chambers. A. Buchanan replied that they are fairly consistent at ~0.72 mm/min for timber. S. Winter stated that LVL is not timber and the new model over-estimates some of the results. He discussed the control of temperature range within a chamber and suggested the need to check the small furnace because furnace can influence the results of the experiment.

J. König stated in EC5 different charring rates for timber and LVL was needed. From Finland the timber and LVL numbers were the same. Some conductivity values are not conductivity values. They are a combination of various parameters which are simplified as effective values. These are results of calibration. Expect LVL and wood to behave differently as influenced by glue-line and thinner char layers because of less insulation provided by char layer. M. Fragiacomo replied measurements were taken of char layer. In the model, no reduction of thickness is assumed and one will look into this further.

S Aicher stated that multilayer composites with differences of density in the layer will contribute to the difference.

J. Köhler commented when judging about differences between approaches, one needs to consider the uncertainties to get an overview of what is important and what is not important.

A. Frangi commented ETH calculates the properties of solid timber not LVL up to 300C after which it is not important. There is a need to check the equipment to 300C. Ten minute difference in results can occur which can make a lot of difference in charring rate.

11 ANY OTHER BUSINESS

R. Steiger thanked the sponsors of the 42nd CIB W18 meeting and the EMPA and ETH team. He also thanked the candidates for their participation.

Master copy of the paper and pdf files with any corrections should be send to R Görlacher at the end of September 2009. Some of the papers will be renumbered. Changes to papers only needed if errors were identified.

External peer review of T. Poutanen’s paper will be sought before consideration for publication in CIB W18 meeting book.

J. Munch Andersen demonstrated Danish software for timber connections with dowel type fasteners according to N 1995-1-1 with gaps filled in with traditional Danish design methods.

12 VENUE AND PROGRAMME FOR NEXT MEETING

A. Buchanan invited the CIB W18 meeting to come to Christchurch New Zealand at the end of August 2010.

M. Fragiacomo invited the CIB W18 meeting to come to Italy in 2011.

The meeting venues for the next few years are: New Zealand (2010), Sardinia Italy (2011), and Växjo (2012).

13 CLOSE

The chair thanked the speakers for their presentations and the delegates for their participation. He also thanked R. Steiger and the host team (EMPA and ETH) for their efforts to organize an excellent meeting.

14. Peer Review of Papers for the CIB-W18 Proceedings

14. Peer review of papers for the CIB-W18 Proceedings

Experts involved:

Members of the CIB-W18 "Timber Structures" group are a community of experts in the field of timber engineering.

Procedure of peer review

- Submission of manuscripts: all members of the CIB-W18 group attending the meeting receive the manuscripts of the papers at least four weeks before the meeting. Everyone is invited to read and review the manuscripts especially in their respective fields of competence and interest.

- Presentation of the paper during the meeting by the author

- Comments and recommendations of the experts, discussion of the paper

- Comments, discussion and recommendations of the experts are documented in the minutes of the meeting and are printed on the front page of each paper.

- Final acceptance of the paper for the proceedings with
  - no changes
  - minor changes
  - major changes
  - or reject

- Revised papers are to be sent to the editor of the proceedings and the chairman of the CIB-W18 group

- Editor and chairman check, whether the requested changes have been carried out.

15. List of CIB-W18 Papers, Dübendorf, Switzerland 2009

List of CIB-W18 Papers, Dübendorf, Switzerland 2009

16. Current List of CIB-W18(A) Papers

CURRENT LIST OF CIB-W18(A) PAPERS

Technical papers presented to CIB-W18(A) are identified by a code CIB-W18(A)/a-b-c, where:

a denotes the meeting at which the paper was presented. Meetings are classified in chronological order:

1 Princes Risborough, England; March 1973
2 Copenhagen, Denmark; October 1973
3 Delft, Netherlands; June 1974
4 Paris, France; February 1975
5 Karlsruhe, Federal Republic of Germany; October 1975
6 Aalborg, Denmark; June 1976
7 Stockholm, Sweden; February/March 1977
8 Brussels, Belgium; October 1977
9 Perth, Scotland; June 1978
10 Vancouver, Canada; August 1978
11 Vienna, Austria; March 1979
12 Bordeaux, France; October 1979
13 Otaniemi, Finland; June 1980
14 Warsaw, Poland; May 1981
15 Karlsruhe, Federal Republic of Germany; June 1982
16 Lillehammer, Norway; May/June 1983
17 Rapperswil, Switzerland; May 1984
18 Beit Oren, Israel; June 1985
19 Florence, Italy; September 1986
20 Dublin, Ireland; September 1987
21 Parksville, Canada; September 1988
22 Berlin, German Democratic Republic; September 1989
23 Lisbon, Portugal; September 1990
24 Oxford, United Kingdom; September 1991
25 Åhus, Sweden; August 1992
26 Athens, USA; August 1993
27 Sydney, Australia; July 1994
28 Copenhagen, Denmark; April 1995
29 Bordeaux, France; August 1996
30 Vancouver, Canada; August 1997
31 Savonlinna, Finland; August 1998
32 Graz, Austria, August 1999
33 Delft, The Netherlands; August 2000
34 Venice, Italy; August 2001
35 Kyoto, Japan; September 2002
36 Colorado, USA; August 2003
37 Edinburgh, Scotland, August 2004
38 Karlsruhe, Germany, August 2005
39 Florence, Italy, August 2006
40 Bled, Slovenia, August 2007
41 St. Andrews, Canada 2008
42 Dübendorf, Switzerland 2009

b	denotes the subject:

1	Limit State Design
2	Timber Columns
3	Symbols
4	Plywood
5	Stress Grading
6	Stresses for Solid Timber
7	Timber Joints and Fasteners
8	Load Sharing
9	Duration of Load
10	Timber Beams
11	Environmental Conditions
12	Laminated Members
13	Particle and Fibre Building Boards
14	Trussed Rafters
15	Structural Stability
16	Fire
17	Statistics and Data Analysis
18	Glued Joints
19	Fracture Mechanics
20	Serviceability
21	Test Methods
100	CIB Timber Code
101	Loading Codes
102	Structural Design Codes
103	International Standards Organisation
104	Joint Committee on Structural Safety
105	CIB Programme, Policy and Meetings
106	International Union of Forestry Research Organisations

c	is simply a number given to the papers in the order in which they appear:

Example:	CIB-W18/4-102-5 refers to paper 5 on subject 102 presented at the fourth meeting of W18.

Listed below, by subjects, are all papers that have to date been presented to W18. When appropriate some papers are listed under more than one subject heading.

LIMIT STATE DESIGN

1-1-1	Limit State Design - H J Larsen
1-1-2	The Use of Partial Safety Factors in the New Norwegian Design Code for Timber Structures - O Brynildsen
1-1-3	Swedish Code Revision Concerning Timber Structures - B Noren
1-1-4	Working Stresses Report to British Standards Institution Committee BLCP/17/2
6-1-1	On the Application of the Uncertainty Theoretical Methods for the Definition of the Fundamental Concepts of Structural Safety - K Skov and O Ditlevsen
11-1-1	Safety Design of Timber Structures - H J Larsen
18-1-1	Notes on the Development of a UK Limit States Design Code for Timber - A R Fewell and C B Pierce
18-1-2	Eurocode 5, Timber Structures - H J Larsen
19-1-1	Duration of Load Effects and Reliability Based Design (Single Member) - R O Foschi and Z C Yao
21-102-1	Research Activities Towards a New GDR Timber Design Code Based on Limit States Design - W Rug and M Badstube
22-1-1	Reliability-Theoretical Investigation into Timber Components Proposal for a Supplement of the Design Concept - M Badstube, W Rug and R Plessow
23-1-1	Some Remarks about the Safety of Timber Structures - J Kuipers
23-1-2	Reliability of Wood Structural Elements: A Probabilistic Method to Eurocode 5 Calibration - F Rouger, N Lheritier, P Racher and M Fogli
31-1-1	A Limit States Design Approach to Timber Framed Walls - C J Mettem, R Bainbridge and J A Gordon
32 -1-1	Determination of Partial Coefficients and Modification Factors- H J Larsen, S Svensson and S Thelandersson
32 -1-2	Design by Testing of Structural Timber Components **-** V Enjily and L Whale
33-1-1	Aspects on Reliability Calibration of Safety Factors for Timber Structures – S Svensson and S Thelandersson
33-1-2	Sensitivity studies on the reliability of timber structures – A Ranta-Maunus, M Fonselius, J Kurkela and T Toratti
41-1–1	On the Role of Stiffness Properties for Ultimate Limit State Design of Slender Columns– J Köhler, A Frangi, R Steiger

TIMBER COLUMNS

2-2-1	The Design of Solid Timber Columns - H J Larsen
3-2-1	The Design of Built-Up Timber Columns - H J Larsen
4-2-1	Tests with Centrally Loaded Timber Columns - H J Larsen and S S Pedersen
4-2-2	Lateral-Torsional Buckling of Eccentrically Loaded Timber Columns- B Johansson
5-9-1	Strength of a Wood Column in Combined Compression and Bending with Respect to Creep - B Källsner and B Norén
5-100-1	Design of Solid Timber Columns (First Draft) - H J Larsen
6-100-1	Comments on Document 5-100-1, Design of Solid Timber Columns - H J Larsen and E Theilgaard
6-2-1	Lattice Columns - H J Larsen
6-2-2	A Mathematical Basis for Design Aids for Timber Columns - H J Burgess

SYMBOLS

PLYWOOD

STRESS GRADING

STRESSES FOR SOLID TIMBER

16-6-1 Size Factors for Timber Bending and Tension Stresses - A R Fewell

16-6-2 Strength Classes for International Codes - A R Fewell and J G Sunley

17-6-1 The Determination of Grade Stresses from Characteristic Stresses for BS 5268: Part 2 - A R Fewell

17-6-2 The Determination of Softwood Strength Properties for Grades, Strength Classes and Laminated Timber for BS 5268: Part 2 - A R Fewell

18-6-1 Comment on Papers: 18-6-2 and 18-6-3 - R H Leicester

18-6-2 Configuration Factors for the Bending Strength of Timber - R H Leicester

18-6-3 Notes on Sampling Factors for Characteristic Values - R H Leicester

18-6-4 Size Effects in Timber Explained by a Modified Weakest Link Theory- B Madsen and A H Buchanan

18-6-5 Placement and Selection of Growth Defects in Test Specimens - H Riberholt

18-6-6 Partial Safety-Coefficients for the Load-Carrying Capacity of Timber Structures - B Norén and J-0 Nylander

19-6-1 Effect of Age and/or Load on Timber Strength - J Kuipers

19-6-2 Confidence in Estimates of Characteristic Values - R H Leicester

19-6-3 Fracture Toughness of Wood - Mode I - K Wright and M Fonselius

19-6-4 Fracture Toughness of Pine - Mode II - K Wright

19-6-5 Drying Stresses in Round Timber - A Ranta-Maunus

19-6-6 A Dynamic Method for Determining Elastic Properties of Wood - R Görlacher

20-6-1 A Comparative Investigation of the Engineering Properties of "Whitewoods" Imported to Israel from Various Origins - U Korin

20-6-2 Effects of Yield Class, Tree Section, Forest and Size on Strength of Home Grown Sitka Spruce - V Picardo

20-6-3 Determination of Shear Strength and Strength Perpendicular to Grain - H J Larsen

21-6-1 Draft Australian Standard: Methods for Evaluation of Strength and Stiffness of Graded Timber - R H Leicester

21-6-2 The Determination of Characteristic Strength Values for Stress Grades of Structural Timber. Part 1 - A R Fewell and P Glos

21-6-3 Shear Strength in Bending of Timber - U Korin

22-6-1 Size Effects and Property Relationships for Canadian 2-inch Dimension Lumber - J D Barrett and H Griffin

22-6-2 Moisture Content Adjustements for In-Grade Data - J D Barrett and W Lau

22-6-3 A Discussion of Lumber Property Relationships in Eurocode 5 - D W Green and D E Kretschmann

22-6-4 Effect of Wood Preservatives on the Strength Properties of Wood - F Ronai

23-6-1 Timber in Compression Perpendicular to Grain - U Korin

24-6-1 Discussion of the Failure Criterion for Combined Bending and Compression - T A C M van der Put

24-6-3 Effect of Within Member Variability on Bending Strength of Structural Timber - I Czmoch, S Thelandersson and H J Larsen

24-6-4 Protection of Structural Timber Against Fungal Attack Requirements and Testing- K Jaworska, M Rylko and W Nozynski

24-6-5 Derivation of the Characteristic Bending Strength of Solid Timber According to CEN-Document prEN 384 - A J M Leijten

25-6-1 Moment Configuration Factors for Simple Beams- T D G Canisius

25-6-3 Bearing Capacity of Timber - U Korin

25-6-4 On Design Criteria for Tension Perpendicular to Grain - H Petersson

25-6-5 Size Effects in Visually Graded Softwood Structural Lumber - J D Barrett, F Lam and W Lau

26-6-1 Discussion and Proposal of a General Failure Criterion for Wood - T A C M van der Put

27-6-1 Development of the "Critical Bearing": Design Clause in CSA-086.1 - C Lum and E Karacabeyli

27-6-2 Size Effects in Timber: Novelty Never Ends - F Rouger and T Fewell

27-6-3 Comparison of Full-Size Sugi (Cryptomeria japonica D.Don) Structural Performance in Bending of Round Timber, Two Surfaces Sawn Timber and Square Sawn Timber - T Nakai, H Nagao and T Tanaka

28-6-1 Shear Strength of Canadian Softwood Structural Lumber - F Lam, H Yee and J D Barrett

28-6-2 Shear Strength of Douglas Fir Timbers - B Madsen

28-6-3 On the Influence of the Loading Head Profiles on Determined Bending Strength - L Muszyñsky and R Szukala

28-6-4 Effect of Test Standard, Length and Load Configuration on Bending Strength of Structural Timber- T Isaksson and S Thelandersson

28-6-5 Grading Machine Readings and their Use in the Calculation of Moment Configuration Factors - T Canisius, T Isaksson and S Thelandersson

28-6-6 End Conditions for Tension Testing of Solid Timber Perpendicular to Grain - T Canisius

29-6-1 Effect of Size on Tensile Strength of Timber - N Burger and P Glos

29-6-2 Equivalence of In-Grade Testing Standards - R H Leicester, H O Breitinger and H F Fordham

30-6-1 Strength Relationships in Structural Timber Subjected to Bending and Tension - N Burger and P Glos

30-6-2 Characteristic Design Stresses in Tension for Radiata Pine Grown in Canterbury - A Tsehaye, J C F Walker and A H Buchanan

30-6-3 Timber as a Natural Composite: Explanation of Some Peculiarities in the Mechanical Behaviour - E Gehri

31-6-1 Length and Moment Configuration Factors - T Isaksson

31-6-2 Tensile Strength Perpendicular to Grain According to EN 1193 - H J Blaß and M Schmid

31-6-3 Strength of Small Diameter Round Timber - A Ranta-Maunus, U Saarelainen and H Boren

31-6-4 Compression Strength Perpendicular to Grain of Structural Timber and Glulam - L Damkilde, P Hoffmeyer and T N Pedersen

31-6-5 Bearing Strength of Timber Beams - R H Leicester, H Fordham and H Breitinger

32-6-1 Development of High-Resistance Glued Robinia Products and an Attempt to Assign Such Products to the European System of Strength Classes - G Schickhofer and B Obermayr

32-6-2 Length and Load Configuration Effects in the Code Format - T Isaksson

32-6-3 Length Effect on the Tensile Strength of Truss Chord Members - F Lam

32-6-4 Tensile Strength Perpendicular to Grain of Glued Laminated Timber - H J Blaß and M Schmid

32-6-5 On the Reliability-based Strength Adjustment Factors for Timber Design - T D G Canisius

34-6-1 Material Strength Properties for Canadian Species Used in Japanese Post and Beam Construction - J D Barrett, F Lam, S Nakajima

35-6-1 Evaluation of Different Size Effect Models for Tension Perpendicular to Grain Design - S Aicher, G Dill-Langer

35-6-2 Tensile Strength of Glulam Perpendicular to Grain - Effects of Moisture Gradients - J Jönsson, S Thelandersson

36-6-1 Characteristic Shear Strength Values Based on Tests According to EN 1193 - P Glos, J Denzler

37-6-1 Tensile Strength of Nordic Birch - K H Solli

37-6-2 Effect of Test Piece Orientation on Characteristic Bending Strength of Structural Timber - P Glos, J K Denzler

37-6-3 Strength and Stiffness Behaviour of Beech Laminations for High Strength Glulam - P Glos, J K Denzler, P W Linsenmann

37-6-4 A Review of Existing Standards Related to Calculation of Characteristic Values of Timber - F Rouger

37-6-5 Influence of the Rolling-Shear Modulus on the Strength and Stiffness of Structural Bonded Timber Elements - P Fellmoser, H J Blass

38-6-1 Design Specifications for Notched Beams in AS:1720 - R H Leicester

38-6-2 Characteristic Bending Strength of Beech Glulam - H J Blaß, M Frese

38-6-3 Shear Strength of Glued Laminated Timber - H Klapp, H Brüninghoff

39-6-1 Allocation of Central European hardwoods into EN 1912 - P Glos, J K Denzler

39-6-2 Revisiting EN 338 and EN 384 Basics and Procedures - R Steiger, M Arnold, M Fontana

40-6-1 Bearing Strength Perpendicular to the Grain of Locally Loaded Timber Blocks - A J M Leijten, J C M Schoenmakers

40-6-2 Experimental Study of Compression and Shear Strength of Spruce Timber - M Poussa, P Tukiainen, A Ranta-Maunus

40-6-3 Analysis of Tension and Bending strength of Graded Spruce Timber - A Hanhijärvi, A Ranta-Maunus, H Sarkama, M Kohsaku, M Poussa, J Puttonen

41-6-1 Design of Inclined Glulam Members with an End Notch on the Tension Face - A Asiz, I Smith

41-6-2 A New Design Approach for End-notched Beams - View on Code - K Rautenstrauch, B Franke, S Franke, K U Schober

41-6-3 The Design Rules in Eurocode 5 for Compression Perpendicular to the Grain - Continuous Supported Beams - H J Larsen, T A C M van der Put, A J M Leijten

41-6-4 Size Effects in Bending – J K Denzler, P Glos

42-6-1 Variability of Strength of European Spruce - A Ranta-Maunus, J K Denzler

42-6-2 Impact Loaded Structural Timber Elements Made from Swiss Grown Norway Spruce - R Widmann, R Steiger

42-6-3 Modelling the Bending Strength of Timber Components –Implications to Test Standards - J Köhler, M Sandomeer, T Isaksson, B Källsner

TIMBER JOINTS AND FASTENERS

1-7-1 Mechanical Fasteners and Fastenings in Timber Structures - E G Stern

4-7-1 Proposal for a Basic Test Method for the Evaluation of Structural Timber Joints with Mechanical Fasteners and Connectors - RILEM 3TT Committee

4-7-2 Test Methods for Wood Fasteners - K Möhler

5-7-1 Influence of Loading Procedure on Strength and Slip-Behaviour in Testing Timber Joints - K Möhler

5-7-2 Recommendations for Testing Methods for Joints with Mechanical Fasteners and Connectors in Load-Bearing Timber Structures - RILEM 3 TT Committee

5-7-3 CIB-Recommendations for the Evaluation of Results of Tests on Joints with Mechanical Fasteners and Connectors used in Load-Bearing Timber Structures - J Kuipers

6-7-1 Recommendations for Testing Methods for Joints with Mechanical Fasteners and Connectors in Load-Bearing Timber Structures (seventh draft) - RILEM 3 TT Committee

6-7-2 Proposal for Testing Integral Nail Plates as Timber Joints - K Möhler

6-7-3 Rules for Evaluation of Values of Strength and Deformation from Test Results - Mechanical Timber Joints - M Johansen, J Kuipers, B Norén

6-7-4 Comments to Rules for Testing Timber Joints and Derivation of Characteristic Values for Rigidity and Strength - B Norén

7-7-1 Testing of Integral Nail Plates as Timber Joints - K Möhler

7-7-2 Long Duration Tests on Timber Joints - J Kuipers

7-7-3 Tests with Mechanically Jointed Beams with a Varying Spacing of Fasteners - K Möhler

7-100-1 CIB-Timber Code Chapter 5.3 Mechanical Fasteners;CIB-Timber Standard 06 and 07 - H J Larsen

9-7-1 Design of Truss Plate Joints - F J Keenan

9-7-2 Staples - K Möhler

11-7-1 A Draft Proposal for International Standard: ISO Document ISO/TC 165N 38E

12-7-1 Load-Carrying Capacity and Deformation Characteristics of Nailed Joints - J Ehlbeck

12-7-2 Design of Bolted Joints - H J Larsen

12-7-3 Design of Joints with Nail Plates - B Norén

13-7-1 Polish Standard BN-80/7159-04: Parts 00-01-02-03-04-05.
"Structures from Wood and Wood-based Materials. Methods of Test and Strength Criteria for Joints with Mechanical Fasteners"

13-7-2 Investigation of the Effect of Number of Nails in a Joint on its Load Carrying Ability - W Nozynski

13-7-3 International Acceptance of Manufacture, Marking and Control of Finger-jointed Structural Timber - B Norén

13-7-4 Design of Joints with Nail Plates - Calculation of Slip - B Norén

13-7-5 Design of Joints with Nail Plates - The Heel Joint - B Källsner

13-7-6 Nail Deflection Data for Design - H J Burgess

13-7-7 Test on Bolted Joints - P Vermeyden

13-7-8 Comments to paper CIB-W18/12-7-3 "Design of Joints with Nail Plates"- B Norén

13-7-9 Strength of Finger Joints - H J Larsen

13-100-4 CIB Structural Timber Design Code. Proposal for Section 6.1.5 Nail Plates - N I Bovim

19-15-1 Connections Deformability in Timber Structures: A Theoretical Evaluation of its Influence on Seismic Effects - A Ceccotti and A Vignoli

20-7-1 Design of Nailed and Bolted Joints-Proposals for the Revision of Existing Formulae in Draft Eurocode 5 and the CIB Code - L R J Whale, I Smith and H J Larsen

20-7-2 Slip in Joints under Long Term Loading - T Feldborg and M Johansen

20-7-3 Ultimate Properties of Bolted Joints in Glued-Laminated Timber - M Yasumura, T Murota and H Sakai

20-7-4 Modelling the Load-Deformation Behaviour of Connections with Pin-Type Fasteners under Combined Moment, Thrust and Shear Forces - I Smith

21-7-1 Nails under Long-Term Withdrawal Loading - T Feldborg and M Johansen

21-7-2 Glued Bolts in Glulam-Proposals for CIB Code - H Riberholt

21-7-3 Nail Plate Joint Behaviour under Shear Loading - T Poutanen

21-7-4 Design of Joints with Laterally Loaded Dowels. Proposals for Improving the Design Rules in the CIB Code and the Draft Eurocode 5 - J Ehlbeck and H Werner

21-7-5 Axially Loaded Nails: Proposals for a Supplement to the CIB Code - J Ehlbeck and W Siebert

22-7-1 End Grain Connections with Laterally Loaded Steel Bolts A draft proposal for design rules in the CIB Code - J Ehlbeck and M Gerold

22-7-2 Determination of Perpendicular-to-Grain Tensile Stresses in Joints with Dowel-Type Fasteners - A draft proposal for design rules - J Ehlbeck, R Görlacher and H Werner

22-7-3 Design of Double-Shear Joints with Non-Metallic Dowels A proposal for a supplement of the design concept - J Ehlbeck and O Eberhart

22-7-4 The Effect of Load on Strength of Timber Joints at high Working Load Level - A J M Leijten

22-7-5 Plasticity Requirements for Portal Frame Corners - R Gunnewijk and A J M Leijten

22-7-6 Background Information on Design of Glulam Rivet Connections in CSA/CAN3-086.1-M89 - A proposal for a supplement of the design concept - E Karacabeyli and D P Janssens

22-7-7 Mechanical Properties of Joints in Glued-Laminated Beams under Reversed Cyclic Loading - M Yasumura

22-7-8 Strength of Glued Lap Timber Joints - P Glos and H Horstmann

22-7-9 Toothed Rings Type Bistyp 075 at the Joints of Fir Wood - J Kerste

22-7-10 Calculation of Joints and Fastenings as Compared with the International State - K Zimmer and K Lissner

22-7-11 Joints on Glued-in Steel Bars Present Relatively New and Progressive Solution in Terms of Timber Structure Design - G N Zubarev, F A Boitemirov and V M Golovina

22-7-12 The Development of Design Codes for Timber Structures made of Compositive Bars with Plate Joints based on Cyclindrical Nails - Y V Piskunov

22-7-13 Designing of Glued Wood Structures Joints on Glued-in Bars - S B Turkovsky

23-7-1 Proposal for a Design Code for Nail Plates - E Aasheim and K H Solli

23-7-2 Load Distribution in Nailed Joints - H J Blass

24-7-1 Theoretical and Experimental Tension and Shear Capacity of Nail Plate Connections - B Källsner and J Kangas

24-7-2	Testing Method and Determination of Basic Working Loads for Timber Joints with Mechanical Fasteners - Y Hirashima and F Kamiya
24-7-3	Anchorage Capacity of Nail Plate - J Kangas
25-7-2	Softwood and Hardwood Embedding Strength for Dowel type Fasteners - J Ehlbeck and H Werner
25-7-4	A Guide for Application of Quality Indexes for Driven Fasteners Used in Connections in Wood Structures - E G Stern
25-7-5	35 Years of Experience with Certain Types of Connectors and Connector Plates Used for the Assembly of Wood Structures and their Components- E G Stern
25-7-6	Characteristic Strength of Split-ring and Shear-plate Connections - H J Blass, J Ehlbeck and M Schlager
25-7-7	Characteristic Strength of Tooth-plate Connector Joints - H J Blass, J Ehlbeck and M Schlager
25-7-8	Extending Yield Theory to Screw Connections - T E McLain
25-7-9	Determination of k_{def} for Nailed Joints - J W G van de Kuilen
25-7-10	Characteristic Strength of UK Timber Connectors - A V Page and C J Mettem
25-7-11	Multiple-fastener Dowel-type Joints, a Selected Review of Research and Codes - C J Mettem and A V Page
25-7-12	Load Distributions in Multiple-fastener Bolted Joints in European Whitewood Glulam, with Steel Side Plates - C J Mettem and A V Page
26-7-1	Proposed Test Method for Dynamic Properties of Connections Assembled with Mechanical Fasteners - J D Dolan
26-7-2	Validatory Tests and Proposed Design Formulae for the Load-Carrying Capacity of Toothed-Plate Connectored Joints - C J Mettem, A V Page and G Davis
26-7-3	Definitions of Terms and Multi-Language Terminology Pertaining to Metal Connector Plates - E G Stern
26-7-4	Design of Joints Based on in V-Shape Glued-in Rods - J Kangas
26-7-5	Tests on Timber Concrete Composite Structural Elements (TCCs) - A U Meierhofer
27-7-1	Glulam Arch Bridge and Design of it's Moment-Resisting Joints - K Komatsu and S Usuku
27-7-2	Characteristic Load - Carrying Capacity of Joints with Dowel - type Fasteners in Regard to the System Properties - H Werner
27-7-3	Steel Failure Design in Truss Plate Joints - T Poutanen
28-7-1	Expanded Tube Joint in Locally DP Reinforced Timber - A J M Leijten, P Ragupathy and K S Virdi
28-7-2	A Strength and Stiffness Model for the Expanded Tube Joint - A J M Leijten
28-7-3	Load-carrying Capacity of Steel-to Timber Joints with Annular Ring Shanked Nails. A Comparison with the EC5 Design Method - R Görlacher
28-7-4	Dynamic Effects on Metal-Plate Connected Wood Truss Joints - S Kent, R Gupta and T Miller
28-7-5	Failure of the Timber Bolted Joints Subjected to Lateral Load Perpendicular to Grain - M Yasumura and L Daudeville
28-7-6	Design Procedure for Locally Reinforced Joints with Dowel-type Fasteners - H Werner
28-7-7	Variability and Effects of Moisture Content on the Withdrawal Characteristics for Lumber as Opposed to Clear Wood - J D Dolan and J W Stelmokas

28-7-8 Nail Plate Capacity in Joint Line - A Kevarinmäki and J Kangas

28-7-9 Axial Strength of Glued-In Bolts - Calculation Model Based on Non-Linear Fracture Mechanics - A Preliminary Study - C J Johansson, E Serrano, P J Gustafsson and B Enquist

28-7-10 Cyclic Lateral Dowel Connection Tests for seismic and Wind Evaluation - J D Dolan

29-7-1 A Simple Method for Lateral Load-Carrying Capacity of Dowel-Type Fasteners - J Kangas and J Kurkela

29-7-2 Nail Plate Joint Behaviour at Low Versus High Load Level - T Poutanen

29-7-3 The Moment Resistance of Tee and Butt - Joint Nail Plate Test Specimens - A Comparison with Current Design Methods - A Reffold, L R J Whale and B S Choo

29-7-4 A Critical Review of the Moment Rotation Test Method Proposed in prEN 1075 - M Bettison, B S Choo and L R J Whale

29-7-5 Explanation of the Translation and Rotation Behaviour of Prestressed Moment Timber Joints - A J M Leijten

29-7-6 Design of Joints and Frame Corners using Dowel-Type Fasteners - E Gehri

29-7-7 Quasi-Static Reversed-Cyclic Testing of Nailed Joints - E Karacabeyli and A Ceccotti

29-7-8 Failure of Bolted Joints Loaded Parallel to the Grain: Experiment and Simulation - L Davenne, L Daudeville and M Yasumura

30-7-1 Flexural Behaviour of GLT Beams End-Jointed by Glued-in Hardwood Dowels - K Komatsu, A Koizumi, J Jensen, T Sasaki and Y Iijima

30-7-2 Modelling of the Block Tearing Failure in Nailed Steel-to-Timber Joints - J Kangas, K Aalto and A Kevarinmäki

30-7-3 Cyclic Testing of Joints with Dowels and Slotted-in Steel Plates - E Aasheim

30-7-4 A Steel-to-Timber Dowelled Joint of High Performance in Combination with a High Strength Wood Composite (Parallam) - E Gehri

30-7-5 Multiple Fastener Timber Connections with Dowel Type Fasteners - A Jorissen

30-7-6 Influence of Ductility on Load-Carrying Capacity of Joints with Dowel-Type Fasteners - A Mischler

31-7-1 Mechanical Properties of Dowel Type Joints under Reversed Cyclic Lateral Loading - M Yasumura

31-7-2 Design of Joints with Laterally Loaded Dowels - A Mischler

31-7-3 Flexural Behaviour of Glulam Beams Edge-Jointed by Lagscrews with Steel Splice Plates - K Komatsu

31-7-4 Design on Timber Capacity in Nailed Steel-to-Timber Joints - J Kangas and J Vesa

31-7-5 Timber Contact in Chord Splices of Nail Plate Structures - A Kevarinmäki

31-7-6 The Fastener Yield Strength in Bending - A Jorissen and H J Blaß

31-7-7 A Proposal for Simplification of Johansen`s Formulae, Dealing With the Design of Dowelled-Type Fasteners - F Rouger

31-7-8 Simplified Design of Connections with Dowel-type fasteners - H J Blaß and J Ehlbeck

32-7-1 Behaviour of Wood-Steel-Wood Bolted Glulam Connections - M Mohammad and J H P Quenneville

32-7-2 A new set of experimental tests on beams loaded perpendicular-to-grain by dowel-type joints- M Ballerini

32-7-3 Design and Analysis of Bolted Timber Joints under Lateral Force Perpendicular to Grain - M Yasumura and L Daudeville

32-7-4 Predicting Capacities of Joints with Laterally Loaded Nails - I Smith and P Quenneville

32-7-5 Strength Reduction Rules for Multiple Fastener Joints - A Mischler and E Gehri

32-7-6 The Stiffness of Multiple Bolted Connections - A Jorissen

32-7-7 Concentric Loading Tests on Girder Truss Components - T N Reynolds, A Reffold, V Enjily and L Whale

32-7-8 Dowel Type Connections with Slotted-In Steel Plates **-** M U Pedersen, C O Clorius, L Damkilde, P Hoffmeyer and L Esklidsen

32-7-9 Creep of Nail Plate Reinforced Bolt Joints - J Vesa and A Kevarinmäki

32-7-10 The Behaviour of Timber Joints with Ring Connectors - E Gehri and A Mischler

32-7-11 Non-Metallic, Adhesiveless Joints for Timber Structures - R D Drake, M P Ansell, C J Mettem and R Bainbridge

32-7-12 Effect of Spacing and Edge Distance on the Axial Strength of Glued-in Rods - H J Blaß and B Laskewitz

32-7-13 Evaluation of Material Combinations for Bonded in Rods to Achieve Improved Timber Connections - C J Mettem, R J Bainbridge, K Harvey, M P Ansell, J G Broughton and A R Hutchinson

33-7-1 Determination of Yield Strength and Ultimate Strength of Dowel-Type Timber Joints – M Yasumura and K Sawata

33-7-2 Lateral Shear Capacity of Nailed Joints – U Korin

33-7-3 Height-Adjustable Connector for Composite Beams – Y V Piskunov and E G Stern

33-7-4 Engineering Ductility Assessment for a Nailed Slotted-In Steel Connection in Glulam– L Stehn and H Johansson

33-7-5 Effective Bending Capacity of Dowel-Type Fasteners **-** H J Blaß, A Bienhaus and V Krämer

33-7-6 Load-Carrying Capacity of Joints with Dowel-Type Fasteners and Interlayers - H J Blaß and B Laskewitz

33-7-7 Evaluation of Perpendicular to Grain Failure of Beams caused by Concentrated Loads of Joints – A J M Leijten and T A C M van der Put

33-7-8 Test Methods for Glued-In Rods for Timber Structures – C Bengtsson and C J Johansson

33-7-9 Stiffness Analysis of Nail Plates – P Ellegaard

33-7-10 Capacity, Fire Resistance and Gluing Pattern of the Rods in V-Connections – J Kangas

33-7-11 Bonded-In Pultrusions for Moment-Resisting Timber Connections – K Harvey, M P Ansell, C J Mettem, R J Bainbridge and N Alexandre

33-7-12 Fatigue Performance of Bonded-In Rods in Glulam, Using Three Adhesive Types - R J Bainbridge, K Harvey, C J Mettem and M P Ansell

34-7-1 Splitting Strength of Beams Loaded by Connections Perpendicular to Grain, Model Validation – A J M Leijten, A Jorissen

34-7-2 Numerical LEFM analyses for the evaluation of failure loads of beams loaded perpendicular-to-grain by single-dowel connections – M Ballerini, R Bezzi

34-7-3 Dowel joints loaded perpendicular to grain - H J Larsen, P J Gustafsson

34-7-4 Quality Control of Connections based on in V-shape glued-in Steel Rods – J Kangas, A Kevarinmäki

34-7-5 Testing Connector Types for Laminated-Timber-Concrete Composite Elements – M Grosse, S Lehmann, K Rautenstrauch

34-7-6 Behaviour of Axially Loaded Glued-in Rods - Requirements and Resistance, Especially for Spruce Timber Perpendicular to the Grain Direction – A Bernasconi

34-7-7 Embedding characteristics on fibre reinforcement and densified timber joints - P Haller, J Wehsener, T Birk

34-7-8 GIROD – Glued-in Rods for Timber Structures – C Bengtsson, C-J Johansson

34-7-9 Criteria for Damage and Failure of Dowel-Type Joints Subjected to Force Perpendicular to the Grain – M Yasumura

34-7-10 Interaction Between Splitting and Block Shear Failure of Joints – A J M Leijten, A Jorissen, J Kuipers

34-7-11 Limit states design of dowel-fastener joints – Placement of modification factors and partial factors, and calculation of variability in resistance – I Smith, G Foliente

34-7-12 Design and Modelling of Knee Joints - J Nielsen, P Ellegaard

34-7-13 Timber-Steel Shot Fired Nail Connections at Ultimate Limit States - R J Bainbridge, P Larsen, C J Mettem, P Alam, M P Ansell

35-7-1 New Estimating Method of Bolted Cross-lapped Joints with Timber Side Members - M Noguchi, K Komatsu

35-7-2 Analysis on Multiple Lag Screwed Timber Joints with Timber Side Members - K Komatsu, S Takino, M Nakatani, H Tateishi

35-7-3 Joints with Inclined Screws - A Kevarinmäki

35-7-4 Joints with Inclined Screws - I Bejtka, H J Blaß

35-7-5 Effect of distances, Spacing and Number of Dowels in a Row an the Load Carrying Capacity of Connections with Dowels failing by Splitting - M Schmid, R Frasson, H J Blaß

35-7 6 Effect of Row Spacing on the Capacity of Bolted Timber Connections Loaded Perpendicular-to-grain - P Quenneville, M Kasim

35-7-7 Splitting Strength of Beams Loaded by Connections, Model Comparison - A J M Leijten

35-7-8 Load-Carrying Capacity of Perpendicular to the Grain Loaded Timber Joints with Multiple Fasteners - O Borth, K U Schober, K Rautenstrauch

35-7-9 Determination of fracture parameter for dowel-type joints loaded perpendicular to wooden grain and its application - M Yasumura

35-7-10 Analysis and Design of Modified Attic Trusses with Punched Metal Plate Fasteners - P Ellegaard

35-7-11 Joint Properties of Plybamboo Sheets in Prefabricated Housing - G E Gonzalez

35-7-12 Fiber-Reinforced Beam-to-Column Connections for Seismic Applications - B Kasal, A Heiduschke, P Haller

36-7-1 Shear Tests in Timber-LWAC with Screw-Type Connections - L Jorge, H Cruz, S Lopes

36-7-2 Plug Shear Failure in Nailed Timber Connections: Experimental Studies - H Johnsson

36-7-3 Nail-Laminated Timber Elements in Natural Surface-Composite with Mineral Bound Layer - S Lehmann, K Rautenstrauch

36-7-4 Mechanical Properties of Timber-Concrete Joints Made With Steel Dowels - A Dias, J W G van de Kuilen, H Cruz

36-7-5 Comparison of Hysteresis Responses of Different Sheating to Framing Joints - B Dujič, R Zarnić

36-7- 6 Evaluation and Estimation of the Performance of the Nail Joints and Shear Walls under Dry/Humid Cyclic Climate - S Nakajima

36-7-7 Beams Transversally Loaded by Dowel-Type Joints: Influence on Splitting Strength of Beam Thickness and Dowel Size - M Ballerini, A Giovanella

36-7-8 Splitting Strength of Beams Loaded by Connections - J L Jensen

36-7-9 A Tensile Fracture Model for Joints with Rods or Dowels loaded Perpendicular-to-Grain - J L Jensen, P J Gustafsson, H J Larsen

36-7-10 A Numerical Model to Simulate the Load-Displacement Time-History of Mutiple-Bolt Connections Subjected to Various Loadings - C P Heine, J D Dolan

36-7-11 Reliability of Timber Structures, Theory and Dowel-Type Connection Failures - A Ranta-Maunus, A Kevarinmäki

37-7-1 Development of the "Displaced Volume Model" to Predict Failure for Multiple-Bolt Timber Joints - D M Carradine, J D Dolan, C P Heine

37-7-2 Mechanical Models of the Knee Joints with Cross-Lapped Glued Joints and Glued in Steel Rods - M Noguchi, K Komatsu

37-7-3 Simplification of the Neural Network Model for Predicting the Load-Carrying Capacity of Dowel-Type Connections - A Cointe, F Rouger

37-7-4 Bolted Wood Connections Loaded Perpendicular-to-Grain- A Proposed Design Approach - M C G Lehoux, J H P Quenneville

37-7-5 A New Prediction Formula for the Splitting Strength of Beams Loaded by Dowel Type Connections - M Ballerini

37-7-6 Plug Shear Failure: The Tensile Failure Mode and the Effect of Spacing - H Johnsson

37-7-7 Block Shear Failure Test with Dowel-Type Connection in Diagonal LVL Structure - M Kairi

37-7-8 Glued-in Steel Rods: A Design Approach for Axially Loaded Single Rods Set Parallel to the Grain - R Steiger, E Gehri, R Widmann

37-7-9 Glued in Rods in Load Bearing Timber Structures - Status regarding European Standards for Test Procedures - B Källander

37-7-10 French Data Concerning Glued-in Rods - C Faye, L Le Magorou, P Morlier, J Surleau

37-7-11 Enhancement of Dowel-Type Fasteners by Glued Connectors - C O Clorius, A Højman

37-7-12 Review of Probability Data for Timber Connections with Dowel-Type Fasteners - A J M Leijten, J Köhler, A Jorissen

37-7-13 Behaviour of Fasteners and Glued-in Rods Produced From Stainless Steel - A Kevarinmäki

37-7-14 Dowel joints in Engineered Wood Products: Assessment of Simple Fracture Mechanics Models - M Snow, I Smith, A Asiz

37-7-15 Numerical Modelling of Timber and Connection Elements Used in Timber-Concrete-Composite Constructions - M Grosse, K Rautenstrauch

38-7-1 A Numerical Investigation on the Splitting Strength of Beams Loaded Perpendicular-to-grain by Multiple-dowel Connections – M Ballerini, M Rizzi

38-7-2 A Probabilistic Framework for the Reliability Assessment of Connections with Dowel Type Fasteners - J Köhler

38-7-3 Load Carrying Capacity of Curved Glulam Beams Reinforced with self-tapping Screws - J Jönsson, S Thelandersson

38-7-4 Self-tapping Screws as Reinforcements in Connections with Dowel-Type Fasteners- I Bejtka, H J Blaß

38-7-5 The Yield Capacity of Dowel Type Fasteners - A Jorissen, A Leijten

38-7-6 Nails in Spruce - Splitting Sensitivity, End Grain Joints and Withdrawal Strength - A Kevarinmäki

38-7-7 Design of Timber Connections with Slotted-in Steel Plates and Small Diameter Steel Tube Fasteners - B Murty, I Smith, A Asiz

39-7-1 Effective in-row Capacity of Multiple-Fastener Connections - P Quenneville, M Bickerdike

39-7-2 Self-tapping Screws as Reinforcements in Beam Supports - I Bejtka, H J Blaß

39-7-3 Connectors for Timber-concrete Composite-Bridges - A Döhrer, K Rautenstrauch

39-7-4 Block Shear Failure at Dowelled Double Shear Steel-to-timber Connections - A Hanhijärvi, A Kevarinmäki, R Yli-Koski

39-7-5 Load Carrying Capacity of Joints with Dowel Type Fasteners in Solid Wood Panels - T Uibel, H J Blaß

39-7-6 Generalised Canadian Approach for Design of Connections with Dowel Fasteners - P Quenneville, I Smith, A Asiz, M Snow, Y H Chui

40-7-1 Predicting the Strength of Bolted Timber Connections Subjected to Fire - M Fragiacomo, A Buchanan, D Carshalton, P Moss, C Austruy

40-7-2 Edge Joints with Dowel Type Fasteners in Cross Laminated Timber - H J Blaß, T Uibel

40-7-3 Design Method against Timber Failure Mechanisms of Dowelled Steel-to-Timber Connections - A Hanhijärvi, A Kevarinmäki

40-7-4 A EYM Based Simplified Design Formula for the Load-carrying Capacity of Dowel-type Connections - M Ballerini

40-7-5 Evaluation of the Slip Modulus for Ultimate Limit State Verifications of Timber-Concrete Composite Structures - E Lukaszewska, M Fragiacomo, A Frangi

40-7-6 Models for the Predictions of the Ductile and Brittle Failure Modes (Parallel-to-Grain) of Timber Rivet Connections - M Marjerrison, P Quenneville

40-7-7 Creep of Timber and Timber-Concrete Joints. - J W G van de Kuilen, A M P G Dias

40-7-8 Lag Screwed Timber Joints with Timber Side Members- K Komatsu, S Takino, H Tateishi

41-7-1 Applicability of Existing Design Approaches to Mechanical Joints in Structural Composite Lumber - M Snow, I Smith, A Asiz, M Ballerini

41-7-2 Validation of the Canadian Bolted Connection Design Proposal - P Quenneville, J Jensen

41-7-3 Ductility of Moment Resisting Dowelled Joints in Heavy Timber Structures - A Polastri, R Tomasi, M Piazza, I Smith

41-7-4 Mechanical Behaviour of Traditional Timber Connections: Proposals for Design, Based on Experimental and Numerical Investigations. Part I: Birdsmouth - C Faye, P Garcia, L Le Magorou, F Rouger

41-7-5 Embedding Strength of European Hardwoods - U Hübner, T Bogensperger, G Schickhofer

42-7-1 Base Parameters of Self-tapping Screws - G Pirnbacher, R Brandner, G Schickhofer

42-7-2 Joints with Inclined Screws and Steel Plates as Outer Members - H Krenn, G Schickhofer

42-7-3 Models for the Calculation of the Withdrawal Capacity of Self-tapping Screws - M Frese, H J Blaß

42-7-4 Embedding Strength of New Zealand Timber and Recommendation for the NZ Standard - S Franke, P Quenneville

42-7-5 Load Carrying Capacity of Timber-Wood Fiber Insulation Board – Joints with Dowel Type Fasteners - G Gebhardt, H J Blaß

42-7-6 Prediction of the Fatigue Resistance of Timber-Concrete-Composite Connections - U Kuhlmann, P Aldi

42-7-7 Using Screws for Structural Applications in Laminated Veneer Lumber - D M Carradine, M P Newcombe, A H Buchanan

42-7-8 Influence of Fastener Spacings on Joint Performance - Experimental Results and Codification - E Gehri

42-7-9 Connections with Glued-in Hardwood Rods Subjected to Combined Bending and Shear Actions - J L Jensen, P Quenneville

LOAD SHARING

3-8-1 Load Sharing - An Investigation on the State of Research and Development of Design Criteria - E Levin

4-8-1 A Review of Load-Sharing in Theory and Practice - E Levin

4-8-2 Load Sharing - B Norén

19-8-1 Predicting the Natural Frequencies of Light-Weight Wooden Floors - I Smith and Y H Chui

20-8-1 Proposed Code Requirements for Vibrational Serviceability of Timber Floors - Y H Chui and I Smith

21-8-1 An Addendum to Paper 20-8-1 - Proposed Code Requirements for Vibrational Serviceability of Timber Floors - Y H Chui and I Smith

21-8-2 Floor Vibrational Serviceability and the CIB Model Code - S Ohlsson

22-8-1 Reliability Analysis of Viscoelastic Floors - F Rouger, J D Barrett and R O Foschi

24-8-1 On the Possibility of Applying Neutral Vibrational Serviceability Criteria to Joisted Wood Floors - I Smith and Y H Chui

25-8-1 Analysis of Glulam Semi-rigid Portal Frames under Long-term Load - K Komatsu and N Kawamoto

34-8-1 System Effect in Sheathed Parallel Timber Beam Structures – M Hansson, T Isaksson

35-8-1 System Effects in Sheathed Parallel Timber Beam Structures part II. - M Hansson, T Isaksson

39-8-1 Overview of a new Canadian Approach to Handling System Effects in Timber Structures - I Smith, Y H Chui, P Quenneville

DURATION OF LOAD

3-9-1 Definitions of Long Term Loading for the Code of Practice - B Norén

4-9-1 Long Term Loading of Trussed Rafters with Different Connection Systems - T Feldborg and M Johansen

5-9-1 Strength of a Wood Column in Combined Compression and Bending with Respect to Creep - B Källsner and B Norén

6-9-1 Long Term Loading for the Code of Practice (Part 2) - B Norén

6-9-2 Long Term Loading - K Möhler

6-9-3 Deflection of Trussed Rafters under Alternating Loading during a Year - T Feldborg and M Johansen

7-6-1 Strength and Long Term Behaviour of Lumber and Glued-Laminated Timber under Torsion Loads - K Möhler

7-9-1 Code Rules Concerning Strength and Loading Time - H J Larsen and E Theilgaard

17-9-1 On the Long-Term Carrying Capacity of Wood Structures - Y M Ivanov and Y Y Slavic

18-9-1 Prediction of Creep Deformations of Joints - J Kuipers

19-9-1 Another Look at Three Duration of Load Models - R O Foschi and Z C Yao

19-9-2 Duration of Load Effects for Spruce Timber with Special Reference to Moisture Influence - A Status Report - P Hoffmeyer

19-9-3 A Model of Deformation and Damage Processes Based on the Reaction Kinetics of Bond Exchange - T A C M van der Put

19-9-4 Non-Linear Creep Superposition - U Korin

19-9-5 Determination of Creep Data for the Component Parts of Stressed-Skin Panels - R Kliger

19-9-6 Creep an Lifetime of Timber Loaded in Tension and Compression - P Glos

19-1-1 Duration of Load Effects and Reliability Based Design (Single Member) - R O Foschi and Z C Yao

19-6-1 Effect of Age and/or Load on Timber Strength - J Kuipers

19-7-4 The Prediction of the Long-Term Load Carrying Capacity of Joints in Wood Structures - Y M Ivanov and Y Y Slavic

19-7-5 Slip in Joints under Long-Term Loading - T Feldborg and M Johansen

20-7-2 Slip in Joints under Long-Term Loading - T Feldborg and M Johansen

22-9-1 Long-Term Tests with Glued Laminated Timber Girders - M Badstube, W Rug and W Schöne

22-9-2 Strength of One-Layer solid and Lengthways Glued Elements of Wood Structures and its Alteration from Sustained Load - L M Kovaltchuk, I N Boitemirova and G B Uspenskaya

24-9-1 Long Term Bending Creep of Wood - T Toratti

24-9-2 Collection of Creep Data of Timber - A Ranta-Maunus

24-9-3 Deformation Modification Factors for Calculating Built-up Wood-Based Structures - I R Kliger

25-9-2 DVM Analysis of Wood. Lifetime, Residual Strength and Quality - L F Nielsen

26-9-1 Long Term Deformations in Wood Based Panels under Natural Climate Conditions. A Comparative Study - S Thelandersson, J Nordh, T Nordh and S Sandahl

28-9-1 Evaluation of Creep Behavior of Structural Lumber in Natural Environment - R Gupta and R Shen

30-9-1 DOL Effect in Tension Perpendicular to the Grain of Glulam Depending on Service Classes and Volume - S Aicher and G Dill-Langer

30-9-2 Damage Modelling of Glulam in Tension Perpendicular to Grain in Variable Climate - G Dill-Langer and S Aicher

31-9-1 Duration of Load Effect in Tension Perpendicular to Grain in Curved Glulam - A Ranta-Maunus

32-9-1 Bending-Stress-Redistribution Caused by Different Creep in Tension and Compression and Resulting DOL-Effect - P Becker and K Rautenstrauch

32-9-2 The Long Term Performance of Ply-Web Beams - R Grantham and V Enjily

36-9-1 Load Duration Factors for Instantaneous Loads - A J M Leijten, B Jansson

39-9-1 Simplified Approach for the Long-Term Behaviour of Timber-Concrete Composite Beams According to the Eurocode 5 Provisions - M Fragiacomo, A Ceccotti

TIMBER BEAMS

4-10-1 The Design of Simple Beams - H J Burgess

4-10-2	Calculation of Timber Beams Subjected to Bending and Normal Force - H J Larsen
5-10-1	The Design of Timber Beams - H J Larsen
9-10-1	The Distribution of Shear Stresses in Timber Beams - F J Keenan
9-10-2	Beams Notched at the Ends - K Möhler
11-10-1	Tapered Timber Beams - H Riberholt
13-6-2	Consideration of Size Effects in Longitudinal Shear Strength for Uncracked Beams - R O Foschi and J D Barrett
13-6-3	Consideration of Shear Strength on End-Cracked Beams - J D Barrett and R O Foschi
18-10-1	Submission to the CIB-W18 Committee on the Design of Ply Web Beams by Consideration of the Type of Stress in the Flanges - J A Baird
18-10-2	Longitudinal Shear Design of Glued Laminated Beams - R O Foschi
19-10-1	Possible Code Approaches to Lateral Buckling in Beams - H J Burgess
19-2-1	Creep Buckling Strength of Timber Beams and Columns - R H Leicester
20-2-1	Lateral Buckling Theory for Rectangular Section Deep Beam-Columns - H J Burgess
20-10-1	Draft Clause for CIB Code for Beams with Initial Imperfections - H J Burgess
20-10-2	Space Joists in Irish Timber - W J Robinson
20-10-3	Composite Structure of Timber Joists and Concrete Slab - T Poutanen
21-10-1	A Study of Strength of Notched Beams - P J Gustafsson
22-10-1	Design of Endnotched Beams - H J Larsen and P J Gustafsson
22-10-2	Dimensions of Wooden Flexural Members under Constant Loads - A Pozgai
22-10-3	Thin-Walled Wood-Based Flanges in Composite Beams - J König
22-10-4	The Calculation of Wooden Bars with flexible Joints in Accordance with the Polish Standart Code and Strict Theoretical Methods - Z Mielczarek
23-10-1	Tension Perpendicular to the Grain at Notches and Joints - T A C M van der Put
23-10-2	Dimensioning of Beams with Cracks, Notches and Holes. An Application of Fracture Mechanics - K Riipola
23-10-3	Size Factors for the Bending and Tension Strength of Structural Timber - J D Barret and A R Fewell
23-12-1	Bending Strength of Glulam Beams, a Design Proposal - J Ehlbeck and F Colling
23-12-3	Glulam Beams, Bending Strength in Relation to the Bending Strength of the Finger Joints - H Riberholt
24-10-1	Shear Strength of Continuous Beams - R H Leicester and F G Young
25-10-1	The Strength of Norwegian Glued Laminated Beams - K Solli, E Aasheim and R H Falk
25-10-2	The Influence of the Elastic Modulus on the Simulated Bending Strength of Hyperstatic Timber Beams - T D G Canisius
27-10-1	Determination of Shear Modulus - R Görlacher and J Kürth
29-10-1	Time Dependent Lateral Buckling of Timber Beams - F Rouger
29-10-2	Determination of Modulus of Elasticity in Bending According to EN 408 - K H Solli
29-10-3	On Determination of Modulus of Elasticity in Bending - L Boström, S Ormarsson and O Dahlblom

ENVIRONMENTAL CONDITIONS

LAMINATED MEMBERS

8-12-1 Testing of Big Glulam Timber Beams - H Kolb and P Frech

8-12-2 Instruction for the Reinforcement of Apertures in Glulam Beams - H Kolb and P Frech

8-12-3 Glulam Standard Part 1: Glued Timber Structures; Requirements for Timber (Second Draft)

9-12-1 Experiments to Provide for Elevated Forces at the Supports of Wooden Beams with Particular Regard to Shearing Stresses and Long-Term Loadings - F Wassipaul and R Lackner

9-12-2 Two Laminated Timber Arch Railway Bridges Built in Perth in 1849 - L G Booth

9-6-4 Consideration of Combined Stresses for Lumber and Glued Laminated Timber - K Möhler

11-6-3 Consideration of Combined Stresses for Lumber and Glued Laminated Timber (addition to Paper CIB-W18/9-6-4) - K Möhler

12-12-1 Glulam Standard Part 2: Glued Timber Structures; Rating (3rd draft)

12-12-2 Glulam Standard Part 3: Glued Timber Structures; Performance (3 rd draft)

13-12-1 Glulam Standard Part 3: Glued Timber Structures; Performance (4th draft)

14-12-1 Proposals for CEI-Bois/CIB-W18 Glulam Standards - H J Larsen

14-12-2 Guidelines for the Manufacturing of Glued Load-Bearing Timber Structures - Stevin Laboratory

14-12-3 Double Tapered Curved Glulam Beams - H Riberholt

14-12-4 Comment on CIB-W18/14-12-3 - E Gehri

18-12-1 Report on European Glulam Control and Production Standard - H Riberholt

18-10-2 Longitudinal Shear Design of Glued Laminated Beams - R O Foschi

19-12-1 Strength of Glued Laminated Timber - J Ehlbeck and F Colling

19-12-2 Strength Model for Glulam Columns - H J Blaß

19-12-3 Influence of Volume and Stress Distribution on the Shear Strength and Tensile Strength Perpendicular to Grain - F Colling

19-12-4 Time-Dependent Behaviour of Glued-Laminated Beams - F Zaupa

21-12-1 Modulus of Rupture of Glulam Beam Composed of Arbitrary Laminae - K Komatsu and N Kawamoto

21-12-2 An Appraisal of the Young's Modulus Values Specified for Glulam in Eurocode 5- L R J Whale, B O Hilson and P D Rodd

21-12-3 The Strength of Glued Laminated Timber (Glulam): Influence of Lamination Qualities and Strength of Finger Joints - J Ehlbeck and F Colling

21-12-4 Comparison of a Shear Strength Design Method in Eurocode 5 and a More Traditional One - H Riberholt

22-12-1 The Dependence of the Bending Strength on the Glued Laminated Timber Girder Depth - M Badstube, W Rug and W Schöne

22-12-2 Acid Deterioration of Glulam Beams in Buildings from the Early Half of the 1960s - Prelimination summary of the research project; Overhead pictures - B A Hedlund

22-12-3 Experimental Investigation of normal Stress Distribution in Glue Laminated Wooden Arches - Z Mielczarek and W Chanaj

22-12-4 Ultimate Strength of Wooden Beams with Tension Reinforcement as a Function of Random Material Properties - R Candowicz and T Dziuba

23-12-1 Bending Strength of Glulam Beams, a Design Proposal - J Ehlbeck and F Colling

23-12-2 Probability Based Design Method for Glued Laminated Timber - M F Stone

23-12-3 Glulam Beams, Bending Strength in Relation to the Bending Strength of the Finger Joints - H Riberholt

23-12-4 Glued Laminated Timber - Strength Classes and Determination of Characteristic Properties - H Riberholt, J Ehlbeck and A Fewell

24-12-1 Contribution to the Determination of the Bending Strength of Glulam Beams - F Colling, J Ehlbeck and R Görlacher

24-12-2 Influence of Perpendicular-to-Grain Stressed Volume on the Load-Carrying Capacity of Curved and Tapered Glulam Beams - J Ehlbeck and J Kürth

25-12-1 Determination of Characteristic Bending Values of Glued Laminated Timber. EN-Approach and Reality - E Gehri

26-12-1 Norwegian Bending Tests with Glued Laminated Beams-Comparative Calculations with the "Karlsruhe Calculation Model" - E Aasheim, K Solli, F Colling, R H Falk, J Ehlbeck and R Görlacher

26-12-2 Simulation Analysis of Norwegian Spruce Glued-Laminated Timber - R Hernandez and R H Falk

26-12-3 Investigation of Laminating Effects in Glued-Laminated Timber - F Colling and R H Falk

26-12-4 Comparing Design Results for Glulam Beams According to Eurocode 5 and to the French Working Stress Design Code (CB71) - F Rouger

27-12-1 State of the Art Report: Glulam Timber Bridge Design in the U.S. - M A Ritter and T G Williamson

27-12-2 Common Design Practice for Timber Bridges in the United Kingdom - C J Mettem, J P Marcroft and G Davis

27-12-3 Influence of Weak Zones on Stress Distribution in Glulam Beams - E Serrano and H J Larsen

28-12-1 Determination of Characteristic Bending Strength of Glued Laminated Timber - E Gehri

28-12-2 Size Factor of Norwegian Glued Laminated Beams - E Aasheim and K H Solli

28-12-3 Design of Glulam Beams with Holes - K Riipola

28-12-4 Compression Resistance of Glued Laminated Timber Short Columns- U Korin

29-12-1 Development of Efficient Glued Laminated Timber - G Schickhofer

30-12-1 Experimental Investigation and Analysis of Reinforced Glulam Beams - K Oiger

31-12-1 Depth Factor for Glued Laminated Timber-Discussion of the Eurocode 5 Approach - B Källsner, O Carling and C J Johansson

32-12-1 The bending stiffness of nail-laminated timber elements in transverse direction- T Wolf and O Schäfer

33-12-1 Internal Stresses in the Cross-Grain Direction of Wood Induced by Climate Variation – J Jönsson and S Svensson

34-12-1 High-Strength I-Joist Compatible Glulam Manufactured with LVL Tension Laminations – B Yeh, T G Williamson

34-12-2 Evaluation of Glulam Shear Strength Using A Full-Size Four-Point Test Method – B Yeh, T G Williamson

34-12-3 Design Model for FRP Reinforced Glulam Beams – M Romani, H J Blaß

34-12-4 Moisture induced stresses in glulam cross sections – J Jönsson

34-12-5 Load Carrying Capacity of Nail-Laminated Timber under Concentrated Loads – V Krämer, H J Blaß

34-12-6 Determination of Shear Strength Values for GLT Using Visual and Machine Graded Spruce Laminations – G Schickhofer

34-12-7 Mechanically Jointed Beams: Possibilities of Analysis and some special Problems – H Kreuzinger

35-12-1 Glulam Beams with Round Holes – a Comparison of Different Design Approaches vs. Test Data - S Aicher L Höfflin

36-12-1 Problems with Shear and Bearing Strength of LVL in Highly Loaded Structures - H Bier

36-12-2 Weibull Based Design of Round Holes in Glulam - L Höfflin, S Aicher

37-12-1 Development of Structural LVL from Tropical Wood and Evaluation of Their Performance for the Structural Components of Wooden Houses. Part-1. Application of Tropical LVL to a Roof Truss - K Komatsu, Y Idris, S Yuwasdiki, B Subiyakto, A Firmanti

37-12-2 Reinforcement of LVL Beams With Bonded-in Plates and Rods - Effect of Placement of Steel and FRP Reinforcements on Beam Strength and Stiffness - P Alam, M P Ansell, D Smedley

39-12-1 Recommended Procedures for Determination of Distribution Widths in the Design of Stress Laminated Timber Plate Decks - K Crews

39-12-2 In-situ Strengthening of Timber Structures with CFRP - K U Schober, S Franke, K Rautenstrauch

39-12-3 Effect of Checking and Non-Glued Edge Joints on the Shear Strength of Structural Glued Laminated Timber Beams - B Yeh, T G Williamson, Z A Martin

39-12-4 A Contribution to the Design and System Effect of Cross Laminated Timber (CLT) - R Jöbstl, T Moosbrugger, T Bogensperger, G Schickhofer

39-12-5 Behaviour of Glulam in Compression Perpendicular to Grain in Different Strength Grades and Load Configurations - M Augustin, A Ruli, R Brandner, G Schickhofer

40-12-1 Development of New Constructions of Glulam Beams in Canada - F Lam, N Mohadevan

40-12-2 Determination of Modulus of Shear and Elasticity of Glued Laminated Timber and Related Examination - R Brandner, E Gehri, T Bogensperger, G Schickhofer

40-12-3 Comparative Examination of Creep of GTL and CLT-Slabs in Bending - R A Jöbstl, G Schickhofer,

40-12-4 Standard Practice for the Derivation of Design Properties of Structural Glued Laminated Timber in the United States - T G Williamson, B Yeh

40-12-5 Creep and Creep-Rupture Behaviour of Structural Composite Lumber Evaluated in Accordance with ASTM D 6815 - B Yeh, T G Williamson.

40-12-6 Bending Strength of Combined Beech-Spruce Glulam - M Frese, H J Blaß

40-12-7 Quality Control of Glulam: Shear Tests of Glue Lines - R Steiger, E Gehri

41-12-1 Paper withdrawn by the author

41-12-2 Bending Strength of Spruce Glulam: New Models for the Characteristic Bending Strength - M Frese, H J Blass,

41-12-3 In-Plane Shear Strength of Cross Laminated Timber - R A Joebstl, T Bogensperger, G Schickhofer

41-12-4 Strength of Glulam Beams with Holes - Tests of Quadratic Holes and Literature Test Results Compilation - H Danielsson, P J Gustafsson

42-12-1 Glulam Beams with Holes Reinforced by Steel Bars – S Aicher, L Höfflin

42-12-2 Analysis of X-lam Panel-to-Panel Connections under Monotonic and Cyclic Loading - C Sandhaas, L Boukes, J W G van de Kuilen, A Ceccotti

42-12-3 Laminating Lumber and End Joint Properties for FRP-Reinforced Glulam Beams - T G Williamson, B Yeh

43-12-4 Validity of Bending Tests on Strip-Shaped Specimens to Derive Bending Strength and Stiffness Properties of Cross-Laminated Solid Timber (CLT) - R Steiger, A Gülzow

42-12-5 Mechanical Properties of Stress Laminated Timber Decks - Experimental Study - K Karlsson, R Crocetti, R Kliger

PARTICLE AND FIBRE BUILDING BOARDS

7-13-1 Fibre Building Boards for CIB Timber Code (First Draft)- O Brynildsen

9-13-1 Determination of the Bearing Strength and the Load-Deformation Characteristics of Particleboard - K Möhler, T Budianto and J Ehlbeck

9-13-2 The Structural Use of Tempered Hardboard - W W L Chan

11-13-1 Tests on Laminated Beams from Hardboard under Short- and Longterm Load - W Nozynski

11-13-2 Determination of Deformation of Special Densified Hardboard under Long-term Load and Varying Temperature and Humidity Conditions - W Halfar

11-13-3 Determination of Deformation of Hardboard under Long-term Load in Changing Climate - W Halfar

14-4-1 An Introduction to Performance Standards for Wood-Base Panel Products - D H Brown

14-4-2 Proposal for Presenting Data on the Properties of Structural Panels - T Schmidt

16-13-1 Effect of Test Piece Size on Panel Bending Properties - P W Post

20-4-1 Considerations of Reliability - Based Design for Structural Composite Products - M R O'Halloran, J A Johnson, E G Elias and T P Cunningham

20-13-1 Classification Systems for Structural Wood-Based Sheet Materials - V C Kearley and A R Abbott

21-13-1 Design Values for Nailed Chipboard - Timber Joints - A R Abbott

25-13-1 Bending Strength and Stiffness of Izopanel Plates - Z Mielczarek

28-13-1 Background Information for "Design Rated Oriented Strand Board (OSB)" in CSA Standards - Summary of Short-term Test Results - E Karacabeyli, P Lau, C R Henderson, F V Meakes and W Deacon

28-13-2 Torsional Stiffness of Wood-Hardboard Composed I-Beam - P Olejniczak

TRUSSED RAFTERS

4-9-1 Long-term Loading of Trussed Rafters with Different Connection Systems - T Feldborg and M Johansen

6-9-3 Deflection of Trussed Rafters under Alternating Loading During a Year - T Feldborg and M Johansen

7-2-1 Lateral Bracing of Timber Struts - J A Simon

9-14-1 Timber Trusses - Code Related Problems - T F Williams

9-7-1 Design of Truss Plate Joints - F J Keenan

10-14-1 Design of Roof Bracing - The State of the Art in South Africa - P A V Bryant and J A Simon

11-14-1 Design of Metal Plate Connected Wood Trusses - A R Egerup

12-14-1 A Simple Design Method for Standard Trusses - A R Egerup

13-14-1 Truss Design Method for CIB Timber Code - A R Egerup

13-14-2 Trussed Rafters, Static Models - H Riberholt

13-14-3	Comparison of 3 Truss Models Designed by Different Assumptions for Slip and E-Modulus - K Möhler
14-14-1	Wood Trussed Rafter Design - T Feldborg and M Johansen
14-14-2	Truss-Plate Modelling in the Analysis of Trusses - R O Foschi
14-14-3	Cantilevered Timber Trusses - A R Egerup
14-7-5	The Effect of Support Eccentricity on the Design of W- and WW-Trusses with Nail Plate Connectors - B Källsner
15-14-1	Guidelines for Static Models of Trussed Rafters - H Riberholt
15-14-2	The Influence of Various Factors on the Accuracy of the Structural Analysis of Timber Roof Trusses - F R P Pienaar
15-14-3	Bracing Calculations for Trussed Rafter Roofs - H J Burgess
15-14-4	The Design of Continuous Members in Timber Trussed Rafters with Punched Metal Connector Plates - P O Reece
15-14-5	A Rafter Design Method Matching U.K. Test Results for Trussed Rafters - H J Burgess
16-14-1	Full-Scale Tests on Timber Fink Trusses Made from Irish Grown Sitka Spruce - V Picardo
17-14-1	Data from Full Scale Tests on Prefabricated Trussed Rafters - V Picardo
17-14-2	Simplified Static Analysis and Dimensioning of Trussed Rafters - H Riberholt
17-14-3	Simplified Calculation Method for W-Trusses - B Källsner
18-14-1	Simplified Calculation Method for W-Trusses (Part 2) - B Källsner
18-14-2	Model for Trussed Rafter Design - T Poutanen
19-14-1	Annex on Simplified Design of W-Trusses - H J Larsen
19-14-2	Simplified Static Analysis and Dimensioning of Trussed Rafters - Part 2 - H Riberholt
19-14-3	Joint Eccentricity in Trussed Rafters - T Poutanen
20-14-1	Some Notes about Testing Nail Plates Subjected to Moment Load - T Poutanen
20-14-2	Moment Distribution in Trussed Rafters - T Poutanen
20-14-3	Practical Design Methods for Trussed Rafters - A R Egerup
22-14-1	Guidelines for Design of Timber Trussed Rafters - H Riberholt
23-14-1	Analyses of Timber Trussed Rafters of the W-Type - H Riberholt
23-14-2	Proposal for Eurocode 5 Text on Timber Trussed Rafters - H Riberholt
24-14-1	Capacity of Support Areas Reinforced with Nail Plates in Trussed Rafters - A Kevarinmäki
25-14-1	Moment Anchorage Capacity of Nail Plates in Shear Tests - A Kevarinmaki and J. Kangas
25-14-2	Design Values of Anchorage Strength of Nail Plate Joints by 2-curve Method and Interpolation - J Kangas and A Kevarinmaki
26-14-1	Test of Nail Plates Subjected to Moment - E Aasheim
26-14-2	Moment Anchorage Capacity of Nail Plates - A Kevarinmäki and J Kangas
26-14-3	Rotational Stiffness of Nail Plates in Moment Anchorage - A Kevarinmäki and J Kangas
26-14-4	Solution of Plastic Moment Anchorage Stress in Nail Plates - A Kevarinmäki
26-14-5	Testing of Metal-Plate-Connected Wood-Truss Joints - R Gupta

26-14-6 Simulated Accidental Events on a Trussed Rafter Roofed Building - C J Mettem and J P Marcroft

30-14-1 The Stability Behaviour of Timber Trussed Rafter Roofs - Studies Based on Eurocode 5 and Full Scale Testing - R J Bainbridge, C J Mettern, A Reffold and T Studer

32-14-1 Analysis of Timber Reinforced with Punched Metal Plate Fasteners- J Nielsen

33-14-1 Moment Capacity of Timber Beams Loaded in Four-Point Bending and Reinforced with Punched Metal Plate Fasteners – J Nielsen

36-14-1 Effect of Chord Splice Joints on Force Distribution in Trusses with Punched Metal Plate Fasteners - P Ellegaard

36-14-2 Monte Carlo Simulation and Reliability Analysis of Roof Trusses with Punched Metal Plate Fasteners - M Hansson, P Ellegaard

36-14-3 Truss Trouble – R H Leicester, J Goldfinch, P Paevere, G C Foliente

40-14-1 Timber Trusses with Punched Metal Plate Fasteners - Design for Transport and Erection - H J Blaß

STRUCTURAL STABILITY

8-15-1 Laterally Loaded Timber Columns: Tests and Theory - H J Larsen

13-15-1 Timber and Wood-Based Products Structures. Panels for Roof Coverings. Methods of Testing and Strength Assessment Criteria. Polish Standard BN-78/7159-03

16-15-1 Determination of Bracing Structures for Compression Members and Beams - H Brüninghoff

17-15-1 Proposal for Chapter 7.4 Bracing - H Brüninghoff

17-15-2 Seismic Design of Small Wood Framed Houses - K F Hansen

18-15-1 Full-Scale Structures in Glued Laminated Timber, Dynamic Tests: Theoretical and Experimental Studies - A Ceccotti and A Vignoli

18-15-2 Stabilizing Bracings - H Brüninghoff

19-15-1 Connections Deformability in Timber Structures: a Theoretical Evaluation of its Influence on Seismic Effects - A Ceccotti and A Vignoli

19-15-2 The Bracing of Trussed Beams - M H Kessel and J Natterer

19-15-3 Racking Resistance of Wooden Frame Walls with Various Openings - M Yasumura

19-15-4 Some Experiences of Restoration of Timber Structures for Country Buildings - G Cardinale and P Spinelli

19-15-5 Non-Destructive Vibration Tests on Existing Wooden Dwellings - Y Hirashima

20-15-1 Behaviour Factor of Timber Structures in Seismic Zones. - A Ceccotti and A Vignoli

21-15-1 Rectangular Section Deep Beam - Columns with Continuous Lateral Restraint - H J Burgess

21-15-2 Buckling Modes and Permissible Axial Loads for Continuously Braced Columns- H J Burgess

21-15-3 Simple Approaches for Column Bracing Calculations - H J Burgess

21-15-4 Calculations for Discrete Column Restraints - H J Burgess

21-15-5 Behaviour Factor of Timber Structures in Seismic Zones (Part Two) - A Ceccotti and A Vignoli

30-15-3 Seismic Force Modification Factors for the Design of Multi-Storey Wood-Frame Platform Construction - E Karacabeyli and A Ceccotti

30-15-4 Evaluation of Wood Framed Shear Walls Subjected to Lateral Load - M Yasumura and N Kawai

31-15-1 Seismic Performance Testing On Wood-Framed Shear Wall - N Kawai

31-15-2 Robustness Principles in the Design of Medium-Rise Timber-Framed Buildings - C J Mettem, M W Milner, R J Bainbridge and V. Enjily

31-15-3 Numerical Simulation of Pseudo-Dynamic Tests Performed to Shear Walls - L Daudeville, L Davenne, N Richard, N Kawai and M Yasumura

31-15-4 Force Modification Factors for Braced Timber Frames - H G L Prion, M Popovski and E Karacabeyli

32-15-1 Three-Dimensional Interaction in Stabilisation of Multi-Storey Timber Frame Buildings - S Andreasson

32-15-2 Application of Capacity Spectrum Method to Timber Houses - N Kawai

32-15-3 Design Methods for Shear Walls with Openings - C Ni, E Karacabeyli and A Ceccotti

32-15-4 Static Cyclic Lateral Loading Tests on Nailed Plywood Shear Walls - K Komatsu, K H Hwang and Y Itou

33-15-1 Lateral Load Capacities of Horizontally Sheathed Unblocked Shear Walls – C Ni, E Karacabeyli and A Ceccotti

33-15-2 Prediction of Earthquake Response of Timber Houses Considering Shear Deformation of Horizontal Frames – N Kawai

33-15-3 Eurocode 5 Rules for Bracing – H J Larsen

34-15-1 A simplified plastic model for design of partially anchored wood-framed shear walls – B Källsner, U A Girhammar, Liping Wu

34-15-2 The Effect of the Moisture Content on the Performance of the Shear Walls – S Nakajima

34-15-3 Evaluation of Damping Capacity of Timber Structures for Seismic Design – M Yasumura

35-15-1 On test methods for determining racking strength and stiffness of wood-framed shear walls - B Källsner, U A Girhammar, L Wu

35-15-2 A Plastic Design Model for Partially Anchored Wood-framed Shear Walls with Openings - U A Girhammar, L Wu, B Källsner

35-15-3 Evaluation and Estimation of the Performance of the Shear Walls in Humid Climate - S Nakajima

35-15-4 Influence of Vertical Load on Lateral Resistance of Timber Frame Walls - B Dujič, R Žarnić

35-15-5 Cyclic and Seismic Performances of a Timber-Concrete System - Local and Full Scale Experimental Results - E Fournely, P Racher

35-15-6 Design of timber-concrete composite structures according to EC5 - 2002 version - A Ceccotti, M Fragiacomo, R M Gutkowski

35-15-7 Design of timber structures in seismic zones according to EC8- 2002 version - A Ceccotti, T Toratti, B Dujič

35-15-8 Design Methods to Prevent Premature Failure of Joints at Shear Wall Corners - N Kawai, H Okiura

36-15-1 Monitoring Light-Frame Timber Buildings: Environmental Loads and Load Paths – I Smith et al.

36-15-2 Applicability of Design Methods to Prevent Premature Failure of Joints at Shear Wall Corners in Case of Post and Beam Construction - N Kawai, H Isoda

36-15-3 Effects of Screw Spacing and Edge Boards on the Cyclic Performance of Timber Frame and Structural Insulated Panel Roof Systems - D M Carradine, J D Dolan, F E Woeste

36-15-4 Pseudo-Dynamic Tests on Conventional Timber Structures with Shear Walls - M Yasumura

36-15-5 Experimental Investigation of Laminated Timber Frames with Fiber-reinforced Connections under Earthquake Loads - B Kasal, P Haller, S Pospisil, I Jirovsky, A Heiduschke, M Drdacky

36-15-6 Effect of Test Configurations and Protocols on the Performance of Shear Walls - F Lam, D Jossen, J Gu, N Yamaguchi, H G L Prion

36-15-7 Comparison of Monotonic and Cyclic Performance of Light-Frame Shear Walls - J D Dolan, A J Toothman

37-15-1 Estimating 3D Behavior of Conventional Timber Structures with Shear Walls by Pseudodynamic Tests - M Yasumura, M Uesugi, L Davenne

37-15-2 Testing of Racking Behavior of Massive Wooden Wall Panels - B Dujič, J Pucelj, R Žarnić

37-15-3 Influence of Framing Joints on Plastic Capacity of Partially Anchored Wood-Framed Shear Walls - B Källsner, U A Girhammar

37-15-4 Bracing of Timber Members in Compression - J Munch-Andersen

37-15-5 Acceptance Criteria for the Use of Structural Insulated Panels in High Risk Seismic Areas - B Yeh, T D Skaggs, T G Williamson Z A Martin

37-15-6 Predicting Load Paths in Shearwalls - Hongyong Mi, Ying-Hei Chui, I Smith, M Mohammad

38-15-1 Background Information on ISO STANDARD 16670 for Cyclic Testing of Connections - E Karacabeyli, M Yasumura, G C Foliente, A Ceccotti

38-15-2 Testing & Product Standards – a Comparison of EN to ASTM, AS/NZ and ISO Standards – A Ranta-Maunus, V Enjily

38-15-3 Framework for Lateral Load Design Provisions for Engineered Wood Structures in Canada - M Popovski, E Karacabeyli

38-15-4 Design of Shear Walls without Hold-Downs - Chun Ni, E Karacabeyli

38-15-5 Plastic design of partially anchored wood-framed wall diaphragms with and without openings - B Källsner, U A Girhammar

38-15-6 Racking of Wooden Walls Exposed to Different Boundary Conditions - B Dujič, S Aicher, R Žarnić

38-15-7 A Portal Frame Design for Raised Wood Floor Applications - T G Williamson, Z A Martin, B Yeh

38-15-8 Linear Elastic Design Method for Timber Framed Ceiling, Floor and Wall Diaphragms - Jarmo Leskelä

38-15-9 A Unified Design Method for the Racking Resistance of Timber Framed Walls for Inclusion in EUROCODE 5 - R Griffiths, B Källsner, H J Blass, V Enjily

39-15-1 Effect of Transverse Walls on Capacity of Wood-Framed Wall Diaphragms - U A Girhammar, B Källsner

39-15-2 Which Seismic Behaviour Factor for Multi-Storey Buildings made of Cross-Laminated Wooden Panels? - M Follesa, M P Lauriola, C Minowa, N Kawai, C Sandhaas, M Yasumura, A Ceccotti

39-15-3 Laminated Timber Frames under dynamic Loadings - A Heiduschke, B Kasal, P Haller

39-15-4 Code Provisions for Seismic Design of Multi-storey Post-tensioned Timber Buildings - S Pampanin, A Palermo, A Buchanan, M Fragiacomo, B Deam

40-15-1	Design of Safe Timber Structures – How Can we Learn from Structural Failures? - S Thelandersson, E Frühwald
40-15-2	Effect of Transverse Walls on Capacity of Wood-Framed Wall Diaphragms—Part 2 - U A Girhammar, B Källsner
40-15-3	Midply Wood Shear Wall System: Concept, Performance and Code Implementation - Chun Ni, M Popovski, E Karacabeyli, E Varoglu, S Stiemer
40-15-4	Seismic Behaviour of Tall Wood-Frame Walls - M Popovski, A Peterson, E Karacabeyli
40-15-5	International Standard Development of Lateral Load Test Method for Shear Walls - M Yasumura, E Karacabeyli
40-15-6	Influence of Openings on Shear Capacity of Wooden Walls - B Dujič, S Klobcar, R Žarnić
41-15-1	Need for a Harmonized Approach for Calculations of Ductility of Timber Assemblies - W Muñoz, M Mohammad, A Salenikovich, P Quenneville
41-15-2	Plastic Design of Wood Frame Wall Diaphragms in Low and Medium Rise Buildings - B Källsner, U A Girhammar
41 15-3	Failure Analysis of Light Wood Frame Structures under Wind Load - A Asiz, Y H Chui, I Smith
41-15-4	Combined Shear and Wind Uplift Resistance of Wood Structural Panel Shearwalls B Yeh, T G Williamson
41-15-5	Behaviour of Prefabricated Timber Wall Elements under Static and Cyclic Loading – P Schädle, H J Blass
42-15-1	Design Aspects on Anchoring the Bottom Rail in Partially Anchored Wood-Framed Shear Walls - U A Girhammar, B Källsner
42-15-2	New Seismic Design Provisions for Shearwalls and Diaphragms in the Canadian Standard for Engineering Design in Wood - M Popovski, E Karacabeyli, Chun Ni, P Lepper, G Doudak
42-15-3	Stability Capacity and Lateral Bracing Force of Metal Plate Connected Wood Truss Assemblies - Xiaobin Song, F Lam, Hao Huang, Minjuan He
42-15-4	Improved Method for Determining Braced Wall Requirements for Conventional Wood-Frame Buildings - Chun Ni, H Rainer, E Karacabeyli

FIRE

12-16-1	British Standard BS 5268 the Structural Use of Timber: Part 4 Fire Resistance of Timber Structures
13-100-2	CIB Structural Timber Design Code. Chapter 9. Performance in Fire
19-16-1	Simulation of Fire in Tests of Axially Loaded Wood Wall Studs - J König
24-16-1	Modelling the Effective Cross Section of Timber Frame Members Exposed to Fire - J König
25-16-1	The Effect of Density on Charring and Loss of Bending Strength in Fire - J König
25-16-2	Tests on Glued-Laminated Beams in Bending Exposed to Natural Fires - F Bolonius Olesen and J König
26-16-1	Structural Fire Design According to Eurocode 5, Part 1.2 - J König
31-16-1	Revision of ENV 1995-1-2: Charring and Degradation of Strength and Stiffness - J König
33-16-1	A Design Model for Load-carrying Timber Frame Members in Walls and Floors Exposed to Fire - J König

33-16-2 A Review of Component Additive Methods Used for the Determination of Fire Resistance of Separating Light Timber Frame Construction - J König, T Oksanen and K Towler

33-16-3 Thermal and Mechanical Properties of Timber and Some Other Materials Used in Light Timber Frame Construction - B Källsner and J König

34-16-1 Influence of the Strength Determining Factors on the Fire Resistance Capability of Timber Structural Members – I Totev, D Dakov

34-16-2 Cross section properties of fire exposed rectangular timber members - J König, B Källsner

34-16-3 Pull-Out Tests on Glued-in Rods at High Temperatures – A Mischler, A Frangi

35-16-1 Basic and Notional Charring Rates - J König

37 - 16 - 1 Effective Values of Thermal Properties of Timber and Thermal Actions During the Decay Phase of Natural Fires - J König

37 - 16 - 2 Fire Tests on Timber Connections with Dowel-type Fasteners - A Frangi, A Mischler

38-16-1 Fire Behaviour of Multiple Shear Steel-to-Timber Connections with Dowels - C Erchinger, A Frangi, A Mischler

38-16-2 Fire Tests on Light Timber Frame Wall Assemblies - V Schleifer, A Frangi

39-16-1 Fire Performance of FRP Reinforced Glulam - T G Williamson, B Yeh

39-16-2 An Easy-to-use Model for the Design of Wooden I-joists in Fire - J König, B Källsner

39-16-3 A Design Model for Timber Slabs Made of Hollow Core Elements in Fire - A Frangi, M Fontana

40-16-1 Bonded Timber Deck Plates in Fire - J König, J Schmid

40-16-2 Design of Timber Frame Floor Assemblies in Fire - A Frangi, C Erchinger

41-16-1 Effect of Adhesives on Finger Joint Performance in Fire - J König, J Norén, M Sterley

42-16-1 Advanced Calculation Method for the Fire Resistance of Timber Framed Walls -S Winter, W Meyn

42-16-2 Fire Design Model for Multiple Shear Steel-to-Timber Dowelled Connections - C Erchinger, A Frangi, M Fontana

42-16-3 Comparison between the Conductive Model of Eurocode 5 and the Temperature Distribution Within a Timber Cross-section Exposed to Fire - M Fragiacomo, A Menis, P Moss, A Buchanan, I Clemente

STATISTICS AND DATA ANALYSIS

13-17-1 On Testing Whether a Prescribed Exclusion Limit is Attained - W G Warren

16-17-1 Notes on Sampling and Strength Prediction of Stress Graded Structural Timber - P Glos

16-17-2 Sampling to Predict by Testing the Capacity of Joints, Components and Structures - B Norén

16-17-3 Discussion of Sampling and Analysis Procedures - P W Post

17-17-1 Sampling of Wood for Joint Tests on the Basis of Density - I Smith, L R J Whale

17-17-2 Sampling Strategy for Physical and Mechanical Properties of Irish Grown Sitka Spruce - V Picardo

18-17-1 Sampling of Timber in Structural Sizes - P Glos

18-6-3 Notes on Sampling Factors for Characteristic Values - R H Leicester

19-17-1 Load Factors for Proof and Prototype Testing - R H Leicester

19-6-2	Confidence in Estimates of Characteristic Values - R H Leicester
21-6-1	Draft Australian Standard: Methods for Evaluation of Strength and Stiffness of Graded Timber - R H Leicester
21-6-2	The Determination of Characteristic Strength Values for Stress Grades of Structural Timber. Part 1 - A R Fewell and P Glos
22-17-1	Comment on the Strength Classes in Eurocode 5 by an Analysis of a Stochastic Model of Grading - A proposal for a supplement of the design concept - M Kiesel
24-17-1	Use of Small Samples for In-Service Strength Measurement - R H Leicester and F G Young
24-17-2	Equivalence of Characteristic Values - R H Leicester and F G Young
24-17-3	Effect of Sampling Size on Accuracy of Characteristic Values of Machine Grades - Y H Chui, R Turner and I Smith
24-17-4	Harmonisation of LSD Codes - R H Leicester
25-17-2	A Body for Confirming the Declaration of Characteristic Values - J Sunley
25-17-3	Moisture Content Adjustment Procedures for Engineering Standards - D W Green and J W Evans
27-17-1	Statistical Control of Timber Strength - R H Leicester and H O Breitinger
30-17-1	A New Statistical Method for the Establishment of Machine Settings - F Rouger
35-17-1	Probabilistic Modelling of Duration of Load Effects in Timber Structures - J Köhler, S Svenson
38-17-1	Analysis of Censored Data - Examples in Timber Engineering Research - R Steiger, J Köhler
39-17-1	Possible Canadian / ISO Approach to Deriving Design Values from Test Data - I Smith, A Asiz, M Snow, Y H Chui

GLUED JOINTS

20-18-1	Wood Materials under Combined Mechanical and Hygral Loading - A Martensson and S Thelandersson
20-18-2	Analysis of Generalized Volkersen - Joints in Terms of Linear Fracture Mechanics - P J Gustafsson
20-18-3	The Complete Stress-Slip Curve of Wood-Adhesives in Pure Shear - H Wernersson and P J Gustafsson
22-18-1	Perspective Adhesives and Protective Coatings for Wood Structures - A S Freidin
34-18-1	Performance Based Classification of Adhesives for Structural Timber Applications - R J Bainbridge, C J Mettem, J G Broughton, A R Hutchinson
35-18-1	Creep Testing Wood Adhesives for Structural Use - C Bengtsson, B Källander
38-18-1	Adhesive Performance at Elevated Temperatures for Engineered Wood Products - B Yeh, B Herzog, T G Williamson
39-18-1	Comparison of the Pull–out Strength of Steel Bars Glued in Glulam Elements Obtained Experimentally and Numerically - V Rajčić, A Bjelanović, M Rak
39-18-2	The Influence of the Grading Method on the Finger Joint Bending Strength of Beech - M Frese, H J Blaß

FRACTURE MECHANICS

21-10-1	A Study of Strength of Notched Beams - P J Gustafsson
22-10-1	Design of Endnotched Beams - H J Larsen and P J Gustafsson

23-10-1 Tension Perpendicular to the Grain at Notches and Joints - T A C M van der Put

23-10-2 Dimensioning of Beams with Cracks, Notches and Holes. An Application of Fracture Mechanics - K Riipola

23-19-1 Determination of the Fracture Energie of Wood for Tension Perpendicular to the Grain - W Rug, M Badstube and W Schöne

23-19-2 The Fracture Energy of Wood in Tension Perpendicular to the Grain. Results from a Joint Testing Project - H J Larsen and P J Gustafsson

23-19-3 Application of Fracture Mechanics to Timber Structures - A Ranta-Maunus

24-19-1 The Fracture Energy of Wood in Tension Perpendicular to the Grain - H J Larsen and P J Gustafsson

28-19-1 Fracture of Wood in Tension Perpendicular to the Grain: Experiment and Numerical Simulation by Damage Mechanics - L Daudeville, M Yasumura and J D Lanvin

28-19-2 A New Method of Determining Fracture Energy in Forward Shear along the Grain - H D Mansfield-Williams

28-19-3 Fracture Design Analysis of Wooden Beams with Holes and Notches. Finite Element Analysis based on Energy Release Rate Approach - H Petersson

28-19-4 Design of Timber Beams with Holes by Means of Fracture Mechanics - S Aicher, J Schmidt and S Brunold

30-19-1 Failure Analysis of Single-Bolt Joints - L Daudeville, L Davenne and M Yasumura

37 - 19 - 1 Determination of Fracture Mechanics Parameters for Wood with the Help of Close Range Photogrammetry - S Franke, B Franke, K Rautenstrauch

39-19-1 First Evaluation Steps of Design Rules in the European and German codes of Transverse Tension Areas - S Franke, B Franke, K Rautenstrauch

SERVICEABILITY

27-20-1 Codification of Serviceability Criteria - R H Leicester

27-20-2 On the Experimental Determination of Factor k_{def} and Slip Modulus k_{ser} from Short- and Long-Term Tests on a Timber-Concrete Composite (TCC) Beam - S Capretti and A Ceccotti

27-20-3 Serviceability Limit States: A Proposal for Updating Eurocode 5 with Respect to Eurocode 1 - P Racher and F Rouger

27-20-4 Creep Behavior of Timber under External Conditions - C Le Govic, F Rouger, T Toratti and P Morlier

30-20-1 Design Principles for Timber in Compression Perpendicular to Grain - S Thelandersson and A Mårtensson

30-20-2 Serviceability Performance of Timber Floors - Eurocode 5 and Full Scale Testing - R J Bainbridge and C J Mettem

32-20-1 Floor Vibrations - B Mohr

37 - 20 - 1 A New Design Method to Control Vibrations Induced by Foot Steps in Timber Floors - Lin J Hu, Y H Chui

37 - 20 - 2 Serviceability Limit States of Wooden Footbridges. Vibrations Caused by Pedestrians - P Hamm

TEST METHODS

31-21-1 Development of an Optimised Test Configuration to Determine Shear Strength of Glued Laminated Timber - G Schickhofer and B Obermayr

31-21-2 An Impact Strength Test Method for Structural Timber. The Theory and a Preliminary Study - T D G Canisius

35-21-1 Full-Scale Edgewise Shear Tests for Laminated Veneer Lumber- B Yeh, T G Williamson

39-21-1 Timber Density Restrictions for Timber Connection Tests According to EN28970/ISO8970 - A Leijten, J Köhler, A Jorissen

39-21-2 The Mechanical Inconsistence in the Evaluation of the Modulus of Elasticity According to EN384 - T Bogensperger, H Unterwieser, G Schickhofer

40 - 21 - 1 ASTM D198 - Interlaboratory Study for Modulus of Elasticity of Lumber in Bending - A Salenikovich

40 - 21 - 2 New Test Configuration for CLT-Wall-Elements under Shear Load - T Bogensperger, T Moosbrugger, G Schickhofer

41-21-1 Determination of Shear Modulus by Means of Standardized Four-Point Bending Tests - R Brandner, B Freytag, G Schickhofer

CIB TIMBER CODE

2-100-1 A Framework for the Production of an International Code of Practice for the Structural Use of Timber - W T Curry

5-100-1 Design of Solid Timber Columns (First Draft) - H J Larsen

5-100-2 A Draft Outline of a Code for Timber Structures - L G Booth

6-100-1 Comments on Document 5-100-1; Design of Solid Timber Columns - H J Larsen and E Theilgaard

6-100-2 CIB Timber Code: CIB Timber Standards - H J Larsen and E Theilgaard

7-100-1 CIB Timber Code Chapter 5.3 Mechanical Fasteners; CIB Timber Standard 06 and 07 - H J Larsen

8-100-1 CIB Timber Code - List of Contents (Second Draft) - H J Larsen

9-100-1 The CIB Timber Code (Second Draft)

11-100-1 CIB Structural Timber Design Code (Third Draft)

11-100-2 Comments Received on the CIB Code - U Saarelainen; Y M Ivanov, R H Leicester, W Nozynski, W R A Meyer, P Beckmann; R Marsh

11-100-3 CIB Structural Timber Design Code; Chapter 3 - H J Larsen

12-100-1 Comment on the CIB Code - Sous-Commission Glulam

12-100-2 Comment on the CIB Code - R H Leicester

12-100-3 CIB Structural Timber Design Code (Fourth Draft)

13-100-1 Agreed Changes to CIB Structural Timber Design Code

13-100-2 CIB Structural Timber Design Code. Chapter 9: Performance in Fire

13-100-3a Comments on CIB Structural Timber Design Code

13-100-3b Comments on CIB Structural Timber Design Code - W R A Meyer

13-100-3c Comments on CIB Structural Timber Design Code - British Standards Institution

13-100-4 CIB Structural Timber Design Code. Proposal for Section 6.1.5 Nail Plates - N I Bovim

14-103-2 Comments on the CIB Structural Timber Design Code - R H Leicester

15-103-1 Resolutions of TC 165-meeting in Athens 1981-10-12/13

21-100-1 CIB Structural Timber Design Code. Proposed Changes of Sections on Lateral Instability, Columns and Nails - H J Larsen

22-100-1 Proposal for Including an Updated Design Method for Bearing Stresses in CIB W18 - Structural Timber Design Code - B Madsen

22-100-2 Proposal for Including Size Effects in CIB W18A Timber Design Code - B Madsen

22-100-3 CIB Structural Timber Design Code - Proposed Changes of Section on Thin-Flanged Beams - J König

22-100-4 Modification Factor for "Aggressive Media" - a Proposal for a Supplement to the CIB Model Code - K Erler and W Rug

22-100-5 Timber Design Code in Czechoslovakia and Comparison with CIB Model Code - P Dutko and B Kozelouh

LOADING CODES

4-101-1 Loading Regulations - Nordic Committee for Building Regulations

4-101-2 Comments on the Loading Regulations - Nordic Committee for Building Regulations

37-101-1 Action Combination Processing for the Eurocodes Basis of Software to Assist the Engineer - Y Robert, A V Page, R Thépaut, C J Mettem

STRUCTURAL DESIGN CODES

1-102-1 Survey of Status of Building Codes, Specifications etc., in USA - E G Stern

1-102-2 Australian Codes for Use of Timber in Structures - R H Leicester

1-102-3 Contemporary Concepts for Structural Timber Codes - R H Leicester

1-102-4 Revision of CP 112 - First Draft, July 1972 - British Standards Institution

4-102-1 Comparsion of Codes and Safety Requirements for Timber Structures in EEC Countries - Timber Research and Development Association

4-102-2 Nordic Proposals for Safety Code for Structures and Loading Code for Design of Structures - O A Brynildsen

4-102-3 Proposal for Safety Codes for Load-Carrying Structures - Nordic Committee for Building Regulations

4-102-4 Comments to Proposal for Safety Codes for Load-Carrying Structures - Nordic Committee for Building Regulations

4-102-5 Extract from Norwegian Standard NS 3470 "Timber Structures"

4-102-6 Draft for Revision of CP 112 "The Structural Use of Timber" - W T Curry

8-102-1 Polish Standard PN-73/B-03150: Timber Structures; Statistical Calculations and Designing

8-102-2 The Russian Timber Code: Summary of Contents

9-102-1 Svensk Byggnorm 1975 (2nd Edition); Chapter 27: Timber Construction

11-102-1 Eurocodes - H J Larsen

13-102-1 Program of Standardisation Work Involving Timber Structures and Wood-Based Products in Poland

17-102-1 Safety Principles - H J Larsen and H Riberholt

17-102-2 Partial Coefficients Limit States Design Codes for Structural Timberwork - I Smith

18-102-1 Antiseismic Rules for Timber Structures: an Italian Proposal - G Augusti and A Ceccotti

18-1-2 Eurocode 5, Timber Structures - H J Larsen

19-102-1 Eurocode 5 - Requirements to Timber - Drafting Panel Eurocode 5

19-102-2 Eurocode 5 and CIB Structural Timber Design Code - H J Larsen

19-102-3 Comments on the Format of Eurocode 5 - A R Fewell

19-102-4 New Developments of Limit States Design for the New GDR Timber Design Code - W Rug and M Badstube

19-7-3 Effectiveness of Multiple Fastener Joints According to National Codes and Eurocode 5 (Draft) - G Steck

19-7-6 The Derivation of Design Clauses for Nailed and Bolted Joints in Eurocode5 - L R J Whale and I Smith

19-14-1 Annex on Simplified Design of W-Trusses - H J Larsen

20-102-1 Development of a GDR Limit States Design Code for Timber Structures - W Rug and M Badstube

21-102-1 Research Activities Towards a New GDR Timber Design Code Based on Limit States Design - W Rug and M Badstube

22-102-1 New GDR Timber Design Code, State and Development - W Rug, M Badstube and W Kofent

22-102-2 Timber Strength Parameters for the New USSR Design Code and its Comparison with International Code - Y Y Slavik, N D Denesh and E B Ryumina

22-102-3 Norwegian Timber Design Code - Extract from a New Version - E Aasheim and K H Solli

23-7-1 Proposal for a Design Code for Nail Plates - E Aasheim and K H Solli

24-102-2 Timber Footbridges: A Comparison Between Static and Dynamic Design Criteria - A Ceccotti and N de Robertis

25-102-1 Latest Development of Eurocode 5 - H J Larsen

25-102-1A Annex to Paper CIB-W18/25-102-1. Eurocode 5 - Design of Notched Beams - H J Larsen, H Riberholt and P J Gustafsson

25-102-2 Control of Deflections in Timber Structures with Reference to Eurocode 5 - A Martensson and S Thelandersson

28-102-1 Eurocode 5 - Design of Timber Structures - Part 2: Bridges - D Bajolet, E Gehri, J König, H Kreuzinger, H J Larsen, R Mäkipuro and C Mettem

28-102-2 Racking Strength of Wall Diaphragms - Discussion of the Eurocode 5 Approach - B Källsner

29-102-1 Model Code for the Probabilistic Design of Timber Structures - H J Larsen, T Isaksson and S Thelandersson

30-102-1 Concepts for Drafting International Codes and Standards for Timber Constructions - R H Leicester

33-102-1 International Standards for Bamboo – J J A Janssen

35-102-1 Design Characteristics and Results According to EUROCODE 5 and SNiP Procedures - L Ozola, T Keskküla

35-102-2 Model Code for the Reliability-Based Design of Timber Structures - H J Larsen

36-102-1 Predicted Reliability of Elements and Classification of Timber Structures - L Ozola, T Keskküla

36-102-2 Calibration of Reliability-Based Timber Design Codes: Choosing a Fatigue Model - I Smith

38-102-1 A New Generation of Timber Design Practices and Code Provisions Linking System and Connection Design - A Asiz, I Smith

38-102-2 Uncertainties Involved in Structural Timber Design by Different Code Formats - L Ozola, T Keskküla

38-102-3 Comparison of the Eurocode 5 and Actual Croatian Codes for Wood Classification and Design With the Proposal for More Objective Way of Classification - V Rajcic A Bjelanovic

39-102-1 Calibration of Partial Factors in the Danish Timber Code - H Riberholt

41 - 102 - 1 Consequences of EC 5 for Danish Best Practise - J Munch-Andersen

41 - 102 - 2 Development of New Swiss standards for the Assessment of Existing Load Bearing Structures – R Steiger, J Köhler

41 – 102 - 3 Measuring the CO2 Footprint of Timber Buildings – A Buchanan, S John

INTERNATIONAL STANDARDS ORGANISATION

3-103-1 Method for the Preparation of Standards Concerning the Safety of Structures (ISO/DIS 3250) - International Standards Organisation ISO/TC98

4-103-1 A Proposal for Undertaking the Preparation of an International Standard on Timber Structures - International Standards Organisation

5-103-1 Comments on the Report of the Consultion with Member Bodies Concerning ISO/TC/P129 - Timber Structures - Dansk Ingeniorforening

7-103-1 ISO Technical Committees and Membership of ISO/TC 165

8-103-1 Draft Resolutions of ISO/TC 165

12-103-1 ISO/TC 165 Ottawa, September 1979

13-103-1 Report from ISO/TC 165 - A Sorensen

14-103-1 Comments on ISO/TC 165 N52 "Timber Structures; Solid Timber in Structural Sizes; Determination of Some Physical and Mechanical Properties"

14-103-2 Comments on the CIB Structural Timber Design Code - R H Leicester

21-103-1 Concept of a Complete Set of Standards - R H Leicester

JOINT COMMITTEE ON STRUCTURAL SAFETY

3-104-1 International System on Unified Standard Codes of Practice for Structures - Comité Européen du Béton (CEB)

7-104-1 Volume 1: Common Unified Rules for Different Types of Construction and Material - CEB

37-104-1 Proposal for a Probabilistic Model Code for Design of Timber Structures - J Köhler, H Faber

CIB PROGRAMME, POLICY AND MEETINGS

1-105-1 A Note on International Organisations Active in the Field of Utilisation of Timber - P Sonnemans

5-105-1 The Work and Objectives of CIB-W18-Timber Structures - J G Sunley

10-105-1 The Work of CIB-W18 Timber Structures - J G Sunley

15-105-1 Terms of Reference for Timber - Framed Housing Sub-Group of CIB-W18

19-105-1 Tropical and Hardwood Timbers Structures - R H Leicester

21-105-1 First Conference of CIB-W18B, Tropical and Hardwood Timber Structures Singapore, 26 - 28 October 1987 - R H Leicester

INTERNATIONAL UNION OF FORESTRY RESEARCH ORGANISATIONS

7-106-1 Time and Moisture Effects - CIB W18/IUFRO 55.02-03 Working Party

CIB-W18/42-1-1

INTERNATIONAL COUNCIL FOR RESEARCH AND INNOVATION IN BUILDING AND CONSTRUCTION

WORKING COMMISSION W18 - TIMBER STRUCTURES

CALCULATION OF PARTIAL SAFETY FACTORS

T Poutanen

Tampere University of Technology

FINLAND

Presented by T Poutanen

H.J. Larsen stated that if the paper is correct, then it points out that there is something wrong with the Eurocode. What the author will do about it, as the partial saftety factors issue is outside the scope of CIB W18. T. Poutanen answered that this issue is indeed difficult. He added that the variability in timber is high compared to other building materials. Eurocode is good for steel and penalizes timber; therefore, there is excessive safety in timber.

J. Munch-Andersen said that he is not convinced whether the results are right because there would have been more failures in steel structures. T. Poutanen said that since the safety margin in codes is so high, steel failures are not observed even if the factors were wrong.

J. Köhler commented that the approach is conceptually wrong because it uncoupled the design with the load combination process. For example a given beam designed to carry gravity load will have to be sized differently if additional live load is applied in combination. He suggested that the paper needs to explain how this work relates to how other people's work is done.

A. Ranta-Maunus stated that he does not understand why loads are considered as dependent and why material is dependent on the load. There are no references to scientific literature as this is something the author has created. T. Poutanen answered that this is mathematics and that loads become dependent when applied to the member simultaneously.

H.J. Blass concluded that there are critical questions related to this work.

H.J. Blass announced the formation of a small subgroup to consider the suitability of papers for publication in the CIB W18 proceedings. Not all papers accepted for presentation will necessarily be published in the proceedings.

(Remark: the paper was not accepted for publication in the proceedings according to the peer review procedure given in chapter 14 of the proceedings)

INTERNATIONAL COUNCIL FOR RESEARCH AND INNOVATION
IN BUILDING AND CONSTRUCTION

WORKING COMMISSION W18 - TIMBER STRUCTURES

MACHINE STRENGTH GRADING – A NEW METHOD FOR DERIVATION OF SETTINGS

R Ziethén
SP Trätek Borås

C Bengtsson
SP Trätek, Borås and
School of Technology and Design, Växjö University

SWEDEN

Presented by C Bengtsson

H.J. Blass stated that very conservative settings could result if different settings were not available for a single grade. In the case where different settings for one grade are currently set if the number of grades produced in a mill is different is an important issue.
C. Bengtsson answered that it is not good to have a complicated system where people do not understand how it works. She agrees that the proposed process could be conservative and it is possible to consider the issues in question.
M. Sandomeer states that output control or monitor process is also possible to be considered to improve grading process.
A. Jorissen asked whether not having different settings for the same grade is practically wrong. C. Bengtsson answered that it is not practically wrong but we currently have a large combination and it is too complicated.
A. Ranta-Maunus said that when considering only the 5th percentile value this is not wrong but when considering the lower tail, it may be incorrect. He agrees with H.J. Blass that it is not fully economical and work should be done.
J. Köhler stated that it is important to rethink the issue of grading with output control system. It may be an issue for the code writing body. It is also important to look into lower tails rather than just 5th percentile.
C. Bengtsson answered that it is possible to consider the issues as additional work.

Machine strength grading – a new method for derivation of settings

Rune Ziethén
SP Trätek, Box 857, SE-501 15 Borås, Sweden

Charlotte Bengtsson
SP Trätek, Box 857, SE-501 15 Borås, Sweden and
School of Technology and Design, Växjö University, SE-351 95 Växjö, Sweden

1 Abstract

This paper presents and analyses a new method for derivation of setting values for strength grading machines. The method uses a model for the relationship between indicating property (measured by a grading machine, IP) and the grade determining property (GDP). This model is of course not perfect and by summarising the errors in the model a confidence interval for the model can be calculated. The confidence interval is used for creating a prediction interval. The lower limit of the prediction interval, the prediction limit, is used to predict the GDP.

The prediction limit method is analysed and evaluated by well defined input data. It is shown that fewer experimental data than required by the method in EN 14081-2 today is needed to determine reliable settings but the producer is awarded with less conservative settings with an increased number of experimental data. A weak correlation between IP and GDP or a high coefficient of variation also results in conservative settings. The settings are not dependent on average strength of the raw material used for deriving the settings.

2 Background and introduction

One workpackage (WP) of the ongoing Gradewood project deals with "Modelling and development of grading procedures". The work presented in this paper is part of this WP. As the present standard for derivation of settings for grading machines, EN 14081, is complicated and also questioned, due to its complexity, other methods are evaluated. One of the results of the Gradewood project will be a concept of an improved machine strength grading standard. The method for calculating settings according to EN 14081 is denoted the "cost matrix method". This method was presented by Rouger (1997).

The procedure today if a grading machine producer wants settings to be used for grading timber to be CE-marked is roughly as follows:

- Sample test material for actual growth areas according to EN 14081. Collect IP-values from the grading machine. Test according to EN 408 (bending or tension) and evaluate characteristic values according to EN 384.
- Calculate settings according to the cost matrix method in EN 14081. Report to CEN TC124/TG1. In the revised version of EN 14081 there is a detailed description of what should be in the report.

- CEN TC124/TG1 evaluates the report. If the report is ok an ITT-report containing the settings is issued.
- The content of the ITT-report is included in EN 14081, part 4, when it is revised.

The main motivations for looking at alternatives to the present method according to EN 14081 are:

- The cost matrix method is complicated. As a consequence of this the interpretation of the standard is difficult and presently there are only few persons around Europe who have detailed knowledge on how to use the metod. As result of the difficulties to interpret/understand the method, the decisions by TG 1 change from meeting to meeting.
- The cost matrix method allows for different settings for the same strength class. This is of course in line with the theory behind the method but in practice this fact leads to confusion. It is difficult to explain for producers and users of graded timber that different settings can be used depending on if the strongest material is "creamed off" or if it is included.
- The building code uses the 5^{th} percentile value of the strength as a characteristic value. This has also affected the grading standard where the requirement on the graded material is based on the 5^{th} percentile for each grade in each grade combination. However, what is interesting from a safety point of view is not the number of pieces below the required value but the probability of getting pieces with strength lower than what is covered by the partial coefficients in the building code. The relation between the 5^{th} percentile and really low values is based on the assumption of a log-nomal distribution of the strength which is valid for a saw-falling population of timber. When the timber is graded this relation is disturbed and the validity of the assumption can be questioned.
- The method in EN 14081 is sensible for single observations (outliers) in the data set used for calculation of settings. One of the requirements is that minimum 0,5 % or 5 pieces must be graded as rejects. In the tail of the distribution of IP-values the difference between the IP-values can be considerable, see Figure 1. This means that one single observation can have a big influence on the settings for the low strength-classes. As example, the value within the ring in Figure 1 lowers the minimum setting in this example from 7000 to 6640 i.e. about 5%.
- The timber used for derivation of settings must of course be representative for the actual timber source. The fact that the cost matrix method is sensible for single observations together with the difficulties connected to representative sampling is a weakness of the present method.
- There are examples when the cost matrix method gives illogical results. Table 1 below gives examples of elementary cost factors for two grade combinations. It is recognised as more severe if a piece is wrongly upgraded from reject to C30 or from C18 to C30 when C30 and C18 are graded together than if the same piece is wrongly upgraded to C30 when C30 is graded on its own. This may require higher settings for C30 in the first case.
- Recent studies indicate that the method in EN 14081 does not produce structural timber with promised grade determining properties in all cases, see Ranta-Maunus and Denzler (2009).

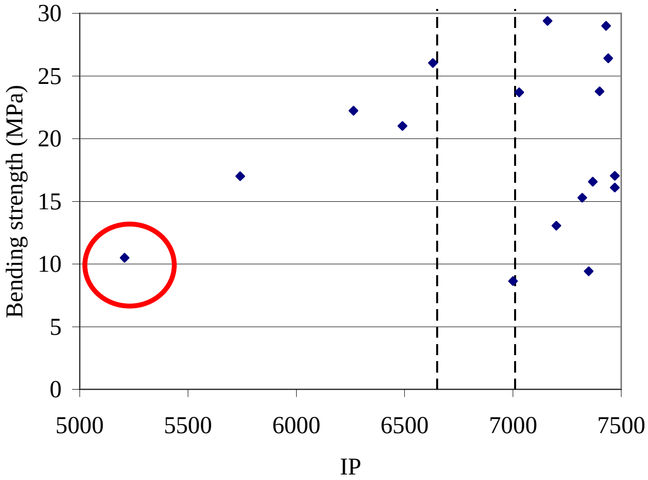

Figure 1. Example of the lower tail of one strength versus IP data set.

Table 1. Elementary cost matrices for a) grade combination C30-C18-reject, b) grade combination C30-reject.

Optimum grade	Assigned grade		
	C30	C18	Rej
C30	0		
C18	2,22	0	
Rej	4,07	1,11	0

a)

Optimum grade	Assigned grade	
	C30	Rej
C30	0	
Rej	1,11	0

b)

Some of the shortcomings of the present EN 14081 was pointed out and discussed by Bengtsson and Fonselius (2003). Even if there is now a revised version of EN 14081 on its way and this revised version is in many cases clearer than the present version there is still a need for a more transparent standard containing methods for derivation of settings for grading machines.

2.1 Objective of this paper

The objective of this paper is to present a method for deriving settings for grading machines which is based on probabilistic theory rather than 5th percentiles. The intention is that the method should be stable which means unsensible for single outlaying observations and stable for variation in incoming raw material to be graded. The method should give settings which are safe indepentently of grade combination. Further, the method should be transparent for the users so that it is suitable for a system with attestation of conformity (AC) level 2+.

3 Analysis

3.1 Proposed method

A method for calculation of settings based on prediction intervals is proposed. Prediction intervals are suitable when future single values shall be estimated based on past or present data. This is the case when settings for grading machines are used.

The relation between IP measured by a grading machine and the grade determining property (GDP) can be represented by a linear regression model: $GDP = \beta_0 + \beta_1 \cdot IP$

The uncertainties of the linear regression can be described by a confidence interval. An expanded confidence interval, the prediction interval, is used to predict a single GDP from IP-values. The lower limit of the prediction interval is the prediction limit.

3.2 Theory

The general expression for a linear regression model is:

$$Y(x) = \beta_0 + \beta_1 x + \varepsilon \qquad \text{eq. 1}$$

The error term,ε, and the regression coefficients, β_0 and β_1, are determined by minimizing the sum of errors using the least square method.

Each error e_i (residual) is given by eq. 2.

$$e_i = Y_i - \left\lfloor \hat{\beta}_0 + \hat{\beta}_1 x_i \right\rfloor \qquad \text{eq. 2}$$

The variance of the error e_i is calculated according to eq. 3. Further the variance of the coefficients, β_0 and β_1, are calculateded, see for example Jørgensen (1993), resulting in variance for the regression model, eq. 4, and confidence interval for the regression model, eq 5.

$$\hat{\sigma}^2 = \frac{1}{n-2}\sum_{i=1}^{n} e_i^2 = \frac{1}{n-2}\sum_{i=1}^{n}\left(Y_i - \left[\hat{\beta}_0 + \hat{\beta}_1 x_i\right]\right)^2 \qquad \text{eq. 3}$$

$$Var[\hat{y}(x)] \approx \hat{\sigma}^2 \left(\frac{(x-\bar{x})^2}{\sum_{i=1}^{n}(x_i - \bar{x})^2} + \frac{1}{n} \right) \qquad \text{eq. 4}$$

$$Conf\,\mathrm{int}[\hat{y}(x)] \approx \pm t \cdot \sqrt{\hat{\sigma}^2 \left(\frac{(x-\bar{x})^2}{\sum_{i=1}^{n}(x_i - \bar{x})^2} + \frac{1}{n} \right)} \qquad \text{eq. 5}$$

t is taken from the student t-distribution with n-2 degrees of freedom.

When the regression model is used to predict a value y*(x) the variance for the predicted value is larger than the confidence interval. The variance for the predicted value is given by eq. 6 and the prediction interval for a predicted value y*(x) is calculated according to eq. 7.

$$Var\left[y^*(x)\right] \approx \hat{\sigma}^2 \left(\frac{(x-\bar{x})^2}{\sum_{i=1}^{n}(x_i-\bar{x})^2} + \frac{1}{n} + 1 \right) \qquad \text{eq. 6}$$

$$y^*(x) = \hat{\beta}_0 + \hat{\beta}_1 x \pm \hat{\sigma} \cdot t \cdot \sqrt{\frac{(x-\bar{x})^2}{\sum_{i=1}^{n}(x_i-\bar{x})^2} + \frac{1}{n} + 1} \qquad \text{eq. 7}$$

t is taken from the student t-distribution with n-2 degrees of freedom.

If the number of observations used for the regression is large, the first two terms under the root-sign in eq. 6 can be neglected. The equation for the prediction interval is then given by eq. 8.

$$y^*(x) = \hat{\beta}_0 + \hat{\beta}_1 x \pm \hat{\sigma} \cdot t \qquad \text{eq. 8}$$

The prediction interval can be calculated for any linear regression. The prediction interval is two sided so to get an estimation of the lower 5^{th}-percentile prediction limit the student t-factor for a 90%-prediction interval is used. In Figure 2a the 5^{th}-percentile prediction interval for a linear model is shown and in Figure 2b the same prediction interval for a logarithmic regression model.

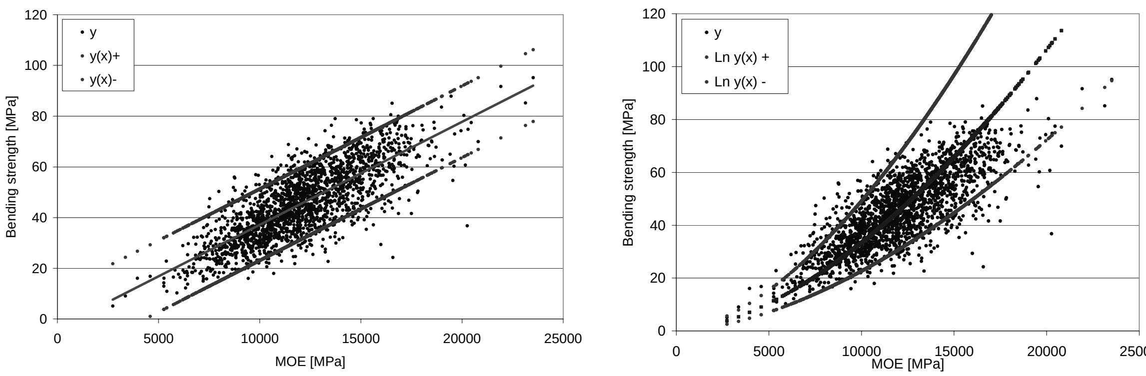

a) b)

Figure 2. Prediction limit for a) a linear model and b) a logarithmic model between MOE and bending strength.

3.3 Data used for the analysis

The calculations in this paper are all carried out on computer-generated data sets. The properties varied are: mean value, coefficient of variation (COV) and coefficient of determination (r^2). All eight data sets were generated with assistance from the University of Ljubljana. Each data set consists of 20 000 observations and four variables. The variables are strength (MOR in MPa), modulus of elasticity (MOE in MPa), density (kg/m^3) and indicating property (IP). The IP is a variable without units and it is not intended to imitate any specific mechanical or physical property. The data sets are denoted based on MOR with three labels “mean - COV - r^2”.

The generated data sets were chosen to fit the distributions defined by COST Action E24 (JCSS probabilistic model code www.jcss.ethz.ch):

- MOR log-normal distribution

- MOE log-normal distribution
- Density normal distribution
- IP log-normal distribution

The properties of the master data set are based on experience from tests both regarding mean value, COV and correlation (mainly from Gradewood WP 2). The properties for the master data set are presented in Table 2.

Table 2a) Basic statistics and b) correlations (r^2) for the master data set, 45-35-50.

	MOR	**MOE**	**Dens**	**IP**
Av. value	44,9	12 503	450	14 788
COV	35%	26%	12%	22%

a)

	MOR	**MOE**	**Dens**	**IP**
MOR	1			
MOE	0,57	1		
Dens	0,17	0,26	1	
IP	0,48	0,65	0,10	1

b)

Group one is data sets with varying mean value of MOR, constant COV (35 %) and constant coefficient of determination between MOR and IP (0,5), see Table 3.

Table 3. Basic statistics for data sets with different mean values of MOR. r^2 is coefficient of determination between each property and IP.

	Data set 30-35-50				**Data set 45-35-50**				**Data set 60-35-50**			
	MOR	MOE	Dens	IP	MOR	MOE	Dens	IP	MOR	MOE	Dens	IP
Av. value	30,1	8390	400	10405	44,9	12503	450	14788	60,1	16512	560	19218
COV	35%	26%	11%	20%	35%	26%	12%	22%	35%	26%	12%	21%
r^2	0,49	0,67	0,10	1	0,48	0,65	0,10	1	0,49	0,66	0,10	1

Group two is data sets with varying COV of MOR, constant mean value (45 MPa) and constant coefficient of determination between MOR and IP (0,5), see Table 4. Data set 45-35-50 is the same as in Table 3.

Table 4. Basic statistics for data sets with different COV. r^2 is coefficient of determination between each property and IP.

	Data set 45-20-50				**Data set 45-50-50**			
	MOR	MOE	Dens	IP	MOR	MOE	Dens	IP
Av. value	45,0	12492	450	14793	45,3	12547	451	14825
COV	20%	15%	7%	13%	50%	37%	17%	33%
r^2	0,50	0,67	0,10	1	0,48	0,66	0,10	1

Group three is data sets with varying coefficient of determination between MOR and IP, constant mean value (45 MPa) and constant COV (35%), see Table 5. Data set (45-35-50) is the same as in Table 3.

Table 5. Basic statistics for data sets with different coefficient of determination (r^2) between MOR and IP. r^2 is coefficient of determination between each property and IP.

	Data set 45-35-10				**Data set 45-35-30**				**Data set 45-35-70**			
	MOR	MOE	Dens	IP	MOR	MOE	Dens	IP	MOR	MOE	Dens	IP
Av. value	45,2	12526	451	14815	45,0	12502	450	14806	45,1	12532	450	14842
COV	35%	26%	11%	10%	35%	26%	11%	17%	35%	26%	11%	26%
r^2	0,10	0,39	0,10	1	0,29	0,53	0,10	1	0,69	0,80	0,10	1

3.4 Characteristic values

To evaluate the prediction limit method the grades C24, C30 and C40 were used with grade determining properties according to EN 338 and EN384, see Table 6.

Table 6. Grade determining properties for grades used in present paper

Grade	MOR [MPa]	MOE [MPa]	Density [kg/m^3]
C24	21,4	10450	350
C30	26,8	11400	380
C40	40,0	13300	450

4 Results

For analysis of the proposed prediction limit method 1000 observations out of the 20 000 within each data set were chosen. In all analyses below the logarithm of the values are used in the linear regressions. In the examples shown here the lower 5th percentile is used as prediction limit but it is of course possible to use any percentile level as prediction limit when calculating settings. Settings are shown for the cases when MOR, MOE or density are used as grade determining property. Settings for MOE are determined from the regression lines as the requirement on MOE is the average value. However, the discussion around the evaluation of the proposed method is concentrated on settings based on MOR.

4.1 Influence of variation in raw material

4.1.1 Mean value

Table 7 shows basic statistics for the raw material (group one) used for calculation of the settings in Table 8. It can be seen that the settings are undependent of variation in mean value of the raw material used for the calculation. For the data set with the highest average strength the settings look strange when density is used as grade determining property. The reason for this is that the average value of the density for this data set is probably set to high which gives a strange relation between density and IP.

In Figure 3 the linear regression lines and the 5 percent prediction limits are plotted for the data sets with different mean values of strength. From the Figure it can also be seen that the average strength values of the data have a very limited influence on the prediction lines.

Table 7. Basic statistics for a) sub data set 30-35-50, b) sub data set 45-35-50 and c) sub data set 60-35-50.

	MOR	MOE	Dens	IP
Av.	29,5	8288	398	10335
5th perc.	16,4	5380	334	7295
COV	35%	27%	11%	21%
Min.	10,9	3194	284	5930

a)

	MOR	MOE	Dens	IP
Av.	45,0	12496	454	14776
5th perc.	24,2	8019	368	10038
COV	35%	26%	12%	22%
Min.	12,2	5403	289	6463

b)

	MOR	MOE	Dens	IP
Av.	59,7	16479	559	19210
5th perc.	32,7	10485	445	13688
COV	35%	26%	12%	21%
Min.	18,7	7548	316	10677

c)

Table 8. Settings for C24, C30 and C40 calculated for a) sub data set 30-35-50, b) sub data set 45-35-50 and c) sub data set 60-35-50.

Grade	MOR	MOE	Dens
C24	11 300	13 100	12 900
C30	13 700	14 300	17 100
C40	19 200	16 600	22 700

a)

Grade	MOR	MOE	Dens
C24	11 200	12 400	11 100
C30	13 800	13 600	17 000
C40	19 800	16 000	25 000

b)

Grade	MOR	MOE	Dens
C24	11 500	12 500	1 300
C30	13 900	13 600	6 600
C40	19 500	15 800	13 700

c)

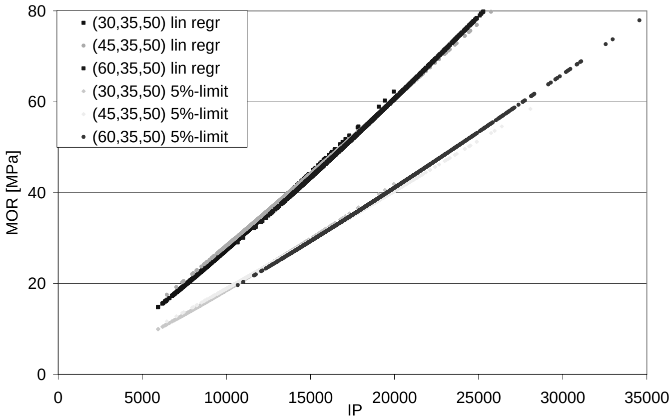

Figure 3. Regression line and 5 percent prediction limit for the three data sets with different mean values of strength.

4.1.2 Coefficient of variation

Table 9 shows settings for the data set with an average strength of 45 MPa and a coefficient of determination between strength and IP of 0,5 (group two). The COV for the strength varies from 20% to 50%. It can be seen that a higher coefficient of variation results in more conservative settings. The COV for MOE and density are changed proportional to the COV for strength. Therefore, the COV for density in sub data set 45-20-50 is as low as 7% and no single values are below 350 kg/m³. This combined with a low coefficient of determination between IP and density gives unrealistic values for settings based on density. The problem is a result of the unrealistic properties of the generated data set and not due to the method of analysis.

Table 9. Settings for C24, C30 and C40 calculated for a) sub data set 45-20-50, b) sub data set 45-35-50 and c) sub data set 45-50-50.

Grade	MOR	MOE	Dens
C24	9 500	12 400	3 700
C30	11 600	13 600	9 800
C40	16 700	15 900	18 200

a)

Grade	MOR	MOE	Dens
C24	11 200	12 400	11 100
C30	13 800	13 600	17 000
C40	19 800	16 000	25 000

b)

Grade	MOR	MOE	Dens
C24	12 700	12 300	16 600
C30	15 700	13 500	21 900
C40	22 900	16 000	29 000

c)

From Figure 4 it can be seen that the linear regression is not effected by the COV of the GDP. However, an increased COV results in a wider prediction interval and a lower predicted strength for the same IP.

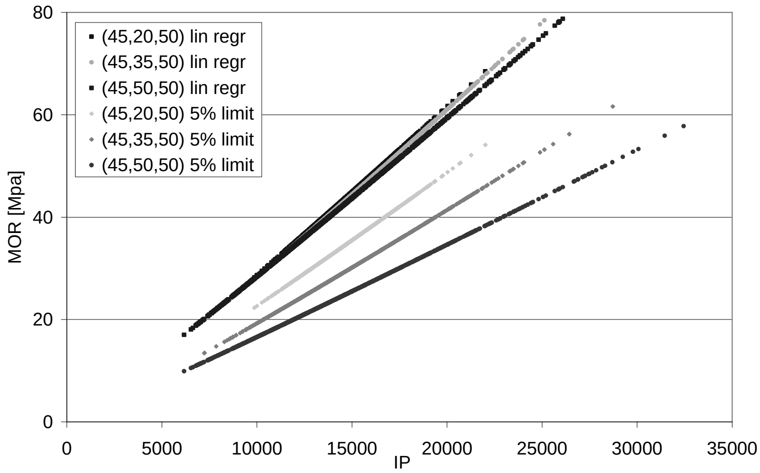

Figure 4. Regression line and 5 percent prediction limit for three data sets with different COV.

4.1.3 Correlation between IP and grade determining property

Tables 10 and 11 show settings for the data sets (group three) with varying coefficient of determination between IP and MOR. The coefficient of determination varies between 0,1 and 0,7. The analysis shows that a lower coefficient of determination results in more conservative settings. The influence of coefficient of determination is more pronounced for high strength classses.

Table 10. Settings for C24, C30 and C40 calculated for a) sub data set 45-35-70, b) sub data set 45-35-50

Grade	MOR	MOE	Dens
C24	10 300	12 200	8 100
C30	12 600	13 500	16 100
C40	17 900	16 000	26 900

a)

Grade	MOR	MOE	Dens
C24	11 200	12 400	11 100
C30	13 800	13 600	17 000
C40	19 800	16 000	25 000

b)

Table 11. Settings for C24, C30 and C40 calculated for a) sub data set 45-35-30, b) sub data set 45-35-10

Grade	MOR	MOE	Dens
C24	11 900	12 800	11 100
C30	14 600	13 800	15 800
C40	21 300	15 900	22 200

c)

Grade	MOR	MOE	Dens
C24	12 700	13 500	12 700
C30	15 600	14 200	15 300
C40	22 900	15 500	18 800

d)

4.2 Stability of settings

One thousand observations were randomly chosen 200 times out of the data set 45-35-50. Settings were calculated for these 200 sub data sets. Average values and COV for the settings from these calculations are shown in Table 12. The proposed method seems to produce stable settings, especially when MOR or MOE are used as grade determining property.

Table 12. a) Settings based on MOR, b) settings based on MOE and c) settings based on density

Grade	Av.	COV [%]
C24	11 112	1,4
C30	13 619	1,1
C40	19 581	1,4

a)

Grade	Av.	COV [%]
C24	12 415	0,6
C30	13 583	0,5
C40	15 921	0,6

b)

Grade	Av.	COV [%]
C24	11 753	4,7
C30	17 585	3,1
C40	25 445	4,2

c)

4.3 Characteristic properties of graded material

Settings based on MOR according to Table 12a above were used for grading all the data sets. C24, C30, C40 were graded as single grades and C24 and C30 were graded together. Examples of grading results are shown in Tables 13 and 14. The last rows in these tables show characteristic value for C24 when it is graded in combination with C30.

It can be noted that the settings in Table 12a are more conservative than what is usually determined by the cost matrix method.

Table13. Characteristic values of graded material. Figures in bold indicate that the required value is not fulfilled. a) Data set 45-35-50, b) data set 45-50-50.

Grade	MOR [MPa]	MOE [MPa]	Dens. [kg/m^3]	Yield [No. obs]
C24	27,1	13 003	367	17 733
C30	31,2	14 120	**375**	12 122
C40	43,4	17895	**398**	1 650
C24 - C30	23,6	10 588	354	5 611

a)

Grade	MOR [MPa]	MOE [MPa]	Dens. [kg/m^3]	Yield [No. obs]
C24	23,8	13 827	**337**	15 409
C30	27,9	15 199	**346**	10 737
C40	**37,6**	19 158	**363**	3 035
C24 - C30	**20,2**	10 674	**321**	4 672

b)

Data set 45-35-50 in Table 13a can be regarded as “the normal” and if the COV decreases (to 20%) all required values are fulfilled. On the other hand, if the COV increases, as in Table 13b, more required values are not fulfilled. If the average strength of the data set increases (to 60 MPa) all required values are fulfilled.

Table 14. Characteristic values of graded material. Figures in bold indicate that the required value is not fulfilled. a) Data set 45-35-10, b) data set 45-35-70.

Grade	MOR [MPa]	MOE [MPa]	Dens. [kg/m^3]	Yield [No. obs]
C24	24,4	12 536	370	19 955
C30	25,8	13 240	**377**	15 742
C40	**36,9**	19 833	421	37
C24-C30	**21,3**	**9 906**	350	4 213

a)

Grade	MOR [MPa]	MOE [MPa]	Dens. [kg/m^3]	Yield [No. obs]
C24	29,3	13 283	375	16 764
C30	34,5	14 426	382	11 609
C40	48,8	18 100	**401**	2 300
C24-C30	26,0	10 708	363	5 155

b)

The “bad” grading machine, results found in Table 14a, with r^2=0,1 results in fulfilled required values and a high yield for C24 as single grade but when higher grades are involved the yield drops and the required values are not fulfilled.

4.4 Influence of number of observations

Figure 5 shows settings calculated with the prediction limit method as a function of the number of observations used for the calculation. Data set 45-35-50 was used and settings based on MOR were calculated for C24, C30 and C40. It can be seen that C24 is very little affected by the number of observations but for the higher grades the method gives more conservative values for fewer observations.

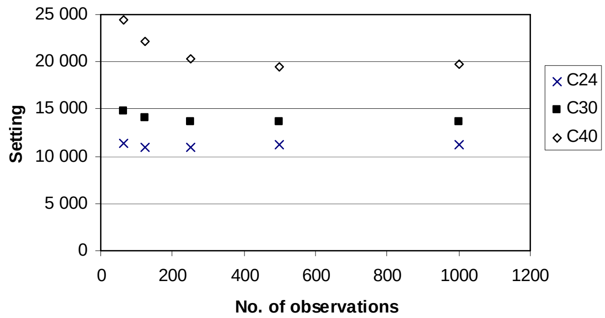

Figure 5. Settings based on MOR calculated with the prediction limit method as function of number of observations used for the calculation.

5 Conclusions and recommendations

The evaluation of the proposed prediction limit method for calculation of settings has shown that:

- The calculated settings are not dependent on average strength of the raw material
- A higher COV of the raw material results in more conservative settings
- Weak correlation between indicating property and grade determining property results in more conservative settings
- Few observations for calculation of settings results in more conservative settings

The method is simple and based on common statistical theory. Such a simple method is transparent for the users and well suited for a European standard. Some grading machines on the market today operate with multiple settings and the prediction limit method can be adopted also to this case. The method gives one setting for each grade independently of grade combination. Depending on the percentile level chosen the calculated settings result in graded material with different safety levels.

The prediction limit studied in this paper is the lower 5% limit and the achieved characteristic values of the graded material are compared to the characteristic values according to EN338. The prediction limit method opens for a possibility to calculate another limit such as the lower 1% or lower 0,1 % limit and compare the result to other required values. It is the combination of confidence level of the prediction limit and the required value that defines the safety for the end user of the graded timber.

In the comparison between the achieved characteristic values after grading based on the prediction limit and the requirements in EN338 it is mainly the density that fails to be fulfilled. One reason for that is obviously the poor correlation between strength and density since the settings were determined based on the relation between IP and MOR. Other reasons can be an unrealistically chosen density in the data sets or an unrealistic required density in EN338.

The authors of this paper recommend a deeper analysis of the prediction limit method for calculation of settings for grading machines. In connection to this also new requirements for the graded material are needed.

6 Acknowledgement

This work was mainly carried out within the Gradewood project, WoodWisdom-Net Project 112006B and Vinnova Dnr 2007-0126. The financial support is gratefully acknowledged. Comprehensive contributions to this paper was given by Prof. Goran Turk, University of Ljubljana, who prepared the data sets.

7 References

Bengtsson, C. and Fonselius, M.: Settings for strength grading machines – evaluation of the procedure according to prEN 14081, part 2, CIB W18, proceedings paper 36-5-1, Colorado, USA, 2003.

Jørgensen, B.: The theory of linear models, CRC Press, 1993.

Ranta-Maunus, A. and Denzler, J.:Variability of strength of European spruce, CIB W18, proceedings paper 42-6-1, Zürich, Switzerland, 2009.

Rouger, F.: A new statistical method for the establishment of machine settings, CIB W18, proceedings paper 30-17-1, Vancouver, Canada, 1997.

EN 384 Structural timber – Determination of characteristic values of mechanical properties

EN 338 Structural timber – Strength classes

EN 14081 Timber structures – Strength graded structural timber with rectangular cross section, part 1-4

CIB-W18/42-6-1

INTERNATIONAL COUNCIL FOR RESEARCH AND INNOVATION IN BUILDING AND CONSTRUCTION

WORKING COMMISSION W18 - TIMBER STRUCTURES

VARIABILITY OF STRENGTH OF EUROPEAN SPRUCE

A Ranta-Maunus

VTT

FINLAND

J K Denzler

Holzforschung Austria

AUSTRIA

Presented by A Ranta-Maunus

S. Aicher stated that when looking at the strong decrease in strength and stiffness when comparing 175 mm to 225 mm width, it may be related to sawing pattern of the logs; otherwise, this information may also concern the timber resources in central Europe. A. Ranta-Maunus answered that sawing pattern may be a problem but forest management practice is also an important issue where other countries may have different approach compared to Scandinavia. H.J. Blass stated that the forest management practice is different in central Europe as they do not harvest trees from the same age group therefore large sizes timber from Central Europe should still be okay in terms of strength properties.

J.W.G. van de Kuilen received clarification of the procedures by checking subsamples with large specimens.

G. Schickhofer and R. Steiger received confirmation that k_v (EN 384) was used. A. Ranta-Maunus commented that he did not like the factor.

Variability of strength of European spruce

Alpo Ranta-Maunus

VTT, Finland

Julia K. Denzler

Holzforschung Austria, Austria

1 Introduction

Unlikely of most other species, European spruce (*Picea abies*) has quite similar properties independently of the growth area. However, mechanical properties of spruce can be variable depending on the growth conditions, forestry management practices, dimensions and sawing patterns.

In Europe, machine strength grading is normally based on the so called "machine control" method defined in EN 14081. This implies that same settings are used for spruce grown within an administrative growth area. Until now, a growth area is defined as a country or a combination of countries. When settings are determined, minimum 4 sub-samples representative for the growth area are tested. There is a limit how much properties of each combination of all-but-one sub-samples can deviate. This method takes care that settings are safe as long as a producer of timber receives its material regularly from the total growth area and as long as the material chosen for determination of settings was representative.

There is no limit how much lower the mechanical properties of a single graded sub-sample representing a region or dimension can be. Obviously this may result in situations where the production of a sawmill can have significantly different properties from the values given in EN 338, at least for limited periods of time.

This paper wants to clarify if there are great differences in the properties of spruce grown in different countries and therefore, if the division into different growth areas as given in EN 14081-4 today is appropriate.

2 Materials and methods

2.1 Materials

2.1.1 General

This study is based on the two sources: Gradewood-project material and strength grading data of a big sawmill using grading machine GoldenEye 706.

2.1.2 Gradewood project material

Gradewood project is an ongoing European project where existing laboratory measurement data all over Europe was combined and analysed [RANTA-MAUNUS ET AL., 2009]. In this paper, results of 15 000 specimens of spruce from Nordic and Central European countries have been analysed. The dimensions varied as typical of various countries. Generally the sampling was intended to be representative for a country. In case of North-West Russia, sampling was random including also logs with lower quality than normally used for sawn timber.

2.1.3 GoldenEye 706 material

The readings of the strength grading equipment GoldenEye 706 at a saw mill in Eastern Finland during period 10/2008-03/2009 were analysed. In total 150 000 boards run through the machine during this period. The dimensions varied between $w = 75$ mm and $w = 225$ mm in width and $t = 40$ mm to $t = 50$ mm in thickness. In this paper, the results are focused on three widths ($w = 75$ mm, $w = 175$ mm, $w = 225$ mm) because dimensions from $w = 75$ mm to $w = 175$ mm give quite similar results whereas the widths of $w = 200$ mm and $w = 225$ mm give lower mechanical values. These three dimension had in total 40 000 boards which have been analysed in this paper.

2.2 Methods

2.2.1 Gradewood project analysis

For all specimens reported in this paper, the laboratory measurements included density, local modulus of elasticity (*MOE*), moisture content and bending strength (*MOR*). To get comparable results the data was adapted to a height of $h = 150$ mm with the k_h-factor given in EN 384 and to a moisture content of $u = 12\%$. The specimens were all tested in bending with a span s = 18*height and the loading heads placed in the third points of the span. The grade determining defect was placed in between the loading heads. Testing was made by different laboratories in several projects during a period from 1990 to 2008. Therefore, there may be some differences in testing practices even if all participants informed that they followed standards EN 408 and EN 384 or equivalent.

To analyse the relationship of *MOE* and *MOR* for different countries, the specimens were divided into bandwidths with approximate limits given in Tab. 1.

Tab. 1: Bandwidths of local *MOE*.

name of *MOE* bandwidth in N/mm²	min. *MOE* in N/mm²	max *MOE* in N/mm²
5 000		<= 6 250
7 500	> 6 250	<= 8 750
10 000	> 8 750	<= 11 250
12 500	> 11 250	<= 13 750
15 000	> 13 750	<= 16 250
17 500	> 16 250	

For each bandwidth the average *MOE* (E_{mean}), the average bending strength ($f_{m,mean}$) and the characteristic bending strength ($f_{m,k}$) were calculated. $f_{m,k}$ is calculated based on the best estimate 5 percentile of Normal distribution fitting.

2.2.2 GoldenEye 706 material analysis

The strength grading machine GoldenEye 706 uses X-Ray radiation to determine sizes, knots (in this investigation *MKP,* Machine Knot Parameter is used) and density of a board via grey scale image, and combines this information to a frequency measurement to determine dynamic modulus of elasticity E_{dyn}. Using this information the machine estimates the bending strength of each board by calculating its indicating property $f_{m,mod}$ for bending strength with an equation based on linear multi-regression.

An estimate of bending strength of each board is generated on statistical basis ($f_{m,sim}$). Numerical simulation is made as follows:

$$f_{m,sim} = f_{m,mod} + \varepsilon \quad (1)$$

where random error ε is a normally distributed variable having zero mean. Standard deviation of ε can be estimated based on the statistical condition that variance of a sum equals the sum of variances:

$$\mathrm{var}\, f_m = \mathrm{var}\, f_{m,mod} + \mathrm{var}\, \varepsilon \quad (2)$$

For simplicity, we choose a constant standard deviation of ε, σ = 6 N/mm^2 ($\varepsilon = N(0;6)$) which satisfies eqn.(2) when COV of $f_{m,mod}$=0.22, COV of f_m=0.26 and $f_{m,mean}$ = 43 N/mm^2. Variation of strength can be larger for high values of $f_{m,mod}$, but the adopted value corresponds well to the variation of the lower half of Nordic material. Fig. 1 shows the simulated strength values $f_{m,sim}$ calculated with the described methods versus the indicating property $f_{m,mod}$ for specimens with a height of h = 225 mm as an example.

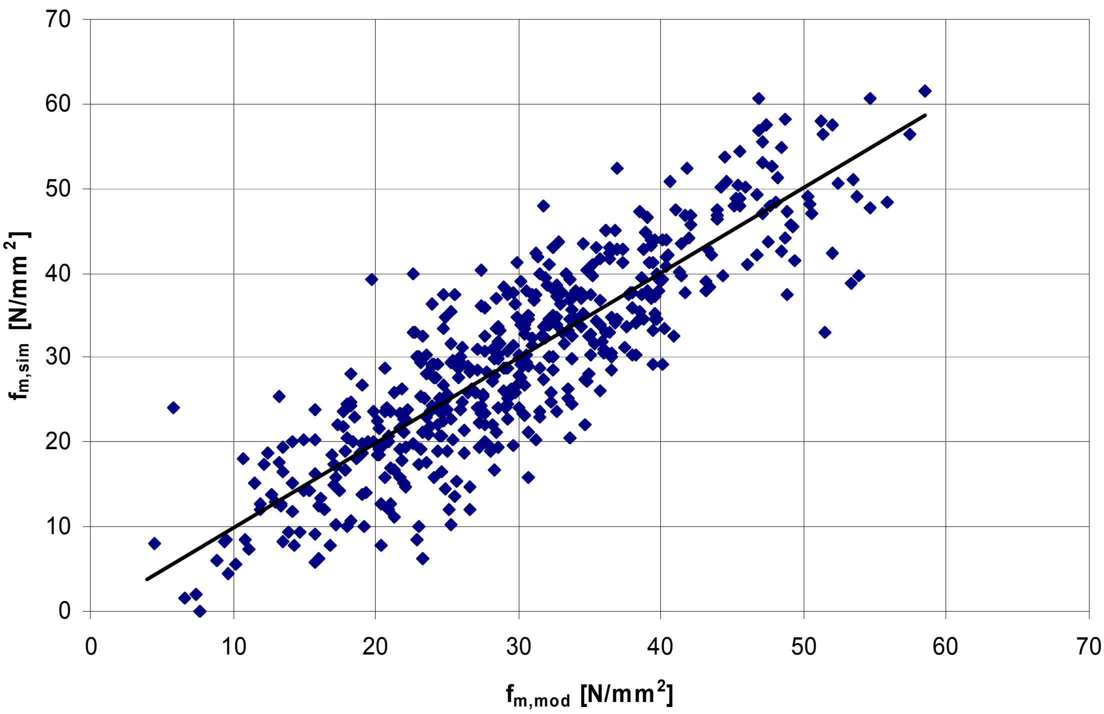

Fig. 1: Simulated strength values versus indicating property for h = 225 mm, n = 500 specimens of sample "low".

To illustrate possible quality changes, the moving average of $f_{m,mod}$ of 500 consecutive boards has been calculated and the samples of 500 with the lowest and the highest moving average have been analysed.

3 Results

3.1 Variation between countries

Tab. 2 summarizes the averages of mechanical properties of European spruce grown in main producing countries. Fig. 2 shows the mean bending strength versus mean *MOE* for different countries within the chosen bandwidths. Fig. 3 shows the same for characteristic bending strength.

Tab. 2: Average mechanical properties divided by country.

country	n	modulus of elasticity		density		bending strength	
		E_{mean} in N/mm²	COV in %	ρ_{mean} in kg/m³	COV in %	$f_{m,mean}$ in N/mm²	COV in %
SWE	4 393	12300	21.8	435	11.5	44.8	29.8
RUS (N-W)	1 031	11500	21.6	427	10.0	42.4	28.3
FIN	2 846	12000	20.9	440	9.3	44.1	26.4
GER	3 538	12100	25.6	441	10.9	41.5	33.9
FRA	1 740	11800	28.2	443	na	42.3	35.1

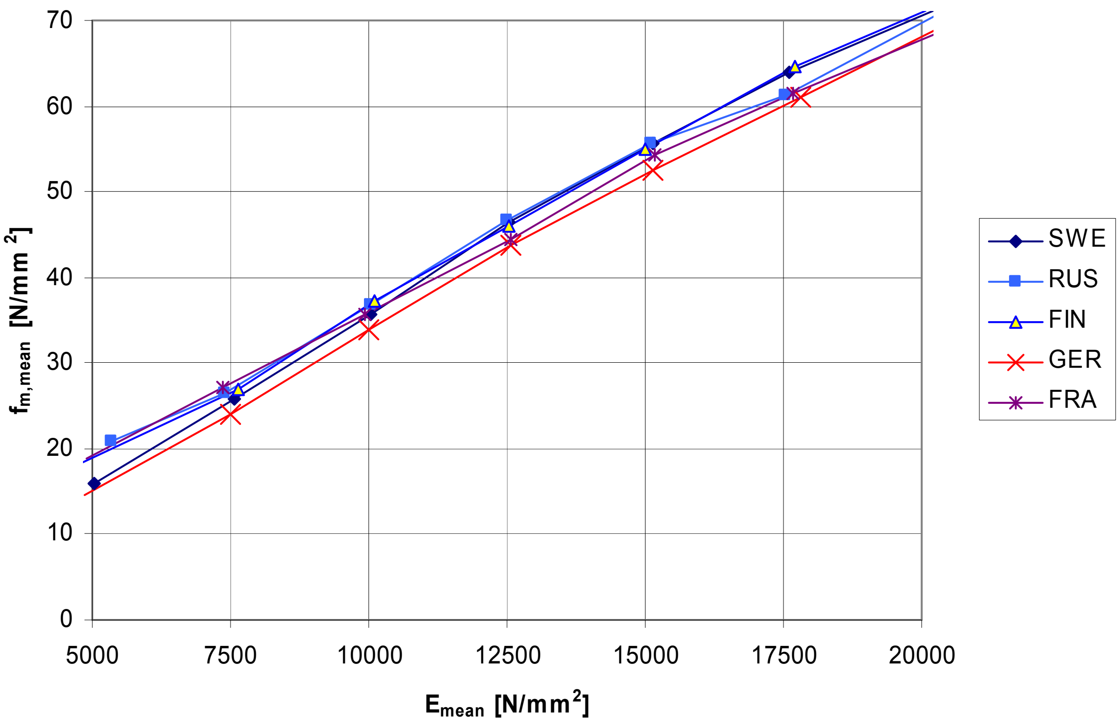

Fig. 2: Mean bending strength versus mean modulus of elasticity for different countries, n = 13 548 specimens.

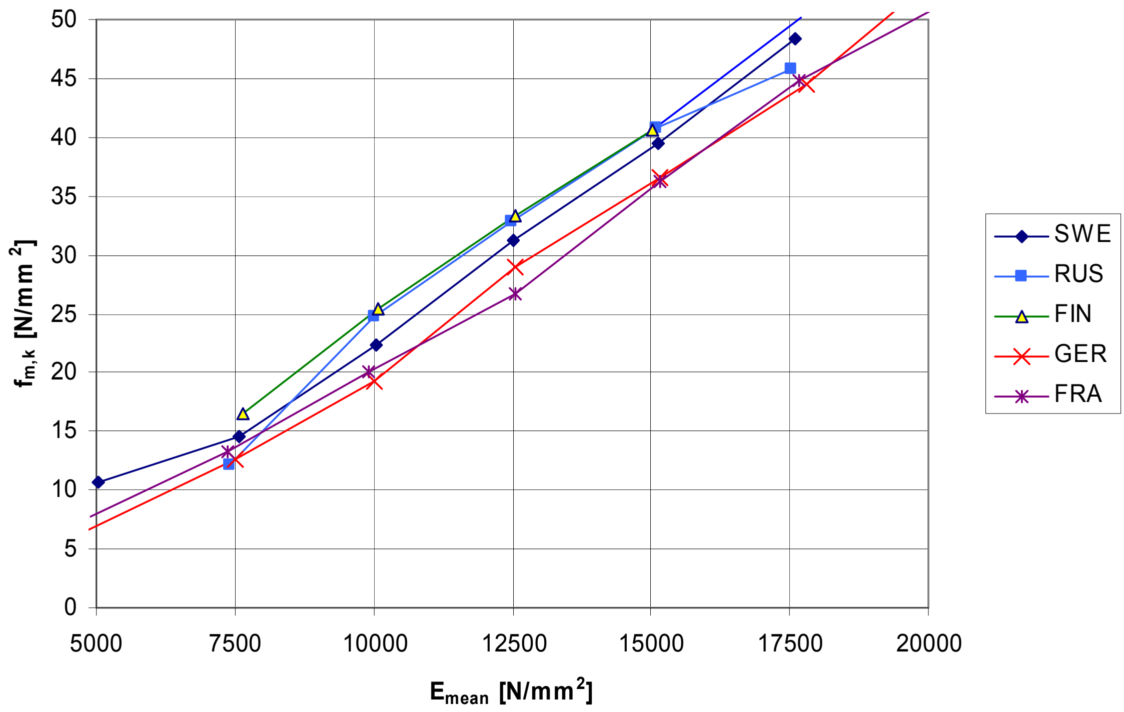

Fig. 3: Characteristic bending strength versus mean modulus of elasticity for different countries and bandwidths of *MOE*, $n = 13\ 548$ specimens.

Within the chosen bandwidths the mechanical properties of spruce on mean level are quite similar for the different countries. The average strength varies between $f_{m,mean} = 41.5$ N/mm² and $f_{m,mean} = 44.8$ N/mm². More differences can be observed in characteristic values (Fig. 3). For bandwidth $E_{mean} = 12\ 500$ N/mm² minimum $f_{m,k} = 27$ N/mm² and maximum $f_{m,k} = 33$ N/mm² can be observed. To clarify if these variations are a result of the variation within or between countries, the variation within countries is determined in the following.

3.2 Variation within countries

Tab. 3 summarises the variation within some countries by selecting a few samples which are different from country averages in Tab. 2.

Tab. 3 shows the number of specimens, mean modulus of elasticity, mean density and mean and characteristic bending strength for these samples. Much more variation is observed between small local sample values than between large samples which are intended to represent average properties in a country.
Exceptionally high values are obtained in most of the samples shown. Low values are shown on three first lines of the table representing central Slovenia, North Germany and South Sweden. Another sample from South Sweden shows clearly higher MOE, density and strength. One conclusion of this table could be that small samples are not easily representative for the region or, if they are, quality of timber is highly variable within a country and also within small regions in countries.

Tab. 3: Examples of mechanical properties of spruce grown in smaller regions: some selected samples with low or high values, n = 2072 specimens.

country	region	n	E_{mean} in N/mm²	ρ_{mean} in kg/m³	$f_{m,mean}$ in N/mm²	$f_{m,k}$ in N/mm²
SLO	central	293	11 300	463	34.4	20.0
GER	north	456	11 200	449	36.4	14.2
SWE	south	234	11 700	359	38.4	19.9
SWE	north-east	40	13 800	454	51.2	29.1
GER	central south	118	12 900	396	44.2	26.9
GER	central south	237	13 200	452	45.6	22.2
SWE	south	178	13 200	481	47.4	28.7
SWE	north-east	79	12 400	406	51.2	33.1
SWE	central	182	13 900	437	51.9	29.1

3.3 Variation within a sawmill

To determine variation within a sawmill the GoldenEye 706 readings of 150 000 boards were used.

Tab. 4 shows the averages and *COV*'s of E_{dyn}, ρ and $f_{m,mod}$. The grading machine provides a prediction of bending strength $f_{m,mod}$ for each specimen. To show the variability of the material the predicted bending strength $f_{m,mod}$ of 500 specimens was calculated as a moving average for three different dimensions.

Fig. 4 illustrates the variation of predicted bending strength between and within dimensions. The maximum average predicted bending strength of 500 is $f_{m,mod,max}$ = 48 N/mm². The specimens with a height of h = 225 mm have a predicted bending strength around $f_{m,mod,h=225}$ = 35 N/mm².

Tab. 4: Average properties of boards with different widths, n = 150 000 specimens. Numbers in parenthesis are mean values of numbers shown for all widths.

width in mm	n	$E_{dyn,mean}$ in N/mm²	*COV* in %	ρ_{mean} in kg/m³	*COV* in %	$f_{m,mod,mean}$ in N/mm²	*COV* in %
75	17 334	12 800	17	461	11	43.4	22
100	53 473	12 800	16	460	10	42.6	22
125	13 829	12 700	16	449	10	41.7	22
150	42 609	12 500	17	447	11	42.3	22
175	7 867	13 000	15	461	9	43.8	20
200	22 900	11 600	17	423	10	39.2	24
225	16 065	10 600	18	401	10	35.6	27
all	156 743	(12 300)	(17)	(443)	(10)	(41.2)	(22)

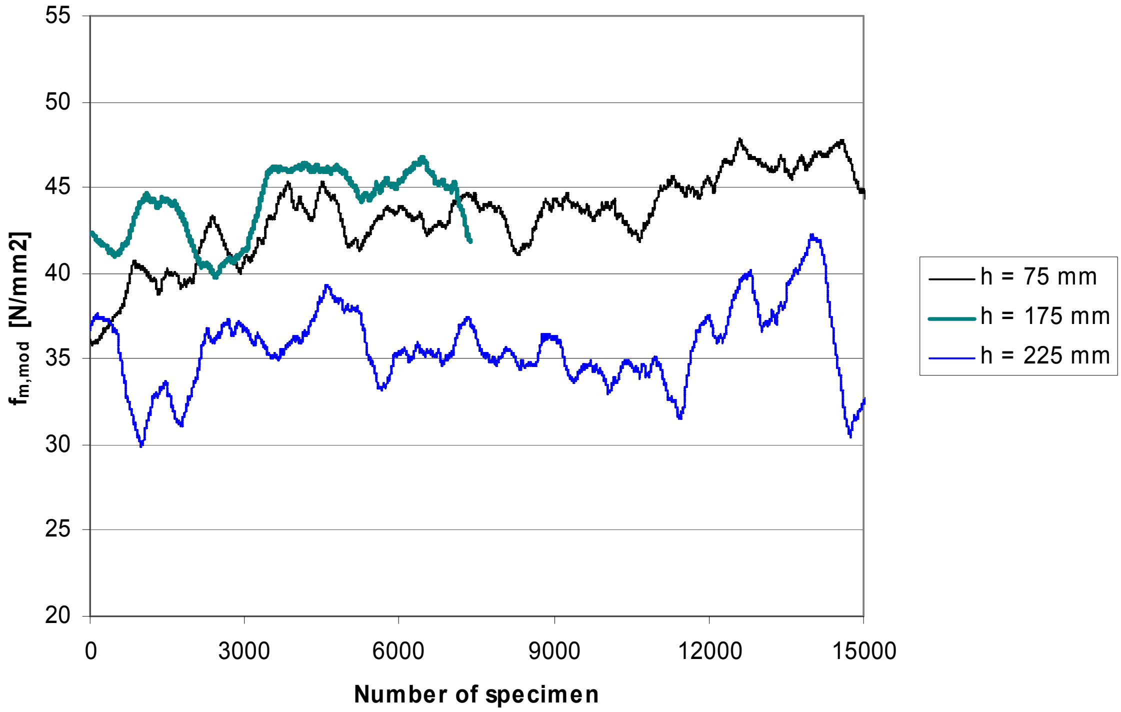

Fig. 4: Moving average of predicted bending strength of 500 consecutive specimens versus number of specimen for three different heights, $n = 40\,000$ specimens.

In order to study properties of strength graded timber, the boards were virtually graded by using existing settings for solid timber given in Table 10-7 of EN 14081-4:2008-08 for GoldenEye 706.

In a first step, all boards with widths $w = 75$ mm, $w = 175$ mm and $w = 225$ mm were graded to C27. Settings used in grading were: $f_{m,mod} > 20.3$ N/mm², $E_{mod} > 5\ 500$ N/mm², $\rho_{mod} > 340$ kg/m³. 99% of boards of widths $w = 75$ mm and $w = 175$ mm fulfil the requirements of strength class C27, whereas the yield is 90% for width $w = 225$ mm.

To show the variation of strength within a strength class, the bending strength values were simulated: The characteristic values calculated for all specimens within the strength class ("all"), and separately for the 500 specimen samples corresponding to the maximum ("high") and minimum quality ("low") were determined.

Tab. 5 shows the results for different dimensions in comparison to the required characteristic values of strength class C27. With respect to EN 384 the required strength values given in EN 338 can be reduced for machine graded timber in strength classes equal or lower than C30 using the k_v-factor ($k_v = 1.12$), With respect to EN 338 the required mean *MOE* given in EN 338 can be reduced to 95% of the one required for the grade.

The specimens with a height of $h = 75$ mm and $h = 175$ mm graded to strength class C27 fulfil these requirements. However, the boards with a height of $h = 225$ mm did not normally fulfil the requirements of the given characteristic values, and for "low" 500 boards, characteristic strength was only $f_{m,k} = 16.7$ N/mm^2.

Additionally, the specimens with a height of $h = 225$ mm were graded to strength class combination C40 & C24. Settings for C40 are $f_{m,mod}$>48.9, E_{mod}>12 000, ρ_{mod}>410 and for C24 $f_{m,mod}$>16.0, E_{mod}> 5 500, ρ_{mod}>320.

Tab. 6 shows the results. In C40 the characteristic values fulfil the requirements within acceptable limits. In case of C24 the results are generally below standard values, simulated characteristic bending strength being as low as 14.2 N/mm^2 for the lowest quality sample.

To compare the results to "visual grading", another grading method was tested on the same material. The X-ray knot parameter (*MKP*) was limited two times: *MKP* < 2500 and *MKP* < 4000. Average of *MKP* is from 2400 to 3000, depending on the dimension

Tab. 7and Tab. 8 show the results. These visual grades did not correlate to the equivalent C-classes. The evaluated characteristic values are quite different depending on the quality of incoming material.

Tab. 5 to Tab. 8 give also the 5 percentile values of *IP*, $f_{m,mod,k}$. These values are an option to estimate the quality level of a sample in comparison to other samples graded with the same settings and the same equation. E_{mean} and ρ_k in tables are in fact the modelled values $E_{mod,mean}$ and $\rho_{mod,k}$, which are considered to be as accurate as destructive testing values.

Tab. 5: Properties of boards graded to C27 and EN 338/384 requirement.

h in mm	specimens		$f_{m,mod,k}$ in N/mm^2	$f_{m,sim,k}$ in N/mm^2	E_{mean} in N/mm^2	ρ_k in kg/m^3	yield in %
EN 338/384: C27				24.1	10 925	370	
225	all	1-16061	23.7	20.4	10 500	353	90
	low	1029-1528	21.9	16.7	9 550	352	81
	high	14074-14573	29.8	27.9	11 900	367	99
175	all	1-7867	30.1	27.3	12 700	393	99
	low	2500-2999	29.0	24.9	11 700	393	99
	high	6500-6999	34.1	29.9	13 800	406	100
75	all	1-17334	28.9	26.0	12 300	386	99
	low	1-500	24.3	21.2	10 300	378	97
	high	12602-13101	35.2	30.9	13 700	416	100

Tab. 6: Properties of boards with $h = 225$ mm graded to combination C40 & C24.

strength class	specimens		$f_{m,mod,k}$ in N/mm^2	$f_{m,sim,k}$ in N/mm^2	E_{mean} in N/mm^2	ρ_k in kg/m^3	yield in %
EN 338/384: C 40				40.0	13 300	420	
C 40	all	1-16061	49.2	41.2	14 300	418	8
	low	1029-1528	51.3	45.0	14 700	446	2
	high	14074-14573	50.1	42.7	14 700	441	15
EN 338/384: C 24				21.4	10 450	340	
C 24	all	1-16061	21.1	18.1	9 900	342	89
	low	1029-1528	18.5	14.2	8 900	346	86
	high	14074-14573	30.0	27.8	11 500	364	85

Tab. 7: Properties of 500 consecutive boards graded to *MKP* < 2500.

h in mm	specimens		$f_{m,mod,k}$ in N/mm^2	$f_{m,sim,k}$ in N/mm^2	E_{mean} in N/mm^2	ρ_k in kg/m^3	yield in %
225	low	1029-1528	28.7	25.7	11100	360	26
	high	14074-14573	38.1	34.0	12700	378	52
175	low	2500-2999	37.7	31.7	13000	403	37
	high	6500-6999	42.6	37.5	14400	419	45
75	low	1-500	32.3	28.2	11200	387	52
	high	12602-13101	41.1	36.6	14300	428	67

Tab. 8: Properties of 500 consecutive boards graded to *MKP* < 4000.

h in mm	specimens		$f_{m,mod,k}$ in N/mm^2	$f_{m,sim,k}$ in N/mm^2	E_{mean} in N/mm^2	ρ_k in kg/m^3	yield in %
225	low	1029-1528	22.9	17.4	9600	347	69
	high	14074-14573	32.0	29.0	12000	368	92
175	low	2500-2999	31.1	27.1	11900	392	89
	high	6500-6999	36.7	31.1	13500	410	94
75	low	1-500	25.5	21.4	10300	373	90
	high	12602-13101	36.8	32.7	13800	417	95

4 Conclusions

The average mechanical properties of spruce timber grown in Sweden, Finland, North-West Russia, Germany and France are reported. The averages and the relation of mean strength and mean stiffness are quite similar in different countries. Larger differences are observed in the characteristic values which are obviously caused by larger *COV* in more southern countries. These differences support on general level the idea of having different settings for different growth areas. However, the variation between countries is smaller than the variation within countries or even within a saw mill. One dimension in Finland had nearly the same average properties as another dimension in Central Slovenia, which had the lowest strength values of all regions within Gradewood-project.

The results reveal that the strength grading according to "machine control" method of standard EN 14081-2 does not produce structural timber with promised strength properties for all customers in every case. When the saw falling material has lower quality than the one used in determination of settings, also the graded material has lower properties, at least when grading is made to grades allowing high yield. In the example analysed, in the worst case the simulated characteristic bending strength of a 500 specimen sample of 150 000 was 60% of the characteristic strength value used in structural design, and one of the dimensions (h = 225 mm) was generally weaker than the design value. A similar problem was observed in "visual grading" when grading was based on X-ray knot parameter.

These results are in line with some recent reports. BACHER (2009) shows results from another saw mill which are at least qualitatively similar to Fig. 4. BRÄNNSTRÖM (2009) found a case in which only 61% of the target strength is reached based on one of the initial subsamples having remarkably lower strength values. He also suggest another method for determination settings based on decision trees which would improve safety and simultaneously also improve economy of timber producers.

Modern grading machines can record a lot of data and observe the change of quality of timber. This information could be used for adjusting settings. SANDOMEER ET AL (2008) have suggested a principle for adjustable settings for output control method. Self adjusting settings could be used also for machine control method when adequate research information is available.

Acknowledgements

This work is part of Gradewood-project which is based on a feasibility study made by the European wood industries under the Roadmap 2010 Building With Wood programme, and this project is supported by the industry via CEI-Bois. The Gradewood-project belongs to the Wood Wisdom.Net-programme and is funded by national technology development bodies: TEKES (Finland), Vinnova (Sweden), Federal Ministry of Education and Research (Germany), Ministry of Agriculture (France), and Slovenian Research Agency (Slovenia).

Stora Enso Timber and MiCROTEC are owners of the strength grading data of a sawmill and they kindly forwarded the data to be analysed.

The contributions from funding organisations and other support are gratefully acknowledged.

References

RANTA-MAUNUS, A.(ed) (2009). Strength of European timber. Part 1. Analysis of growth areas based on existing test results. VTT Publication 706, VTT, Finland. 174 p. http://www.vtt.fi/inf/pdf/publications/2009/P706.pdf

BRÄNNSTRÖM, M. (2009). Integrated strength grading. Doctoral thesis. Luleå University of technology; Sweden. 62 p.

BACHER, M. (2009). GoldenEye 706 Quality shifts. Cost Action E53, Topic 4: Quality control in production of wood and wood based material. Meeting in Bled, Slovenia. 5p.

SANDOMEER, M., KÖHLER, J.; FABER, M.H. (2008). Probabilistic output control for structural timber – Modelling approach. Proc. of CIB-W18 Meeting, Paper 45-5-1. St.Andrews-by-the-Sea, New Brunswick, Canada. 12 p.

EN 384:2004-01 Structural timber – Determination of characteristic values of mechanical properties and density. European Committee for Standardization (CEN). 15 p.

EN 338:2003-04 Structrual timber – Strength classes. European Committee for Standardization (CEN). 9 p.

EN 408:2003-08 Timber structures – Structural timber and glues laminated timber – Determination of some physical and mechanical properties. European Committee for Standardization (CEN). 34 p.

EN 14081-4:2008-08 Timber structures – Strength graded structural timber with rectangular cross section – Part 4: Machine grading – Grading machine settings for machine controlled systems. European Committee for Standardization (CEN). 69 p.

INTERNATIONAL COUNCIL FOR RESEARCH AND INNOVATION
IN BUILDING AND CONSTRUCTION

WORKING COMMISSION W18 - TIMBER STRUCTURES

IMPACT LOADED STRUCTURAL TIMBER ELEMENTS MADE FROM SWISS GROWN NORWAY SPRUCE

R Widmann

R Steiger

Empa, Swiss Federal Laboratories for Materials Testing and Research
Duebendorf

SWITZERLAND

Presented by R Widmann

F. Lam commented that the shape and size of the loading tub/head will influence results. Also the influence of the inertia load of the beam was not considered without mounting an accelerometer on the specimen. R. Widmann agreed that the shape of the loading head has an influence. Although the influence of the inertia loads were not considered, the results seem reasonable.

H.J. Larsen stated in the case of impact loading on scaffolding planks where the plank may break from a person jumping on it. The interaction of the human body is very important and in this study, the loading head is very stiff. R. Widmann agreed the specific case of a man jumping on a board will influence the response. Successive drops at increasing heights are also tests specified in test standards; it is a good method for specific cases but will not address the general problem of impact strength of material.

J.W.G. van de Kuilen stated that the impact speed k_{mod} factor of 1.3 is reasonable. R. Widmann stated that without considering the comments from F. Lam, his results indicated ~ 1.27 so the k_{mod} of 1.3 seems reasonable.

A. Jorissen received confirmation about the integrals of force versus deformation and force versus time and the relationship between them.

The possibility of needing to develop individual test methods for different applications is discussed.

Impact loaded structural timber elements made from Swiss grown Norway spruce

Robert Widmann
René Steiger
Empa, Swiss Federal Laboratories for Materials Testing and Research
Duebendorf, Switzerland

1 Introduction

The consideration of an impact load is rather a scarce scenario when designing structural timber members. Vehicle impact on timber guardrails or on unprotected bridge columns as well as impact of stones and/or snow on respective wooden barriers are common examples. The unintentional impact of falling/jumping persons on wooden scaffold boards or planks and its sometimes fatal consequences was the motivation for research project carried out at Empa. No design codes exist in Switzerland and Europe to cover this kind of loading and literature only delivers few data for impact bending strength of structural timber elements. In addition the application of e.g. the existing k_{mod} factor according to Eurocode 5 for such cases is questionable and in literature [1] it is also discussed if the published factor is correct for impact loadings in general.

Hence, a test program was initiated in order to obtain basic data about impact bending behaviour of large sized members in order to support the development of adequate regulations in regulations and codes.

2 Existing data about impact strength

Impact bending resistance of wood is relatively easy to determine as long as it is tested on small clear specimens, e.g. according to the German standard DIN 52189-1. With the use of a pendulum impact hammer many specimens can be tested within a short time. Therefore a lot of data are published about impact bending resistance of different wood species. Literature covering the (mechanical) properties of wood species, e.g. Sell [2], Bodig [3] and wood handbook [4] include data about impact resistance in tabulated form. However, these were obtained on small clear specimens and are somehow linked to the used test method. Therefore these data can be used for comparison of the impact bending behaviour of different wood species but not the prediction of the impact strength of structural timber members like beams and boards.

In a literature review of impact bending strength of timber and joints Leijten [5] summarizes existing work done on this topic. Important contributions were made by

Madsen [6] and Jansson [7], who developed also an analysis that considers the energy input induced by an impact loading as well as the inertial forces occurring during impact loading. Leijten [1] and Bocchio et al. [8] tested several wood species with the background of their possible use for guardrails along highways. In comparison to tests with small clear specimens the existing data about impact bending resistance of big size specimens rely mostly on impact bending strength (stress) and not on impact work. A part of the already published data will be discussed further down in results and discussion.

A major obstacle for the comparison of published data is the absence of standardized procedures for the execution and analysis of (instrumented) impact bending tests with large size specimens. Important parameters like available impact energy (speed, mass of impact hammer), geometry of loading heads and supports, geometry of specimens (cross section, span), kind of measured data and procedures used for their acquisition and analysis vary from study to study. This study will widen the variation of parameters even more. Therefore a considerable amount of this paper is also dedicated to the used methods.

3 Experimental

3.1 General Considerations

For the analyse of impact bending resistance the impact bending strength as well as the impact bending energy (toughness, work) were considered. The tests were designed to clarify the influence of several parameters on the impact bending resistance of timber structural members and in particular of:

- member geometry: span, cross section, slenderness, bending stiffness
- moisture content (scaffold boards)
- static and dynamic MOE
- static bending strength and static rupture energy
- knots

The data analyse is still ongoing. Therefore in this paper only a part of the mentioned parameters are discussed.

3.1 Material

The tests were executed with square cut timber beams and with boards made of Swiss grown Norway Spruce (*Picea abies*). The 130 square cut timber beams with dimensions of $l \cdot b \cdot h = 5000 \cdot 80 \cdot 120\text{mm}^3$ were ordered as strength class C24 and the 45 boards with dimensions of $l \cdot b \cdot h = 4000 \cdot 330 \cdot 45\text{mm}^3$ as “scaffold boards”. Before testing, the beams and boards were cut and the beams were also planed. Due to geometrical restrictions of test equipment the maximum width of the specimens was 130mm and the maximum length (span) was 2200 mm. Therefore the boards were cut into quarters and the beams were cut into halves or thirds. An overview of the used boards and beams is given in Table 1 and Table 2. The densities refer to the stated moisture contents. For the comparison of impact bending strength and static bending strength twin specimens were used.

Table 1: Overview of the tested square cut beams. (e –edgewise, f – flatwise, i – impact load, s – static)

Series	n	l_{eff}	b	h	λ	ρ	u	E_{dyn}
		[mm]	[mm]	[mm]	[ ]	[kg/m³]	[%]	GPa
s-208-e	27	2080	80	110	18.9	470 ± 42	14.5 ± 1.1	16.0 ± 2.6
s-172-e	21	1720	80	110	15.6	453 ± 34	14.1 ± 1.6	15.0 ± 2.2
s-148-e	27	1480	80	110	13.5	440 ± 55	11.7 ± 1.3	13.4 ± 2.2
s-148-f	27	1480	110	80	18.5	439 ± 58	12.4 ± 1.4	13.4 ± 2.6
s-136-e,i	48	1360	71	110	12.4	451 ± 52	13.7 ± 2	15.8 ± 3.0
s-136-f,i	48	1360	110	71	19.2	456 ± 55	13.2 ± 1.5	15.8 ± 3.0
s-136-e,s	48	1360	71	110	12.4	448 ± 50	13.4 ± 1.6	15.2 ± 3.2
s-136-f,s	48	1360	110	71	19.2	450 ± 54	13.4 ± 1.5	15.3 ± 3.0

Table 2: Overview of the tested boards. (mc – high moisture content).

Series	n	l_{eff}	b	h	λ	ρ	u	E_{dyn}
		. [mm]	[mm]	[mm]	[ ]	[kg/m³]	[%]	GPa
b-208	60	2080	130	50	41.6	459 ± 44	10.5 ± 1.1	16.0 ± 2.4
b-136	60	1360	130	50	27.2	453 ± 41	10.6 ± 1.2	16.0 ± 2.3
b-172-mc	30	1720	130	50	34.4	464 ± 28	20.5 ± 2.3	14.1 ± 1.2
b-136-mc	30	1360	130	50	27.2	465 ± 33	20.7 ± 1.9	14.5 ± 1.3

The used slenderness ratios λ can be compared to standardized values for static bending tests like in EN 408 with λ = 18 (to 15) for static 4-point bending tests and to impact loading tests of small clear specimens according to DIN 52189-1 with λ = 12.

3.2 Impact testing

The tests were executed in a drop weight impact testing machine made by Dynatup as shown in Figure 1. In general with this machine drop heights of about 2.00m and drop hammer masses between about 90kg to 200kg can be realized. The machine is initially not foreseen for impact bending tests and therefore had to be adapted for this purpose. This adaptation reduced the possible drop height to about 1.35m and with this a maximum capacity of impact energy was available like follows:

$$E_{pot} = m \cdot g \cdot h_0 = 200\text{kg} \cdot 9.81\text{m/s}^2 \cdot 1.35\text{m} \approx 2650\text{J} \qquad \text{Eq. 1}$$

The drop height h_0 could be adjusted continuously and for the tests they were varied from minimum 1.00 m to maximum 1.25 m. This resulted in impact speeds of 4.43 m/s^2 up to 4.95 m/s^2. For the tests the mass of the impact weight was varied between 90.2 kg and 132.8 kg and in combination with the mentioned impact speeds the applied impact energies ranged from 890 J to 1640 J.

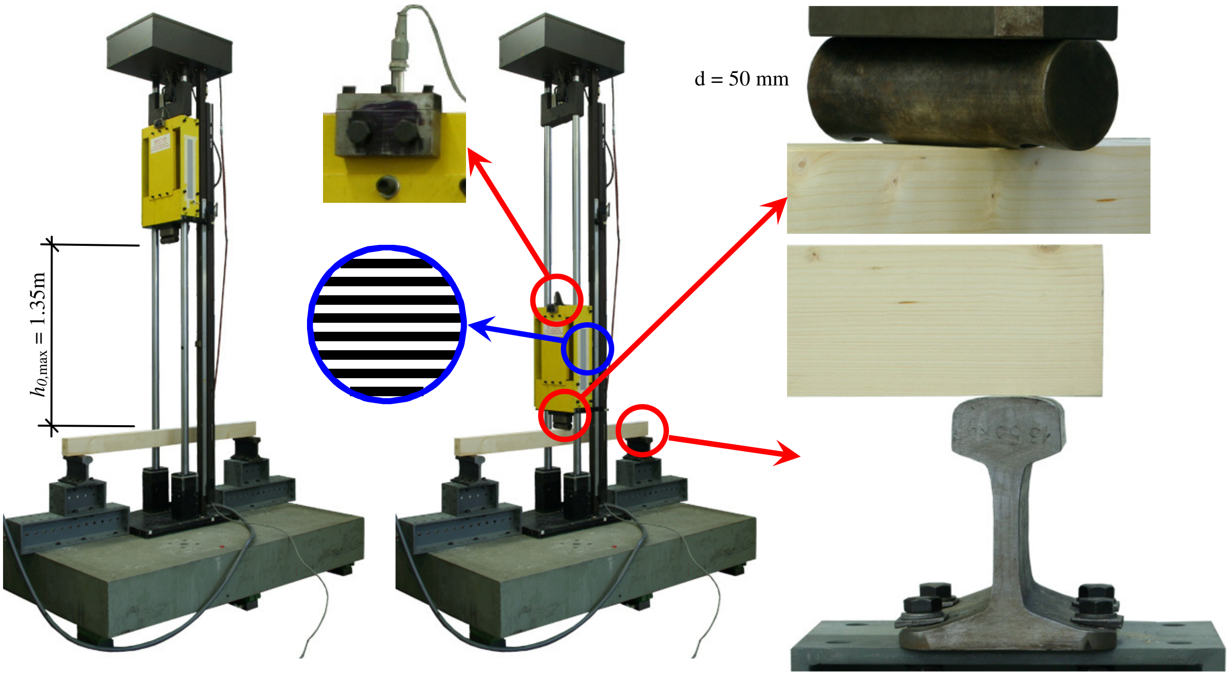

Figure 1: Drop weight impact testing machine used for the tests. The span of the beams was varied from 1.36m to 2.08m and the maximum possible drop height was 1.35m (max 1.25m was used). Highlighted details are the acceleration sensor, target for speed measurement, loading head and support.

Tests with a drop weight are more difficult to analyse compared to tests with a pendulum. After release of a pendulum hammer at a defined height and its travel to the specimen positioned at the bottom point of the hammers circular pathway it will lose a specific energy for breaking the specimen. As a consequence the hammer won't reach its initial height anymore. The difference of the height reached after rupture of the specimen and the initial height correlates to the energy loss due to breaking the specimen and can be directly and easily read from appropriate scales.

A comparatively easy possibility for drop weight tests is a set up where a hammer of a given mass is dropped upon a beam from successively increased heights until rupture occurs or the beam deflects a certain distance (successive blows, Hatt-Turner test). The height of the maximum drop or the drop that causes failure is then given as a comparative value for the ability to absorb shocks that cause stresses beyond the proportional limit [4]. However, effects of premature damage due to preceding loadings in such a series can have a strong influence on the results of these tests. Therefore instrumented drop weights are more suitable as they permit to determine the impact resistance with a single loading of the specimen (single blow test). In addition the mentioned tests methods only deliver impact energy (work) but don't provide data about impact strength, e.g. in terms of impact bending stress. This also requires instrumented impact tests in order to acquire data about the applied force during an impact. This force can be measured directly via a load cell or indirectly using acceleration sensors. These kinds of measurements are tricky however, as sensitivity, natural frequency and damping ratios of the sensors can effect the results.

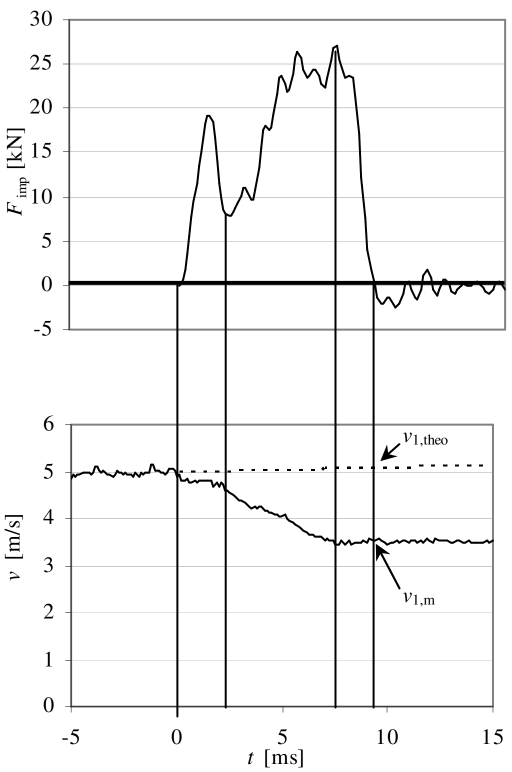

Figure 2: Impact force and speed of drop hammer against time for a beam with a span of 1.48m.

A standard instrumentation for impact hammers is an accelerometer. The characteristics of the used accelerometer, in particular its natural frequency, is an important factor. Sensitivity and natural frequency have to be adapted to the intended use as they might strongly influence the results [9]. For our tests an accelerometer was attached to the drop weight as shown in Figure 1. The above mentioned restrictions to the use of accelerometers lead the desire to verify the obtained results with an independent method. Therefore the displacement of the drop weight was measured at the same time. A photocell detecting the luminance difference of a spot illuminated bar target that was attached to the drop hammer (Figure 1) permitted to record the displacement with a resolution of 0.5 mm. Both data, acceleration a and displacement w_m of the drop weight, were registered with a frequency of 50 kHz. The directly measured displacement w_m could be compared to the displacement w_i obtained by integration of the accelerometer signal as a measure for determination of the quality of the measured data.

This permitted to determine the impact resistance in form of mechanical work $W_{imp,i}$ applied for the rupture of the specimen as well as independently from that in form of loss of kinetic energy ΔE_{kin} of the drop weight due to impact loading of the specimen (Figure 2).

Integration of force – displacement: $$W_{imp,i} = \int_{w=0}^{max} F(w_i)dw_i \qquad \text{with:} \quad w_i(t) = \iint a(t)dt \qquad \text{Eq. 2}$$

Kinetic energy: $$W_{imp,k} = \Delta E_{\text{kin}} = 0.5 \cdot m \cdot \left(v_{1,theo}^2 - v_{1,m}^2\right) \qquad \text{Eq. 3}$$

with $v_{1,theo}$ is the theoretically undisturbed speed of the drop weight without an obstacle (specimen) and $v_{1,m}$ the measured speed of the drop weight at the time/position of rupture as is shown in Figure 2.

A comparison of the results obtained by both methods showed a very good correlation as can be seen in Figure 3. For the further analysis the impact energy derived by the mechanical work was used:

Impact energy used for analysis: $$W_{imp} = W_{imp,i} \qquad \text{Eq. 4}$$

A certain difficulty was the definition of the rupture. For specimens that showed a strong immediate drop of the impact force from maximum to zero – a brittle failure – rupture could be defined relatively easy (Figure 4, left). Specimens that did not fail immediately showed a more ductile failure as is shown in Figure 4, right. This was in particular true for the boards. Time to failure and displacement at failure increased significantly. Often the specimens did not fail completely and the two parts were held together with a tiny very flexible remaining cross section at the compression side of the beam/board. This caused a further reduction of hammer energy and therefore affected also the results of the registered impact energy.

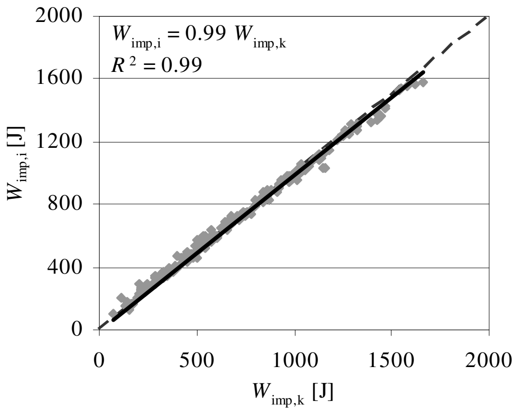

Figure 3: Correlation of impact energy derived by integration of mechanical work $W_{imp,i}$ and by loss of kinetic energy $W_{imp,k}$ of square cut beams.

In many cases with ductile failure and in particular for the boards the maximum force was already reached at the first initial impact. Therefore the point of maximum force could not be taken for the definition of rupture. For the analysis it was decided to use a consistent rupture criterion in defining rupture at the point/time of the end of the last registered impulse with the maximum force of which reaching 50% or more of the overall maximum impact force (see Figure 4). On base of this the average time to failure varied between 12 ms for series with low slenderness ratios and 30 ms for series with high slenderness ratios.

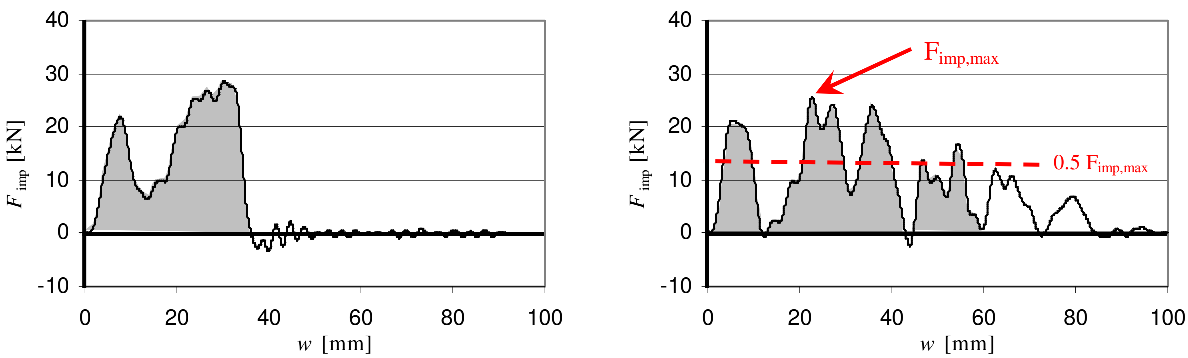

Figure 4: Load – deformation graphs for a specimen with brittle failure mode (left) and a specimen with ductile failure mode (right). With increasing slenderness $\lambda = l/h$ of the specimens and particular for the boards a tendency to a more ductile behaviour could be observed. The shaded areas highlight the line integral over impact force F_{imp} and the displacement of the drop weight w. The upper limit for integration was set to the end of the last impulse that showed a peak load of at least 0.5 $F_{imp,max}$.

For the determination of the impact bending strength possible inertia effects according to Johansson [7] were not considered. The impact bending strength was calculated with the maximum value of the recorded force on base of normal single span beam theory.

The static tests were executed as 3-point bending tests on a standard testing machine. The loading rate was applied load governed and was taken as in EN 408 resulting in nominal times to rupture from 300 s± 120 s. Maximum load, modulus of rupture and rupture energy were registered. The rupture was defined as the point/time when the loading level had decreased to 50% of maximum load.

4 Results and discussion

4.1 Maximum Force

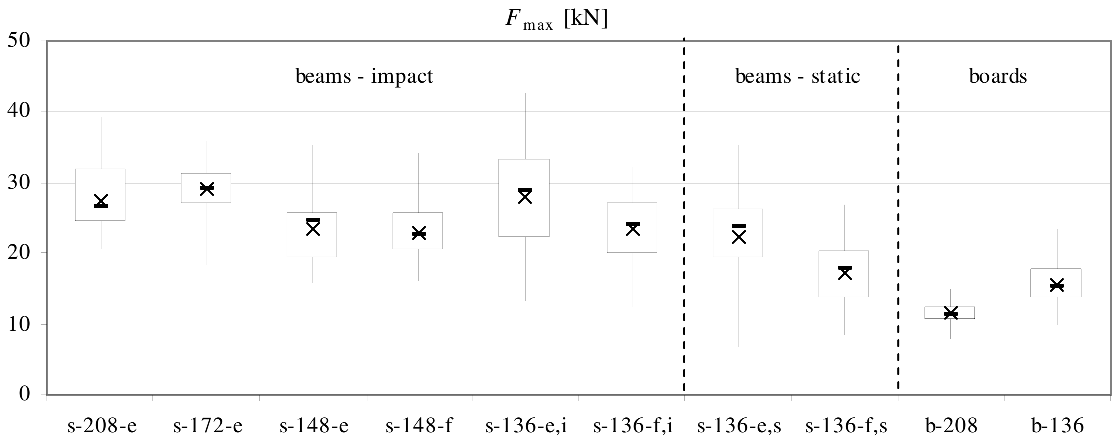

Figure 5: Maximum force recorded for the impact and static bending tests. Board with high moisture content are not shown. In general the boxplots indicate quartiles, mean (x), minimum and maximum values as well as the median (-).

Maximum impact forces of the beams did not differ as would be expected from static bending tests. The mean values of beams with longer clear span were at a same level or even higher than of beams with a shorter span.

Johanssen reported impact bending tests with beams of Spruce with cross sections $b \cdot h = 38 \cdot 89\ mm^2$ and a clear span of 1095 mm ($\lambda = 12.3$). For tests the material was assigned to two classes (with and without knots/inclination of grain) and grouped to be tested with three different drop heights resulting in three different (target-) failure times. In the tests mean failure loads of 13.5 kN – 16.5 kN (better class) and 11.9 kN – 13.8 kN (class with knots) were obtained. For shorter times to failure higher impact failure loads were observed.

4.2 Bending Strength

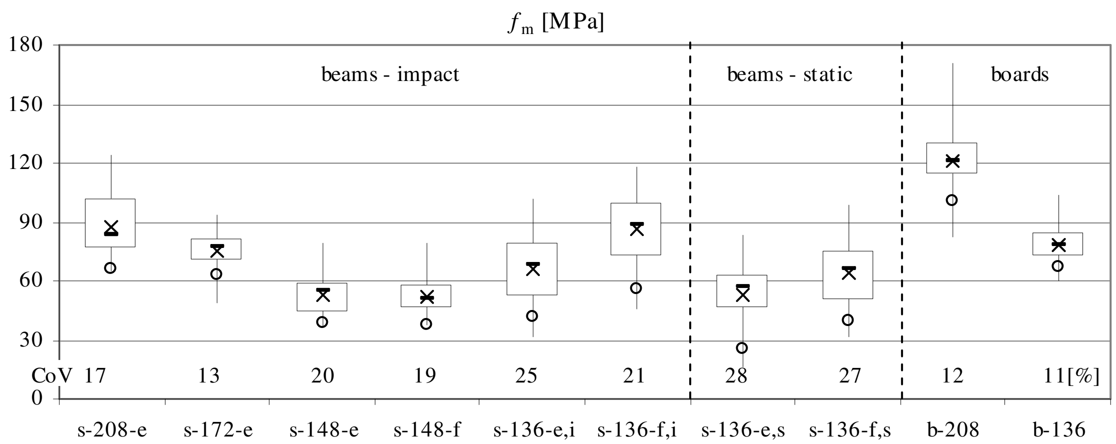

Figure 6: Impact and static bending strength. The 5-percentile values are marked by "o" and the respective value for static series s-136-e,s indicates that the material was in the range of the ordered strength class C 24 .

The impact bending strength as shown in Figure 6 was determined on base of the registered maximum Force without the consideration of inertia effects.

The impact strength of the series with a span of 1360mm can be compared directly with the corresponding static bending strength. It shows that for both orientations – flatwise and edgewise – the impact bending strength is higher (see also further down). Remarkably is the very high impact bending strength of the board series with a span of 2080 mm. For about 80% of all specimens within these series the maximum load was recorded at the initial impulse compared to only 14 % of the board series with a span of 1360 mm.

It is difficult to compare the obtained values with values from literature. Leijten [1] reports about flatwise impact bending of - among others – softwood species Douglas Fir and commercial Larch specimens with cross sections of $130 \cdot 40$ mm^2 and a clear span of 1400 mm ($\lambda = 35$). Leijten obtained average static bending strengths of 72.2 MPa and 55.1 MPA and impact bending strengths of 63.8 MPa and 24.3 MPA respectively. In particular the mean impact bending strength of the Larch specimens is considerably lower than the values obtained in our tests for Spruce. It is doubted that these big differences can only be attributed to inertia effects.

According to Sell [2] the impact resistance in terms of mean impact work for these species (small clear specimens) range from 3.7 J/cm^2 – 6.0 J/cm^2 and 5.0 J/cm^2 – 7.5 J/cm^2 respectively (4.0 J/cm^2 – 5.0 J/cm^2 for Spruce).

The above mentioned failure loads obtained in impact bending tests with Spruce specimens by Johansson lead to mean impact bending strengths without consideration of inertia effects ranging from 64.9 MPa to 90.0 MPa (CoV 16% - 33%) and are with this in the range of our test data.

4.3 Impact and static work

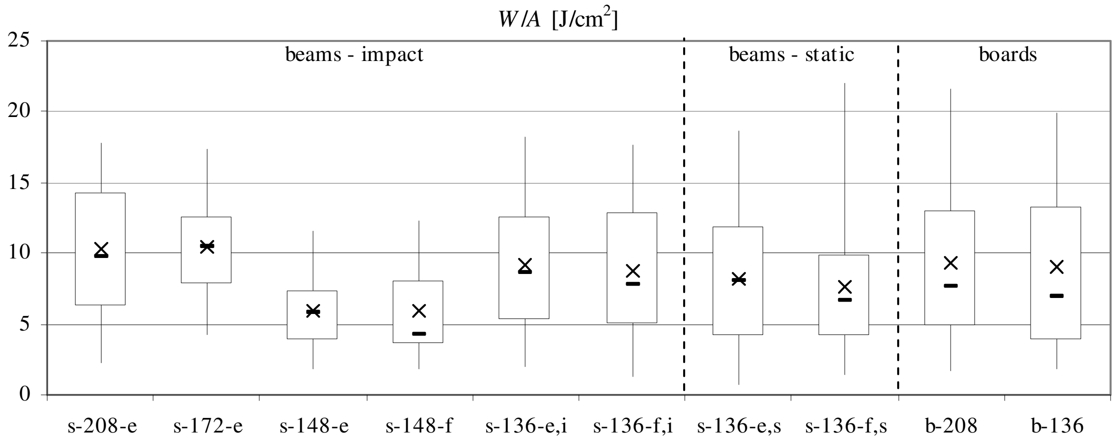

Figure 7: Work to rupture for impact and static bending.

Impact work was another important consideration for the impact resistance. In literature it is often normalized to the cross section of the specimens which was done here too, same for the static work. From Figure 7 it can be seen that the mean values of most series did not differ significantly from each other, except the two series with a span of 1480 mm. The very same series also showed the lowest impact bending strength. A reason for this could be that the dynamic MOE of these two series were lower compared to the other series (see Table 1). Literature [2] gives for spruce, based on tests with small clear specimens values of 4 J/cm^2 to 5 J/cm^2. Compared to the published impact works the values obtained from the tests with the large sized specimens are clearly higher.

4.4 Correlations

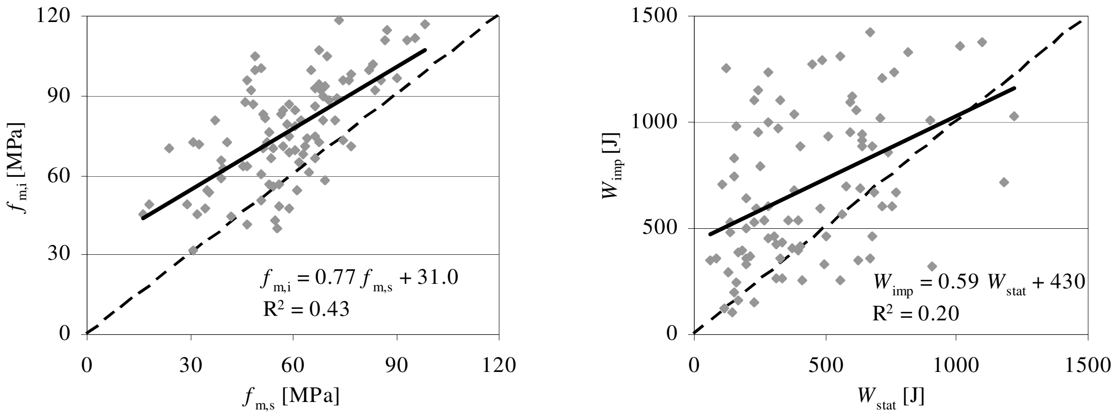

Figure 8: Impact- compared to static bending strength (left) and impact- compared with static work (right) for twin samples of square cut beams with span l_{eff} = 1360mm.

In Figure 8 the impact bending strength $f_{m,i}$ is compared with the static bending strength $f_{m,s}$ for the $n = 48$ twin specimens. It can be seen that the impact bending strength is higher than the static bending strength. A linear fit with an intercept at the point of origin leads to $f_{m,i} = 1.27 f_{m,s}$ with $R^2 = 0.24$, indicating that impact bending strength exceeds static bending strength by about 27% in average. It has to be noted, that inertia forces were not considered for this approach. Regarding the rupture energy the correlation between static bending and impact bending is less pronounced but impact work exceeds static work as well.

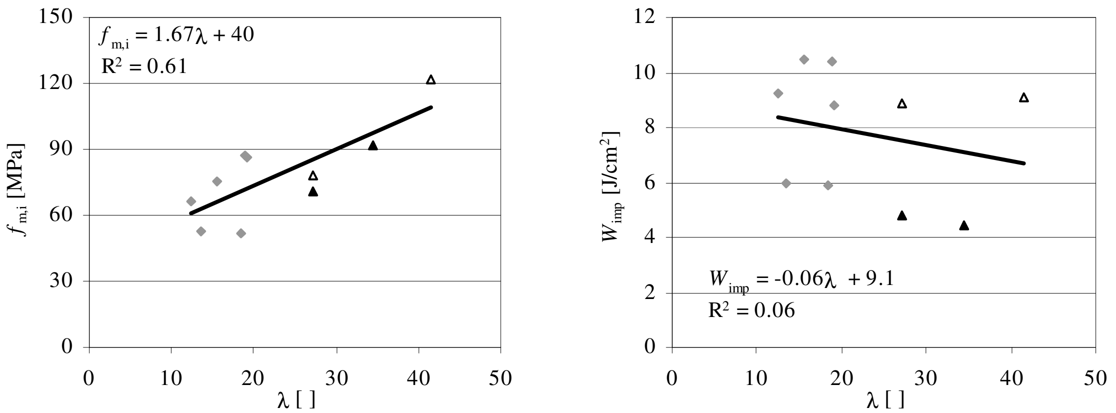

Figure 9: Impact bending strength (left) and impact work (right) against slenderness ratio on base of mean values of all series. Triangles represent boards (solid triangles = high moisture content). Whereas slenderness of the beams and boards seem to have an influence on impact bending strength this cannot be observed for the impact work.

According to Figure 9 an influence of the slenderness ratio on the impact bending strength can be assumed. A higher slenderness leads to a higher impact bending strength which is in particular well visible for the boards. However, this cannot be concluded for the impact work which seems to be independent from λ. In literature [10] it is stated based on tests with small specimens that there is an influence of λ on impact work. It is possible that effects of features like knots and angle of grain superimpose a possible effect of λ on impact work.

4.4 Short remark on duration of load

The data obtained by our tests cannot be used for duration of load classifications without further analysis.

In EC 5 it is stated that the load duration classes are characterised by the effect of a constant load acting for a certain period of time in the life of a structure. Whereas for short term loads the accumulated duration of characteristic load is defined by a period of less than one week there is no indication about the duration of load for instantaneous loads.

It can be questioned if impact (bending) loads in general are in terms of "a constant load acting for a certain period of time" according to the standard. The load in form of force or stress is not constant during impact bending. Only an average ("constant") loading rate (or stress rate) can be determined for impact loadings, e.g. on base of time to failure and force/stress at failure. In addition impact loads are usually characterized by its impact energy in J and not its force in kN. It is also clear that for impact loadings other parameters like inertia effects must be considered.

A solution could be that impact loads are assigned to a own specific load duration class or even better that impact loading in general is treated separately from static loading and relevant load duration classes. In this context a clear definition of load duration for instantaneous loads, a respective possible differentiation from impact loads and a standardisation of procedures to obtain relevant data would certainly help to overcome the existing uncertainties regarding the effects of load duration on strength properties of timber.

5 Summary and Conclusions

The impact bending and static bending tests with square cut beams and boards from Swiss grown Norway Spruce and a related research showed that:

- The used methods and technologies for the determination of impact energy in form of impact work and loss of kinetic energy worked well and the respective data correlated well. However, the determination of the point/time of rupture on base of the data was not easy.
- Impact bending strength – determined with a standard approach without consideration of inertia effects – was higher than static bending strength and impact work was higher than static work. High slenderness ratios lead to higher bending strength but this could not be observed for impact work.
- On base of the obtained data no conclusion in regard of load duration classes according to EC5 can be drawn.
- Data analysis is still ongoing in order to evaluate the influence of other parameters on the impact bending behaviour.
- Data from different sources are difficult to compare as tailor made equipments was used for the respective tests. The results of our tests only partly match published

results. One of the reasons for this could be that inertia effects were not (yet) considered in our analysis.

- If data of impact tests should be used for the determination of load duration factors like k_{mod} a minimum of standardization of test method(s), equipment as well as of analyze-tools should be available. This would also be helpful for further research activities and could be a research topic itself at the same time.

6 Literature und Standards

6.1 Literature

1. Leijten, A.J.M. *Load duration factors for instantanous loads*. in *CIB - W18 Meeting Thirty-Six*. 2003. Colorado.
2. Sell, J., *Eigenschaften und Kenngrössen von Holzarten*, ed. S.A.f.d.H. LIGNUM. 1997, Zuerich, Switzerland: Baufachverlag Lignum.
3. Bodig, J. and J.A. Benjamin, *Mechanics of Wood and Wood Composites*. 1982, Malabar: Krieger Publishing Company.
4. *Wood Handbook*. 1999: Forest Products Laboratory General Technical Report FPL-GTR-113.
5. Leijten, A.J.M. *Literature review of impact strength of timber and joints*. in *World Timber Engineering WCTE*. 2000. Whistler, Canada.
6. Madsen, B., *The Effect of Impact Loading*, in *Structural Behaviour of Timber*. 1992, Timber Engineering Ltd.: North Vancouver.
7. Jansson, B. *Impact Loading of Timber Beams*. in *1st RILEM Symposium on Timber Engineering*. 1999. Stockholm, Sweden: RILEM Publications s.a.r.l.
8. Bocchio, N., P. Ronca, and J.-W. van de Kuilen. *Impact Loading Tests on Timber beams*. in *Innovative Wooden Structures and Bridges*. 2001. Lahti, Finland.
9. Krech, H., *Grösse und zeitlicher Ablauf von Kraft und Durchbiegung beim Schlagbiegeversuch an Holz und ihr Zusammenhang mit der Bruchschlagarbeit.* Holz als Roh- und Werkstoff, 1960. **18**(3): p. 95-105.
10. Kollmann, F., *Principles of wood science and technology*. Vol. 1. 1968, Berlin: Springer.

6.2 Standards

DIN 52189-1: *Testing of wood; Impact bending test; Determination of impact bending strength*, DIN German Institute for Standardization, 1981

EN 408: Timber structures - *Structural timber and glued laminated timber - Determination of some physical and mechanical properties*, CEN Comité Européen de Normalisation, 2003

EN 1995-1-1: *Eurocode 5 - Design of timber structures - Part 1-1: General - Common rules and rules for buildings*, CEN Comité Européen de Normalisation, 2004

7 Acknowledgement

The presented work was/is supported by the Swiss Federal Funds for the Support of Forest and Wood research.

INTERNATIONAL COUNCIL FOR RESEARCH AND INNOVATION
IN BUILDING AND CONSTRUCTION

WORKING COMMISSION W18 - TIMBER STRUCTURES

MODELLING THE BENDING STRENGTH OF TIMBER COMPONENTS – IMPLICATIONS TO TEST STANDARDS

J Köhler
M Sandomeer

SWITZERLAND

T Isaaksson
B Källsner

SWEDEN

Presented by J Köhler

F. Lam commented that the factors developed from Isaksson's data are applicable to high quality timber. Lower quality material with more variability will behave differently; H.J. Larsen and J. Köhler discussed the issue of bias being prescribed in the standard and the issue of whether there is a need to change the test standard to remove the bias. They also discussed the fact that limited data is available when testing more than one section within a piece and the majority of the data in Europe were obtained based on the existing test standard.
J. Munch-Anderson stated that if ones test the specimen with randomly placed weak point, it would be difficult to account for different load conditions.
J Köhler commented that the "bias" needs to be specified. J.W.G van de Kuilen stated that in many wood species in the world the weak section cannot be determined.

Modelling the Bending Strength of Timber Components – Implications to Test Standards

Jochen Köhler, Markus Sandomeer, Tord Isaaksson, Bo Källsner

1 Abstract

The present paper focuses on the prediction and modelling of the bending capacity of timber structural elements. The standardisation of test procedures is the prerequisite to compare and aggregate data of timber strength and stiffness related properties on a national and international scale. Concepts of hierarchical modelling are applied to link the information from (mainly standardized) tests to a generic and probabilistic description of the strength and stiffness related capacities in structures; differing in terms of size, climate and load characteristics. A model framework is suggested where three different hierarchical levels of spatial variation of the bending capacity are differentiated, namely the macro variability between different lots of timber structural elements, the meso variability within one lot of structural timber elements and the micro variability within one particular structural element. The results of standard tests are reflecting the variability of strength properties at a meso level. It is discussed how the suggested model framework might be utilized for the consistent representation of test data.

The paper is concluded with a comparison of the impact of weak sections on different standardized test procedures. Monte Carlo simulation technique is used to test generated test data virtually according to three different test standards: EN 408, ASTM D 4761 and AUS/NZ 4063. Possible implications for further developments of test standards for the timber bending strength are discussed.

2 Introduction

A model framework is suggested where three different hierarchical levels of spatial variation of the timber load bearing capacity are differentiated, namely the variability between different lots of timber structural elements (macro level), the variability within one lot of timber structural elements (meso level) and the variability within one particular structural element (micro level), Figure 1.

At the market timber is represented as a graded material; i.e. timber material for structural purposes is associated to a certain grade or strength class. Various grading schemes are calibrated to identify timber grades, i.e. sub-populations of timber elements for which the strength class requirements are fulfilled. The statistical characteristics of the material properties of these sub-populations are strongly dependent on the properties of the timber supply which is used for initial calibration of the particular grading procedure which is applied (Faber et al. (2004)). This means that for different sub-populations - all assigned to the same timber grade, but by applying different grading schemes and/or using different ungraded material - the statistical properties of the material properties might be different, although the target fractile values are similar. According to the scheme in Figure 1 this variation is termed macro variation. A recent study on a large European database has confirmed that the macro variations for graded structural timber are significant, Ranta-Maunus, Denzler (2009).

In a design situation it is typically known what timber strength class will be utilized in the structure but in general it is not differentiated in regard to the timber origin, species, grading scheme, etc. That means that the relevant population that has to be considered during a design situation is only defined by the timber strength class that is utilized, i.e. modelling the macro level variability.

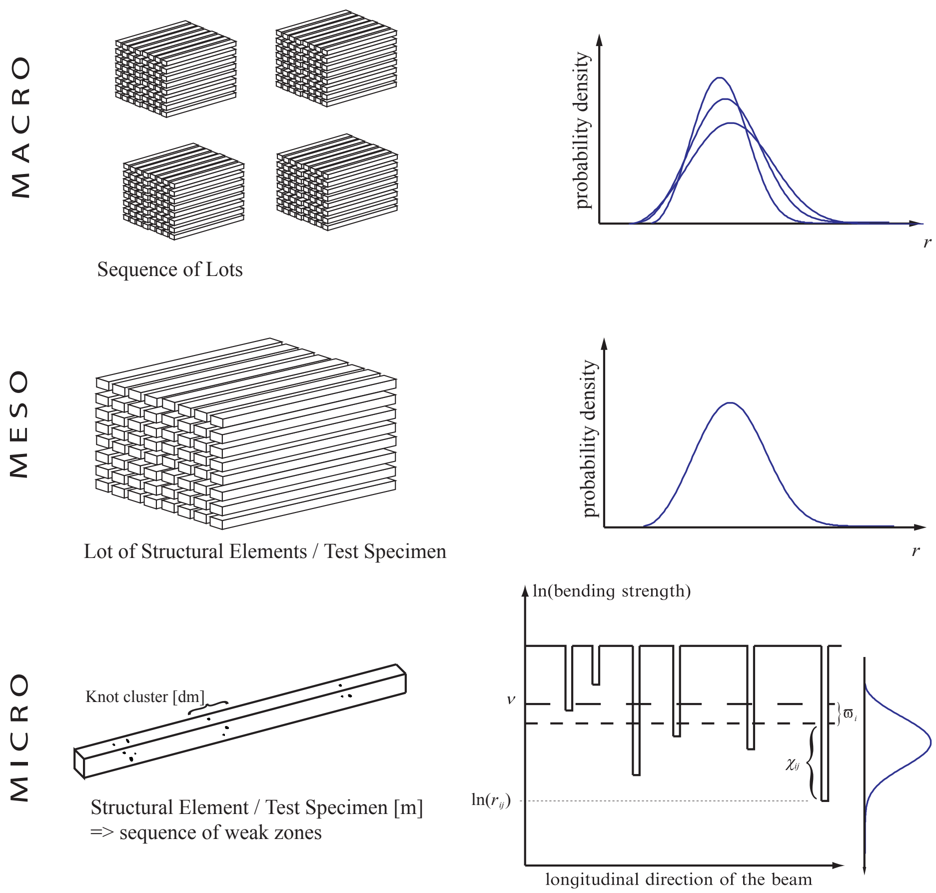

Figure 1 *Different scales of modelling of timber material properties.*

Samples of standardized test specimens or a lot of structural elements on a construction side are in general not representing the overall population of the corresponding timber strength class. The sample is biased mainly due to the specific origin or the timber species and the particular grading scheme that is applied to identify the grade. The variations between standardized timber test specimens or structural elements of the corresponding sub-population are modelled at the meso level.

At the micro-level the irregularities in the timber material itself are represented. These are basically uncontrollable as they originate from natural variability such as the random distribution of knots fissures and grain deviations. The geometrical scale of these irregularities could be measured in μm at wood cell level or in cm if knots and weak sections are considered. Micro level variations earned considerable attention in research activities in the last decade, mainly in connection with investigations of the so-called size effect, i.e. the size-dependency of material properties.

For the evaluation of the reliability and robustness of timber structures the variability of timber material properties on all three levels has to be considered. In the remainder of this paper it is discussed how to relate information on standardized test data with the variability on the macro scale and on the micro scale.

3 Normative Representation of Timber Bending Strength

In timber engineering strength material properties are defined at a component scale (meso level), i.e. as the load bearing capacity of standard test specimen.

For any interpretation and further use of strength properties as they are evaluated according to standard test procedures, three key aspects have to be taken into account that are crucial for the definition of strength properties:

- Definition of test set up: dimension, loading mode and time, conditioning.
- Sampling: the definition and representation of a population of interest.
- Representation of the sample: methodology for estimating the 5%-fractile values.
- Emplacement of test results into hierarchical modelling approach.

3.1 Definition of Test Set Up: dimension, loading mode and time, conditioning.

In general test standards comprise the specification of the test set up, dimensions, the loading history and climate conditions until failure. The bending strength according to the international standard ISO 13910 is determined with a test configuration illustrated in Figure 2. The load q is applied with constant rate until collapse of the beam. The maximum load $q_{\max}$ is observed. The projected test time to failure t_f is also specified as 60 seconds. The reference moisture content of the test specimen at the time of testing shall be consistent with a surrounding climate corresponding to a temperature of 20°C and 65% relative humidity. Furthermore, ISO 13910 specifies that a test specimen shall be selected from random locations within a piece of timber.

The bending strength r_m is expressed in stress, assuming homogeneous ideal elastic material and pure bending as:

$$r_m = \frac{qa}{h^2 b} \tag{1}$$

where q is the applied load, h and b are the larger and smaller dimension of the cross section, respectively. a represents the total length of the span.

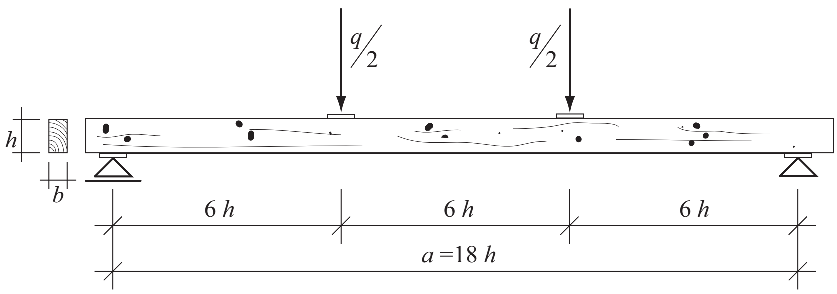

Figure 2 Typical bending test configuration. b , h *are the specified dimensions,* q *is the load applied until failure.*

Most test standards are based on ISO 13910, however, considerable differences exist that are summarized in Table 1 for three standards, European Standards EN 408 and EN 384, ASTM D 4761-05 and D 1990-91 and Australian/New Zealand Standard, AS/NZ 4063:1992.

Table 1: An overview comparison between different bending strength test procedures; differences to ISO 13910 are shaded.

Origin/Code	Geometry 4-point bending (Figure 2)	Climate/Moisture Content	Loading/Time to failure	Bias
ISO 13910	span = 18h	Conditioned at Temp.: 20°C Rel. Hum: 65%	Ramp load, Time to failure: Approx. 60 s	-
Europe: EN 408 and EN 384	span = 18h h = 150 mm	Conditioned at Temp.: 20°C Rel. Hum: 65%	Ramp load, Time to failure: 300 s ± 120 s	(By judgment) weakest section in the middle. Tension side random.
North America: ASTM D 4761-05	span = 17h- 21h h = 150 mm	Moisture Content: 13%	Ramp load, Time to failure: 60 s ~ (10s, 600s)	(By judgment) weakest section within supports. Tension side random.
AUS/NZ: AS/NZ 4063:1992	span = 18h h = 150 mm	Conditioned at Temp.: 20°C Rel. Hum: 65%	Ramp load, Time to failure: 300 s ± 120 s	-

3.2 Sampling: definition and representation of a population of interest.

The sample of test specimen should represent the defined population of interest. The population might be defined in terms of the timber species, timber source, timber grade and method of grading. The sample is representative, if the sample is drawn randomly from the population. According to ISO 13910 and EN 384 random sampling has to be applied and the minimum sample size is 40. It is emphasized that the timber origin of each sample, and therefore also for the population should be fixed. All other indicators that might have an effect on the strength should be represented equally distributed – in the sample and in the population.

3.3 Representation of the sample: methodology for estimating the 5%-fractile values.

In general, the characteristic values of strength properties are estimated based on the outcomes of standardized test. Several techniques to estimate the 5%-fractile value based on test data exist and a considerable variety of these methods are prescribed in standards as e.g. EN 384 and ISO 13910, both valid for solid timber.

The method according the European standard EN 384 relies on stratified sampling, i.e. a sample is subdivided into at least $j = 5$ sub-samples of size $n_j > 40$ and for each sub-sample the 5%-fractile value $x_{05,j}$ is assessed based on order statistics. The value $\overline{x}_{05}$ is estimated as the weighted mean value of the 5%-fractile values of the sub-samples as $\overline{x}_{05} = \sum_j n_j x_{05,j} / \sum_j n_j$. The characteristic value x_k is estimated as $x_k = \min(\overline{x}_{05}, 1.2 \min_j x_{05,j})$.

According to ISO 13910 the sample 5%-fractile value x_{05} is also assessed based on order statistics. The parameters w and k of the 2-parameter Weibull distribution are calibrated to the data with explicit consideration of the lower tail data. The lower tail is defined with the threshold value x_G corresponding to the lower 15% of the data. v_{tail} is introduced as a approximation of the coefficient of variation of the Weibull distribution as $v_{tail} = k^{-0.92}$. The characteristic value is given as $x_k = (1 - 2.7 v_{tail} / \sqrt{n}) x_{05}$, where n is the sample size.

3.4 Emplacement of the results of standard tests in the hierarchical modelling scheme

The standardisation of test procedures is the prerequisite to compare and aggregate data of timber strength and stiffness related properties on a national and international scale. The results of standard tests are reflecting the variability of strength properties at a meso scale (compare with the scheme in Figure 1). Although test standards prescribe that sampling has to be performed in a way that a defined population has to be represented, the proper representation of the population of interest in design – the population of a strength grade – cannot be reached with a single test program. A recent study by Ranta Maunus and Denzler (2009) confirms that the variability of the statistical properties of different test samples is significant.

4 Modelling the Macro-Variability of Bending Strength

A possible method to quantify macro material variations is demonstrated in Rackwitz and Müller (1977), where the macro variability of concrete is analysed. Concrete from a particular grade but from several different producers is analysed. The sample moments of each sub-population are quantified and functional relationships between the sample moments are derived. A similar scheme can be realized for graded timber by taking timber from different regions and graded to the same grade but identified by different grading schemes. Alternatively the macro variability can be explicitly assessed if the applied grading scheme can be formalized to a probabilistic framework which takes into account all uncertainties involved into the grading procedure, see e.g. Sandomeer et al. (2008).

A straightforward approach to represent hierarchical data by means of hyperparameters is introduced in the following:

A material property is considered as a random variable X which is described by a probability density function with a given set of parameters $\boldsymbol{\theta}$; $\boldsymbol{\theta} = \left(\theta_1, \theta_2, ..., \theta_n\right)^T$

$$f_X\left(x|\boldsymbol{\theta}\right) \tag{2}$$

E.g. for the normal distribution θ_1 would be the mean value μ and θ_2 the standard deviation σ. In the following, μ and σ are used for illustrative reasons.

On the meso level the parameters of the probability density function (e.g. μ and σ) can be estimated based on sample observations, whereas the accuracy of the estimates is a function of the number of available observations. The uncertainty associated with the parameter estimates due to the limited number of observations becomes small if the number of observations arises; for illustrative reasons this uncertainty is ignored here.

On the macro level, suppose that the outcome of the assessment of, say, sample 1 are estimates of the parameters $\hat{\boldsymbol{\theta}}_1 = \left(\mu_1, \sigma_1\right)^T$ and m different samples are assessed, then the variability between the different samples can be assessed by modelling the realizations of the different parameter sets $\hat{\boldsymbol{\theta}}_1, \hat{\boldsymbol{\theta}}_2, ..., \hat{\boldsymbol{\theta}}_m$ at the macro level as random variables itself.

This model setup corresponds to a *hierarchical model* as described in more detail in the Probabilistic Model Code of the Joint Committee on Structural Safety (JCSS) [8]. The model allows for a differentiated treatment of macro and meso variability. Issues like the proper representation of populations of graded timber could be assessed directly on the macro level , i.e. statistical properties of the distribution parameters itself.

4.1 Representation of data

According to modern design codes as the Eurocodes (EN 1990:2002) characteristic values for strength related material properties have to be introduced as predictive values of the 5%-fractile. The general form of the predictive p %-fractile value can be given as:

$$x_{p,pred} = F_{X,pred}^{-1}\left(p\right) \quad \text{with} \quad F_{X,pred}\left(x\right) = \int\int f_X\left(x\middle|\boldsymbol{\theta}\right) f''_{\boldsymbol{\Theta}}\left(\boldsymbol{\theta}\middle|\hat{\mathbf{x}}\right) d\boldsymbol{\theta} dx \tag{3}$$

where $\hat{\mathbf{x}}$ are the sample observations, $\boldsymbol{\theta}$ are the parameters of the distribution function. The parameters $\boldsymbol{\theta}$ are realisations of the random vector $\boldsymbol{\Theta}$ with the posterior joint probability density function $f''_{\boldsymbol{\Theta}}\left(\boldsymbol{\theta}\middle|\hat{\mathbf{x}}\right)$. Equation (3) can be generally solved by reliability methods as FORM/SORM or numerical integration, however, an analytical solution exists, e.g. for the case where X is normally distributed. In this case the predictive value of the p %-fractile $x_{p,pred}$ is given as:

$$x_{p,pred} = \overline{x} + t_p\left(\nu\right) s\sqrt{1 + 1/n} \tag{4}$$

where $\overline{x}$ is the sample mean, s the sample standard deviation, n is the sample size and ν is defined by $\nu = n - 1$. $t_p\left(\nu\right)$ is the p %-fractile value of the t-distribution with ν degrees of freedom.

Equation (4) can be utilized to handle the case where data is assumed to follow a lognormal distribution simply by logarithmic transformation.

The described scheme facilitates the consistent representation of the information that is contained by the data, i.e. statistical uncertainties are considered and sample characteristics can be consistently related to the (required) characteristics of the entire population of a grade.

5 Modelling the micro variability of the bending strength

For modelling the variations of strength related timber material properties within a component, the variability on a micro scale has to be taken into account. In general, assumptions about the micro system behaviour of the material are providing guidelines for the development of stochastic material models. Structural timber material is a compound material with different load bearing behaviour for different loading modes. For the most relevant loading modes as bending and tension parallel to the main fibre direction, the load bearing behaviour might be classified as brittle.

5.1 Timber as an ideal brittle material

An ideal brittle material is defined as a material that fails if a single particle fails, see e.g. Bolotin (1969). The strength of the material is thus governed by the strength of the 'weakest' particle; therefore the model for ideal brittle materials is also called the weakest link theory, Weibull (1939). Over the last 40 years, the ideal brittle material model has been widely applied to study the tension, bending, bending shear and compression strength variability of various wood products including sawn and glued laminated timber. However, whenever the theory is utilised to explain some observed phenomena, inconsistencies to the theory have been noticed.

In Bohannan (1966) one of the first studies is published, showing that size effects and load configuration effects on the bending strength of clear wood specimen could be explained by the weakest link theory for brittle materials. In Madsen and Stinson (1982), the width effect on the bending strength of structural timber is studied. Their results suggest that bending strength increases as the member width becomes larger, which is contrary to the concept of a weakest link fracture process. It is suggested in Madsen and Buchanan (1986) that this inconsistency could result from visual grading rules which limit knot sizes on the wide and narrow faces of the member. These rules tend to limit the maximum size of knots for a fixed member depth independent of member width. In the same study it is suggested to consider size effects on the strength of timber separately depending on every single dimension of the member, i.e. to consider width, height and length effects on timber beams separately. In Madsen (1992) it is shown that the bending strength of sawn timber of constant thickness varies with member length and loading condition in a manner consistent with the ideal brittle material model.

In Barrett et al. (1975) and subsequently in Colling (1986) the perfectly brittle material model is successfully applied to model tension perpendicular to the grain failure modes in curved and pitched tapered beams and connections. These studies confirm that the Weibull model has wide application in modelling of wood fracture especially for tension perpendicular to the grain.

In Foschi and Barrett (1975) and in Colling (1986) it is confirmed that shear strength of beams varies with member size and the effects are quantified by using the ideal brittle material model. A normative representation of this effect is suggested in Larsen (1986).

In Barrett and Fewell (1990) Canadian, US and European species data is analysed and length effect factors for bending and tension are derived by also using the ideal brittle material model. An important result of these studies is the observation that length effects in tension and bending are very similar; i.e. inductively it was concluded that the bending and tension strength of structural timber is both governed by the ultimate tension strength. On the other hand in Rouger and Fewell (1994) it is found that 60-90% of the bending specimens considered in this study showed ductile failure mode governed by the compression side.

There is an ongoing list of further literature and many applications of the ideal brittle material model for timber can be found. However, the results of these investigations are delivering partly contrary results; contrary in regard to the value of quantified parameters, as e.g. the scale parameter of the Weibull model, but also in regard to the observed phenomena. This can be explained by the variability of the timber material at a macro scale, i.e. different species and grades exhibit different size effects (Rouger and Fewell (1994)); but also by the fact that the assumptions underlying the theory of ideal brittle fracture are not strictly fulfilled when considering timber. Timber is referred to as an orthotropic material; strength and stiffness properties are depending on the stress direction in a timber solid. Therefore the theory can only be used for individual loading modes for which the stress direction can be assumed to be constant, i.e. timber components loaded to tension perpendicular or parallel to the grain, shear along the grain or pure bending of beam shaped timber specimen. The latter loading mode includes tension and compression and has to be considered with caution because the failure mode in compression is not brittle. The material irregularities are in the scale of μm if the fibre configuration is considered or in the scale of dm when considering major defects as knots and grain deviations. The latter ones are almost in the same scale as structural components, which is in conflict of the basic assumption of the brittle material model, i.e. a material with a big number of defects, identical distributed and independent. Timber material is not statistically homogeneous.

In summary it can be concluded that the ideal brittle material model can be used in some cases as an empirical model basis which describes the major phenomenon, but where the parameters, i.e. scale and shape parameters do not have any physical meaning; but can be derived by fitting to experimental data. Especially for tension perpendicular to the grain the physical deviations to the initial theory seem to be small.

5.2 Weak section models for special load cases for timber structural elements

A typical timber structural element is of beam shape which means that its longitudinal extension is much larger than its transversal extensions and the main fibre direction is orientated along the longitudinal (main) axis of the element. These elements are mainly loaded in tension, compression and/or bending along the main axis. According to the inhomogeneous structure of these elements due to major defects such as knots and grain deviations, the direct application of the ideal brittle material model is questionable. Therefore, an alternative model for the variation of strength and stiffness related material properties is desirable. In regard to the modelling of the variation of the modulus of elasticity (MOE) several references can be found in the literature, see e.g. in Kass (1975), Suddarth and Woeste (1977) and Foschi and Barrett (1980). In Kline et al. (1986) a probabilistic approach to describe the lengthwise variation of bending stiffness is introduced. As illustrated in Figure 3 timber beams are divided in segments of identical length and the stiffness of segment 2 to segment $n-1$ is measured with a 4-point bending test. The correlation between the MOE_i's of the different segments is investigated and quantified by the so-called *Lag-k* serial correlation. The *Lag-k* serial correlation is the correlation of an observation from segment i and an observation from segment $i+k$; e.g. if $k=2$, *Lag-k* means the correlation of the MOE of segments 2 and 4 or of the segments 3 and 5 etc. For realisations $x_1, x_2, x_3, \ldots, x_n$ of the $MOE = X$; the *Lag-k* serial correlation ρ_k is defined as:

$$\rho_k = \frac{\sum_{i=1}^{n-k}\left(x_i - \bar{x}\right)\left(x_{i+k} - \bar{x}\right)}{\sum_{i=1}^{n}\left(x_i - \bar{x}\right)^2} \tag{5}$$

with $\bar{x}$ being the sample mean value of X . It is found that the serial correlation decreases with increasing k . The lengthwise variation of X is modelled by a second order Markov model as:

$$X_{i+1} = \beta_0 X_i + \beta_1 X_{i-1} + \varepsilon_{i+1} \tag{6}$$

where β_i, $i=1,2$ are regression coefficients and $\boldsymbol{\varepsilon}$ is the vector of random errors. The variables are assumed to be normal distributed with mean $\mu = 0$ and unknown standard deviation σ_ε .

Similar approaches are utilised to describe the lengthwise variation of tension and bending strength. Obviously only every second section can be tested destructively (compare Figure 3). In Showalter et al. (1987), Lam and Varoglu (1991) the tension strength is considered, in Czmoch (1991) the bending strength is considered; all studies find decreasing serial correlation with increasing k .

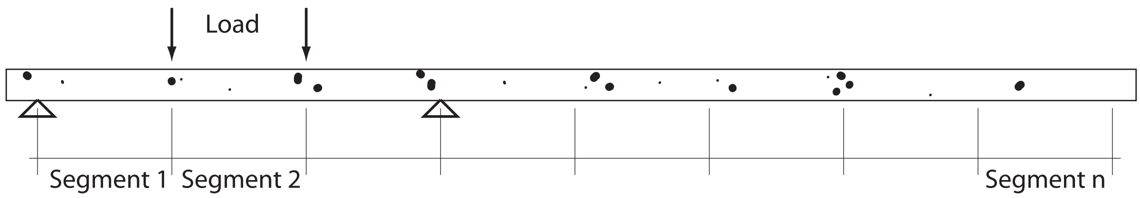

Figure 3 Separation in segments and test arrangement.

As seen in Figure 3 the regular segmentation does not facilitate the explicit consideration of observable irregularities in the beams. Examples for such observable irregularities are knots and knot clusters. In Riberholt and Madsen (1979) it is observed that low bending strength and bending stiffness coincides with the presence of knots and knot clusters. In this study it is assumed that failure can only occur at such weak sections and due to the discrete distribution of knots and knot clusters. An idealised model is proposed in terms of discrete weak sections separated by strong sections – sections of clear wood, see Figure 4. Furthermore equicorrelation of the strength of weak sections is assumed, which means that the correlation between the strength of weak sections is independent on their distance over the length of the beam.

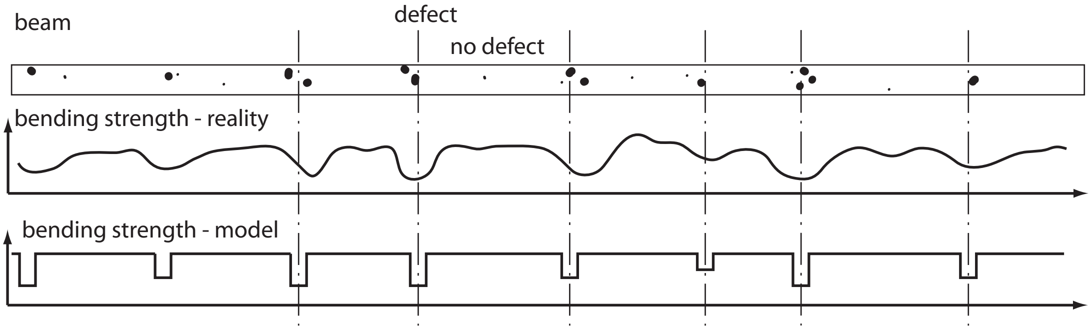

Figure 4 Bending strength of a timber beam; implied reality and as in the proposed model (Riberholt, Madsen (1979)).

Failure of one single weak section is determining the strength of the entire component and consequently the component can be modelled as a series system of weak sections. The strength of the weak section is described by a random variable whereas the location of the weak sections is modelled as an arrival 'time' of a Poisson process. The parameters of the Poisson process are estimated by direct measurements of the distances of knots and knot clusters. The parameters of the distribution function of the weak section strength is estimated indirectly; through measurements of the bending stiffness as an indicator for bending strength or by existing bending strength tests according to EN 408.

The proposed model for the variation of bending strength properties is investigated by Czmoch et al (1991). Here the length and load configuration effect of beams is studied and it is found that the available experimental information to verify the parameters of the proposed model is insufficient. This issue is considered in Isaksson (1999). Based on the ideas in Riberholt and Madsen (1979) and Czmoch et al (1991) a model for modelling the within member variation is suggested and the model parameters are estimated based on experiments on Norway spruce. The "Isaksson-model" appears as a quite promising basis for the consistent representation of timber bending and tension properties, if the basic assumption about the discrete appearance of knot clusters along the beam holds for the corresponding timber species of interest. In the following the model is summarized as it is represented in the JCSS Probabilistic Model Code (JCSS (2006), Köhler et al. (2005)).

The bending moment capacity $r_{m,0}$ at a particular point j in component i of a structure/batch is given as:

$$r_{m,0} = r_{m,\mathrm{ij}} = \exp\left(\nu + \varpi_i + \chi_{ij}\right) \tag{7}$$

where ν is the unknown logarithm of the mean of all sections in all components, ϖ_i is the difference between the logarithm of the mean of the sections within a component i and ν . ϖ is normal distributed with mean $\mu = 0$ and standard deviation σ_{ϖ} . χ_{ij} is the difference between the strength of weak section j in the beam i and the value $\nu + \varpi_i$. χ is normal distributed with mean $\mu = 0$ and standard deviation σ_{χ} . ϖ and χ are statistically independent.

Accordingly $R_{m,0}$ is a lognormal distributed random variable.

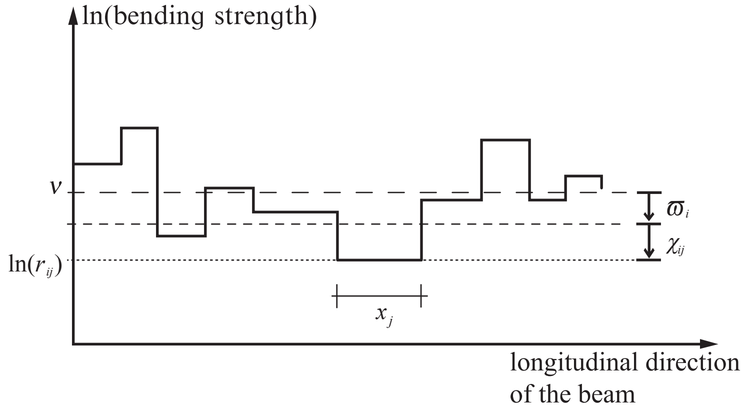

Figure 5 Modelling of the longitudinal variation of bending strength of a timber beam, Isaksson (1999).

The bending moment capacity $R_{m,0}$ is assumed to be constant within one segment (compare Isaksson (1999)). The discrete section transition is assumed to be Poisson distributed, thus the section length follows an exponential distribution.

The exponential distribution is given as:

$$F_X(x) = 1 - \exp(-\lambda x) \tag{8}$$

For Nordic spruce the following information basis can be given (Isaksson (1999)):

The variation of the logarithm of the bending capacity $\ln(R_{m,0})$ is related by 60% to the variable ϖ and by 40% to the variable χ. The expected length of a section is $1/\lambda = 480mm$.

A similar study on the lengthwise variation of bending strength is reported in Källsner and Ditlevsen (1994, 1997), Ditlevsen and Källsner (2004). Out of 26 beams 197 weak sections are identified and tested in regard to their bending strength by cutting them out, finger joining them between two pieces of stronger wood and testing them in a four point bending arrangement. A particular feature of this study is that unintentionally a large fraction of the test specimen did not fail in the section of interest, i.e. failure took place in the finger joints or in the stronger wood. Due to the censored data special methods are introduced to consider the observations properly. However, the results are in general consistent with the results presented in Isaksson (1999). A hierarchical model is introduced with two levels to represent the variation of bending strength within and between members. The $Lag-k$ correlation is found to be constant, i.e. equicorrelation is assumed. An interesting closed form analytical expression for the distribution function of the bending strength with any given number of weak section is provided in Ditlevsen and Källsner (2004).

The model presented in Equation (7) has hierarchical character; the variables ν, ϖ_i, χ_{ij} are representing the macro, meso and mirco variability as introduced in the chapter above. However, the representation of the macro variability is restricted to model a population with fixed variance and variable mean values of the corresponding sub-populations.

The presented model for the lengthwise variation of the bending strength has been successfully applied to assess the system performance of timber structures, Hansson and Thelandersson (2002), Hansson and Ellegaard (2006).

A drawback for the model might be the difficulty to collect data to feed the model with sufficient experimental evidence. The corresponding test set ups are complex, see Isaksson (1999) and Källsner and Ditlevsen (1994, 1997) and information from tests of standard test specimen cannot be directly utilized to update the parameters of the model.

However, the relation between the strength of weak sections and the strength of standard test specimen might be related based on the model. The corresponding study delivers furthermore interesting insights about the comparability of test results from different standards.

6 Comparison of the results of test standards

The fact that different test standards exist (in terms of different test specifications, but also differences in the data processing) makes the direct comparison of information provided by following different procedures impossible. Especially the different prescriptions for the relative placement of the weakest sections in the test set ups introduce considerable bias.

The European standard requires placing the weakest section in the middle, high stressed region. According to the US standard the weakest section has to be placed within the supports and following the Australian standard the weakest section shall be placed at random. The difference between the test standards in regard to placing the test specimen is illustrated in Figure 6. In the Figure the weakest section is indicated by a knot cluster. It can easily be imagined that the effect between the different specifications becomes larger when the length of the entire specimen increases. In practice it is in general not clear how long the specimen is.

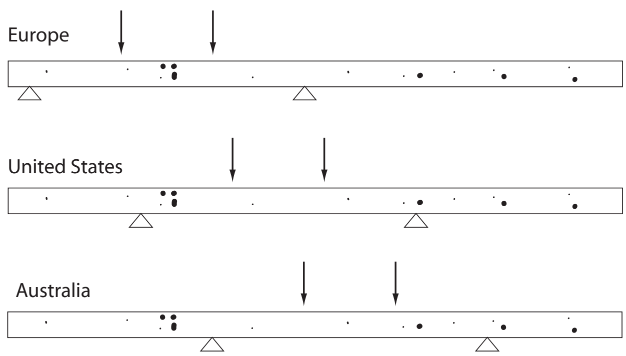

Figure 6 Illustration of the effect of different weak section placing specifications; Europe (EN 384, weak section between load application), United States (ASTM D 4761-05, weak section between supports), Australia (AS 4063:1992, weak section at random).

To illustrate the effect of the weak section placing specification the model derived in Isaksson (1999) is utilized for simulations. The model is used as it is presented in Chapter 5.2. The Monte Carlo Simulation technique (see e.g. Melchers (2001)) is used for the simulation of the random variables in the model. It is assumed that the beams have a length of 5 m. 1000 bending components are generated with a weak section distribution as indicated in Chapter 5.2. The components are virtually tested according to the three different bending strength test specifications. The obtained data is utilized to calibrate the parameters of a lognormal distribution. The corresponding distribution functions are plotted together with the distribution function of the strength of the weak sections in Figure 7. The parameters of the distribution functions are given in Table 2.

The distribution functions illustrated in Figure 7 show the difference between the bending moment capacity of test specimen and the bending moment capacity of all weak sections. It is underlined that these results correspond to the specific set up test range 2.7m, beam length 5m, perfect identification of the weakest section within a beam and beam properties as evaluated in Isaksson (1999) and summarized above.

An interesting question within the probabilistic modelling of timber material properties and for the further application of the Isaaksson Model is how to relate measurements on test specimen $r_{m,s}$ to the properties of weak sections $r_{m,0}$. For the given example a simple relation is found with the form:

$$r_{m,0} = r_{m,s}^{\vartheta} \tag{9}$$

The parameter ϑ is calibrated for different test standards by using the least squares technique. The results are given in Table 3.

Table 2 Parameter for lognormal distribution corresponding to Figure 7.

	ξ	δ
Weak sections	56.28	0.247
Europe	45.68	0.213
United States	50.36	0.247
Australia	51.95	0.232

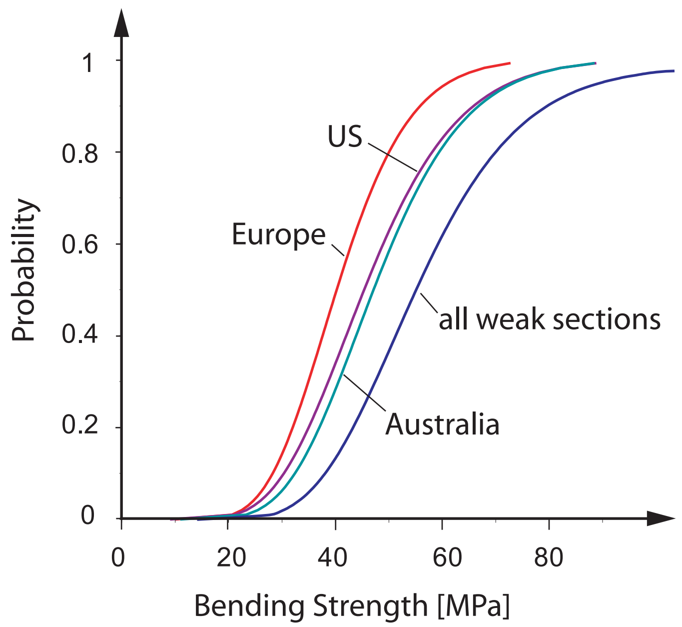

Figure 7 Distribution Functions of simulated bending test specimen according to different national test standards.

Table 3 ϑ-values for the estimation of the strength of weak sections.

See Equation (9)	*EN*	*US*	*AUS*
$\vartheta =$	*1.05*	*1.03*	*1.02*

According to Equation (9) the parameters of the lognormal distribution can be related as:

$$\begin{aligned} \xi_{r_{m,0}} &= \left(\xi_{r_{m,s}}\right)^{\vartheta} \\ \delta_{r_{m,0}} &= \left(\delta_{r_{m,s}}\right)\vartheta \end{aligned} \tag{10}$$

It should be underlined that the given example is based on the within component bending moment capacity variation model and the corresponding model parameters as presented in Isaksson (1999) and above.

7 Conclusions and discussion

The probabilistic analysis as well as the calibration of partial safety and modification factors for timber structures require reasonable probabilistic models and limit state equations. Probabilistic models of the load bearing performance of structural timber elements are to a large degree based on empirical data. A major challenge of ongoing and future research is to find ways to link the information from (mainly standardized) tests to a generic and probabilistic description of the strength and stiffness related capacities in structures. The aim of the present paper is to discuss a possible approach to accommodate for the hierarchical character of timber material properties in general. The principle way of thinking is exemplified by considering the bending capacity.

The bending strength is defined on an element level, i.e. as the capacity of standardized test specimen. Most test standards for the bending strength are based on ISO 13910, i.e. the principle test set up is equal. However, small differences in terms of the placement of the weakest section in the test configuration and the prescribed time to failure might be significant if the data is interpreted and used as a basis for the assessment of the performance of timber material elements in structures.

Especially the intended placement of the weakest section has provoked much discussion among researchers in the last decades since it introduces significant bias to the destructive test results. It might be discussed whether it is useful to have by definition a conservative estimate of the bending strength. The major drawback and the main contra argument against this strategy is that it introduces a “gray area” to the data. For the following reasons:

- The length of the entire beams is not specified. If the test length is e.g. 2.7 m it is a large difference whether the weakest section can be chosen from a 3 m beam (not possible) of a 5 m beam. If the weakest section is near the edge of the entire beam it cannot be placed between the load cylinders.
- The weakest section is identified by individual judgement. The real weakest section might not coincide with the weakest section selected. This doubt is confirmed by Leicester et al. (1998) where a rather low significance of the weakest section estimated was found.

A possible way to represent test data on a maco level is suggested. Samples should be represented with the corresponding predictive 5% fractile values. This information can be consistently used in line with the presented macro/meso representation with hyperparameters.

The presented model for the within member variability of the bending strength has a large potential to consistently represent the length effect of slender timber structural elements. However, the data basis for the model is rather thin and the model parameters are expected to depend strongly on species, growing conditions and sawing pattern of the corresponding timber resource.

For the modelling of size effects for the cross section direction, the Weibull theory seems promising although the long history of empirical research in that direction did not yet converge to a common set of model parameters. The effect of grading procedures and origin of the timber seems to be significant.

8 References

ISO 13910:2005 Structural Timber – Characteristic Values of strength-graded timber – Sampling, full-size testing and evaluation.

EN 408: European Standard: Timber structures - Structural Timber - Determination of some physical and mechanical properties. Comité Européen de Normalisation, Brussels, Belgium, 2004.

AS/NZ 4063:1992 Structural Timber – Characteristic values for strength graded timber.

Joint Committee of Structural Safety (JCSS, 2009). Probabilistic Model Code, Internet Publication: www.jcss.ethz.ch.

EN 1990:2002 Basis of structural design. Comité Européen de Normalisation, Brussels, Belgium, 2002.

Barrett J. D. and Fewell A. R. (1990). Size factors for the bending and tension strength of structural lumber. Proceedings of the 23th Meeting, International Council for Research and Innovation in Building and Construction, Working Commission W18 – Timber Structures, CIB-W18, Paper No. 23-10-3, Lisbon, Portugal, 1990.

Barrett J. D., Foschi R. O. and Fox S. P. (1975). Perpendicular to the grain strength of douglas fir. Canadian Journal of Civil Engineering. 2(1) pp. 50-57.

Bohannan B. (1966). Effect of size on bending strength of wood members. USDA Forest Service, Research Paper FPL 56, Forest Products Laboratory, Madison, WI.

Bolotin V. V. (1969). Statistical Methods in Structural Mechanics. Holden-Day Series in Mathematical Physics.

Colling F. (1986). Influence of volume and stress distribution on the shear strength and tensile strength perpendicular to the grain. Proceedings of the 19th Meeting, International Council for Research and Innovation in Building and Construction, Working Commission W18 – Timber Structures, CIB-W18, Paper No. 19-12-3, Florence, Italy, 1986.

Czomch I. (1991). Lengthwise variability of bending stiffness of timber beams. Proceedings of the International Timber Engineering Conference, London, UK , Vol.2, pp. 2158-2165.

Ditlevsen O. and Källsner B. (2004). Statistical series system size effects on bending strength of timber beams. Reliability and Optimization of Structural Systems – Maes & Huyse (eds). Taylor and Francis Group, London.

Faber M. H., Köhler J. and Sørensen, J. D. (2004). Probabilistic modelling of graded timber material properties. Journal of Structural Safety, 26(3), pp. 295-309.

Foschi R. O. and Barrett J. D. (1980). Glued laminated beam strength: A model. ASCE Journal of Structural Division 106 (ST8).

Hansson M., Ellegaard P. (2006) System reliability of timber trusses based on non-linear structural modelling. Materials and Structures 39 (pp593-600).

Hansson M., Thelandersson S. (2002) Assessment of probabilistic system effects on the reliability of timber trusses. Materials and Structures, Vol 35, (pp573-578).

Isaksson T. (1999). Modelling the Variability of Bending Strength in Structural Timber. PhD-thesis, Lund Institute of Technology, Report TVBK-1015.

Källsner B. and Ditlevsen O. (1994). Lengthwise bending strength variation of structural timber. IUFRO Sydney, Australia.

Källsner B. and Ditlevsen O. (1997). Experimental verification of a weak zone model for timber bending. IUFRO S5.02 Timber Engineering, pp. 389-404, Copenhagen, Denmark.

Kass A. J. (1975). Middle ordinate method measures stiffness variations within pieces of lumber. Forest Products Journal 25(3), pp. 33-41.

Kline D. E., Woeste F. E. and Bendtsen B. A. (1986). Stochastic model for the modulus of elasticity of lumber. Wood and Fiber Science, 18(2), pp. 228-238.

Köhler J. (2005). Reliability of Timber Structures. Dissertation. Swiss Federal Institute of Technology.

Lam F. and Varoglu E. (1991). Variation of tensile strength along the length of timber, Part 1 and 2. Wood Science and Technology 25, pp. 351-360 and pp. 449-458.

Larsen H. J. (1986). Eurocode 5 and CIB structural design code. Proceedings of the 19th Meeting, International Council for Research and Innovation in Building and Construction, Working Commission W18 – Timber Structures, CIB-W18, Paper No. 19-102-2, Florence, Italy, 1986.

Leicester R.H., Breitinger H. and Fordham H. (1998). A comparison of In-Grade test procedures. Proceedings of the 31st Meeting, International Council for Research and Innovation in Building and Construction, Working Commission W18 – Timber Structures, CIB-W18, Paper No. 31-5-2, Savonlinna, Finland, 1998.

Madsen B. (1992). Structural Behaviour of Timber. Timber Engineering Ltd., Vancouver, Canada.

Madsen B. and Buchanan A. H. (1986). Size effects in timber explained by a modified weakest link theory. Canadian Journal of Civil Engineering 13(2), pp. 218-232.

Madsen B. and Stinson T. (1982). In-grade testing of timber four or more inches in thickness. Tech. Rept. Univ. of British Colombia, Dept. of Civil Engineering, Vancouver, B. C.

Melchers R. (1999). Structural Reliability: Analysis and Prediction. Ellis Horwood, Chichester, UK.

Rackwitz R. and Müller K. F. (1977). Zum Qualitätsangebot von Beton, II. Beton, 27(10), pp. 391-393.

Ranta-Maunus, A. and Denzler, J.:Variability of strength of European spruce, CIB W18, proceedings paper 42-6-1, Zürich, Switzerland, 2009.

Riberholt H. and Madsen P. H. (1979). Strength of timber structures, measured variation of the cross sectional strength of structural lumber. Report R 114, Struct. Research Lab., Technical University of Denmark.

Rouger F. and Fewell A. R. (1994). Size effects in timber: Novelty never ends. Proceedings of the 27th Meeting, International Council for Research and Innovation in Building and Construction, Working Commission W18 – Timber Structures, CIB-W18, Paper No. 27-6-2, Sydney, Australia, 1994.

Sandomeer M. K., Köhler J., Faber M. H. (2008). Probabilistic output control of structural timber - Modelling Approach. Proceedings of the 41st Meeting, International Council for Research and Innovation in Building and Construction, Working Commission W18 - Timber Structures, CIB-W18, Paper No. 41-5-1, St. Andrews, Canada, 2008.

Showalter K. L., Woeste F. E. and Bendtsen B. A. (1987). Effect of length on tensile strength in structural timber. Forest Products Laboratory, Research paper FPL-RP-482. Madison, Wisconsin.

Suddarth S. K. and Woeste F. E. (1977). Influence of variability in loads and modulus of elasticity in wood column strength. Wood Science 20(2), pp. 62-67.

INTERNATIONAL COUNCIL FOR RESEARCH AND INNOVATION IN BUILDING AND CONSTRUCTION

WORKING COMMISSION W18 - TIMBER STRUCTURES

BASE PARAMETERS OF SELF-TAPPING SCREWS

G Pirnbacher

Graz University of Technology

R Brandner

Competence Center holz.bau forschungs gmbh

G Schickhofer

Graz University of Technology

AUSTRIA

Presented by G Pirnbacher

H.J. Blass commented that changing definition of f_{ax} or f_1 in Eurocode would make things difficult.
A. Jorissen questioned whether r^2=0.3 is enough. He also asked about the safety of the realized connection. G. Pirnbacher answered that the low r^2 values are inherent to the material properties.
H.J. Blass received confirmation that the tests were performed with the screw direction parallel to grain and the long term strength effect was not considered.
J.W. G. van de Kuilen discussed the fact that in machine grading, the overall density of the board is considered rather than the density of the individual specimen and asked what would be the influence of this effect. G. Pirnbacher answered that r^2 values would decrease because of the variability of density.

Base Parameters of self-tapping Screws

G PIRNBACHER

Graz University of Technology, Institute for Timber Engineering and Wood Technology

Austria / Europe

R BRANDNER

Competence Center holz.bau forschungs gmbh

Austria / Europe

G SCHICKHOFER

Graz University of Technology, Institute for Timber Engineering and Wood Technology

Austria / Europe

1 Introduction

According to EN 1382:1999 [1] the axial withdrawal strength of fasteners in timber is determined by means of a standardised test under tightly regulated loading conditions and exact rules for the moisture content of the specimens (thereby also limiting the possible climatic conditons during preparation and/or storage of the test pieces). The axial resistance is the primary mechanism defining connections that employ axially loaded screws as load carrying members – in general the dowel-type effect of the screw is not taken into account for the design of the connection. Variations of the moisture content, the temperature at “screw-in” and/or “pull-out” and wether the screw is pre-drilled or not are not considered in the design rules at all. Other parameters like the effective length and the angle between the screw axis and the grain are taken into account in the different rules available in the diverse codes like EN 1995-1-1:2004-11[2] and –A1 [3] and DIN 1052:2008 [4] and technical approvals.

2 State of the Art

In current regulations the withdrawal resistance depends on the density, the diameter and the length [2], [3], [4] and [8]. The basic relation found for the shear strength of screws follows this formula:

$$f_{ax} = A \cdot d^B \cdot l_{ef}^C \cdot \rho_k^D$$

Table 1: Parameters of current regulations concerning f_{ax}

regulatory document	A	d^B	l_{ef}^C	ρ_k^D
EN 1995-1-1:2004/A1 [3]	0.52	-0.5	-0.1	0.8
DIN 1052:2004 [4]	$(60 \div 80) \cdot 10^{-6}$	0.0	0.0	2.0
SIA 265:203 [8]	$30 \cdot 10^{-3} \cdot \pi^{-0.2}$	-0.2	-0.2	1.0

This research program is aimed at these basic influencing parameters and adds several more like temperature and moisture content. Cockrell [7] reported moisture effects of 1.5% in average for screws Nr. 6, 8 and 10 in various wood species. These screws were of the diameters 3.5 to 4.8 mm and had an effective thread length of 20 mm. These values do not match the sizes used in current constructive practice, so their applicability has to be questioned and verified for modern screws. Newlin and Gahagan [9] stated that the relation between withdrawal capacity and penetration is linear.

The study presented in the following pages was designed and carried out to draw a picture of the visited parameters and their influence.

3 Scope

To provide a solid frame of reference and foundational knowledge of the influence of diverse parameters a broad test programme aimed specifically at the basic parameters has been initiated at the Competence Center holz.bau forschungs gmbh and the Institute for Timber Engineering and Wood Technology at Graz University of Technology. The aim is to provide knowledge about the influence of following basic parameters:

- the moisture content
- the temperature at “screw-in” and “pull-out”
- the influence of screw diameter
- the influence of slenderness
- the influence of the embedment of the threaded part
- the influence of the angle between the screw axis and the grain
- the influence of pre-drilling
- all tests conducted with solid and glue laminated timber

The final count of withdrawal experiments considered in the statistical analysis is 5524; all parameters studied were investigated parallel and perpendicular to the grain.

4 Test program

For the initial study a matched sample setup was choosen. The material used was sitka spruce, with strength classes of C24 (ordered as grading class S10) for solid timber and GL28h for GLT. The single specimens were cut from beams and grouped into matched samples by means of the specimen weight. This lead to very coherent groups to start with, and resulted in comparable distributions for the small scale density samples (good matches for the mean values were achieved), although the initial matching was done by weight of the whole specimen.

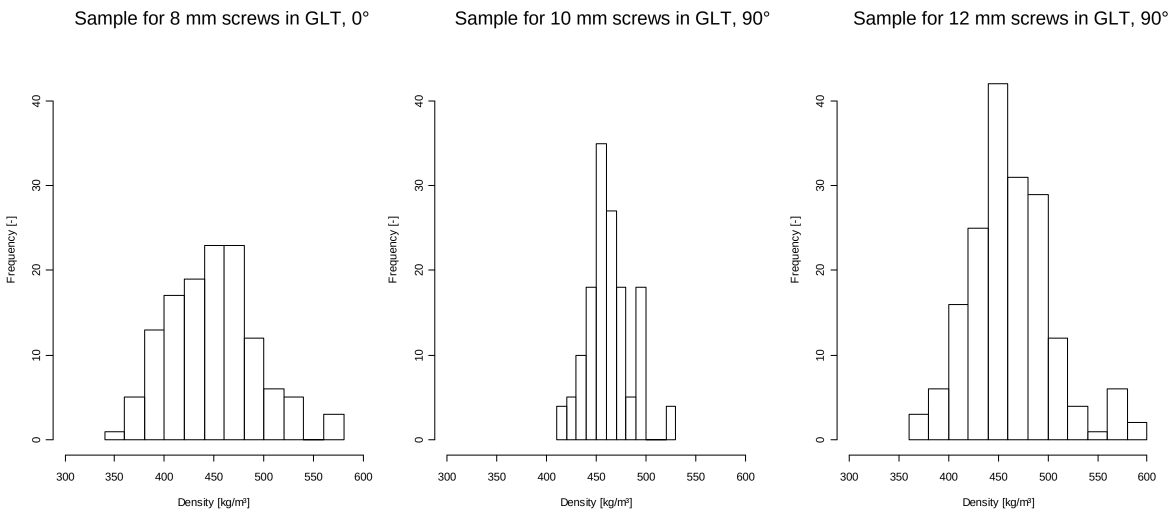

Figure 1: Histograms of density at 12% mc for selected samples (reference volume = $4d \cdot 4d \cdot l_{ef}$)

The samples were cut from the length of beams (100/280 mm or 120/180 mm with 4000 mm (solid timber) or 8000 mm (GLT) length) in length steps of 180 mm. Areas with concentrations of knots were cut out at the time of preparation. These single blocks were then weighted and grouped into test samples. In each single "block" sufficient volume for at least 5 experiments was provided. This made it possible that each single "block" accommodated all variations of the parameter(s) – e.g. the moisture values of 0% (kiln dry), 6%, 12% and 20% were tested in each block of this group. For each instance of the timber properties of a block – in one small volume of timber: max. 100 · 280 · 180 mm or 5,04 dm³ – resistance values of all parameter variations are obtained. Taking into account that obvious areas inappropriate for testing were cut out during specimen preparation quite homogenous properties for each block can be assumed.

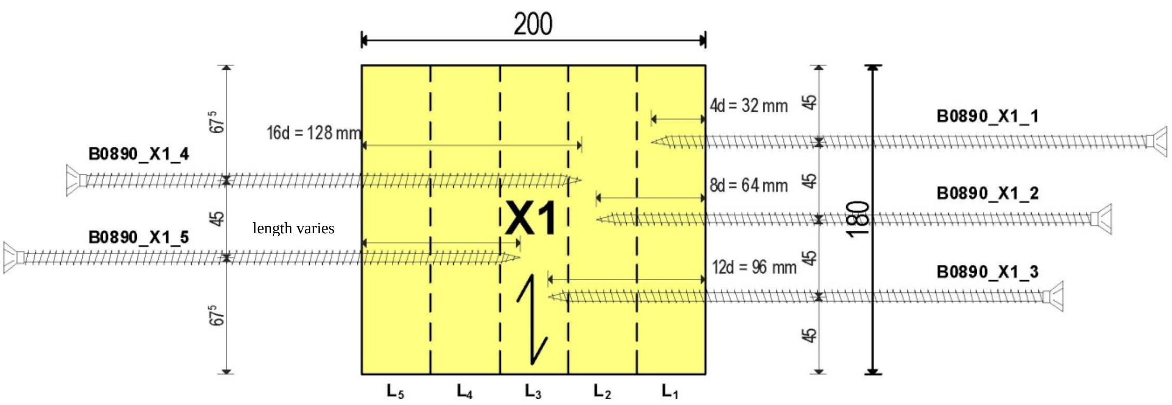

Figure 2: Overview of test design in one "block", e.g. of the sample B0890 [5]

Following levels for each single parameter were tested during the study:

Table 2: Overview of the parameter variations including planned levels and associated parameters held constant

Variation of parameter	Screw Diam. [mm]	Parameter values (constants or mean values)	Constant Values
Moisture **C**ontent [%]	8	0%, 6%, 12%, 20%	T,D,EL,EM,AG,PD
Temperature [°C]	8	-20°, 0°, 20°, 50° C	MC,D,EL,EM,AG,PD
Diameter	8,10,12	8, 10, 12 mm	MC,T,SL,EM,AG,PD
Effective **L**ength [mm]	8,10,12	**SL**enderness of 4, 8, 12, 15d	MC,T,D,EM,AG,PD
EMbedment [mm]	8	0, …, 240 mm	MC,T,D,EL,AG,PD
Angle to the **G**rain [deg]	8	0° …/12,5°/… 90°	MC,T,D,EL,EM,PD
Pre**D**rilling [yes/no]	8	0° …/12,5°/… 90°	MC,T,D,EL,EM,AG

(Further on single parameters will be referenced by the initials bolded in Table 2)

The withdrawal tests were done with screws from the manufacturer WÜRTH – an ASSY II; 8x400/100 mm screw (all series except ‘EL’) – and with Screws from SPAX – here SPAX-S with diameters from 8 to 12 mm were used (inside Sample ‘EL’). The partially threaded screw from WÜRTH was choosen because the error source of unintentional variations in the effective length (measurement, marking and screw-in errors) is eliminated by design because of the given length of the threaded part. The SPAX-S was choosen where a deviation from this rule became necessary, precisely in the ‘EL’ series where the effective length was varied.

The pull-out loading was performed by means of two test rigs. One was a Proceq Z-25FS concrete adhesion tester with a maximum load of 25 kN, which allowed the recording of deflection and force used for all samples with only 8 mm screws. Further tests – all samples including screws of diameters of 10 mm and 12 mm (because these reach higher withdrawal resistances than the 25 kN limit for the smaller setup) – were conducted on the LIGNUM-UNI-275, a test rig manufactured by Zwick-Roell, with a maximum force of 275 kN. All pull-out tests were carried out with a load distribution plate interlocked beween the “block” and the test rig. This plate guaranteed the same load distribution on both used test rigs and also defined the unloaded area around the screw. The hole in the plate was defined with a diameter of 4d (a slight deviation from EN 1382 [1] which defines “no part may be nearer than 3d”).

Figure 3: Test rigs: photos of the setup in the Lignum-Uni-275 and a picture of the Proceq Z-25FS tester

After the experimental work was finished every single "block" was cut into small density specimens of the dimensions $4d \cdot 4d \cdot l_{ef}$ for the determination of the moisture content and the density. For selected groups, where the small cubes slightly overlapped (groups where all diameters were tested), a plate ($40 \cdot 180 \cdot 200$ mm or 1.44 dm³) enveloping the 4 to 5 smaller cubes was cut (this leads according to earlier research [5] to a maximum error of ~∓2% of the density when compared to small scale samples). Additionally the annual rings as well as – after splitting the affected specimens – the interpenetration length of screws and present knots (not the knot diameter) were recorded.

Figure 4: Selected small scale density and moisture specimens with clear wood, a knot and a resin inclusion

5 Analysis

The analysis was carried out with the statistics package R 2.9.1 [10] and as additional tools Excel and Tinn-R are applied. For all series the applicability of the Gaussian distribution has been verified or assured by partially applying transformations (a logarithmisation has been choosen) to the subsamples. If not stated otherwise all following sections have been normalised to a reference value that has been choosen as one of the values common to the standard climate for homogenisation of the test samples. The reference parameter values are 12% moisture content as reference value for moisture variation, 20° Celsius as reference for temperature influence, the 90° values of the stresses for the angle and pre-drilling section, the diameter of 8 mm for the influence of screw diameter and finally the values of the stresses reached at 15 mm embedment of the thread for the section concerning the effect of embedment. Additionally the normalization parameters are given in each figure inside the y-axis labels. The aim of the statistical analysis was to provide good description of the effects at mean level (and at the 5% fractile for the HANKINSON relation). As method to get usable mean value models an outlier treatment has been performed following two premises: all outliers directly accountable to branches or resin inclusions as well as errors during trial or measurement have been generally removed. Any remaining outliers – not accountable to deviations inside the specimens or from the reference test procedure – were removed if they are outside a range of ∓ three times the IQR from the mean values (this is a removal of absolute extreme values). For each parameter a representative sample was singled out and is shown in the appropriate section.

5.1 Influence of the timber's moisture content

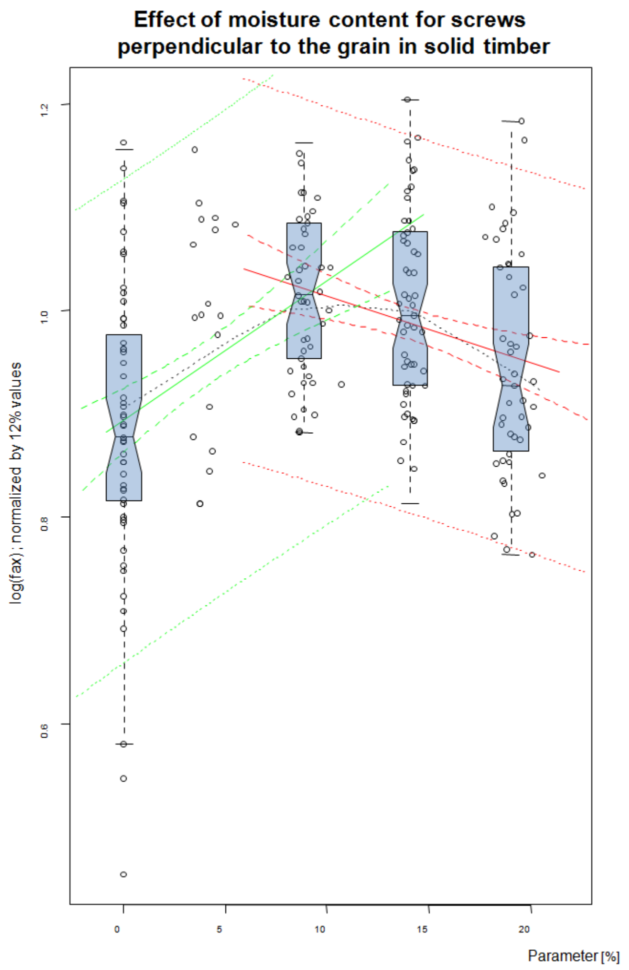

Figure 5: Effect of moisture content for solid timber, perpendicular to the grain

This section was designed to include tests at four levels of moisture content inside the specimens. The planned levels included 20%, 12%, 7% and 0% (kiln-dry) and were tested in this sequence. Due to hysteresis effects in homogenisation the exact planed values were not reached but mean values of 0%, 9%, 14% and 19% were present in the tested specimens. Subsamples inside this section were glue laminated timber and solid timber with screws in directions parallel and perpendicular to the grain. Figure 5 shows the effect for screws perpendicular to the grain in solid timber. Visible is a split into two distinctive modes: for m.c. levels below 10% a sharply increasing quota of brittle failures – splitting of the whole "block" – was observed, additionaly cracks inside the specimens formed earlier and lead on the median level to a decrease to a niveau of 88% when referenced to the values at 12% m.c.

In specimens with a moisture content above 10% a steady decrease of f_{ax} can be observed and can be described using a linear function of the form:

$$k_{mc} = 1{,}078 - 0{,}0065 * m.c.[\%] \quad \text{for m.c. levels >12\%}$$

can be given. To put this relation into numbers: leading from the point of reference at 12% m.c. the decrease in shear strength (obtained with the shell area of the thread) is -5% at a moisture content of 20%. For moisture values above the fibre saturation this relation has yet to be verified (a linear extrapolation would lead to - 12% at 30% m.c.). As moisture contents below 7-8% are seldom in practical use it seems possible to suggest a k_{mc} moisture correction of the following form:

$$k_{mc} = \begin{cases} 1.00 \\ 1.00 - 0.0065 * (u[\%] - 12) \end{cases} \; for \; \begin{cases} 8\% \leq m.c. \leq 12\% \\ 12\% < m.c. \leq 20\% \end{cases}$$

For service class 1 and 2 the k_{mod} factors are of the same value, due to this fact an inclusion of $k_{mc} = 0.95$ for the use of screws in connections exposed to service class 2 is proposed.

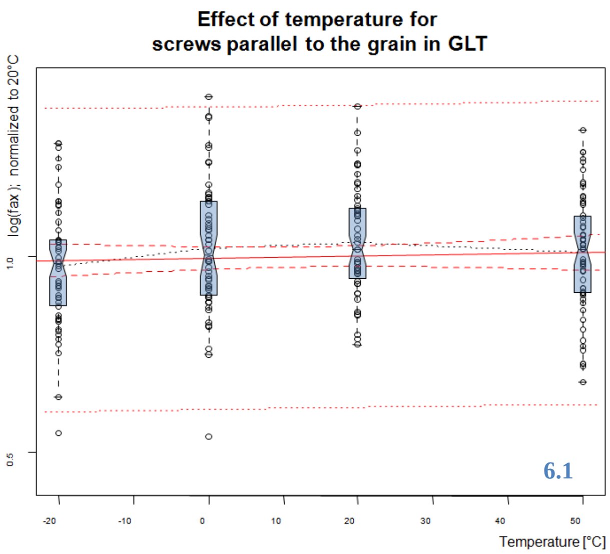

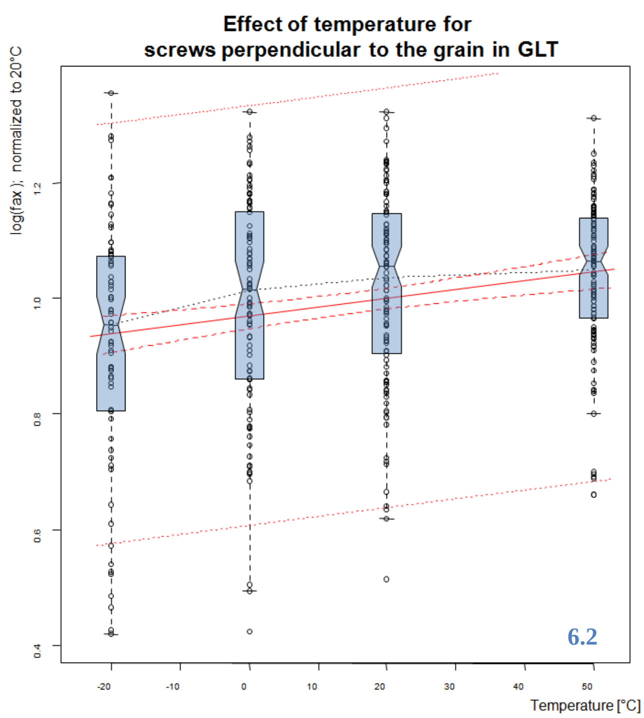

5.2 Influence of temperature

This section was designed to include tests with temperatur levels of 50°, 20°, 0° and -20° Celsisus (in this order). The specific subsamples show small differences. For screws parallel to the grain – both in GLT and solid timber – no noticeable effect of temperature on the strength is apparent (Fig. 6.1). For screws perpendicular to the grain the two materials show contrarian tendencies. Glue laminated timber shows a slight increase with temperature (+0.15% per degree Celsius) (Fig. 6.2) whereas solid timber shows a decrease with same incline (-0.15% per degree Celsius) (Fig. 6.3). This is possibly an effect of orientation in relation to the annual rings, but this assumption is yet to be verified. In GLT the tests were performed in radial direction, whereas in solid timber the tests were done in tangential direction due to the way the beams were cut from the stem. In the generalised description the model shows no dependency of strength on temperatures up to 50° Celsius (the two effects for perpendicular screws annul each other).

Figure 6.1 and 6.2: Effect of temperature for GLT; 0°(1) and 90°(2)

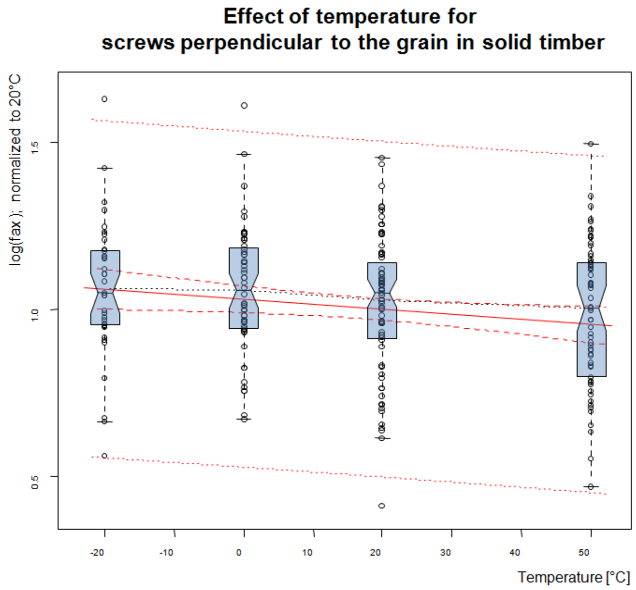

Figure 6.3: Effect of temperature for solid timber; perpendicular to the grain

A temperature correction is therefore proposed in the following form:

$$k_{temp} = 1.00 \qquad \text{for -20° to +50° C}$$

The quota of brittle failures sharply increases starting from temperatures near 0° Celsius. The complete reserves had to be included into this subsample because test specimens suffered severe brittle splitting failures during screw-in. Whole specimens split apart at penetration lengths between two to four times the screw diameter.

In order to complete the tests the specimens were secured against splitting by applying restrictions over the smaller side during srew-in. After the screw was completely screwed into the specimen these restrictions were removed and the standardised test performed. Due to this fact it is advised to install screws at temperatures above 5° Celsius.

5.3 Diameter

The samples aimed at the effect of the diameter were done with screws of the diameters 8 mm, 10 mm and 12 mm with constant slenderness l/d of 12. The shear strengths were normalized by the values obtained at a diameter of 8 mm and plotted in Figure 7.1 (a slight horizontal offset has been added to allow optical separation of the subsamples: GLT90°: red (solid), GLT00°: blue (dash-dot), VH90°: green (dashed), VH00° magenta (dash-double-dot)). Apparent is the coherent behaviour of the four subsamples. Each material/direction pair shows a similar trend over the diameter. In Figure 7.2 a generalised model ist shown combining the four subsamples.

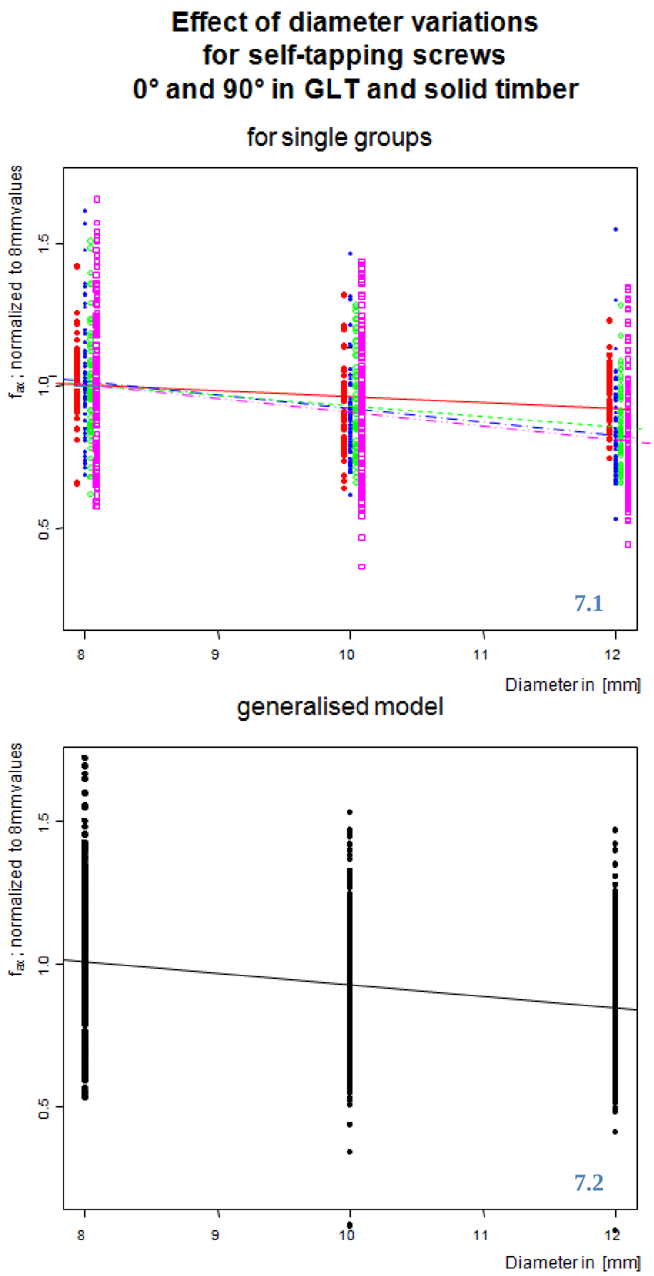

Figure 7: Effect of the screw diameter

Table 3: Dependency of f_{ax} on diameter in [mm]

d [mm]	normalized f_{ax} [%] linear	normalized f_{ax} [%] potential
8	1,00	1,00
10	0,92	0,91
12	0,84	0,84

The linear model takes the form of:

$$f_{ax,diam} = k_{diam} \cdot f_{ax,diam=8mm} \quad \text{with} \quad k_{diam} = 1{,}322 - 0{,}0402 * d \qquad \text{d in [mm]}$$

This relation can be alternatively formulated in potential form as:

$$k_{diam} = 2{,}44 * d^{-0{,}428} \qquad \text{d in [mm]}$$

This relation was included in the potential form in the modeling of f_{ax} as a function of density in section 5.7. The inclusion was done as summand to the density effect, because the normalization (congruence of normalized behaviour) in chapter 5.3 shows that the effect of the diameter can be described independently from density, material and angle to the grain.

5.4 Effective length

This parameter [5] was examined in detail with primary groups by diameter (d = 8, 10 and 12 mm) and subgroups by material (GLT, solid timber) and angle to the grain (90° and 0°). In each of these samples length steps of 4d, 8d, 12d and 15d (the planned length of 16d lead to high quotas of screw failure) were tested. The samples show coherent behaviour and one of the samples (B1290) was singled out and is shown in Figure 8.

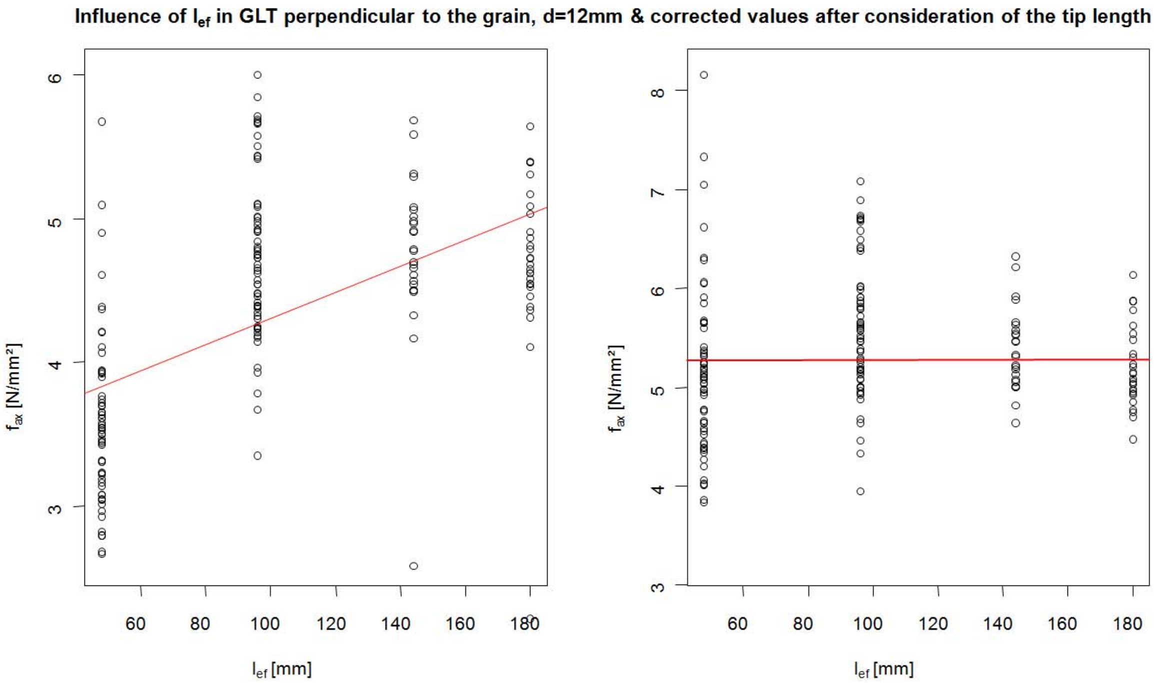

Figure 8: Length Correction of subsample B1290 – GLT, 12 mm screws perpendicular to the grain

The premise of this correction is very simple: If the trendline in the scatterplot is horizontal no influence of length is present. This can be very easily put into an equation $k_{length} = k_{length}(min|slope|)$ where the slope is obtained using a linear model of the form $f_{ax}[\%] = slope * l_{korr} + B$ and $l_{korr} = l_{thread} - k_{length} \cdot d$. This relation has been optimized for all subsamples at hand. The results of these calculations are given in Table 4:

Table 4: Optimised length correction by subtraction of tip length, results over subsamples ("B" denotes GLT, "K" denotes solid timber)

Subsample [material|d|angle]	k_{length}	Angle	$k_{length,\ mean(angle)}$	$k_{length,\ mean}$
B0890	1.20	90°	1.15	1.17
B1090	0.93			
B1290	1.22			
K0890	1.30			
K1090	1.04			
K1290	1.18			
B0800	1.59	0°	1.21	
B1000	1.58			
B1200	0.91			
K0800	1.45			
K1000	0.80			
K1200	0.92			

The length correction by subtracting $1{,}17 \cdot d$ from the thread length to include the effect of the tip was included in the modeling of f_{ax} as a function of density in section 5.7 by calculating the input f_{ax} values with this correction applied.

$$k_{length} = 1{,}17 \cdot d$$

5.5 Effects of angle to the grain and pre-drilling

Another test series aimed at determining the influence of pre-drilling and of the angle to the grain. The aim was to check the applicability of the HANKINSON relation for axially loaded screws. It was possible to include pre-drilled and self-tapping screws (of the same type) in this sample. The angle values included in this series are 0°, 12.5°, 25°, 37.5°, 45°, 72.5° and 90° between screw axis and grain direction.

Table 5: Shear strength ratio between parallel and perpendicular to the grain

	ratio $f_{ax,90°} / f_{ax,0°}$		
Type	mean-level	median-level	5% fractile level
pre-drilled	1,20	1,25	1,45
self-tapping	1,26	1,28	1,50

In Figure 8 the angle dependency of the shear strength (normalized by the 90° values) is shown. The Hankinson relation as given in EN1995-1-1:A1 [3] describes the mean values good. If the line is shifted to the 5% values a slight undermatching for the 5% fractile values for angles lower than 72.5° is apparent. A slight modification to the Hankinson relation leading to the following formula fits the values between 0° and 72.5°:

$$k_{Hankinson,modified} = \frac{1}{\sin(\alpha)^{2,2} + 1{,}30 \cdot \cos(\alpha)^{2,2}}$$

This modified Hankinson relation includes the slower degradation for angles between 60° and 90° while still describing the drop down to the 0° values reliably.

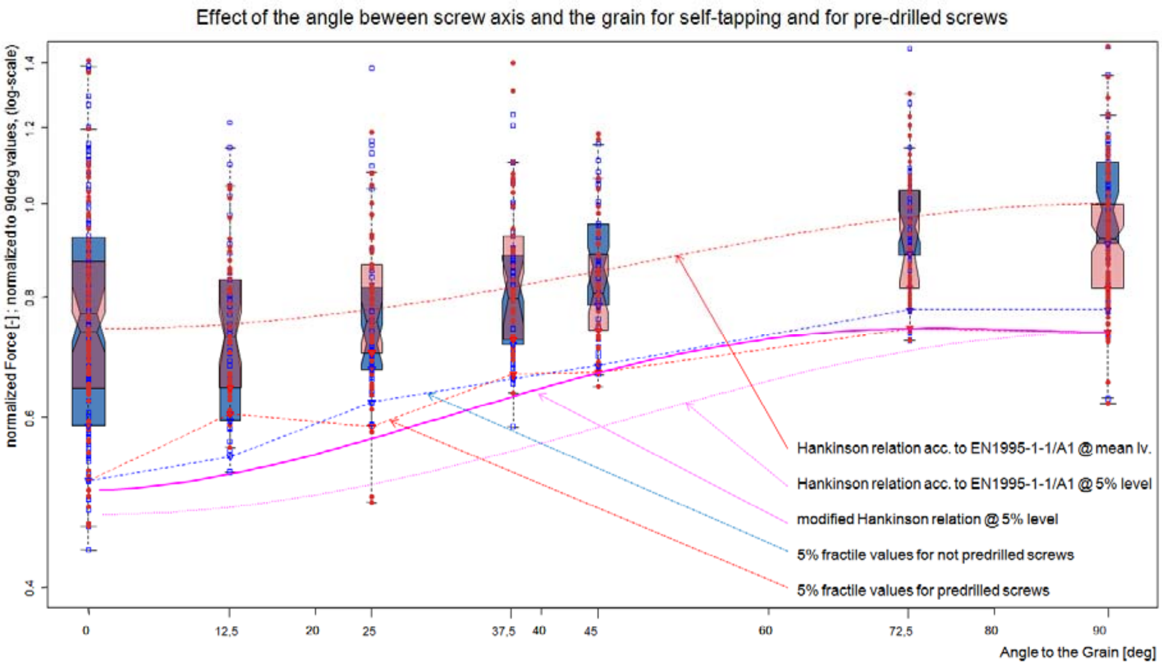

Figure 9: Hankinson relation for axially loaded screws, d = 8 mm

Table 6 shows that no differentiation between pre-drilled or self-tapping screws is necessary. Screws of the same type in homogenous material (distance between tests was 5d) show difference in shear strength of only 1.3% at the 5% fractile level.

Table 6: Ratios of f_{ax} between pre-drilled and self-tapping screws

	ratio of $f_{ax,self\text{-}tapping}$ / $f_{ax,pre\text{-}drilled}$	
angle	mean-level	5% fractile level
90.0°	1.071	1.057
75.2°	1.068	1.045
45.0°	1.065	1.016
37.5°	1.045	0.988
25.0°	0.946	1.061
12.5°	1.005	0.903
00.0°	1.047	1.020
mean(angles)	**1.035**	**1.013**

5.6 Embedment

This section features a different test setup than all other parameter studies. Over the length of two GLT beams a rasterization of 116 rows of three holes each was applied. Each row was then tested with a different embedment depth. Applied depths were 0 mm, 15 mm, 30 mm, 100 mm, 170 mm and 240 mm measured from the surface to the starting point of the thread.

The analysis shows a steep decline when the embedment drops below 2d. The mean value for not embedded screws is 4.62 N/mm² (partially threaded screws with d = 8 mm and l_{thread} = 100 mm) while the screws embedded 15 mm into the wood reach a value of 5.21 N/mm². This is a difference of $k_{emb,15mm}$=1.13 or 13% when referenced to the $f_{ax,0mm}$ values ($f_{ax,15mm}$ is the normalization reference value for Figure 10).

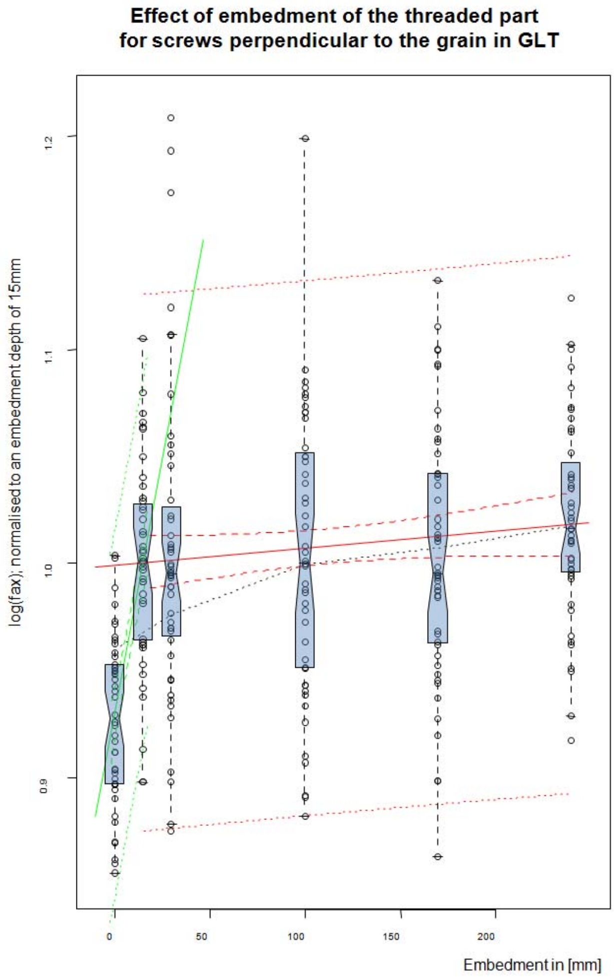

Figure 10: Effect of thread embedment into the wood

The shown value of 1.13 for k_{emb} is conservative as the trend shows a monotone increase with growing embedment depth. With the highest embedment depth of l_{emb} = 240mm the factor reaches a maximum value of $k_{emb,240mm}$ = 5,43/4,62 = 1,18.

As the tests used in section 5.7 (modelling of f_{ax} as function of density) were perfomed without embedment the correction k_{emb} can be calculated as shown above. With these values a mean factor to include embedment can be set as:

$$k_{emb} = 1.15 \quad \text{if } l_{emb} \geq 2d$$

5.7 Withdrawal resistance – circumferential shear resistance f_{ax}

With all tests carried out under constant climate (and the temperature series which shows no effect of temperature) a combined model for the influence of the density was created. Included in the modeling are the length correction shown in chaper 5.4 (included in the calculation of $f_{ax,test}$) and the diameter influence shown in chapter 5.3 inside the proposed model fitted to the data.

The choosen basic model describes the shear strength as a linear function of the density and an additional summand based on the diameter effect. This basic dependency was put into the regression for a linear model performing a least squares fit of the coefficients:

$$f_{ax} \sim A \cdot \rho_{test} + B \cdot d \cdot (2{,}44 * d^{-0{,}428}) + C = A \cdot \rho_{test} + B \cdot (2{,}44 * d^{0{,}572}) + C$$

Figure 11 shows the scatterplots and the regression lines achieved with this formula.

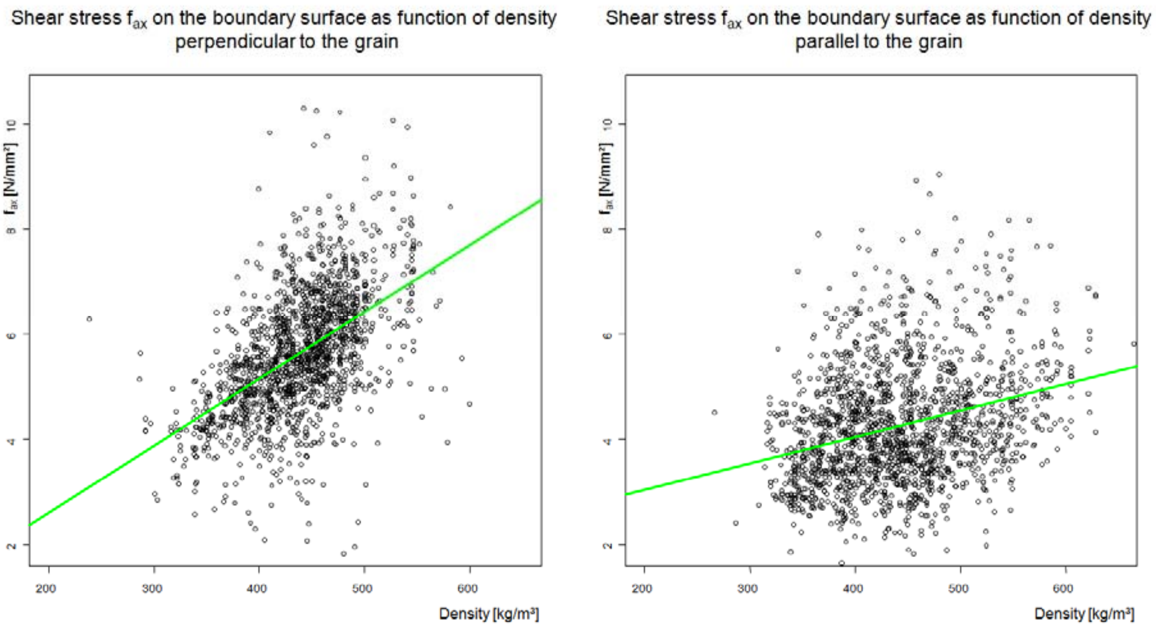

Figure 11: Scatterplots with regression lines for the models with 90° and 0° to the grain

Table 7 shows the coefficients and R^2 values obtained from the linear models. Parameter A can be directly interpreted as N/mm² per kg/m³ while Parameter C is the basic offset of the linear function. For perpendicular screws we get a value of 1.35 N/mm² for each 100 kg/m³ of density, while for parallel screws this value is 0.54 N/mm² per 100 kg/m³ of density. On the other hand the offset with a value of 5.92 N/mm² is very high for screws parallel to the grain indicating a very small influence of density.

The ratio of mean density shows the comparability of the two samples for parallel and perpendicular to the grain. The ratio of $f_{ax,90}/f_{ax,0}$ of 1.32 shows the validity of the Hankinson relation clearly.

Table 7: Regression values obtained by fitting the basic relation to test data

	model for 90° to the grain	model for 00° to the grain
Parameter A	0.01353	0.00538
Parameter B	-0.28147	-0.45875
Parameter C	2.18888	5.92460
R^2 (without d-term)	0.32 (0.27)	0.20 (0.08)
Ratio of mean density	1.009	
Ratio of mean f_{ax}	0.75 (for Hankinson relation: 1.32)	

6 Conclusion

The parameters researched show significant effects on the withdrawal resistance of screws. Most prominent ist the effect of embedment with an increase of at least 15% starting from only 15 mm embedment of the thread into the wood.

Additionally the effect of embedment covers other effects – e.g. the effect of the angle to the grain (earlier research without consideration of embedment indicated no effect between 90° and even below 45°). The inclusion of the embedment depth is proposed in the following form:

$$k_{emb} = 1.15 \quad \text{if } l_{emb} \geq 2d$$

The moisture content shows an influence of 0.65% per percent of moisture content. The proposed correction takes the form of:

$$k_{mc} = \begin{cases} 1.00 \\ 1.00 - 0.0065 * (u[\%] - 12) \end{cases} \quad for \quad \begin{cases} 8\% \leq m.c. \leq 12\% \\ 12\% < m.c. \leq 20\% \end{cases}$$

The diameter has an effect of about -12.5% between the diameters of 8 mm and 12 mm. The relation included in the modelling of f_{ax} as function of density is:

$$k_{diam} = 2{,}44 * d^{-0{,}428} \quad \text{d in [mm]}$$

The length can be considered by deducting the tip from the thread length, where the correction is diretly related to the diameter and proposed in the form of:

$$l_{korr} = l_{thread} - k_{length} \cdot d \quad with$$

$$k_{length} = 1{,}17 \cdot d$$

The temperature does not exert a quantifiable effect on the withdrawal resistance.

$$k_{temp} = 1.00 \quad \text{for -20° to +50° C}$$

A modified Hankinson relation optimized to describe the 5% fractile can be formulated by an adjustment of the exponents from the original value of 2.0 to 2.2 as follows:

$$k_{Hankinson,modified} = \frac{1}{\sin(\alpha)^{2,2} + 1{,}30 \cdot \cos(\alpha)^{2,2}}$$

The dependency from density shows clearly in the regression analysis. An example of the obtained mean value model shall be given here:

$$f_{ax,mean,90} = 0.01353 \cdot \rho_{test} - 0.28147 \cdot (2{,}44 * d^{0{,}572}) + 2.18888$$

$$\text{with } \rho_{mean} = 450\ kg/m^3 \text{ and } d = 8\ mm$$

$$f_{ax,mean,90} = 0.01353 \cdot 450 - 0.28147 \cdot (2{,}44 * 8^{0{,}572}) + 2.18888$$

$$f_{ax,mean,90} = 6.09 - 2.26 + 2.18 = 6.02\ N/mm^2$$

The investigated effects show clear trends and can be normalized across material and angle to the grain variations. Summing all single effects up and considering observations during testing an optimized screw for load carrying joints with steel plates and screws under an angle of 45° can be derived. This screw includes a strengthened shaft of about 3d length under the head in order to minimize the curb effect of the steel plate's edge. Then an additional free length of about 1,5d is added to reach the optimal embedment depth of 2d below the surface. Finally a thread length of about 18-20d is applied to the screw. As lower bound 18d are suggested because the critical length that marks the transition of withdrawal failure to screw failure is at around 16d (depending on steel strength). If the effect of embedment is taken into account this length could even be reduced to 14 – 16d.

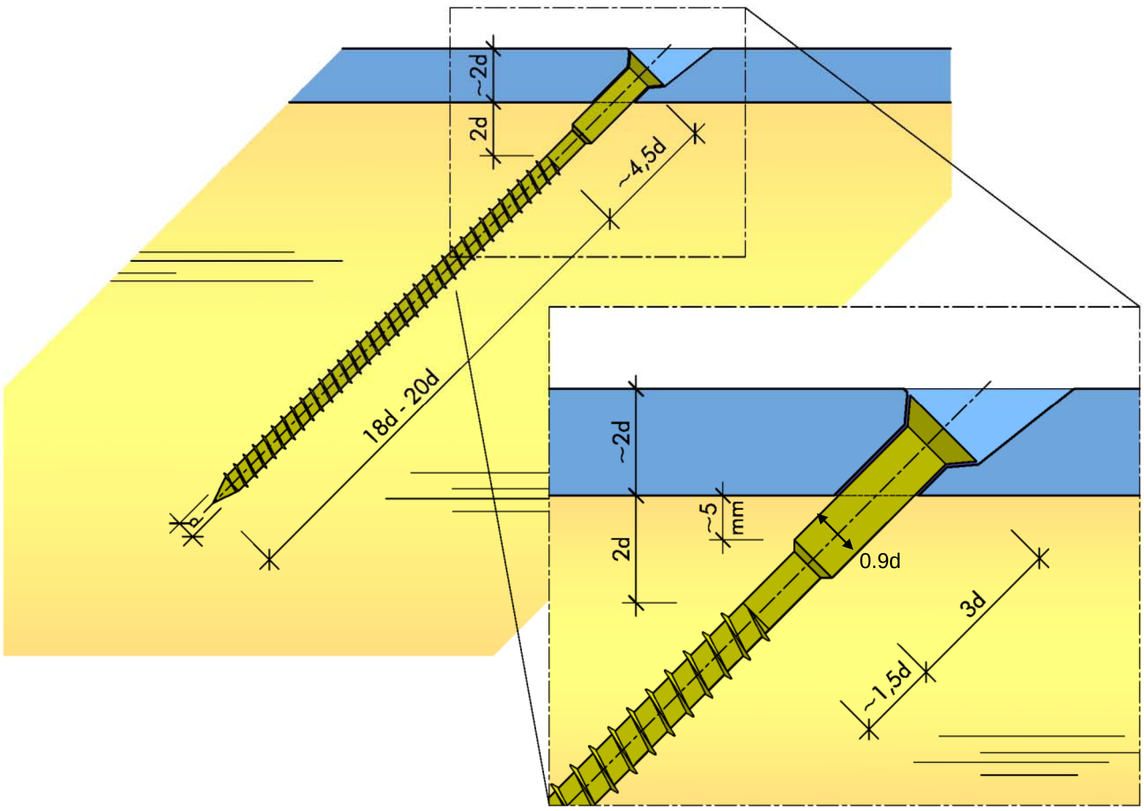

Figure 12: Optimized screw geometry for load carrying steel plate connections

Based on the research concerning moisture content and feedback from practical use it is proposed to limit screws to applications inside the serviceclass 1 and 2.

7 Acknowledgements

The research within the projects P06-II FV and 1.2.1_screw_long_term is financed by the competence centre holz.bau forschungs gmbh and performed in collaboration with the Institute for Timber Engineering and Wood Technology of the Graz University of Technology and several partners from Industry, notably the Association of the Austrian Wood Industries. The project is sponsored by the Federal ministry of Economics and Labour and the Styrian Business Promotion Agency Association.

Special thanks go to all the people carrying out the immense number of trials that amounted in this area. These are B. Heissenberger, for preparing all the specimens and cutting them up later; T. Kröpfl, G. Flatscher, U. Hübner, the Bacc-Gang (aka Tick, Trick & Track) and all the other Students participating in carrying out the trials and collection of additional information needed in the analysis.

Additional thanks go to the Würth Handelsges.m.b.H., especially Mr. G. Fessl – the company Würth was so kind to provide the screws used in this research project.

8 Reference

[1] EN 1382:1999 Timber structures. Test methods. Withdrawal capacity of timber fasteners.

[2] EN 1995-1-1:2004-11 Eurocode 5 - Design of timber structures - Part 1-1 General - Common rules and rules for buildings.

[3] EN 1995-1-1:2004-11:A1 Eurocode 5 - Design of timber structures - Part 1-1 General - Common rules and rules for buildings.

[4] DIN 1052:2008-12 Entwurf Berechnung und Bemessung von Holzbauwerken - Allgemeine Bemessungsregeln und Bemessungsregeln fuer den Hochbau.

[5] GAICH, A., RINGHOFER A., WALLNER R.: Ausziehwiderstand selbstbohrender Holzschrauben in Abhängigkeit der Eindrehlänge, Baccalaureate submitted at the Institute for Timber Engineering and Wood Technology, Graz University of Technology.

[7] COCKRELL, R., A Study of the Screw-Holding Properties of Wood. Technical Publication No. 44, New York State College of Forestry, Syracuse, 1933.

[8] SIA 265:2003 Timber Structures.

[9] NEWLIN J.A., GAHAGAN J.M., Lag-Screw Joints: Their Bahaviour and Design. USDA. Technical Bulletin BNo. 597, Wahsington DC, 1938.

[10] R Development Core Team (2009). R: A language and environment for statistical computing. R Foundation for Statistical Computing, Vienna, Austria. ISBN 3-900051-07-0, URL http://www.R-project.org.

CIB-W18/42-7-2

INTERNATIONAL COUNCIL FOR RESEARCH AND INNOVATION IN BUILDING AND CONSTRUCTION

WORKING COMMISSION W18 - TIMBER STRUCTURES

JOINTS WITH INCLINED SCREWS AND STEEL PLATES AS OUTER MEMBERS

H Krenn
G Schickhofer

Graz University of Technology

AUSTRIA

Presented by H Krenn

S. Aicher received confirmation of how the overlap distance of 4d was measured. He commented that the moment caused by the misalignment of the shear forces of the screws and the reaction would only level out if there are a large number of rows and the 4d overlap might not be appropriate if there are few screws. H. Krenn responded that there are different provisions in the paper for cases with few screws.

R. Crocetti commented that the splitting problem can be resolved by installing reinforcement perpendicular to grain. H. Krenn agrees.

P. Quenneville questioned why there is a split and H. Krenn explained via free body diagram.

Joints with inclined Screws and Steel Plates as outer Members

H. Krenn, G. Schickhofer
Graz University of Technology, Austria

1 Introduction

The load-carrying capacity of connections with dowel-type fasteners and steel plates as outer member of a single shear connection, determined on the basis of Johansen's yield theory, is limited by the embedding strength of the timber member and the bending capacity of the fastener. The use of self-tapping screws with continuous threads with the screw axis perpendicular to the axis of the timber member is very inefficient because of the limited diameter and the relatively small bending capacity of the screws.

The application of inclined screws that are arranged under an angle of 45° between screw axis and member axis was presented by Bejtka & Blass [1] as well as Kevarinmäki [6] in 2002. They showed that the load-carrying capacity and the stiffness of timber-to-timber connections in these joints is a lot higher compared to common shear connections due to the high withdrawal capacity of the screws. Going one step further, the additional use of steel plates with special holes, incorporating the geometry of the screw head, leads to a further increase in load-carrying capacity and stiffness of this steel-to-timber connection. The ultimate load of these joints is then mainly limited by the withdrawal capacity and the tensile capacity of the screw as well as the friction between the steel plate and the timber member. These parameters are relatively well known, whereas the influence of the number of fasteners in such a connection is in question.

This paper will present the results of tests of joints with inclined screws in glued laminated timber and steel plates as outer members. Some aspects of the influence of the number of fasteners will be discussed and a proposal for design rules for single-shear joints with inclined screws will be presented. General considerations about the joint geometry and the screw arrangement will conclude the publication.

2 Steel-to-timber joints with inclined screws

Timber-to-timber joints with fully- or partially-threaded self-tapping screws have been commonly used in modern timber construction over the last decade and the available publications on this topic contain sufficient mechanical models for the design of these joints. The economic advantage lies in their easy application and the designer benefits from the very high load-carrying capacity as well as from the high stiffness of these joints (as long as the screws are principally loaded axially). The wide field of application is ranging from secondary- main-beam connections over the reinforcement of existing structures (carried out as mechanically jointed beams or columns) to simple tension joints of two wood members (see [1] and [6]).

A few years ago, some engineers started to use steel plates as outer members of the above described tension joints. The angle between screw axis and grain direction of the wood was fixed with 45° due to the following considerations: The highest stiffness and considerable load-carrying capacity are reported for joints with screws under this angle. Furthermore the special hole geometry, incorporating the geometry of the screw head, requires a certain width of the steel plates, which lead to the same angle under economical considerations. Additionally, this type of connection can be applied to nodes of trusses, where the steel tension members of the truss are connected to the timber chords. Another application is the establishment of a rigid connection of columns at their base, which opens up more opportunities for timber construction. All of the above mentioned fields of application are capable of replacing common steel-to-timber connections with dowel-type fasteners. Figure 1 shows two examples in existing structures.

Figure 1: Examples of joints with inclined screws and steel plates as outer members

Figure 2 shows a schematic sketch of a steel-to-timber tension joint with inclined self-tapping screws with a single shear plane. This type of connection can either be executed as a symmetrical connection (tension joint) or as a non-symmetrical connection (truss node). The angle β is defined as the angle between screw axis and grain direction.

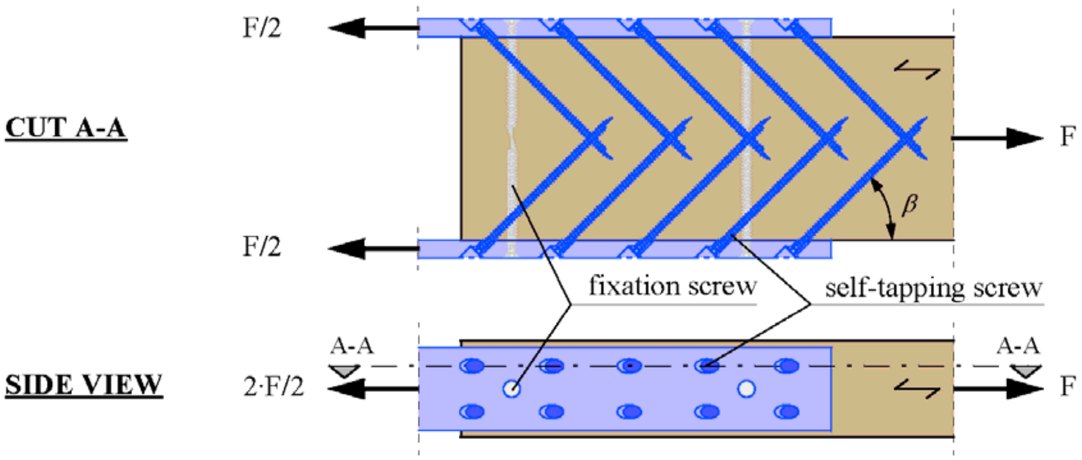

Figure 2: Symmetric steel-to-timber joint with inclined self-tapping screws

Steel-to-timber connections with inclined screws typically consist of three parts: the timber member, the outer steel members with a special hole geometry (see Figure 3) and the self tapping screws with a thread along the complete length of the screw and countersunk head. The assembling procedure usually starts with a fixation of the steel plate on the timber member with at least two screws, screwed in perpendicular to the grain, to prevent a sliding of the steel plate during the assembly. Subsequently, the screws responsible for the load transfer are preferably screwed-in in a symmetric pattern, to avoid deviations from the system line and guarantee a uniform loading of the screws. The screws are generally inserted without pre-drilling, but with the use of a template to roughly ensure the direction of the screw. The end and edge distances as well as the spacing between the screws shall satisfy the requirements in the technical approvals for the particular screw. It should be taken care, that the points of two opposite screws do not touch each other in the middle of the timber member.

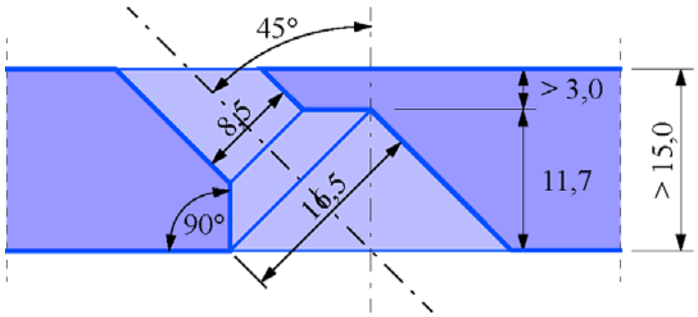

Figure 3: Detail of the hole geometry in the steel plates for an angle β of 45° (in mm)

The ultimate load of these joints is limited by the withdrawal capacity and the tensile capacity of the screw as well as the friction between the steel plate and the timber member. These parameters are relatively well-known, whereas the influence of the number of fasteners in such a connection is still in question. Due to the interest of some engineers specialised in timber engineering who were already applying this type of connection, a research programme in cooperation with the Association of the Austrian Wood Industries was started in 2006. The main topics were the investigation of the load-carrying behaviour incorporating the withdrawal resistance, the time-dependant behaviour (DOL) and an investigation of the influence of the number of screws in a connection (group effect – n_{ef}).

This paper is concentrating on the influence of the number of fasteners in a connection and will present the results of the tests as well as a mechanical model for the design of joints with inclined screws and outer steel plates.

3 Tests with steel-to-timber joints with inclined screws

In consequence of the bibliographical work, it became clear that neither a single scientific publication on steel-to-timber joints with inclined screws could be found, nor a test standard for testing this type of connection was (and still is) available. The next step was to develop a suitable test set-up and to investigate the influence parameters, which are obviously the withdrawal strength (which implicates the density of the wood in the first line) and the tensile capacity of the screws. The splitting of the timber member was the third important parameter, to be considered in the tests. As the focus of this work lied on the investigation of the group effect, no withdrawal tests were performed.

Based on the preliminary work, approximately 600 tension tests with joints in full size have been conducted in at the Institute of Timber Engineering and Wood Technology of the Graz University of Technology. Although several different test series were performed (described in [8]), only three representative test series will be discussed within this paper.

3.1 Materials and Methods

3.1.1 Timber

All tests were performed with glued laminated timber declared as strength class GL 28h built up with lamellas from Norway Spruce (Picea abies). After tension tests of the basic material (25 single boards were provided in addition to the gluelam beams) as well as the measurement of the density of the gluelam beams, it became clear, that the available material should be correctly classified as GL 24. Nevertheless, the 5%-value of the density – as governing influence parameter for connections – exceeded the required value of 410 kg/m³ in all test series.

Two different types of cross-sections were delivered: 284 beams with the dimension 2000 x 70 x 210 mm for the tests at an angle of 45° degrees between screw axis and grain direction (series 1) and 95 beams with the dimension 2000 x 70 x 150 mm for the tests at an angle of 30° (series 2). The test specimens for test series 3 were built up from remaining beams of series 1 and glued together and subsequently planed in the laboratory to a total cross section of 1000 x 200 x 200 mm. The test specimens were stored under constant climate (20/65) until the test.

For test series 2 with the partially threaded screws, density samples were taken in the area of the threaded part. Uncertainties may have occurred since it was just possible to measure the density for two opposing screws, due to the overlap of the screws in the beam axis. In the other test series no density samples were taken because of the failure mode head-tear off and because it was nearly impossible to cut specimens without damaging the circular saw with the remaining parts of the screws in the wood.

Test series	Screw	Test set-up	Dimensions of specimens (l x b x h) in [mm]	Type of joint
1	Type A1	T-S-T	2000 x 70 x 210	single row, β = 45°
2	Type A2	T-S-T	2000 x 70 x 150	single row, β = 30°
3	Type A1	S-T-S	1000 x 200 x 200	single and multiple row, β = 45°
T-S-T … timber-steel-timber (see Figure 5a) S-T-S … steel-timber-steel (see Figure 5b)				

Table 1: Overview of the dimensions of the test samples and the screws in use

3.1.2 Screws

Two types of self-tapping screws were used during the tests described in this paper, one with a thread along the whole length and one partially-threaded screw. All the screws used in the tests were equipped with a countersunk head. The spacing and the distances of the screws satisfied the requirements of the technical approvals.

Tension tests were carried out with three randomly selected screws from each package of screws used in test series 3 where the load-displacement-behaviour was recorded as well. The screws used in test series 1 and 2 were not specially tension tested.

The results of the tension tests showed good correspondence to the values given in the technical approval. The 5%-value of the ultimate capacity of the screws was 26055 N and exceeded the value given in the technical approval by 13 %. The coefficient of variation within the series of tested screws was 1.65 %.

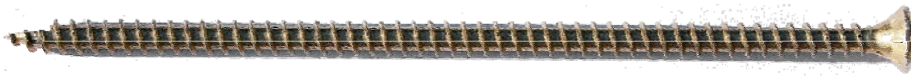

Type A1: 8 x 200 mm, fully threaded

Type A2: 8 x 200/84 mm, partially threaded

Figure 4: Screws used in the tests

3.1.3 Test set-up

All tests were performed as full size tension tests in the laboratory of the Institute with a displacement-controlled tension testing machine, whereas the timber members of test series 1 and 2 were directly fixed in the clamping device of the machine. For test series 3, a configuration with steel tension rods plus load sharing plates was developed and adjusted to the situation at the testing machine. A sketch and a photogrph of the two test set-ups are given in Figure 5.

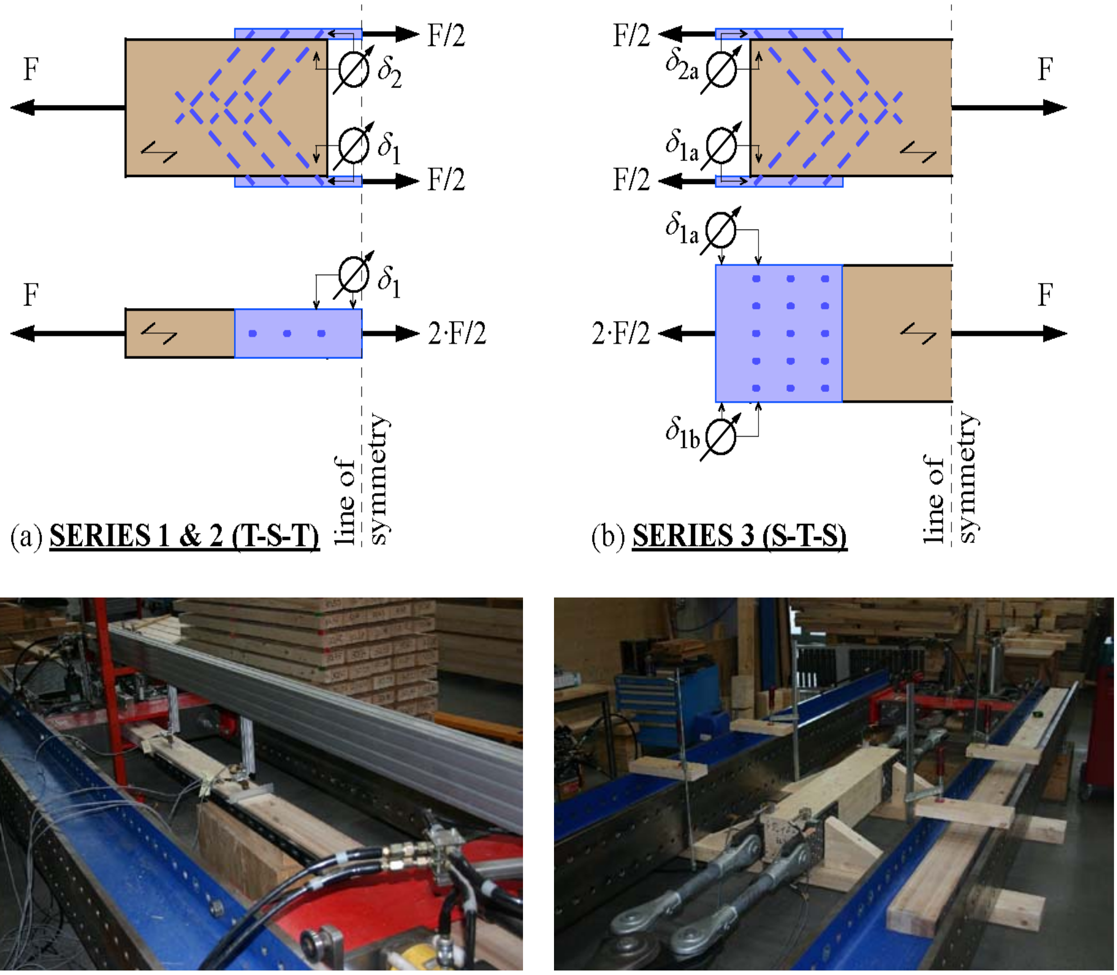

Figure 5: Test set-up for (a) single-row tests and (b) multiple-row tests

The following list contains more detailed information about the two test set-ups.

> **T-S-T:** Two joints were tested and due to the direct connection between the connections 1 and 2, both failed together. For this test series, only one timber member was exchanged after each test, the other part was made of ash-gluelam because of the high capacity and the stiffness. This part was fixed to each steel plate with eight screws. By this provision, many test specimens and even more screws have been saved and the required testing time was minimised.
>
> The drawback of the current configuration was that the load in each steel plate was not exactly identifiable (there might have been some differences in the stiffness of the ash-gluelam member). For the interpretation of the test results an equal load distribution among the two joints was assumed, as the aim of this study lied in the determination of the group effect and therefore the error should only be of relative magnitude.
>
> **S-T-S:** Four joints were tested simultaneously, and after the failure of one joint, it was reinforced with $n + 1$ screws, where n is the initial number of screws in the joints. Afterwards, the specimen was tested again, and this was repeated until all four joints failed.
>
> The benefit from this configuration lied in the ability to arrange the scews both in a row parallel to the grain and perpendicular to the grain. In addition, the test set-up was statically determined so the forces in each joint were known exactly (some tests were conducted with strain gauges applied to the steel rods for verification and the tests confirmed the assumptions).

The forces were measured with the integrated load cell of the tension testing machine and the slip between the steel plates and the timber member was measured with inductive displacement transducers (one per joint for the series T-S-T and two per joint for the series S-T-S). The measuring point on the surface of the timber member was located 20 mm from the end as well as from the edge of the timber that means before the first screw in the joint. At that point, the total force in the joint was completely within the steel member. The relative displacement δ includes the elongation of the steel plate, which is negligible in comparision to the slip of the joint.

3.2 Test results

In general, it has to be stated, that the maximum load was reached at a slip δ between the timber member and the steel plate of 3 to 4 mm, whereas the capacity dropped off to zero immediately in the cases of head tear off and/or splitting of the wood. In the cases of withdrawal of the screw, the displacement could be increased, without a further increase in the capacity. A slip of 15 mm according to EN 26891 was in no case observed.

In the following Tables 2 to 4, the results of the tests are presented. In the first row, the number of tests performed in each series is given, followed by the mean value of the capacity per side ($R_{v,test}$ / 2) and the coefficient of variation (over all failure modes!). In the grey shaded rows 4 and 5, the 5%-values (LND) over the number of screws and the effective number over the number of screws are displayed. Row 6 shows the failure modes (***w*** for withdrawal, ***h*** for head tear off, ***s*** for splitting and ***t*** for tension failure of the timber member). The mean values of the densitiy of the timber members can be found in the last row.

Number of screws n_{screw}	1	2	3	4	6	8 [1)]
n_{test}	20	20	20	20	20	5
$R_{v,test,mean}$ [kN]	24.85	48.59	69.74	92.63	135.41	163.51
COV [%]	5.8	6.9	6.4	5.8	7.0	5.1
$R_{v,test,05}$ / n_{screw} [kN]	22.18	21.20	20.44	20.66	19.65	18.00
n_{ef} / n_{screw} [2)]	1.00	0.94 / 1.00	1.08 / 0.94	1.00 / 1.01	- / 0.97	- / -
Failure mode (***w***/***h***/***s***/***t***)	14/6/0/0	7/13/0/0	9/11/0/0	4/10/6/0	0/9/9/2	0/0/1/4
ρ_{mean} [kg/m^3]	442	441	437	442	438	444

[1)] Not taken into account for the interpretation of the test results because of the governing failure mode ***t***.

[2)] First value: withdrawal; second value: head tear off

Table 2: Results of test series 1 (single row, $\beta = 45°$)

Number of screws n_{screw}	1	2	3	4	5	6	7
n_{test}	10	10	10	10	10	10	7
$R_{v,test,mean}$ [kN]	13.86	24.82	38.69	55.57	65.75	82.51	91.43
COV [%]	11.0	7.1	11.0	10.5	6.5	11.0	10.8
$R_{v,test,05}$ / n_{screw} [kN]	10.99	10.59	10.15	11.10	11.48	10.79	10.09
n_{ef} / n_{screw}	1.00	0.96	0.92	1.01	1.04	0.98	0.92
Failure mode (***w***/***h***/***s***/***t***)	10/0/0/0	10/0/0/0	10/0/0/0	10/0/0/0	10/0/0/0	9/0/0/1	7/0/0/0
ρ_{mean} [kg/m^3]	462	448	455	467	442	462	461

Table 3: Results of test series 2 (single row, $\beta = 30°$)

In test series 3, tests with a single row as well as multiple rows were performed up to a maximum of 8 screws per joint. The notation in the header of the following table e. g. 1 x 5 means one row with five screws in a row. No density is given for this series because all screws failed in head tear off.

Number of screws n_{screw}	1 x 1	1 x 3	1 x 5	2 x 1	3 x 1	5 x 1	2 x 4	4 x 2
n_{test}	92	32	20	40	32	19	12	12
$R_{v,test,mean}$ [kN]	27.79	85.17	138.35	56.36	83.82	139.80	218.16	219.76
COV [%]	7.4	5.3	4.2	5.0	5.5	5.1	4.1	4.9
$R_{v,test,05}$ / n_{screw} [kN]	24.36	25.67	25.47	25.67	25.17	25.32	24.93	24.76
n_{ef} / n_{screw}	1.00	1.05	1.05	1.05	1.03	1.04	1.02	1.02

Table 4: Results of test series 3 (single and multiple row, $\beta = 45°$)

As result of these tests, it can be concluded, that the influence of the number of fasteners on the capacity of the joints is rather small and therefore hard to identify. The variation lies between 5 and 10 % and usually decreases with the number of screws in the failure mode ***h***, which may be caused by the ductile behaviour of the screw in tension. In the failure mode ***w***, the variation is nearly constant (series 1 & 2). In general, the influence of the number of screws is larger for the failure mode **withdrawal** than for **tension failure** of the screw.

In Figure 6, the normalised test results are displayed (5%-values on the basis of a log-normal distribution incorporating the number of tests) and the current function of EN 1995-1-1 for axially loaded screws is given as reference. The solid green line indicates the proposal for the reduction factor n_{ef}. Orange symbols indicate a withdrawal failure, purple symbols a tension failure and the grey ones are test results from other test series not discussed in detail within this publication.

The values in the graph were calculated according to the following procedure: the 5%-value of tests with *n* screws was divided by the 5%-value of tests with one screw in one specific series, where all values were separated with respect to the failure mode.

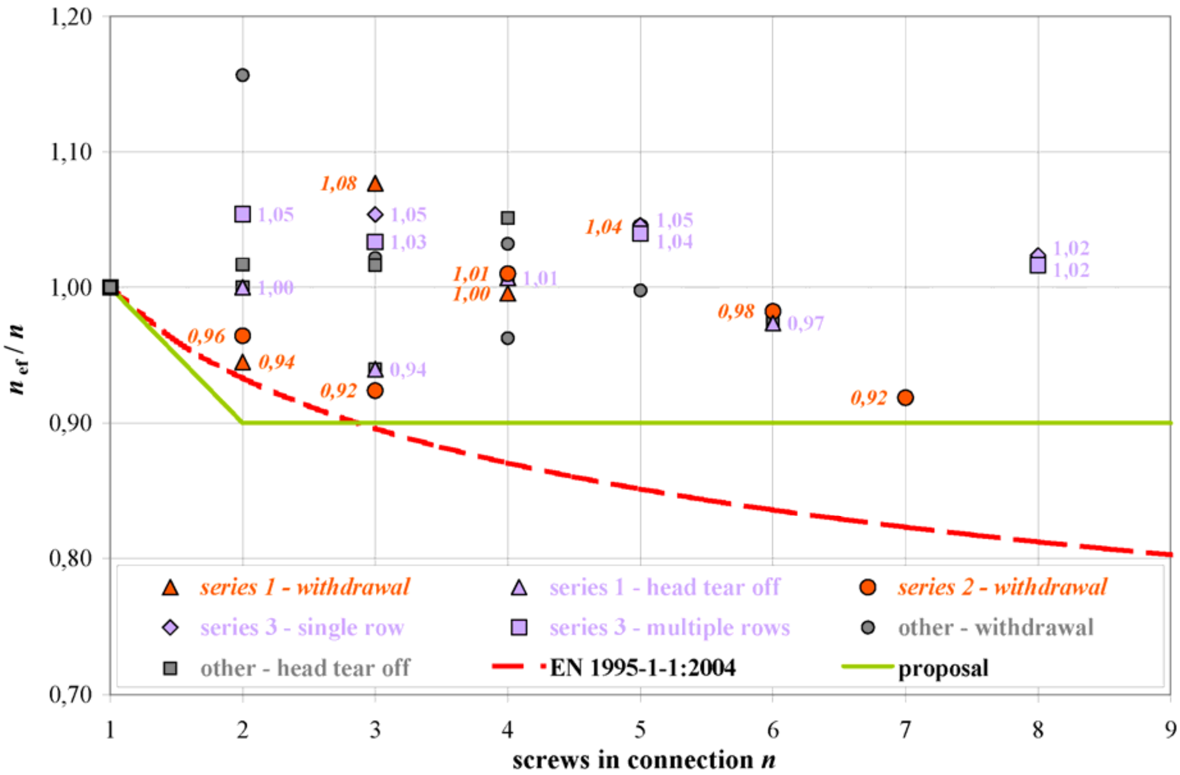

Figure 6: Influence of the number of screws on the capacity of the joint

The stiffness of the joints showed a differing result: Apart from the high variation (ranging from 84 % for one screw to 24 % for five screws) the evaluation between 10 % and 40 % of the maximum load showed a clear dependence of the stiffness from the number of screws in the joint. This behaviour is displayed in the subsequent Figure 7, incorporating the results from test series 1 and 3. Due to the generally very high stiffness in steel-to-timber joints with inclined screws, the influence of the number of fasteners on the stiffness in the connection may be disregarded, since the stiffness of a single 8 x 200 mm screw amounts to approximately 30 kN/mm. This value is rather large in comparison to dowel-type fasteners with a comparable diameter loaded perpendicular to their axis.

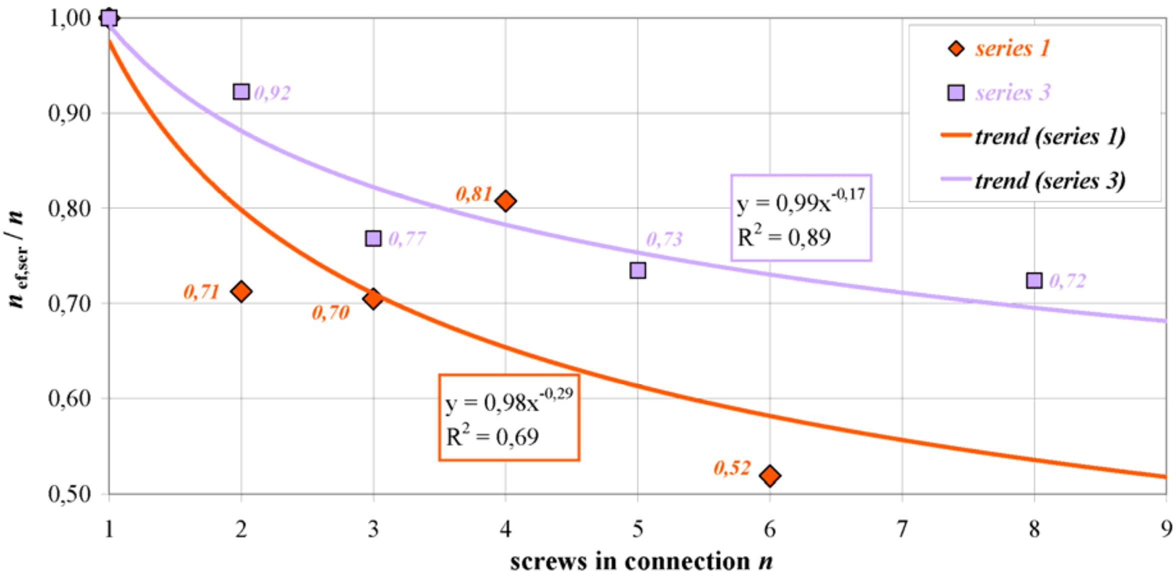

Figure 7: Influence of the number of screws on the stiffness of the joint

4 Design proposal for steel-to-timber joints with inclined screws

In fact, there are no design procedures for steel-to-timber joints with inclined screws available in the current standards. Bejtka & Blass [1] as well as Kevarinmäki [6] proposed design models for timber-to-timber joints with inclined screws, where the first one is an extension of the Johansen-Theory incorporating the withdrawal resistance of the screw and the friction between the surfaces. The second model omits the contribution of the dowel effect and therefore only consideres the axial forces in a simple truss-model.

4.1 Truss-model for the single screw

The above described truss-model turned out to be very suitable for the calculation of the capacity of steel-to-timber joints and could be the prefered design model because of its simplicity. In consequence of the small displacements in the shear-plane (δ_{max} = 3 - 4 mm, the dowel effect should be neglected. However, the friction resistance in the interface between the timber member and the steel plate should be taken into account since it is activated, as soon as the joint is loaded. For joints with stiff end plates and relatively stiff side members it should be regarded that the contact pressure in the interface between timber and steel is no more mandatory if the timber is subjected to moisture changes (shrinkage). Indeed, this may only be the case for a certain length, but the effect should be kept in mind.

The kinetic friction coefficient for timber-to-timber joints is given with 0.26 in [6] and 0.23 in [2]. The value in the current standards is 0.25 [4]. From a recalculation of test series 3 where all parameters were known (note the neglection of the dowel effect) except for the coefficient of friction, a value for μ of 0.32 could be found. Anyway, it is recommended to use μ = 0.25 for the calculation of the joint capacity.

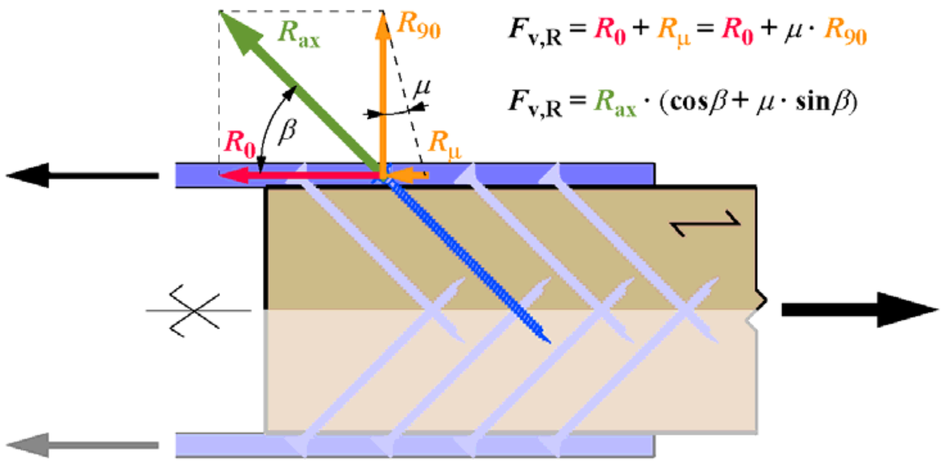

Figure 8: Truss-model for calculation of the capacity of steel-to-timber joints

A comparison of the test results with the results of a calculation of the load-carrying capacity $F_{v,R,05}$ (force in the shear plane) according to this proposal and the results of the tension tests of the screws (capacity of the screw: $R_{t,u,test,05}$ = 26055 N, coefficient of friction: $\mu = 0.25$) yields the following results:

For failure mode ***h*** in test series 1: $F_{v,R,05}$ / $R_{v,test,05}$ = 1,02

For test series 3 (failure mode ***h***): $F_{v,R,05}$ / $R_{v,test,05}$ = 0,95

These comparisons show good correlation and allow the assumption that the proposed truss-model is suitable for the design of steel-to-timber joints with inclined screws.

4.2 Structural detailing

The screws responsible for the load transfer shall be of the same type and size and all screws shall be placed under the same angle β between screw axis and grain direction. The screws shall be arranged in such a way, that no eccentricities to the system line occur. The length of the threaded part of the screw in the wood shall exceed 16 - 20 *d*, in order to induce the failure mode head tear off. The screwing moment shall be between 60 % and 80 % of the characteristic torsion capacity of the screw which can be ensured by the use of a torque wrench. The screw spacing and the end and edge distances shall satisfy the requirements of the technical approvals for the screws.

The ductility in steel-to-timber joints with inclined screws is generally limited and shall therefore be assigned to the steel parts in the connection (e. g. end plates). For the failure mode head tear off, a limited amount of load redistribution is possible because of the ductile behaviour of the screw in tension.

The points of the screws shall overlap at least 4 *d* in the system axis of the timber member (in a symmetrical joint) as shown in Figure 9a. Otherwise splitting along the axis will occur as a consequence of considerable tension stresses perpendicular to the grain. Figure 9b shows the utilisation ratio with respect to the stresses perpendicular to the grain resulting from a linear elastic finite element analysis with different loading configurations and missing overlap. The loads (shear, compression or tension force or bending moment) applied to the body for the analysis, would lead to a utilisation ratio equal to unity. All calculations are based on the characteristic stresses.

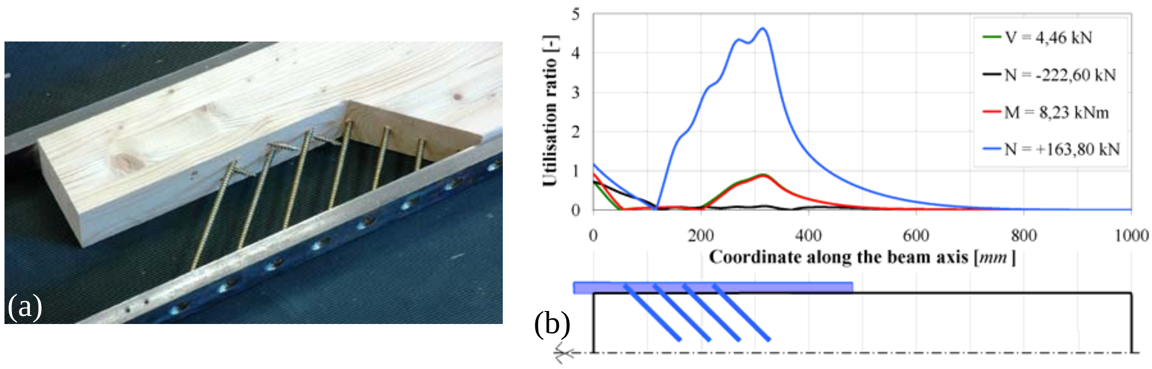

Figure 9: Overlap of the screws in the axis of the timber member (a) and the consequences of a missing overlap (b)

4.3 Effective number of fasteners

In general, the effective number of fasteners is influenced by many parameters (see [5]). It can be assumed that, if the geometrical requirements like spacing and distances as well as the slenderness of the fastener are fulfilled, the effective number of fasteners only depends on the number of fasteners in the joint, in particular, the number of fasteners in a row. This statement is valid at least for connections with dowel-type fasteners, but has to have some relevance to joints with inclined screws as well.

Since the current standards do not specifically cover joints with inclined screws, it is not quite clear, which value for n_{ef} is to be used. In consequence of the fact, that the screws are mainly loaded axially, it can be argued that the sections dealing with axially loaded screws in the standards are to be applied. In the relevant clause of Eurocode 5 [4], a value for $n_{ef} = n^{0.9}$ is given, in the German Standard DIN 1052 [3], no reduction of the number of screws is required. The current practice of timber engineers, who are familiar with this type of joint, is to reduce the number of screws by approximately 10 - 15 % with a maximum of about 15 screws in a row.

From the tests carried out in this study it can be concluded, that a reduction with a global factor of 0.9 is sufficient and on the safe side for the calculation of the capacity of the joint. If the tension failure of the screw (head tear off) can be ensured, this factor approaches the value 1.0 (on the safe side) and can even be slightly higher, up to a value of 1.05 (test series 3). With utmost probability it can be assumed that this increase arises due to the ductile behaviour of the screws in tension (system effect). For design in the serviceability limit state, a value of n to the power of 0.8 was found, since the influence of the number of fasteners on the stiffness of the joint was clearer to see. In fact, it should be questioned, if it is necessary to account for this influence, since the stiffness of a single screw (in the shear plane) amounts to 30 kN/mm, a considerably higher value than for dowel-type fasteners.

5 Conlusions

The test results of this study showed that steel-to-timber joints with inclined self-tapping screws yield a very high load-carrying capacity and an even more impressive stiffness. A simple truss-model, incorporating the axial resistance of the screw and the friction in the interface between timber member and steel plate, is sufficient for reliable design of these joints (although the dowel effect could be observed to some extent). In the ultimate limit state, the effective number of screws shall be taken into account with $n_{ef} = 0.9 \cdot n \cdot m$ with the number of screws n in a row and the number of rows m. In the serviceability limit state, the group effect might be accounted for with $n_{ef,ser} = (n \cdot m)^{0.8}$. All of these results are only valid, if the personnel for the fabrication of these joints is well trained and the deviations from the plan are minimised.

For structural detailing, the geometry of the steel members (e. g. rigid end plate) shall be taken into account. Furthermore an overlap of the screws in the axis of the timber member of at least 4 d is essential for symmetrical tension joints – otherwise a tension failure perpendicular to the grain could occur. In addition, it is recommended to choose an embedment length of the threaded part in the wood with at least 16 - 20 d, so the withdrawal capacity exceeds the tensile capacity of the screw sufficiently, and the screws fail in tension. The width of the steel plates depends on the applied screws, in particular on the head diameter of the screws with a countersunk head. For a screw diameter of 8 mm, a width of the steel plate of 15 mm shall be the minimum.

6 Acknowledgements

The research work within this project is financed by the competence centre holz.bau forschungs gmbh and performed in collaboration with the Institute for Timber Engineering and Wood Technology of the Graz University of Technology and the partners from industry, the Association of the Austrian Wood Industries and Holzcluster Steiermark GmbH. The project is fostered through the funds of the Federal Ministry of Economics and Labour, the Federal Ministry of Transport, Innovation and Technology, the Styrian Business Promotion Agency Association and the province of Styria.

7 References

[1] BEJTKA, I., BLASS, H.J. (2002): Joints with inclined Screws. In: Proceedings CIB-W18/35-7-5. Kyoto, 2002.

[2] BLASS, H.J., BEJTKA, I. (2001): Screws with continuous threads in timber connections. In: Proceedings PRO 22: International RILEM Symposium on Joints in Timber Structures. Stuttgart, pp.193-201, 2001.

[3] DIN 1052:2008 Design of timber structures – General rules and rules for buildings.

[4] EN 1995-1-1:2004 Eurocode 5 – Design of timber structures – Part 1-1: General – Common rules and rules for buildings.

[5] JORISSEN, A. (1998): Double shear timber connections with dowel type fasteners. Dissertation, TU Delft, 1998.

[6] KEVARINMÄKI, A. (2002): Joints with inclined Screws. In: Proceedings CIB-W18/35-7-4. Kyoto, 2002.

[7] KRENN, H., SCHICKHOFER, G. (2007): Traglast von auf Zug beanspruchten Schraubenverbindungen mit Stahlblechen. In: Tagungsband 6. Grazer Holzbau-Fachtagung ´07. TU Graz, 2007 (in German).

[8] KRENN, H. (2009): Selbstbohrende Holzschrauben in hoch beanspruchten Bereichen. Research Report, holz.bau forschungs gmbh, Graz, 2009 (in German).

CIB-W18/42-7-3

INTERNATIONAL COUNCIL FOR RESEARCH AND INNOVATION IN BUILDING AND CONSTRUCTION

WORKING COMMISSION W18 - TIMBER STRUCTURES

MODELS FOR THE CALCULATION OF THE WITHDRAWAL CAPACITY OF SELF-TAPPING SCREWS

M Frese
H J Blaß

Lehrstuhl für Ingenieurholzbau und Baukonstruktionen
Universität Karlsruhe (TH)

GERMANY

Presented by M Frese

J.W. G. van de Kuilen received confirmation that the pitch was not included because it did not have significant effect.
G Schickhofer questioned whether there is a difference in performance between different producers. M. Frese responded that the main aim of the paper is to create a model to explain the behaviour independently of the producer. H.J. Blass stated that 15 to 20 producers were considered in Universität Karlsruhe and it seems there are no major differences between producers.
G Schickhofer commented that the model indicates that the code values are too conservative. He asked whether the model will be used. H.J. Blass agreed that the model can be used. In some cases there is a 100% increase in characteristic values.

Models for the calculation of the withdrawal capacity of self-tapping screws

M. Frese and H.J. Blaß
Lehrstuhl für Ingenieurholzbau und Baukonstruktionen
Universität Karlsruhe (TH)

Abstract Equations to calculate the withdrawal capacity of self-tapping screws, arranged in softwood, were determined. Based on results of 1850 withdrawal tests and by means of a regression analysis one equation for the withdrawal resistance and two further equations for the withdrawal parameter (resistance over nominal screw diameter and penetration depth) were derived. Nominal screw diameter, penetration depth and characteristic density of the softwood used are the independent variables in the equations, which are valid for an angle from 45° to 90° between the screw axis and the grain.
The equation for the withdrawal resistance delivers, also in comparison with code rules, the most favourable values. It enables, more accurately than until now, the estimation of the withdrawal resistance for wood screws with geometrical properties similar to those of the screws used for the tests. Hence, the benefit of this study is the reduction in testing, which is currently necessary for technical approvals.

1 Introduction

1.1 Preface

The application of wood screws (abbr. „screws“) has increased in the recent years, also because of the fast and successful further development of self-tapping screws. Due to the preferred insertion of screws at an angle α to grain (Fig. 1), the focus is on the load-carrying behaviour of screws loaded in tension, and less on the load-carrying capacity of screws loaded perpendicular to their axis. For load-bearing wood connections standard screws or screws approved by national technical approval are used: Standard screws are specified in DIN 96, DIN 97 or DIN 571 and have threads and screw tips according DIN 7998. Screws with national technical approval are usually self-tapping short or full threaded screws, with a length up to 600 mm and nominal diameters up to 14 mm. The variety of self-tapping screws brought about quite a number of technical approvals.

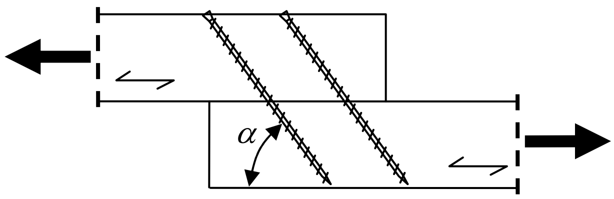

Fig. 1 Self-tapping screws inserted at an angle α to grain and loaded in tension

DIN 1052 and EN 1995-1-1 include various equations and methods for the calculation of the characteristic values of the withdrawal resistance $R_{ax,k}$. This value describes the calculational resistance concerning withdrawal. According DIN 1052 a screw has to be classified into one of the three load-carrying capacity categories. By this classification the characteristic value of the withdrawal parameter (in DIN 1052: $f_{1,k}$) can be calculated and afterwards the withdrawal resistance of the screws. From an experimental point of view the withdrawal parameter is a maximal withdrawal strength related to penetration depth and nominal diameter. In EN 1995-1-1 the characteristic value of the withdrawal parameter (in it $f_{ax,k}$) can be calculated directly or in specific cases it can be determined by withdrawal tests according EN 14592. Then the withdrawal resistance can be determined. Up to present both methods in DIN 1052 resp. EN 1995-1-1 have required extensive testing. Hence the aim of this study was to determine the withdrawal resistance resp. withdrawal parameter of self-tapping screws from various manufacturers by means of calculation models. The advantage of the equations is a reduction in testing of the screws concerning their withdrawal capacity. Due to a meanwhile quite extensive data collection of test results, obtained from approval procedures or research, it seemed useful to determine new models for the withdrawal resistance directly, or indirectly by means of the withdrawal parameter. Thus a new calculation model would refer to current test results and would be of high universal validity, as screws from various manufacturers are included in the data collection.

The following study describes all essential steps of modeling to the equations. The equations (or models) depend on the penetration depth ℓ_{ef}, the nominal diameter d and the characteristic density ρ_k (of a selected softwood strength class according EN 338). They are applicable for an angle α between 45° and 90°. Finally, it will be shown, that currently valid equations can often have very differing results when it comes to building practice. Therefore the study also aims at optimizing the calculation of the withdrawal capacity.

1.2 Technical standard

In comparison with standard screws, self-tapping screws with national technical approval have the following advantages or qualities:

1. The d_k/d-relation is lower, on average about 0.65 (Fig. 2), for screws with threads according DIN 7998 on average 0.70. The special shape of the thread region allows a high load transmission into the surrounding wood.

2. Generally they are hardened after rolling the thread. Hardening increases the yield moment, the torsional strength and the tensile bearing capacity. The stiffness of the connection increases, the danger of "slipping" decreases. Therefore the holes do not have to be pre-drilled.

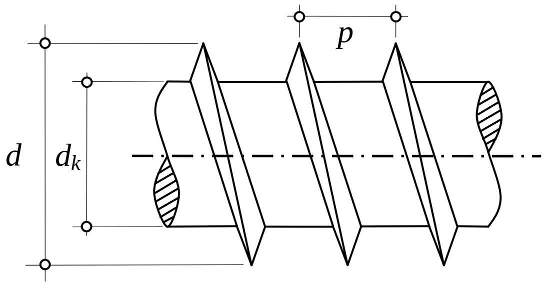

Fig. 2 Detail of a screw thread: denotations nominal diameter d (= nominal screw size), thread-root diameter d_k and thread pitch p

The equations (from code rules and publications**)** to calculate the characteristic withdrawal resistance $R_{ax,k}$ (in N) are briefly presented below; the resistance against head pull-through is excluded:

$$R_{ax,k} = \frac{f_{1,k} \cdot d \cdot \ell_{ef}}{\sin^2 \alpha + \frac{4}{3} \cdot \cos^2 \alpha} \qquad (45° \le \alpha \le 90°)\,, \tag{1}$$

$$R_{ax,k} = \frac{0.52 \cdot d^{0,5} \cdot \ell_{ef}^{0,9} \cdot \rho_k^{0,8}}{1.2 \cdot \cos^2 \alpha + \sin^2 \alpha} \qquad (0° \le \alpha \le 90°) \tag{2}$$

$$R_{ax,k} = \frac{n_{ef} \cdot f_{ax,k} \cdot d \cdot \ell_{ef} \cdot k_d}{1.2 \cdot \cos^2 \alpha + \sin^2 \alpha} \qquad \begin{pmatrix} 6\,\mathrm{mm} \le d \le 12\,\mathrm{mm} \\ 0.60 \le d_k / d \le 0.75 \\ \alpha \ge 30° \end{pmatrix} \tag{3}$$

Insert $f_{1,k}$ and $f_{ax,k}$ in MPa, d and ℓ_{ef} in mm and ρ_k in kg/m³.
Eq. (1) according DIN 1052 indicates the characteristic withdrawal resistance $R_{ax,k}$ depending on the characteristic withdrawal parameter $f_{1,k}$, the nominal diameter d, the penetration depth ℓ_{ef} and the angle α. The variable $f_{1,k}$ (in Mpa), depending on the load-carrying category (TFK), is calculated by the characteristic density:

$$\begin{aligned} &\mathrm{TFK\,1:}\ f_{1,k} = 60 \cdot 10^{-6} \cdot \rho_k^2 \\ &\mathrm{TFK\,2:}\ f_{1,k} = 70 \cdot 10^{-6} \cdot \rho_k^2\ . \\ &\mathrm{TFK\,3:}\ f_{1,k} = 80 \cdot 10^{-6} \cdot \rho_k^2 \end{aligned}$$

The characteristic density must be inserted in kg/m³, but maximally 500 kg/m³. The screws are tested according to EN 1382 resp. following DIN 1052, appendix C, and classified into load-carrying categories.
Blaß et al. 2006 analysed about 800 withdrawal tests. They suggest Eq. (2) to calculate the characteristic withdrawal resistance. The regulation in EN 1995-1-1 was based on this equation. In it the withdrawal resistance is calculated with Eq. (3). Additionally the number of screws n of an axially loaded group of screws is included. For screws with nominal diameters between 6 and 8 mm the withdrawal capacity is reduced with the non-dimensional factor k_d.
The variables n_{ef}, $f_{ax,k}$ (in MPa) und k_d in (3) are calculated by

$$n_{ef} = n^{0.9}\,, \qquad f_{ax,k} = 0.52 \cdot d^{-0.5} \cdot \ell_{ef}^{-0.1} \cdot \rho_k^{0.8}\,, \qquad k_d = \min \begin{cases} d/8 \\ 1 \end{cases}. \tag{4}$$

The unit of d and ℓ_{ef} is mm, of ρ_k kg/m³. For d_k/d-relations out of [0.60;0.75] there is a variation in EN 1995-1-1 differing from Eq. (3). It is valid for an experimentally obtained withdrawal parameter $f_{ax,k}$.

2 Modeling

2.1 Data collection and database

The data collection of the Lehrstuhl für Ingenieurholzbau und Baukonstruktionen is based on more than 2400 withdrawal tests (Fig. 3). Observations to the following parameters – not always complete – are included: 1. angle α, 2. nominal diameter d, 3. thread-root diameter d_k, 4. thread pitch p, 5. penetration depth ℓ_{ef}, 6. density ρ and 7. withdrawal resistance R_{ax}.

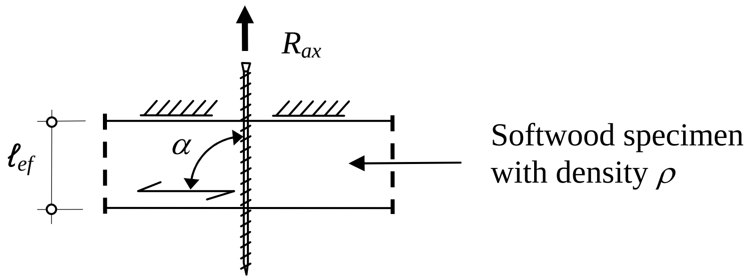

Fig. 3 Screw withdrawal test, schematic

A preliminary multiple regression analysis (from R_{ax} on the parameters 1 to 6) showed, that the thread pitch p has no major influence on the withdrawal resistance. For the screws tested, p is between 2 and 8 mm, on average 4.4 mm. Therefore p was not included in the data for the models. The data only include observations on angles greater than/equal to 45°, also to take into consideration the different load-carrying mechanism between screws inserted parallel to the grain and screws with angles between 45° und 90°. Based on the two conditions, of the 2400 datasets a total of 1847, with the same number of observations per parameter, are available. The statistics of the parameters recorded, of the d_k/d-relation and of the withdrawal parameter are shown in Table 1. Based on these data any of the following statistical analyses are performed.

Table 1 Statistics of the parameters recorded

Line	Explanatory variable		N	$\bar{x}$	s	Min	Max
1	α	°	1847	75	19.1	45	90
2	d	mm		8	2.34	4.00	14.0
3	d_k	mm		5.2	1.53	2.56	9.70
4	ℓ_{ef}	mm		61	25.5	18.8	140
5	ρ	kg/m³		431	39.7	325	602
6	d_k/d	-		0.65	0.0426	0.559	0.700
	Response variable						
7	R_{ax}	N	1847	9150	5093	1533	32100
8	$f_{ax} = R_{ax}/(d \cdot \ell_{ef})$	MPa		19	3.44	8.84	33.6

In Fig. 4 the dependencies between the values of those parameters are shown, which are most relevant as explanatory variable in the following regression equations. The corresponding coefficients of determination (r^2) are shown on the bottom right in the diagrams. The variance inflation factors (VIF) in Table 2 are the results, if for any of the explanatory variables a regression on the other explanatory variables is undertaken. The VIFs are clearly below 10. Hence it is proven to a large extent, that there is no collinearity (Chatterjee and Price 1995) among the values of the parameters nominal diameter, penetration depth and softwood density.

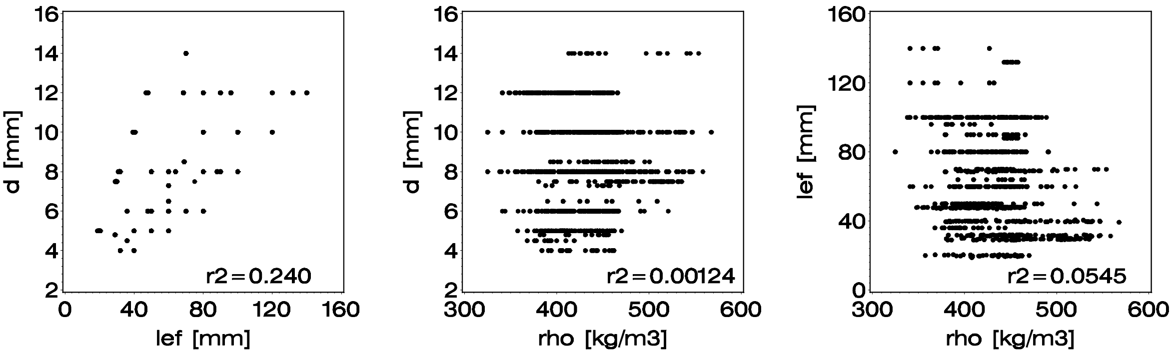

Fig. 4 Scatter plots: dependencies between the values of the parameters nominal diameter, softwood density and penetration depth

Table 2 Variance inflation factors (VIF) showing that there is no collinearity among the crucial explanatory variables

Regression from	N	r^2	$VIF=1/(1-r^2)$
d on ℓ_{ef} and ρ	1847	0.264	1.36
ℓ_{ef} on d and ρ		0.303	1.43
ρ on d and ℓ_{ef}		0.084	1.09

2.2 Identification of statistically relevant models

Basis function is a rational function of multiple variables of second order. Independent terms are not only the variables in Table 1, ll. one to six, linear and quadratic, but also their cross products, without product $d \cdot d_k/d$, though. Altogether they are 26 terms. Regression from the logarithmized withdrawal resistance $\ln(R_{ax})$, respectively from the logarithmized withdrawal parameter $\ln(f_{ax})$ on these terms, in which the number of terms in the model was increased from 1 to 25, resulted in Table 3. It shows, in extracts, for one to three terms in the model the three combinations with the highest coefficient of determination, sorted according to quantity. For four of the terms it shows the best combination, respectively. The models selected for further observations are marked with arrows. As expected, the nominal diameter d and the thread-root diameter d_k are almost equal as explanatory variable. There is no indication, that angle α is relevant in the value range [45°;90°] in a calculation model with a limited number of terms. The last line of Table 3 shows the highest coefficients of determination for models with 25 terms. It becomes obvious, that the limitation to three resp. two terms in the model is mechanically logical and suitable for practical application. Logarithmizing of the regressand R_{ax} resp. f_{ax} eliminates- to be shown below – the existing non-constant variance of errors (Chatterjee and Price 1995).

Table 3 Model selection, number of observations used 1847

	Regression from ln(R_{ax})		Regression from ln(f_{ax})	
Number of terms in the model	r²	Selected terms	r²	Selected terms
1	0.825 0.821 0.811	$\ell_{ef} \cdot \rho$ $d_k \cdot \ell_{ef}$ $d \cdot \ell_{ef}$	0.263 0.249 0.241	d d^2 $d_k \cdot \ell_{ef}$
2	0.920 0.916 0.913	$d, \ell_{ef} \cdot \rho$ $\ell_{ef}, d \cdot \rho$ $d_k, \ell_{ef} \cdot \rho$	$\rightarrow$ 0.458 0.455 0.452	d, ρ $\rho, d \cdot \rho$ d, ρ^2
3	$\rightarrow$ 0.942 0.937 0.935	$\ell_{ef}, d \cdot \rho, \ell_{ef}^2$ $\ell_{ef}, d_k \cdot \rho, \ell_{ef}^2$ $\ell_{ef}, d \cdot \ell_{ef}, d \cdot \rho$	0.481 0.475 0.475	d, ρ, d^2 d, d^2, ρ^2 d_k, ρ, d_k^2
4	0.945	$\ell_{ef}, d, \rho, \ell_{ef}^2$	0.490	$d, \rho, \alpha \cdot \rho, d^2$
25	0.954	all terms[a]	0.555	all terms[b]
[a]without d_k resp. [b]without $(d_k)^2$ due to the close linear relation between d_k and d				

2.2.1 Regression from ln(R_{ax})

By excluding observations with standard errors e out of [-3;3] the number of observations was reduced from 1847 to 1838 after a preliminary regression from ln(R_{ax}) on ℓ_{ef}, $d \cdot \rho$ and $(\ell_{ef})^2$. By means of the criterion for exclusion $|e| > 3$ (Hartung et al. 2005) some measured values, which were caused e.g. by irregularities in the test, should be excluded. This results in a slightly lower distribution of errors.

Eq. (5) specifies the functional correlation for the final regression. The coefficient of determination is 0.945, the standard deviation of errors 0.1365. Fig. 5 shows observed values dependent on predicted values according to Eq. (5): Fig. 5a) shows logarithmic and b) true values. Their dispersion follows a normal distribution between the depicted 99% confidence limits. With it the conditions for the application of the least squares method to estimate the coefficient in Eq. (5) are given. Fig. 5b) shows the non-constant variance of the true values. The points are distributed in a funnel-formed way around the regression straight line. Thus logarithmizing is a suitable method to stabilize the variance. The individual density is explanatory variable in Eq. (5). Consequently the equation is suitable for specific cases, in which the density of the wood is obtained by measurement to estimate R_{ax} individually.

$$\ln(R_{ax}) = 6.739 + 0.03257 \cdot \ell_{ef} + 2.148 \cdot 10^{-4} \cdot d \cdot \rho - 1.171 \cdot 10^{-4} \cdot \ell_{lef}^2 + e \qquad (5)$$

$$n = 1838 \qquad \mathrm{r}^2 = 0.945 \qquad e : \mathrm{N}(0; 0.1365)$$

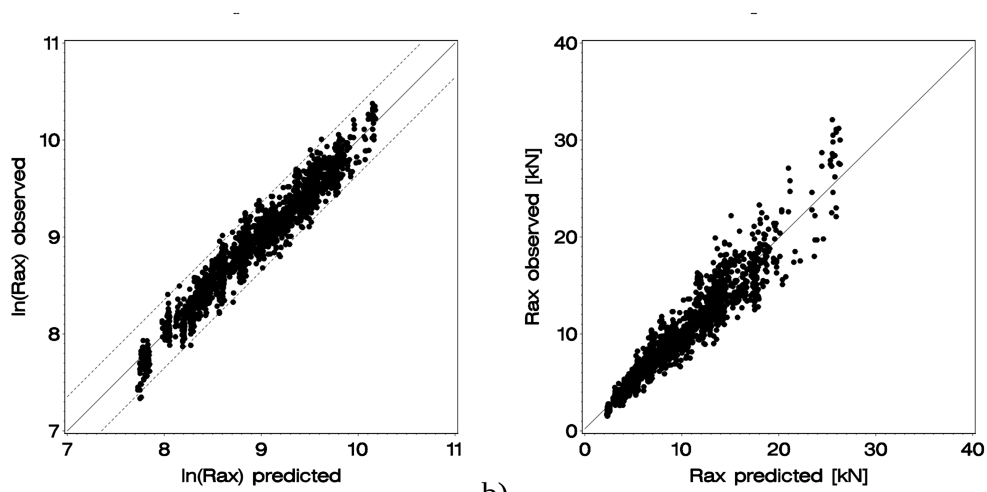

a) b)

Fig. 5 Regression Eq. (5): experimental and predicted value for the axial withdrawal resistance; logarithmic a) and true values b)

2.2.2 Regression from ln(f_{ax})

Eq. (6) specifies the functional correlation of the final regression from the logarithmized withdrawal parameter ln(f_{ax}) on d and ρ. The reduced number of observations 1839 and Fig. 6 can be explained analogically to the derivation of Eq. (5). A constant variance of errors e, which follows a normal distribution, is only valid with limitations: For lower predicted values the distribution is somewhat less than for higher ones. Thus the basic condition of the constant variance of errors for the least squares method is not fulfilled. The coefficient of determination 0.466 might be somewhat distorted. In this model the individual density is explanatory variable.

$$\ln(f_{ax}) = 2.359 - 0.04172 \cdot d + 2.039 \cdot 10^{-3} \cdot \rho + e \qquad (6)$$

$n = 1839 \qquad \mathrm{r}^2 = 0.466 \qquad e : \mathrm{N}(0; 0.1331)$

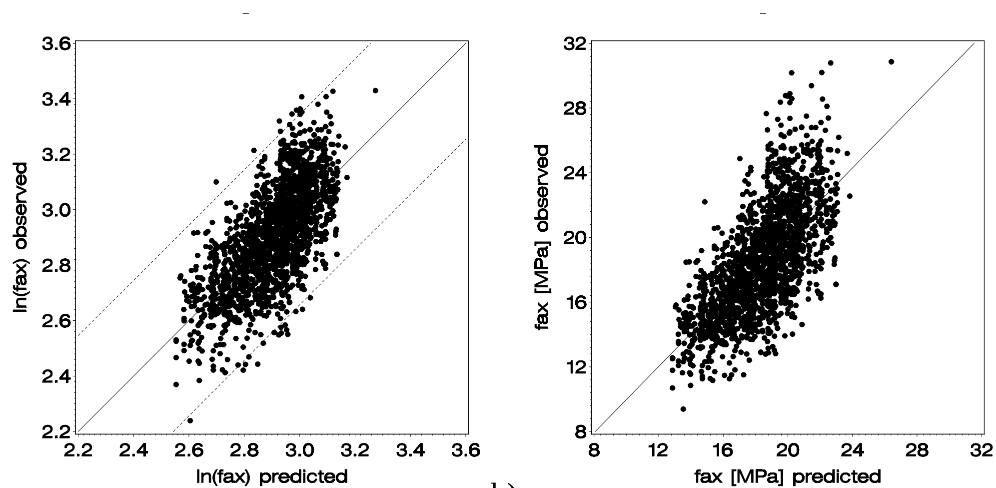

a) b)

Fig. 6 Regression Eq. (6): experimental and predicted value for the axial withdrawal parameter; logarithmic a) and true values b)

2.3 Models depending on characteristic density

In both regression Eqs. (5) and (6) the individual density is the explanatory variable, based on about 12% wood moisture content. The error *e* follows a normal distribution. For practical applications like design, a dependence on the characteristic density ρ_k is required, though. Both equations are suitable – due to a largely constant variance of errors – to determine the withdrawal resistance resp. the withdrawal parameter empirically. By means of simulated density values for selected strength classes and simulated errors, the dependence on the characteristic density may be determined numerically. For this purpose with both models, (5) and (6), 42 d-ℓ_{ef}-combinations were tested for the six strength classes C14, C18, C24, C30, C40 and C50 according EN 338. The 6 x 7 combinations include the elements according definition (7). That means altogether 252 tests per model. In every test 1000 R_{ax}- resp. f_{ax}-values were simulated by means of density values resp. errors, which follow a normal distribution. Classifications (8) and (9) show normal distributions. Naturally with model (6) testing various nominal diameters would be sufficient, as the penetration depth ℓ_{ef} in model (6) is no explanatory variable. The application of the same 42 combinations only results in a multiplication of the simulated values per nominal diameter. The result is not falsified, though.

$$\begin{aligned} d &= \{4, 6, 8, 10, 12, 14\,[\text{mm}]\} \\ \ell_{ef} &= \{20, 40, 60, 80, 100, 120, 140\,[\text{mm}]\} \end{aligned} \tag{7}$$

$$\begin{array}{ll} \text{C14} & \rho : \text{N}(350; 36.4) \\ \text{C18} & \rho : \text{N}(380; 36.4) \\ \text{C24} & \rho : \text{N}(420; 42.4) \\ \text{C30} & \rho : \text{N}(460; 48.5) \\ \text{C40} & \rho : \text{N}(500; 48.5) \\ \text{C50} & \rho : \text{N}(550; 54.5) \end{array} \tag{8}$$

$$\begin{array}{ll} R_{ax,k} & e : \text{N}(0; 0.1365) \\ f_{ax,k} & e : \text{N}(0; 0.1331) \end{array} \tag{9}$$

Based on the 1000 simulated individual values the characteristic value, $R_{ax,k}$ and $f_{ax,k}$, was determined, respectively. Fig. 7 shows exemplarily the distribution of the simulated individual values $R_{ax,k}$ and $f_{ax,k}$ for strength class C24, for a nominal diameter of 8 mm and a penetration depth of 60 mm (only required for $R_{ax,k}$). As expected, the distribution in Fig. 7a) and b) follows a normal distribution. Altogether 252 simulated characteristic values of the withdrawal resistance $R_{ax,k}$ and of the withdrawal parameter $f_{ax,k}$ for various d-ℓ_{ef}-combinations and various strength classes per model were available. A new regression from the simulated characteristic values on the variables in Eqs. (5) and (6), now with ρ_k, eliminates the error terms and results in the favoured dependence on the characteristic density. The withdrawal resistance is given by:

$$\boxed{\ln(R_{ax,k}) = 6.54 + \ell_{ef} \cdot (0.03265 - 1.173 \cdot 10^{-4} \cdot \ell_{ef}) + 2.35 \cdot 10^{-4} \cdot d \cdot \rho_k} \tag{10}$$

and the withdrawal parameter accordingly:

$$\boxed{\ln(f_{ax,k}) = 2.182 - 0.04175 \cdot d + 2.21 \cdot 10^{-3} \cdot \rho_k}. \tag{11}$$

Fig. 8 shows the correlation between the simulated characteristic values $R_{ax,k}$ resp. $f_{ax,k}$ and the predicted values according Eqs. (10) and (11). The simulated characteristic values can be determined almost perfectly by the two equations. The coefficients of determination are 1.000 resp. 0.997. This results in the possibility to estimate the characteristic withdrawal resistance resp. withdrawal parameter for any strength class.

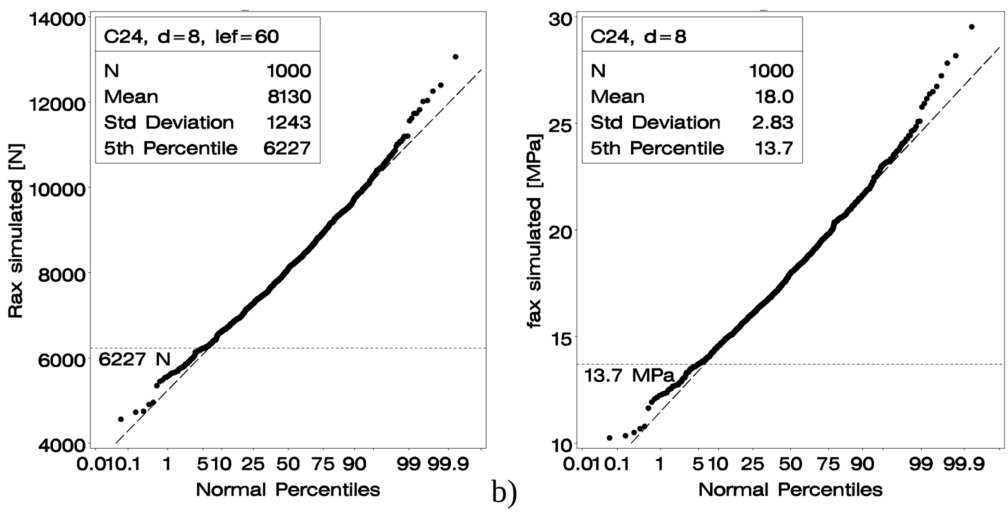

a) b)

Fig. 7 Simulation results for R_{ax} a) and f_{ax} b); the characteristic value $R_{ax,k}$ and $f_{ax,k}$, respectively, can be exemplarily determined from the distributions. Values refer to strength class C24 and d-ℓ_{ef} -combination 8/60 and 8, respectively.

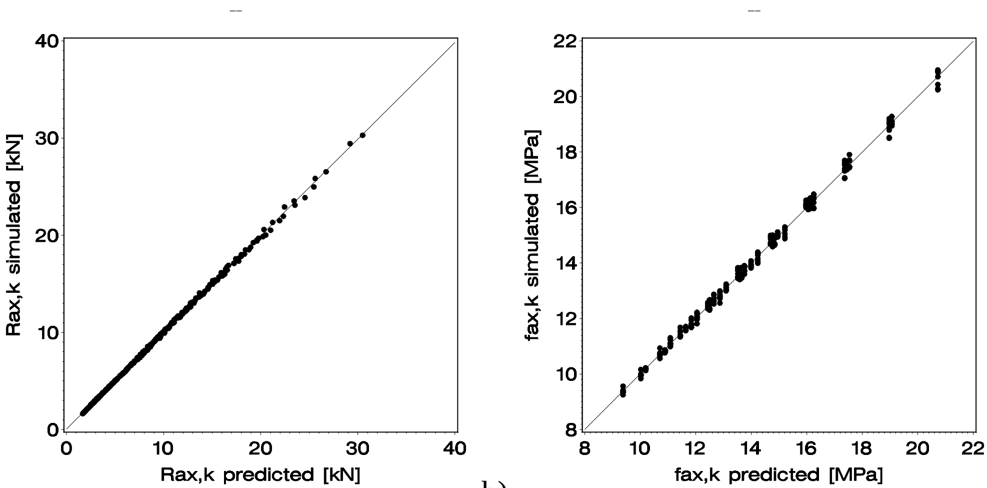

a) b)

Fig. 8 Regression Eqs. (10) and (11): simulated and predicted value for the axial withdrawal resistance a) and the axial withdrawal parameter b)

2.4 Application of a conventional non-linear basis function

In the following an elementary function (12) will be presented, which in practical application requires few arithmetic operations to calculate the withdrawal parameter f_{ax}. It refers to Eq. (4), without the penetration depth ℓ_{ef}. Of course in a further step the penetration depth ℓ_{ef} must be multiplied – together with the nominal diameter d – by the withdrawal parameter f_{ax}.

$$f_{ax} = A \cdot \rho \cdot d^{B} \tag{12}$$

A non-linear regression from f_{ax} on ρ and d with 1830 observations, i.e. 17 observations with standard errors out of [-3;3], which were excluded after a preliminary regression, delivers the following correlation:

$$f_{ax} = 0.0857 \cdot \rho \cdot d^{-0.3423} + e\,, \tag{13}$$

$$n = 1830 \qquad \mathrm{r}^2 = 0.484 \qquad e : \mathrm{N}(0; 2.388)\,.$$

This model is quite similar to the one in paragraph 2.2.2. Here the variance of errors e is only approximately constant (Fig. 9a), the coefficient of determination might be slightly distorted. The errors follow more or less a normal distribution. Analogically to the simulation process in paragraph 2.3, the coefficient and exponent (13) are fitted in a way, that the characteristic density ρ_k is the explanatory variable. The characteristic withdrawal parameter is expressed by the following equation:

$$\boxed{f_{ax,k} = 0.0872 \cdot \rho_k \cdot d^{-0.4119}}\,. \tag{14}$$

Fig. 9b illustrates the quality of the regression from simulated characteristic withdrawal parameters on the characteristic density (of the six tested strength classes) and various nominal diameters.

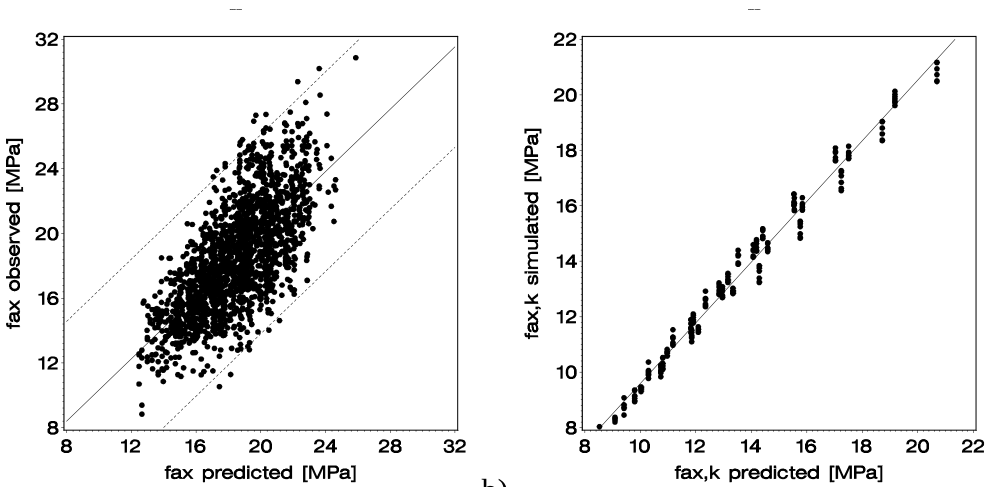

a) b)

Fig. 9 Regression Eq. (13): experimental and predicted value for the axial withdrawal parameter a) and Regression Eq. (14): simulated and predicted value for the characteristic axial withdrawal parameter b)

3 Evaluation of the models

For the evalutation of the models (10), (11) and (14), their predicted values $R_{ax,k}$ for 18 different d-ℓ_{ef} –combinations will be compared. Conditions are: The values of model (10) are the basis to which the $R_{ax,k}$-values of models (11) and (14) are referred. The ratios (15) are used for comparisons. Table 4 shows the 18 evaluated combinations. A less deep penetration depth ℓ_{ef} for smaller nominal diameters and vice versa is taken into account. Hence the possibility of practical application is given. The strength classes C24 and C40 with characteristic densities of 350 resp. 420 kg/m³ are evaluated.

In Fig. 10 the ratios are compared. It becomes obvious, that models (11) and (14) result in similar values, which on average only reach 92% of the values of model (10). There is a high congruence between all models for nominal diameters of 9 mm, i.e. the combinations 4-6 and 13-15. Due to a comparatively high withdrawal capacity, model (10) should be preferred.

$$\eta_{11/10} = \frac{R_{ax,k}\ \text{Eq.}(11)}{R_{ax,k}\ \text{Eq.}(10)}, \quad \eta_{14/10} = \frac{R_{ax,k}\ \text{Eq.}(14)}{R_{ax,k}\ \text{Eq.}(10)} \qquad (15)$$

Table 4 d-ℓ_{ef} –combinations and characteristic softwood density for comparisons between the models

Combination	d in mm	ℓ_{ef} in mm	ρ_k in kg/m³	Strength class
1-3	4	20-40-60	350	C24
4-6	9	40-70-100		
7-9	14	60-100-140		
10-12	4	20-40 60	420	C40
13-15	9	40-70-100		
16-18	14	60-100-140		

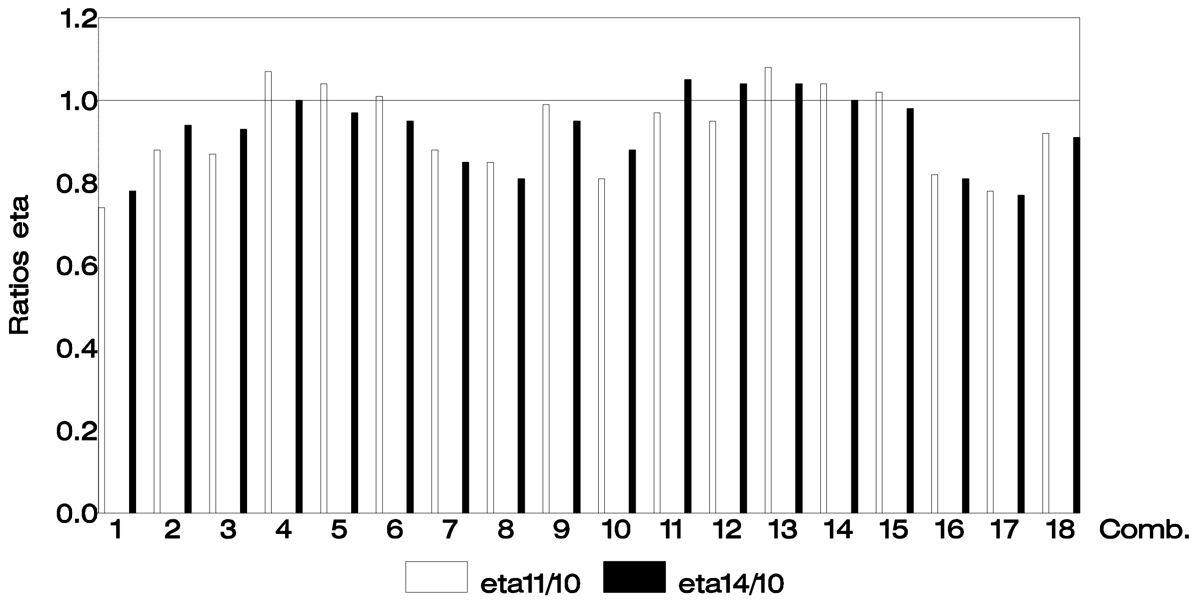

Fig. 10 Model comparison: (11) and (14) with (10) by means of predicted values

For further comparisons with Eqs. (1), (2) and (3) (according DIN 1052, Blaß et al. 2006, EN 1995-1-1) model (10) may continue to be – due to favourable predicted values – the basis for comparison. For the same 18 combinations the corresponding ratios (16) are calculated in Table 4. The angle α is 90°. The predicted values according Eq. (1) are calculated with load-carrying capacity category 3 (TFK=3). The nominal diameters for Eq. (3) are 2 mm higher resp. lower than allowed. Fig. 11 shows the comparison of the ratios: On average the values according Eq. (1) only reach 78% of the level of the values according Eq. (10). Eq. (2) delivers 93% and Eq. (3) only 76%. Partially the ratios are 50%. If the angle α in Fig. 11 was 45°, the percentage would be lower a further 10%.

$$\eta_{1/10} = \frac{R_{ax,k}\ \text{Eq.}(1)}{R_{ax,k}\ \text{Eq.}(10)}, \quad \eta_{2/10} = \frac{R_{ax,k}\ \text{Eq.}(2)}{R_{ax,k}\ \text{Eq.}(10)}, \quad \eta_{3/10} = \frac{R_{ax,k}\ \text{Eq.}(3)}{R_{ax,k}\ \text{Eq.}(10)} \qquad (16)$$

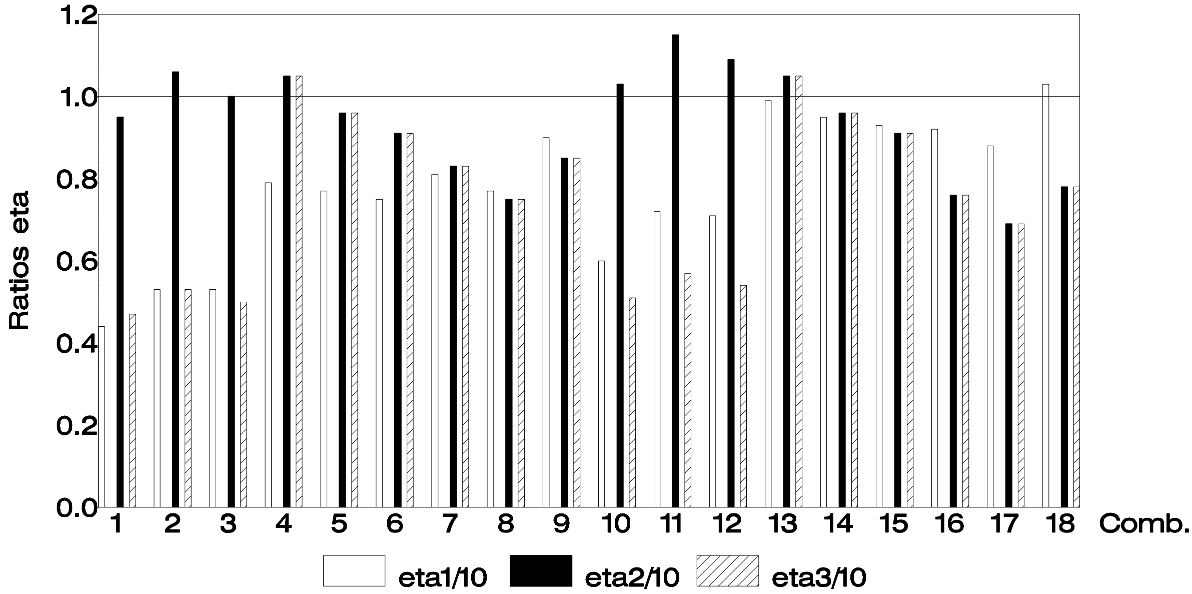

Fig. 11 Model comparison: (1), (2) and (3) with (10) by means of predicted values

The five comparisons show, that the direct modeling of $R_{ax,k}$ with Eq. (10) delivers the highest values. Neither the angle nor the withdrawal parameter is necessary for the calculation. This makes this equation just as applicable as its alternatives. In comparison with EN 1995-1-1 the tolerable range of values for the nominal diameter is wider. The dependence on the characteristic density, obtained by simulations, is consistent concerning the strength classes in EN 338. Hence the reliability of the predicted values increases for a wide range of the characteristic density.

4 Conclusion

Based on results of about 1850 withdrawal tests with self-tapping screws, arranged in softwood, one equation for the withdrawal resistance and two further equations for the withdrawal parameter were derived. Nominal diameter, penetration depth and characteristic density of a strength class in EN 338 are the independent variables in the equation for the withdrawal resistance. In the equations for the withdrawal parameter the independent variables are nominal diameter and characteristic density. The equation for the withdrawal resistance delivers, compared with the equations for the withdrawal parameter, the most favourable values concerning the withdrawal capacity. In comparison with the equations in DIN 1052 and Eurocode 5 the values of this equation are on average 30% higher. Further criteria: The equation is valid for nominal diameters between 4 and 14 mm, for penetration depths between 20 and 140 mm and is applicable independent of the angle between 45° and 90°. The results of the withdrawal tests are based on different types of screws from various manufacturers, therefore the new equations are suitable to calculate the withdrawal capacity of standard self-tapping wood screws. The new equation for the withdrawal resistance increases the load-carrying capacity in a considerable way, with the consequence that the application of self-tapping wood screws for connections inserted at an angle α to grain might be even more attractive in the future.

Literature

Chatterjee S, Price B (1995) Praxis der Regressionsanalyse, 2. Aufl. Oldenbourg Verlag: München, Wien

Blaß HJ, Bejtka I, Uibel T (2006) Tragfähigkeit von Verbindungen mit selbstbohrenden Holzschrauben mit Vollgewinde, Bd. 4. Karlsruher Berichte zum Ingenieurholzbau. Universitätsverlag Karlsruhe, Karlsruhe

Hartung J, Elpelt B, Klösener KH (2005) Statistik, 14. Aufl. Oldenbourg Verlag: München, Wien

DIN 96:1986-12 Halbrund-Holzschrauben mit Schlitz

DIN 97:1986-12 Senk-Holzschrauben mit Schlitz

DIN 571:1986-12 Sechskant-Holzschrauben

DIN 1052:2008-12 Entwurf, Berechnung und Bemessung von Holzbauwerken – Allgemeine Bemessungsregeln und Bemessungsregeln für den Hochbau

DIN 7998:1975-02 Gewinde und Schraubenenden für Holzschrauben

EN 338:2003 Bauholz für tragende Zwecke – Festigkeitsklassen

EN 1382:2000-03 Holzbauwerke – Prüfverfahren – Ausziehtragfähigkeit von Holzverbindungsmitteln

EN 1995-1-1:2008-09 Eurocode 5: Bemessung und Konstruktion von Holzbauteilen – Teil 1-1: Allgemeines – Allgemeine Regeln und Regeln für den Hochbau

EN 14592:2002 Holzbauwerke – Stiftförmige Verbindungsmittel – Anforderungen

CIB-W18/42-7-4

**INTERNATIONAL COUNCIL FOR RESEARCH AND INNOVATION
IN BUILDING AND CONSTRUCTION**

WORKING COMMISSION W18 - TIMBER STRUCTURES

EMBEDDING STRENGTH OF NEW ZEALAND TIMBER AND RECOMMENDATION FOR THE NZ STANDARD

S Franke

P Quenneville

University of Auckland

NEW ZEALAND

Presented by P Quenneville

J.W. G. van de Kuilen received confirmation that the diameter can be ignored in one of the cases.
H.J. Larsen stated that he has no doubt that it is useful to get the data but he questioned the distinction between acquiring data and knowledge; where knowledge acquisition needs research. He asked what the research content of the paper is. P. Quenneville agreed that the paper does not have a high level of new research content. However the new data is needed to address code changes issues in New Zealand therefore it is valuable. It is also important to confirm applicability of EC5 provisions for New Zealand engineers.
A. Buchanan stated since LVL and lumber are the same radiata pine material in New Zealand, he questioned why there is a difference. P. Quenneville stated that they are different materials because of density difference.
H.J. Blass commented that density of individual specimens was used in the development of the equation and there are other significant factors which can be masked by this approach. For the final proposal in the code equation additional procedures are needed. P. Quenneville agreed.

Embedding strength of New Zealand timber and recommendation for the NZ standard

Dr. Steffen Franke, Prof. Pierre Quenneville
University of Auckland, New Zealand

1 Introduction

For all connections it is important to predict the failure strength as accurately as possible. This includes both the ductile and in some cases especially in timber construction, the brittle failure as well. For the calculation of the ductile failure strength, the European Yield Model (EYM) is used in many standards and accepted as a very accurate model. It forms the basis of the European timber standard Eurocode 5, EN 1995-1-1:2004. The development of this is based on a multitude of embedding and joint tests with different European and North American wood species by many researchers. Furthermore a continuous adaptation and improvement is reported overseas such as in Hübner et al. 2008 [7]. The most important parameters for the EYM are the fastener yield moment and the timber embedding strength, which are known for most of the softwoods and tropical hardwoods.

In the current NZ timber standard NZS 3603:1993 [10], the design concept for bolted connections is not based on the EYM and depends only on the diameter and the timber thickness. It doesn't predict the different types of failure and overestimates the joint strength partially. There are no embedding strength values, which can be used for the Johansen's yield theory to estimate the yield strength of joints. Furthermore, no formulas are available for the design of joints with the engineered wood product Laminated Veneer Lumber (LVL), which uses becomes more important in structural members. To implement the EYM design concept in the current New Zealand design standard for mechanical connections, it is thus necessary to investigate the material behaviour and to determine the embedment values for Radiata Pine timber and also for Radiata Pine LVL, the two main products used in New Zealand constructions.

Embedding tests parallel, perpendicular and under various load-to-grain angles with different dowel diameters with LVL were conducted and compiled together with results of NZ Radiata Pine to build a database of embedding strength values to implement the European Yield Model into the NZ standard. The embedding strength was evaluated using the 5 %-offset method, the extended proportional limit load according to DIN 52192 and the maximum load, which is either the ultimate load or the load at 5 mm displacement, according to EN 383:1993 and ISO/DIS 10984-2 respectively. For the embedding strength from Radiata Pine lumber, results from other researchers were used. There is also a comparison with the predicted embedding failure from Eurocode 5. Moreover, the paper presents a comparison of the different available test standards for determining the dowel embedding strength.

2 Material and methods

2.1 Test standards

There are different test standards for testing the embedding strength of wood for dowel-type fasteners, the ASTM D 5764-97a, the ISO/DIS 10984-2 and EN 383:1993. A summary and comparison of the specific procedures are given below.

<u>ASTM D 5764-97a</u>

The ASTM standard provides a full-hole and a half-hole testing setup, as shown in Figure 1 and Figure 2. The minimum specimen dimensions are 38 mm or 2*d* in thickness and a maximum of 50 mm or 4*d* for the width and length, independent of the load-to-grain angle, where *d* is the dowel diameter.

The test is conducted as to reach the maximum load in 1 to 10 min, using a constant rate of testing of usually 1.0 mm/min. There is no further information about the loading procedure. The results are given as the yield load, determined using the 5 %-offset method, the proportional limit load and the ultimate load. The embedding strength, calculated from the yield load, is given by:

$$f_h = \frac{F_{yield}}{b \cdot t} \tag{1}$$

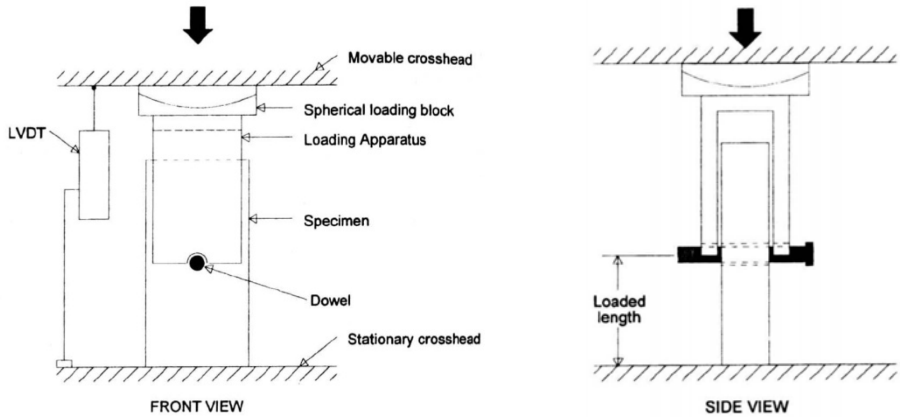

Figure 1: Test configuration full-hole test, ASTM D 5764-97a [1]

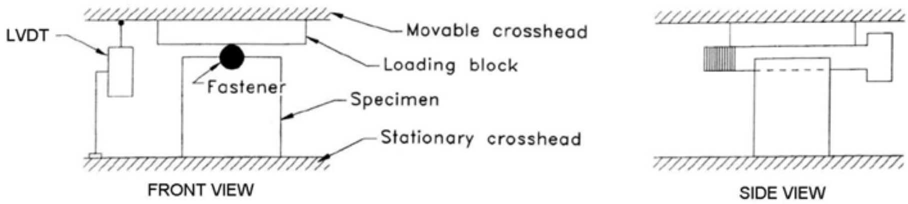

Figure 2: Test configuration half-hole test, ASTM D 5764-97a [1]

<u>ISO/DIS 10984-2</u>

The tests according to the international standard shall be carried out using a full-hole test shown in Figure 3a, but it is a requirement of the test to avoid bending of the fastener under test. Thus it also allows using a half-hole test shown in Figure 3b. The minimum specimen dimensions for tests parallel and perpendicular to grain can be found in Figure 4.

The loading procedure to be used consists of one preload cycle from $0.4{\cdot}F_{max,est}$ to $0.1{\cdot}F_{max,est}$ and the force is to be increased or decreased at a constant rate. The maximum load is to be reached within 300 ± 120 s. The standard includes formulas to calculate the embedding strength, where F_{max} is either the ultimate load or the load at 5 mm displacement, and the foundation modulus as below, where w is the displacement:

$$f_h = \frac{F_{\max}}{b \cdot t} \tag{2}$$

$$K = \frac{0.4 f_{h,est}}{w_{i,\mathrm{mod}}} = \frac{0.4 f_{h,est}}{4/3 \cdot \left(w_{0.4 \cdot F} - w_{0.1 \cdot F} \right)} \tag{3}$$

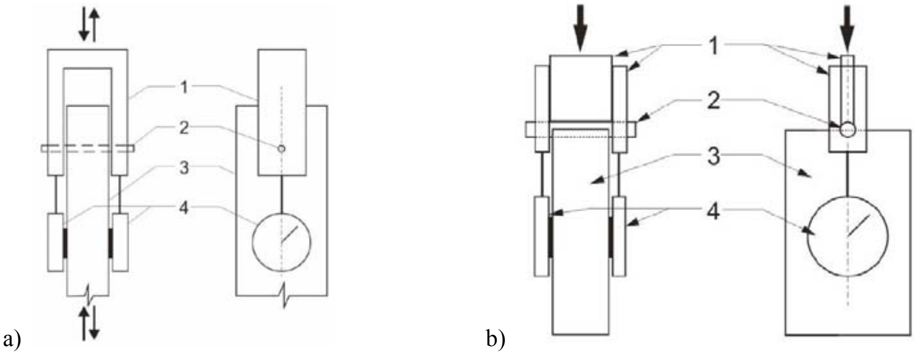

Figure 3: Test configuration: a) full-hole, b) half-hole, ISO/DIS 10984-2 [8]
1. Steel apparatus, 2. Fastener, 3. Test piece, 4. Displacement gauge attached to the test piece

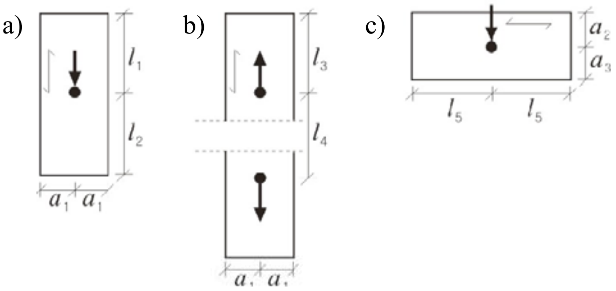

a) Compression parallel to grain
b) Tension parallel to grain
c) Compression perpendicular to grain
for dowels or bolts:
$a_1 = 3d$
$a_2 = a_3 = 5d$
$l_1 = l_2 = l_3 = 3d$
$l_4 = 30d$
$l_5 = 10d$

Figure 4: Sizes of test specimen, ISO/DIS 10984-2 [8]

EN 383:1993 or DIN EN 383:2007

The European testing standard is equal to the ISO/DIS 10984-2, except that it does not provide the half-hole test alternative.

2.2 Test series and specimen

LVL from Radiata Pine

The embedding tests series conducted include a total of 244 tests with LVL and a dowel diameter d of 8, 12, 16, and 20 mm. They comprise load-to-grain angles α of 0°, 22.5°, 45°, 67.5° and 90° for each dowel diameter. Additional to this, a test series with two dowels were conducted to investigate the influence of dowel spacing on the embedding strength for loading angles of 0° and 90° for all dowel diameters. For this the minimum distance of 3d was used for the bolt spacing. As a result of the splitting observed on the specimens with both one and two dowels for the 90° loading angle, further tests were done using specimen having twice the end distance requirement. The labelling of each test is based to the following definition:

LVL-E0-1x12-01

Specimen number

Bolt diameter: Ø 8, **12**, 16, 20 mm

Number of bolts: 1, 2

Load-to-grain angle: **0°**, 22.5°, 45°, 90°

Embedment test

Wood product: Radiata Pine, **LVL**

The tests were conducted according to the ASTM D 5764-97a as a half-hole test (Figure 2 and Figure 5) which involves pushing a bolt so that no bending effects are observed. All specimens were cut from billets of 46 mm thickness, so that for all test series, a constant thickness of 46 mm and a constant height of 70 mm were used. The width of the specimens depends on the dowel diameter, the number of dowels and the load-to-grain angle. The number, sizes and densities of all groups are shown in Table 1. The specimens were conditioned to 20 °C and 65 % relative humidity.

Table 1: Number, sizes and density of embedding test with LVL

Diameter	**Load-to-grain angle**	**No. of dowel**	**No. of specimen**	**Width [mm]**	**Height [mm]**	**Thickness [mm]**	**Density [kg/m³]**	
							Mean	**CV [%]**
d = 8 mm	α = 0°	1	12	120	70	46	608	2.0
		2	6	150	70	46	610	3.5
	α = 22.5°	1	6	110	70	46	619	2.2
	α = 45°	1	6	100	70	46	585	2.2
	α = 67.5°	1	6	90	70	46	619	2.2
	α = 90°	1	12 (+2)	80 (160)	70	46	599	1.9
		2	6 (+2)	104 (200)	70	46	603	2.1
d = 12 mm	α = 0°	1	12	120	70	46	600	2.5
		2	12	150	70	46	603	2.9
	α = 22.5°	1	6	120	70	46	607	2.0
	α = 45°	1	6	120	70	46	611	1.9
	α = 67.5°	1	6	120	70	46	602	2.1
	α = 90°	1	12 (+2)	120 (240)	70	46	571	0.8
		2	12 (+2)	150 (270)	70	46	596	3.7
d = 16 mm	α = 0°	1	12	120	70	46	600	3.5
		2	6	150	70	46	574	2.0
	α = 22.5°	1	6	130	70	46	587	2.2
	α = 45°	1	6	140	70	46	586	1.4
	α = 67.5°	1	6	150	70	46	601	2.9
	α = 90°	1	12 (+2)	160 (320)	70	46	613	1.9
		2	6 (+2)	208 (400)	70	46	608	1.5
d = 20 mm	α = 0°	1	12	120	70	46	587	3.8
		2	6	150	70	46	585	3.0
	α = 22.5°	1	6	140	70	46	586	3.4
	α = 45°	1	6	160	70	46	581	2.0
	α = 67.5°	1	6	180	70	46	584	2.0
	α = 90°	1	12 (+2)	200 (400)	70	46	604	1.5
		2	6 (+2)	260(500)	70	46	588	1.4
Total or average			244				597	

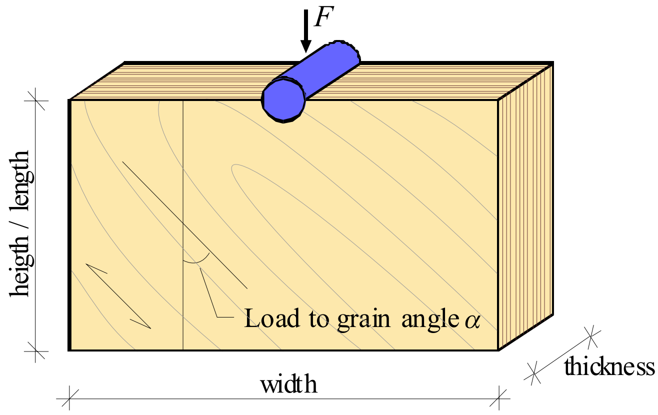

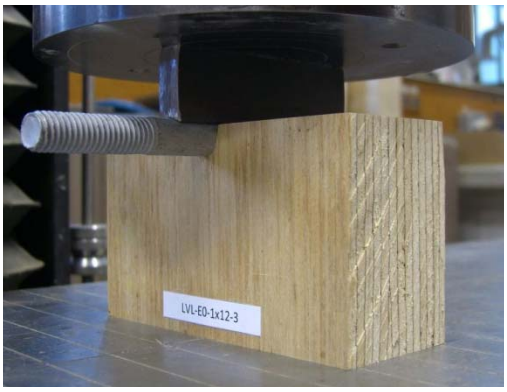

Figure 5: Definition of embedding tests variables and photo of test specimen during the test

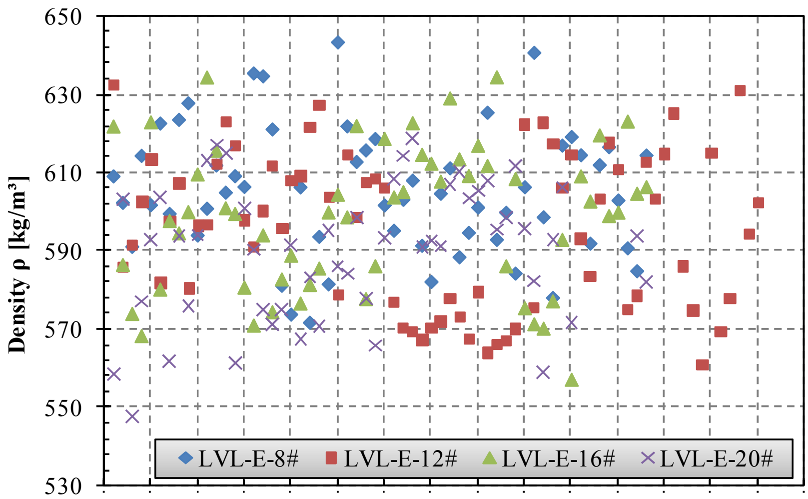

Figure 6: Density distribution over all tests

Radiata Pine

For a comparison of the test results of LVL with results of Radiata Pine lumber, results of a student project done by Suffiad 2008 [15] and Mills 2008 [9] were used. The tests were also carried out following the ASTM D 5764-97a procedure as a half-hole test with dowel diameters *d* of 10 mm, 16 mm and 20 mm. Referring to Figure 5, the dimensions were constant for all dowel diameters inside each of the series with 0° and 90° loading angle, as shown in Table 2. The strength is calculated using the yield strength with the 5 %-offset method.

Table 2: Number, sizes and density of embedding test with Radiata Pine lumber, from [15] and [9]

Diameter	Load-to-grain angle	No. of dowel	No. of specimen	Width [mm]	Height [mm]	Thickness [mm]	Density [kg/m³]	
							Min	Max
d = 10 mm	α = 0°	1	35	45	90	45	412	637
	α = 90°	1	32	120	80	45	340	553
d = 16 mm	α = 0°	1	30	45	90	45	431	674
	α = 90°	1	31	120	80	45	348	512
d = 20 mm	α = 0°	1	30	45	90	45	424	633
	α = 90°	1	30	120	80	45	350	547

3 Results and discussion

3.1 Evaluation methods of the embedding strength

In Figure 7 are shown typical load-displacement curves for the series with one 16 mm dowel. The curves represent the average curve of each group, depending on the load-to-grain angle. For all dowel diameters, the curves show a linear increase of the load up to the proportional limit. After the yielding point, curves are almost constant for α = 0° or increasing slightly for α = 22.5°, 45° but increase significantly for α = 67.5° and 90°.

For each test, the following characteristics as shown in Figure 8 were evaluated: the stiffness K_{ser} (as the slope of a line between approx. 10 % and 40 % of the maximum load), the slope/stiffness T after the yield point (as the slope of a line fitted to the load-displacement), the proportional limit load F_{prop}, the yield load $F_{5\%}$, and the maximum load F_{max}, either as the ultimate load (mostly for α = 0° and 22.5°) or the load at 5 mm displacement (mostly for $\alpha \geq$ 45°). The proportional limit load is defined as the contact point of the test data and a line with a slope of $2/3 \cdot K_{ser}$ according to DIN 52192. The 5 %-offset method, according to EN 383 and ISO 10984 respectively, was adopted to evaluate the yield load. Based on the relation given at equation (2), the embedding strength is calculated to the 5 % yield embedding strength $f_{h,\alpha,5\%}$ and the maximum embedding strength $f_{h,\alpha,max}$ in this paper respectively, where α is the load-to-grain angle.

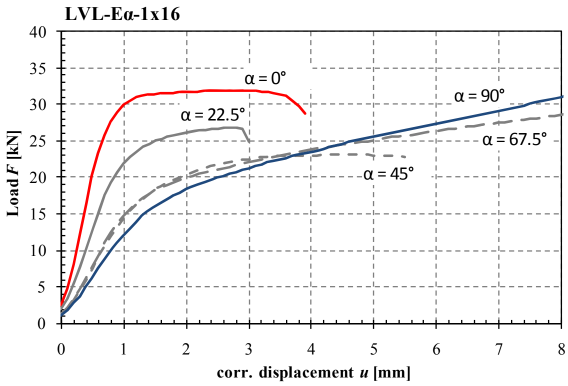

Figure 7: Typical load vs. displacement curves

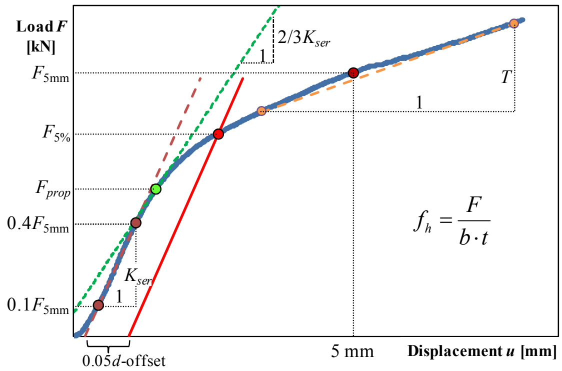

Figure 8: Evaluating embedding strength

3.2 Embedding strength

<u>*LVL from Radiata Pine*</u>

Table 3 shows the mean values and the coefficient of variation of the yield and maximum embedding strength for each test series depending on the dowel diameter, the number of dowels and the load-to-grain angle. The last row includes the ratio between the yield and maximum embedding strengths. There are only very small variations between the yield strength of 1 and 2 dowels with a maximum difference of ± 6 %, which is within the same range as the coefficient of variation. This is also valid for K_{ser}. Also the load-displacement curves of all tested longer specimens are within the range of the shorter specimens, so that the results of one dowel, two dowels, the short and the long specimens are examined as one group “Eα” together in the further discussion and comparison with the Eurocode 5.

The mean values of the yield embedding strength $f_{h,\alpha,5\%}$ and the maximum embedding strength $f_{h,\alpha,max}$ are compared as a function of the dowel diameter in Figure 9. Both show a reduction in the strength values with an increase of the dowel diameter. The dependency of the embedding strength on the load-to-grain angles was more significant for the yield embedding strength. For dowel diameters $d \leq 8$ mm, we observed a sensitive influence on the strength values for α = 0° and 22.5°. This was also observed within current investigations on the embedding strength of nails. All embedding strength values vs. density are shown in Figure 10. The strength values have a visible positive correlation with the density, but the relative small range of the investigated density from LVL (mostly 560 kg/m³ to 620 kg/m³) is to be taken into account.

Table 3: Embedding strength results [MPa] of LVL

Diameter	**Load-to-grain angle**	**No. of dowel**	**Yield strength $f_{h,\alpha,5\%}$**		**Max. strength $f_{h,\alpha,max}$**		**$f_{h,\alpha,max}/f_{h,\alpha,5\%}$**
			Mean	**CV [%]**	**Mean**	**CV [%]**	
d = 8 mm	α = 0°	1	40.8	6.6	43.7	6.8	1.07
		2	40.6	5.8	46.1	6.3	1.13
	α = 22.5°	1	37.5	9.1	41.1	8.1	1.09
	α = 45°	1	28.7	7.8	37.2	7.7	1.29
	α = 67.5°	1	31.2	8.2	52.0	5.4	1.67
	α = 90°	1	29.4	6.3	49.1	5.2	1.67
		2	29.4	9.9	42.4	7.5	1.44
d = 12 mm	α = 0°	1	47.2	4.7	47.9	4.3	1.02
		2	47.0	8.9	48.1	9.0	1.02
	α = 22.5°	1	43.2	5.3	46.4	5.4	1.07
	α = 45°	1	33.5	3.5	41.6	2.5	1.24
	α = 67.5°	1	28.3	7.5	38.3	9.0	1.35
	α = 90°	1	26.5	6.5	36.7	7.3	1.39
		2	28.1	7.3	36.9	8.0	1.32
d = 16 mm	α = 0°	1	42.6	5.4	43.6	5.7	1.02
		2	39.2	3.0	40.4	3.7	1.03
	α = 22.5°	1	34.9	4.3	36.4	5.1	1.04
	α = 45°	1	29.0	4.6	33.5	6.2	1.16
	α = 67.5°	1	27.6	8.5	34.2	8.1	1.24
	α = 90°	1	27.2	7.8	35.1	6.7	1.29
		2	27.1	4.9	34.3	5.4	1.26
d = 20 mm	α = 0°	1	40.3	5.9	40.6	5.7	1.01
		2	41.9	5.6	42.4	5.3	1.01
	α = 22.5°	1	33.2	7.9	33.8	8.3	1.02
	α = 45°	1	28.0	5.1	29.9	3.8	1.07
	α = 67.5°	1	24.6	8.0	28.7	9.6	1.17
	α = 90°	1	27.5	5.5	33.2	6.0	1.21
		2	25.8	6.6	30.7	7.7	1.19

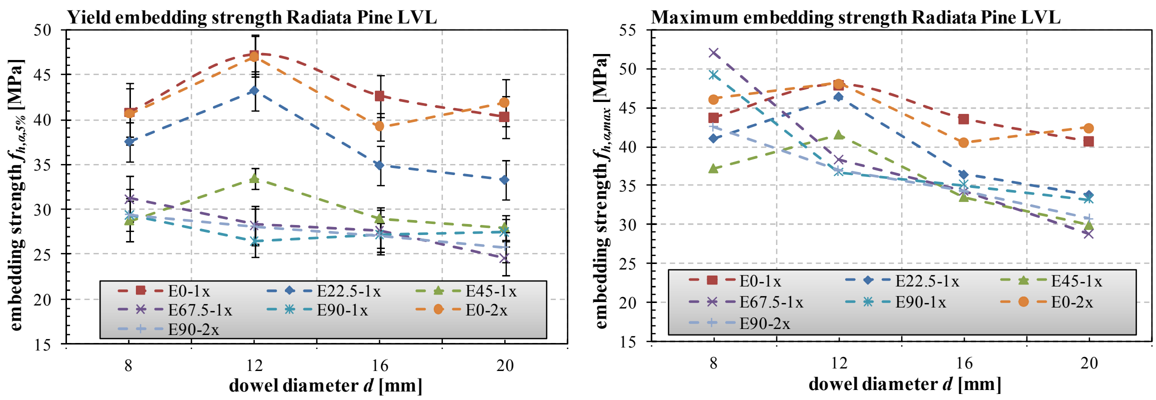

Figure 9: Yield and maximum embedding strength vs. dowel diameter for LVL

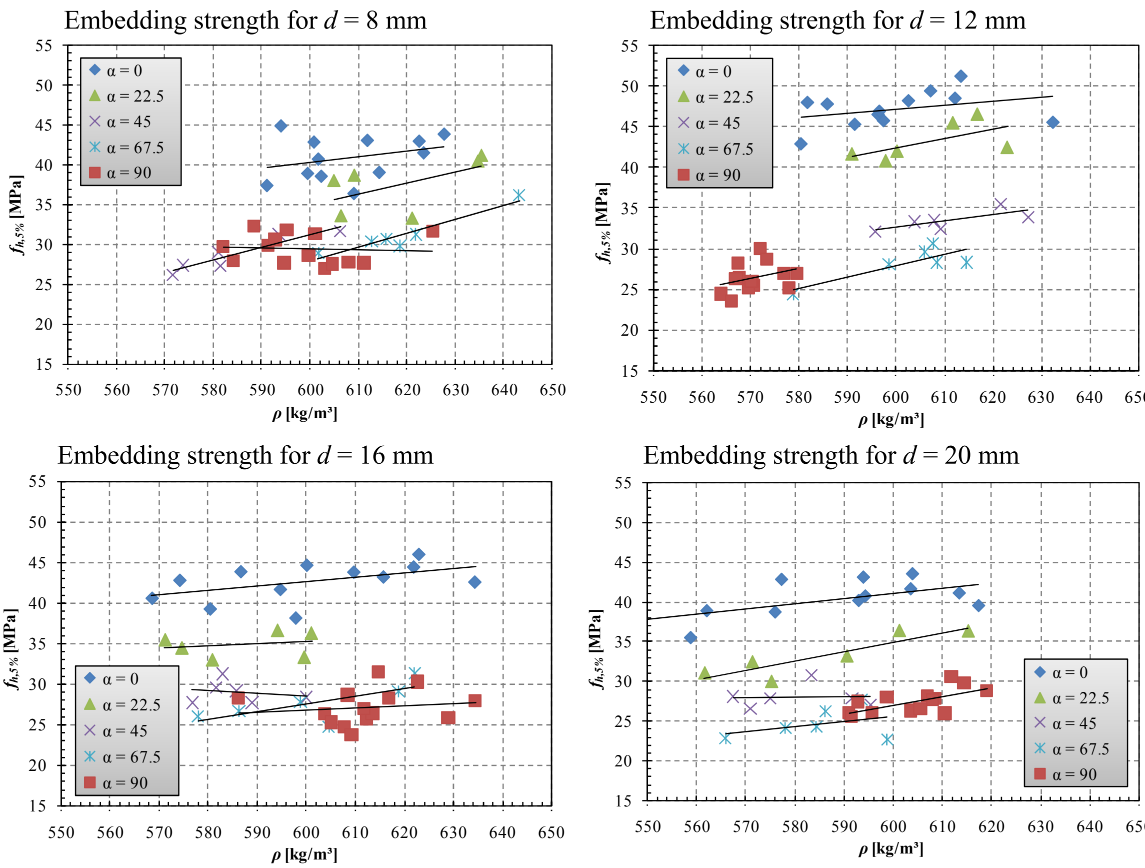

Figure 10: Embedding strength vs. density for d = 8 mm, 12 mm, 16 mm and 20 mm for all loading angles in Radiata Pine LVL

Radiata Pine

Table 4 shows the mean values and the coefficient of variation of the yield embedding strength $f_{h,\alpha,5\%}$ for the test series depending on the dowel diameter d and the load-to-grain angle α. Figure 11 contains the mean values of the yield embedding strength $f_{h,\alpha,5\%}$ as a function of the dowel diameter. The results are constant regardless of the dowel diameter, which agrees with studies for other species of wood by Sawata 2002 [13] and Harada 1999 [6], whereas in a previous study by Whale et al. 1987 [16], the embedding strength decreases as the dowel diameter increases.

Table 4: Embedding strength results [MPa] of Radiata Pine lumber

Diameter	Load-to-grain angle	No. of dowel	Yield strength $f_{h,\alpha,5\%}$	
			Mean	CV
d = 10 mm	α = 0°	1	34.6	15.8 %
	α = 90°	1	18.0	18.6 %
d = 16 mm	α = 0°	1	35.2	15.0 %
	α = 90°	1	16.9	17.6 %
d = 20 mm	α = 0°	1	34.0	16.3 %
	α = 90°	1	17.9	16.6 %

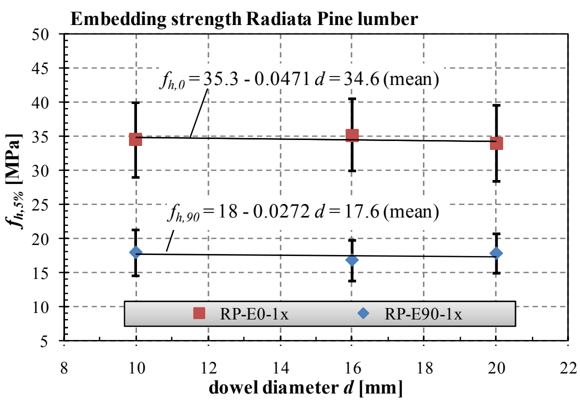

Figure 11: Yield embedding strength vs. dowel diameter for Radiata Pine lumber (mean value, standard deviation and linear regression)

3.3 Embedding strength vs. Eurocode 5

The comparison of the mean test values with the corresponding embedding strengths according to the Eurocode 5 formulas are shown in Figure 12 for LVL and in Figure 13 for Radiata Pine lumber. Each of the left graphs shows the embedding results for α = 0° and 90° in comparison with the embedding strength by EC 5 (for LVL for one and two dowels separately), whereas each of the right graphs show the embedding strength $f_{h,0}$ and the reduction factor k_{90} as well as their linear regression (for LVL as one group for one and two dowels together). The embedding strength was calculated using:

$$f_{h,0} = 0.082\left(1 - 0.01d\right)\rho \tag{4}$$

$$f_{h,a} = \frac{f_{h,0}}{k_{90} \cdot \sin^2 \alpha + \cos^2 \alpha} \tag{5}$$

where

$$k_{90} = \begin{cases} 1.35 + 0.015d & \text{for softwood} \\ 1.30 + 0.015d & \text{for LVL} \\ 0.90 + 0.015d & \text{for hardwood} \end{cases}, \tag{6}$$

and d is the dowel diameter, ρ the mean density of 597 kg/m³ for LVL and 527 kg/m³ for Radiata Pine lumber and α the load-to-grain angle.

For the LVL results shown in Figure 12, there is a good agreement for the average, especially for the 12 mm dowel for both the embedding strength $f_{h,0}$ and the reduction factor k_{90}. The decreasing of the yield embedding strength is smaller than the prediction of the Euro-

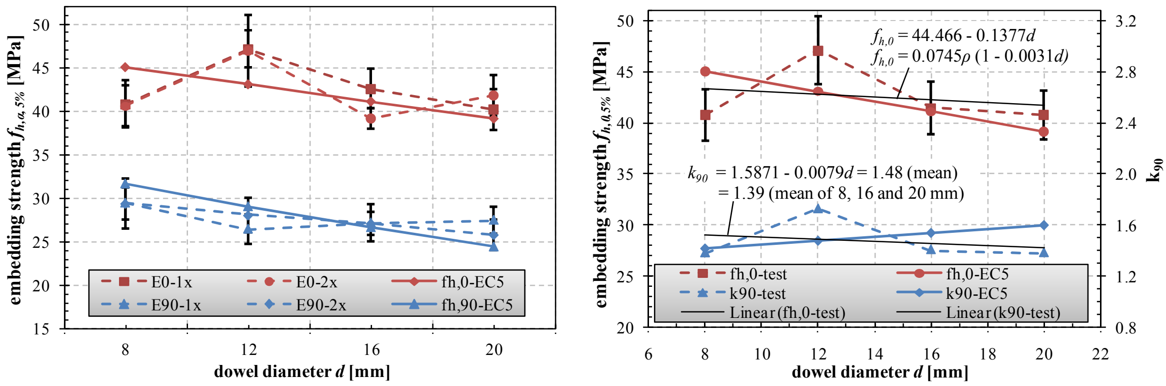

Figure 12: Comparison of the test results with the Eurocode 5 for Radiata Pine LVL

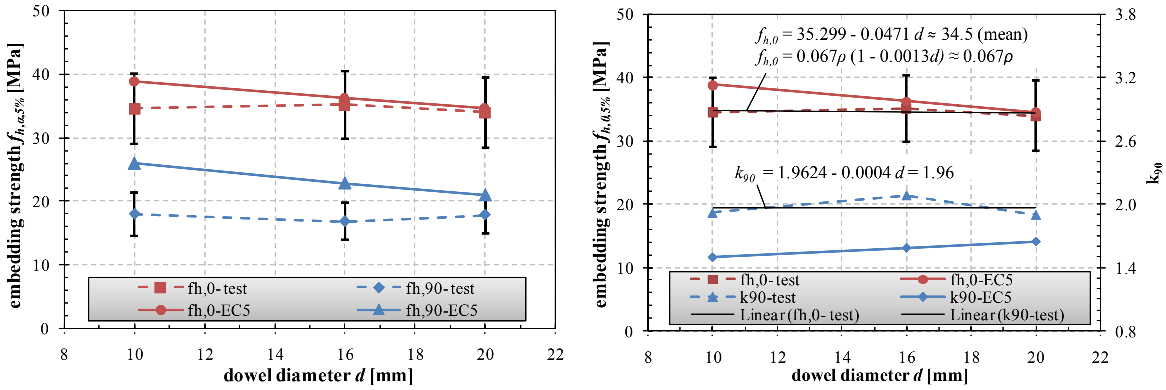

Figure 13: Comparison of the test results with the Eurocode 5 for Radiata Pine lumber

code, whereas the reduction factor k_{90} is opposite in trend, but quite constant regardless of the dowel diameter. For Radiata Pine lumber results shown in Figure 13, there is good agreement only for the embedding strength $f_{h,0}$ for the bigger dowel diameter. For the smaller diameters, the EC5 overestimates the embedding strength $f_{h,0}$. The reduction factor $k_{90,}$ evaluated by EC 5, is much lower than the evaluated factor based on the test results.

4 Conclusions

Based on the current results from Radiata Pine LVL, the formulas of EC 5 for estimating the embedding strength $f_{h,0}$ for LVL can be used, but it needs further tests to check the sensitive strength behaviour of dowels with a diameter of 8 mm or smaller and to ensure these results. We propose to use a constant factor of 1.4 for the reduction factor k_{90}, which is about the mean value of the three lower values of the 8 mm, 16 mm and 20 mm dowels, cp. Figure 12. A summary is given with the equations (7), (8) and (9).

Based on the results for Radiata Pine, lumber we propose to estimate the embedding strength $f_{h,0,k}$ and the reduction factor k_{90} regardless to the dowel diameter as a constant value as follow:

$$f_{h,0,k} = \begin{cases} 0.067\rho_k & \text{for Radiata Pine lumber} \\ 0.082\left(1-0.01d\right)\rho_k & \text{for Radiata Pine LVL} \end{cases} \tag{7}$$

$$f_{h,\alpha,k} = \frac{f_{h,0,k}}{k_{90}\cdot\sin^2\alpha+\cos^2\alpha} \tag{8}$$

where

$$k_{90} = \begin{cases} 2.0 & \text{for Radiata Pine lumber; softwood} \\ 1.4 & \text{for Radiata Pine LVL} \end{cases} \tag{9}$$

and

ρ_k is the characteristic timber density in kg/m³
d is the bolt or dowel diameter in mm
α is the load-to-grain angle.

5 Literature

[1] ASTM D 5764-97a: *Standard Test Method for Evaluating Dowel-Bearing Strength of Wood and Wood-Base Products*. ASTM International, West Conshohocken, USA

[2] Ehlbeck, J.; Werner, H. (1992): *Tragfähigkeit von Laubholzverbindungen mit stabförmigen Verbindungsmitteln.* Techn. Report, Versuchsanstalt für Stahl, Holz und Steine der Universität Karlsruhe, Abt. Ingenieurholzbau, Karlsruhe

[3] EN 1995-1-1:2004: *Eurocode 5 – Design of timber structures, Part 1-1: General - Common rules and rules for buildings.* European Committee for Standardization (CEN), Brussels

[4] EN 383:1993: *Timber structures – Test methods. Determination of embedding strength and foundation values for dowel type fasteners.* European Committee for Standardization (CEN), Brussels

[5] EN 408:2004: *Timber structures - Structural timber and glued laminated timber - Determination of some physical and mechanical properties.* European Committee for Standardization (CEN), Brussels

[6] Harada, M. Et al. (1999): *Dowel-bearing test of glued laminated timber with a drift-pin.* Summary of technical paper, annual meeting, Architectural institute of Japan

[7] Hübner, U.; Bogensperger, T.; Schickhofer, G. (2008): *Embedding Strength of European hardwoods*. In: Proceedings of CIB-W18, Paper 41-7-5, St. Andrews, Canada

[8] ISO/DIS 10984-2: *Timber structures - Dowel-type fasteners - Part 2: Determination of embedding strength and foundation values*. International Organization for Standardization, Geneva

[9] Mills, M. (2008): *Bolted timber connections.* Internal research report, Department of Civil and Environmental Engineering, University of Auckland, New Zealand

[10] NZS 3603:1993: *TIMBER STRUCTURES STANDARD.* Standards New Zealand

[11] Patton-Mallory, M.; Pellicane, P.; Smith, F. W. (1997): *Modelling bolted connections in wood*: review. In: Journal of Structural Engineering, vol. 123, no. 8, pp. 1054-1062

[12] Patton-Mallory, M.; Cramer, S.; Smith, F.W.; Pellicane, P. (1997): *Nonlinear material models for analysis of bolted wood connections.* In: Journal of Structural Engineering, vol. 123, no. 8, pp. 1063-1070

[13] Sawata, K.; Yasumura M. (2002): *Determination of embedding strength of wood for dowel-type fasteners*. In: Journal of Wood and Sciences 48, pp. 138-146

[14] Snow, M.; Smith, I.; Ballerini, M. (2008): *Applicability of existing design approaches to mechanical joints in structural composite lumber.* In: Proceedings of CIB-W18, Paper 41-7-1, St. Andrews, Canada

[15] Suffiad, J. (2008): *Bolted timber connections perpendicular to the grain.* Internal research report, Department of Civil and Environmental Engineering, University of Auckland, New Zealand

[16] Whale, L.R.J.; Smith, I.; Larsen, H.J. (1987): *Design of nailed and bolted joints proposals for the revision of existing formulae in draft Eurocode 5 and the CIB code.* In: Proceedings of the CIB-W18 meetings, paper 25-7-2

CIB-W18/42-7-5

INTERNATIONAL COUNCIL FOR RESEARCH AND INNOVATION
IN BUILDING AND CONSTRUCTION

WORKING COMMISSION W18 - TIMBER STRUCTURES

LOAD-CARRYING CAPACITY OF TIMBER - WOOD FIBER INSULATION BOARD - JOINTS WITH DOWEL TYPE FASTENERS

G Gebhardt

H J Blaß

Lehrstuhl für Ingenieurholzbau und Baukonstruktionen

Universität Karlsruhe

GERMANY

Presented by G Gebhardt

B. Dujic asked whether one can add the contribution of WFIB with respect to adding different normal sheathing. He said the normal sheathing may have higher stiffness so its contribution in roof application will be minimal. He received clarification of the shear flow in plane and asked about the shear modulus of WFIB. G. Gebhardt said that the shear modulus of WFIB ranges from 50 N/mm^2 to 250 N/mm^2. H.J. Blass said that the thickness of WFIB in roof application is high so that it can contribute to the overall stiffness and confirmed that thick plate connections will fail first but thinner plates may have different mode of failure. H.J. Blass added that shear wall and diaphragm tests will be conducted.

T. Poutanen asked what would happen if one add adhesive. G. Gebhardt answered that initial stiffness would increase. H.J. Blass added that this was tried already and failure will be in the panels.

S. Winter commented that this panel is used commonly in roof applications and doubt the stiffness will be enough for roof construction because there are usually many smaller sub-plates which means that you do not have a continuous plate. H.J. Blass said that they are trying WF/WF connections to make it into one big sheet with mechanical fasteners.

Load-Carrying Capacity of Timber - Wood Fibre Insulation Board - Joints with Dowel Type Fasteners

G. Gebhardt, H.J. Blaß

Lehrstuhl für Ingenieurholzbau und Baukonstruktionen

Universität Karlsruhe, Germany

1 Introduction

So far wood fibre insulation boards (WFIB) are used as thermal and acoustic insulation in timber constructions. As wood-based panels, WFIB are suited for the transfer of loads caused by wind and earthquakes in timber frame constructions. Until present this task has been undertaken by plywood, particle boards and OSB. This new field of application of WFIB has been analysed in a research project at the Universität Karlsruhe.

In this paper a proposal is given to calculate the load-carrying capacity of timber-WFIB-joints with dowel type fasteners. For this purpose the load-carrying capacity of joints in timber and WFIB may be determined according to Johansen's yield theory and an extension of this theory. Tests were carried out to estimate the embedding strength of nails in WFIB and the crown pull-through resistance of staples in WFIB. The test results verified the calculation model and the stiffness properties of timber-WFIB-joints were evaluated.

2 Characteristics of WFIB

WFIB can be fabricated in two different manufacturing processes: In both the wood chips are thermo-mechanically pulped.

In the wet process the wood fibres are mixed with water and further aggregate into a suspension. Afterwards the boards are formed and dried. For the bonding of the wood fibres only the wood´s own cohesiveness (predominantly lignin resin) is used. Due to the high use of energy for the drying process, boards with higher thicknesses are manufactured by gluing raw single-layer boards to multilayer boards. At this raw single-layer boards with different densities may be combined.

In the dry process the wood fibres are dried and sprayed with PUR resin. Afterwards the boards are formed and the resin hardens. In this process boards with thicknesses up to 240 mm may be manufactured as single-ply boards.

WFIB may be used in different parts of buildings. In roofs, rain-tight sub plates (RTSP) are fixed as sub decking. A further insulation is possible as above-rafter or interim-rafter insulation with universal insulation boards (UIB). In walls, plaster baseboards (PB) may be used in composite thermal insulation systems.

11 different WFIB of three different manufacturers were selected to analyse the characteristics needed for the use as sheathing of shear walls. The nominal density range was 110 kg/m^3 up to 270 kg/m^3. The densities and moisture contents of the tested boards were determined. The measured moisture content range was 7.3% to 10.3%. Characteristic densities are proposed for the different types of WFIB and given in table 1.

Table 1 Proposed characteristic densities of WFIB

WFIB type	Characteristic density in kg/m^3
Rain-tight sub plate (RTSB)	200
Plaster baseboard (PB)	150
Universal insulation board (UIB)	150 100

3 Embedding strength

Several dowel type fasteners may be used for the attachment of WFIB on the studs or rafters. In roofs, nails are commonly driven in through the counter battens. In walls, staples are commonly used. An alternative for staples are special screws.

For the calculation of timber-WFIB-connections according to Johansen's yield theory [1] the embedding strength of WFIB is required. Apart from the embedding strengths of the connected parts, the load-carrying capacity depends on the geometry of the connection (thicknesses of the connected parts and diameter of the fastener) and the yield moment of the fastener.

Tests with nails were carried out according to EN 383 [2] to determine the embedding strength of mechanical fasteners in WFIB. In preliminary tests an influence of the angle between force direction and production direction had not been identified. 608 embedment tests with five diameters (d = 3.1/3.4/3.8/4.6/5.0 mm) were performed. The embedding strength correlates with the measured density of the test specimen. In figure 1 the embedding strength is plotted vs. the density. The correlation coefficient is r = 0.880.

There is a smaller correlation between the embedding strength and the thickness of the boards. A negative correlation exists between the embedding strength and the diameter of the fastener. Due to a correlation between the density and the thickness and the higher correlation between embedding strength and thickness, the parameters diameter and density are considered in the calculation model for the embedding strength. By means of a multiple regression analysis, equation (1) could be derived to estimate the embedding strength f_h of WFIB.

$$f_{\mathrm{h}} = 18.5 \cdot 10^{-5} \cdot \rho^{2.04} \cdot d^{-0.74} \qquad \text{in N/mm}^2 \qquad (1)$$

where ρ is the density of the WFIB in kg/m^3 and d the diameter of the fastener in mm

In figure 2 the tested embedding strength values are plotted vs. the calculated embedding strength values. The correlation coefficient is r = 0.916. The slope of the regression straight is m = 1.02 and the y-intercept is b = -0.090.

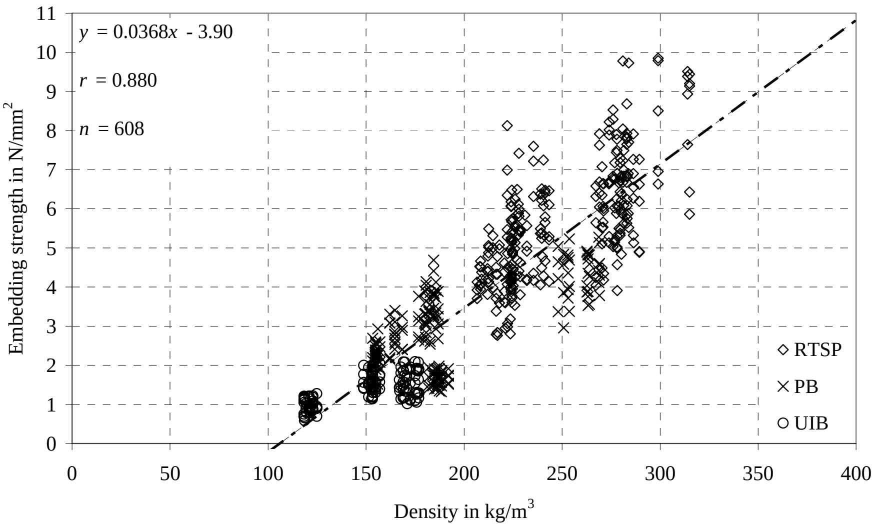

Figure 1 Embedding strength vs. density

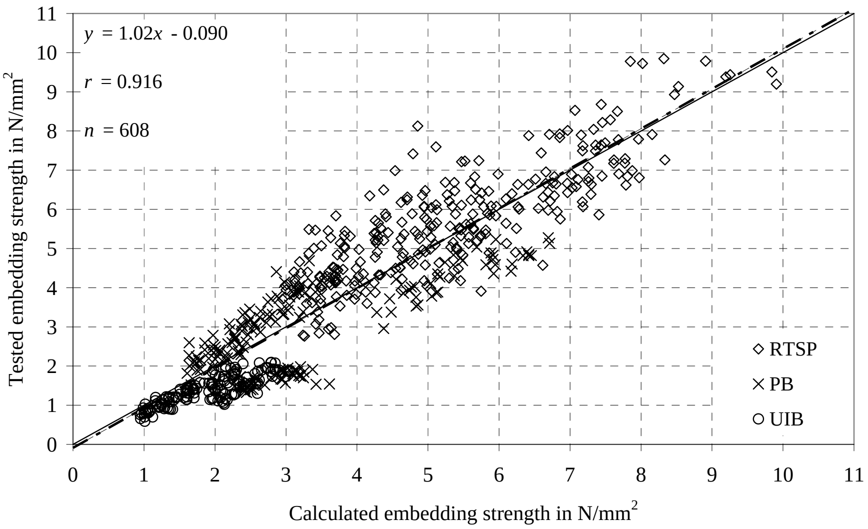

Figure 2 Tested embedding strength vs. calculated embedding strength

Characteristic values of the embedding strength may be calculated considering the proposed characteristic densities for the different types of WFIB (equation (2)).

$$
\begin{array}{lll}
\text{RTSP} & \rho_k = 200\ \text{kg/m}^3 & f_{h,k} = 8.88 \cdot d^{-0.75} \\
\text{PB} & \rho_k = 150\ \text{kg/m}^3 & f_{h,k} = 4.25 \cdot d^{-0.75} \\
\text{UIB} & \rho_k = 150\ \text{kg/m}^3 & f_{h,k} = 3.53 \cdot d^{-0.75} \\
\text{UIB} & \rho_k = 100\ \text{kg/m}^3 & f_{h,k} = 1.57 \cdot d^{-0.75}
\end{array}
\quad \text{in N/mm}^2 \qquad (2)
$$

4 Crown pull-through resistance

The load-carrying capacity may be calculated according to Johansen's yield theory considering the geometry of the connection (thicknesses of the connected parts and diameter of the fastener), the embedding strengths of the members (for WFIB presented in chapter 3) and the yield moment of the fastener. The load-carrying capacity may be increased if the fastener can be loaded axially apart from loading laterally. The increasing value depends on the withdrawal strength of the fastener in the first part and the head/crown pull-through resistance in the second part. In order to calculate the rope effect the crown pull-through resistance of staples in WFIB was examined.

According to EN 1383 [4] about 100 tests with RTSP and PB were carried out. For each of the 15 different WFIB at least four tests were performed. The displacement at maximum load correlates with the thickness of the WFIB. In figure 3 the displacement at maximum load is plotted vs. the thickness of the WFIB. The correlation coefficient is r = 0.893. The slope of the regression straight is m = 0.500 and the y-intercept is b = 0.115.

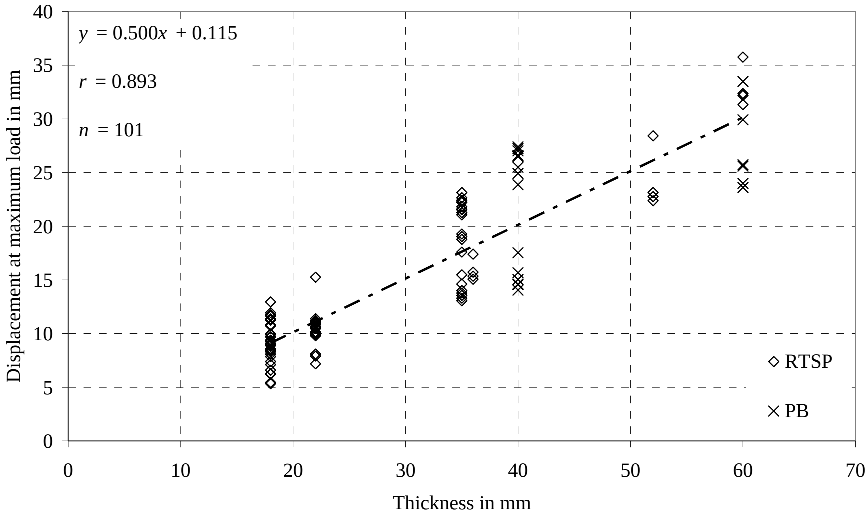

Figure 3 Displacement at maximum load vs. thickness

By means of a multiple regression analysis, equation (3) could be derived to estimate the crown pull-through resistance $R_{ax,2}$ of staples in WFIB.

$$R_{ax,2} = 0.040 \cdot \rho^{1.17} \cdot t^{0.95} \quad \text{in N} \qquad (3)$$

where ρ is the density of the WFIB in kg/m^3 and t the thickness of the WFIB in mm

In figure 4 the tested crown pull-through resistance values are plotted vs. the calculated crown pull-through resistance values. The correlation coefficient is r = 0.814. The slope of the regression straight is m = 1.01 and the y-intercept is b = -0.01. Test results of one RTSP with relative high thickness and density could not be explained by the regression model but test values are greater than calculated values. To explain thicker WFIB with higher densities further tests are needed.

Characteristic values of the crown pull-through resistance may be calculated considering the proposed characteristic densities for the different types of WFIB (equation (4)).

$$R_{\mathrm{ax,2}} = 0.032 \cdot \rho_{\mathrm{k}}^{1.17} \cdot t^{0.95} \qquad \text{in N} \qquad (4)$$

where ρ_{k} is the characteristic density of WFIB in kg/m^3

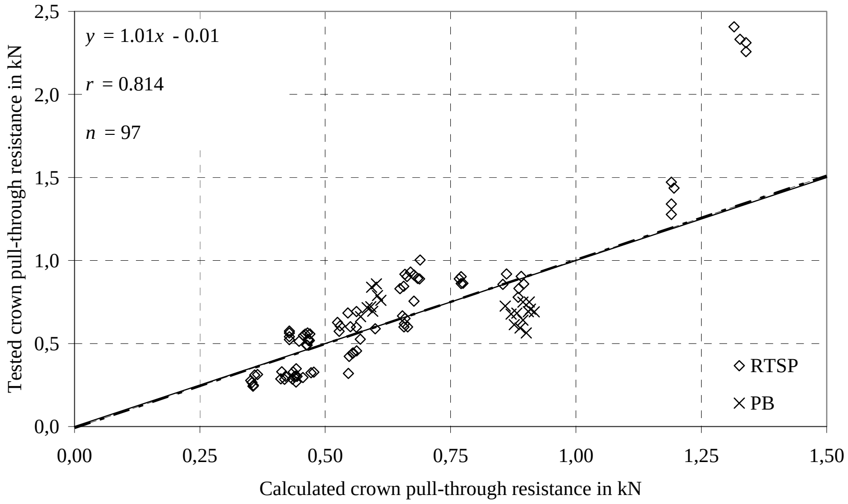

Figure 4 Tested crown pull-through resistance vs. calculated crown pull-through resistance

5 Calculation model for Timber - Wood Fibre Insulation Board – Joints

The load-carrying capacity may be calculated according to Johansen's yield theory considering the different failure mechanisms. If the fastener is driven in through a counter batten, in failure modes 1a and 2b an extension of the existing equations is necessary. In failure modes 1a and 2b the embedding strength in the counter batten is reached and this effect increases the load-carrying capacity. The load path is from the stud into the sheathing board. There is no resulting load in the counter batten. Force and moment equilibrium, considering the existing embedding strength distribution and the yield moment, deliver equation (5) for extended failure mode 1a and equation (6) for extended failure mode 2b. The failure modes activating the influence of the counter batten are shown in figure 5.

$$R = \frac{f_{h1} \cdot t_1 \cdot d}{1+\beta_2}\left[\sqrt{\beta_2 + 2\beta_2^2\left[1+\left(\frac{t_2}{t_1}\right)+\left(\frac{t_2}{t_1}\right)^2\right]+\beta_2^3\left(\frac{t_2}{t_1}\right)^2+\beta_2\cdot\beta_3\left(1+\beta_2\right)\left(\frac{t_3}{t_1}\right)^2} - \beta_2\left(1+\frac{t_2}{t_1}\right)\right] \quad (5)$$

$$R = \frac{f_{h1} \cdot t_2 \cdot d}{1 + 2\beta_2} \left[\sqrt{2\beta_2^2 \left(1 + \beta_2\right) + \frac{4\beta_2 \left(1 + 2\beta_2\right) M_y}{f_{h1} \cdot d \cdot t_2^2} + \beta_2 \cdot \beta_3 \left(1 + 2\beta_2\right) \left(\frac{t_3}{t_2}\right)^2} - \beta_2 \right] \qquad (6)$$

where t_3 is the thickness of the counter batten and $f_{h,3}$ is the embedding strength of the counter batten

and $\beta_2 = \frac{f_{h2}}{f_{h1}}$, $\beta_3 = \frac{f_{h3}}{f_{h1}}$

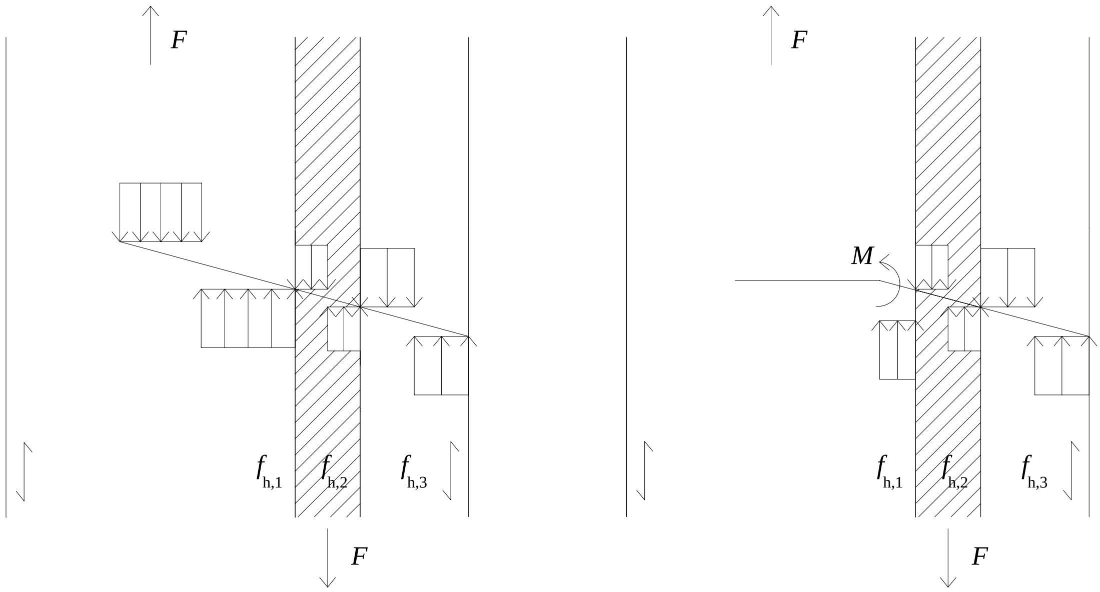

Figure 5 Extended failure modes 1a and 2b according to Johansen's yield theory

6 Tests with Timber-WFIB-Joints

In order to verify the results obtained in the tests presented in chapter 3 and 4 and to examine the stiffness of joints, further tests were performed. Nails and staples were used as fasteners. Staples may be driven directly into the WFIB or through the counter batten like nails. In figure 6 the test specimens for the tests with nails and staples are shown. The relative deformations between WFIB and stud were measured at each of the four fasteners. The tests were carried out according to EN 26891 [5], firstly force-controlled and afterwards displacement-controlled. The maximum load was reached at a displacement of 15 mm. The analysis of the joint stiffness requires linear load-displacement behaviour up to 40% of the maximum load. In the tests non-linear load-displacement behaviour was observed. Due to this the analysis of the stiffness was calculated for a constant displacement of 0.3 mm.

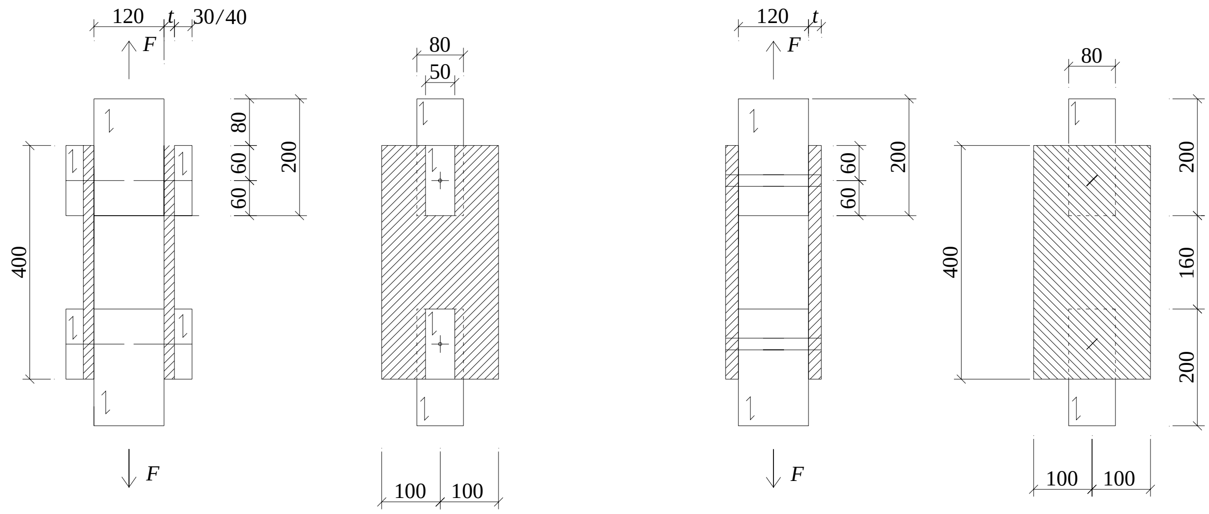

Figure 6 Test specimens for tests with nails and staples

6.1 Tests with nails

27 tests with nails and RTSP were performed. RTSP of three manufacturers in three thicknesses respectively and two nail diameters were used. The load-carrying capacity may be obtained according to Johansen's yield theory considering the results in the presented tests and the extended calculation model. The yield moments of the nails were evaluated according to EN 409 [6]. The embedding strength of WFIB was determined in previous tests (see chapter 3) and the embedding strength of the timber was calculated according to DIN 1052 [7] considering the evaluated densities. Although failure mode 1b was authoritative, failure mode 3 was observed in the tests. This may be explained by friction between the joint members. The withdrawal resistance and the pull-through resistance were calculated according to DIN 1052. In figure 7 the tested load-carrying capacity is plotted vs. the calculated load-carrying capacity.

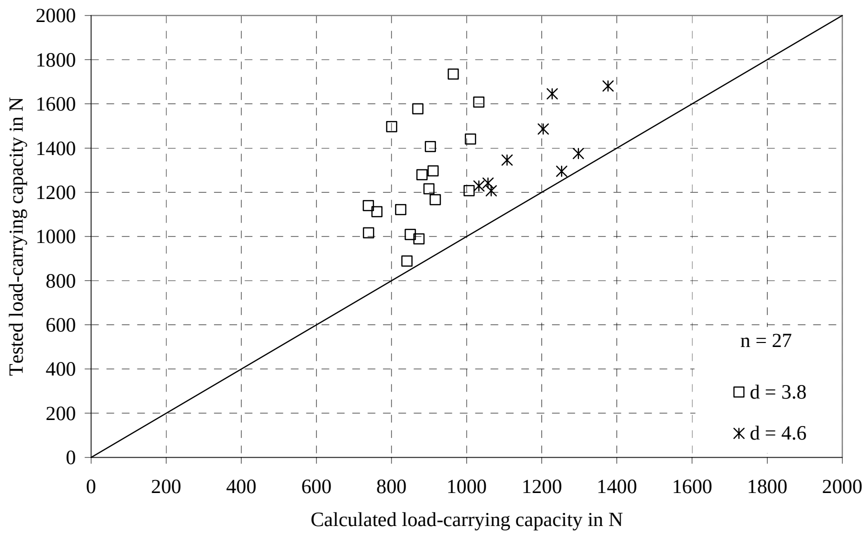

Figure 7 Tested load-carrying capacity vs. calculated load-carrying capacity for nails

6.2 Tests with staples driven in through counter battens

27 tests with staples and RTSP were performed. RTSP of three manufacturers in three thicknesses respectively were used. The load-carrying capacity may be obtained according to Johansen's yield theory considering the results in the presented tests and the extended calculation model. The yield moments of the staples were evaluated according to EN 409 [6]. The embedding strength of staples in WFIB was calculated according to equation (1) assuming the validity for diameters smaller than the tested ones and the embedding strength of the timber according to DIN 1052 [7] considering the evaluated densities. The withdrawal resistance was calculated according to DIN 1052. In figure 8 the tested load-carrying capacity is plotted vs. the calculated load-carrying capacity.

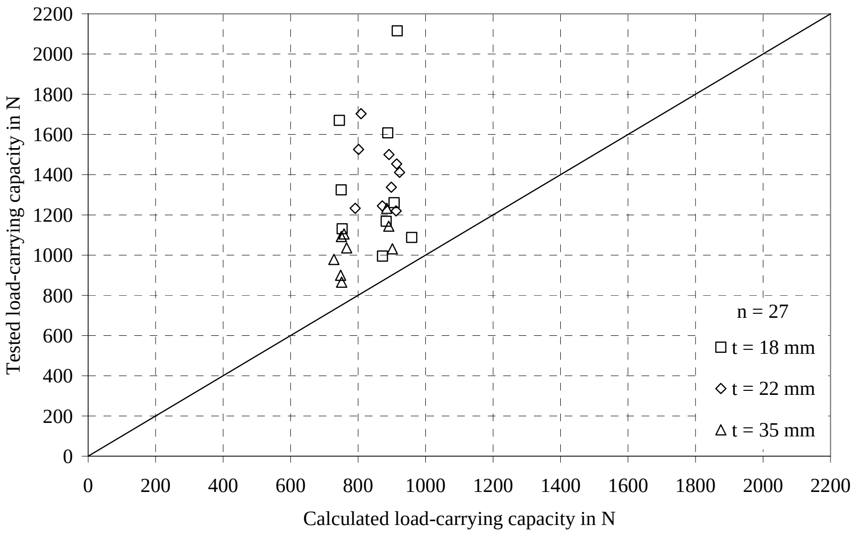

Figure 8 Tested load-carrying capacity vs. calculated load-carrying capacity for staples driven in through counter battens

6.3 Tests with staples driven in directly

36 tests with staples and RTSP/PB were performed. RTSP and PB of three manufacturers were used. The load-carrying capacity may be obtained according to Johansen's yield theory considering the results in the presented tests. The yield moments of the staples were evaluated according to EN 409 [6]. The embedding strength of staples in WFIB was calculated according to equation (1) assuming the validity for diameters smaller than the tested ones and the embedding strength of timber according to DIN 1052 [7] considering the evaluated densities. The pull-through resistance was determined in previous tests (see chapter 4). In figure 9 the tested load-carrying capacity is plotted vs. the calculated load-carrying capacity.

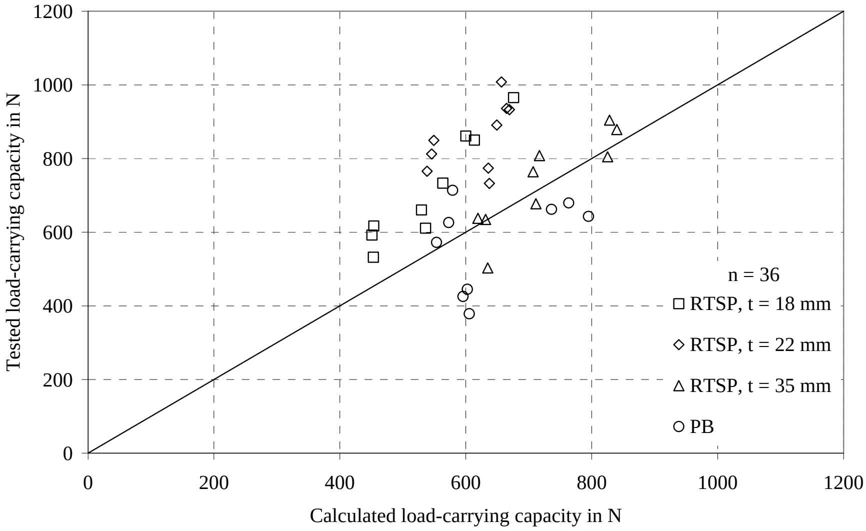

Figure 9 Tested load-carrying capacity vs. calculated load-carrying capacity for staples driven in directly

6.4 Stiffness of timber-WFIB-joints

By means of a multiple regression analysis, equation (7) could be derived to calculate the stiffness of a timber-WFIB-joint. In figure 10 the tested stiffness is plotted vs. the calculated stiffness. The correlation coefficient is r = 0.814. The slope of the regression straight is m = 1.01 and the y-intercept is b = -0.01.

$$K_{\text{ser}} = 1.25 \cdot \rho_{\text{WFIB}}^{0.80} \cdot \rho^{0.30} \cdot t^{-0.32} \cdot d^{1.29} \qquad \text{in N/mm} \qquad (7)$$

where ρ_{WFIB} is the density of the WFIB in kg/m^3, ρ is the density of the timber in kg/m^3, t is the thickness of the WFIB in mm and d is the diameter of the fastener in mm

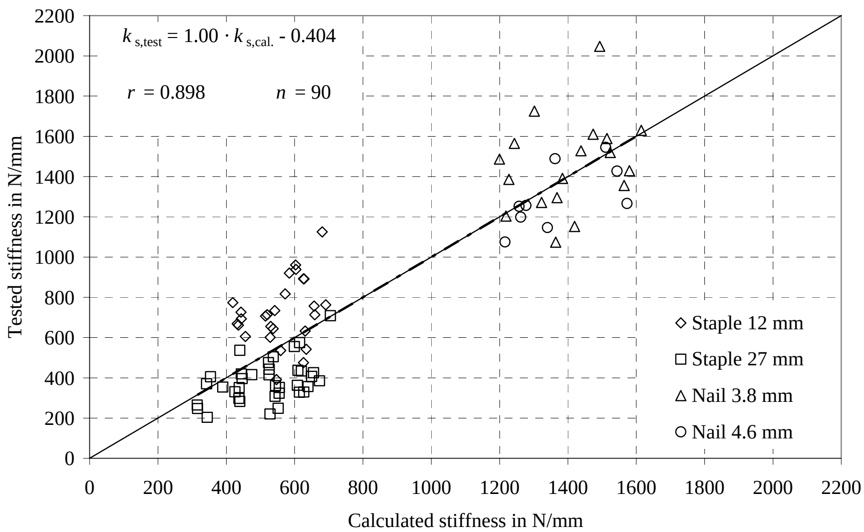

Figure 10 Tested stiffness vs. calculated stiffness

7 Conclusions

The embedding strength of nails in WFIB was tested. As result of a multiple regression analysis, the embedding strength may be calculated considering the density of the WFIB and the diameter of the fastener. In further tests, the pull-through resistance of staples in WFIB was examined. The pull-through resistance depends on the thickness and the density of the WFIB. To consider the influence of a counter batten in the failure modes according to Johansen's yield theory, the equations for two failure modes were extended. The results of the previous tests were used to calculate predictive values of the load-carrying capacity of timber-WFIB-joints tested in further tests. The stiffness of timber-WFIB-joints may be calculated depending on the densities of the joint members, the thickness of the WFIB and the diameter of the fastener. With these results the load-carrying and displacement characteristics of timber-WFIB-joints may be evaluated and further be used for the calculation of shear walls with WFIB sheathing.

8 References

[1] Johansen, K. W.: Theory of timber connections. International Association of bridge and structural Engineering, Bern. P. 249-262

[2] EN 383:1993: Timber structures; Test methods; Determination of embedding strength and foundation values for dowel type fasteners

[3] Blaß, H. J.; Gebhardt, G.: Holzfaserdämmplatten – Trag- und Verformungsverhalten in aussteifenden Holztafeln. Karlsruher Berichte zum Ingenieurholzbau, Band 14, Lehrstuhl für Ingenieurholzbau und Baukonstruktionen (Ed.), Universität Karlsruhe (TH), will be published in 2009

[4] EN 1383:1999: Timber structures; Test methods; Pull through resistance of timber fasteners

[5] EN 26891:1999: Timber structures; Joints made with mechanical fasteners; General principles for the determination of strength and deformation characteristics

[6] EN 409:1993: Timber structures – Test methods – Determination of the yield moment of dowel type fasteners

[7] DIN 1052:2004: Design of timber structures – General rules and rules for buildings

CIB-W18/42-7-6

INTERNATIONAL COUNCIL FOR RESEARCH AND INNOVATION IN BUILDING AND CONSTRUCTION

WORKING COMMISSION W18 - TIMBER STRUCTURES

PREDICTION OF THE FATIGUE RESISTANCE OF TIMBER-CONCRETE-COMPOSITE CONNECTIONS

U Kuhlmann

P Aldi

Institute of Structural Design/Universität Stuttgart

GERMANY

Presented by P Aldi

H.J. Blass received confirmation that the groove joints failed in shear. He asked how you would design such a case. P. Aldi said that code values would be used and uniform distribution of shear stress would be considered which is higher than values in the standard. A simplified model will be used as there is not much literature available.

They discussed the fact that results are dependent on the geometry and the static resistance of the timber uses kfatigue info from the code. H.J. Blass stated that this still needs shear strength information of the material; the approach needs more work.

J. Köhler asked whether the temperature was measured. P. Aldi gave a positive response in which the temperature was measured and there was small difference especially with low frequency. J. Köhler asked about the issue of accumulative time to loading and DOL effect in timber.

P. Aldi said that there are load duration models in timber but these are not the main points of the thesis.

P. Crocetti asked whether a modified shape of the groove would give better results. P. Aldi agreed that one can have the benefit. Some references however show the case with different angles and there seemed to be little impact. He said that in this case there are some compression forces in the notch. Also the theory under predicted the test results which shows there must be some compression.

M. Fragiacomo stated that the inclined surface with shrinkage of timber may create a gap so it may not be reliable. P. Aldi said that they have been trying to develop a model. H.J. Blass questions whether there will be a separating layer between the concrete and timber. There may be a gluing effect between timber and concrete. This means that the influence of inclination will not be strong.

Prediction of the fatigue resistance of timber-concrete-composite connections

Prof. Dr.-Ing. U. Kuhlmann, Ing. P. Aldi
Institute of Structural Design/Universität Stuttgart, Germany

1 Introduction

Lack of knowledge about the fatigue behavior of the interface between timber and concrete may be regarded as one of the difficulties of the further spread of timber-concrete-composite structures (TCC-structures) for the construction of road bridges. The first objective of this study is an analysis of the fatigue strength of TCC-beams, in which the joint between the two single sections of timber and concrete is achieved by either grooved connections or crosswise glued-in rebars. These fastening methods seem to be suitable for bridges due to their relative high stiffness as well as strength values. An investigation about the fatigue resistance of such kind of connections might also help to spread the application of TCC-beams for the construction of small or middle span composite bridges.

Load standards, like EN1991-2 [1] or the German DIN-FB 101 [2], state a number of fatigue verifications for road bridges, which have to be included in the design calculation of bridges. For the timber parts of these structures, certain information about fatigue strength is included in Annex A of EN 1995-2 [3], or in DIN 1074, Anhang C [14]. Within these codes the information is limited to pure timber elements, timber-timber joints and steel-timber connections. There is no information about the fatigue resistance of connections between timber and concrete.

2 Previous works and motivation

Investigations concerning ultimate load capacity and stiffness of the mentioned timber-concrete connections have been reported in a number of publications, but only a few of them refer to the fatigue strength of TCC constructions. A very short review of the results contained in these reports (see [4], [5] and [6]) was presented in [8]. The results of another new investigation have been published in 2008. Two series of symmetrical pulsating push-out tests were carried out in Brazil by J.C. Molina [7]. The specimens had been produced with rebars glued-in solid wood with two different geometrical arrangements. In one series the fasteners have been installed perpendicular to the timber-concrete interface, in the other series with an inclination of 45°. For each set a number of 3 specimens were tested. The significant research data taken from the mentioned four publications are summarized in the Table 1. Only one of the 19 reported tests failed due to fatigue (see Tab. 1, the specimen named “CP01”). The other specimens were loaded with more than 10^6 cycles and in some cases more than $2{\cdot}10^6$ cycles without any collapse. The results of these investigations are not easy to compare to each other, considering that geometries (symmetrical or asymmetrical push-out specimens), materials (in three papers the use of softwood is reported, in one hardwood) and applied methods (i.e. the used load frequency) were different. Under these conditions it is quite difficult to gain sufficient information in order to draw an S-N line for the tested connections. However without such an S-N curve a general verification of a TCC structure under fatigue loading is not possible.

Tab. 1 Available fatigue research data for TCC connections (cp. [4], [5], [6] and [7])

References	Series	Number of Specimens	Maximal Load F_{max}	Load Ratio $R=F_{min}/F_{max}$	Applied Cycles
[4]	Xp$^{(*)}$	1	0.27·Fult	0.06	$1.0 \cdot 10^6$
	Xe$^{(*)}$	1	0.23·Fult	0.06	$2.1 \cdot 10^6$
	VN$^{(*)}$	1	0.17·Fult	0.06	$1.2 \cdot 10^6$
	XN$^{(*)}$	1	0.17·Fult	0.06	$1.7 \cdot 10^6$
[5]	$^{(+)}$	3	0.44·Fult	0.43	$>2.0 \cdot 10^6$
[6]	S$^{(-)}$	2	0.35·Fult	0.17	$>2.0 \cdot 10^6$
	K$^{(\#)}$	2	0.35·Fult	0.17	$>2.0 \cdot 10^6$
	X$^{(*)}$	2	0.35·Fult	0.17	$>2.0 \cdot 10^6$
[7]	CP06$^{(*)}$	1	0.3·Fult	0.167	$2.0 \cdot 10^6$
	CP07$^{(*)}$	1	0.4·Fult	0.125	$2.0 \cdot 10^6$
	CP10$^{(*)}$	1	0.5·Fult	0.100	$2.0 \cdot 10^6$
	CP04$^{(+)}$	1	0.3·Fult	0.167	$2.0 \cdot 10^6$
	CP08$^{(+)}$	1	0.4·Fult	0.125	$2.0 \cdot 10^6$
	CP01$^{(+)}$	1	0.5·Fult	0.100	$7.7 \cdot 10^5$

$^{(*)}$ = 45° inclined glued-in rebars; $^{(+)}$ = rebars perpendicular to the timber – concrete interface; $^{(-)}$ = special steel connector; $^{(\#)}$ = grooved connection.

3 Experimental investigations

3.1 Push-out tests

3.1.1 Materials and methods

The push-out tests have been carried out using two different types of connectors: notches and crosswise glued-in rebars. During the first phase of the testing program a series of monotonic tests was carried out to get the mean values of the ultimate load capacity and stiffness of the connectors.

The timber elements have been produced with glulam of the strength class GL32h (according to [9] and [10]). The concrete strength class was C30/37 (in accordance with [11]). These materials have been used for both test series. The glued-in rebars for the X-connector series were made of steel BSt 500 (cp. [11]) and had a nominal diameter of 16 mm.

The specimens consisted of three main parts: two identical external reinforced concrete slabs simulating the concrete deck of the bridge and a middle timber element simulating the timber beam. The geometry of the push-out test series is shown in Fig. 1. The groove had a length of $l_v = 200$ mm and a depth of $t_v = 40$ mm. For the specimens with crosswise glued-in rebars the connection between timber and concrete was realized with steel elements positioned with a 45° angle between their main axis and the timber-concrete shear surface. The rebars were glued-in with a two components epoxy resin.

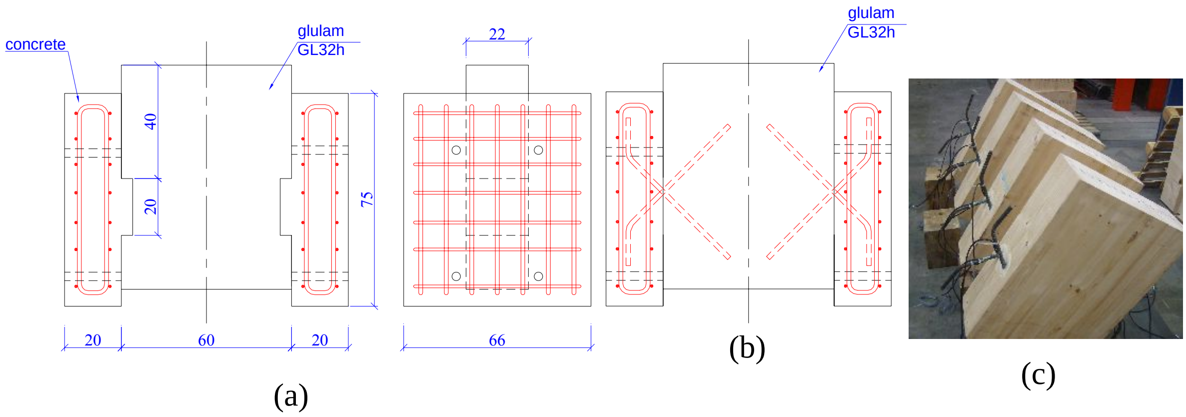

Fig. 1 Geometry of the push-out specimens

The load was applied on top of the timber element parallel to the grain (cp. Fig. 2). A steel I-profile and a steel plate were placed between the load actuator and the glulam for a better load distribution.

Fig. 2 Specimen under load

To determine the relative slip between timber and concrete, 4 inductive transducers were placed in the lower part of each specimen (cf. Fig. 2). Assuming that the stiffness at the interface on the right side and on the left side of the specimen was approximately equal, the mean value of the measured slip was used to determine the slip modulus of the connection. Furthermore on both sides of the specimen 4 additional transducers were installed: two near the connectors (notches or glued rebars) and two in the upper part of the specimen. Thereby, it was possible to observe the distribution of the slip in vertical direction. Two strain gauges were placed at every glued-in rebar, to investigate if the glued-in rebars were under tension (or alternatively under compression) or if an additional moment occurred in the connectors (compare Fig. 1 (c)).

The same set up was used for both, the monotonic and the fatigue tests. The only difference was the application of a larger number of transducers for the slip measurement during the static tests. Furthermore the strain gauges applied on the rebars of the X-connectors were only in the reference tests and not in the pulsating ones.

3.1.2 Monotonic reference tests

The load for the determination of the mean value of the ultimate load capacity and the stiffness was applied according to the testing standard DIN EN 26891 [12]. In the diagram of Fig. 3(a) a typical load-slip curve for the specimens with grooved connection is shown. All the values obtained with the 12 transducers applied on the specimen “N2” are visible. A photo of a notched specimen at the end of the test, with cracked parts of the glulam beam is presented in Fig. 3(b). The same mechanical behaviour has been observed during the experiments of all the reference tests with notched connection. After an initial phase of regular growth of displacement the failure has been reached, due to the formation and immediate propagation of a crack between the concrete notch and the upper edge of the timber. The formation of this kind of shear plane in the timber appeared first on one side of the specimen and nearly simultaneously the same happened on the other side.

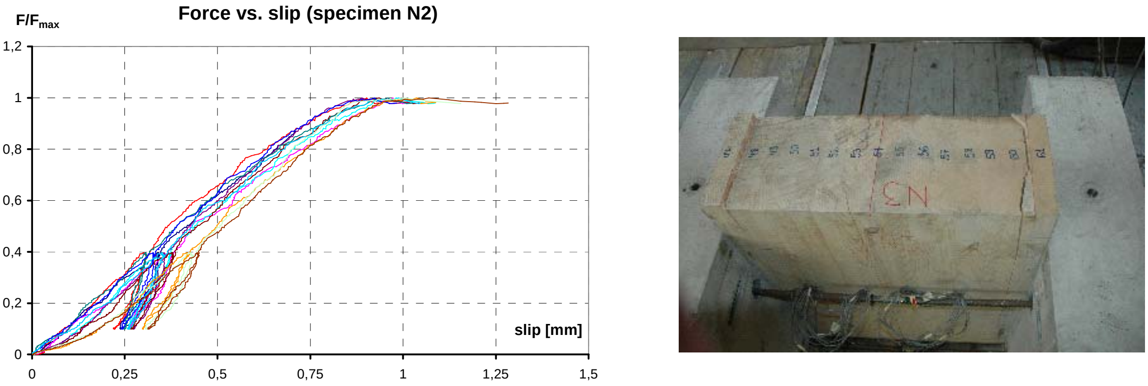

(a) (b)

Fig. 3: Results of a reference test with grooved connections

Very small slip values between timber and concrete have been recorded by the inductive transducers until the specimen suddenly failed in a brittle manner. Not only the failure mechanisms were the same, but also the ultimate load measured for each notch during the three different tests were very close to each other.

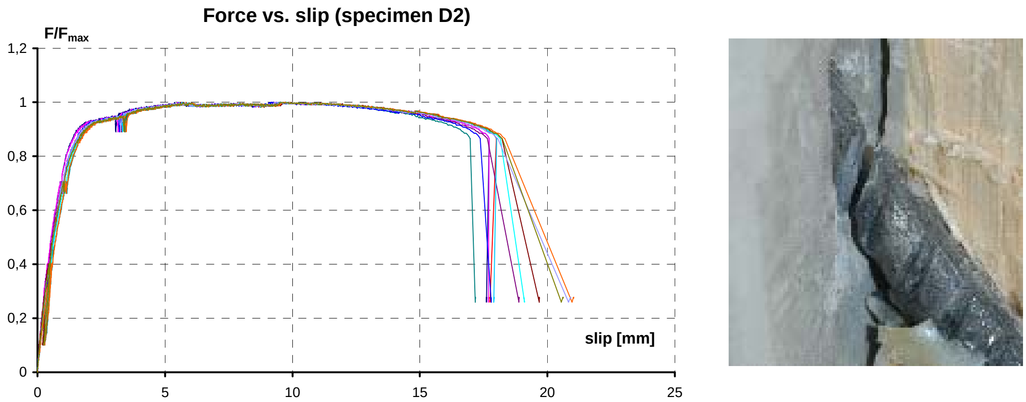

(a) (b)

Fig. 4: Results of a reference test (X-connector)

In the case of the X-connectors a very ductile behaviour has been observed during the tests. This is also visible in the diagram of Fig. 4(a), where the slips between concrete and timber are shown against the force measured by the load cell during the test of the specimen “D2”. The failure occurred after reaching the ultimate tension stress in the rebars. Only the rebars under tensile stress failed (cp. Fig. 4 (b)).

Tab. 2 Summary of the push-out reference tests

Specimen	F_{ult}/VBM	k_i/VBM	k_s/VBM
	[kN]	[kN/mm]	[kN/mm]
N1	250.15	364.1	377
N2	251.77	271.0	311
N3	288.55	400.8	471.8
mean values	**263.49**	**345.3**	**386.6**
D1	255.33	158.2	151.5
D2	224.45	196.6	184.5
D3	229.38	180.3	172.9
mean values	**236.39**	**178.37**	**169.63**

Neither failure of the timber fiber nor of the epoxy resin nor of the concrete has been observed in the tests. Also the stiffness values were very similar within the three tests. The mean value of the stiffness is about 50 % of the value observed for the notched details. In this case very similar ultimate load values have been measured. A summary of the results obtained from the reference tests is listed in Table 2

3.1.3 Pulsating fatigue tests

The fatigue tests were performed under load control. Before the application of the pulsating load, a "static" pre-load was applied on the specimens. The form of the fatigue load was a sine wave with a frequency value of about 2.5÷3 hertz. Only compressive forces were applied, a reversed loading with tension forces has not been examined. A load ratio "R" of 0.1 (for each test) has been chosen in order to reach a relative high slope for the S-N curve, see [3] or [14]. Thus a high damage of the used materials (for pulsating compression loads) is ensured. In Fig. 5 (a) a typical diagram of the measured slips vs. the number of cycles for the specimen "N8" with grooved connection is presented.

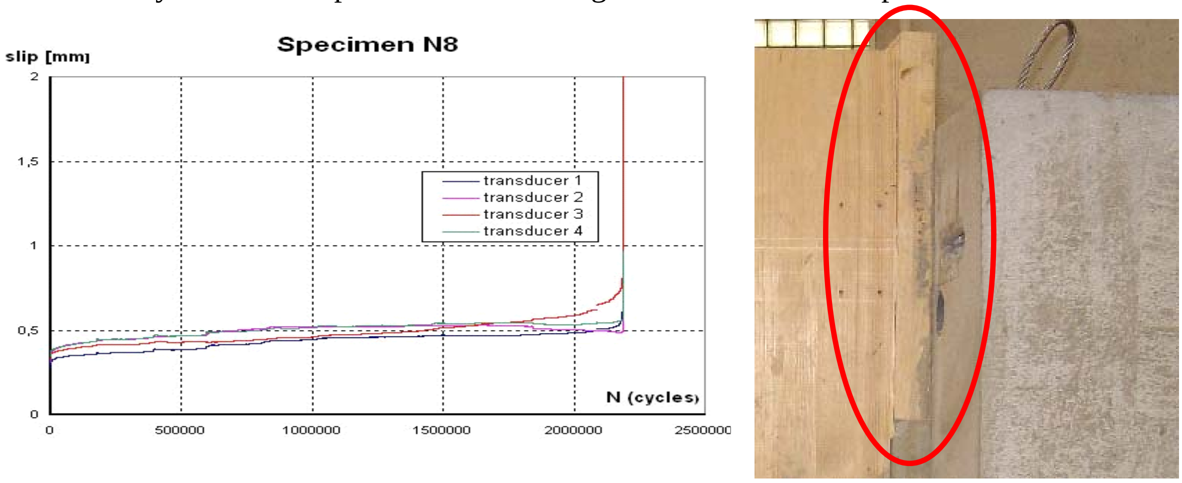

(a) (b)

Fig. 5: Results of a pulsating test (grooved connection): shear failure.

For the fatigue tests only four transducers, placed in the middle of the concrete notch (or at the crossing point of the rebars, for the X-connectors) were used. In Fig. 5(a) the maximum slip values for each cycle related to the higher force values applied to the specimen are shown. The initial slip values correspond to the elastic behaviour of the material. After an initial phase of fast slip development, the relative displacement values tend to increase almost constantly until about $1.7 \cdot 10^6$ cycles. During this phase the crack was propagating starting from the edge of the notch. Just before the failure the slip values, on the side of the propagation of the crack, increased very rapidly, while on the other side the slip remained nearly constant. The failure mechanism, a shear failure of the timber board at the notch, was the same as observed in the monotonic reference tests. A photo of a cracked specimen after the fatigue test is shown in Fig. 5(b).

The collapse mechanism of the specimens with glued-in rebars also was the same as in the corresponding reference tests. The steel rebars under tension failed and neither the timber nor the concrete nor the epoxy resin appeared to be severely damaged at the end of the fatigue test (cp. Fig. 6). The main difference compared to the static tests was the sudden failure without any previous signs of incipient collapse while during the reference tests a long ductile phase and a corresponding high deformation of the specimens have been observed.

Fig. 6: Fatigue failure mechanism -X-connector

A summary of the results obtained from the fatigue push-out tests is presented in Tab. 3. Two tests are marked as run-out. In these cases the tests were stopped after more than $6{\cdot}10^6$ cycles, with visible damage (crack) of the timber, but without a complete failure. The value of the residual carrying capacity has then been determined with a further static test.

Tab. 3 Summary of the push-out fatigue tests

Specimen	F_{max}/VBM	Cycles to failure	Residual carrying capacity	
Grooved connection	[kN]		[kN]	
N4	197,6	4400	-	
N5	197,6	4910	-	
N6	197,6	1820	-	
N7	131,7	48000	-	
N8	131,7	2220000	-	
N9	131,7	686500	-	
N10	110	991800	-	
N12	110	*6403531**	210	(run out)
N13	110	650000	-	
X-Connector				
D5	169,8	4570	-	
D6	169,8	4790	-	
D7	169,8	640	-	
D8	113,2	62000	-	
D9	113,2	184200	-	
D10	113,2	62600	-	
D11	64	1440000	-	
D12	64	1410000	-	
D13	64	*6081900**	224.7	(run out)

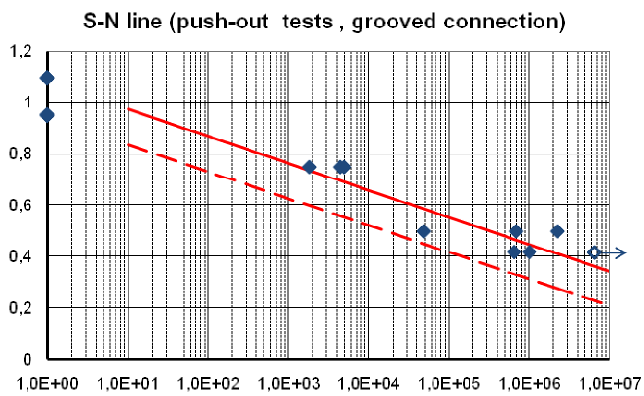

Fig. 7: S-N curve for the notched connection (push-out tests, red lines giving mean values and 95% fractile)

Fig. 7 shows the obtained S-N curve for the grooved specimens. The y-axis represents the ratio between the applied forces and the mean value obtained with the monotonic tests; on the x-axis the cycles to failure for each performed test are given in a logarithmic scale. The line in the diagram, based on the results of 11 tested push-out speci-mens, has been calculated by means of a linear regression and the least squares method without considering the run-out test, however taking into account the mean static value.

Following the same procedure the fatigue strength in the form of an S-N line has also been calculated based on the results of the specimens with glued-in rebars. The curve followed the corresponding line of fatigue resistance of reinforcing steel as given in EN 1992-1-1 ([13]).

3.2 Beam Tests

3.2.1 General

In order to transfer the S-N-lines obtained in the push-out tests to the calculation of a road bridge with timber-concrete-composite beams, a control seems to be important. The fatigue behaviour of the composite beam has to be similar to the behaviour of the previous tested push-out specimens, even if the direction of the applied forces in a beam differs from the situation in a push-out test. Therefore 9 TCC-beams with grooved connection have been tested with a three point bending scheme. The aim of these tests was to obtain shear failure in the interface of timber and concrete and to compare the number of cycles to failure of the beam with the obtained S-N line of the connection.

3.2.2 Materials and methods

The materials used for the production of the 9 composite beams were of the same strength class used for the push-out specimens. Test geometry and the set-up are shown in Fig. 8. The slip between timber and concrete was measured at the middle of each notch (on both sides of the timber) and also at each end of the beam. In addition a number of transducers were used for recording the vertical deflections and the horizontal movements of the specimen. Three beams were loaded monotonically to quantify the ultimate load capacity. A pulsating vertical load was applied on the other six specimens with a force ratio "R" chosen to 0.1 for each beam. Also for the beams the fatigue test were started after the application of a "static" pre-loading phase.

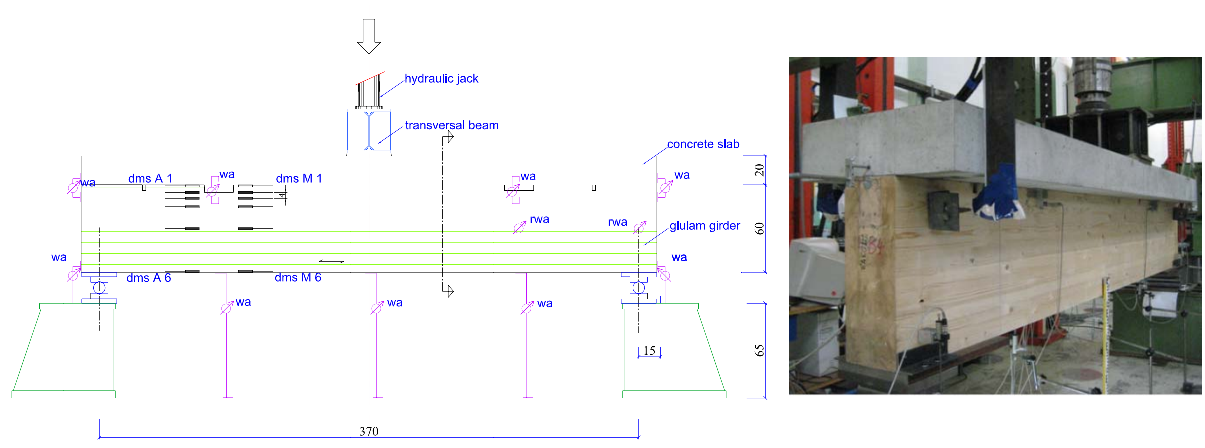

Fig. 8 Geometry and set-up of the beam tests

3.2.3 Results

Two of three monotonically loaded specimens failed as planned due to the formation of a crack parallel to the grain near the contact surface between timber and concrete at the edge of the notch (see Fig. 9 (a)). The third specimen reached a higher value of ultimate load capacity, however showed a different failure mechanism: a shear failure occurred at the support of the beam in the middle of the section (see Fig. 9 (b)). There also was a higher scatter of the ultimate loads of the beam tests in comparison to the push-out tests.

The expected failure, shear timber failure at the notch, could be observed for the majority of specimens under fatigue load. One of the six fatigue loaded beams was a run-out. After

$2{\cdot}10^6$ cycles and with a visible crack, this test was stopped. The residual load capacity tested afterwards reached the same order as the monotonic load test, see Table 4, where a summary of both, monotonic and pulsating beam tests, is given.

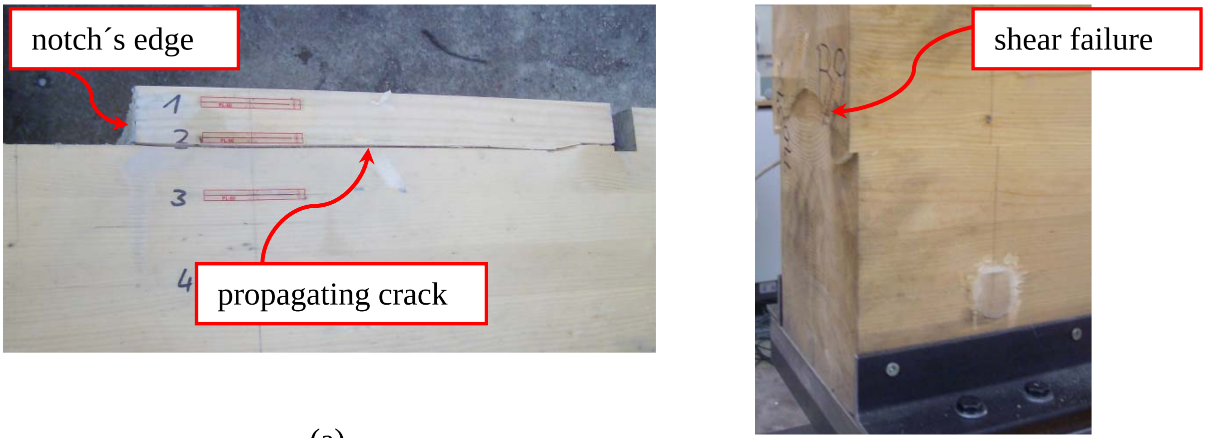

(a) (b)

Fig. 9 Failure mechanisms of the monotonic tests

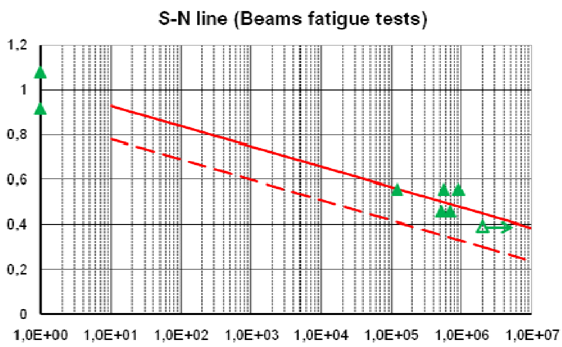

Fig. 10 S-N line of the beam tests including mean regression line and 95% survival probability

In the Fig. 10 the S-N-line for the beams is presented showing at the y-axis the applied forces divided by the mean value obtained with the monotonic testcharacteristic strength, on the x-axis the cycles to failure in a logarithmic scale. The S-N line in the diagram has been calculated by means of a linear regression and the least squares method without considering the run-out test, however taking into account the corresponding mean static value.

Tab. 4 Summary of the beam tests (monotonic and fatigue)

Specimen (beams)	Ultimate load capacity	Applied F_{max} (hydraulic jack)	Cycles to failure	Residual carrying capacity	
Grooved connection	[kN]	[kN]		[kN]	
B1	611.00	-	-	-	
B8	718.16	-	-	-	
B9	*820.00**	-	-	-	(shear failure at the support)
B6	-	369	120000	-	
B4	-	369	548850	-	
B2	-	369	904950	-	
B3	-	304	694250	-	
B7	-	304	516200	-	
B5	-	259,4	*2000000**	738.48	(run out)

4 Comparison with rules in EN 1995-2

As the failure of the notched connection tests is a timber shear failure, it seems reasonable to compare the obtained experimental results with the S-N line for shear in timber given in [3], [14]. In the diagram of Fig. 11 the blue line represents the values according to EN 1995-2, Annex A, equation (A.4) or DIN 1074, Anhang C, equation (C.5). This equation:

$$k_{fat} = 1 - \frac{1-R}{a(b-R)} log_{10}(\beta \cdot N_{obs}) \geq 0 \quad (1)$$

has been used to calculate the values of cycles to failure. The parameters "a" and "b" have been set to 6.7 and 1.3 respectively (for shear) and β has been taken as 3 (substantial consequences in case of failure is assumed here). The red line represents the regression line based on the observed data from the push-out tests (the same as in Fig. 7). The results of the push-out tests are given as blue dots. The dashed line in the diagram represents the limit above which one may expect a 95% survival probability (with a 95% confidence) for a next possible test also based on the push-out tests. The results of the beam tests are given as green triangles and show a convincing accordance with the tendency of the push-out results.

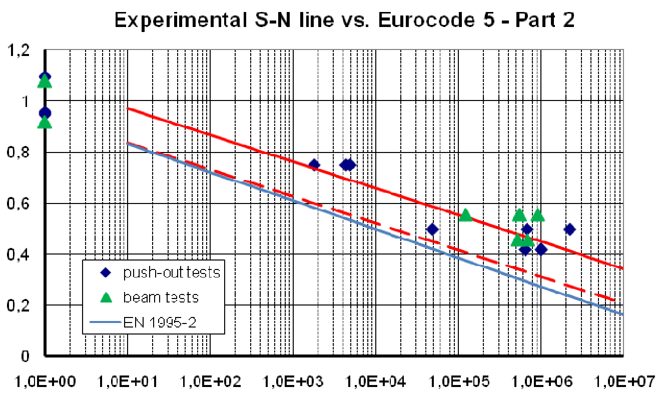

Fig.11 Experimental S-N-line vs. indication of Eurocode for timber in shear

At least in the range of applied load cycles, which is important for the fatigue resistance (>10^4), the use of the above mentioned parameter values in eq. (1), according to EN 1995-2, leads to a safe estimation of the number of cycles to failure. Thus a prediction of the connection lifetime with eq. (1) could be considered as safe for the failure mode of timber shear failure at the notch according to § 3.1.2. Similar conclusions may be drawn for the fatigue behavior of X-Connectors.

5 Conclusions

Neither S-N curves nor other analytical means are currently available to predict the lifetime of timber-concrete-composite structures under pulsating load. Two new series of investigations based on shear fatigue tests have been carried out with the aim to obtain a sufficient number of data about the fatigue behavior of the timber-concrete shear interface in composite structures. A first preliminary S-N curve for the notch in grooved TCC structures, based on symmetrical push-out tests, has been presented. A number of composite beam tests were carried out to confirm the results obtained with the push-out tests. Furthermore a comparison with the rule given in EN 1995-2 indicates the possibility to use the available S-N line for timber shear faitugue failure for grooved connections with the investigated geometry. This would lead to a safe prediction of the number of cycles to failure for the connection and will be useful for the fatigue verification of TCC structures in road bridges.

Acknowledgements

The research has been financially supported by the German Society for Wood Research (DGfH) and by the German Federation of Industrial Research Associations (AiF). These two Institutions are gratefully acknowledged.

6 References

[1] EN1991-2, *Eurocode 1: Actions on structures - Part 2: Traffic loads on bridges,* CEN, September 2003

[2] DIN Fachbericht 101, *Einwirkungen auf Brücken*, Beuth Verlag, 2009.

[3] EN1995-2 *Eurocode 5: Design of timber structures - Part 2: Bridges,* CEN, August 2004.

[4] Tommola, J.; Salokangas, L. and Jutila, A., *Wood- Concrete Composite Bridges: Tests on Shear Connectors,* Technical report, Helsinki University of Technology, Laboratory of Bridge Engineering, Nordic Timber Bridge Project,1999.

[5] Davids, W.; Dagher, H.; Sanchez, O. and Weaver, C. (2005), *Bridge with Composite Concrete Deck and Glued Laminated Girders Strengthened with Fiber-Reinforced-Polymer,* Technical report, Advanced Engineered Wood Composites Center - University of Maine, 2005.

[6] Döhrer A. and Rautenstrauch K., "Connectors for timber-concrete composite-bridges", Paper 39-7-3, *Proceedings of CIB – W18,* Florence, 2006

[7] Molina, J. C., *Análise do comportamento dinâmico da ligação formada por barras de aço coladas para tabuleiros mistos de madeira e concreto para pontes,* PhD thesis, Escola de Engenharia de Sao Carlos da Universidade de Sao Paulo, 2008.

[8] Kuhlmann, U. Aldi, P., *Fatigue of timber-concrete-composite beams: characterization of the connection behaviour trough push-out tests* WCTE 2008 Miyazaki, Japan, 2008.

[9] DIN 1052, *Entwurf, Berechnung und Bemessung von Holzbauwerken - Allgemeine Bemessungsregeln und Bemessungsregeln für den Hochbau,* DIN - Deutsches Institut für Normung e. V., 2008.

[10] DIN EN 1194, *Brettschichtholz - Festigkeitsklassen und Bestimmung charakteristischer Werte*, DIN - Deutsches Institut für Normung e.V., 1999.

[11] DIN 1045-1, *Tragwerke aus Beton, Stahlbeton und Spannbeton - Teil 1: Bemessung und Konstruktion,* DIN - Deutsches Institut für Normung e. V, 2001.

[12] DIN EN 26891, *Holzbauwerke – Verbindungen mit mechanischen Verbindungsmitteln, Allgemeine Grundsätze für die Ermittlung der Tragfähigkeit und des Verformungsverhaltens,* DIN – Deutsches Institut für Normung e.V., 1991.

[13] DIN EN 1992 1-1, *Eurocode 2: Design of concrete structures - Part 1-1: General rules and rules for buildings,* CEN European Committee for Standardization, 2004.

[14] DIN 1074, *Holzbrücken* , DIN – Deutsches Institut für Normung e.V., 2006.

CIB-W18/42-7-7

**INTERNATIONAL COUNCIL FOR RESEARCH AND INNOVATION
IN BUILDING AND CONSTRUCTION**

WORKING COMMISSION W18 - TIMBER STRUCTURES

USING SCREWS FOR STRUCTURAL APPLICATIONS IN LAMINATED VENEER LUMBER

D M Carradine

M P Newcombe

A H Buchanan

University of Canterbury, Christchurch

NEW ZEALAND

Presented by D M Carradine

H.J. Blass discussed about the EC5 values and the model assumptions at the pivot point. He asked whether there is compression stresses perpendicular to grain there. Given the pivoting deformation the other screws may have minor impact. He also asked how the thickness of the steel plate was chosen. D.M. Carradine answered that the design of the steel plate was based on bending for all different types of specimens.

E Gehri discussed shearing out failure of the timber and commented that the behaviour of the timber is important because of group action as this is part of the failure.

A. Ceccotti stated that the self centering idea is a good one and asked whether there are plans to study other cases such as wall system. D.M. Carradine responded that this will be considered.

Tuomo Poutanen stated that this technique looks expensive and asked whether a study on the cost of these joints will be carried out. D.M. Carradine agreed that this could be expensive.

F. Lam commented that average values should not be compared against characteristic values.

K. Crews stated that there are also interests in cost of repair after an earthquake and the speed of construction is okay.

Using Screws for Structural Applications in Laminated Veneer Lumber

D. M. Carradine, M. P. Newcombe and A. H. Buchanan
University of Canterbury
Christchurch, New Zealand

Abstract

There is a large body of research currently underway in New Zealand investigating the behaviour and design of multi-storey and long-span structures utilizing laminated veneer lumber (LVL) as beam, column and wall components. Screws have significant potential for use as fasteners for a myriad of connections throughout these buildings. While considerable research has been conducted on the use of screws in solid timber and glue laminated timber (glulam), there is currently a lack of data on the behaviour of screws when used with LVL. In many cases screws are installed parallel to the laminations (and glue-lines) and subjected to withdrawal loading, so it is necessary to determine appropriate configurations of screws that can be safely used in these situations. Monotonic testing on double shear screwed connections in LVL has been performed on specimens with varying screw configurations, LVL thickness and member depth. Direct withdrawal tests of screws installed into the edge grain of LVL, parallel to the glue lines were conducted using varying screw penetration depth, screw spacing and numbers of screws. Comparisons are drawn between existing standards for determining screw connection capacity typically used for solid timber and glue laminated material and the capacities of the screwed connections in LVL. Recommendations are made for calculating LVL connection strength using screws as well as the limitations of existing design code predictions when using screws installed parallel to glue lines in LVL.

1. Introduction

In an effort to increase the use of timber for structural applications throughout New Zealand and Australia, research is being conducted on the behaviour and design of multi-storey and long-span timber buildings using a patented post-tensioned timber system to create moment resisting frames and wall systems. These building systems incorporate large timber sections, constructed of laminated veneer lumber (LVL), held together using steel post-tensioning tendons. These buildings have significant potential to compete with current forms of construction in concrete and steel (Smith, 2008) and allow for open floor plans suitable in a large range of commercial or office type structures. Additionally, these buildings have the ability to re-centre themselves after a seismic event, and the inclusion of energy dissipating devices allows for energy absorption and dynamic damping during an earthquake.

Past and continued experimental research on post-tensioned LVL buildings in New Zealand has focused primarily on building components including beam-column joints, and timber-concrete floor systems (Iqbal et al., 2008 and Yeoh et al., 2008). Currently a 2/3 scale two-storey structure using this technology has been designed, fabricated by regional glue laminators and erected at the University of Canterbury as shown in Figure 1. This building will be tested over the next several months to assess the structural integrity of the system when subjected to biaxial pseudo-static lateral loading. In order to accommodate the necessary movement of the structure due to lateral loads and to minimise damage to the floors during rocking, innovative connections between beams and floor joists and supporting post-tensioned frame and wall systems were required. These connections were designed using locally available self-drilling screws to be hung from corbels, which were screwed to the larger building components as seen in Figure 2, using methods provided in ANZ Standard 3603 (SNZ, 1993) and the Timber Design Guide (Buchanan, 2006) based on methods for designing connections in solid sawn timber and glue laminated timber. The design of these connections using LVL have been based on the assumption that the behaviour under load will be the same as solid sawn timber, but research has indicated that caution should be exercised when using existing design standards for structural composite lumber products, such as LVL (Snow et al., 2008). Additionally, because the screws in many of these connections have been installed parallel to the glue lines in the LVL and are subject to withdrawal loading, there is concern that failure modes of these connections have not been accurately covered in standard timber design methods.

Figure 1. 2/3 Scale Post-Tensioned Test Structure at the University of Canterbury

Figure 2. Hanging Beam/Floor Joist Connections

Several studies have been conducted on the behaviour of screws for connections and reinforcement in solid timber and glue laminated structures. Inclined screws in timber were tested and modelled by Bejkta and Blaß (2002). Newcombe et al. (2009) expanded on this work by testing laterally loaded connections between LVL floor joists and laminated LVL framing members using screws installed at 90º and 45º. These connections provided adequately strong, stiff and ductile connections intended for use with multiple storey timber structures using LVL. Jöhnsson and Thelandersson (2005) investigated the effectiveness of screws used for reinforcement against perpendicular to grain stresses in curved glue laminated structures. Bejkta and Blaß (2005) tested dowel connections in timber with screws as reinforcement and developed a model to predict the behaviour of these connections. They also verified the effectiveness of screws as reinforcement in timber supports using tests and developed a model (Bejkta and Blaß, 2006). All three previously mentioned studies verified the effectiveness of using screws as reinforcement in timber.

Because LVL is a proprietary product, very few research projects aimed at quantifying its behaviour have been performed. Kairi (2004) investigated bolted connections in LVL fabricated with the laminations oriented diagonally. Hummer et al. (2006) included LVL in a study on tension perpendicular to grain strength, which concluded that LVL was weaker than solid timber in tension perpendicular to grain loading. Bier (2003) provided test data and discussion on issues raised regarding highly loaded structures fabricated from LVL. In general, LVL manufacturers publish design values for their products, but this does not include values for screws installed parallel to the glue lines subject to withdrawal. This lack of information creates a distinct need for testing and validation of design methods for screwed connections in LVL in order to further the use of rocking connections in LVL structures.

2. Experimental Methods and Materials

The objectives of the project were on the one hand to assess the actual capacity of the rocking connections designed for the current demonstration building constructed at the University of Canterbury, and secondly to determine the withdrawal strength of screws installed parallel to the glue lines of LVL, for comparison with published design recommendations.

2.1. Connection Testing

The testing configuration utilised for the connection tests was double shear as shown in Figure 3. Due to the unique nature of the connections, ASTM Standard D 7147 – 05 Standard Specification for Testing and Establishing Allowable Loads for Joist Hangers (ASTM, 2008a) was used as a guideline for test procedures. Loads were applied to joist members using a 250 mm x 250 mm steel plate attached to the cross head of an Avery testing frame and were applied at a consistent rate such that failure did not occur before 5 minutes. Displacement measurements were obtained at both ends of the joist member with respect to the LVL end blocks. Load and displacement data were obtained using a computer controlled data acquisition system.

Testing configurations are described in Table 1, below. Screws were locally purchased self-drilling, 14 Gauge Type 17 screws having a shank diameter of 5.3 mm. Observations indicated that splitting could occur when installing the screws, therefore tests were also conducted with screws installed in pre-drilled holes having a diameter consistent with Eurocode 5 (EC5, 1994) and NZS 3603 (SNZ, 1993) recommendations. The LVL used came primarily from one of the two major LVL manufacturers in New Zealand, although a partial set of tests was also performed using LVL from the other manufacturer for comparison. Sample sizes were a minimum of three, with most having between five and nine specimens tested. The specimens using the other LVL manufacturer contained only two specimens each and were used only as a spot check of possible difference between the two manufacturers. Sample sizes were kept small due to the complexity of the connections and for the reason that once effective connection configurations were determined, additional testing would be conducted using larger sample sizes.

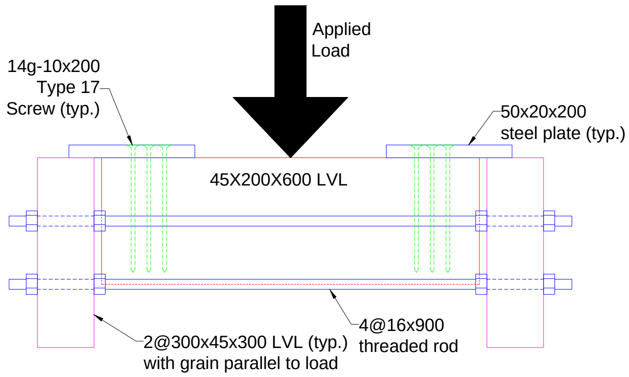

Figure 3. LVL Connection Testing Configuration

Table 1. LVL Connection Testing Configurations

Configuration	Joist Thickness (mm)	Number Of Screws per Side	Depth of Joist (mm)	Steel Plate Dimensions (mm)	Screw Length (mm)
1	45	3	200	20x50x200	200
2	45	3	100	20x50x200	100
3	65	7	200	25x50x342	200
4	3x65	28	200	2@25x125x342	150

As testing progressed on these initial four connection types, other connection possibilities became apparent and were tested also. Configuration 2 from Table 1 was tested using 6 mm diameter high tensile strength threaded rods and a 6 mm thick steel plate beneath the joist instead of relying on the withdrawal or tensile capacity of the screws but this was not included in the results as the capacity was based on threaded rod capacity. Additionally it was observed that the first screw in the row of three used for Configuration 1 was the screw taking most of the load, therefore Configuration 1A reconfigured the three screws so that the first row contained two screws rather than one as shown in Figure 4 and was only testing using pre-drilled holes. Additional tests were also performed to assess the capacities of the LVL corbels, but this will be the focus of a separate paper.

Figure 4. LVL Test Connection Configuration 1A

2.2. Withdrawal Testing

Direct withdrawal tests of 14 Gauge Type 17 screws installed into the edge of LVL members parallel to the glue line were conducted using ASTM D 1761-06 (ASTM, 2008b) as a guideline. LVL used was from a single New Zealand supplier and were prisms 200 mm deep and 400 mm long using the apparatus shown in Figure 5. In all cases screws were installed at the centre top face of the prisms, with the screws installed parallel to the glue lines and perpendicular to the top face. Configurations were varied based on number of screws (1, 2, 3 and 5), penetration depth (40, 60 and 80 mm), screw spacing (25 and 50 mm) and LVL thickness (45 and 65 mm). Table 3 describes the specific screw withdrawal combinations tested. Most withdrawal tests were conducted without pre-drilling, but some configurations using 65 mm thick LVL were pre-drilled to assess the effects.

Figure 5. Direct Withdrawal Testing Apparatus for Screws in LVL

Table 2. LVL Screw Withdrawal Testing Configurations

Number of Screws	LVL Thickness (mm)	Screw Spacing (mm)	Penetration Depth (mm)
1	45 and 65	0	40, 60 and 80
2	45 and 65	25 and 50	60 and 80
3	45 and 65	25 and 50	60 and 80
5	45 and 65	25 and 50	60 and 80

2.3. Supplemental Testing

In addition to withdrawal and double shear connection tests describe above, moisture content specimens were obtained from tested specimens and examples of 200 mm long 14 gauge Type 17 wood screws in tension to determine the average ultimate capacity of 17.56 kN.

3. Results and Comparisons

Presented in this section are experimental test values for double shear connection capacity and withdrawal strength tests performed, and descriptions of failure mechanisms observed. Comparisons are provided between average test data and predicted design capacities from NZS 3603:1993 (SNZ, 1993).

3.1. Connection Testing Results

Testing previously described was conducted on a series of connections subject to double shear and averages of each configuration are presented in Table 3, which represent the applied loads for each side of the tested specimens. Failure modes for Configurations 1 and 1A were primarily due to screw breakage, most often starting with the outermost screws. Configuration 2 specimens began splitting upon installing the screws when no pre-drilling was done, contributing to screw withdrawal as the mode of failure, which was similar for the specimens with pre-drilling, although the lack of splitting in pre-drilled specimens resulted in greater ultimate connection capacity. Small splits were also observed between fasteners following installation of screws for Configuration 3 specimens without pre-drilling, and both pre-drilled and non pre-drilled specimens failed as a result of a combination of withdrawal and screw breakage, although screw breakage was considered to be the primary and limiting failure mode. Configuration 4 specimens failed as a result of perpendicular to grain splitting of the LVL at the plane where the screws ended.

Table 3. LVL Double Shear Connection Testing Results and Comparisons with Design Standard Values

Configuration	Average Test Capacity With No Pre-Drilling (kN)	Average Test Capacity With Pre-Drilling (kN)	NZS 3603 Design Strength (kN)
1	12.44	12.45	4.31
1A	NA	19.70	7.58
2	8.33	11.57	3.26
3	17.78	19.46	9.17
4	NA	43.87	27.60

While the data obtained provided verification that these screwed LVL connections were sufficiently strong, experimental observations suggested that the behaviour of these double shear connections was more complex than simple withdrawal of the fasteners, but also incorporated aspects of bending as the steel plate was displaced and some amount of shear due to the lateral movement of the steel plate in connections where a notch prevented the free rotation of the plate. In order to design these connections it was assumed that the steel plates were rotating about the inside corner of the steel plate and that the distribution of load to the line of fasteners would be linear due to the relative stiffness of the steel plate. It is worth noting that the strength reduction factor used for determining capacities of connections was 0.7, the most stringent in NZS 3603 (SNZ, 1993) and resulted in very conservative design values. Comparisons with test capacities provided acceptable factors of safety, but decreased as the number of screws per connection was increased. Pre-drilling holes did not have a significant effect on Configuration 1, but the capacity of Configurations 2 and 3 increased by 39% and 9.5%, respectively when pre-drilled holes were used.

3.2. Screw Withdrawal Testing Results

Screw withdrawal testing from the edge of LVL was conducted as previously detailed and averages of each configuration are presented in Table 4. Failure mode for all single screw withdrawal tests was withdrawal of the screw from the LVL. Screw withdrawal continued to be a failure mode when two and three screws were installed at 50 mm spacings, but when spacings were reduced to 25 mm a type of plug shear failure was observed where a segment of timber was removed from the region between the screws as load was applied. Examples of this failure mode are shown in Figure 5. None of the screws fractured during withdrawal testing.

Table 4. Average Screw Withdrawal Parallel to the Glue Line from LVL Testing Results and Comparisons with Design Standard Values

Number of Screws	Penetration Depth (mm)			Screw Spacing (mm)		LVL Thick-ness (mm)		Average Testing Withdrawal Strength (kN)	Eurocode 5 Withdrawal Strength (kN)	NZS 3603 Design Withdrawal (kN)
	40	60	80	25	50	45	65			
1	X					X		7.3	8.6	3.2
1	X						X	8.0	8.6	3.2
1		X				X		11.5	12.3	4.8
1		X					X	10.6	12.3	4.8
1			X			X		16.0	15.8	6.4
1			X				X	13.1	15.8	6.4
2		X		X		X		19.4	23.0	9.5
2			X	X		X		25.8	29.5	12.7
2		X			X	X		20.8	23.0	9.5
2		X		X			X	15.7	23.0	9.5
2			X	X			X	21.7	29.5	12.7
2			X		X		X	25.1	29.5	12.7
2		X			X		X	17.0	23.0	9.5
3		X		X			X	21.2	33.2	14.3
3*		X		X			X	22.2	33.2	14.3
3			X	X			X	27.2	42.5	19.1
3*		X			X		X	23.5	33.2	19.1
5		X		X			X	22.2	52.5	23.9
5*		X		X			X	25.1	52.5	23.9
5			X	X			X	32.2	67.4	31.8

*Pre-drilled Specimens Tested

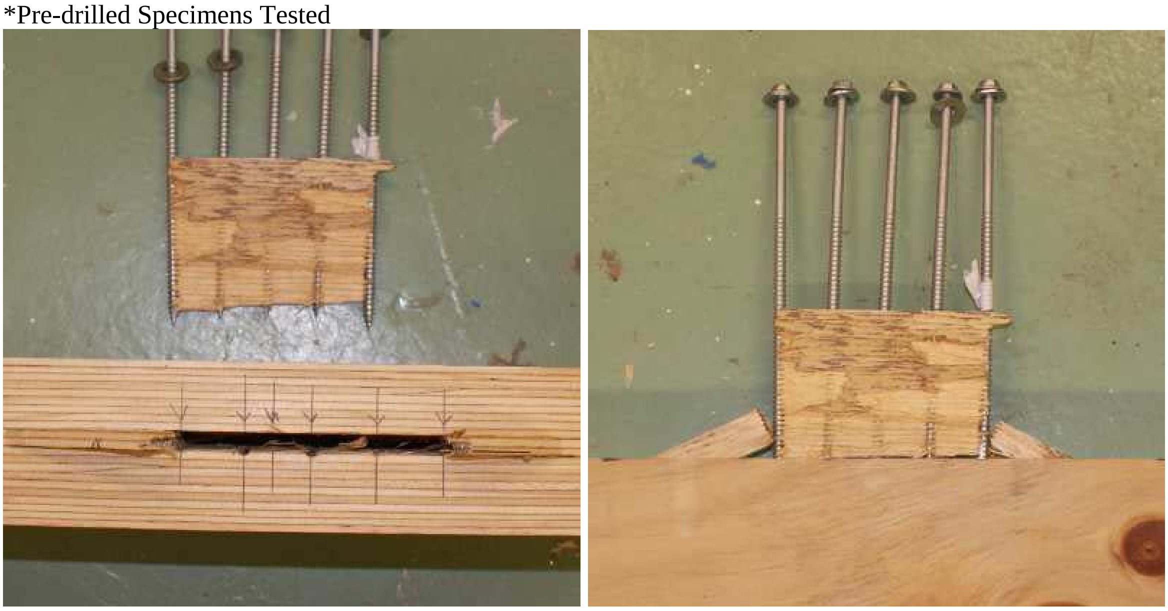

Figure 5. Shear Plug Failures Observed During Screw Withdrawal Tests from LVL

Direct screw withdrawal tests in LVL provided data on behaviour of these connections subject to withdrawal loads and on the effects of connection parameters. Loads clearly increased in a very predictable fashion with increases in penetration depth. Pre-drilling resulted in slightly increased strength values and 65 mm thick LVL consistently had lower withdrawal strength values that 45 mm thick LVL. Increased fastener spacing from 25 mm to 50 mm also provided slightly increased strength. The strength increases with increased numbers of screws decreased as the number of screws went from two to three to five. Specimens having more than two screws installed 40 mm deep into 45 mm thick LVL were prone to perpendicular to grain splitting of the LVL which was attributed to the length of the specimens, therefore only 65 mm thick was used for specimens having more than two screws. Penetrations deeper than 80 mm also resulted in screw failures and were not included within these data presented.

Screw withdrawal test data comparisons with design values obtained from Eurocode 5 (EC5, 1994) and NZS 3603 (SNZ, 1993) suggest that there are some connection predictions which are unconservative. A significant number of Eurocode 5 predictions were greater than experimental test values. This over estimation of connection capacity increased as the number of screws increased as can be seen in Table 4. The same trend is seen in design predictions from NZS 3603, but most of the values in this case tend to be less than the experimental strengths and for single screws a reasonable factor of safety is achieved. Five screw withdraw strength predictions from NZS 3603 are nearly equal to the experimental strengths but without any margin of safety.

4. Recommendations and Future Research

Analysis of results from testing screwed connections in LVL where fasteners were installed parallel to the glue lines has provided valuable information on the behaviour of these connections which are being used for rocking timber systems for multi-storey and long span structures. Due to the lack of design information on these types of connections in LVL it was necessary to test structural connections for capacity in double shear in order to verify the strength experimentally. Design values obtained using NZS 3603 were considered adequate and allowed for factors of safety between 1.6 and 3.5. While these connections have been shown to be effective for this application, it is recommended that different connections with screws in LVL be similarly investigated.

Predicted screw withdrawal values from Eurocode 5 and NZS 3603 were considered unconservative especially when larger numbers of screws were used. Because increased fastener spacing resulted in only minimal strength increases, it is recommended that designers exercise caution when predicting the strength of screwed connections subject to withdrawal loads parallel to the glue lines using multiple fasteners. Spacing between multiple fasteners needs to be researched further in order to understand the plug shear failure mode described previously and to determine at what spacing this will no longer be a consideration. Screw placement should also be manipulated and tested, such as staggering rather than installing fasteners in a continuous line, as a means of avoiding this failure mode, which reduced direct withdrawal capacity.

It is recommended that investigations on the differences between solid timber, glulam and LVL be conducted for inclusion of appropriate factors for adjusting design capacities to account for the structural behaviour of LVL as a building material. Timber does not exhibit the plug shear failures observed in LVL, possibly due to rolling shear failure of laminations within LVL once the screws have been installed and this requires further research. Similarly, the effects of using different thicknesses of LVL should be investigated as current codes do not differentiate between them, even though withdrawal tests indicated that thicker LVL had lower withdrawal capacities.

Connections are being developed currently which will have screws installed into the end grain of the LVL, parallel to the glue lines and the longitudinal axis of the member. Corbel connections and the effects of different spacing, screw configuration on splitting at the time of installation are also under investigation at the time of writing this paper. Screws installed diagonally to the face of installation will also be tested and analysed for future connection studies.

5. Conclusions

Experimental testing of screwed connections in LVL designed for rocking timber building systems has shown that design methods in NZS 3603 (SNZ, 1993) provide acceptable predictions of connection failure when loaded vertically. Subsequent testing on a 2/3 scale 2-storey demonstration building at the University of Canterbury will assess the lateral load behaviour of the screwed connections and provide data for the design of these structures. NZS 3603 provided conservative values for these connections due to inherent uncertainty of the fastening method reflected in the standard as well as the assumptions that the designers made in order to predict the behaviour of connections that have never been tested or used in practice. Development of connections similar to these and also for gravity resisting systems that do not require the ability to rock are currently underway and will be presented in future papers.

Direct withdrawal testing of self-drilling 14 gauge Type 17 screws installed in the edge of LVL members parallel to the glue lines provided data indicating that Eurocode 5 (EC5, 1994) and NZS 3603 (SNZ, 1993) predictions of withdrawal strength tended to be unconservative particularly when more than a single screw was installed in a row along the length of the LVL. It was observed that a possible failure mode where a plug of timber between the screws was removed as withdrawal loads were applied is a concern for designers and needs to be investigated because the spacing requirements from both model building codes did not keep this from occurring. Designers should exercise caution when designing these types of connections unless very conservative assumptions are used for the distribution of forces to screws.

6. Acknowledgements

The authors would like to acknowledge the significant contributions of Emmanuel Roubin and Sviatoslov Malko, visiting students from France earning Masters Degrees in Structural Engineering. Emmanuel and Sviatoslov conducted the connection testing and performed analyses and comparisons while fulfilling requirements for their degrees. Their help was fundamental for the completion of this testing programme and was greatly appreciated.

7. References

American Society for Testing and Materials (ASTM) Standards. 2008a. *ASTM D 7147-05 Standard Specification for Testing and Establishing Allowable Loads for Joist Hangers*. West Conshohocken, PA: ASTM.

American Society for Testing and Materials (ASTM) Standards. 2008b. *ASTM D 1761-06 Standard Test Methods for Mechanical Fasteners in Wood*. West Conshohocken, PA: ASTM.

Bejkta, I. and H. Blaß. 2002. Joints with Inclined Screws. CIB-W18 Conference Proceedings: Paper 35-7-4, Kyoto, Japan.

Bejkta, I. and H. Blaß. 2005. Self-Tapping Screws as Reinforcements in Connections with Dowel-type Fasteners. CIB-W18 Conference Proceedings: Paper 38-7-4, Karlsruhe, Germany.

Bejkta, I. and H. Blaß. 2006. Self-Tapping Screws as Reinforcements in Beam Supports. CIB-W18 Conference Proceedings: Paper 39-7-2, Florence, Italy.

Bier, H. 2003. Problems with Shear and Bearing Strength of LVL in Highly Loaded Structures. CIB-W18 Conference Proceedings: Paper 36-12-1, Estes Park, Colorado, USA.

Buchanan, A. H. 2007. *Timber Design Guide*. Timber Design Federation, Wellington, New Zealand.

EC5. 1994. *Eurocode 5: Design of Timber Structures*, ECS, English version.

Hummer, T., J. Dolan and M. Wolcott. 2006. Tension Perpendicular to Grain Strength of Wood, Laminated Veneer Lumber and a Wood Plastic Composite. World Conference on Timber Engineering Proceedings, Portland, Oregon, USA.

Iqbal, A., S. Pampanin and A. Buchanan. 2008. Seismic Behaviour of Prestressed Timber Columns Under Bi-Directional Loading. Proceedings, World Conference on TimberEngineering, Miyazaki, Japan.

Jöhnsson, J. and S. Thelandersson. 2005. Load Carrying Capacity of Curved Glulam Beams Reinforced with Self Tapping Screws. CIB-W18 Conference Proceedings: Paper 38-7-3, Karlsruhe, Germany.

Kairi, M. 2004. Block Shear Failure Test with Dowel-Type Connection in Diagonal LVL Structure. CIB-W18 Conference Proceedings: Paper 37-7-7, Edinburgh, Scotland.

Newcombe, M., W.A. van Beerschoten, D. Carradine, S. Pampanin, A. Buchanan, B. Deam and M. Fragiacomo. 2009. Experimental Testing of Timber-Concrete Composite Floor Diaphragms. Proceedings, New Zealand Society for Earthquake Engineering Conference, Christchurch, New Zealand.

Smith, T. 2008. "Feasibility of Multi Storey Post Tensioned Timber Buildings: Detailing, Cost and Construction," Master of Engineering Thesis, University of Canterbury, Christchurch, New Zealand.

Snow, M., I. Smith, A. Asiz and M. Ballerini. 2008. Applicability of Existing Design Approaches to Mechanical Joints in Structural Composite Lumber. CIB-W18 Conference Proceedings: Paper 41-7-1, St. Andrews, Canada

Standards New Zealand (SNZ). 1993. *New Zealand Standard NZS 3603:1993 Timber Structures Standard.* Standards New Zealand, Wellington, New Zealand.

Yeoh, D., E. Chuan, M. Fragiacomo, A. Buchanan, K. Crews, J. Haskell and B. Deam. 2008. Development of Semi-Prefabricated Timber-Concrete Composite Floors in Australasia. Proceedings, World Conference on Timber Engineering, Miyazaki, Japan.

**INTERNATIONAL COUNCIL FOR RESEARCH AND INNOVATION
IN BUILDING AND CONSTRUCTION**

WORKING COMMISSION W18 - TIMBER STRUCTURES

INFLUENCE OF FASTENERS SPACINGS ON JOINT PERFORMANCE - EXPERIMENTAL RESULTS AND CODIFICATION

E Gehri

ETH Zürich

SWITZERLAND

Presented by E Gehri

H.J. Blass asked on what basis was the influence of edge distance considered and will one consider the reduction of edge distance? E. Gehri stated yes. The screws can be long and if they are not installed correctly they can go through to the outside of the beam,

A. Jorissen discussed the accumulation of stresses perpendicular to grain and shear; if the spacing is reduced, their influence can increase. The friction between dowel/timber glued-in-rods/timber and screw/timber is different which can influence the stresses. He commented that he can't see why the screws would react the same way as glue-in rod. Finally laterally loaded fastener versus withdrawal behavior was discussed.

P. Quenneville asked how one can say that the measured values are statistically different for the 4th group of a/H. E. Gehri said that it is based on engineered judgment. G. Schickhofer also added that there are recognized group and system effects which support the engineered judgment.

J. Jensen said that the glue effect factor for glued in rods is failing in yielding and not rod in withdrawal and group effect in yielding will not occur. He said that in Eurocode 1st failure is in yielding mode then wood failure mode. In practice you can't get glued in length long enough for yielding to occur; therefore, wood withdrawal failure is occurring. H.J. Blass asked whether there were withdrawal failures or yielding failure of the rods. E. Gehri answered only withdrawal failures were noted.

CIB-W18/42-7-8

Influence of fasteners spacings on joint performance - Experimental results and codification

E. Gehri – ETH Zürich

Introduction

Engineer's first aim is to connect timber pieces together in the most efficient way; that includes performance, economy and reliability. Starting from the known behaviour of a joint – for a given geometry and fasteners arrangement – the performance can be established in relation to load-carrying capacity, stiffness and ductility.

For the evaluation of the above mentioned properties more or less standardized procedures may be applied. Due to the complexity of such a joint (different parameters involved, different failure modes possible) and the lack of reliable strength models the analysis of the influence of fasteners (and of fasteners spacings) is here quite impossible.

Therefore evaluation of fasteners starts mostly from the behaviour of a single or individual fastener; in many cases test procedures are only directed to a single property like the embedding strength (case for dowel-type fasteners) or the withdrawal strength (case for axially loaded screws) for a determined species and wood density. In a second step the interaction in a multiple fastener connection is than considered.

Basically such derived values are only valid for the test geometry and configuration used. The application for actual joint design may be problematic, if the behaviour of the fastener in a joint does not follow the assumed behaviour of an individual fastener.

The **load-carrying capacities** of fasteners are in the Codes generally given in function of fasteners spacings, edges and end distances. In certain cases they are furthermore linked to the number of fasteners acting in a row or in a group. The **stiffness** is implicitly assumed to be independent of fasteners spacing (which is not true). The important and safety relevant property **ductility** has even not found recognition in the Codes; fasteners spacings may highly affect the ductility of a joint.

The weak points in a timber structure are often the joints. Generally the joint presents a lower load-carrying capacity than the two parts to be jointed. Highest performance is linked to an undisturbed (smooth) flux of forces in direction of the fibres. This is achieved the nearest by finger-jointing. More indicated – since a rather smooth flux of forces is possible – are glued-in rods. A near steady flow of shear forces is originated around the rod.

Typical joints with lateral load transmission

The most used mechanically jointing systems are of the dowel type. Limiting wood property on the load-carrying capacity of dowel type fasteners is the embedding strength (local compression strength). They are very efficient for compression joints, but less suitable for tension joints, due to the unfavourable load path.

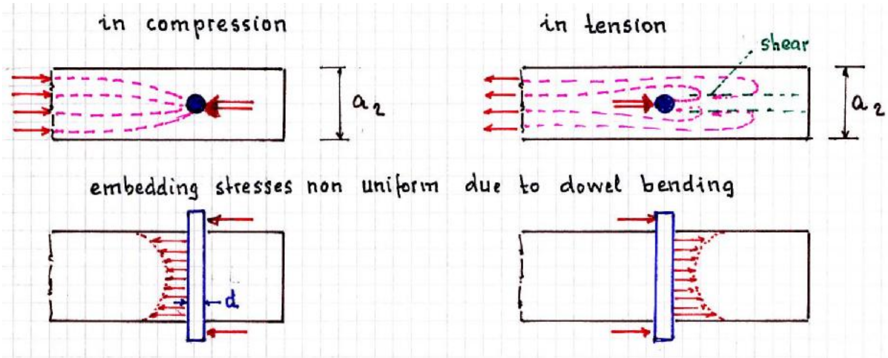

Fig. 1: Load path by lateral load transmission

The load is laterally transmitted through the dowel (originating in the dowel bending and shear) into the timber section. For an individual dowel highest values are obtained with stocky dowels (more uniform embedding). Basically all embedding strength tests are done with very stocky dowels. Test configurations are furthermore such to avoid splitting of the specimen, through use of enough end length and width a_2.

The hole for introducing the dowel into to the timber member leads to an important reduction of the effective section. For a spacing of rows perpendicular to grain $a_2 = 4 \cdot d$ the reduction represents 25%; the minimum possible spacing for dowels is fixed to $a_2 = 3 \cdot d$.

Since in practice more slender dowels are used (stocky dowels should be avoided due to the very brittle failure mode) the embedding is no more uniform. Nevertheless the values found with stocky dowels are used in the strength models. Since the models are finally calibrated, this is of less importance; the embedding strength (or the directly correlated wood density) is used as indicator of the wood property.

Implications of spacings

- Case dowel type connection

What are the implications of spacings on the load-carrying capacity of the individual fastener, which is obtained by the usual test procedure? Experience has shown that by using an adequate (large) spacing, interference may be avoided. To achieve performance corresponding to the net section (joint area) with dowel-type fasteners a longer connection will result. Depending on the stiffness of the fastener and the level of fabrication tolerances an uneven distribution (in length, in a row of fasteners) must be additionally considered.

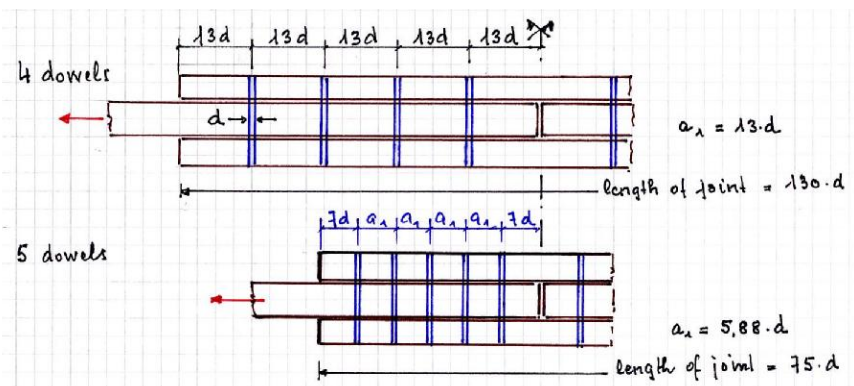

Fig. 2: Dowelled joints of same strength, but different length and number of dowels

In practice shorter connections and therefore shorter spacings are preferred; this leads to a reduction of load-carrying capacity per fastener (which may be compensated by increasing the number of fasteners in a row).

Actual Codes consider this by introducing an effective number of fasteners n_{ef} (acting in a row parallel to grain) or by using a reduction factor $k_n = n_{ef}/n$.

EN 1995-1-1

$$n_{ef} = \min\left[n\,;\, n^{0.9}\cdot\sqrt[4]{\frac{a_1}{13\cdot d}}\right] \qquad \text{or} \qquad k_n = n^{-0,1}\cdot (a_1/13\cdot d)^{0,25} \leq 1$$

DIN 1052 uses the same formulation, but instead of 13·d only a value of 10·d. Minimum spacing a_1 is fixed in both Codes to 5·d.

From the above relationship it may be seen, that the reduction is depending:

- on the number of dowels (in a row); this considers mainly the uneven distribution of forces; important in case of brittle failure modes
- on the spacing a_1; this considers mainly the interference of the neighbouring fasteners on the timber (splitting) strength; by increasing the spacing a_1 to 13·d (or 10·d) the second term becomes 1; only the number of dowels in a row is affecting; this effect can even be reduced by increasing more a_1; e.g. with a_1=20·d and n=3 no reduction ($k_n \approx 1$)

- Case axially loaded fasteners inserted parallel to grain

Most research has been done on the behaviour of a single acting fastener. For timber structures and their connections always a group of fasteners has to be considered. To obtain the desired performance in the timber element to be connected, a dense application of the fasteners is normally needed. From figure 3 it can be seen, that spacing less than 3 to 4 times the diameter may be required for connections parallel to the grain.

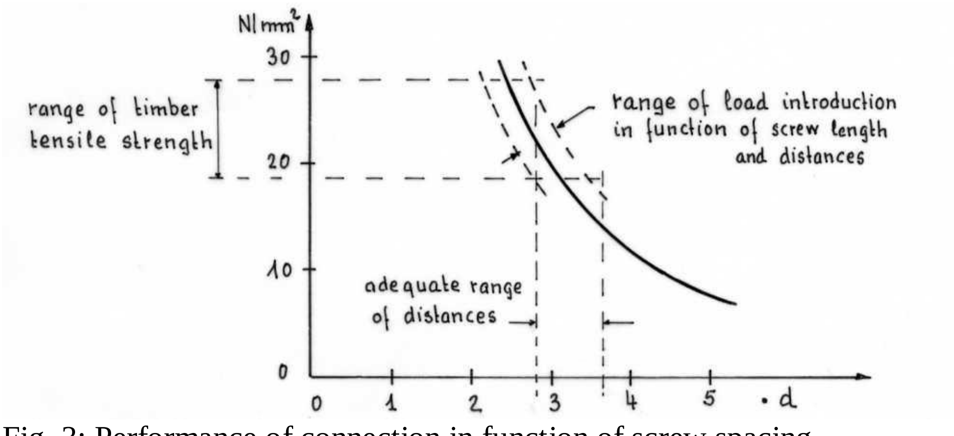

Fig. 3: Performance of connection in function of screw spacing

Tests on glued-in rods and on screws inserted parallel to grain and axially loaded (they behave similar since the load transfer is by shear) have shown, that the optimum relationship of spacing to diameter (or size of timber specimen to diameter) is about 5. Larger spacings do not increase the load-carrying capacity; smaller spacings results in a decrease.

Earlier research (Gehri/2001) had shown that the observed group effect was partly due to an inadequate basis of comparison (not the same rations A_{timber} to A_{steel}).

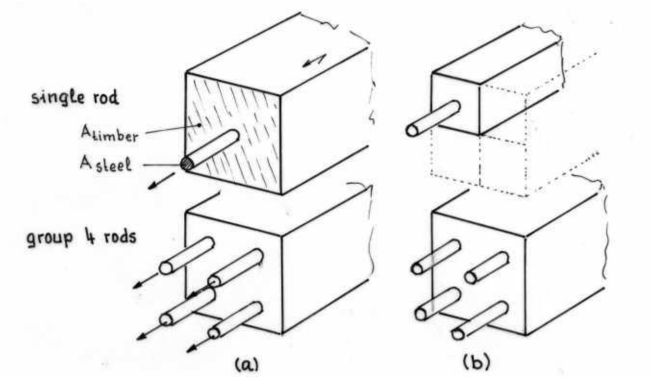

(a) with different ratios
A_{timber} to A_{steel}
therefore different stress levels in the timber member

(b) with same ratios and same stress level

Fig. 4: Testing procedures: (a) – usual; (b) – correct basis for comparison

Tests made with screws parallel to the grain with variation of the ratio A_{timber} to A_{steel} showed a relationship according to figure 5. The smaller the timber section, the higher the stress level in the timber and therefore the higher the strain difference between timber and rod, the lower the apparent nominal shearing strength. Note that no splitting occurred. The values correspond always to a pull out failure.

Fig. 5: Effect of cross-section on the pull-out strength of screws (with normalized density and related to section 40 by 40 mm)

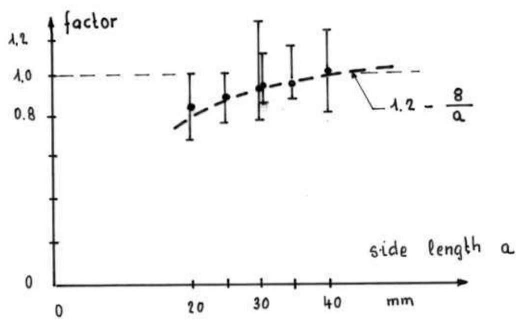

The above relationship (established for screws with d_a = 7,5 mm) $k_{red} = 1{,}2 - (8/a) \leq 1$ can be written in more generalised form $k_{red} = 0{,}57 \cdot (a/d)^{0{,}35} \leq 1$; which leads to the same results. Newer research by Steiger et al (2007) confirmed the validity of the relationship also for glued-in rods. Similar results were published by Blass/Blasewitz (1999). They proposed the following relationship: $k_{red} = 0{,}68 + 0{,}064 \cdot (a/d) \leq 1$.

From this, we can conclude that the optimum relationship a/d is equal to about 5. Larger timber dimensions will not increase the withdrawal strength for axially loaded bars (screws or glued-in rods) parallel to the grain. As long as the group of fasteners shows the same relationship of distance between fastener to diameter of fastener (or a / d), no group effect must be expected: e.g. under these condition $n_{ef} = n$ or $k_{red} = 1$.

From the above it may be concluded, that for connections with glued-in rods or screws, inserted parallel to the grain, no group effect needs to be considered, if the values of the individual rods or screws are based on the same ratio A_{timber} to A_{steel} (or a/d –ratio).

For smaller ratios of a/d than 5, the following reduction has to be used:

$$k_{red} = 0{,}57 \cdot (a / d)^{0{,}35} \leq 1 \quad \text{or} \quad k_{red} = (a / 5 \cdot d)^{0{,}35} \leq 1$$

The second expression is written in the same format as for the lateral loaded dowels, where the reduction part due to spacing is given by $k_{red,spacing} = (a_1 / 13 \cdot d)^{0{,}25}$.

Note: For practical cases values of k_{red} are between 0,85 and 1,0 for axially loaded bars and about 0,80 to 0,85 for lateral loaded dowels. Since for lateral loaded dowels also a $k_{red,number}$ has to be considered, the reduction is therefore more important..

Note: DIN 1052 does not allow the use of screws in end grain (axially loaded parallel to grain); the use of glued-in rods is limited to strengthening measures.

Experimental verification with axially loaded screws parallel to grain

- Scope

The above mentioned studies have shown, that for axially loaded screws or glued-in rods inserted parallel to the grain no group effect has to be considered; furthermore that the influence of reduced spacings than the optimum ones is quite small and can be taken in account by the following expression: $\mathbf{k_{red} = (a / 5 \cdot d)^{0,35} \leq 1.}$ The expression is assumed to be valid for both cases:

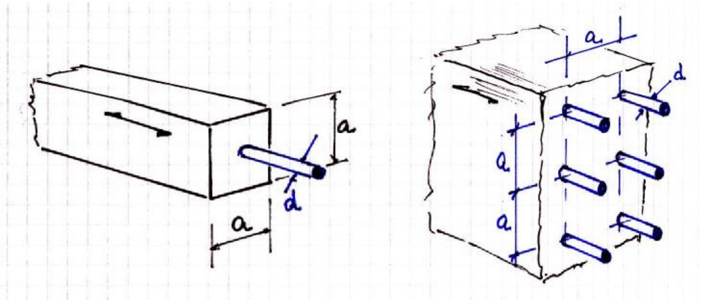

individual screw group of screws

with same ratio A_{timber} / A_{steel} or same ratio a / d

Fig. 6: Cases to be considered

By adequate concept of the experiments the proof of above statements should be possible.

Since the goal was only to show the effect of spacing on the withdrawal strength of the screw, other factors were – as possible – eliminated, by using:

- same type of screw (same diameter and same inserting length)
- timber with similar properties in each test series
- the failure mode should always be by pull-out without splitting of the timber (this was achieved by an adequate preboring and limiting the slenderness to ≤ 15).

- Specimens

The timber used was spruce (Picea abies Karst.); for smaller sections up to 60 by 60 mm from solid timber, for section 125 by 125 mm from glued-laminated timber, composed of 3 boards of nearest possible density (the density was determined for each board before manufacturing). The material chosen was as free as possible of major defects (mainly knots), to achieve the lower bond of withdrawal strength. Knots – even small ones or only near to the screw – will drastically increase the withdrawal capacity. The highest values may therefore not be considered. By sawing or splitting the specimens after testing, this could be proven. Note that the number of culls was rather small; this is due to the fact that double specimens were used. The probability to have on both sides – with the material chosen – a knot was therefore much smaller.

A commercial available self-tapping screw of diameter d_a = 10 mm was used. The pre-boring with diameter of 6 mm corresponded to the core diameter. The effective length used was in all cases equal and determined to 130 mm.

Below are given the dimensions of the specimens, the parameters a/d, the timber dimensions, number of screws and the number of specimens tested.

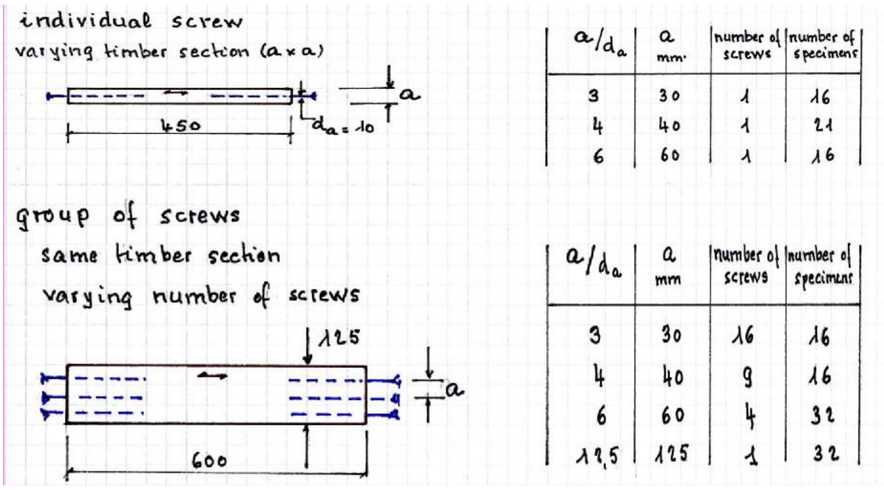

a/d_a	a mm	number of screws	number of specimens
3	30	1	16
4	40	1	21
6	60	1	16

a/d_a	a mm	number of screws	number of specimens
3	30	16	16
4	40	9	16
6	60	4	32
12,5	125	1	32

Table 1: Dimensions of specimens; number of specimens (double number of connections)

The timber used had a moisture content of about 10% (small variations).

The density of the glued laminated specimens varied between 380 and 500 kg/m^3; from each 5,0 m long bar 8 specimens of quite identical density were obtained; from each bar two specimens were than assigned to each series. The result was an identical density distribution for each series.

- Test results for individual screws

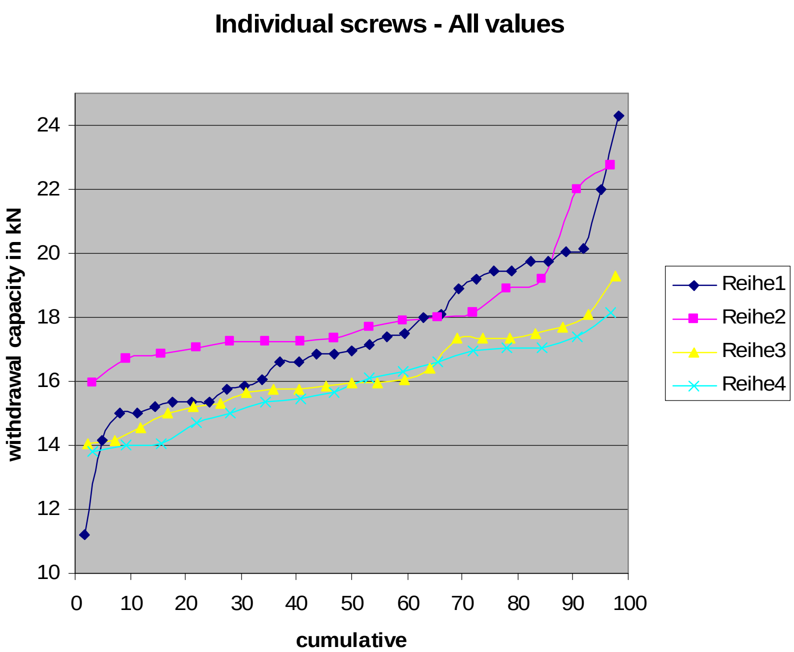

(Reihe 1 to 4) with d/a: 12,5; 6; 4 and 3

Fig 7: Withdrawal capacity of individual screws with varying a/d_a

- Test results for group of screws

The differences between the series a/d=6 (with 4 screws) and a/d=4 (with 9 screws) are very small, only for a/d=3 (with 16 screws) a clear difference is shown.

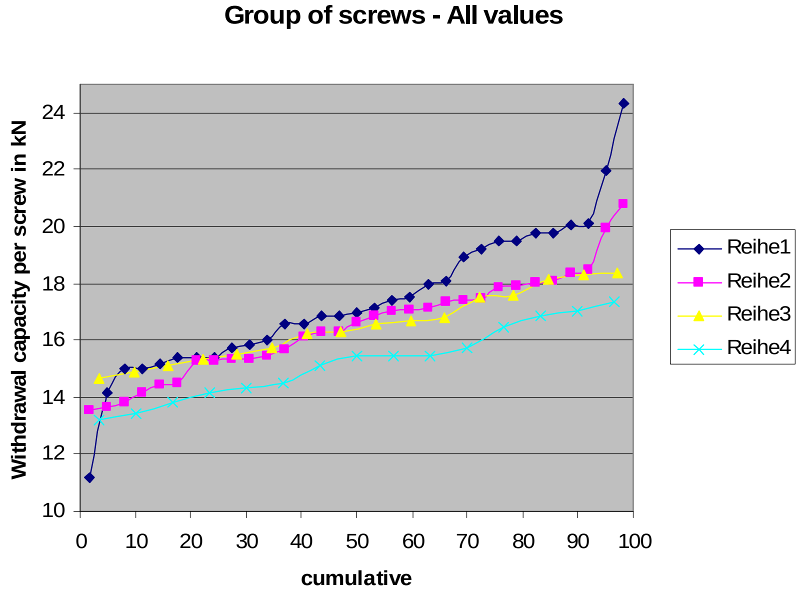

(Reihe 1 to 4) with d/a: 12,5; 6; 4 and 3

Fig. 8: Withdrawal capacity of group of screws with varying a/d_a

- Effect of spacings on the withdrawal strength

As can be seen from figures 7 and 8, both series (individual screws and group of screws) show similar behaviour when related to the same ratios of areas or stiffness (or a/d_a).

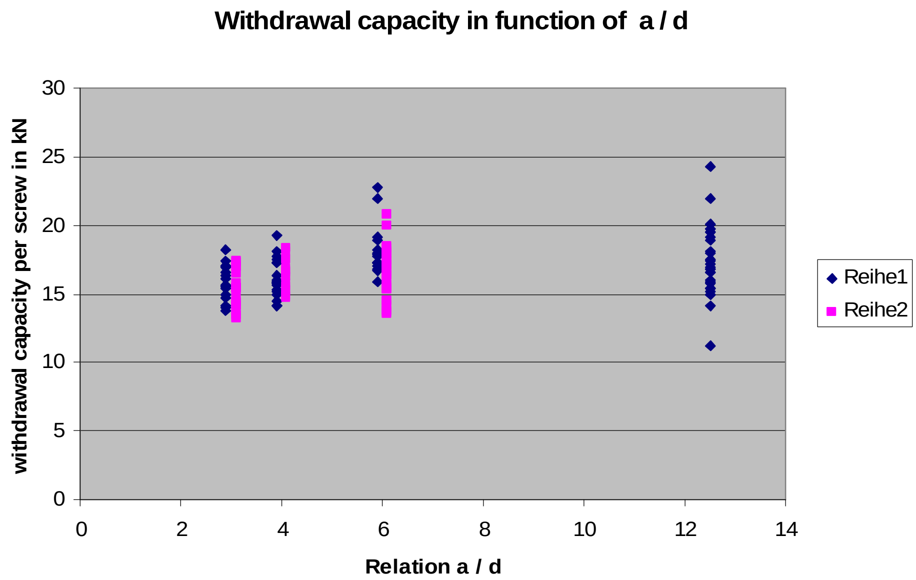

left column: individual screws right column: group of screws

Fig. 9: Effect of a/d_a on the withdrawal strength

For a/d ≈ 5 a threshold will be found. The decrease of withdrawal strength (per fastener) with decreasing spacing a/d can conservatively be approached by the equation $k_{red} = (a / 5 \cdot d)^{0,35}$.

For a spacing of a/d=3 the value of k_{red} becomes 0,84. The withdrawal strength of the individual fastener (in the connexion with a group of fasteners) is reduced by this factor, but – and that is the most important fact – the withdrawal capacity for the same timber section is increased by a factor of $(5/3)^2 \cdot 0,84 = 2,4$.

- Number of fasteners and variability

From figure 9 it is already perceptible that with increasing number of screws in a connection the extreme values – as found in the individual tests – will disappear. Since – by practical reasons – no tests were made with larger number of screws and a/d > 5 - the available tests values were "transformed" to the level of the individual screw by dividing with the corresponding k_{red}. The result is shown in figure 10, here with $k_{red} = (a / 5 \cdot d)^{0,25}$.

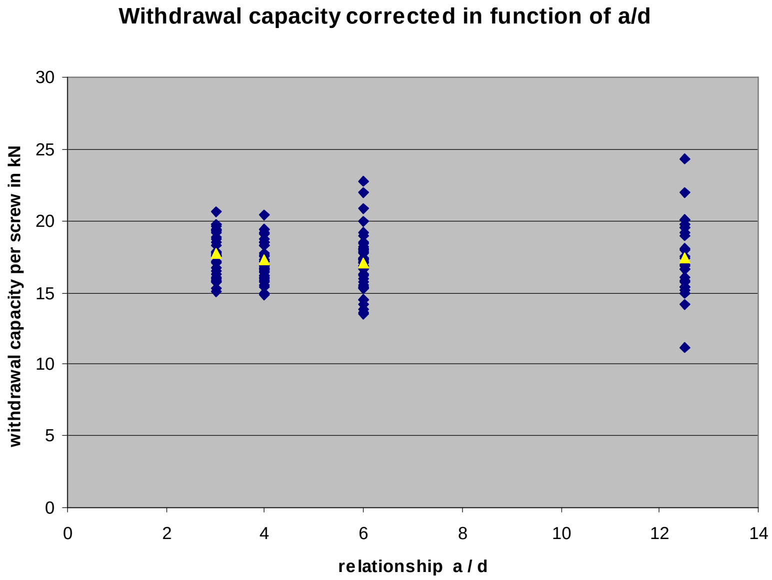

Fig. 10: Corrected withdrawal capacities (distribution and mean values)

Spacing requirements and Codes

-General

Independent of the type of load transfer (lateral load as for dowels and axially load as for screws or glued-in rods) there is a threshold value of spacing between fasteners. For dowels this value may be fixed to $a_1 = 13 \cdot d$ (in DIN 1052 a lower value of $10 \cdot d$ was fixed, to comply with the requirements for nails); for axially loaded screws and glued-in rods inserted parallel to grain a value of $a = 5 \cdot d$ is justified. Greater spacings do not lead to higher values; smaller spacings lead to a reduction of strength.

The reduction of strength – compared to the strength of fasteners with spacings greater than the threshold spacing – may be expressed by: $k_{red} = n^{-\alpha} \cdot (a / a_{threshold})^{\beta}$

For dowels the following values should be assumed:

$\alpha = -0,1$ with n = number of dowels in a row parallel to grain

$\beta = 0,25$

$a_{threshold} = 13 \cdot d$

$\mathbf{k_{red} = n^{-0,1} \cdot (a / 13 \cdot d)^{0,25}}$

For screws and glued-in rods axially loaded and inserted parallel to the grain the following values should be considered:

$\alpha = 0$ no influence of number of fasteners on the withdrawal strength

$\beta = 0{,}35$

$a_{threshold} = 5 \cdot d$

$\mathbf{k_{red} = (a / 5 \cdot d)^{0,35}}$

According to the test results on screws (see figure 10) a lower exponent of 0,25 (same value as for dowels) could be used. As long as no other research is available – for safety reasons – a higher exponent or a stronger reduction is proposed.

- Codification

For **dowel-type connections** the Codes have generally introduced the threshold distance on which the strength of the individual dowel is based (reference basis). There are some differences about the correct threshold value. During the discussions for Eurocode 5 a value of 14·d had been postulated for dowels; later on the value was reduced to 13·d. For smaller spacings a reduction factor k_{red} has to be introduced: $\mathbf{k_{red,spacing} = (a / a_{threshold})^{0,25}}$.

In addition – for taking in account the uneven load distribution – the number of dowels acting in a row parallel to the grain has to be considered. For joints with ductile behaviour no influence; for joints with very brittle behaviour the reduction is not enough high. This may be the case for small values of a; according to most Codes values down as 5·d are allowed. They may behave very brittle. The Swiss Code for the design of timber structures SIA 265:2003 foresees therefore a minimum of 7·d.

For **axially loaded screws** inserted parallel to the grain Eurocode 5 fixes the **minimum spacings to 4·d.** No threshold value is given. We may assume that the withdrawal strength given in the Code corresponds to this spacing. Following DIN 1052 screws in end grain are simply not allowed, therefore no specifications needed.

For **glued-in rods** inserted parallel to the grain DIN 1052 fixes the **minimum spacings to 5·d,** value that corresponds to the threshold value, as has been shown (and known at the time of writing down the above Code). Nobody seemed to be aware about the implications of such formulation, which results in a very poor performance of the connection. The same spacing rules were proposed 2002 to be included in Eurocode 5-1-1. To avoid such a disastrous formulation in Eurocode 5 the complete annexe “glued-in rods” had to be skipped from the Code.

In both cases – screws and glued-in rods axially loaded and inserted parallel to the grain – the threshold (or reference) value may be assumed equal to 5·d. For smaller spacings a reduction factor k_{red} has to introduced: $\mathbf{k_{red} = (a / 5 \cdot d)^{0,35}}$ **.** Smaller spacings down to about 2,5·d are possible; the use of such small spacings may lead to an earlier splitting. In such a case the strength model on withdrawal is no more valid. Tests with a/d as small as 2,8 and suitable design detailing have proven that splitting can be avoided.

The poor performance of glued-in rods according to DIN 1052 (due to the required minimum spacing of 5·d) tempts to use longer rods (of higher steel strength). This has no sense, as can be seen from the tests made under GIROD (see e.g. Gustafsson et al /2001). After certain length or better slenderness of the rod only slightly increase results. The change of the curves corresponds to a specific deformation ε of about 3%o of the steel rod. It is known that the specific tension failure deformation of spruce is about of that size (mean value).

- Conclusion
In view of the great importance of a correct formulation of the spacing requirements for the performance of connections with axially loaded screws and glued-in rods inserted parallel to the grain the actual Codes have to be adapted.

Acknowledgements

Thanks goes to the "neue Holzbau AG, Lungern" for all the free delivered "hardware" and to my friend and personal assistant dipl. Bauing. ETHZ Peter Haas for preparing and testing the great number of specimens.

Literature

Blass, H. and Laskewitz, B. (1999): Effect of spacing and edge distance on the axial strength of glue-in rods. CIB-W18/32-7-2.

Gehri, E. (2001): Ductile behaviour and group effect of glued-in steel rods. In: Joints in timber structures. Proceedings RILEM – PRO 22.

Gustafsson, P.-J., Serrano, E., Aicher, S. and Johansson, C.-J. (2001): A strength design equation for glued-in rods. In: Joints in timber structures. Proceedings RILEM – PRO 22.

Steiger et al. (2007): Pull-out strength of axially loaded steel rods bonded in glulam parallel to the grain. Materials and Structures 40:1. 69-78.

CIB-W18/42-7-9

INTERNATIONAL COUNCIL FOR RESEARCH AND INNOVATION IN BUILDING AND CONSTRUCTION

WORKING COMMISSION W18 - TIMBER STRUCTURES

CONNECTIONS WITH GLUED-IN RODS SUBJECTED TO COMBINED BENDING AND SHEAR ACTIONS

J L Jensen

P Quenneville

School of Engineering

The University of Auckland

NEW ZEALAND

Presented by J L Jensen

H.J. Blass commented that there is information from Karlsruhe on steel rod under pure shear mode where shear failures were observed. He received explanation of one of the test configuration where almost the entire section has dowels covering it. Here he/h would be close to one as k approaches infinity where dowel load bearing capacity would be in terms of bending and embedment.
E. Gehri asked how would one control the gluing of the rods. J.L. Jensen said that in testing the rod were pulled.
R. Crocetti asked what would be the advantage of using hard wood rod and whether the placement of the rod has been optimized for shear capacity. J.L. Jensen said that the steel rods can corrode and the connection is intended to take large moment.
R. Steiger commented that since the paper only deals with hardwood dowel the title should be adjusted (Remark: done by the author).
S. Aicher stated that tension perpendicular to grain stress can be expected in bending in location near the tension rods close to the bending tension edge. This behaviour is commonly seen in steel rods. The bending stiffness of the hardwood dowel is more compatible with the timber member hence you did not get such a failure mode. He asked what would the efficiency of a joint with lots of dowels be. In design you have to make reduction according to the hole created by the rods. Therefore the efficiency would be low. H.J. Blass said that this is a wrong engineering assumption which explains the good observed efficiency in the connector.
A. Buchanan asked whether the equation would be applicable to glulam to steel connections. He stated that glued-in rod with crosswise reinforcement was used in Sydney. J.L. Jensen said that this was thought of but was not done. A. Buchanan also stated that B. Madsen did similar work in UBC with 45 degree steel rods and this work should be considered. J.L. Jensen said that wood-steel situation would give different solutions.
U. Kuhlmann said that it would be nice to have such joints in the code for timber to timber as well as timber to other materials. In this work material values were assumed and were specific to the tested material (eg G); therefore, more work is needed to get a general solution. The glued-in-rod perpendicular as reinforcement is effective. J.L. Jensen agreed.

Connections with glued-in rods subjected to combined bending and shear actions

Jørgen L. Jensen and Pierre Quenneville

School of Engineering, The University of Auckland, New Zealand

1 Introduction

Glued-in rods have in recent years been widely used in timber structures. Such connections provide an efficient means of transferring moments, and they are architecturally attractive. During the last decade, numerous research papers have been produced on this topic, but nevertheless, design rules for glued-in rods have not been accepted into the major design codes. In the final draft of EC5, a previously included informative annex on glued-in steel rods has been removed.

The vast majority of research papers on glued-in rods have concentrated on withdrawal of single rods, usually steel rods. Relatively little attention has been paid to materials other than steel, and very little attention has been paid to applications of glued-in rods to connections as used in real life. Of the few research papers on moment-resisting connections, virtually all have focused on pure bending. No research (other than reported in the present paper) seems to have attempted quantifying the strength of moment-resisting connections with glued-in rods subjected to combinations of bending and shear, nor did the now removed annex from EC5 deal with combined bending and shear and possible splitting problems.

2 Design equations

Expressions for the withdrawal failure load and stiffness of a single rod are given based on a simple fracture mechanics model (Johansson et al., 1995; Jensen et al., 2001; Gustafsson and Serrano, 2001).

Based on the withdrawal strength and stiffness of single rods, a simple theoretical model for moment-resisting joints subjected to pure bending is given (Jensen et al., 1999; Sasaki et al., 2002; Jensen et al., 2004).

The splitting strength of symmetrical moment-resisting joints subjected to pure shear loading is given based on a fracture mechanics model (Jensen et al., 2003; Jensen and Gustafsson, 2004).

Empirical failure criteria for arbitrary combinations of bending and shear actions are proposed based on testing (Jensen et al., 2004).

2.1 Withdrawal of a single rod

A single rod subjected to withdrawal is shown in Fig. 1. The applied load is denoted P and the slip between the rod and the wood at x = 0 is denoted δ. The load-slip relationship is assumed to be linear and given by

$$P = K_i \delta \tag{1}$$

A simple model based on the Volkersen-theory and quasi-non-linear fracture mechanics (Johansson et al., 1995; Jensen et al., 2001; Gustafsson and Serrano, 2001) gives the following failure load, P_u

$$\frac{P_\mathrm{u}}{\pi d l_i f_\mathrm{v}} = \begin{cases} \dfrac{(1+\alpha)\sinh\omega}{\omega(\alpha+\cosh\omega)} & \text{for } \alpha \leq 1 \\ \dfrac{(1+\alpha)\sinh\omega}{\omega(1+\alpha\cosh\omega)} & \text{for } \alpha \geq 1 \end{cases} \tag{2}$$

and the stiffness

$$\frac{K_i}{\pi d l_i f_\mathrm{v}} = \frac{f_\mathrm{v}}{2\mathcal{G}_\mathrm{f}} \frac{(1+\alpha)\sinh\omega}{\omega(1+\alpha\cosh\omega)} \tag{3}$$

where

$$\alpha = \frac{EA}{E_\mathrm{r} A_\mathrm{r}} \quad , \quad \omega = \sqrt{\frac{1+\alpha}{\alpha}} \sqrt{2 \frac{l_i^2 f_\mathrm{v}^2}{d E_\mathrm{r} \mathcal{G}_\mathrm{f}}} \tag{4}$$

E: Modulus of elasticity (MOE) of the wood

E_r: MOE of the rod

A: Cross section area of the wood

A_r: Cross section area of the rod

d: Diameter of the rod

l_i: Glued-in length of the rod

f_v: Shear strength of the bond-line

$\mathcal{G}_\mathrm{f}$: Fracture energy of the bond-line

Other (e.g. empirical) expressions for the withdrawal failure load, P_u, and stiffness, K_i, than Eqs. (2) and (3) may be used in the model for pure bending of moment-resisting joints if preferred.

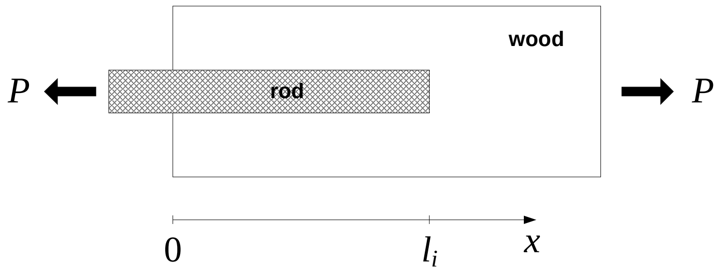

Fig. 1 *Withdrawal of a single rod*

2.2 Pure bending

Simple mechanical models similar to those used for design of reinforced concrete beams may be applied to moment-resisting connections with glued-in rods for design of pure bending (Komatsu et al., 1997; Sasaki et al., 2002; Batchelar, 2007). However, tests clearly revealed that the usual assumption that plane cross sections remain plane is not fulfilled in timber beams with glued-in rods in multiple layers; the whole dowel group in the tension side turned out to be subjected to the same slip (Jensen et al., 1999; Sasaki et al., 2002), as shown in Fig. 3. This effect was not due to the yielding of the rods since rods of hardwood were used in the tests.

The experimental fact that a whole group of rods in the tension side acts like just one rod makes it possible to derive a mechanical model for pure bending of timber beams with glued-in rods, which is even simpler than the models used for reinforced concrete beams.

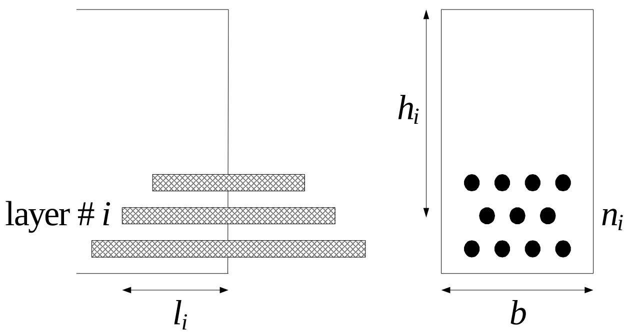

Fig. 2 *Geometry of connection subjected to pure bending*

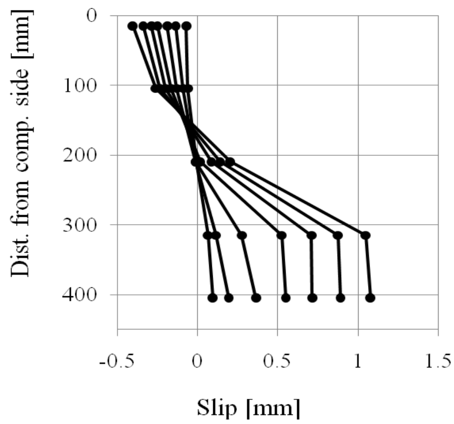

Fig. 3 *Slip distribution in specimen A1(Fig. 5)measured with displacement transducers*

At this point, it is convenient to introduce the following parameters:

$$K_{\mathrm{G}} = \sum_{i=1}^{N} n_i K_i \quad , \quad l_{\mathrm{G}} = \frac{1}{K_{\mathrm{G}}} \sum_{i=1}^{N} n_i K_i l_i \quad , \quad h_{\mathrm{G}} = \frac{1}{K_{\mathrm{G}}} \sum_{i=1}^{N} n_i K_i h_i$$
$$h_0 = \frac{K_{\mathrm{G}} l_{\mathrm{G}}}{bE} \quad , \quad h_{\mathrm{c}} = h_0 \left(\sqrt{1 + \frac{2h_{\mathrm{G}}}{h_0}} - 1 \right) \tag{5}$$

where

N: Number of layers of rods in the tension side

n_i: Number of rods in the i^{th} layer

K_i: Withdrawal stiffness of the rods in the i^{th} layer

l_i: Glued-in length of the rods in the i^{th} layer

h_i: Depth of the i^{th} layer of rods calculated from the edge of the beam in the compression side

b: Width of the beam

E: MOE of the beam in parallel-to-grain direction.

K_{G}: Withdrawal stiffness of group of rods

l_{G}: Glued-in length of the group of rods

h_{G}: Depth of the group of rods in the tension side calculated from the edge of the beam in the compression side

h_{c}: Depth of the neutral axis calculated from the edge of the beam in the compression side

The failure moment, M_{u}, is given by

$$M_{\mathrm{u}} = \nu K_{\mathrm{G}} \frac{2\mathcal{G}_{\mathrm{f}}}{f_{\mathrm{v}}} \left(h_{\mathrm{G}} - \tfrac{1}{3} h_{\mathrm{c}} \right) \tag{6}$$

The factor ν in Eq. (6) is an effectiveness factor introduced to make it possible to account for a group effect, i.e. the effect that the withdrawal failure load per rod in a group of rods may be less than the withdrawal load of a single rod. Such an effect was observed experimentally (Koizumi et al., 1998a) and may be due to a weakest-link effect.

The rotational stiffness, $R = M/\theta$, where M is the applied moment and θ is the rotation, is given by

$$R = \tfrac{1}{2} K_{\mathrm{G}} \left(h_{\mathrm{G}} - h_{\mathrm{c}} \right) \left(h_{\mathrm{G}} - \tfrac{1}{3} h_{\mathrm{c}} \right) \tag{7}$$

2.3 Pure shear

A symmetrical joint as shown in Fig. 4 is considered and assumed subjected to pure shear loading. Unless reinforced in one way or another, connections with glued-in rods may be very vulnerable to splitting due to tensile stresses perpendicular to grain.

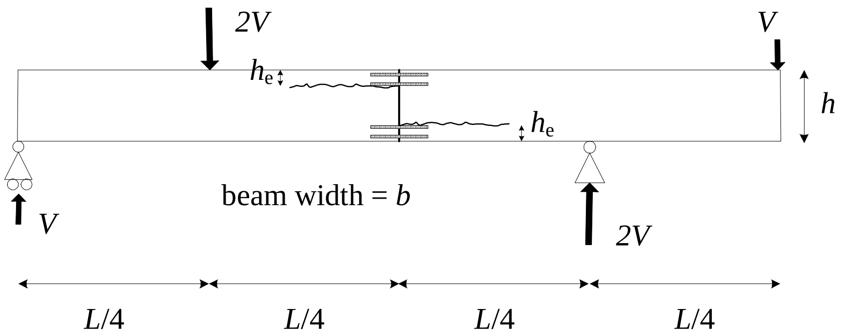

Fig. 4 *Loading, geometry and crack pattern of symmetrical joint subjected to pure shear*

A lower-bound value, $V_{\mathrm{u,L}}$, and an upper-bound value, $V_{\mathrm{u,U}}$, of the shear failure load of an un-reinforced symmetrical joint as shown in Fig. 4 subjected to pure shear may be given by (Jensen et al. 2003; Jensen and Gustafsson 2004):

$$V_{\mathrm{u,L}} = \gamma\mu V_{\mathrm{u,LEFM}} \quad , \quad V_{\mathrm{u,U}} = \gamma V_{\mathrm{u,LEFM}}$$

$$V_{\mathrm{u,LEFM}} = \kappa b\sqrt{\tfrac{20}{3} G \mathcal{G}_{\mathrm{f}}^{\mathrm{I}} h_{\mathrm{e}}} \tag{8}$$

$$\gamma = \frac{\sqrt{2\zeta+1}}{\zeta+1} \quad , \quad \mu = \frac{\zeta+1}{2\zeta+1} \quad , \quad \zeta = \frac{5}{\sqrt{3}}\frac{G}{E}\sqrt{\frac{E}{h_{\mathrm{e}}}\frac{2\mathcal{G}_{\mathrm{f}}^{\mathrm{I}}}{f_{\mathrm{t}}^{2}}}$$

$$\kappa = \frac{1}{1-3\left(\dfrac{h_{\mathrm{e}}}{h}\right)^{2}+2\left(\dfrac{h_{\mathrm{e}}}{h}\right)^{3}}$$

where

b: Width of the beam

h_{e}: Depth of group of rods, see Figs. 4 and 5

h: Total depth of beam

G: Shear modulus of the beam

E: MOE of the beam in the parallel-to-grain direction

$\mathcal{G}_{\mathrm{f}}$: Mode I fracture energy of the beam

f_{t}: Tensile strength perpendicular to grain of the beam

The lower-bound value was derived assuming that the dowel group can rotate freely at the junction of the two beam ends, and the upper-bound value was derived assuming that the dowel group is fully fixed against rotations at the junction of the two beam ends.

2.4 Combined bending and shear

Arbitrary combinations of applied moment, *M*, and shear force, *V*, may be handled by applying simple empirical failure criteria (V_u and M_u being ultimate values for pure actions)

$$\frac{V}{V_u} + \frac{M}{M_u} \le 1 \tag{9}$$

or

$$\left(\frac{V}{V_u}\right)^2 + \left(\frac{M}{M_u}\right)^2 \le 1 \tag{10}$$

3 Comparison with experimental data

Experiments were conducted on moment-resisting connections subjected to pure bending and pure shear in order to validate the theoretical models given in sections 2.2 and 2.3, and on connections subjected to combinations of bending and shear in order to be able to suggest an appropriate empirical failure criterion for combined actions.

All experiments reported here used rods of hardwood. The design equations should preferably also be verified for connections using steel rods with larger diameters and glued-in lengths, but may be anticipated to be of general validity since they are based on theoretical considerations.

3.1 Withdrawal of a single rod

Detailed information on experiments on withdrawal of single hardwood rods as used in the moment-resisting joints reported below may for instance be found in (Koizumi et al., 1998a), (Koizumi et al., 1998b), and (Koizumi et al., 2004).

3.2 Pure bending

Glulam beams with 100x200 mm^2 and 120x420 mm^2 cross sections were tested in four-point bending, in which the joints were subjected to pure moment. Rods of hardwood were used, and a number of different rod configurations were tested. It should be noted that not all tested joints were symmetrical; In most cases only a small number of rods were used in the compression side. In all cases the holes were made 1 mm larger than the rods.

Glulam beams were made of Japanese cedar (*Cryptomeria japonica*) with an MOE of approximately 10 GPa. A special MOE of 7.3 GPa, obtained by compression tests of two blocks of wood, end-grain against end-grain, was used in the calculation of moment capacity and rotational stiffness of the joint since special conditions apply to the compression zone of the connection. The moisture content of the beams varied between 11-15%.
Rods were made of hard maple (*Acer saccharum*) with an MOE of approximately 15 GPa. The adhesive used was one-component polyurethane. The following values of bond-line parameters were used: $\mathcal{G}_f^{II}$ = 2.9 N/mm, f_v = 7.6 MPa.

Test results and calculated joint strengths are given in Table 1. Further details on moment-resisting joints with glued-in hardwood rods subjected to pure bending may be found in (Sasaki et al., 1999) and (Sasaki et al., 2002).

Table 1 *Pure bending. Specimen characteristics and results*

Specimen	**A1**	**A2**	**C1**	**C2**	**C3**	**C4**	**C5**
Rod diameter, *d* [mm]	12	12	8	8	8	12	12
Beam depth, *h* [mm]	420	420	200	200	200	200	200
Beam width, *b* [mm]	120	120	100	100	100	100	100
No. of layers of rods, *N*	3	5	1	2	3	1	2
No. of rods per layer	5	5	6	6	6	4	4
h_1 [mm]	402	396	184	184	184	182	182
h_2 [mm]	378	372	-	168	168	-	158
h_3 [mm]	354	348	-	-	152	-	-
h_4 [mm]	-	324	-	-	-	-	-
h_5 [mm]	-	300	-	-	-	-	-
l_1 [mm]	120	120	80	80	80	120	120
l_2 [mm]	110	110	-	48	48	-	72
l_3 [mm]	100	100	-	-	48	-	-
l_4 [mm]	-	90	-	-	-	-	-
l_5 [mm]	-	80	-	-	-	-	-
No. of specimens tested, N_{repl}	3	2	3	6	3	5	7
MOR_T [MPa]	25.1	30.0	12.8	19.4	24.7	17.8	29.4
MOR_T/MOR_C	1.25	1.03	1.12	1.01	0.95	1.26	1.24

MOR_T: Modulus of rupture determined by testing. MOR_C: Modulus of rupture determined by calculation based on $v = 0.8$.

3.3 Pure shear

A total of eight different joints as shown in Fig. 5 were subjected to pure shear loading in a test set-up as shown in Figs. 4 and 7.

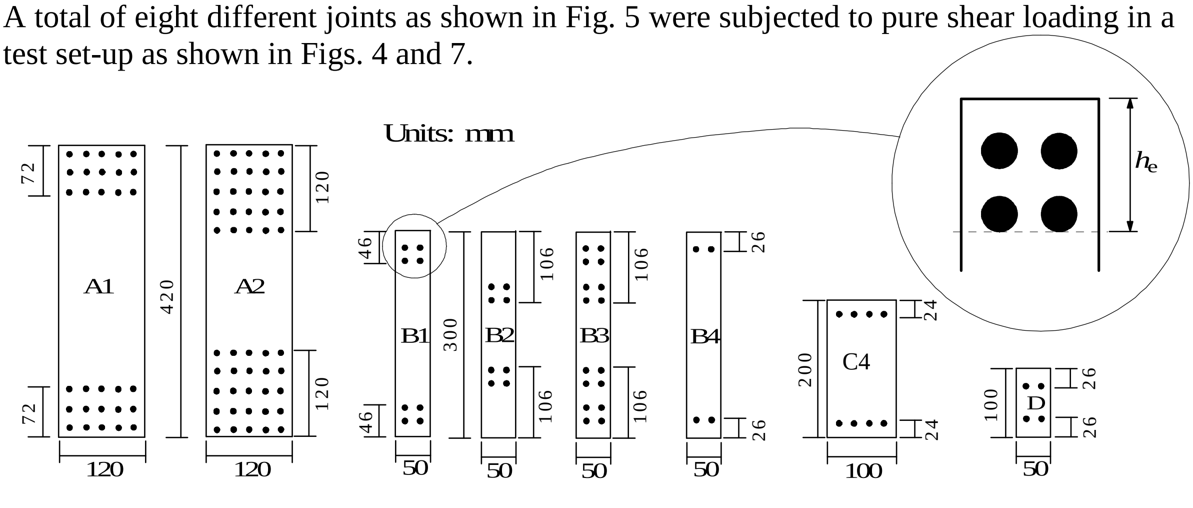

Fig. 5 *Geometry of joints tested in pure shear*

All glulam beams tested in pure shear were made of Japanese cedar (*Cryptomeria japonica*). The dynamic MOE is given in Table 2. The moisture content was 12-13%.

Rods were all 12 mm in diameter, made of the same hard maple (*Acer saccharum*) as used in the bending tests. The adhesive used was the same one-component polyurethane as used in the bending tests.
The mode I fracture energy was determined using Double-Cantilever-Beam-specimens, and the tensile strength perpendicular to grain was determined using hour-glass shaped specimens with 10x10 mm^2 minimum cross section. The DCB-specimens and tensile strength specimens were cut from non-damaged parts of beams already tested in pure shear without special selection to avoid defects such as knots and cut in such a way that failure in all types of specimens occurred in the same lamina of the glulam beam. The fracture energy was found to be $\mathcal{G}_f^I = 0.28 \pm 0.14$ N/mm, and the tensile strength to be $f_t = 4.1 \pm 1.3$ MPa.

Further details on the pure shear tests can be found in (Jensen and Gustafsson, 2004).

Table 2 *Pure shear. Specimen characteristics and results*

Specimen	N_{repl}	MOE [MPa]	b [mm]	h [mm]	h_e [mm]	κ	V_u [kN]		
							Test	$V_{u,L}$	$V_{u,U}$
A1	3	8670	120	420	72	1.08	31.5 ± 4.2	25.7	32.0
A2	6	9310	120	420	120	1.25	51.3 ± 8.2	41.4	50.0
B1	3	8340	50	300	46	1.07	7.3 ± 0.9	8.0	10.3
B2	3	8340	50	300	106	1.40	12.9 ± 2.2	17.2	20.7
B3	6	9950	50	300	106	1.40	19.8 ± 2.9	18.5	22.5
B4	3	9950	50	300	26	1.02	7.0 ± 0.6	5.7	7.8
C4	7	8300	100	200	24	1.04	11.0 ± 1.2	10.4	14.0
D	3	9950	50	100	26	1.20	6.9 ± 0.8	6.7	9.1

Calculations based on $G = E/18$. N_{repl} is number of specimens tested. Test results given as mean ± standard deviation.

3.4 Combined bending and shear

Specimens A2 and C4 as shown in Fig. 5 were tested in a 3-point test set-up, in which the location of the joint was varied in order to obtain different combinations of moment and shear force.
Test results (each data point represents the mean value of three specimens) are shown in Fig. 6 along with the failure criteria given in Eqs. (9) and (10). M_u is the mean value of the failure moment in case of pure bending as obtained by testing (Table 1) and V_u is the mean value of the shear failure load in case of pure shear as obtained by testing (Table 2).

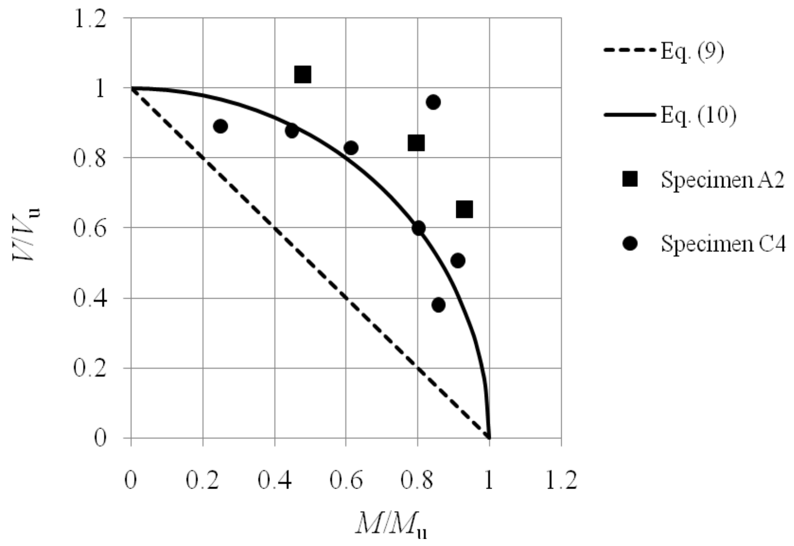

Fig. 6 *Test results of joints subjected to combined bending and shear*

Fig. 7 is for all beams tested in pure bending, pure shear and combined bending and shear to show the comparison of theoretical to experimental failure loads. Notice that the failure load here is the total load applied to a specimen by the testing machine. For the beams subjected to pure shear, the theoretical lower-bound value has been chosen for specimens B2, B4, C4 and D since these configurations obviously do not allow considerable moment to be transferred by the cracked beam parts, while the theoretical upper-bound value has been chosen for specimens A1, A2, B1 and B3. For the specimens A2 and C4 subjected to combined bending and shear, the theoretical failure loads have been calculated using the theoretical values of V_u and M_u and using Eq. 10 with the equality sign.

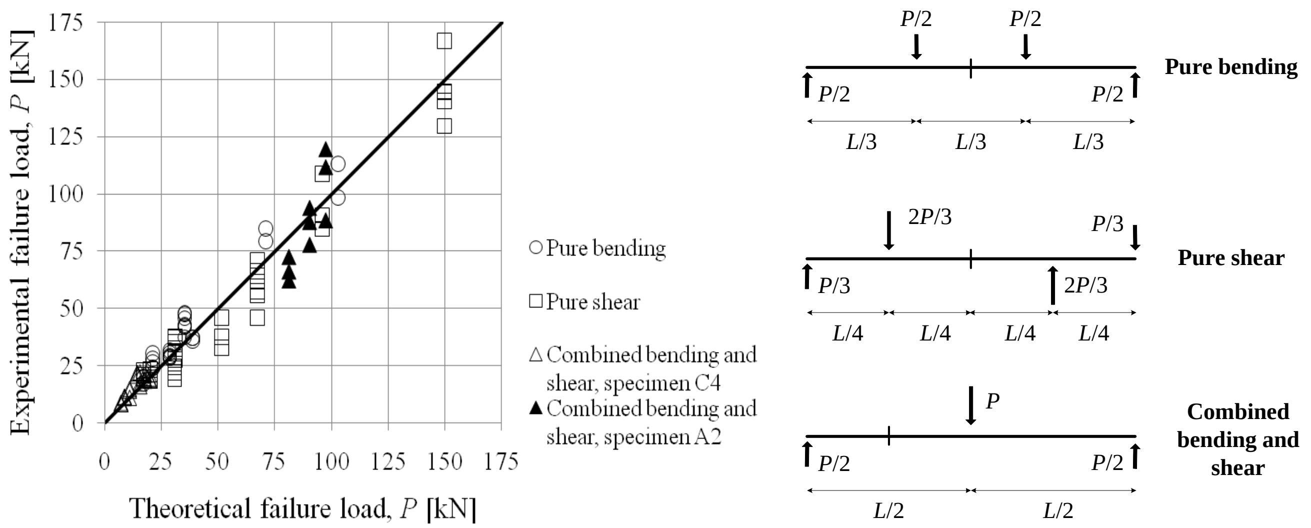

Fig. 7 *Comparison of experimental and theoretical failure loads for pure bending, pure shear, and combined actions*

3.5 Shear reinforcement

Non-reinforced joints are vulnerable to shear loads. Shear reinforcement may be applied in various ways to improve the resistance against splitting. Screws or glued-in rods may be used if space permits it. Alternatively, a plate of plywood (or other materials) may be glued on to the ends of the jointed beams.

Specimens of type A2 and C4 (see Fig. 5) were reinforced by means of plywood plates. The specimens (three replications, i.e. 12 specimens in total) were tested in pure shear to see the improvement in shear strength, and in pure bending to see if the reinforcement might influence the bending capacity.

In case of the C4 specimens, a 9-mm plywood plate was glued on to each end of the glulam beams before drilling the holes for the rods. A double layer of plastic film was inserted between the two plywood plates when gluing the beams together. This was done in order to ensure that shear forces were transferred only via the rods so as to give a conservative estimate of the effect of the reinforcement.

In case of the A2 specimens, a 28-mm plywood plate was glued on to the end of one glulam beam before drilling the holes for the rods. No plywood plate was glued on to the second beam. A double layer of plastic film was inserted between the plywood plate on the one beam-end and the end-grain of the other beam when gluing the two beams together.

In table 3 is the strength of reinforced joints compared with that of non-reinforced joints. It should be noted that the number of tested specimens is low and the variation in test results fairly high in some cases (particularly pure bending of reinforced A2 specimens), and that the tests on reinforced A2 specimens subjected to pure shear had to be terminated prematurely due to excessive damage at loading points and supports, see Fig. 8.

Table 3 *Effect of reinforcement*

Specimen	Pure bending, M_u [kNm]		Pure shear, V_u [kN]	
	Un-reinforced	Reinforced	Un-reinforced	Reinforced
A2	105.8	82.3	51.3	72.6*
C4	11.9	9.6	11.0	31.3

* Experiments terminated before failure in joint due to excessive damage at supports and loading points

Fig. 8 *Support of reinforced A2 specimen subjected to pure shear*

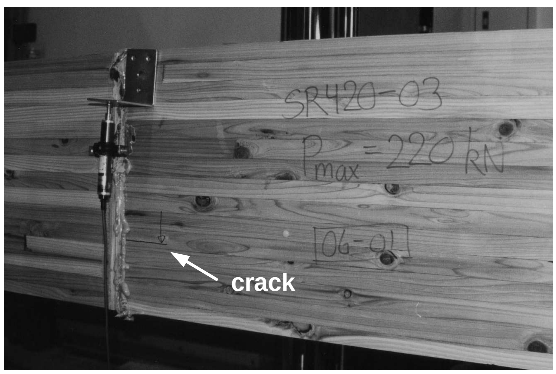

Fig. 9 *Crack in reinforced A2 specimen*

In the reinforced A2 specimens, cracks developed at the location shown in Fig. 9. The cracks occurred in the beams, which did not have a plywood plate glued on to the end. However, the cracks extended very slowly at increasing load levels and did not cause catastrophic failure before the tests had to be terminated due to damage at the loading points and supports. No cracks were observed in the beams, which had plywood plates glued on to the ends.

In the reinforced C4 specimens (9-mm plywood plates glued on to both beam ends), no splitting was observed. Failure occurred due to bending/shear in the hardwood rods as shown in Fig. 10. It should also be noted from Fig. 10, that the double layered plastic film effectively prevented the beam ends from being glued together and thereby transferring shear loads.

Fig. 11 *Shear reinforced C4 specimen after testing*

4 Conclusions

Glued-in rods are widely used for moment resisting connections. However, no design rules are given in EC5. Future editions of EC5 should preferably contain guidelines not only for withdrawal of single rods, but also for moment resistance, shear resistance, and resistance to combined actions of moment and shear.
Simple models suitable for practical design have been derived for pure moment and pure shear actions based on fracture mechanics, and combined actions have been considered empirically for connections with rods of hardwood. Test show good agreement between theoretical and experimental failure loads. It is believed that the presented models with minor alterations can be adopted for rods of steel, aluminum and other materials.

Considerable increase of the shear strength may be obtained in simple ways, e.g. by gluing plywood plates on to the beam ends. Reinforcement by means of screws may prove efficient for this purpose as well.

5 References

[1] Johansson C. J., Serrano E, Gustafsson P. J., Enquist B. 1995. Axial strength of glued-in bolts – Calculation model based on non-linear fracture mechanics – A preliminary study. In: Proceeding of the international council for building research studies and documentation, CIB-W18A, Meeting Twenty Eight, Copenhagen, Denmark, paper 28-7-9.

[2] Jensen J. L., Koizumi A., Sasaki T., Tamura Y., Iijima Y. 2001. Axially loaded glued-in hardwood dowels. Wood Science and Technology, Vol. 35, pp. 73-83.

[3] Gustafsson P. J., Serrano E. 2001. Glued-in rods for timber structures – Development of a calculation model. Report TVSM-3056, Division of Structural Mechanics, Lund University, Sweden, p. 83.

[4] Jensen J. L., Koizumi A., Sasaki T. 1999. Timber joints with glued-in hardwood dowels. In: Proceedings of Pacific Timber Engineering Conference, Forest Research Bulletin 212, Rotorua, New Zealand, pp. 100-107.

[5] Sasaki T., Koizumi A., Jensen J.L., Iijima Y., Komatsu K., 2002. End joint with glued-in hardwood dowels in timber construction II. Bending properties of beams jointed with multiple rows of dowels. *Mokuzai Gakkaishi*, Vol. 48, No. 1, pp. 23-31. (In Japanese).

[6] Jensen J. L., Koizumi A., Sasaki T. 2004. Moment-resisting joints with hardwood dowels glued-in parallel to grain. In: Proceedings of the 8th World Conference on Timber Engineering, Lahti, Finland, pp. 239-245.

[7] Jensen J. L., Gustafsson, P. J., Larsen H. J. 2003. Beam splice joints with rods and dowel joints analysed by a perpendicular-to-grain tensile fracture model. In: Proceeding of the international council for building research studies and documentation, CIB-W18A, Meeting Thirty Six, Colorado, United States of America, paper 36-7-9.

[8] Jensen J. L., Gustafsson P. J. 2004. Shear strength of beam splice joints with glued-in rods. Journal of Wood Science, Vol. 50, pp. 123-129.

[9] Komatsu K., Koizumi A., Jensen J., Sasaki T., Iijima Y., 1997. Flexural behaviour of GLT beams end-jointed by glued-in hardwood dowels. In: Proceeding of the international council for building research studies and documentation, CIB-W18A, Meeting Thirty, Vancouver, Canada, paper 30-7-1.

[10] Batchelar M., 2007. Timber frame moment joints with glued-in steel rods – A designer’s perspective. NZ Timber Design Journal, Vol. 15, No.2.

[11] Koizumi A., Jensen J.L., Sasaki T., Iijima Y., Tamura Y., 1998. Withdrawal properties of hardwood dowels in end joints II. Effects of dowel diameters, Young’s moduli of adherends, dowel spacings, and numbers of dowels. *Mokuzai Gakkaishi*, Vol. 44, No. 2, pp. 109-115. (In Japanese).

[12] Koizumi A., Jensen J.L., Sasaki T., Iijima Y., Tamura Y., 1998. Withdrawal properties of hardwood dowels in end joints I. Evaluation of shear performance of adhesives. *Mokuzai Gakkaishi*, Vol. 44, No. 1, pp. 41-48. (In Japanese).

[13] Koizumi A., Sasaki T., Matsuki Y., 2004. The effects of cure time and humidity cycles on withdrawal strength of the hardwood dowel joints. *Mokuzai Gakkaishi*, Vol. 50, No. 4, pp. 248-254. (In Japanese).

[14] Sasaki T., Koizumi A., Jensen J.L., Iijima Y., Tamura Y., Komatsu K., 1999. End joint with glued-in hardwood dowels in timber construction I. Bending properties of glulams jointed with single row of dowels. *Mokuzai Gakkaishi*, Vol. 45, No. 1, pp. 41-48. (In Japanese).

CIB-W18/42-10-1

INTERNATIONAL COUNCIL FOR RESEARCH AND INNOVATION IN BUILDING AND CONSTRUCTION

WORKING COMMISSION W18 - TIMBER STRUCTURES

RELATIONSHIPS BETWEEN LOCAL, GLOBAL AND DYNAMIC MODULUS OF ELASTICITY FOR SOFT- AND HARDWOODS

G J P Ravenshorst

Delft University of Technology; Delft

THE NETHERLANDS

J W G van de Kuilen

Delft University of Technology; Delft

THE NETHERLANDS

TU München, München

GERMANY

Presented by JWG van de Kuilen

R. Steiger asked why EN384 adjustment equations were not used. He commented that MOE_{local} versus MOE_{global} ratio of 1.15 was found in EMPA study and there is no point of having an equation with a non zero offset. Specimens with low MOE are too much on the safe side. J.W.G. van de Kuilen replied that the current study ratio of 1.13 agrees with the 1.15 factor of EMPA study and agrees with the other comments.

A. Ranta-Maunus stated the results are in-line with Finnish experience and he doesn't believe in the adjustment equation in EN384.

R Steiger asked whether there is any dependency on the frequency of wave propagation such that ultrasonic devices need to be excluded because the results may be wave speed/ equipment dependent. He asked would there be rules to exclude some devices. J.W.G. van de Kuilen replied that damping issues of ultrasonic wave would influence results; therefore, only stress wave results were focused and they have confidence in the data.

Relationships between local, global and dynamic modulus of elasticity for soft- and hardwoods.

G.J.P. Ravenshorst[1], J.W.G. van de Kuilen[2,3],

[1]Delft University of Technology, Delft, The Netherlands.

[2]TU München, München, Germany, [3]CNR Ivalsa, San Michele all'Adige, Italy

Abstract

European Standard EN 408 gives two methods for the determination of the static modulus of elasticity. One is called local modulus of elasticity (MoE-Local) and determined in the shear free central zone in a four-point bending test; the other is called global modulus of elasticity (MoE-global) and determined over the full span length. European Standard EN 384 gives a mathematical relationship between MoE-Local and MoE-global. Both methods are based on displacement measurements on the specimen. The measurements are time consuming and, especially for local MoE, sensitive to measurement errors. It is stated in EN 384 that the determination of global MoE is the preferred method. Because most historical data relates to local MoE the conversion equation is given to determine MoE-global from MoE-local. This conversion equation is mainly based on softwood tests results performed in various laboratories around Europe. In this paper the ratio between local and global MoE is analyzed on a dataset of 1354 tests on a number of European and tropical hardwood species and European spruce from a number of growth locations. As a result a relationship between MoE-global and MoE-local has been derived.

In addition an analysis has been performed on the possibility of replacing the mechanical measurement of MoE by a dynamic MoE measurement. The latter is faster and seems also less sensitive to measurement mistakes. Furthermore, the dynamic MoE is also used more and more in practice for strength grading, since quite a number of grading machines use this principle. Relationships between dynamic MoE and MoE-local and global are given in the paper, based on tests with soft- and hardwoods with densities varying from 350 to 1100 kg/m^3. A proposal for inclusion of this method in EN 408 / EN 384 is made.

1 Introduction

In the last decade the determination of the static Modulus of Elasticity has been the subject of several studies. The principles of MoE-local and MoE-global are shown in figures 1 and 2 respectively. Historically in Europe the MoE-local was determined, since the 2003-version of EN 408 the MoE-global is the preferred method. The conversion equation from MoE-global to MoE-local according to EN 384 reads:

$$MoE_{loc} = 1.3MoE_{glob} - 2690 \qquad (1)$$

Solli (1996) pointed out the problem of twisting in MoE-local measurements when only one measurement on one side of the test piece is performed. To prevent errors due to this effect, measurements on both sides of the beam are necessary of which the average value can be taken. Boström (1997) concluded that the measurement position over the depth of the beam makes a difference in the resulting value of the calculated MoE. In later study Boström (2000) compared tests on Nordic data from different institutes. Tests on different sizes by different institutes gave different ratios for Elocal/Eglobal over the range of MoE values. In a study by Denzler et al (2008) on German softwood the trend in the regression line in the current EN 408 with ratios for Elocal/Eglobal below 1 for lower MoE values increasing to above 1 for higher MoE values was confirmed. They did not find an effect from size or quality, nor species. However, the slope of equation (1) was clearly lower with values between 1.14 and 1.23 as well as the constant being between -452 and -2025 for the different species and subsamples.

All mentioned research report tests on softwood. In this paper tests on a temperate hardwood species (chestnut), on tropical hardwood species and a softwood species (spruce) are reported and discussed. In addition, a third method for determining the MoE, the dynamic MoE, calculated out of the natural frequency of the beam is analyzed.

2 Materials and methods

2.1 Materials

In the research the investigated timber came from the following growth areas:

- European softwoods: spruce (*picea abies*) from Belgium and from Trentino in Northern Italy.

- European temperate hardwood: Chestnut (*castanea*) from Tuscany in Italy

- Tropical hardwoods: cumaru (*dypterix*), massaranduba (*manilkara bidentata*), purpleheart (*peltogyne pubescens*) and tauari vermelho *(couratari spp.)* from Brazil; azobé/ekki (*lophira alata*) from Cameroon.

The average moisture content for the spruce was 12%. For the temperate hardwood species chestnut the average moisture content was around 15% and for the tropical hardwoods the moisture content of individual pieces varied between 12% and 54% with an average of 22%.

From all 1354 pieces, the MoE-local, MoE-global and MoE-dyn were measured. From the 1354 pieces the measurements for the local and global MoE were made at the same time in the test set-up. All tests were performed in a comparable way. The tests were performed by Delft University of Technology (spruce and tropical hardwoods) and CNR Ivalsa in San Michele all´Adige (spruce) and Florence (chestnut).

2.1 Methods

2.2.1 Local Modulus of elasticity according to EN 408

The local Modulus of Elasticity is based on deformation of the shear free centre piece of length 5h of the beam in a four point bending test. The load heads are placed in a way that the beam is divided in three equal parts of 6h, the total span being 18 h. See figure 1

In this study, the measurements for the MoE-local were made in the neutral axis on both sides of the beam.

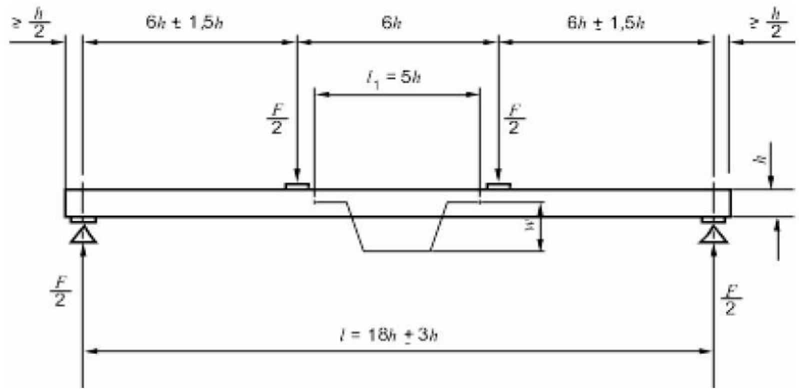

Figure 1. Test set-up for MoE-local according to EN 408

Considerations for MoE-local:

- The deformations are small, between 1-2 mm; that makes that the measurements are sensitive to accuracy errors.
- For softwoods the visually characterized weakest part is placed between the two load points.
- For tropical hardwoods the weak zone is mostly not visually recognizable. This means that the weak zone is randomly present over the specimen length.

2.2.2 Global modulus of elasticity according to EN 408

The MoE-global is based on the deformation of the centre point in the same test setup that is used for the local Modulus of Elasticity. See figure 2.

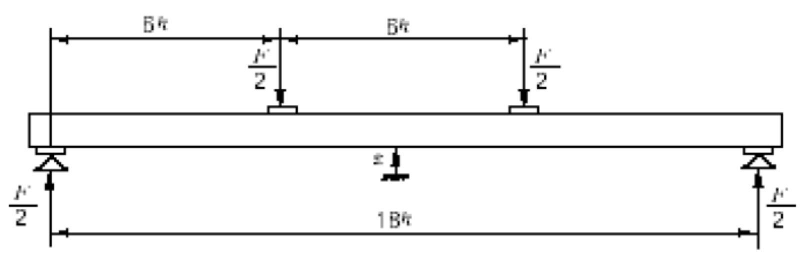

Figure 2. Test set-up for determining the MoE-global according to EN 408.

Considerations for MoE-global:

- The deformation-measurements are made on the bottom side of the beam
- The deformations are relative large (around 15-25 mm from 10% to 40% of the failure load)
- The deformations are caused by bending and shear. In the calculation rule of EN 408 these shear deformations are not included. For both softwoods and hardwoods the ratio between the Modulus of Elasticity parallel to the grain with the mean shear modulus is given as 16 in EN 408. When $MoE_{//}$ would be constant over the total span it would mean that MoE-global gives a result that is 4% less than MoE-local.
- For softwoods the area between the load heads is considered the weakest zone and can be assumed to have a lower MoE than the outer parts. For hardwoods the weakest zone

can be randomly distributed over the length of the beam. As a consequence, a higher value for the ratio local/global would be expected for hardwoods.

- The measurements for the global MOE were made at the centre of the beam on the tension side. The deflections were measured against a fixed point outside the beam with a laser. Measurements were corrected for deformations in the test set-up, for instance the deformation of the steel supporting beam.

2.2.3 Dynamic Modulus of Elasticity based on longitudinal stress waves.

The dynamic modulus of elasticity MoE-dyn is based on vibration measurements of a beam in which a longitudinal stress wave is initiated. Out of these vibration measurements the first natural frequency is determined by using a Fourier Transformation. MoE_{dyn} is calculated according to the equation:

$$E_{dyn} = 4 f^2 \ell^2 \rho$$

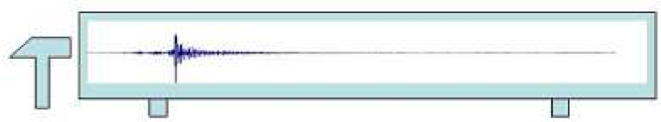

Figure 3. Test set-up for MoE_{dyn}

Considerations for MoE-dynamic:

- The dynamic Modulus of Elasticity is an average value over the whole beam
- The measurements were made at the same moisture content as for E-local and E-global
- The measurement period is only a fraction of that of static tests. In addition, in static tests the determined MoE is dependent on the strain rate applied. As a consequence, differences will be found between laboratories.
- The lengths of the beams during the dynamic tests were larger then the spans in the static tests. This is due to the fact that for softwoods according to EN 384/408 one has to be able to place the weak zone in the centre part of the test set-up. It is current practise that beam lengths are around 4 to 4, 5 meters, so mostly a length of 30h, where the span in the static test is 18h. This means that the MoE-dyn is an average value over the length of 30h. For tropical hardwoods, since the weak zone can hardly be determined visually, mostly only a length of 21h is used, over which the average MoE-dyn is determined.
- By placing the weakest zone in the centre, it may be expected that a larger COV is found for static MoE because of the large difference in MoE between low grade and high grade timber. For the MoE-dyn, there is only one value that takes the average MoE value over the length of the beam thus averaging areas of low and high MoE.
- The measurement for MoE-dyn has been made by stress wave measurement where natural frequency was measured out of longitudinal vibrations. Hanhijärvi et al (2005) reported that the natural frequencies from measurements made by hand and an in-line grading machine on the same set of timber beams did not significantly differ. For the MoE-dyn results in this paper a hand grading device was used; the beams were place on 2 wooden support sticks.

4 Results

In table 1 the results are gathered. For the pieces were all 3 measurements were made the ratio's between the 3 MoEs are given in table 1. For the tropical hardwoods the measurements for each species were combined as one batch. For the chestnut and spruce the batches are divided by origin and size. In table 2 the average values for the 3 species groups tropical hardwoods, chestnut and spruce are given.

Table 1. Mean values for E-local, E-global, Edyn and ratio's E-local/E-global, E-local/Edyn and E-global/Edyn

Wood species	n=	mean Eloc (N/mm^2)	mean Eglob (N/mm^2)	mean Edyn (N/mm^2)	ratio Eloc/Eglob	Ratio Eloc/Edyn	ratio Eglob/Edyn
Tropical hardwoods							
cumaru	192	18838	16060	20476	1,17	0,92	0,78
massaranduba	54	16937	15601	19987	1,09	0,85	0,78
purpleheart	45	18615	15010	19398	1,24	0,96	0,77
Tauari vermelho	51	14309	12697	15496	1,13	0,92	0,82
azobe	111	18116	14993	18721	1,21	0,97	0,80
Chestnut (temperate hardwood)							
Chestnut 1	130	12755	11428	14232	1,12	0,90	0,80
Chestnut 2	170	12838	11550	14262	1,11	0,90	0,81
Spruce							
Spruce BE 1	83	9983	9178	11556	1,09	0,86	0,79
Spruce BE 2	108	10646	9937	11472	1,07	0,93	0,87
Spruce BE 3	44	12316	11187	13074	1,10	0,94	0,86
Spruce BE 4	96	10223	9587	10918	1,07	0,94	0,88
Spruce IT 1	45	12079	9775	13039	1,24	0,93	0,75
Spruce IT 2	41	13007	10187	13011	1,28	1,00	0,78
Spruce IT 3	51	9296	7873	10282	1,18	0,90	0,77
Spruce IT 4	46	9813	9005	11010	1,09	0,89	0,82
Spruce IT 5	40	11382	9536	12076	1,19	0,94	0,79
Spruce IT 6	47	10968	9148	11646	1,20	0,94	0,79

Table 2. Mean values for and coefficients of variation for wood species for E-local, E-global, Edyn and ratio's E-local/E-global, E-local/Edyn and E-global/Edyn

Wood species	n=	mean Eloc (N/mm^2)	Cov Eloc	mean Eglob (N/mm^2)	Cov Eglob	mean Edyn (N/mm^2)	Cov Edyn	ratio Eloc/ Eglob	Ratio Eloc/ Edyn	Ratio Eglob/ Edyn
Tropical hardwoods	453	17363	0,16	14872	0,17	18816	0,13	1,17	0,92	0,79
Chestnut	300	12797	0,18	11489	0,14	14247	0,17	1,11	0,90	0,81
spruce	601	10971	0,20	9541	0,17	11808	0,17	1,15	0,93	0,81
All	1354	13066	0,18	11338	0,17	14156	0,16	1,15	0,92	0,80

5 Analysis

5.1 Ratio MoE-global / MoE-local

In figure 4 the data for MoE-global and MoE-local are plotted for all three dataset combined and linear regression equations are given, in figure 5 the data is plotted for the whole dataset. Figure 4 shows that the relationships between E-global and E-local for the 3 datasets of tropical hardwood, temperate hardwood and European softwood follow the same trend.

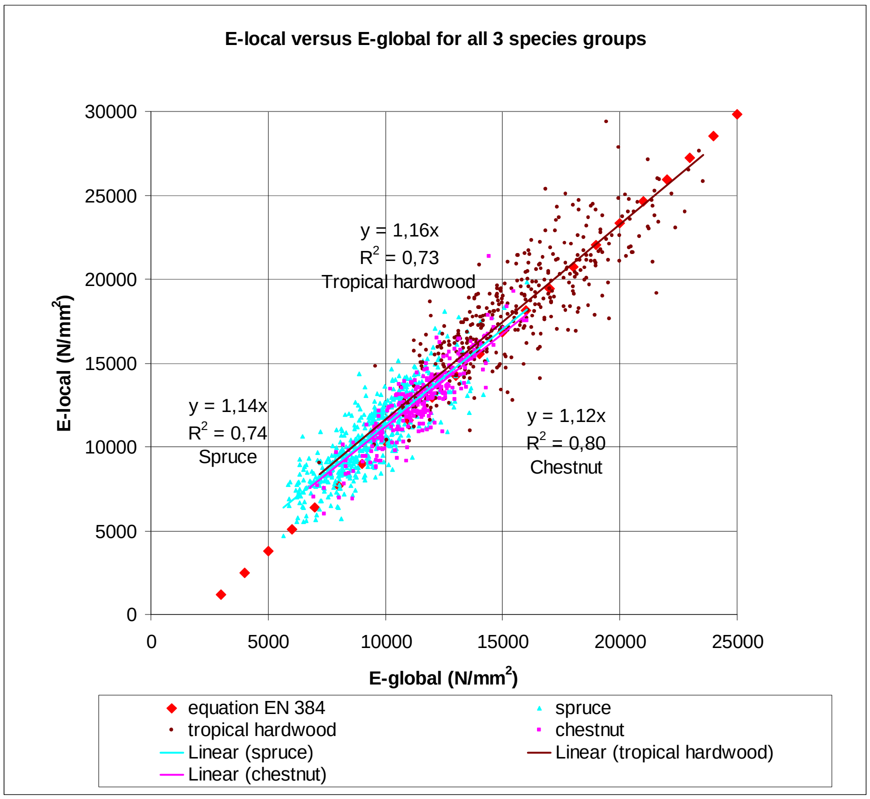

Figure 4. Scatter plots for MoE-global-MoE-local for the 3 datasets

In table 3 the coefficients of determination are listed and two types of linear regression lines are compared. The difference is that in the second regression line the line is forced to go through the origin (0, 0).

Table 3. Regression equations for E-local

	E-local = A *E-global + B				E-local = A * Eglobal	
	A	B	r^2		A	r^2
Equation EN 384	1,3	-2690	1		1,18	0,99
Tropical hardwoods	1,05	1772	0,74		1,16	0,73
Chestnut	1,26	-1672	0,81		1,12	0,80
Spruce	1,16	-239	0,74		1,14	0,74
all data	1,16	-257	0,88		1,14	0,88

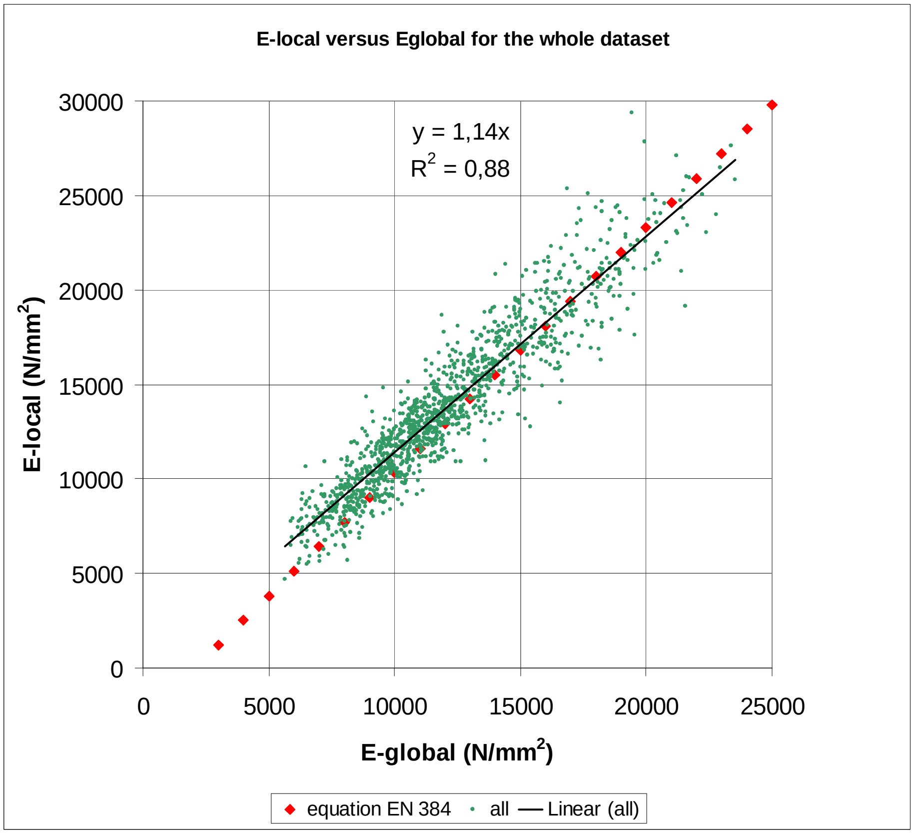

Figure 5. Scatter plot for MoE-global-MoE-local for the whole dataset

Figure 6 shows the average value for individual batches of the same species-size combination. This plot shows that for the mean values the general ratio of is 1, 16, which is in the same order as the value of 1, 14 for all individual pieces. Regarding at batch level, a good prediction of the average MoE-local values out of MoE-global measurements can be made. Figure 7 shows no influence of depth on the mean ratio MoE-Elocal/MoE-global for batches. No clear relation was found.

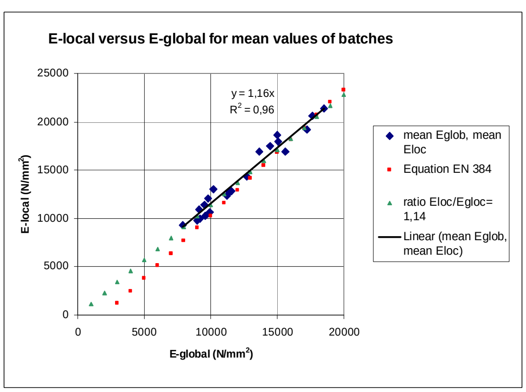

Figure 6. Mean values of MoE-local plotted against MoE-global.

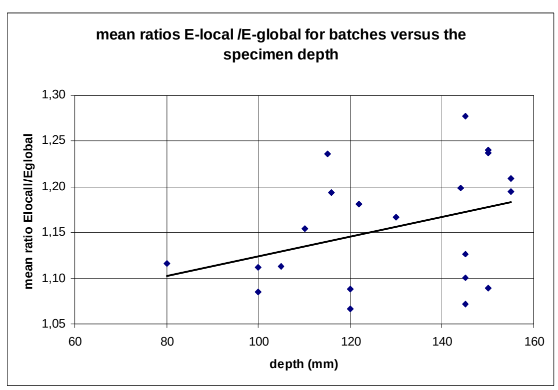

Figure 7. Average values for batches for the ratio MoE-local/MoE-global plotted against the depth of the test pieces.

Table 3 shows that the r^2-values for the regression lines are almost the same, regardless whether the regression line is forced through the origin or not. Although the ratios for MoE-local/MoE-global differ for the 3 datasets, figure 5 shows that the one ratio for pieces out of all three datasets can be used. The ratio between MoE-local/MoE-global for every piece is plotted against the value of MoE-global in figure 8.

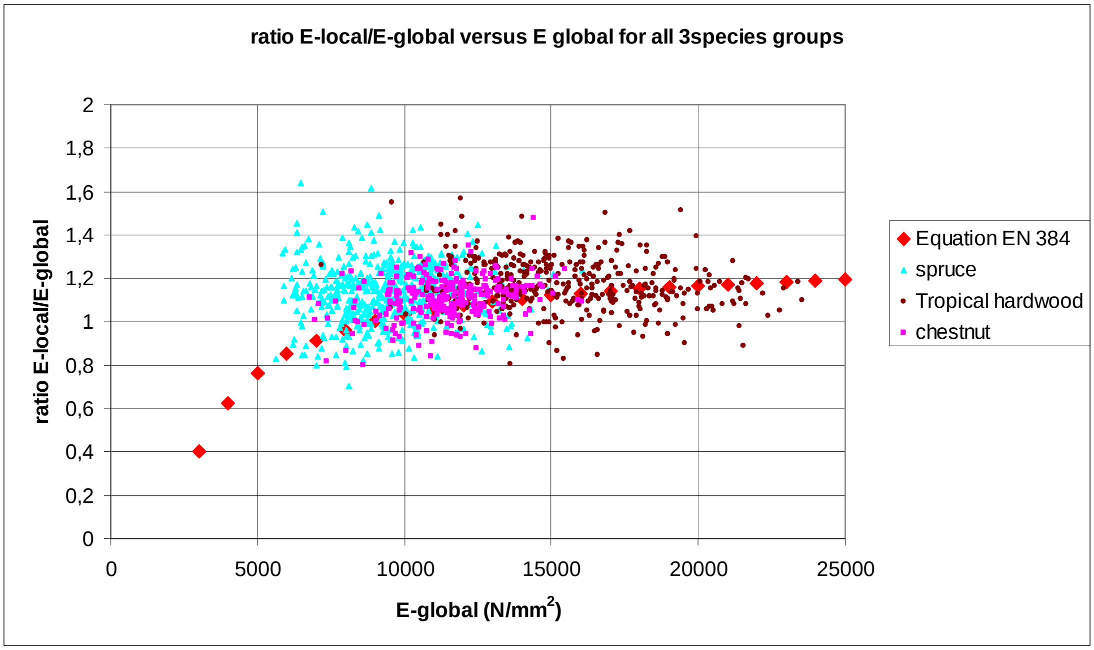

Figure8. Scatter plot of the ratio MoE-local/MoE-global against MoE-global for individual pieces.

Figures 5 and 8 show that the test data in this study do not show the decrease of ratio for MoE-local/MoE-global for the low values of MoE-global as is given in EN 384. There seems to be a larger scatter in the ratio for the low values of E-global, figure 5 shows that the magnitude of the absolute values of MoE-local/MoE-global are the same for the whole range of values for MoE-global.

No significant higher values for the ratio MoE-local/MoE-global for hardwood were found than for spruce and chestnut. However, the coefficient of variation for MoE-local was higher then the covariance for spruce and chestnut, and about the same for tropical hardwood. This could be explained by the position of the visually determined weakest zone in the centre of the test set-up for spruce and chestnut.

5.2 Ratio MoE-global/Edyn and MoE-local/Edyn

In figure 9 the correlation between MoE-dyn and MoE-local is shown and in figure 10 the correlation between MoE-dyn and MoE-global. The correlation between MoE-dyn and MoE-local for all combined data is r^2 = 0, 92 with regression line MoE-local = 0, 92 MoE-dyn. The correlation between MoE-dyn and MoE-global for all combined data is r^2 = 0, 87 with regression line Eglobal = 0, 81 MoE-dyn.

The correlations of MoE-dyn with MoE-global and MoE-local respectively show good consistency. See figure 9 and 10. The moisture content range covered varied between 12% and 54%. The E-local can be predicted out of MoE-dyn with a linear relationship. One single value for the ratio between E-local and MoE-dyn for softwoods and hardwoods is sufficient. The same is the case for E-global. Since the measurements for MoE-dyn are much faster to perform and less sensitive to errors this could be an alternative standardized measurement procedure for E-local and E-global, whereby the following equation is proposed:

$$MoE_{loc} = 0.92 MoE_{dyn} \tag{2}$$

This equation gives the MoE-loc for a moisture content at which MoE-dyn is measured. For strength classification according to EN 384, this MoE-loc has to be adjusted to 12% level as follows:

$$mc_{test} > 18\% \rightarrow MoE_{loc;12\%} = 1.12 MoE_{loc;mc\_test} \tag{3a}$$

$$10\% > mc_{test} > 18\% \rightarrow MoE_{loc;12\%} = (0.96 + (18 - mc_{test}) * 0.02) MoE_{loc;mc\_test} \tag{3b}$$

$$mc_{test} < 10\% \rightarrow MoE_{loc;12\%} = 0.96 MoE_{loc;mc\_test} \tag{3c}$$

Table 2 shows that the covariance for MoE-local is higher than for Edyn. This could be explained by the fact that Edyn gives an average value over the beam.

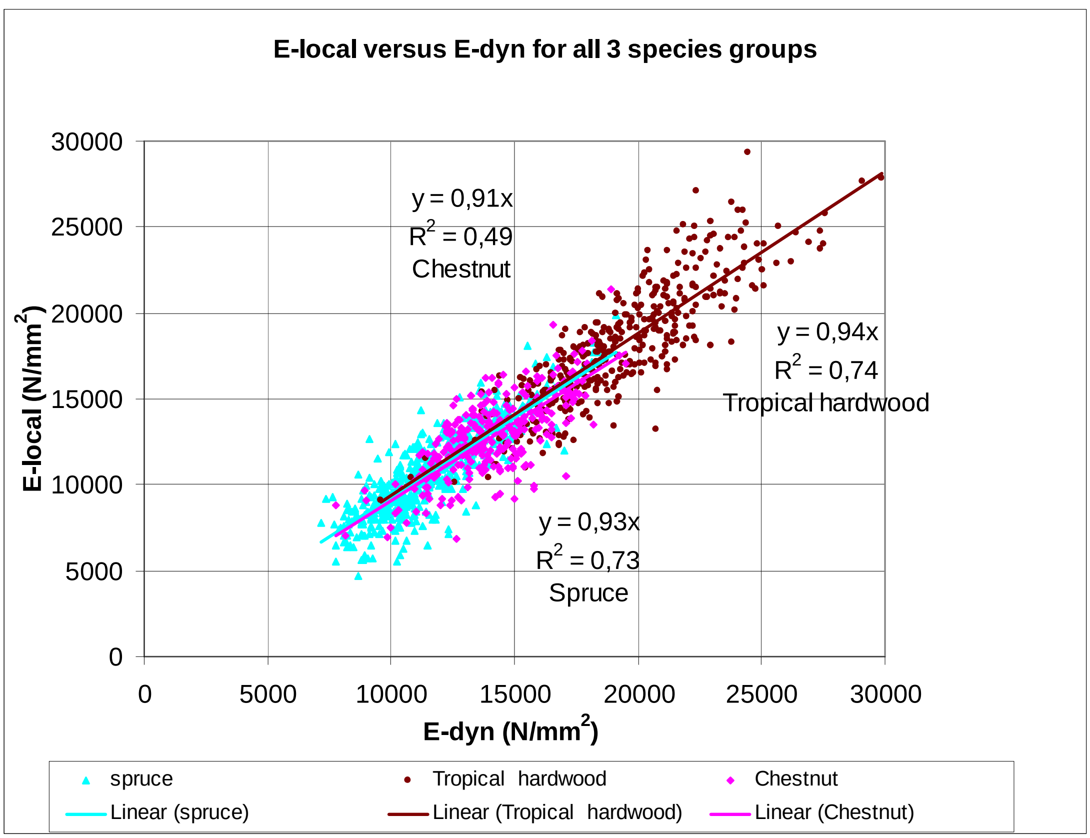

Figure 9. Scatter plots for MoE-dyn-MoE-local for the whole dataset.

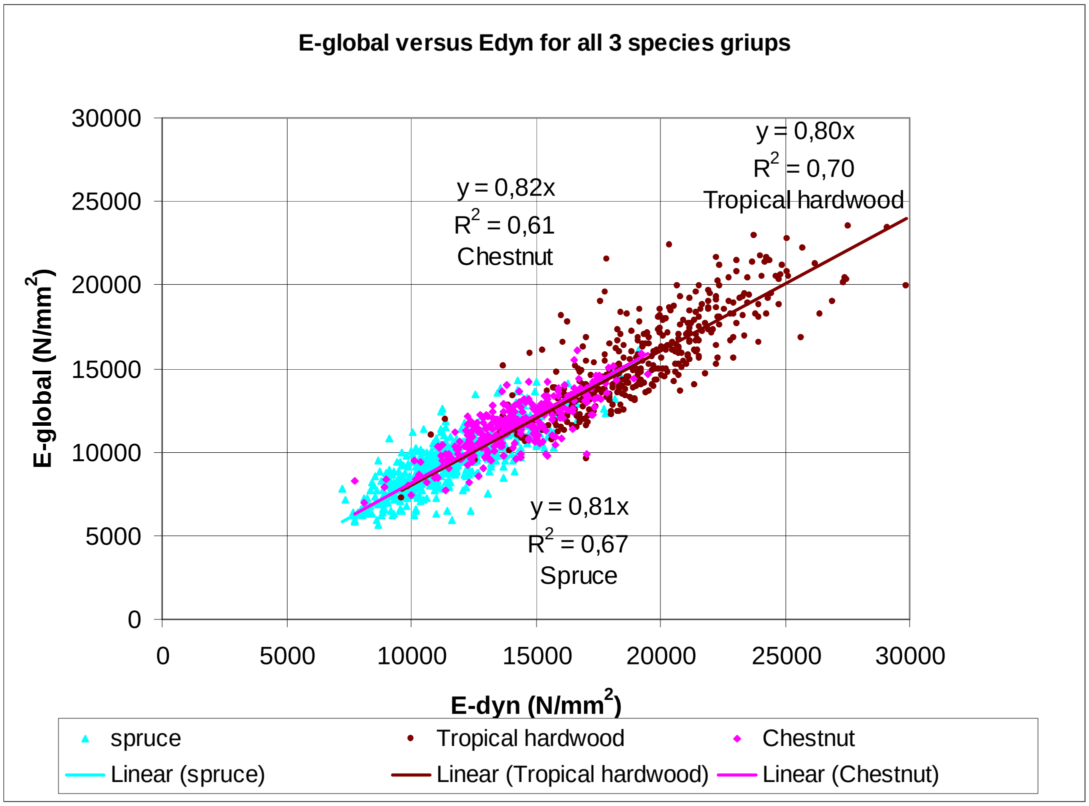

Figure 10 Scatter plots for MoE-dyn-MOEglobal- for the whole dataset.

6 Conclusions

Based on the research the following conclusions can be drawn:

- The ratio of MoE-local/MoE-global follows the same trend for tropical hardwoods, chestnut and spruce and is between 1.12 and 1.16, see figure 7, with an average value of 1.15
- In this study no ratio of MoE-local/MoE-global below 1 was found. No depth influence was found.
- MoE-dyn shows very good correlations with MoE-local and MoE-global for spruce, chestnut and the tropical hardwoods
- MoE-dyn measurements with longitudinal stress waves are easy to perform and with good accuracy. This measurement method could be included in EN 408 as an alternative method to static method. The derived equation (2): MoE-local = 0, 92 MoE-dyn may be used with sufficient accuracy independent of the moisture content. For strength classification according to EN 384, MoE-local has to be adjusted to 12% moisture content after the conversion of MoE-dyn into MoE-local.

7 References

EN 384:2004 Structural Timber – Determination of characteristic values of mechanical properties and density. CEN European Committee for Standardization, Brussels

EN 408:2003 Timber structures – Structural timber and glued laminated timber-Determination of some physical and mechanical properties. CEN European Committee for Standardization, Brussels

Denzler, J.K, Stapel,P. and Glos,P. 2008. Relationships between global and local MOE. CIB W18 paper 41-10-3

Solli, K.H. 1996 Determination of modulus of elasticity in bending according to EN 408. CIB W18 paper 29-10-2.

Boström, L. 1997. Measurement of Modulusof Elasticity in Bending. CIB W18 paper 30-10-2.

Boström, L. and Holmqvist, C. 2000. Determination of the modulus of elasticity in bending- comparison of two methods. World Conference of Timber Engineering , Whistler, Canada

Hanhijärvi, A., Ranta-Maunus, A. and Turk, G. 2005. Potential of strength grading of timber with combined measurement techniques. Report of the Combigrade-project phase 1. VTT Publications 568

CIB-W18/42-12-1

**INTERNATIONAL COUNCIL FOR RESEARCH AND INNOVATION
IN BUILDING AND CONSTRUCTION**

WORKING COMMISSION W18 - TIMBER STRUCTURES

GLULAM BEAMS WITH HOLES REINFORCED BY STEEL BARS

S Aicher

L Höfflin

MPA University Stuttgart

GERMANY

Presented by S Aicher

H.J. Blass asked how to explain the difference between screw in and glue in rods. S. Aicher replied that the difference in results should not be over-interpreted. There is a moment in the rod which makes the design complicated. This can contribute to the differences as there is higher deformability due to the moment.

H.J. Larsen commented that he is impressed with the size of the test program and asked about the shear strength of the cross section. S. Aicher replied that they have tested for the shear strength of the cross section.

H.J. Larsen commented that rather stating that the design method should be improved, reinforcement should be used. S. Aicher said that both issues are important. Even with reinforcement one does not reach capacity which indicates it does not depend on design method. H.J. Blass said that in cases of rectangular hole you would not reach capacity even with reinforcement.

T. Poutanen asked what would happen in the reinforcement situation if the timber dries out. S. Aicher said that the overall failure mechanism will stay the same but initial crack load could be reduced.

J.W.G. van de Kuilen received clarification on the detail of the FEM where the rods were modeled by discretely connected beam elements.

Glulam beams with holes reinforced by steel bars

S. Aicher, L. Höfflin

MPA University Stuttgart, Germany

1 Introduction

The placement of holes in glulam beams represents a frequent necessity in timber construction practice in order to enable the penetration of pipes, wirings and heating tubes. The disturbance of the stress flow around a hole creates tension stresses perpendicular to grain which reduce the load bearing capacity of beams with unreinforced holes, depending on the hole size, considerably. In general a hole reinforcement is inevitable to provide sufficient shear force capacity. Invisible internal reinforcements, such as glued-in steel rods and screws, especially self-tapping screws, are very often preferable from architectural points of view.

The paper reports first on some basic aspects of the stress distribution in the timber and on the rod forces of reinforced holes at two loading stages: i) before crack development and ii) after cross-sectional cracking at the hole edge and subsequent progressive crack extension. Second, the design and construction rules for internal reinforcements, as specified in DIN 1052:2008, are given. Third, first experiments with internally reinforced holes in structural sized glulam beams are presented. The results are discussed in comparison with experimental results on shear force capacities of beams with unreinforced holes and with regard to calculated shear capacities. A preliminary assessment of the applied design rules is given.

2 Stresses perpendicular to grain and rod forces

In the following the relevant stress and rod force distributions are sketched in brief manner for three different hole / reinforcement / crack configurations of glulam beams, being:

- an unreinforced hole (Fig. 1)
- a hole reinforced internally with rods or screws without presence of any major cracks (Fig. 2)
- a reinforced hole with a crack over the entire cross-sectional width, extending from the hole edge beyond the reinforcement bar (Fig. 4)

In all cases, for sake of simplicity, exclusively the primarily damage relevant (damage initiating) stresses perpendicular to grain and the rod normal forces are regarded. However, it should be mentioned, that especially shear stresses in the timber and the bending moment in the steel bar/screw have to assessed for a comprehensive design approach, too.

Figure 1 reveals the typical stress perpendicular to grain distribution in the vicinity of a hole rather close to a support, i.e. with a (rather) small moment vs. shear force ratio M/V (roughly M/V ≈ h to 10h). The stress distribution is characterized by two diagonally opposite tension stress fields in the bending compression part of the beam at the "right" side of the hole (ℓ_A + a, see Fig. 6) and in the bending tension part of the beam at the "left" side of the hole. The tension stress maxima occur at an inclination of about φ = 45° vs. the beam axis. Due to the increased moment, the maximum value at the right hole side is throughout higher depending significantly on the M/V ratio. Diagonally opposite to the tension stress fields similar fields of compression stresses perpendicular to grain occur. The stress distribution given in Fig.1 leads to a typical damage/failure scenario which is always characterized by two distinct major cracks starting at the hole edge at the diagonally opposite locations of the maximum tension stresses perpendicular to grain and extending straight parallel to fibre. Ultimate damage occurs when the tension perpendicular to grain/shear crack located in the bending tension part closer to the support has extended until the support. For details of the stress distributions, failure occurrences and a Weibull theory based design of unreinforced round holes see i.a. (Aicher and Höfflin (2006); Höfflin (2005); Aicher et al. (2007)).

Figure 2 gives a schematic view of stresses perpendicular to grain for a glulam beam with a round hole, internally reinforced by steel bars. The beam dimensions and loading are the same as in Fig.1, so the stress distribution can be compared with regard to shape and magnitude. It is important to note that the reinforcements do not lead to a fundamental change of stress fields as compared to the unreinforced situation. The degree of change in the stress field shape and its magnitude is of course depending on the specific reinforcement configuration (stiffness and distance of the rod from the hole edge). The distribution of the normal force in the rod is given schematically, too.

Figure 3 depicts the decrease of the maximum tension stress perpendicular to grain at the hole edge depending on the diameter d_c of the rod (= rod core). The distance of the rod from the hole edge $a_{1,c}$ (see Fig. 6b) is kept constant. Further, the shift of the location φ of the maximum stress at the hole periphery and the increase of the maximum axial rod force as depending on d_c is depicted.

Figure 4 gives a schematic view of the stress perpendicular to grain of a glulam beam with a hole, internally reinforced by steel rods, now incorporating a major crack parallel to beam axis extending from the hole edge. The onset of the crack is located at the location of the maximum stress perpendicular to grain prior to cracking. A comparison with Fig. 2 reveals, as anticipated, that the stress perpendicular grain in the timber vanishes almost entirely. The resultant of these stresses is taken up by the reinforcement rod. This successive load transfer from the timber to the rod with increasing crack length from the hole edge is depicted in Fig. 5 for two reinforcement configurations V1 and V5 investigated experimentally. The rod force attains a limit value once the crack has propagated beyond a certain distance (~10 - 40 mm) away from the rod.

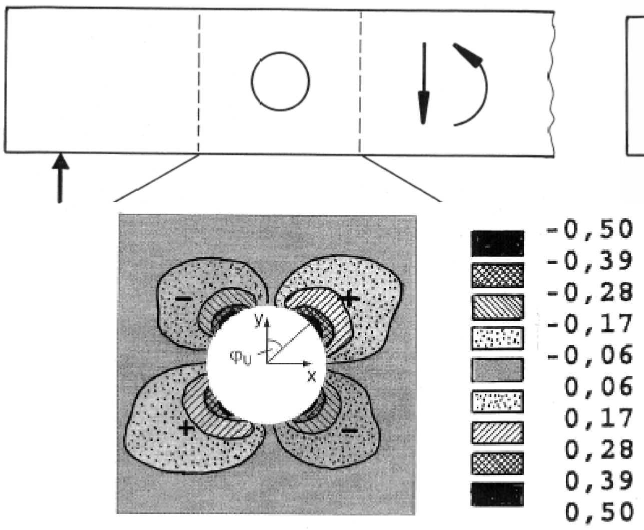

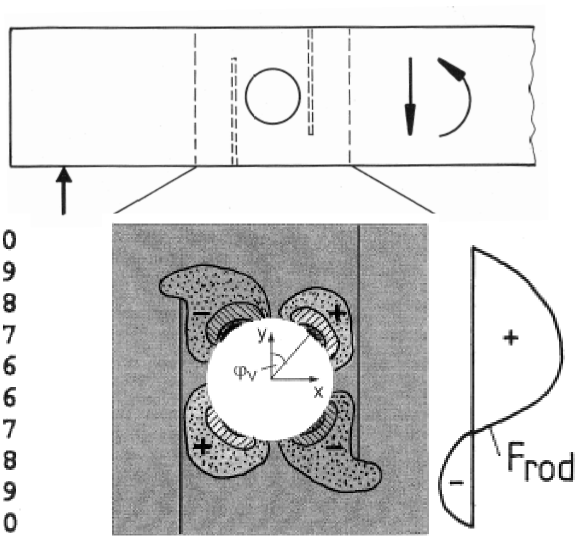

Fig. 1:
Example of distribution of stresses perpendicular to grain in the vicinity of an unreinforced hole in a glulam beam (M/V = 1,5 h; V = 10 kN)

Fig. 2:
Example of distribution of stresses perpendicular to grain in the vicinity of a reinforced hole in a glulam beam (M/V = 1,5 h; V = 10 kN); also given: schematic view of rod force distribution

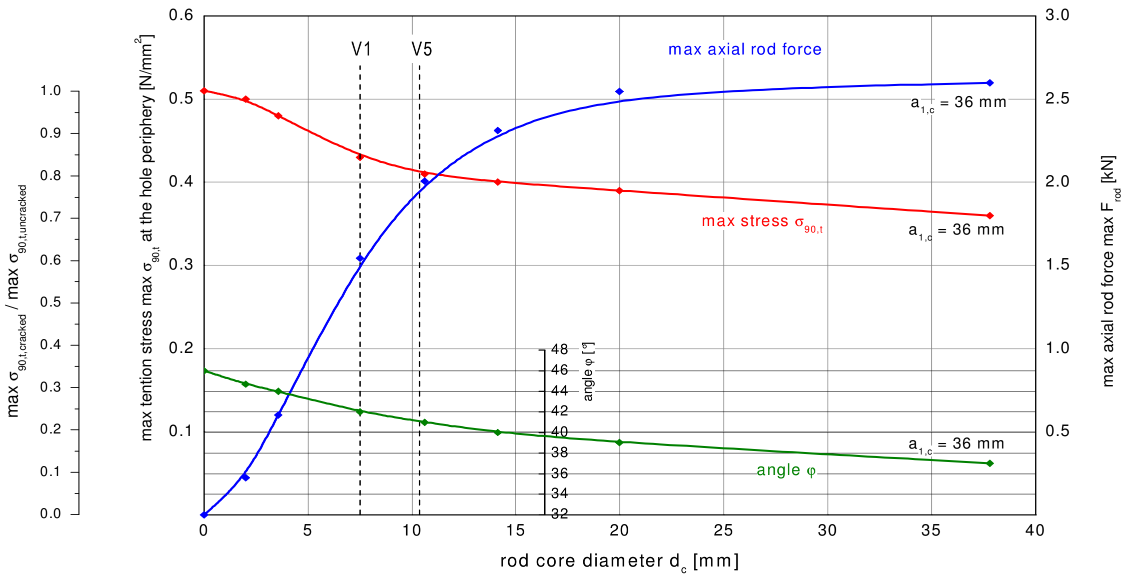

Fig. 3:
Effect of rod diameter on maximum tension stress perpendicular to grain at the hole edge and on the rod force for a glulam beam with internal reinforcements; shear force V = 10 kN; beam dimensions as given in Fig. 8

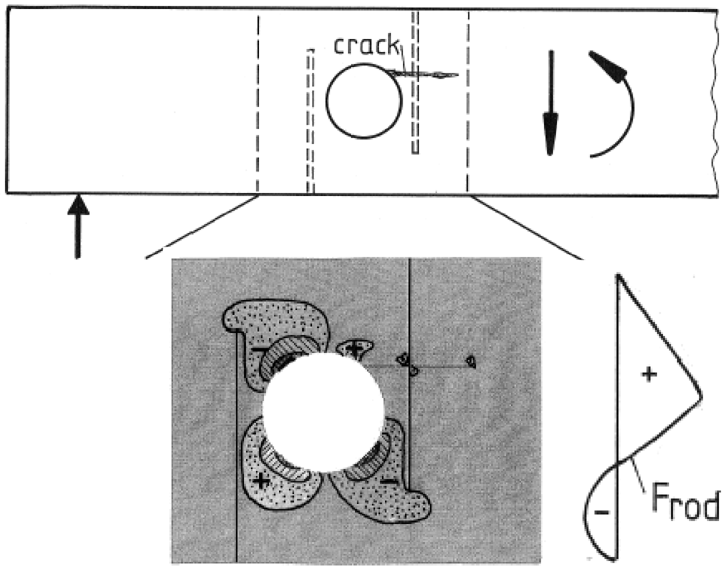

Fig. 4:
Example of distribution of stresses perpendicular to grain in the vicinity of a cracked reinforced hole in a glulam beam (M/V = 1,5 h; V = 10kN); also given: schematic view of rod force distribution

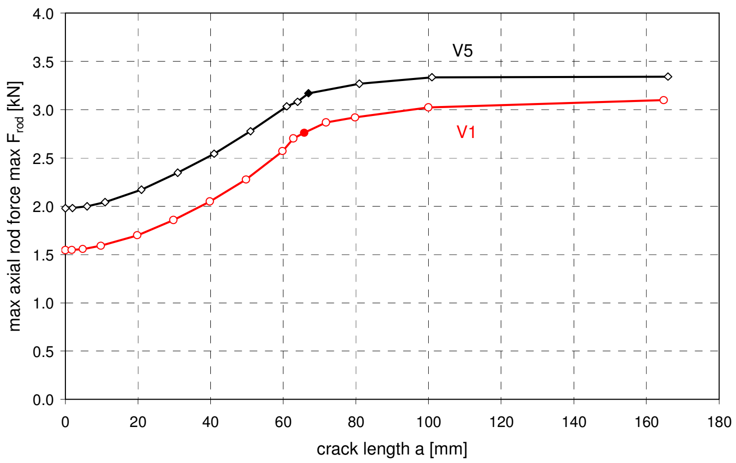

Fig. 5:
Relationship between rod force and crack length starting from the edge of the hole; shear force V = 10 kN; beam dimensions see Fig. 8

The increase of the rod force from the uncracked to the fully cracked stage is roughly denoted by a factor of 1,5 to 2 depending on the reinforcement stiffness and the distance of the rod from the hole edge.

3 Design and construction rules for internally reinforced holes acc. to DIN 1052

Figure 6 gives the geometry notations used in the present German timber design code DIN 1052:2008-10. In detail Fig. 6a specifies the dimensions of the hole within the beam and indicates the relevant crack planes, similarly relevant for unreinforced and reinforced holes. Figure 6 b gives the dimensional notations of the internal reinforcement rods and the respective (edge) distances. The following construction rules/limits for the permissible position and sizes of round holes (see Fig. 6a) apply:

- $\ell_V \geq h$
- $\ell_A \geq h/2$
- $h_{ro(ru)} \geq h/4$

- $h_d \leq 0,3$ h (internal reinforcements, i. e screws, glued-in rods)
- $h_d \leq 0,4$ h (external reinforcements, i. g. glued-on plywood plates)

For the position of the reinforcement bars (d_r = nominal /outer diameter) the following (edge) distances are prescribed:

- $a_{1,c}$: $2,5\ d_r \leq a_{1,c} \leq 4\ d_r$
- a_2: $a_2 \geq 3\ d_r$
- $a_{2,c}$: $a_{2,c} \geq 2,5\ d_r$

The design verification of the rod is given as

$$F_{t,90,d} \leq R_{ax,d} \tag{1}$$

where

$$F_{t,90,d} = F_{t,90,k} \cdot \gamma_L = F_{t,V,d} + F_{t,M,d} \tag{2a}$$

design (d) resp. characteristic (k) tension force perpendicular to grain due to stress disturbance in the hole vicinity

and

$$F_{t,V,d} = \frac{V_d \cdot 0,7 h_d}{4 \cdot h}\left[3 - \frac{(0,7\ h_d)^2}{h^2}\right], \quad F_{t,M,d} = 0,008\ \frac{M_d}{h_r} \tag{2b,c}$$

$$h_r = \min\left\{h_{ro} + 0,15\ h_d\ ; h_{ru} + 0,15 h_d\right\} \tag{3}$$

k_{mod} modification factor for accumulated load duration and service class;

γ_L, γ_M partial safety factors for loading and materials

And on the resistance side, in case of screws

$$R_{ax,d} = R_{ax,k} \cdot (k_{mod} / \gamma_M) \tag{4a}$$

axial design (d) resp. characteristic (k) tension capacity of the rod

In case of (self-tapping) screws the characteristic axial capacity at 90 degrees vs. fiber direction is (head pull through situation not regarded here)

$$R_{ax,k} = \min\left\{f_{1,k} \cdot \ell_{ad} \cdot d_r\ ;\ R_{t,u,k}\right\} \tag{4b}$$

and (ρ_k in kg/m^3)

$$f_{1,k} = 80 \cdot 10^{-6} \cdot \rho_k^2 \quad \text{in N/mm}^2 \tag{4c}$$

characteristic value of pull out parameter of wood screw (load capacity class 3) or of self tapping screw acc. to Z-9.1-519

$R_{t,u,k}$ characteristic axial steel tension load capacity

In case of glued-in rods the design capacity is

$$R_{ax,d} = \min \{\pi \cdot d_r \cdot \ell_{ad} \cdot f_{k1,d} \; ; \; f_{y,d} \cdot A_{ef}\} \qquad (5a)$$

where

$$f_{k1,d} = f_{k1,k} \cdot (k_{mod}\, \gamma_M) \qquad (5b)$$

design (d) resp. characteristic (k) bond strength between rod and timber (values for $f_{k1,k}$ given in Tab. F. 23 of DIN 1052:2008, see below)

$f_{y,d} = f_{y,k} / \gamma_M$ design (d) resp. characteristic (k) yield stress of rod

The effective anchorage length ℓ_{ad} of the rod, accounting for the possible slight eccentricity of the hole vs. mid-depth and the respective minimum value are

$$\ell_{ad} = h_{ru} + 0{,}15\, h_d \quad \text{or} \quad \ell_{ad} = h_{ro} + 0{,}15\, h_d, \quad \ell_{ad,min} = \max\{0{,}5 d_r^2 \,;\, 10 d_r\} \qquad (5c,d)$$

The basic idea of the design equations (1) and (2a-c) is sketched schematically in Fig. 7, which exclusively addresses the redistribution of the shear stresses which can not be transferred in undisturbed manner due to the missing cross-section in the hole area [Kolb and Epple, 1984; Blaß and Steck, 1999a-c].

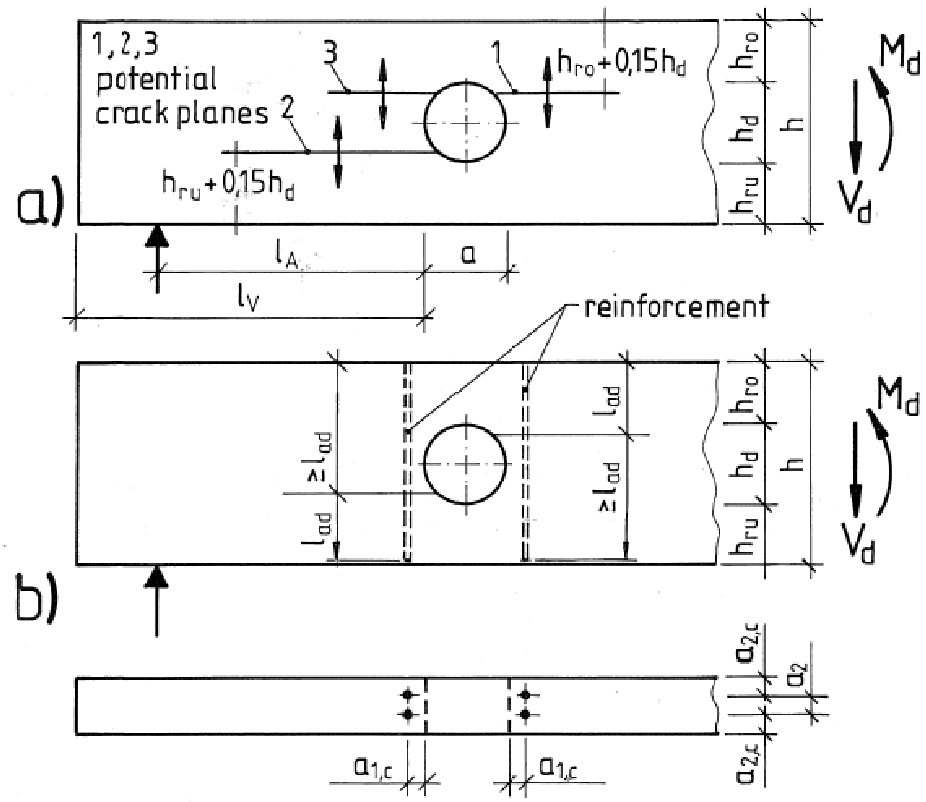

Fig. 6: Geometry notations and endangered/potential crack planes of unreinforced and reinforced glulam beams acc. to DIN 1052:2008

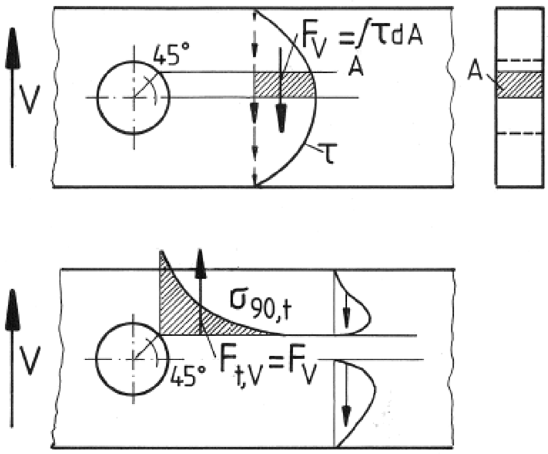

Fig. 7: Schematic illustration of basic idea of DIN 1052 design approach for reinforced holes (exclusively shear force contribution)

In a simplified mechanical model, exclusively regarding internal force equilibrium, the resultant shear force of the shadowed area in Fig. 7 is transferred to the remaining cross-sections in the bending compression and tension parts by a discrete tension force, taken up the steel reinforcement rod. The additional contribution of the bending moment to the rod force results qualitatively perceivable, but not elementary quantifiable, from a tension band perpendicular to the normal stresses flowing around the hole. With increasing hole size the inclination of their force resultants and hence of the component perpendicular to beam axis becomes larger.

4 Experimental program

All tests were performed with homogeneously built-up glulam beams of strength class GL 32h according to EN 1194. All laminations were machine strength graded and conformed to strength class C 35. The beams, manufactured by four different producers, had the same dimensions (width b, depth h and length l) of : 120 mm x 450 mm x 3500 mm. Each beam had a round hole of diameter h_d = 180 mm at the same position, shown in Fig. 8, which gives the test set-up, too. In each test configuration beams of 3 different producers were used. Three different test series, two with reinforced and one with unreinforced holes were performed:

test series V1: Reinforcement of the hole at both sides (regarding beam length) with self tapping screws of nominal/outer diameter of d_r = 12 mm. End grain distance was $a_{1,c} = 3d_r$ = 36 mm. The screws conformed to general German building approval Z-9.1-519.

test series V2: similar to test series V1, but with glued-in steel rods with metric thread. The hole diameter was d_h = 14 mm. The employed adhesive has a general German building approval (Z-9.1-750) for bonding of steel rods in timber / glulam. The strength class of the steel rod was 8.8 according to EN ISO 898-1.

test series U: Unreinforced reference beams with holes.

Test series V1 and V5 comprised 6 specimens and test series U consisted of 7 specimens, whereof four (U1 to U4) had been investigated earlier in the frame of a research project on glulam beams with unreinforced holes (Aicher and Höfflin, 2006).

The position of the hole and the end grain distances of the reinforcements conformed to the construction details specified in DIN 1052:2008 and given above. The investigated ratio of the hole size vs. beam depth, $h_d/h = 0,4$, is inline with the former design code DIN 1052:2004, however does not comply, as mentioned, with the present dimensional prescriptions, limiting the hole size to $h_d/h \leq 0,3$. (Note: as the newly introduced reduction of the permissible relative hole size is exclusively bound to specific stress features at high M/V ratios, the here obtained results can well be considered relevant for the somewhat smaller permissible hole size of $h_d/h = 0,3$.)

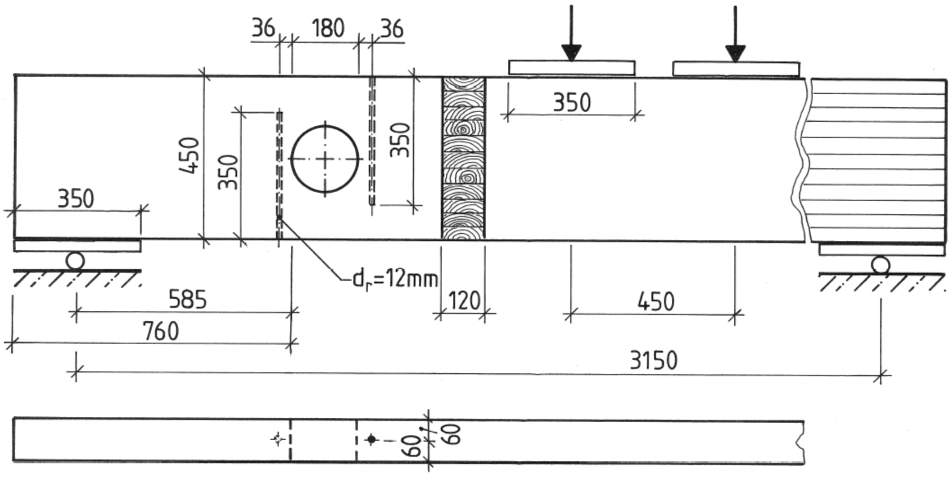

Fig. 8: Dimensions of investigated reinforced (and unreinforced) glulam specimens and test set-up.

The steel reinforcements were chosen in such manner that the shear force capacity of the beams with reinforced holes should at least equal the characteristic shear force capacity of a glulam beam of same dimension and strength class without a hole. Hereby the characteristic shear force capacity was calculated for two cases: i) in very conservative manner, $V_k = V_{k,1}$, by consideration of the crack factor k_{cr}, which normally reflects the effect of aging/climate effects what is not relevant for the test specimens and ii) without consideration of the crack factor what should mirror the virgin characteristic shear capacity $V_k = V_{k,2}$ of the beams.

The shear force capacity of the beam without a hole is (EN 1995-1-1: 2005)

$V_k = 2/3 f_{v,k} \cdot h \cdot b_{ef}$ where $b_{ef} = k_{cr} \cdot b$ and $k_{cr} = 0,67$ (shear) crack factor.

With $f_{v,k} = 3,8\ \mathrm{N/mm^2}$ (characteristic shear strength for GL32h acc. to EN 1194) one obtains

$V_{k,1} = 0,67 \cdot 3,8 \cdot 450 \cdot 120 \cdot 0,67 = 92,1\ \mathrm{kN}$, $V_{k,2} = 137,5\ \mathrm{kN}$.

Then the characteristic bending moments at the right edge of the hole are

$M_{k,1} = 92{,}1 \cdot 0{,}765 = 70{,}46\ \text{kNm},\ M_{k,2} = 105{,}19\ \text{kNm}$

and hence (with $k_r = 35 + 0{,}15 \cdot 180 = 62\ \text{mm}$)

$F_{t,v,k,1} = 18{,}84\ \text{kN}, \quad F_{t,M,k,1} = 3{,}48\ \text{kN}$
and so
$F_{t,90,k,1} = 18{,}84 + 3{,}48 = 22{,}32\ \text{kN}$, $F_{t,90,k,2} = 33{,}32\ \text{kN}$.

The effective anchorage length of the reinforcement screws/bars acc. to eq. (5c) is $l_{ad} = 162\,\text{mm}$. This forwards a characteristic axial tension capacity of the self tapping screw acc. to eq. (4c) (with $R_{t,u,k} = 38\ \text{kN}$, see Z-9.1-519 and $\rho_k = 430\,\text{kg/m}^3$ for GL 32h) of
$R_{ax,k} = 14{,}8 \cdot 162 \cdot 12 = 28{,}8\ \text{kN}$

In case of the glued-in rods the characteristic bond strength for a bond length $\leq 250\,\text{mm}$ acc. to DIN 1052:2008 is maximally $4\ \text{N/mm}^2$, irrespective of the specific adhesive. For the employed adhesive acc. to Z-9.1-750 a more realistic experimentally based value, still conservative, is $f_{k1,k} = 5\ \text{N/mm}^2$. This gives acc. to eq. (5a) a characteristic axial tension capacity of $R_{ax,k} = \pi \cdot 12 \cdot 162 \cdot 5 = 30{,}5\ \text{kN}$.

So, in case of both reinforcement types, screws or glued-in rods: $R_{ax,k} > F_{t,90,k,1}$. With regard to $F_{t,90,k,2}$ the axial rod capacities would be nominally too low but are regarded sufficient for the specific test scenarios.

5 Test results

The primary test results are compiled in Table 1. Given are the shear forces at different damage resp. crack stages:

- V_{init} = shear force associated to the 1st crack visible in the end grain face of the hole
- V_c = shear force associated to the damage state where a crack is first visible on both side faces
- V_u = ultimate shear force capacity

Table 2 presents some relevant ratios of shear force capacities, being i. a. the ratios V_{init}/V_u, V_c/V_u. Further shear forces V_c and V_u are compared with the respective means of test series U with the unreinforced holes ($V_{c,U,mean}$, $V_{u,U,mean}$) and finally, the ultimate shear force capacities are related to the characteristic shear capacities, $V_{k,1}$ and $V_{k,2}$, of the beam without a hole.

The following results are noteworthy:

- Both investigated reinforcement alternatives forwarded significant and comparable shear capacity increases vs. the beams with unreinforced holes at all three regarded shear force levels, V_{init}, V_c and V_u. The largest increase was obtained

for ultimate shear force V_u, where at the level of the mean values, the increases were 55 % and 64 % in case of configurations V1 and V5, respectively.
The smallest shear force increases vs. the unreinforced holes, however still very noticeable, were obtained at the initial crack load level, V_{init}; the increases were 27 % and 41 % in case of V1 and V5, respectively. At the shear force level V_c, the capacity gains were 38 % and 49 % for V1 and V5, respectively.

- The reinforcement alternative V5 (glued-in rod) provided throughout somewhat higher shear force capacities as compared to alternative V1 (self-tapping screw). On the mean value level, the ratios of the shear forces of series V5 vs. V1 were 1,11, 1,08 and 1,06 in case of V_{init}, V_c and V_u.

- On the ultimate shear capacity level, V_u, the result scatter of the V1 and V5 samples, very similar showed a C.O.V of about 9 %, so the stated mean value difference between alternatives V1 and V5 should also hold on the 5percentile level. However, on the V_c and V_{init} shear force level, the scatter of the V5 results was larger what might be explicable by the higher rigidity/brittleness of the glued interface vs. the screwed anchorage conditions.

- The shear force gains of the reinforced holes vs. the unreinforced holes ranged from V_{init} (in average for V1 and V5: + 34 %) to V_c (in average: + 44 %) and V_u (in average: + 60 %). The capacity increase at the mean level is qualitatively in line with the computational results. There it was shown that in the uncracked state up to V_{init} the peak tension stress perpendicular to grain is reduced by a factor of about 1,2 to 1,25 (for the regarded beam/reinforcement configuration).

- The shear force ratios V_{init}/V_u and V_c/V_u which in case of the unreinforced holes are, in average, 0,64 and 0,86, respectively, are lower for the reinforced samples. There, very similar for the V1 and V5 configurations, ratios of $V_{init}/V_u \approx 0{,}52$ and $V_c/V_u \approx 0{,}75$ were obtained.

- A comparison of the ultimate shear force ratio $V_u/V_{k,1}$ of the reinforced configuration V1 reveals that, in average, a level of 0,93 of the characteristic target shear force capacity of the beam without hole (including service life cracks via k_{cr}) was obtained. Minimally a value of 0,84 $V_{k,1}$ has to be stated. This means that the design, which is suggesting that the reinforcement will re-establish the full shear capacity of the beam without hole is about 15 % to 20 % unconservative. In case of reinforcement alternative V5, in average V_u = 0,99 $V_{k,1}$ and minimally $V_{u,min}$ = 0,9 $V_{k,1}$ were obtained. Despite the fact that the results are somewhat better as in case of reinforcement alternative V1, especially the mean value of $V_{u,V5}$ is still about 15 % to 20 % too low.

- The comparison of the shear force capacities V_u with the shear capacity $V_{k,2}$ of a beam without a hole and without service life cracks, reveals that the investigated reinforcements fail considerably to re-establish the shear capacity of the beam without a hole. This is most probably due to fact, that the ultimate load of the beam with a hole, beyond shear force level V_c, is finally determined by a propagating shear crack, which is not hindered by a steel rod acting transverse to the crack plane.

<table>
<tr><th rowspan="3">test series</th><th rowspan="3">specimen No.</th><th rowspan="2">density</th><th colspan="3">shear force
at initial cracking

V_{init}</th><th colspan="3">shear force at fully
develloped
cross-sectional crack
V_c</th><th rowspan="2">ultimate
shear force

V_u</th></tr>
<tr><th colspan="2">crack location</th><th></th><th colspan="2">crack location</th><th></th></tr>
<tr><th>ρ_{12}</th><th>AN[1)]</th><th>AF[2)]</th><th>min. value</th><th>AN[1)]</th><th>AF[2)]</th><th>min. value</th><th></th></tr>
<tr><td>-</td><td>-</td><td>kg/m³</td><td>kN</td><td>kN</td><td>kN</td><td>kN</td><td>kN</td><td>kN</td><td>kN</td></tr>
<tr><td rowspan="10">U</td><td>U/1[3)]</td><td>511</td><td>30,3</td><td>34,0</td><td>30,3</td><td>41,8</td><td>38,3</td><td>38,3</td><td>44,5</td></tr>
<tr><td>U/2[3)]</td><td>466</td><td>27,0</td><td>37,0</td><td>27,0</td><td>45,0</td><td>50,0</td><td>45,0</td><td>53,4</td></tr>
<tr><td>U/3[3)]</td><td>463</td><td>38,0</td><td>48,3</td><td>38,0</td><td>50,6</td><td>48,3</td><td>48,3</td><td>50,6</td></tr>
<tr><td>U/4[3)]</td><td>505</td><td>56,7</td><td>43,3</td><td>43,3</td><td>58,7</td><td>58,7</td><td>58,7</td><td>58,7</td></tr>
<tr><td>U/5</td><td>454</td><td>41,3</td><td>32,4</td><td>32,4</td><td>50,2</td><td>51,1</td><td>50,2</td><td>53,1</td></tr>
<tr><td>U/6</td><td>460</td><td>-</td><td>38,8</td><td>38,8</td><td>44,1</td><td>44,1</td><td>44,1</td><td>54,6</td></tr>
<tr><td>U/7</td><td>458</td><td>-</td><td>33,0</td><td>33,0</td><td>44,8</td><td>42,9</td><td>42,9</td><td>72,3</td></tr>
<tr><td>mean</td><td>474</td><td>38,7</td><td>38,1</td><td>34,7</td><td>47,9</td><td>47,6</td><td>46,8</td><td>55,3</td></tr>
<tr><td>STD</td><td>24</td><td>11,6</td><td>5,9</td><td>5,6</td><td>5,8</td><td>6,6</td><td>6,5</td><td>8,6</td></tr>
<tr><td>COV [%]</td><td>5</td><td>30,0</td><td>15,5</td><td>16,2</td><td>12,0</td><td>13,9</td><td>13,9</td><td>15,6</td></tr>
<tr><td rowspan="9">V1</td><td>V1/1</td><td>467</td><td>39,8</td><td>35,0</td><td>35,0</td><td>67,5</td><td>55,1</td><td>55,1</td><td>77,3</td></tr>
<tr><td>V1/2</td><td>-</td><td>45,7</td><td>35,9</td><td>35,9</td><td>56,1</td><td>72,9</td><td>56,1</td><td>80,5</td></tr>
<tr><td>V1/3</td><td>471</td><td>34,7</td><td>38,7</td><td>34,7</td><td>81,2</td><td>63,8</td><td>63,8</td><td>95,9</td></tr>
<tr><td>V1/4</td><td>437</td><td>52,8</td><td>47,3</td><td>47,3</td><td>65,6</td><td>71,7</td><td>65,6</td><td>80,8</td></tr>
<tr><td>V1/5</td><td>455</td><td>-</td><td>44,9</td><td>44,9</td><td>73,1</td><td>65,6</td><td>65,6</td><td>82,8</td></tr>
<tr><td>V1/6</td><td>444</td><td>67,2</td><td>-</td><td>67,2</td><td>80,0</td><td>80,0</td><td>80,0</td><td>95,7</td></tr>
<tr><td>mean</td><td>455</td><td>47,5</td><td>44,8</td><td>44,2</td><td>70,6</td><td>68,2</td><td>64,4</td><td>85,5</td></tr>
<tr><td>STD</td><td>15</td><td>11,4</td><td>12,0</td><td>12,5</td><td>9,5</td><td>8,6</td><td>9,0</td><td>8,2</td></tr>
<tr><td>COV [%]</td><td>3</td><td>24,0</td><td>26,8</td><td>28,3</td><td>13,5</td><td>12,6</td><td>13,9</td><td>9,6</td></tr>
<tr><td rowspan="9">V5</td><td>V5/1</td><td>451</td><td>40,0</td><td>34,1</td><td>34,1</td><td>75,5</td><td>46,0</td><td>46,0</td><td>83,3</td></tr>
<tr><td>V5/2</td><td>470</td><td>53,3</td><td>26,8</td><td>26,8</td><td>59,9</td><td>-</td><td>59,9</td><td>83,9</td></tr>
<tr><td>V5/3</td><td>470</td><td>56,4</td><td>33,8</td><td>33,8</td><td>70,8</td><td>63,7</td><td>63,7</td><td>83,2</td></tr>
<tr><td>V5/4</td><td>-</td><td>76,0</td><td>-</td><td>76,0</td><td>96,6</td><td>80,4</td><td>80,4</td><td>96,6</td></tr>
<tr><td>V5/5</td><td>-</td><td>59,4</td><td>-</td><td>59,4</td><td>94,6</td><td>78,3</td><td>78,3</td><td>100,2</td></tr>
<tr><td>V5/6</td><td>-</td><td>77,5</td><td>63,4</td><td>63,4</td><td>90,2</td><td>88,7</td><td>88,7</td><td>97,8</td></tr>
<tr><td>mean</td><td>464</td><td>60,4</td><td>39,5</td><td>48,9</td><td>81,3</td><td>71,4</td><td>69,5</td><td>90,8</td></tr>
<tr><td>STD</td><td>11</td><td>14,3</td><td>16,2</td><td>19,9</td><td>14,8</td><td>16,8</td><td>15,8</td><td>8,2</td></tr>
<tr><td>COV [%]</td><td>2,4</td><td>23,6</td><td>41,1</td><td>40,8</td><td>18,2</td><td>23,6</td><td>22,7</td><td>9,0</td></tr>
</table>

1) in bending tension part between support and hole
2) in bending compression part between hole and load
3) see Aicher and Höfflin (2006)

Table 1: Compilation of primary test results of test series V1, V5 with glulam beams with reinforced holes and of test series U with unreinforced holes

test series	specimen No.	shear force ratios					
		$\frac{V_{init}}{V_u}$	$\frac{V_c}{V_u}$	$\frac{V_c}{V_{c,U,mean}}$	$\frac{V_u}{V_{u,U,mean}}$	$\frac{V_u}{V_{k,1}}$	$\frac{V_u}{V_{k,2}}$
U	U/1	0,68	0,86	0,82	0,80	0,48	0,32
	U/2	0,51	0,84	0,96	0,97	0,58	0,39
	U/3	0,75	0,95	1,03	0,92	0,55	0,37
	U/4	0,74	1,00	1,25	1,06	0,64	0,43
	U/5(L1)	0,61	0,95	1,07	0,96	0,58	0,39
	U/5(L2)	0,71	0,81	0,94	0,99	0,59	0,40
	U/6(L3)	0,46	0,59	0,92	1,31	0,79	0,53
	mean	0,64	0,86	1,00	1,00	0,60	0,40
	STD	0,11	0,14	0,14	0,16	0,10	0,06
	COV [%]	17,9	15,9	13,7	15,7	16,0	16,2
V1	V1/1	0,45	0,71	1,18	1,40	0,84	0,56
	V1/2	0,45	0,70	1,20	1,46	0,87	0,59
	V1/3	0,36	0,67	1,36	1,73	1,04	0,70
	V1/4	0,59	0,81	1,40	1,46	0,88	0,59
	V1/5	0,54	0,79	1,40	1,50	0,90	0,60
	V1/6	0,70	0,84	1,71	1,73	1,04	0,70
	mean	0,52	0,75	1,38	1,55	0,93	0,62
	STD	0,12	0,07	0,19	0,15	0,09	0,06
	COV [%]	23,4	9,3	13,8	9,4	9,5	9,8
V5	V5/1	0,41	0,55	0,98	1,51	0,90	0,61
	V5/2	0,32	0,71	1,30	1,52	0,91	0,61
	V5/3	0,41	0,77	1,36	1,50	0,90	0,61
	V5/4	0,79	0,83	1,72	1,75	1,05	0,70
	V5/5	0,59	0,78	1,67	1,81	1,09	0,73
	V5/6	0,65	0,91	1,90	1,77	1,06	0,71
	mean	0,53	0,76	1,49	1,64	0,99	0,66
	STD	0,18	0,12	0,34	0,15	0,09	0,06
	COV [%]	33,7	15,9	22,6	9,0	9,1	8,7

Table 2: Normalized shear force capacities

6 Conclusions

The performed tests with glulam beams with reinforced holes proved that internal, invisible reinforcements by screws or glued-in rods provide a significant, well reproduceable increase of the static short term shear force capacity vs. glulam beams with unreinforced holes. However, the investigated reinforcement configurations did not forward completely the expected load capacity level predicted by the applied DIN 1052 design model. As the final failure mode is a shear failure, as in case of unreinforced beams, it seems worthwhile to attempt a fracture mechanics approach. In ongoing tests further reinforcement and beam size configurations are regarded.

7 References

Aicher, S., Höfflin, L., Reinhardt, H. W. (2007): Round holes in members made of glued laminated timber. Part 2: Load capacity and design (In German). Bautechnik 84, (8), pp. 867 – 880

Aicher, S., Höfflin, L. (2006): Tragfähigkeit und Bemessung von Brettschichtholzträgern mit runden Durchbrüchen – Sicherheitsrelevante Modifikationen der Bemessungsverfahren nach Eurocode 5 und DIN 1052. Research Report ZP 52-5-13.161-1092/04, MPA University Stuttgart

Blaß, H. J., Steck, G. (1999 a - e): Querzugverstärkungen von Holzbauteilen

- Teil 1; Bauen mit Holz 101 (3), pp. 42 – 46
- Teil 2; Bauen mit Holz 101 (4), pp. 44 – 49
- Bemessungsbeispiele; Bauen mit Holz 101 (5), pp. 46 - 50

Kolb, H., Epple, A. (1985): Verstärkungen von durchbrochenen Brettschichtholzbindern. Schlussbericht Forschungsvorhaben I.4 – 34810, Forschungs- und Materialprüfungsanstalt Baden-Württemberg, Stuttgart

Höfflin, L. (2005): Runde Durchbrüche in Brettschichtholzträgern – Experimentelle und theoretische Untersuchungen. PhD thesis. MPA Universität Stuttgart, Schriftenreihe Heft 90, Stuttgart

CIB-W18/42-12-2

INTERNATIONAL COUNCIL FOR RESEARCH AND INNOVATION IN BUILDING AND CONSTRUCTION

WORKING COMMISSION W18 - TIMBER STRUCTURES

ANALYSIS OF X-LAM PANEL-TO-PANEL CONNECTIONS UNDER MONOTONIC AND CYCLIC LOADING

C Sandhaas

J Boukes

Delft University of Technology

THE NETHERLANDS

J W G van de Kuilen

Delft University of Technology

THE NETHERLANDS

Technical University of Munich

GERMANY

A Ceccotti

IVALSA-CNR Trees and Timber Research Institute

ITALY

Presented by C. Sandhaas

H.J. Blass received clarification that the 30 mm deformation was related to 2 connections; therefore, 15 mm per shear connection.

H Zeitter asked and received explanation on why one of the four sets of results was used and whether the specimens were identical. He also asked and received information about the gaps in the wall elements and the results are symmetrical.

B. Dujic stated that he has tested a similar system and the ductility was more than 6. He asked whether one could get 7 or 8 for ductility if the loading was continued. C. Sandhaas said that the expected capacity was almost reached and they discussed why the damping ratio was higher with increasing cycles.

F. Lam commented on the test configuration where the gap closure during testing might lead to friction which can influence the test result.

A. Buchanan initiated discussions about the building system, the rocking mechanisms, the screw quality, storey height, and energy dissipation mechanism.

H. Zeitter further questioned about the gaps between main wall elements and stated that the gap in the test set up should be maintained.

M. Yasumura stated that if the connection is too rigid energy dissipation may not be achieved.

M. Popovski asked about the influence of the floor slab which could prevent rocking movement. C. Sandhaas replied that the floor slab may not be continuous and compression perpendicular to grain stresses and deformations also occur. B. Dujic stated that there are screw connections between the floor and the wall which are quite a lot weaker; therefore, one will have rocking.

I. Smith discussed the concept of ductility.

T. Williamson stated that this type of work is very much needed if the CLT products were to make its way to the US.

Analysis of X-lam panel-to-panel connections under monotonic and cyclic loading

Sandhaas, C.[1]; van de Kuilen, J.-W. G.[2]; Boukes, J.[1]

and

Ceccotti, A.[3]

[1]. Delft University of Technology (NL)

[2]. Delft University of Technology (NL), Technical University of Munich (D),

[3]. IVALSA-CNR Trees and Timber Research Institute, (I)

Abstract

Cross-laminated timber panels (X-lam) are more and more used as construction material for buildings. For a sound and reliable structural analysis in both static and cyclic loading situations, the behaviour of connections between wall panels has to be evaluated. As the X-lam panels are very rigid, these connections are determining significantly the mechanical performance of X-lam buildings.

A typical in-plane wall-to-wall connection makes use of an LVL strip that is mounted as an inlay along the edges of two notched panels and is connected to these two panels by single shear fasteners, for instance self-drilling screws. As a consequence, the static and dynamic behaviour of this connection type differs from panels that are directly connected to each other due to the LVL strip and the subsequent double row of single shear fasteners. The LVL-inlay joints have to be modelled as a serial system of single shear fastener springs.

Therefore, monotonic and cyclic tests on such connections have been undertaken in order to get input parameters for subsequent design models. Bending angles of fasteners have been measured. A comparison of the test results with dynamic measurements and calculations on a 3-storey building has resulted in the conclusion that in-plane wall-to-wall panel connections are an important factor in the structural behaviour of X-lam buildings, especially under dynamic loading such as earthquakes. Design procedures dealing with EC5 and EC8 concerning this connection type are discussed and their applicability is evaluated.

1 Review and scope of research

The building material X-lam, cross-laminated-timber, has been researched at lot in the last couple of years. Most of the material's mechanical properties such as bending strength, strength in-plane or out-of-plane, shear strength or stiffness have been investigated [e. g. 1, 2, 3]. However, in order to design structures using X-lam, information on connection behaviour and design prescriptions must be made available. For instance, the embedment strength of the material is varying through the thickness due to the cross layers. Furthermore, the use of X-lam plates as wall elements with joints to assemble the panels create complex loading situations when loaded in-plane horizontally.

Therefore, newer projects extended the research field on connections in X-lam. In [4], extensive testing series were carried out to investigate the connection behaviour of X-lam. Different fasteners such as nails, bolts and dowels were used which were loaded in shear (Johansen) or axially (pull-out). The joints were situated at the broad side of the material or on the edge. The double-shear connections were timber-timber-connections or timber-steel connections. Also the embedment strength of X-lam was assessed. The derived design procedures in [4] include an extension of the analytical Johansen theory for dowels to account for the different embedment strengths for the parallel and orthogonal layers of X-lam. However, this approach leads to complex equations already when using only a three-layered X-lam. Comparisons with test results showed that the use of smeared embedment strength for the whole thickness is an allowable simplification in order to evaluate the load carrying capacity of a joint with dowels. Empirically derived design prescriptions with such a homogenised embedment strength are summarised in [4] for static loading of dowelled connections in X-lam. It should be stressed however, that static loading is not the only possible loading for X-lam connections.

In this research, X-lam constructions made with massive X-lam panels as wall and floor elements connected with metal fasteners are intended. Research has shown that the X-lam construction system seems to be very suitable for seismic regions [5]. During earthquakes though, the loading is dynamic and reversible. Concepts such as energy dissipation capacity get very important for those types of loading with regard to safety and the applicability of design concepts of Eurocode 8, the European standard for earthquake design [6]. In order to develop dissipative behaviour and hence utilise the potential of X-lam constructions, plastic behaviour must be achieved, unless a fully elastic approach is taken. As the panels are very rigid in-plane, the desired ductile behaviour must be obtained with the connections.

In comparison to timber-frame constructions where a high number of nails connecting the sheathing to the frame are providing the ductile behaviour, the quantity of connections is very much reduced in X-lam structures. This fact makes the single connections important factors in the overall behaviour of the construction. Generally, the different connection types can be identified as safety relevant where no plastic behaviour with high deformations is desired or as important contributors to dissipative behaviour. Examples for the first connection type are the connections of the wall elements in the angles of the building or the connection of the floor elements to the wall elements below. The last connection type, designed for energy dissipation, includes hold-down connections and the connections between adjacent wall elements in one plane. This last connection type differs from a common connection in that they are connecting a vertical joint between (horizontally loaded) wall elements with a LVL strip and subsequently with a double row of single-shear fasteners, mostly self-drilling screws.

Earthquake tests carried out within the research project SOFIE [5] have underlined the significant contribution of these wall-to-wall connections during an earthquake. During full-scale earthquake tests of a three-storey building, these connections deformed considerably without seeming to affect the stability of the buildings. If these deformations have been of plastic nature, they contributed thus to the energy dissipation of the whole structure. It may even be the question if these wall-to-wall connections can be ‘tuned’ in order to guarantee a more ductile or a less ductile behaviour, according to the design wishes.

A closer investigation into this connection type, its design and an evaluation on its dissipation characteristics are consequently needed in order to better understand the static and seismic response of a X-lam building. Furthermore, no research has yet been undertaken including cyclic loading of these connections in X-lam.

2 Test setup

2.1 Test specimen and protocol

One possibility to carry out the wall-to-wall connections is by means of notching the boundaries of the panels, inserting an LVL strip and connecting this inlay by mechanical fasteners to the two adjacent panels. Normally, self-drilling screws are used as fasteners. A drawing of the tested connection is shown on the left in Fig. 1. Two different X-lam panel types were used, both 95mm thick: one panel with three layers and one with five layers. The panels are assembled from spruce planks and were conditioned at 20°C and 65% r. H. The tests were carried out in a climate chamber of TU Delft. On the right, a photo from the same connection in one of the tested buildings is shown to explain the starting point of the research.

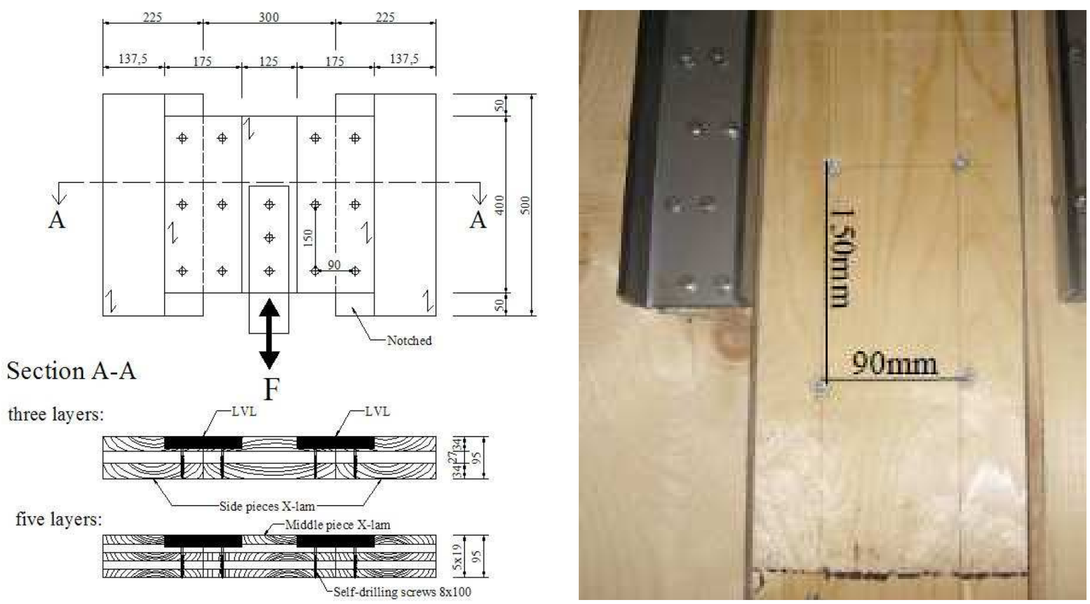

Fig. 1: Tested wall-to-wall connection and photo of connection in SOFIE building [5]

In the tested buildings during the earthquake project SOFIE [5], the wall-to-wall connection was thus carried out with the same parameters such as materials and geometry. However, the wall elements in the building have been 2.95m high and the loading of the connection was typically a horizontal force as shown in Fig. 2. The deformations shown in Fig.2 on the left hand could be observed during the seismic test (possible horizontal slip neglected and rotation exaggerated) in both directions with a maximum slip of 25mm during the earthquake JMA Kobe at 100%.

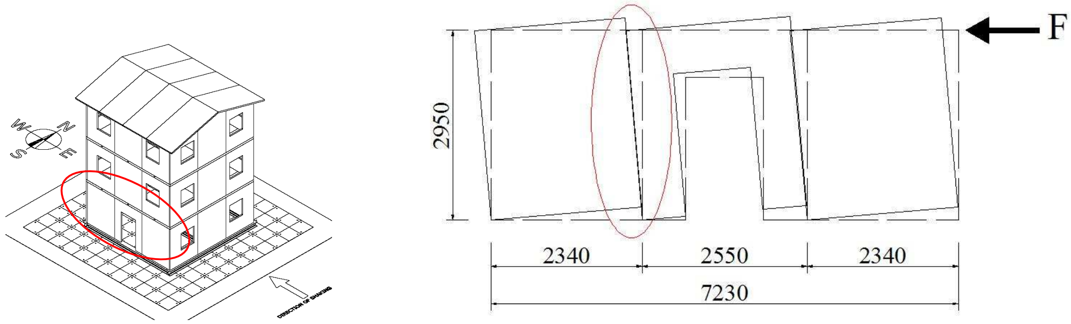

Fig. 2: SOFIE building [5] with identification of connection

For the test setup, it was chosen to test a symmetrical connection with two wall-to-wall connections and a shorter specimen height with only 400mm. The loading was displacement controlled with a speed of 0.2mm/s and carried out according to EN26891 for the monotonic test and EN12512 for the cyclic test. The following Table 1 lists the executed tests.

Table 1: List of tests on wall-to-wall connections

Specimen	Layers X-lam	Test protocol
M5-1	5	EN 26891 (ramp)
Z3-1	3	EN 12512 (cyclic)
Z3-2	3	EN 12512 (cyclic)
Z3-3	3	EN 12512 (cyclic)
Z5-1	5	EN 12512 (cyclic)
Z5-2	5	EN 12512 (cyclic)
Z5-3	5	EN 12512 (cyclic)

After the first monotonic test M5-1, a restraint was added to avoid rotational movement of the side pieces when pulling on the centre X-lam piece. Test M5-1 has then been repeated. Motivation for the added restraint was mainly that also in practice such a rotation is prevented because of the height of the X-lam elements relative to the width of the gap between the LVL strip and the X-lam panel.

2.2 Instrumentation

The deformations were measured with transducers which were attached at the positions shown in Fig. 3 in a front and rear view. The numbers of the different measuring channels given in Table 2 are also noted.

Fig. 3: Test specimen in front and rear view with instrumentation channels

Table 2: Instrumentation

Channel	Measure point
1	force of hydraulic cylinder
2	displacement of hydraulic cylinder
3	horizontal slip between left side panel and LVL (rotation)
4	horizontal slip between right side panel and LVL (rotation)
5	horizontal slip between left side panel and LVL (rotation)
6	vertical slip between steel holder (force input) and specimen
7	vertical slip between left side panel and LVL
8	vertical slip between right side panel and LVL
9	vertical slip between middle panel and right LVL
10	vertical slip between middle panel and left LVL
11	vertical slip between left side panel and middle panel (at rear)
12	vertical slip between right side panel and middle panel (at rear)
14	horizontal slip between right side panel and LVL (rotation)

3 Design

The used screws were self-drilling screws of steel with $f_{u,k}$ = 1000MPa with an outer thread diameter of 8mm and a shank diameter of 5.85mm. The thread root diameter is 5.4mm (d_{ef}=1.1·5.4mm=5.94mm) and the length of the threaded part is 52mm. The holes were not predrilled.

In [4], the homogenised embedment strength for screws in X-lam is only valid for X-lam with layers ≤ 7mm, but it is stated that the embedment strength for connections with screws and nails without predrilling can be assessed by known equations for solid wood as the cross layers do not have any influence. Therefore, the characteristic embedment strength for screws with an effective diameter ≤ 6mm can be established by using the formula for nails without predrilled holes according to EC5 [7]. Bigger diameters depend on the angle between force and grain direction of the outer layer.

However, the mean values were established by using the following formula instead of the characteristic embedment strength from EC5:

$$f_{h,mean} = 0.10 \cdot \rho_{mean} \cdot d_{ef}^{-0.3} \tag{1}$$

This formula is derived from test results assessing the embedment strength of dowel-type fasteners in softwood, European and tropical hardwood [8]. According to [4], the value of ρ_{mean} is taken to 437kg/m^3 which is the lowest ρ_{mean} of all X-lam products per producer. ρ_{mean} of the LVL is according to the producer 510kg/m^3.

The mean withdrawal capacity of self-drilling screws is according to [4]:

$$R_{ax,s,pred} = 0.435 \cdot d_{nom}^{0.8} \cdot l_{ef}^{0.9} \cdot \rho^{0.75} \tag{2}$$

In eq (2), the mean value ρ_{mean} of spruce is taken for the density. Subsequently and according to EC5, the governing load-bearing capacity per shear plane of the connection is resulting to failure mode d (one yield moment in the fastener inside the X-lam panel) with R_{mean}=4.6kN.

To evaluate the total load-bearing capacity of the tested connection, the single shear planes cannot be simply summed up. The double row of fasteners is instead acting in series and the capacity must thus be calculated by taking half the fasteners into account. In the symmetric test setup, this means that 2 times 3 screws are establishing the capacity. Thus 6 shearplanes which results in a total predicted load bearing capacity of 27.6kN of the tested connection.

According to EC5, the initial stiffness of one screw can be calculated as:

$$K_{ser} = \frac{(\sqrt{\rho_{m,1} \cdot \rho_{m,2}})^{1.5}}{23} \cdot d_{ef} \tag{3}$$

Which results in a value of K_{ser} = 2649 N/mm per shear plane per fastener.

4 Results

4.1 Tests

The outcomes in terms of load-slip curves are very similar for all specimens and are nearly symmetric. No difference could be observed for the two different panel types with three or five layers. The results are summed in Table 3 whereas typical load-displacement curves are shown in Fig. 4.

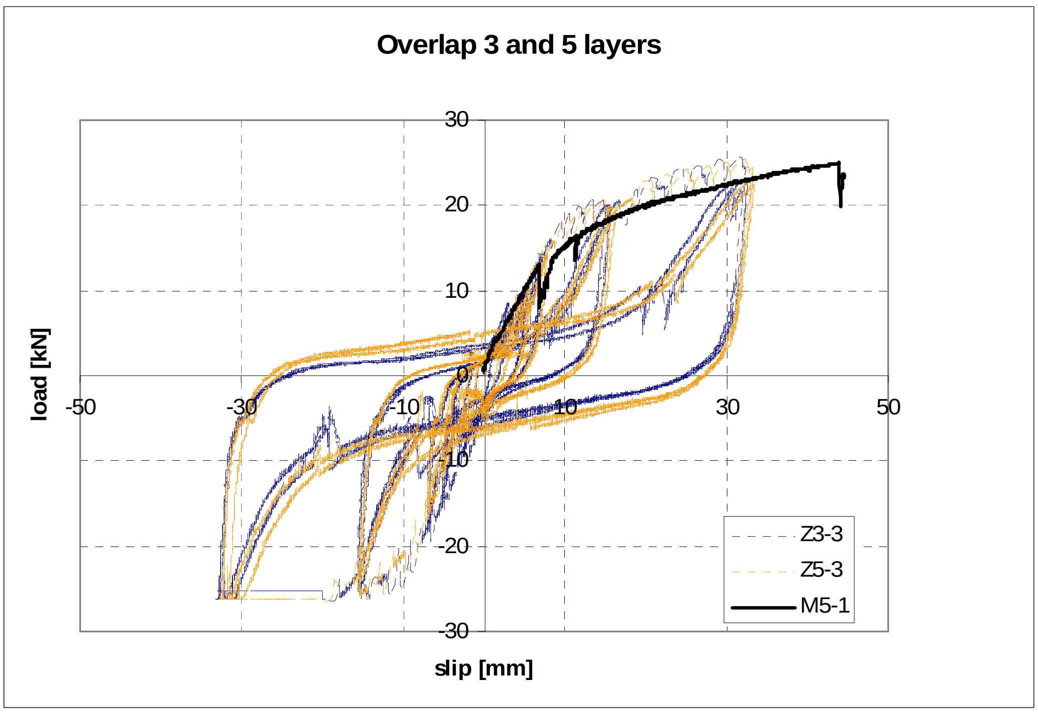

Fig. 4: Typical result of monotonic and cyclic test, overlap of panels with 3 and 5 layers

The first part of the monotonic test covers perfectly the cyclic loops. The load in the second part only reached the degraded peaks of the hysteresis loops, the loading of the second and third cycles of one loading step. The monotonic test forms however a nice envelope curve of the cyclic tests.

It can be observed that this kind of connection is degrading significantly between one loop and the other with a prominent pinching behaviour. The difference in equivalent viscous damping between the first loop of a displacement level and the second loop has about the factor 2.

Table 3: Test results

Specimen	u_{max} test [mm]	F_{max} test [kN]	F_{pred} [kN]	ratio F_{max}/F_{pred}	equivalent viscous damping			
					cycles at 15mm slip		cycles at 30mm slip	
					1st loop	2nd loop	1st loop	2nd loop
M5-1	44.6	25.0	27.6	0.91	-	-	-	-
Z3-1	32.8	26.4	27.6	0.96	18.2%	10.4%	23.1%	12.9%
Z3-2	33.5	27.6	27.6	1.00	18.1%	11.1%	22.8%	13.4%
Z3-3	33.2	26.3	27.6	0.95	18.4%	10.4%	23.4%	13.9%
Z5-1	31.8	27.7	27.6	1.00	16.4%	10.6%	23.6%	15.7%
Z5-2	32.5	28.0	27.6	1.01	16.3%	10.7%	20.9%	12.8%
Z5-3	32.8	26.3	27.6	0.95	17.4%	10.4%	24.1%	15.4%

The very good dissipating qualities of this type of joint could be confirmed with the tests. No brittle failure modes could be observed – no cracks or splitting occurred during the monotonic and cyclic tests. The cyclic tests went up to a displacement of around 30 mm at which the maximum load was reached. This was confirmed by the monotonic tests that did not take more load with larger deformations of up to 45mm; the behaviour of the connections is approximately elastic - ideal plastic.

4.2 Comparison with design equations

As one idea of these tests is to develop a simplified approach for modelling this type of connection without the need of carrying out further tests, calculations with characteristic values are of few importance. Good agreement must be reached between the actually tested connections and the predicted stiffnesses and load carrying capacities.

Fig. 5 shows an X-ray scan of one of the test specimens after the test. First of all, the predicted failure mode is the correct one; one plastic hinge in the part of the screw inside the X-lam panel. Secondly, the bending angles can be measured which were for all tests around 26°.

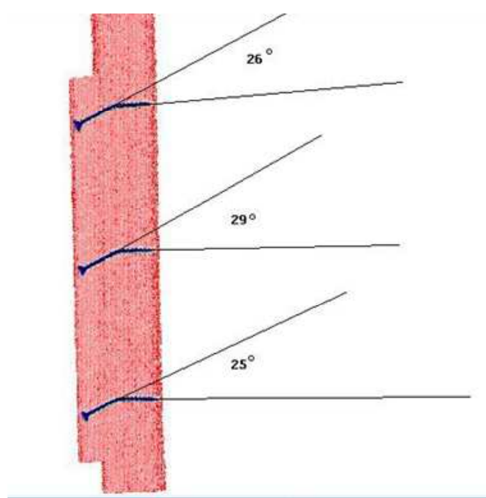

Fig. 5: X-ray of tested specimen with bended screws

The maximum load carrying capacity was well established with the equations of EC5 using the mean values as can be seen in Table 3 with a value of n_{ef}=1. N_{ef}=1 is quite logic when considering the structure of X-lam with its cross layers and a n_{ef}=1 for connections in X-lam was already proposed by [4]. In addition, the line of force changes slightly at each fastener, so splitting along the row of fasteners is not to be expected. Apparently at this stage of research, there is no need in chosing more sophisticated approaches. A closer look must be given into the stiffness prediction which was predicted per screw with 2650N/mm. Fig. 6 shows the tested connection in deformed position. From this drawing, the initial stiffness per screw measured by the test can be derived as shown in eq (4). As the rotational movement has been small due to the restraint added to the test rig, this deformation is neglected. The reference test data are the measured force F and the vertical slip u of the middle piece in relation to the fixed side pieces. By considering these two measurements, the elastic initial stiffness of one screw is calculated.

The initial slip modulus K_{ser} is established by a line going through 40% of the maximum force. A second stiffness K_2 is also taken from the load-slip graphs. K_2 however is visually established as also shown in EN12512 and is hence quite imprecise. However, since COV of stiffness values of timber joints are high (normally over 0.40) this is considered to be sufficiently accurate.

In order to model the X-lam construction type in models such as proposed in [9], usually the connections are modelled as springs with the Florence pinching hysteresis model [10] and the panels are considered as stiff. The data obtained by the testing series described here allow to develop a simplified approach to establish the main parameters of this connection type in order to undertake seismic modelling.

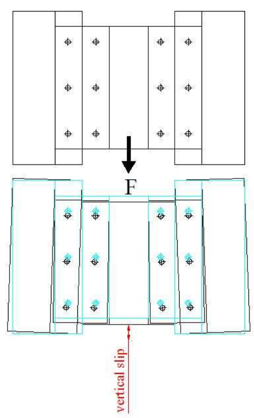

Fig. 6: Drawing of deformed specimen

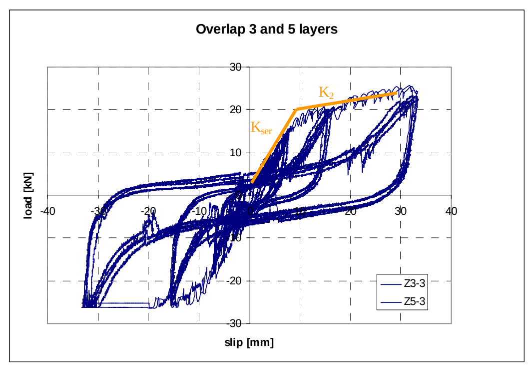

Fig. 7: Load-slip curve with K_{ser} and K_2

The measured stiffness per screw was therefore (assuming that the total force is equally distributed to the two side panels):

$$u = 2 \cdot \left(\frac{0.5F}{3K_{ser}} + \frac{0.5F}{3K_{ser}}\right) = \frac{2F}{3K_{ser}} \Leftrightarrow K_{ser,test} = \frac{2F}{3u} \tag{4}$$

This leads to the values shown in Table 3.

Table 4: Test results in terms of elastic stiffness

Specimen	**$K_{ser, pred}$ [N/mm]**	**$K_{ser, test}$ [N/mm]**	**$K_{2, test}$ [N/mm]**	**difference in [%] $K_{ser, test}/K_{2, test}$**
Z3-1	2649	2029	217	10.7
Z3-2	2649	2230	257	11.5
Z3-3	2649	2505	207	8.3
Z5-1	2649	1900	223	11.8
Z5-2	2649	2333	260	11.1
Z5-3	2649	1559	250	16.0

The stiffness values needed according to the Florence pinching hysteresis model [10] are shown in Fig. 8; the values obtained through a calibration on the testing data for one connection system of 6 screws (one side of the test specimen) are listed in Table 5.

Values taken from tests are displacements U1 and U2 and the two stiffnesses K1 and K2; the other values are approximative and are needed to calibrate the energy dissipation which should be the same for model and test.

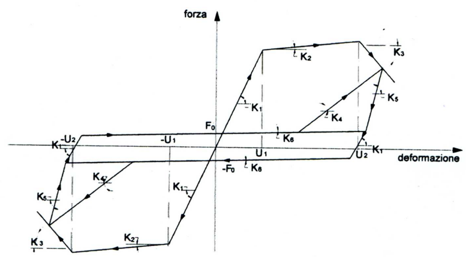

Fig. 8: Florence pinching hysteresis model

Table 5: Values for Florence pinching hysteresis model

U1 [mm]	U2 [mm]	K1 [N/mm]	K2 [N/mm]	K3 [N/mm]	K4 [N/mm]	K5 [N/mm]	K6 [N/mm]	F0 [kN]
4.5	40	1600	180	-560	700	6400	-1	2000

These stiffness values must be adjusted when more than 3 screws over the height are used which is the case in buildings with a higher wall height than the tested 400mm. The relationship can be assumed to be linearly proportional as could be confirmed by the good agreement of slip modulus and load-carrying capacity between test and EC5.

4.3 Summary

The six specimens tested under cyclic loading showed a good agreement of the parameters needed for earthquake modelling such as maximum force, energy dissipation at different cycles of different load levels and initial and “plastic” stiffness, K_{ser} and K_2.

Maximum force and initial stiffness can be calculated with EC5 and mean values whereas the energy dissipation and ratio between initial and plastic stiffness can be derived from test results. Within the needed range of accuracy during earthquake modelling, the values obtained in such a way are precise enough.

This means that this connection type can be rather easily transferred into the Florence pinching hysteresis model [10]. The scatter of the test results is small and the agreement with calculated values is satisfactory. The single correlations between the dissipated energy in different cycles and between K_{ser} and K_2 also have an acceptable small scatter and can be taken from Tables 3 and 4.

5 Conclusions

The load-carrying capacity of this connection type loaded cyclically can be calculated with the Johansen equations defined in EC 5 and the total load-carrying capacity of a whole joint can be established with n_{ef} = 1. No difference could be observed between specimens with 3 or 5 layers. The energy dissipation capacity of the connection type is high as can be seen in Table 3 where the equivalent viscous damping is calculated. Energy dissipation capacity is an important concept for seismic design according to EC8. Furthermore, the impairment of strength in different cycles at one load step is not higher than 20% (see Fig. 4).

As for the testing procedure, the problem of rotational movements when carrying out connection tests should be resolved and praxis oriented restraining scheme should be developed and applied by researchers in order to keep results comparable and applicable. Furthermore, the limit of 30mm of testing protocols may be not sufficient, especially for large diameter dowels. The tested connections could support a displacement of 45mm without rupture which allows good seismic design.

The system values in terms of load-carrying capacity and stiffness found by the tests and calculations can be used for further modelling purposes of this important connection type in seismic design.

6 Acknowledgements

Our thanks go to the companies KLH (Austria), Finnforest (the Netherlands) and Rothoblaas (Italy) for delivering the necessary material free of charge.

7 References

[1] Blaß, H.-J.; Fellmoser, P.: *Design of solid wood panels with cross layers*. Proceedings of the 8th World Conference on Timber Engineering, Volume II, Lahti, Finland, 2004

[2] Jöbstl, R. A.; Moosbrugger, T.; Schickhofer, G.: *In-plane shear strength of cross laminated timber*. Paper 41-12-3, CIB W18 Meeting 41, St. Andrews, Canada, 2008

[3] Gülzow, A.; Gsell, D.; Steiger, R.: *Non-destructive evaluation of elastic parameters of square-shaped cross-laminated solid wood panels, built up symmetrically with 3 layers*. Holz als Roh- und Werkstoff, Volume 66, Issue 1, pp 19-37, 2008 (in German)

[4] Blaß, H.-J.; Uibel, T.: *Tragfähigkeit von stiftförmigen Verbindungsmitteln in Brettsperrholz*. Band 8, Karlsruher Berichte zum Ingenieurholzbau, Lehrstuhl für Ingenieurholzbau und Baukonstruktionen, Universität Karlsruhe, Germany, 2007 (in German)

[5] Ceccotti, A.; Yasumura, M.; Minowa, C.; Lauriola, M. P.; Follesa, M.; Sandhaas, C.: *Which Seismic Behaviour Factor for Multi-Storey Buildings made of Cross-Laminated Wooden Panels?* Paper 39-15-2, CIB W18 Meeting 39, Florence, Italy, 2006

[6] EN 1998-1:2004, Eurocode 8: *Design of structures for earthquake resistance – Part 1: General rules, seismic actions and rules for buildings*. CEN, 2004

[7] EN 1995 1-1:2004, Eurocode 5*: Design of timber structures - Part 1-1: General - Common rules and rules for buildings*. CEN, 2004

[8] Vreeswijk, B.: *Verbindingen in hardhout*. Master Thesis, Faculty of Civil Engineering, Delft University of Technology, 2003 (in Dutch)

[9] Ceccotti, A.: *New Technologies for Construction of Medium-Rise Buildings in Seismic Regions: The XLAM Case*, Structural Engineering International, Volume 18, Issue 2, pp 156-165, 2008

[10] Ceccotti, A.; Vignoli, A.: *A hysteretic behavioural model for semi-rigid joints*. European Earthquake Engineering, Volume 3, pp 3-9, 1989

CIB-W18/42-12-3

**INTERNATIONAL COUNCIL FOR RESEARCH AND INNOVATION
IN BUILDING AND CONSTRUCTION**

WORKING COMMISSION W18 - TIMBER STRUCTURES

LAMINATING LUMBER AND END JOINT PROPERTIES FOR FRP-REINFORCED GLULAM BEAMS

T G. Williamson

Borjen Yeh

APA – The Engineered Wood Association

U.S.A.

Presented by TG Williamson

H.J. Blass asked whether a flat line can be used to represent the stress strain relationship in compression. T.G. Williamson replied yes.
A. Buchanan asked whether the approval involves getting a calculation model approved and a design method approved. T.G. Williamson replied that one can use the APA/University of Maine model and calibrate it with one's data. The University of Maine model is proprietary.
I. Smith and T.G. Williamson discussed the approach to size effect and what can be done as follow up.
J.W.G. van de Kuilen asked how one will handle gluing of the fiber in practice and fire issue. T.G. Williamson answered the gluing of fiber is not as complex as previous cases. Here sanding technique is no longer needed. Fire behaviour was reported in a previous CIBW18 meeting.
S. Aicher stated that in Europe gain of using FR beam was not attractive and design model was not appealing. T.G. Williamson answered that in the past the process and design model for FR beam in US was convoluted. The current system is much simpler and very attractive to manufacturers.
A. Jorissen stated that the gain in stiffness is not that high. T.G. Williamson answered stiffness control 5% of the time especially with camber.
R. Crocetti suggested that the price of carbon fiber must be too high and asked if steel plate was considered. He also asked about $_{m}$ and $_{dol}$ values. T.G. Williamson said hat fiber has the advantage of coming in spool and glass fiber has much lower cost. University of Maine results show DOL and moisture factors have not changed.

Laminating Lumber and End Joint Properties for FRP-Reinforced Glulam Beams

Thomas G. Williamson, P.E. and Borjen Yeh, Ph.D., P.E.
APA – The Engineered Wood Association, U.S.A.

Abstract

Glulam beams reinforced with fibre-reinforced-polymer (FRP) are typically manufactured using graded laminating lumber with FRP reinforcement in the tension zone and have been used in numerous construction projects worldwide. Unfortunately, the layup combinations currently used for manufacturing FRP-reinforced glulam are all proprietary even though an FRP glulam standard, ASTM D 7199, *Standard Practice for Establishing Characteristic Values for Reinforced Glued Laminated Timber (Glulam) Beams Using Mechanics-Based Models*, was published in 2007. This standard resulted from years of joint effort by APA – The Engineered Wood Association and the Advanced Engineered Wood Composites Center (AEWC) of the University of Maine.

A mechanics-based computer model, called ReLam, has been developed by the AEWC for predicting the performance of FRP-reinforced glulam beams in accordance with ASTM D 7199. This model can be used to develop a range of layup combinations for FRP-reinforced glulam beams. As the first step toward the development of these glulam layup combinations, mechanical properties of laminating lumber, including the tensile and compressive strength and moduli, and the end joint tensile strength must be obtained. While the lumber properties for these lumber grades have been published in glulam industry standards, such as AITC 407, *Standard for Alternate Lumber Grades for Use in Structural Glued Laminated Timber*, the basis of those data is more than 20 years old and was in need for an update and reaffirmation. While there are end joint tension data generated daily from the quality control records of each glulam plant, those data are considered proprietary and typically unavailable for general use. In addition, the compressive strength and moduli data are not readily available. As a result, APA initiated a comprehensive study to evaluate four Douglas-fir (DF) laminating lumber grades; 302-24 tension lam, L1, L2, and L3, and two grades of end joints, 302-24 tension lam and L1, from a range of glulam plants in 2008 using current production resources in the U.S.

These laminating lumber properties, including end joint data, not only confirm the historical data for these dominant DF lumber grades and end joints used in today's glulam production in the U.S., but also provide the required data for the development of layup combinations using ReLam. This paper presents the laminating lumber and end joint properties. In addition, the likely FRP-reinforced glulam beam layup combinations at characteristic bending strength and modulus of elasticity values of 43.4 N/mm^2 (6,300 psi) and 13800 N/mm^2 (2.0 x 10^6 psi), and 49.2 N/mm^2 (7,140 psi) and 15200 N/mm^2 (2.2 x 10^6 psi), respectively, are also provided. These FRP-reinforced glulam beams are expected to be highly competitive with steel in non-residential construction markets in the U.S.

1. Introduction

Reinforcing structural glued laminated timbers (glulams) with synthetic fibres for enhanced structural performance is not a new concept and there have been a wide range of applications around the world using fibre-reinforced-polymer (FRP) reinforced glulam. Unfortunately, the design methodology for FRP-reinforced glulam has been kept as proprietary information and is not readily available to general design engineers. Moreover, the development of FRP-reinforced glulam layup combinations for commercial production has not been widely understood. These factors have prohibited a wider application of this technology in the otherwise highly competitive commercial construction market with steel and concrete. In the last decade, staff members of APA – The Engineered Wood Association have been working with at least 3 private consortiums in promoting and advancing this FRP-reinforced glulam technology with limited success.

The main-stream FRP-reinforced glulam methodology in North America is based on the development work championed by the Advanced Engineered Wood Composites Center (AEWC, http://www.aewc.umaine.edu/) of the University of Maine. Working with the AEWC and the ASTM D07 Committee on Wood, APA has been able to standardize the fundamental FRP-reinforced glulam design and manufacturing methodologies in ASTM D 7199 [1], *Standard Practice for Establishing Characteristic Values for Reinforced Glued Laminated Timber (Glulam) Beams Using Mechanics-Based Models*, which was published in 2007. This standard resulted from years of joint effort by the APA and AEWC, but has not been put into practical use except for limited research projects.

A mechanics-based computer model, called ReLam, has been developed by the AEWC for predicting the performance of FRP-reinforced glulam beams [2]. This model can be used to develop a range of layup combinations for FRP-reinforced glulam beams. As the first step toward the development of these glulam layup combinations, mechanical properties of laminating lumber, including the tensile and compressive strength and moduli, and the end joint tensile strength must be obtained. While the lumber properties for these lumber grades have been published in glulam industry standards, such as AITC 407 [3], *Standard for Alternate Lumber Grades for Use in Structural Glued Laminated Timber*, the basis of those data is more than 20 years old and was in need of an update and reaffirmation. While there are end joint tension data generated daily from the quality control records of each glulam plant, those data are considered proprietary and typically unavailable for general use. In addition, the compressive strength and moduli are not readily available. As a result, APA initiated a comprehensive study to evaluate four Douglas-fir (DF) laminating lumber grades; 302-24 tension lam, L1, L2, and L3, and two grades of end joints, 302-24 tension lam and L1, from a range of glulam plants in 2008 using current production resources in the U.S.

The main objective of this study was to develop a database on the characteristic tensile and compressive stresses parallel to grain, and long-span E of major grades of DF laminating lumber for use in the modelling of FRP-reinforced glulam in accordance with ASTM D 7199 and the ReLam model. Characteristic finger joint tensile strengths for the highest 2 grades of laminating lumber were also developed.

2. Materials and Test Methods

2.1 Material Description

Thirty pieces of 4267-mm (14-foot) long 2x6 (38 mm x 140 mm or 1-1/2 inches x 5-1/2 inches net dimension) Douglas-fir sawn lumber specimens for each of 4 Douglas-fir laminating lumber grades; 302-24 tension lam, L1, L2, and L3, were sampled by APA quality services division auditors from 3 major glulam plants; Calvert Company Inc., Washougal, Washington, Cascade Structural Laminators, Chehalis, Washington, and

Rosboro, Springfield, Oregon in April 2008. These specimens were shipped to the APA Research Center in Tacoma, Washington where these lumber specimens were regraded and reclassified as on-grade materials meeting the grade requirements specified in the *Grading Handbook for Laminating Lumber* [4]. A non-destructive long-span E test was conducted on each specimen, followed by destructive tension tests in May 2008.

Thirty pieces of 2438-mm (8-foot) long 2x6 Douglas-fir laminations with a finger joint near the center of the specimen for each of the 2 highest laminating lumber grades, 302-24 tension lam and L1, were sampled by APA auditors from regular production runs at the same glulam plants mentioned above in April 2008. The adhesives used in manufacturing the finger joints were previously qualified by the manufacturers in accordance with the *American National Standard for Structural Glued Laminated Timber*, ANSI/AITC A190.1 [5], using melamine-urea formaldehyde from one plant, and phenol-resorcinol-formaldehyde from the other 2 plants. These specimens were also shipped to the APA Research Center for destructive tension tests in May 2008.

From each of the 4267-m (14-foot) long 2x6 lumber specimens designated for the long-span E and tension tests, 2 specimens of 305-mm (12 inches) in length were cut prior to tension tests. These specimens were regraded for excessive knots and slope of grain, and then square-cut to 191-mm (7-1/2 inches) in length for destructive compression test with a slenderness ratio (length to least radius of gyration) of 17.3 in accordance with ASTM D 198 [6], *Standard Methods of Static Tests of Timbers in Structural Sizes*.

2.2 Test Methods

Tension parallel to the grain tests were conducted in accordance with Sections 24 – 29 of ASTM D 4761 [7], *Standard Test Methods for Mechanical Properties of Lumber and Wood-Base Structural Materials*, using an 2438-mm (8-foot) gauge length for laminating lumbers. A 610-mm (2-foot) gauge length was used for finger-jointed tests. For the long-span E tests, a flatwise center-point bending method with an on-center span of 3810-mm (150 inches) (i.e., the span-to-depth ratio = 100:1) was followed in accordance with AITC Test T116 [8], *Modulus of Elasticity of E-Rated Lumber by Static Loading*. All specimens were tested at as-received conditions (the average moisture content of the specimens from each manufacturer was in the range of 10 to 13%). The moisture content and specific gravity of selected specimens were determined using the oven-drying method specified in ASTM D 4442 [9], *Standard Test Methods for Direct Moisture Content Measurement of Wood and Wood-Base Materials*, and D 2395 [10], *Standard Test Methods for Specific Gravity of Wood and Wood-Based Materials*, after the mechanical testing.

Compression tests were conducted following Sections 12 -19 of ASTM D 198 using a gauge length of 130 mm (5-1/8 inches) with a constant loading rate of 0.38 mm (0.015 in.) per minute. Special attention was made to ensure the contact surfaces were plane and parallel to each other and normal to the long axis of the specimen. To accomplish this, the specimen was square-cut at each end. After trimming the ends, but prior to the mechanical testing, the actual cross-sectional dimension of each specimen was measured at the mid-length to the nearest 0.025 mm (0.001 inch). For the measurement of compressive deformation, two LVDTs were attached to the opposite faces of the specimen at a gauge length of 130 mm (5-1/8 inches). No lateral supports were provided during testing. All specimens were tested at as-received conditions (the average moisture content of the specimens from each manufacturer was in the range of 10 to 13%).

The downward slope (m) of the compressive load and deformation curve, which is required by the ReLam model due to the fact that the compression failure is the predominant failure mode for FRP-reinforced glulam at a high percentage of fibre reinforcement ratio, was determined based on Figure 1 using the relationship between two slopes obtained before and after the ultimate failure load, as shown in Section 3 of ASTM D 7199. The slope before failure was determined in the proportional range of load and deformation curve.

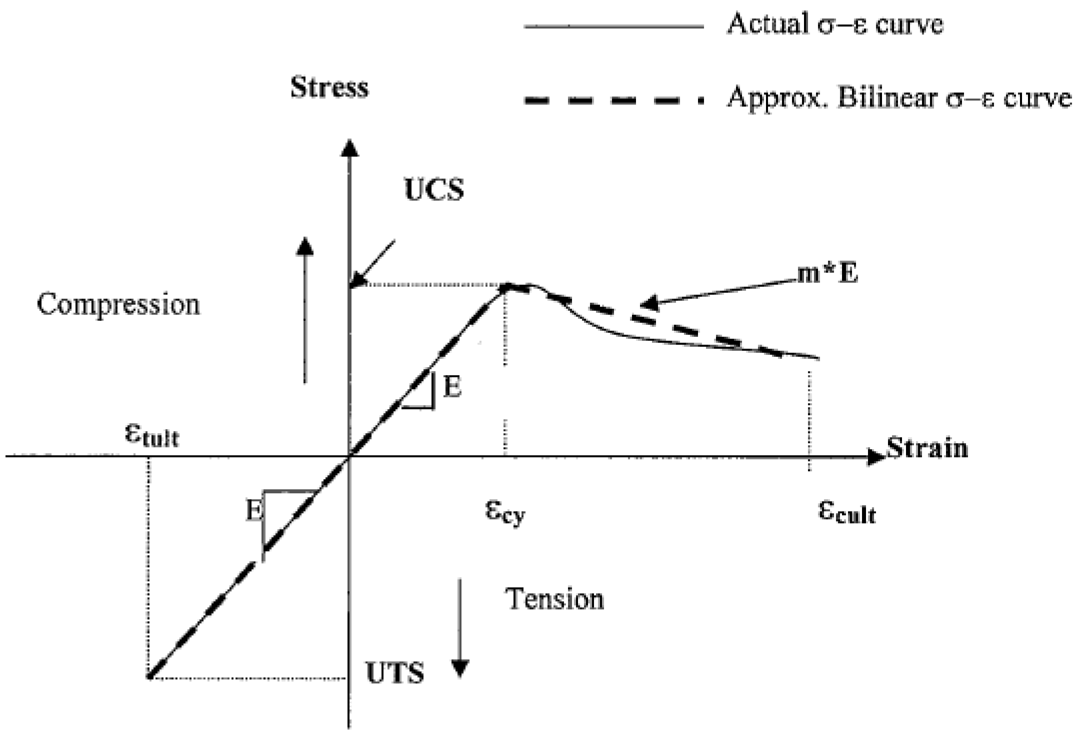

Figure 1. Schematic compressive stress-strain curve (excerpt from ASTM D 7199)

3. Results and Discussions

3.1 Lumber Tension

Test results for lumber tension (2438-mm or 8-foot gauge length) are shown in Table 1. The characteristic tensile strength (5th percentile with 75% confidence) of the lumber, $f_{t,0,l,05}$, of each lumber grade from the combination of 3 glulam plants were determined based on ASTM D 2915 [11], *Standard Practice for Evaluating Allowable Properties for Grades of Structural Lumber*. Figure 2 shows the data distribution of each lumber grade.

Table 1. Summary statistics of lumber tensile strength

Properties	Lumber Tensile Strength			
	302-24	L1	L2	L3
No. of observations	86	90	87	93
$f_{t,0,l,mean}$, N/mm^2 (psi)	48.9 (7093)	30.0 (4354)	20.9 (3026)	14.3 (2073)
Coefficient of variation	0.271	0.293	0.286	0.325
$f_{t,0,l,05}$, N/mm^2 (psi) [(a)]	29.0 (4212)	17.5 (2537)	12.3 (1777)	7.8 (1137)
Published $f_{t,0,l,05}$, N/mm^2 (psi) [(b)]	27.6 (4008)	16.7 (2420)	11.6 (1680)	7.0 (1010)

[(a)] Parametric 5th percentile with 75 percent confidence of laminating lumber (lognormal distribution).
[(b)] Characteristic value of laminating lumber published in AITC 407.

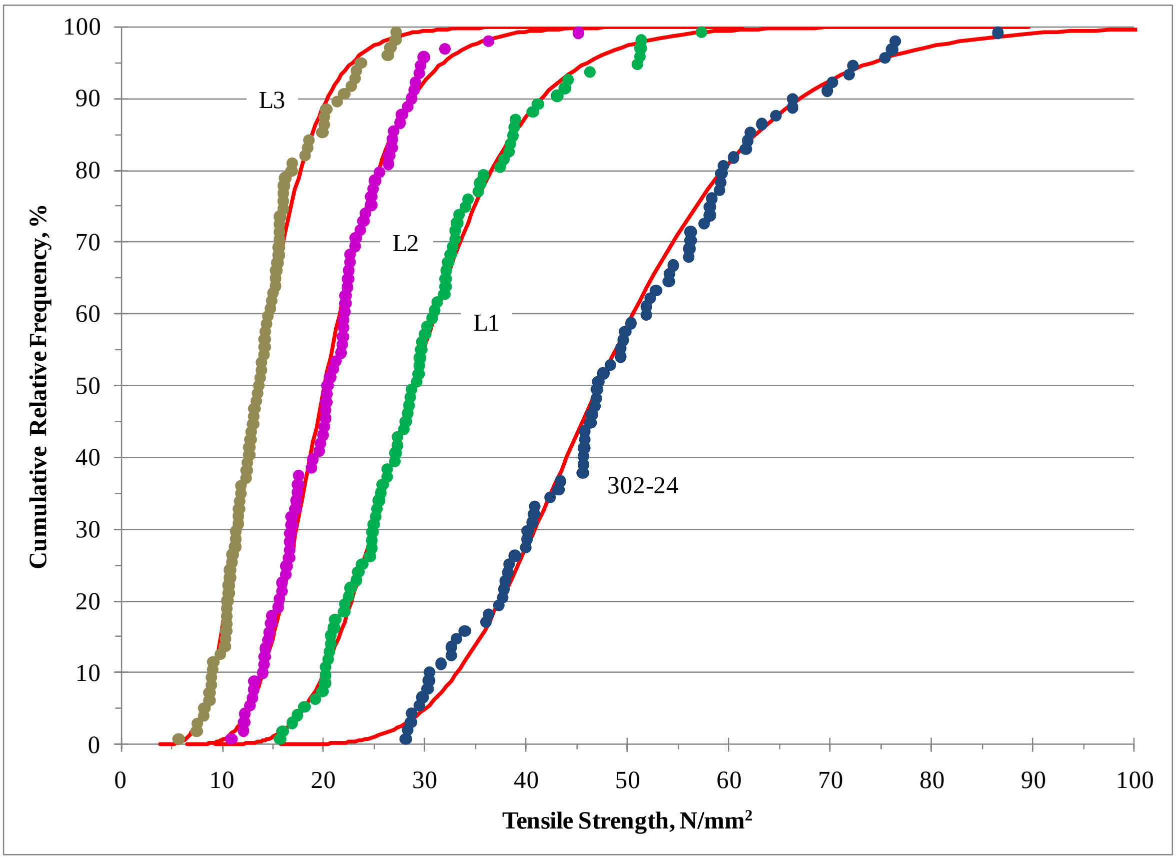

Figure 2. Data distribution of lumber tensile strength based on an assumed log-normal distribution function

As shown in Table 1, the characteristic tensile strength of each lumber grade based on an assumed log-normal distribution meets the currently published characteristic value with a coefficient of variation of between 27 to 33% depending on the relative lumber quality.

3.2 End-Joint Tension

Test results for end joint tension (610-mm or 2-foot gauge length) are shown in Table 2. The characteristic tensile strength (5th percentile with 75% confidence) of the end joints, $f_{t,j,05}$, for each of the two lumber grades from the combination of 3 glulam plants was determined based on ASTM D 2915. The data distribution of end joint tension values for each lumber grade is shown in Figure 3.

Table 2. Summary statistics of end joint tensile strength

Properties	End Joint Tensile Strength	
	302-24	L1
No. of observations	80	88
$f_{t,j,mean}$, N/mm^2 (psi)	35.6 (5165)	30.4 (4416)
Coefficient of variation	0.149	0.183
$f_{t,j,05}$, N/mm^2 (psi)	27.8 (4036) [a]	21.5 (3114) [b]
$f_{t,0,l,05}$, N/mm^2 (psi) [c]	29.0 (4212)	17.5 (2537)
Published $f_{t,0,l,05}$, N/mm^2 (psi) [d]	27.6 (4008)	16.7 (2420)
$f_{t,j,05}/f_{t,0,l,05}$	0.96	1.23

[a] Non-parametric 5th percentile with 75 percent confidence of end joints.
[b] Parametric 5th percentile with 75 percent confidence of end joints (lognormal distribution).
[c] Parametric 5th percentile with 75 percent confidence of laminating lumber (from Table 1).
[d] Characteristic value of laminating lumber published in AITC 407.

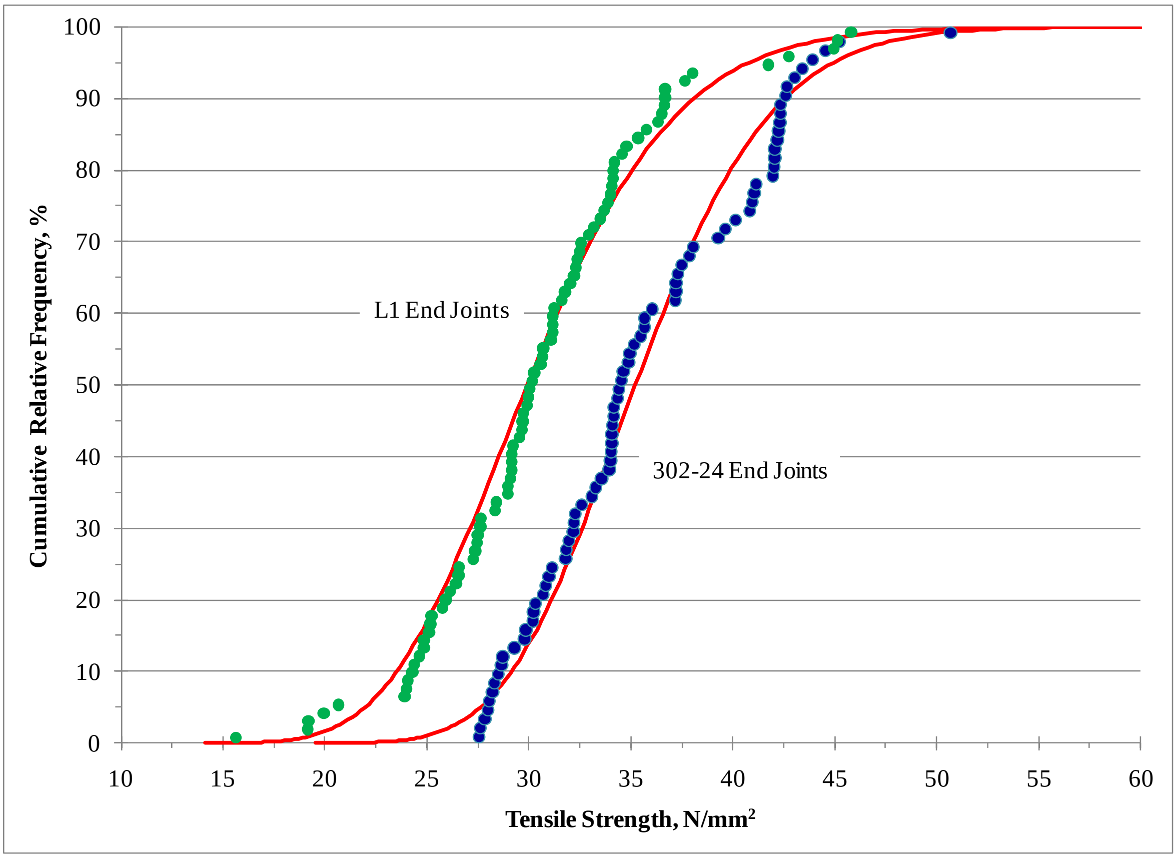

Figure 3. Data distribution of end joint tensile strength based on an assumed log-normal distribution function

As compared to Table 1, Table 2 shows that the end joints have a substantially lower coefficient of variation than the corresponding laminating lumber as is expected. As a result, even though the mean tensile strength of the end joints, $f_{t,j,mean}$, made of high-quality 302-24 tension lams is significantly below the mean tensile strength of the laminating lumber, $f_{t,0,l,mean}$, the characteristic tensile strength of the end joints, $f_{t,j,05}$, remains comparable (within 4%) to the characteristic tensile strength of the laminating lumber, $f_{t,0,l,05}$. On the other hand, for L1 lumber, the mean tensile strength of the end joints is comparable to the mean tensile strength of the laminating lumber. As a result of the reduced coefficient of variation, the characteristic tensile strength of the end joints is substantially higher (23%) than that of the laminating lumber. In all cases, the end joints appear to meet the currently published characteristic value for the laminating lumber.

It is important to note that in the North American glulam standards, the characteristic tensile strength of end joints is required to be only as strong as the characteristic tensile strength of the corresponding lumber. This is different from prEN 14080 [12], *Timber Structures - Glued Laminated Timber and Glued Laminated Solid Timber – Requirements*, which requires the characteristic tensile strength of end joints to be 5 N/mm^2 higher than the characteristic tensile strength of the lumber. While it is entirely possible that some low to medium grades of lumber could have end joints that are 5 N/mm^2 higher than the characteristic tensile strength of the lumber, it is recognized by the North American glulam industry that this requirement is extremely difficult to satisfy for high-quality lumber, such as 302-24 tension laminations and it has been demonstrated through numerous full-scale beam tests to be unnecessary to ensure beam performance.

3.3 Lumber Long-Span E

Table 3 shows test results for lumber long-span E (span-to-depth ratio of 100:1 in flatwise bending). The mean long-span E of the lumber, $LSE_{m,l,mean}$, of each lumber grade can be considered as the shear-free modulus of elasticity. As shown in Table 3, the mean long-span E values of the high-quality 302-24 tension laminations and L2 lumber are substantially higher (15% and 12%, respectively) than the currently published values. The higher long-span E for the 302-24 tension laminations should not be a surprise because the current published long-span E value is assumed to be the same value as the relatively lower quality L1 grade.

Table 3. Summary statistics of lumber long-span E

Properties	Lumber Long-Span E [(a)]			
	302-24	L1	L2	L3
No. of observations	86	90	87	93
$LSE_{m,l,mean}$, kN/mm^2 (10^6 psi)	16.7 (2.42)	14.9 (2.15)	13.1 (1.91)	11.6 (1.69)
Coefficient of variation	0.124	0.154	0.151	0.172
Published $LSE_{m,l,mean}$, kN/mm^2 (10^6 psi) [(b)]	14.5 (2.1)	14.5 (2.1)	11.7 (1.7)	11.0 (1.6)
$LSE_{m,l,mean}$/Published $LSE_{m,l,mean}$	1.15	1.02	1.12	1.06

(a) Tested with a span-to-depth ratio of 100:1 in accordance with ASTM D 4761.
(b) Mean value published in AITC 407.

3.4 Lumber Compression

Table 4 shows the test results for lumber compression based on short-column tests (a slenderness ratio of 17.3) in accordance with ASTM D 198. The characteristic compressive strength (5^{th} percentile with 75% confidence) of the lumber, $f_{c,0,l,05}$, of each lumber grade from the combination of 3 glulam plants were determined based on ASTM D 2915. The data distribution of each lumber grade is shown in Figure 4. Note that there are no currently published compressive strength values for laminating lumber. However, as compared to results shown in Table 1, the characteristic compressive strength of the laminating lumber is 1.6, 2.5, 3.2, and 4.9 times higher than the characteristic tensile strength values, respectively, for 302-24, L1, L2, and L3 laminations. This trend suggests that the compression-to-tension ratio increases with decreasing lumber quality.

Table 4. Summary statistics of lumber compressive strength

Properties	Lumber Compressive Strength			
	302-24	L1	L2	L3
No. of observations	149	145	89	93
$f_{c,0,l,mean}$, N/mm^2 (psi)	56.9 (8260)	53.6 (7774)	51.7 (7506)	50.7 (7357)
Coefficient of variation	0.098	0.108	0.146	0.146
$f_{c,0,l,05}$, N/mm^2 (psi) [(a)]	47.7 (6926)	44.2 (6406)	38.9 (5639)	38.6 (5592)
$f_{c,0,l,05}/f_{t,0,l,05}$ [(b)]	1.6	2.5	3.2	4.9

(a) Parametric 5^{th} percentile with 75 percent confidence of laminating lumber (lognormal distribution).
(b) Based on the results reported in Table 1.

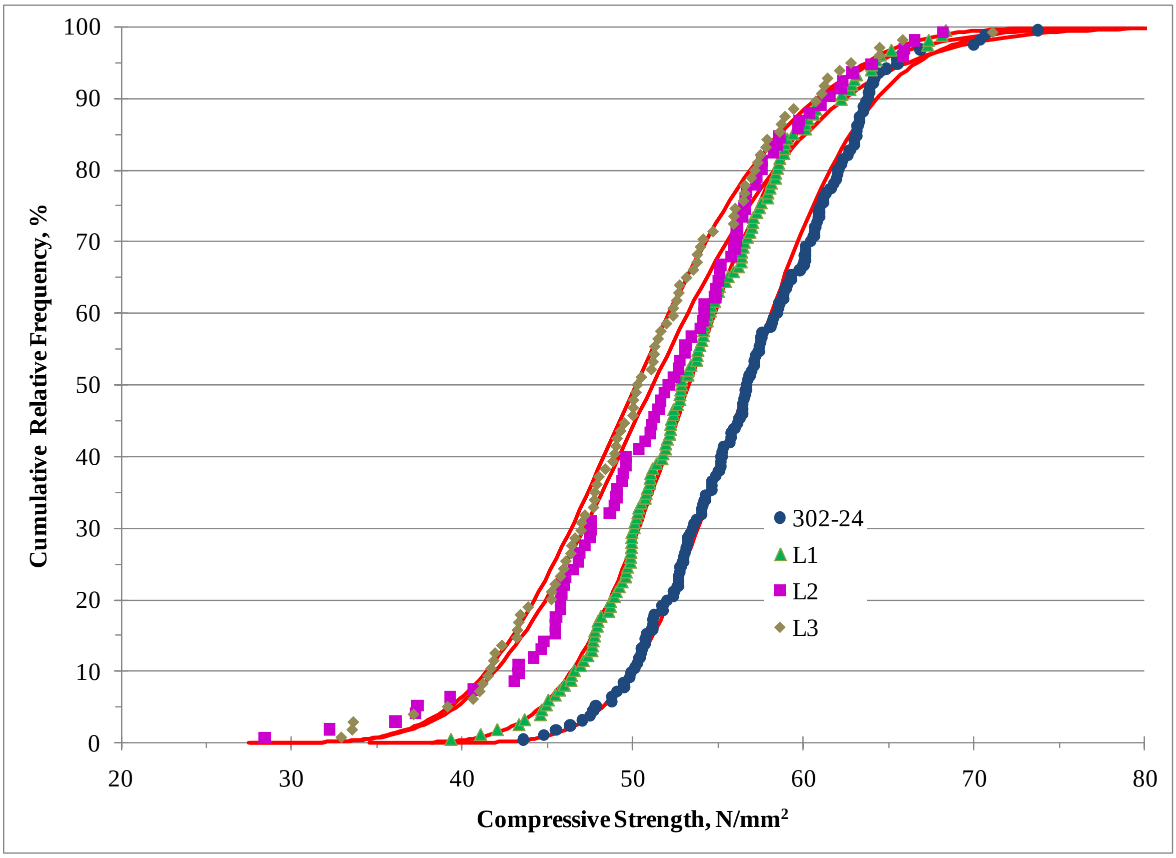

Figure 4. Data distribution of lumber compressive strength based on an assumed log-normal distribution function

The compression moduli and downward slope (m) of the bi-linear compressive stress and strain curve, as shown in Figure 1, are summarized in Table 5. The high coefficient of variation for this property is not a surprise because it is related to the post-failure phenomenon. As a result, the use of this information for computer modelling is highly likely to affect the quality of the simulation. An active investigation is pending for improving the accuracy of the estimate for this property and studying the effect of the coefficient of variation on the quality of the ReLam prediction.

Table 5. Summary statistics of the downward slope of compressive stress and strain curve

Properties	M	
	302-24	L1
No. of observations	47	54
Mean	-0.24	-0.20
Coefficient of variation	0.72	0.55

4. FRP-Reinforced Glulam Layup Combinations

Based on the data obtained from this study, FRP-reinforced glulam layup combinations were generated using the ReLam model. Figure 5 shows two candidate layup combinations with a targeted characteristic bending strength, $f_{m,g,k}$, of 48.3 N/mm^2 (7000 psi) and mean bending modulus of elasticity, $E_{0,g,mean}$, of 14480 N/mm^2 (2.1 x 10^6 psi) based on a reinforcement ratio, ρ (the ratio of the reinforcement to the overall beam volume), of about 3%. These layup combinations are designed to utilize low-grade laminations (mostly L2 and L3) to achieve a bending strength that far exceeds the conventional non reinforced glulam beam.

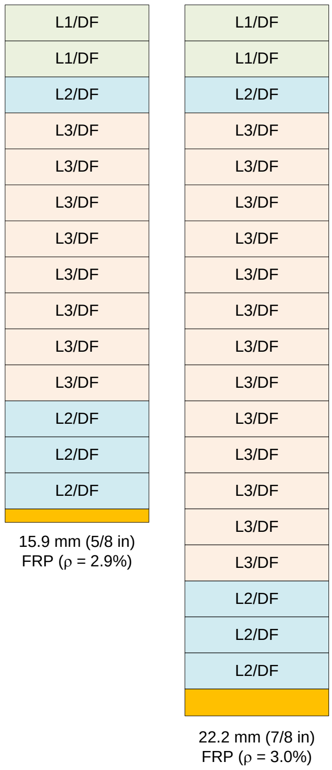

Figure 5. Candidate FRP-reinforced glulam layup combinations at a reinforcement ratio (ρ) of around 3% of the beam depth

The confirmation of the properties for the layup combinations shown in Figure 5 by full-scale beam tests is currently active and will be provided in a separate report when the results become available. Nonetheless, once the ReLam model is confirmed with its methodology and prediction, computer simulations can be conducted to generate FRP-reinforced glulam layup combinations with different reinforcement ratios, wood species, lamination grades, and targeted characteristic beam properties.

5. Conclusions and Recommendations

Results obtained from this study provide the characteristic properties of Douglas-fir laminating lumber that can be used for the modelling of FRP-reinforced glulam in accordance with ASTM D 7199. These data also confirm that the currently published laminating lumber properties are adequate albeit in some cases conservative. For the purpose of the glulam modelling using the bilinear compressive stress and strain curve, further investigation on the accuracy of the estimate for the downward slope after the compression failure will be conducted.

A model analysis was conducted for the development of candidate layup combinations with a targeted characteristic bending strength of 48.3 N/mm^2 (7000 psi) and mean bending modulus of elasticity of 14480 N/mm^2 (2.1×10^6 psi) based on a reinforcement ratio of about 3% utilizing low-grade laminations. The confirmation of the properties for these layup combinations is pending the completion of full-scale beam tests.

Once the confirmation of the ReLam model is completed, APA will pursue obtaining a code evaluation report based on ICC-ES AC280 [13], *Acceptance Criteria for Fiber-Reinforced-Polymer Glued Laminated Timber Using Mechanics Based Models*, on behalf of its manufacturing members. This will allow APA members to be listed on the code evaluation report and significantly expand the use of FRP-reinforced glulam in the U.S.

6. References

1. ASTM International. 2009. Standard Practice for Establishing Characteristic Values for Reinforced Glued Laminated Timber (Glulam) Beams Using Mechanics-Based Models. ASTM D 7199. *Annual Book of ASTM Standards.* Philadelphia, PA.
2. Lindybery, R.F. 2000. *ReLAM: A Nonlinear Probabilistic Model for the Analysis of Reinforced Glulam Beams in Bending*. Ph.D. Dissertation. University of Maine, Orono.
3. American Institute of Timber Construction. 2005. *Standard for Alternate Lumber Grades for Use in Structural Glued Laminated Timber*, AITC 407. Centennial, CO.
4. American Institute of Timber Construction. 2004. *AITC Grading Handbook for Laminating Lumber*. In *Standard Specifications for Structural Glued Laminated Timber of Softwood Species*, AITC 117. Centennial, CO.
5. American National Standards Institute. 2007. *American National Standard for Wood Products - Structural Glued Laminated Timber.* ANSI/AITC A190.1. New York, NY.
6. ASTM International. 2009. Standard Methods of Static Tests of Timbers in Structural Sizes. ASTM D 198. *Annual Book of ASTM Standards.* Philadelphia, PA.
7. ASTM International. 2009. Standard Test Methods for Mechanical Properties of Lumber and Wood-Base Structural Materials. ASTM D 4761. *Annual Book of ASTM Standards.* Philadelphia, PA.
8. American Institute of Timber Construction. 2004. *Test Method T116, Modulus of Elasticity of E-Rated Lumber by Static Loading*. In *Manufacturing Quality Control System Manual*, AITC 200. Centennial, CO.
9. ASTM International. 2009. Standard Test Methods for Direct Moisture Content Measurement of Wood and Wood-Base Materials. ASTM D 4442. *Annual Book of ASTM Standards.* Philadelphia, PA.
10. ASTM International. 2009. Standard Test Methods for Specific Gravity of Wood and Wood-Based Materials. ASTM D 2395. *Annual Book of ASTM Standards.* Philadelphia, PA.
11. ASTM International. 2009. Standard Practice for Evaluating Allowable Properties for Grades of Structural Lumber. ASTM D 2915. *Annual Book of ASTM Standards.* Philadelphia, PA.
12. European Committee for Standardization (CEN). 2009. *Timber Structures - Glued Laminated Timber and Glued Laminated Solid Timber – Requirements*. prEN 14080.
13. ICC Evaluation Service, Inc. 2005. *Acceptance Criteria for Fiber-Reinforced-Polymer Glued Laminated Timber Using Mechanics Based Models*, AC280. Whittier, CA.

CIB-W18/42-12-4

**INTERNATIONAL COUNCIL FOR RESEARCH AND INNOVATION
IN BUILDING AND CONSTRUCTION**

WORKING COMMISSION W18 - TIMBER STRUCTURES

VALIDITY OF BENDING TESTS ON STRIP-SHAPED SPECIMENS TO DERIVE BENDING STRENGTH AND STIFFNESS PROPERTIES OF CROSS-LAMINATED SOLID TIMBER (CLT)

R Steiger

Empa, Swiss Federal Laboratories for Materials Testing and Research

Duebendorf

A Gülzow

Carbo-Link GmbH

Fehraltorf

SWITZERLAND

Presented by R. Steiger

H.J. Blass stated that the difference between shear and rolling shear failure is not apparent. R. Steiger agreed.
J. Köhler stated that multiple parameters can have several optima. R. Steiger said that he took more Eigen frequencies than needed to derive the nine elastic constants.
H.J. Blass and R. Steiger discussed the failure mode of the four-side supported panel with restraint against lifting. H.J. Blass asked whether the rolling shear in the panel compared to strip was compared. R. Steiger said not yet.

Validity of bending tests on strip-shaped specimens to derive bending strength and stiffness properties of cross-laminated solid timber (CLT)

René Steiger
Empa, Swiss Federal Laboratories for Materials Testing and Research
Duebendorf, Switzerland

Arne Gülzow
Carbo-Link GmbH
Fehraltorf, Switzerland

Abstract

Cross-laminated solid timber (CLT) is a panel-shaped engineered wood product, assembled of cross-wise oriented layers of lamellas (mostly softwood). In contrast to other panel-shaped engineered wood products, CLT is not only used as component of structural elements, but rather for load bearing plates and shear panels itself. The application of CLT used as load-bearing plates requires information on strength properties, the design, however, is often governed by serviceability criterions like maximal deflection and vibration susceptibility. Hence, predicting the respective behaviour of such panels requires accurate information about their bending and shear strength as well as their elastic properties.

Regulations regarding the derivation of performance characteristics, evaluation of conformity and (CE-) marking of wood-based panels for use in construction are given in EN 13986. According to this standard bending strength and stiffness of CLT have to be assessed following the procedure in EN 789. The latter requires 4-point bending tests of strip-shaped specimens with a width of 300 mm, cut off the CLT panels. The span has to be taken as 300 mm + 32 · *t*, *t* being the nominal thickness of the CLT panel.

By comparing results of bending tests on strip-shaped specimens and on full panels it is shown, that neither strength nor stiffness properties derived by testing strip-shaped panels are appropriate to assess the respective properties of the original panels. The analysis of the test data covers bending strength, bending MOE parallel and perpendicular to the grain direction of the face layers as well as shear moduli. Rolling shear failures which frequently occurred when testing strip-shaped specimens could not be observed in destructive tests of whole CLT panels. Additionally a verification by carrying out static bending tests (deflection measurements) under different loading situations showed, that the overall stiffness properties (elastic parameters of the stiffness matrix) can, alternatively to EN 789 tests or estimations with the compound theory, be derived directly by a modal analysis of full-size CLT panels.

Keywords

Cross-laminated solid timber, CLT, bending strength / stiffness, failure mode, EN 789, rolling shear, NDE, modal analysis, production control, variation of mechanical properties

1 Introduction

Cross-laminated solid timber (CLT) is a panel-shaped engineered wood product (EWP), assembled of cross-wise oriented layers of lamellas (mostly softwood) which compared to the raw material benefits from homogenised mechanical properties. In contrast to other panel-shaped EWP, CLT is not only used as component of structural elements, but rather for load bearing plates and shear panels itself. As for other load bearing structural elements as well, the design of CLT requires verification of sufficient strength and serviceability. Since in practice the design of plates loaded perpendicular to the plane is often governed by serviceability criterions like maximal deflection and vibration susceptibility, predicting the adequate behaviour of such panels has to be based on accurate information about their elastic properties besides their bending and shear strength.

Regulations regarding the derivation of performance characteristics, evaluation of conformity and (CE-) marking of wood-based panels for use in constructions are given in EN 13986 [1]. There CLT is called “Solid Wood Panel” (SWP) and with regard to deriving the so-called “performance characteristics” bending strength and bending stiffness reference is made to the standard EN 789 [2]. EN 789 asks for 4-point bending tests of strip-shaped specimens with a width of 300 ± 5 mm, cut from the CLT panels. The span has to be taken as 300 mm + 32 · *t*, *t* being the nominal thickness of the CLT panel.

According to EN 789 sampling has to guarantee adequate consideration of variability within the production of the EWP by following certain cutting schemes of the raw plates. Concerning mechanical properties in bending the standard asks for only one specimen per plate and grain direction of the face layers to be tested respectively. The standard EN 13353 [3] being relevant for the requirements on SWP allows this respective test value to be taken as the mean value of the whole panel and for using this value for all statistical calculations where the mean value and the variation of the mean values of the panels are used. It is however said that “the variation within a panel and the according calculations cannot be done” which means that e.g. characteristic values cannot be assigned to SWP based on the procedure described above. According to EN 789 calculation of characteristic 5-percentile values and sampling has to follow the rules of EN 14358 [4]. It is obvious that deriving mechanical properties from one single test is not reliable enough. However, in the course of production control such tests are useful to check e.g. sufficient quality of bonding and can thus serve as a kind of “red light alert”. In scientific studies, tests of strip-shaped specimens may serve to verify assumptions (e.g. Poisson’s ratios, shear moduli, etc.).

When designing CLT panels to be used as plates, bending and shear strength as well as moduli of elasticity (MOE) parallel and perpendicular to the grain direction of the face layers together with shear moduli are needed. These values are usually derived on base of the mechanical properties of the raw material (layers) using the compound theory [5] [6]. Stiffness properties can also be assessed by non-destructive testing of the CLT panels e. g. by a combination of theoretical and experimental modal analysis [7] as will be explained in more detail in 3.1. Bending tests of strip-shaped panels cut from whole plates is another way of evaluating strength and stiffness properties of CLT. Such tests, however, suffer from being destructive, tedious and not in all cases a reliable indicator of the CLT’s real mechanical performance [8] [9].

By comparing results of bending tests of strip-shaped CLT specimens with properties of full panels the presented study aimed to evaluate, if bending strength and flexural stiffness properties of CLT panels can be reliably derived by testing strip-shaped specimens.

2 Material

2.1 Panels

The study comprised of a total of 42 CLT panels with different lay-ups and geometrical dimensions as indicated in Table 1. The panels were supplied by two producers (A and B) and due to totally different ways of production the panels exhibited remarkable differences in appearance and mechanical properties although the raw material was in both cases visually strength graded Norway Spruce (*Picea abies Karst.*).

Table 1: Geometrical properties of investigated CLT panels

Series	Length 1) x Width [m]	Thickness [mm]	Lay-up [mm]	Number of panels
1	2.50 x 2.50	70	Product A and B: 10/50/10	9 of each product
			Product A and B: 25/20/25	3 of each product
2	2.50 x 2.50	110	Product A: 35/40/35	3
			Product B: 20/70/20	3
	4.00 x 2.50	80	Product A: 25/30/25	3
			Product B: 15/50/15	3
		110	Product B: 15/15/20/15/15	3
			Product A: 35/40/35	3

1) direction parallel to the grain of the face layers

The face layers of product A (Fig. 1, left) have according to the manufacturing policy to correspond to strength class C24 (EN 338 [10]), whilst the inner layers can consist of C20 lamellas. In a first step of production “glulam beams” are produced by assembling lamellas (boards, if necessary end-jointed) with a thickness of up to 70 mm. The “glulam” then is vertically cut into planks (the width of them being equal to the height of the “glulam beams”) which oriented flat wise are used as face layers of the CLT panels. The smaller sides of these planks are not bonded. The inner layers of the CLT panels consist of single lamellas with a width of 100 – 150 mm which at their lateral sides are not bonded. If the thickness of the inner layers is ≥ 30 mm, grooves are cut into the inner layers in order to guarantee a sufficient strength of the bond line when processing the panel at low stresses perpendicular with a vacuum press. The moisture content (MC) of the layers is 12 – 14%. All bonds are made with a 1-component-PUR adhesive.

CLT product B (Fig. 1, right) is according to information by the producer made from lamellas of at least strength class C24. In both face and inner layers the width of the lamellas is 25 mm. Before assembling the CLT, planking are produced by side bonding the single 25 mm lamellas. Making sure that there is a sufficient lengthwise overlap of the single planking elements, several planking are bonded glulam-like resulting in “Blockholz” which is then vertically cut into layers being the raw material for the CLT production. All bonds are made with a MUF type adhesive and the MC of the lamellas and layers is 8%. Compared to product A, product B due to smaller sized components of the layers, lacking of grooves and due to bonding of the layers on all sides exhibits a higher degree of homogenization.

Prior to testing in the lab, the panels were stored in climate 20°C / 60% r h, which resulted in an equilibrium moisture content of slightly below 12%. The r h was chosen different from 65% in order to prevent product B from too strong changes in MC.

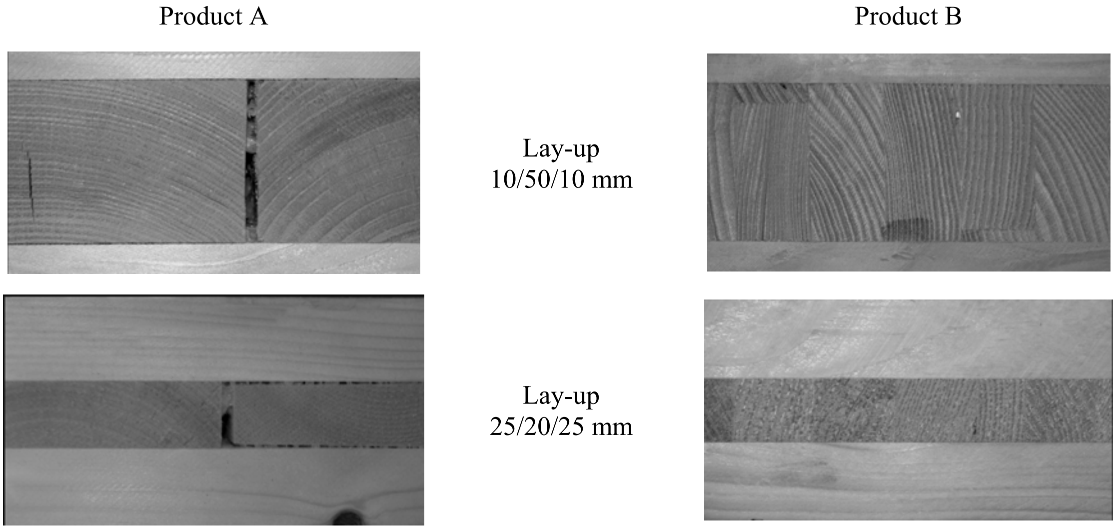

Fig. 1: CLT products A (left) and B (right). Thickness = 70 mm.

2.2 Strip-shaped specimens

The scheme of cutting the strip-shaped specimens parallel and perpendicular to the grain direction of the face layers from the series 1 – CLT panels is shown in Fig. 2 left. The panels were originally produced in rectangular shape and got quadratic after cutting off the strip-shaped specimens. The width of the 5 – 6 strips per direction was 100 mm. In the course of test series 2 two 300 mm wide strips (one per grain direction of the face layers) were cut off each panel according to Fig. 2 right.

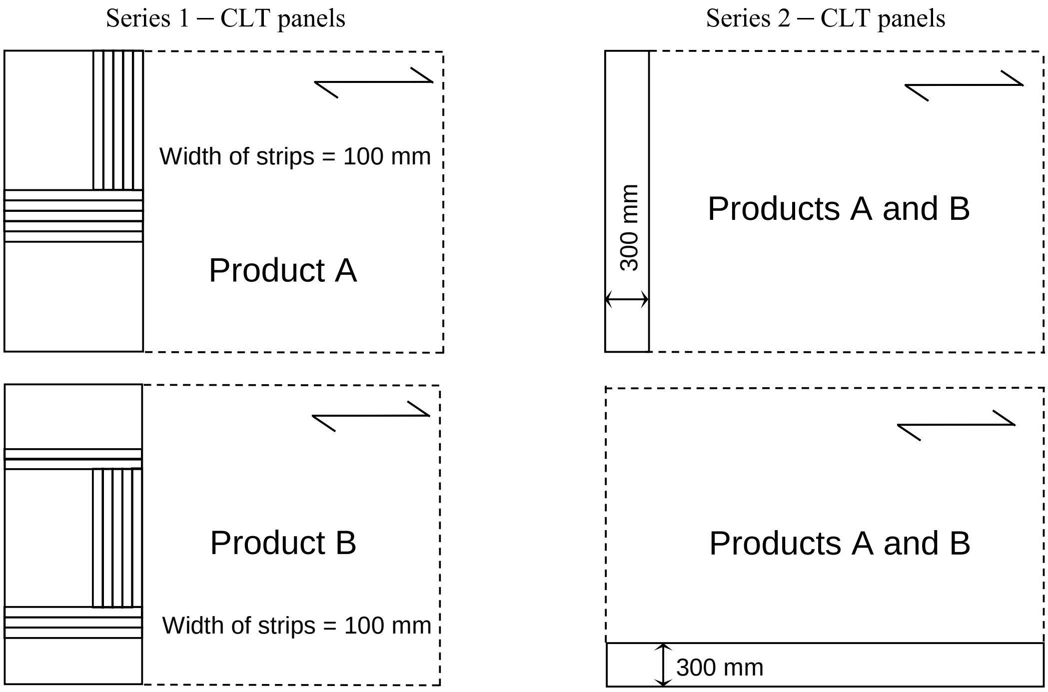

Fig. 2: Scheme of cutting strip-shaped specimens off CLT panels (series 1: left, series 2: right). The arrow sign indicates the grain direction of the face layers.

The strip-shaped specimens as well were stored in climate 20°C / 60% r H in order to have the same MC as the CLT panels.

3 Method

3.1 Evaluation of elastic properties of the CLT panels

To derive stiffness properties of whole CLT panels a method was applied which had recently been studied and further developed at the Swiss Federal Laboratories for Materials Testing and Research, Empa [11]. The method is non-destructive and bases on experimental and theoretical modal analysis. It turned out to be an efficient and accurate technique to determine elastic stiffness elements of panel-shaped EWP [12-16]. The procedure is based on three major steps [17]:

– First, an experimental modal analysis is performed on panels vertically suspended by thin lines: Resonance frequencies $f_{i,exp}$ and mode shapes of the panels are evaluated.

– In a second step, resonance frequencies $f_{i,cal}$ and mode-shapes of the free vibrating, linear elastic panel are described in a theoretical model as functions of the elastic material properties using Reddy's higher order plate theory for the orthotropic case [18]. Since shear deformations play an important role in CLT, a model has to be taken which is able to account for such deformations.

– Finally, the inverse problem is solved by systematically adjusting the unknown stiffness properties until the theoretically calculated resonance frequencies $f_{i,cal}$ match the experimentally measured ones $f_{i,exp}$. In this optimization process, the stiffness values are estimated simultaneously using a parametric model fitting algorithm. In the first few iteration steps the computed and measured frequencies and mode shapes do not necessarily coincide, since the initial values of the material parameters are only rough estimates. Matching of mode shapes therefore is needed. This is done by a procedure based on MAC (Modal Assurance Criterion) values [19] which is a scalar measure of the degree to which two mode shapes are identical (MAC = 1).

In the course of applying and further developing the method at Empa, experiments were first performed under lab conditions on one single plate consisting of 3 layers (10/50/10 mm) and having geometrical dimensions of 1.0 m x 1.5 m x 0.07 m. By an experimental verification with static bending tests it was shown that the method was able to correctly evaluate the relevant stiffness parameters of the CLT panel [20]. This was afterwards shown again for a total of 42 CLT panels of different geometrical dimensions and lay-ups (see Table 1) made by two different producers [21]. In a final step the applicability of the method under industrial conditions (production plant, CLT made for real objects) was proven and the method was further optimised (reduction of number of excitation points and plates supported by air bearings instead of suspending them from lines or cable wires) [11].

The method is capable of deriving two in-plane elastic moduli (E_{11}, E_{22}) and the three shear moduli (G_{12}, G_{13}, G_{23}) of CLT panels with different geometrical dimensions and lay-ups [21]. The directions of the principal axis are shown in Fig. 3. It is difficult to estimate the shear modulus G_{23} (being a combination of rolling shear modulus of the face layers and of shear modulus of the middle layer) by modal analysis since this parameter does not take noticeable influence on the mode shapes and resonance frequencies. Bending tests of strip-shaped specimens with variable span as well are not capable of deriving actual G_{23} values since grooves and layer sides not adhesively bonded exhibit different stiffness when being positioned at free span or near the supports respectively. The bending tests however will let at least confirm the correct range of the G_{23} values derived by modal testing.

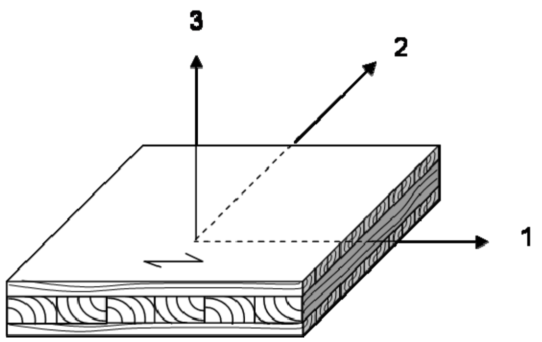

Fig. 3: Principal axis in CLT as used in this paper

3.2 Bending tests of strip-shaped specimens

3.2.1 Strips taken from series 1 – CLT panels to assess bending strength and stiffness as well as failure mode

4-point bending tests to assess bending strength and stiffness as well as type of failure were carried out with a span of 1100 mm and a distance between the loading points of 300 mm (Fig. 4) [22]. Due to restrictions by the available testing machine the width of the specimens was only 100 mm (EN 789 would have required 300 mm!) and thus the span was reduced similarly (EN 789 would have required 2540 mm). The reference loads to determine MOE were 10% and 40% of the assumed failure load and the deformations were measured between the loading points on the upper side of the specimens (Fig. 4). Speed of the loading head was adjusted such that failure was reached after 300 ± 120 seconds.

3.2.2 Strips taken from series 2 – CLT panels to assess bending stiffness

The MOE in bending and the shear modulus were evaluated according to EN 408 [23] with the specimens having dimensions as asked by EN 789. The shear moduli G (below referred to as G_{13} and G_{23}) and the MOE E_m (below referred to as E_{11} and E_{22}) were determined by the variable span method from the apparent MOE $E_{m,app}$ for each test piece [23]. The depth (h) to span (ℓ) ratio was varied between $h/\ell = 0.0037$ and 0.035. The deformations were measured for 10% and 40% of the supposed failure load and the speed of loading was such that each test cycle lasted 1 minute, which is slightly above the test duration asked by EN 408. The test arrangement is shown in Fig. 5. Strips with grooves and cuts (which aim at reducing warping due to changing moisture) have been tested twice with changing orientation of tension and compression side.

[mm]

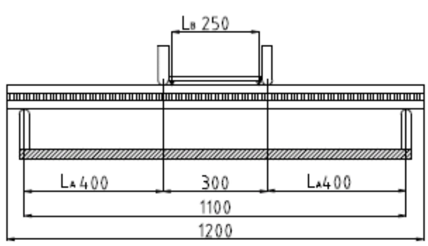

Fig. 4: 4-point bending tests on strip-shaped specimens cut off the series 1 – CLT panels [22]

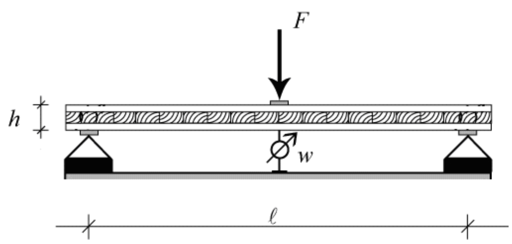

Fig. 5: 3-point bending tests with variable span on strip-shaped specimens cut off the series 2 – CLT panels

4 Results and discussion

4.1 Bending strength, MOE and failure modes of strips cut off the series 1 – CLT panels

Fig. 6 shows a comparison of bending strength recorded along bending tests of whole CLT panels (geometrical dimensions: 2.50 x 2.50 x 0.07 m, lay-ups 10/50/10 mm and 25/20/25 mm) and of respective values derived from strip-shaped specimens (1.20 x 0.10 x 0.07 m) cut off the panels parallel to the grain direction of the face layers (Fig. 2 (left)). The panel tests consisted of 3 different types of loading occurring in practical situations: a) 4 single loads in the centre point of the panels' quadrants, b) 1 single load in the centre of the panel and c) 1 single load in the centre of one quadrant [9]. The bending strength were calculated with the compound theory taking into account all layers [5, 6].

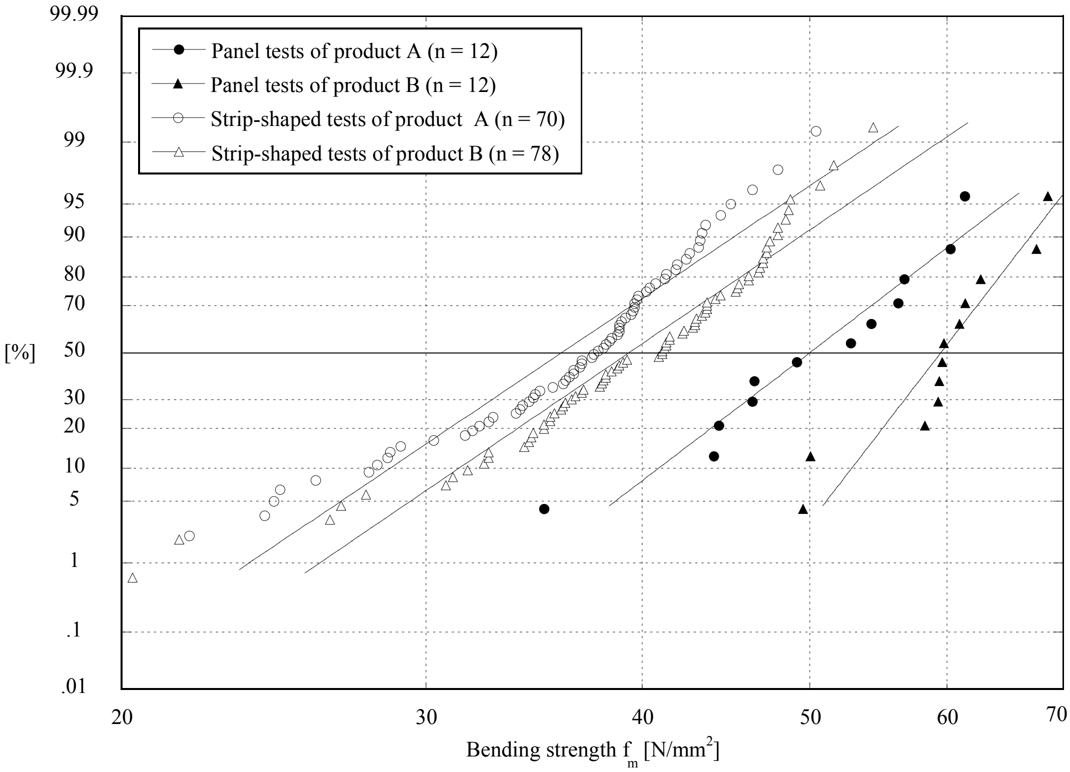

	n	Minimum [N/mm²]	Mean [N/mm²]	Median [N/mm²]	Maximum [N/mm²]	Standard dev. [N/mm²]	5th percentile [N/mm²]	COV [%]
Tests on whole CLT panels 2.50 x 2.50 x 0.07 m with lay-ups 10/50/10 mm and 25/20/25 mm								
Product A	12	35.1	50.7	50.0	61.4	8.20	35.1	16.2
Product B	12	49.6	59.8	59.5	68.6	5.86	48.0	9.80
Tests on strip-shaped specimens 1.20 x 0.10 x 0.07 m								
Product A	70	18.7	36.5	37.6	50.4	6.18	25.5	16.9
Product B	78	20.3	39.9	41.1	54.4	6.71	28.0	16.8

Fig. 6: Comparison of bending strength derived from tests on whole 2.50 m x 2.50 m x 0.07 m CLT panels with lay-ups 10/50/10 mm and 25/20/25 mm [9] and on strip-shaped specimens (width = 100 mm) cut off these panels according to Fig. 2 (left).

For both products bending strength derived from tests on strip-shaped specimens is considerably lower than when performing bending tests on whole panels. Comparing the variation of results (represented by the slope of the linear regression lines) it can be seen that testing of strip-shaped specimens with a width of 100 mm is not capable to correctly account for the higher degree of homogenisation of product B, whereas this difference can clearly be seen when comparing the test results of the whole CLT panels. In the course of the strip tests in 4-point bending shear failures occurred frequently, whereas this was not the case with the gross CLT panels. There, due to comparably lower shear stresses, bending failure on the tension side was predominant (Table 2).

Table 2: Failure modes along the bending tests of strip-shaped specimens and gross CLT panels

Strip-shaped specimens (n_{tot} = 303)			Gross CLT panels (n_{tot} = 24)		
Type of failure	Count	Percentage	Type of failure	Count	Percentage
Bending failure	129	42.6%	Bending failure	22	91.6%
(Rolling) shear failure	97	32%	Shear failure	1	4.2%
Mixed mode	19	6.3%	Punching	1	4.2%
Local defects	58	19.1%			

Fig. 7 shows mean, maximum and minimum values of the MOE E_{11} and E_{22} of 5 – 6 strips per panel and grain direction of the face layers. Left portions of the diagrams (with dark grey background) reflect test results of product A and right portions (light grey background) those of product B. For lay-up 10/50/10 mm the respective sample sizes were with product A: n_{E11} = 57, n_{E22} = 59 and with product B: n_{E11} = 59, n_{E22} = 57. The lay-up 25/20/25 mm sample sizes for product A amounted to: n_{E11} = 18, n_{E22} = 18 and for product B to: n_{E11} = 17, n_{E22} = 18.

The high COV clearly indicate a large variation of the stiffness properties within a CLT panel independent of its lay-up. These big variations result from the heterogeneity of the raw material. Maximum COV of E_{11} of strip test samples within one CLT panel was 16.7% for product A and 18.7% for product B. In case of E_{22} these values are 32.8% (product A) and 12.2% (product B). Respective mean values of COV were for E_{11} 11.6% (product A) and 12.8% (product B) and for E_{22} 14.8% (product A) and 9.6% (product B). The mean values of the strip test samples can be compared to the respective values derived by modal analysis of the whole CLT panel. The biggest difference is 20.6% for strips tested parallel to the grain direction of the face layers (E_{11}) and 13.8% perpendicular to it (E_{22}). Thereby no clear trend of over- or underestimating could be found. Thus it is not possible to derive correct stiffness properties of CLT panels by testing one or a few strip-shaped specimens. In average (mean values of all strip-shaped specimens cut from the same panel) the differences are for E_{11} 10.2% (product A) and 6% (product B) and for E_{22} 6.9% (product A) and 7.8% (product B). This precision would be sufficient for applications in civil engineering but occurring differences up to 15 – 20% in specific cases nevertheless highlight the shortcomings of tests on strip-shaped specimens.

When plotting all series of the CLT panels with lay-up 10/50/10 in normal probability plots (NPP) (Fig. 8) it can be seen that the mean values of the MOE of the strip tests are marginally higher than the ones derived by modal analysis of the whole panel. The difference in E_{11} is +1.5% for product A and +2.7% for product B. In case of E_{22} the respective differences are +5.4% (product A) and +8.3% (product B). Comparing the slopes of the linear regression lines in the NPP, much bigger variability of the strip test samples is obvious. Overall variations are higher in product A than in product B which can be explained by a different degree of homogenization due to the different ways of production and the quality of the raw material (see 2.1). This phenomenon, however, is marked more for MOE E_{11} and E_{22} of the whole panel than for the strip test samples.

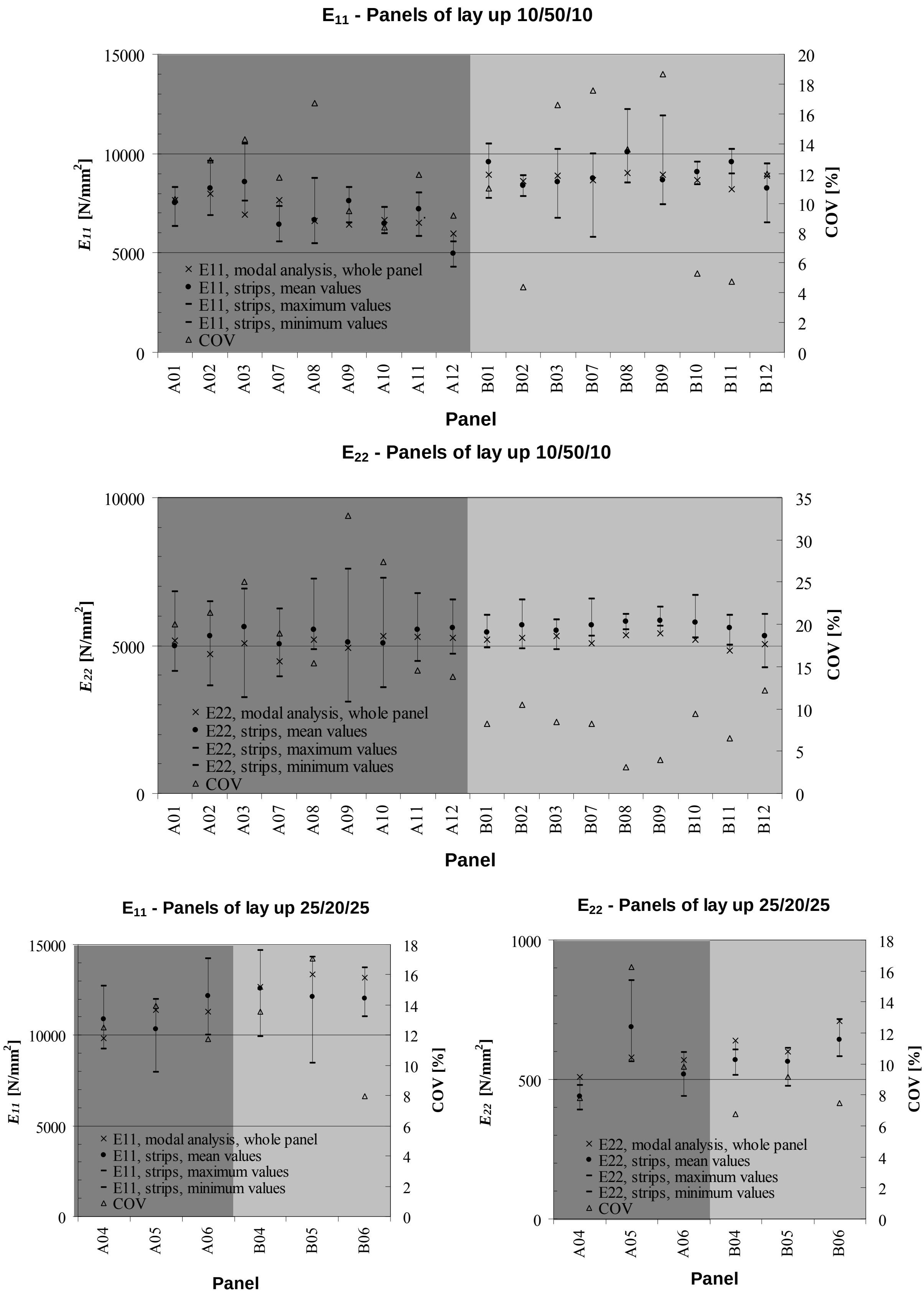

Fig. 7: MOE E_{11}, E_{22} derived by 4-point bending tests of strip-shaped specimens (5 – 6 specimens per series 1 – CLT panel) or by modal analysis together with respective coefficients of variation (COV) and by modal analysis derived MOE values(x-signs).

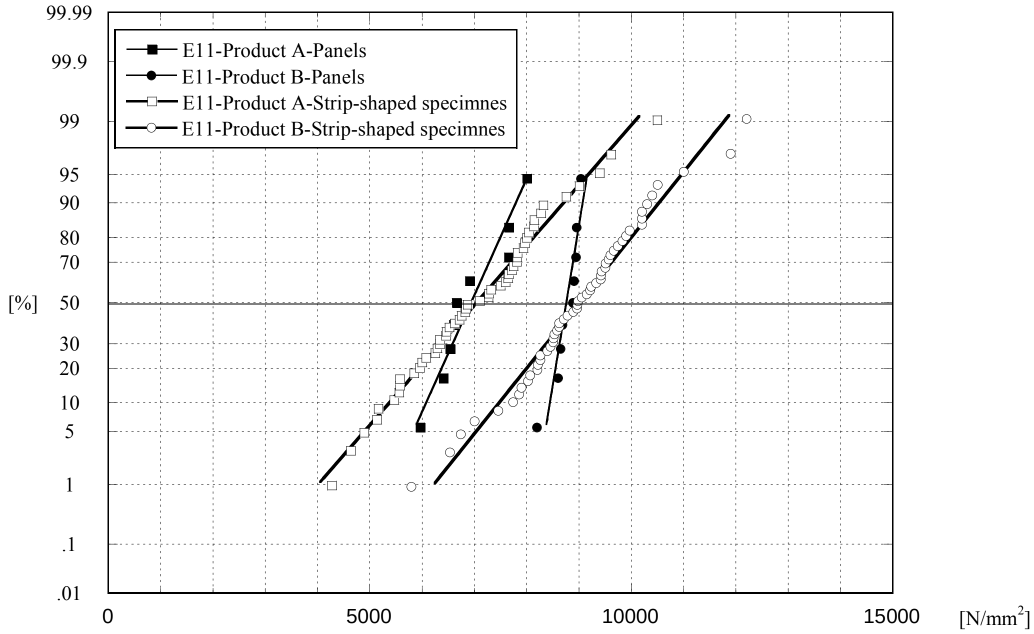

Parameter	E_{11} of product A		E_{11} of product B	
	Panels	Strip-shaped specimens	Panels	Strip-shaped specimens
Sample size	9	52	9	54
Mean value [N/mm^2]	6936	7038	8759	8998
Standard deviation [N/mm^2]	686	1304	260	1201
COV	9.9%	18.5%	3.0%	13.3%

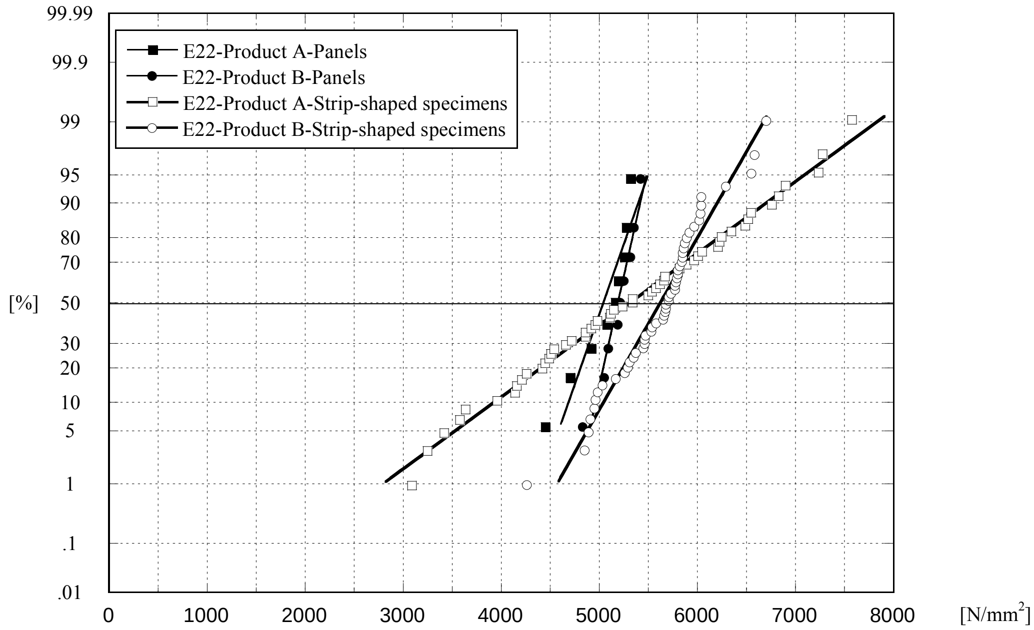

Parameter	E_{22} of product A		E_{22} of product B	
	Panels	Strip-shaped specimens	Panels	Strip-shaped specimens
Sample size	9	53	9	52
Mean value [N/mm^2]	5043	5315	5190	5623
Standard deviation [N/mm^2]	295	1083	180	460
COV	5.8%	20.4%	3.5%	8.2%

Fig. 8: Normal probability plot and statistical parameters of MOE E_{11} and E_{22} derived by 4-point bending tests of strip-shaped specimens (5 – 6 specimens per series 1 – CLT panel) and by modal analysis. (Panels with lay-up 10/50/10 mm only)

4.2 MOE and shear moduli of strips cut off the series 2 – CLT panels

Generally, linear regression lines in plots of $1/E_{m,app}$ versus $(h/\ell)^2$ exhibited high coefficients of determinations which indicates that derived MOE and shear moduli are of high accuracy. However, some single values in the test series with strips oriented perpendicular to the grain direction of the face layers did not fit the trend line well, this being due to opening of layers at lamella contacts which were not glued together (Fig. 9). When such zones in specimens tested at large span ℓ are placed in the middle of the spans, the openings take much more influence on the test results than when being put near the supports in tests with short spans. Consequently respective test results were excluded from analysis and the MOE were derived from tests with 3 aspect ratios h/ℓ only (Fig. 9, right). Another solution might have been to fill the grooves with an adhesive prior to testing.

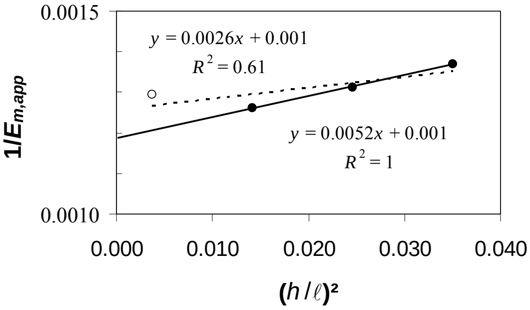

Fig. 9: Deriving of MOE and shear moduli in case of strips perpendicular to the face layers of the CLT panels concentrated only on test results (marked with •) not being influenced by opening of gaps. Test results from strips with open gaps are marked with o.

Fig. 10 shows a comparison of MOE (E_{11}, E_{22}) and shear moduli (G_{13}, G_{23}) derived by modal analysis of the whole CLT panels and by bending tests of strip-shaped specimens cut off the respective panels according to Fig. 2, right. The diagonal line in Fig. 10 indicates the ideal case, where parameters derived by modal analysis would be equal to those derived by static bending tests of the strip-shaped specimens. The results are grouped by type of product and geometrical parameters of the panel as indicated in Table 1 and in the caption of Fig. 10. Overall the differences independent from type of product are small to moderate. Parameter E_{22} even shows a very good agreement. Some big differences are visible between values derived on gross panels and on strip-shaped specimens respectively especially regarding the MOE E_{11} and the shear moduli G_{13} and G_{23}. A closer look on the test data of specimens exhibiting these big differences and on the specimens themselves turned out, that big differences mainly resulted from striking non-homogeneities in the used raw material. The biggest difference in E_{11} (60%) occurred with panel R_0.08_3L_A_P1. A detailed analysis of the reasons for this big difference showed up defects (knots, pitch pockets and deviated grain) (Fig. 11) which partly affected whole layers resulting in a severe reduction of the stiffness of the face layers.

In order to ensure quality of data, specimens with marked cuts and grooves were tested twice with changing orientation of the tension side in bending. Table 3 shows a comparison of respective values. Overall the differences are below 5% except shear modulus G_{13} of panel R_0.08_5L_B_P3 (13.7%), wherefrom it can be concluded that the test procedure did not systematically affect the data. Differences between dynamically (by modal analysis) derived values and such derived by static testing, however, also result from the well-known fact that stiffness parameters derived by means of dynamic methods due to the high speed of action (impulse hammer) are approximately 6% higher than those determined on base of static experiments at comparably lower loading rate [24, 25].

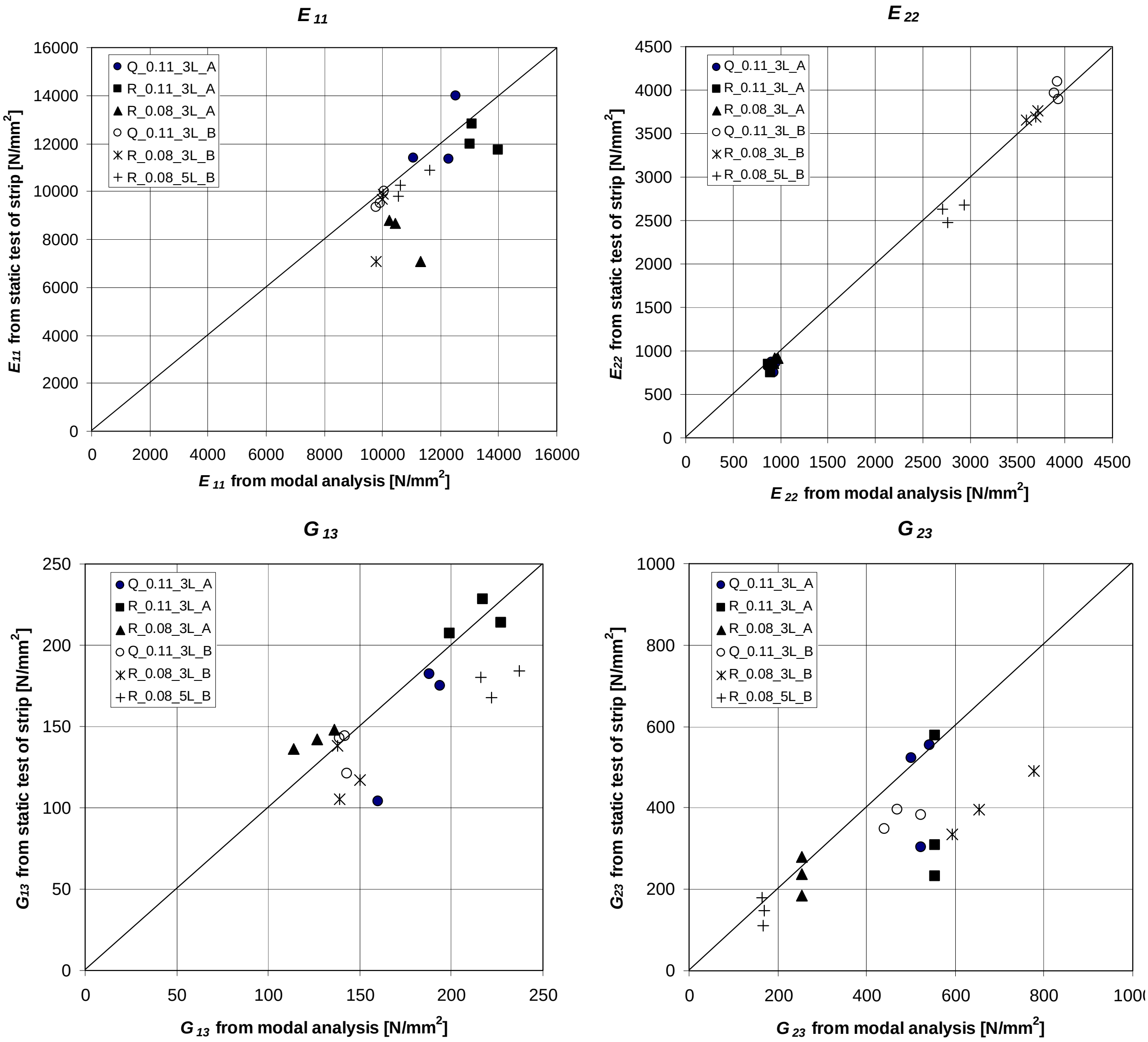

Fig. 10: Comparison of MOE and shear moduli derived by modal analysis of the whole CLT panels and by bending tests of single strip-shaped specimens cut off the respective panel according to Fig. 2, right. (Labels: Q/R = quadric/rectangular panel 2.50 x 2.50 m / 4.00 x 2.50 m, 0.11/0.08 = panel thickness [m], 3L/5L = 3/5 layers, A/B = Product)

Fig. 11: Cross-section view of the strip taken from panel R_0.08_3L_A_P1: Knots, pitch pockets, deviated grain and grooves affect nearly the whole respective layers.

Table 3: Comparison of MOE and shear moduli of strip-shaped specimens with cuts and grooves tested twice with changing orientation of the tension side

Panel	E_{11} [N/mm^2]	ΔE_{11}	G_{13} [N/mm^2]	ΔG_{13}
R_0.08_3L_A_P1a R_0.08_3L_A_P1b	7062 7082	0.3%	138 134	3.0%
R_0.08_3L_A_P2a R_0.08_3L_A_P2b	8681 8628	0.6%	149 145	2.8%
R_0.08_3L_A_P3a R_0.08_3L_A_P3b	8921 8688	2.7%	139 145	4.3%
R_0.08_5L_B_P1a R_0.08_5L_B_P1b	10858 10893	0.3%	170 166	2.4%
R_0.08_5L_B_P2a R_0.08_5L_B_P2b	10277 10277	0%	180 180	0%
R_0.08_5L_B_P3a R_0.08_5L_B_P3a	9579 10020	4.6%	195 172	13.4%

5 Summary and conclusions

Strength properties can best be assigned to CLT by means of the compound theory. However, the mechanical properties (strength and stiffness) of the layers have to be known which means that the raw material has to be strength graded. Deriving stiffness properties of whole CLT panels with modal analysis is a good alternative to estimating them on base of the mechanical properties of the singly layers by means of the compound theory. Especially in cases where the raw material is not strength graded or its mechanical properties are not known with sufficient precision, the modal analysis can help in assigning correct stiffness properties to CLT. After having proven the correctness of the method by static proof loading, the panel properties were compared to bending MOE and shear moduli derived from tests on strip-shaped specimens cut off the CLT panels. One part of the tests additionally focused on bending strength and failure modes. The following conclusions could be drawn:

– Bending strength and stiffness of CLT panels can vary quite strongly within one single panel. For both parameters differences between the strength and stiffness of strip-shaped specimens cut off the panels of up to 100% have been found. Hence it is not possible to derive strength and stiffness properties of CLT panels from bending tests of few or single strip-shaped specimens.
– The accuracy of the test results when performing bending tests of strip-shaped specimens according to EN 789 is increased with increasing sample size. Mean values of at least 5 – 6 specimens better describe the actual bending stiffness of the panels. Average differences then amount to 10% (E_{11}) and 6% (E_{22}) but can still reach 20%. As asked for in EN 789, characteristic values of strength and stiffness properties of CLT have to be derived on samples which fulfill the criteria of EN 14358.
– The variation of the stiffness properties depends on the degree of homogenisation of the actual CLT panel product. The smaller the components (lamellas) are and the less the variation in mechanical properties is (which can be reached by adequate strength grading of the raw material), the better it can be concluded from tests on strip-shaped specimens to the bending strength and stiffness properties of the whole CLT panel.
– Compared to gross CLT panels, local non-homogeneities and faults (knots, pitch pockets, deviated grain, not adhesively bonded contacts, cuts, grooves, cracks) take more influence on the mechanical properties of the strip-shaped specimens. The smaller the width of such specimens is, the more their load-bearing behaviour is affected by local defects and non-homogeneities due to faults in the raw material or due to way of producing the panels.
– The distances between middle layer parts not adhesively bonded at their lateral sides and the number of cuts and grooves, which are aimed at reducing the deformations of the CLT panel in case of changing moisture, take a big influence on the shear moduli. When deriving respective values on base of testing strip-shaped specimens this possible variation has to be taken into account by using empirical relationships.
– When testing strip-shaped specimens in 4-point bending, (rolling) shear failures occur quite frequently, whereas such failure modes could not be observed when testing whole CLT panels to failure in loading situations occurring in practice. There bending failure was dominating. Punching, however, should be regarded, especially with thin panels and products with grooves and layers not adhesively bonded at their lateral sides.
– Single tests on strip-shaped specimens may serve as an instrument of production control especially regarding the quality of bonding. They should, however not be used to derive mechanical properties of CLT panels. In scientific studies testing of strip-shaped cut

offs of CLT should only be carried out on big samples. Geometrical dimensions should not be taken smaller than asked by the standards and generalization of conclusions in most cases is not possible (e.g. type of failure).

6 References

1. CEN (2004): EN 13986: Wood-based panels for use in construction - Characteristics, evaluation of conformity and marking.
2. CEN (2004): EN 789: Timber structures - Test methods - Determination of mechanical properties of wood based panels.
3. CEN (2003): EN 13353: Solid wood panels (SWP) - Requirements.
4. CEN (2006): EN 14358: Timber structures - Calculation of characteristic 5-percentile values and acceptance criteria for a sample.
5. Bodig J., Jayne B. A. (1993): Mechanics of wood and wood composites. Krieger Publishing Company, Malabar, Florida, USA.
6. Blaß H. J., Görlacher R. (2003): Bemessung im Holzbau: Brettsperrholz - Berechnungsgrundlagen. In: Holzbau-Kalender, Bruderverlag, Karlsruhe, Deutschland. 580-598.
7. Steiger R., Gülzow A., Gsell D. (2008): Non-destructive evaluation of elastic material properties of cross-laminated timber. In: Proceedings of COST E53 Conference on "End user's needs for wood material and products", COST, Delft, The Netherlands. 171-182.
8. Jöbstl R. A., Moosbrugger T., Bogensperger T., Schickhofer G. (2006): Paper CIB-W18 39-12-4: A contribution to the design and system effect of cross-laminated timber (CLT). In: Proceedings of CIB-W18 Meeting Thirty-Nine, Florence, Italy.
9. Czaderski C., Steiger R., Howald M., Olia S., Gülzow A., Niemz P. (2007): Versuche und Berechnungen an allseitig gelagerten 3-schichtigen Brettsperrholzplatten. Holz als Roh- und Werkstoff 65 (5) 383-402.
10. CEN (2004): EN 338: Structural timber - Strength classes.
11. Gülzow A. (2008): Zerstörungsfreie Bestimmung der Biegesteifigkeiten von Brettsperrholzplatten - PhD Thesis ETH Nr. 17944. ETH Zurich, Switzerland.
12. Bastos S. F., Borges L., Rochinha F. A. (2002): Numerical and experimental approach for identifying elastic parameters in sandwich plates. Shock and Vibration 9 (4-5) 193-201.
13. Frederiksen P. S. (1997): Numerical studies for the identification of orthotropic elastic constants of thick plates. European Journal of Mechanics a-Solids 16 (1) 117-140.
14. Frederiksen P. S. (1997): Application of an improved model for the identification of material parameters. Mechanics of Composite Materials and Structures 4 (4) 297-316.
15. Frederiksen P. S. (1997): Experimental procedure and results for the identification of elastic constants of thick orthotropic plates. Journal of Composite Materials 31 (4) 360-382.
16. Larsson D. (1997): Using modal analysis for estimation of anisotropic material constants. Journal of Engineering Mechanics-Asce 123 (3) 222-229.
17. Sol H., Hua H., De Visscher J., Vantomme J., De Wilde W. P. (1997): A mixed numerical/experimental technique for the non-destructive identification of the stiffness properties of fibre reinforced composite materials. NDT & E International 30 (2) 85-91.
18. Reddy J. N. (1984): A simple higher-order theory for laminated composite plates. Journal of Applied Mechanics-Transactions of the Asme 51 (4) 745-752.
19. Maia N. M. M., Silva J. M. M. (1997): Theoretical and experimental modal analysis. Research Studies Press etc., Taunton, Somerset, England.
20. Gsell D., Feltrin G., Schubert S., Steiger R., Motavalli M. (2007): Cross-laminated timber plates: Evaluation and verification of homogenized elastic properties. Journal of Structural Engineering 133 (1) 132-138.
21. Gülzow A., Gsell D., Steiger R. (2008): Zerstörungsfreie Bestimmung elastischer Eigenschaften quadratischer 3-schichtiger Brettsperrholzplatten mit symmetrischem Aufbau. Holz als Roh- und Werkstoff 66 (1) 19-37.
22. Howald M., Niemz P. (2006): Massivholzplatten für das Bauwesen - Berichtsteil I/1: Berechnungsmodell für Massivholzplatten - Ermittlung mechanischer Eigenschaften anhand von Ultraschall-Messungen und Biegeversuchen an Kleinproben. Institut für Baustoffe, ETH Zurich, Switzerland.
23. CEN (2003): EN 408: Timber structures - Structural Timber and glued laminated timber - Determination of some physical and mechanical properties.
24. Görlacher R. (1984): Ein neues Messverfahren zur Bestimmung des Elastizitätsmoduls von Holz. Holz als Roh- und Werkstoff 42 (6) 219-222.
25. Machek L., Militz H., Sierra-Alvarez R. (2001): The use of an acoustic technique to assess wood decay in laboratory soil-bed tests. Wood Science and Technology 34 (6) 467-472.

CIB-W18/42-12-5

INTERNATIONAL COUNCIL FOR RESEARCH AND INNOVATION IN BUILDING AND CONSTRUCTION

WORKING COMMISSION W18 - TIMBER STRUCTURES

MECHANICAL PROPERTIES OF STRESS LAMINATED TIMBER DECKS – EXPERIMENTAL STUDY

K Karlsson

R Crocetti

R Kliger

Chalmers University of Technology, Gothenburg

SWEDEN

Presented by K. Karlsson

M. Frese wondered why the drawing shows an unsymmetrical response. K. Karlsson said that the drawing exaggerates the unsymmetrical behaviour.
R. Widmann received clarification that the deflections are relative deflections.

Mechanical Properties of Stress Laminated Timber Decks – Experimental study

Karlsson. K, Crocetti. R, Kliger. R

Chalmers University of Technology, Gothenburg, Sweden

1 Introduction

Timber bridges for road traffic are often designed as stress laminated timber (SLT) decks. SLT decks consist of several individual timber beams placed side by side and then stressed together. The friction generated by the prestress between the surfaces of the laminates makes it possible to consider the beams as a homogeneous timber plate. In EN 1995-2:2004 three models for analysis of timber bridges are suggested, namely:

- Orthotropic plate theory
- Modelling the deck plate by a grid
- Simplified method, calculation with an effective width b_{eff}.

In order to analyze an orthotropic plate, knowledge about material properties in the two main directions of the plate are required. Modulus of elasticity (MOE) and Poisson's ratio in both directions, as well as in-plane shear modulus are required. There is a significant difference between the material parameters of a single beam and the material parameters of several beams acting as a structural system. It is of great importance that the material parameters of such a system are identified. These material parameters for SLT decks have been studied over the last two decades mainly in North America and Australia, but also in Europe to some extent. Due to practical reasons, the transverse MOE and in-plane shear MOE are often expressed as a percentage of the longitudinal MOE. The MOE in the longitudinal direction is commonly a known property for a given timber material.

Modelling the deck plate by a grid also requires knowledge of the material parameters in two main directions of the plate, similar as for orthotropic plate theory.

The third alternative in EN 1995-2:2004 is to design the SLT-deck with a simplified method based on the assumption of a beam with an effective width b_{eff} to carry the loads. This assumption is the basis for simplified hand calculation methods e.g. Ritter (1990), Crews (2002). The method suggested in EN 1995-2:2004 is significantly more conservative than similar international design methods (Crews, 2006).

There are several experimental methods for determining the material parameters of an SLT. Some methods include dynamic measurements, other require several test sequences. In this paper the results of a test series according to a method first suggested by Stephan Tsai in 1965 is shown. Two square timber plates are needed together with knowledge of the longitudinal MOE E_x. Plates are subjected to pure twisting and deflection is measured in the middle of the plate.

This paper is the first part of a larger study with the aim of revising suitable design methods for SLT bridges made of Swedish glulam and designed for Swedish requirements. This is a pilot study for obtaining material parameters for SLT decks.

2 Background

The idea of SLT bridges comes from the technique used in order to repair nail laminated timber bridges. Such a technique was developed in Ontario, Canada in 1976. The result of adding stressed steel bars across the width of the bridge were so succsessfull that research about developing this technique started soon after.

Today the practical solutions may have changed a bit, but the principle is the same. Several laminates, from planks or glulam beams, are placed next to each other with holes drilled straight through at certain spacing. High strength steel bars are used to stress the timber pieces together. For instance, a system with aluminium and/or steel washers and a hard wood plate is used to distribute the prestress from the steel bars to the timber deck in Sweden. The purpose of the prestress is to press the timber pieces together forming a timber deck that behaves like a solid timber plate redistributing stresses from one loaded beam to the neighbouring beams, see Figure 1. This system is highly dependent on the friction between the laminates, and therefore the friction coefficient of timber-to-timber is of great importance.

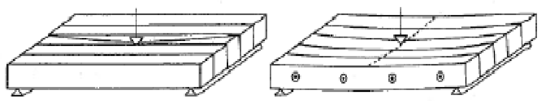

Figure 1 Load distribution as a result of prestress

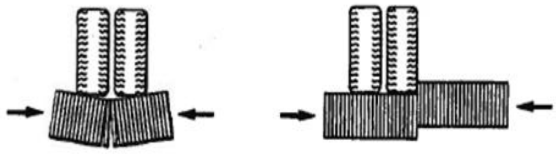

Figure 2 Failure modes for prestress to overcome

The prestress force needs to generate a compressive stress that is larger than the tensile stress from transverse bending moment. If this should not be the case, a gap between the planks or beams would occur and thus a decrease of the contact surface area would take place, see Figure 2 left. Secondly, the prestress must generate a friction stress between laminates larger than any shear stress generated by concentrated loads, e.g. car tyres, se Figure 2 right. The most important for the prestress is to make sure that these two failures described above never occur.

Normally SLT bridges in Sweden are manufactured using glulam beams made of Norway spruce timber. Glulam beams might have larger dimensions than sawn planks, and often also have a higher MOE than sawn planks. This will affect the ratio between E_x and the transverse modulus E_y as well as the ratio between E_x and the in-plane shear modulus G_{xy}. Another difference is that at the time of erection, glulam generally have more controlled and lower moisture content (MC) than sawn timber. The MC of the surfaces will significantly influence the overall behaviour of the SLT bridge.

In EN 1995-2:2004, values for E_y and G_{xy} are suggested to be 2% respectively 6% of E_x. These values are rather large when compared to other international research studies, especially the value of G_{xy} that in EN 1995-2:2004 is suggested to be 6% of E_x. Table 2 shows the results from several international studies conducted over the last two decades.

3 Orthotropic plate theory

Wood is an anisotropic material but the trunk of a tree consists of concentric cylindrical shells. If a small rectangular sample is cut out of a trunk with a pair of faces tangential to the annual rings this sample have three axes of symmetry. The three axes are parallel to the longitudinal, tangential and radial direction. All material parameters are generally expressed in these three directions. (Kollman, Wilfred, 1968)

A well known design model for a plate is Kirchhoff's theory for thin plates. However, to be able to use the model following assumptions, with some additions are to be made: (Szilard, 2004 and Ottosen, Petersson, 1992)

- Stress-strain relationship according to the generalized Hooke's law
- The thickness of the plate is small. At most one tenth of the width or length of the plate
- The transverse deflection is at most one tenth of the thickness
- Normal stress through the plate is neglected
- Plane stress state.

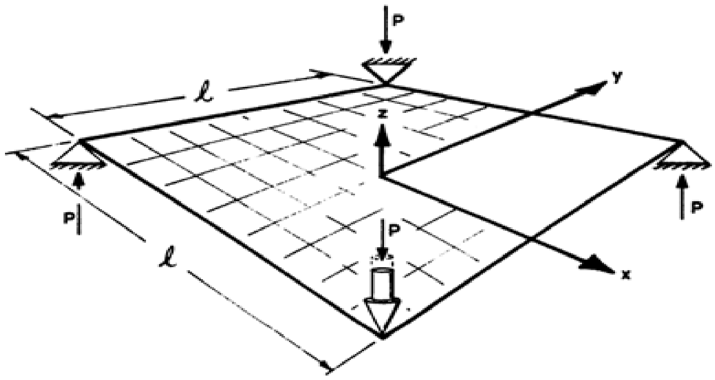

Figure 3 Adopted load and boundary scheme for pure twisting test with corner supports and patch load based on a Cartesian coordinate system with origin in the middle of the plate. (Tsai 1965)

The global directions for a plate are defined in Figure 3. *X* and *Y* are the two axes creating a plane with the direction *Z* perpendicular to this plane.

The differential equation of an orthotropic plate can be written as:

$$D_{11}\frac{\partial^4 w}{\partial x^4} + 2(D_{12} + 2D_{66})\frac{\partial^4 w}{\partial x^2 \partial y^2} + D_{22}\frac{\partial^4 w}{\partial y^4} - p_z = 0 \qquad \text{(Eq.1)}$$

Where: $D_{ij} = \frac{h^3}{12} \cdot C_{ij}^{-1}$

$$C_{11} = \frac{1-\upsilon_{xy}\upsilon_{yx}}{E_x} \qquad C_{12} = \frac{1-\upsilon_{xy}\upsilon_{yx}}{\upsilon_{xy}E_y} = \frac{1-\upsilon_{xy}\upsilon_{yx}}{\upsilon_{yx}E_x} \qquad C_{22} = \frac{1-\upsilon_{xy}\upsilon_{yx}}{E_y} \qquad C_{66} = \frac{1}{G_{xy}} \qquad p_z = 0$$

The general solution to the differential equation (Eq. 1) under uniform bending and twisting moments is:

$$w_z(x,y) = \frac{1}{h^3}(6M_x \cdot (C_{11}x^2 + C_{12}y^2) + 6M_y \cdot (C_{12}x^2 + C_{22}y^2) + 6M_{xy} \cdot (C_{66}xy) + ax + by + c)$$

(Eq. 2)

A test setup to obtain pure twisting of a plate is suggested by Tsai (1965). It consists of three fixed pinned corners and a fourth loaded corner. The pinned corners can rotate freely but cannot move in any lateral directions. The reaction forces in each of the three corners will be of the same magnitude as the applied load in the fourth corner, se Figure 3. This system will stabilize itself when loaded in one corner perpendicular to the plane of the plate. The following moments are generated as a result of a pure twisting test:

$$M_x = M_y = 0 \qquad M_{xy} = \frac{-P}{2}$$

The particular solution (Eq. 3) for the differential equation (Eq. 2) can be obtained if the load and boundary conditions at the supports are known.

$$w_z(0,0) = \frac{3Pl^2}{4h^3} \cdot C_G \qquad \text{Where:} \qquad C_G = C_{16} + C_{26} + C_{66} \qquad \text{(Eq. 3)}$$

For the case of a "0° plate" (notation according to Figure 4), $C_{16} + C_{26} = 0$ and $C_G = C_{66}$

$$G_{xy} = \frac{3Pl^2}{4h^3 w_{z,0^\circ}(0,0)} \quad \text{(Eq. 4)}$$

For the two cases of a "+45° plate" and a "-45° plate" (notation according to Figure 4), $C_{66} = 0$ and $C_G = 2(C_{22} - C_{12})$ respectively $C_G = 2(C_{11} - C_{12})$

$$E_y = \frac{1}{C_{12} + \dfrac{2h^3 w_{z,-45^\circ}(0,0)}{3Pl^2}} \quad \text{and} \quad C_{12} = \frac{1}{E_x} - \frac{2h^3 w_{z,+45^\circ}(0,0)}{3Pl^2} \quad \text{(Eqs. 5,6)}$$

Which one of these two equations that is to be used is depending on the orientation of the plate, i.e. if it is the "+45° plate" or "-45° plate". Testing the "+45° plate" will provide the deformation $w_{z,+45^\circ}$ in the middle of the plate. This deformation value together with a known value of E_x, results in a value for C_{12}, (Eq. 6). The deformation value for the "-45° plate" together with the value for C_{12} will result in a value for E_y (Eq. 5). (Szilard, 2004, Tsai, 1965 and Jónsson, Kruglowa, 2009).

4 Method

Three SLT plates were constructed from glulam beams. Those plates can be seen as three pieces of a SLT-deck with different directions of the main grain direction. Full scale glulam beams were chosen.

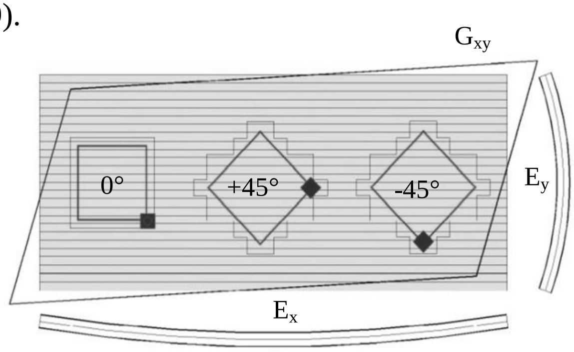

Figure 4 Test specimens seen as pieces of a SLT-deck. Plate names from left: 0°, +45°, -45°

4.1 Geometry and material for the test specimens

The dimensions of the glulam beams for the test specimens were 115x315x6000 mm³. All beams were initially tested for longitudinal MOE. A four-point load test was performed and compared with the results from dynamic testing. The beams had been stored in an indoor climate for a long time prior to testing and had a MC of about 9%. The beams were then cut into correct length and then placed in one of the three plates so the mean value of the longitudinal MOE in all three plates would be as similar as possible. The dimensions of the test specimens can be seen in Figure 5-6. The plates were prestressed to five different prestress levels. The prestressing bars were of commercial type *Dywidag* with a nominal diameter

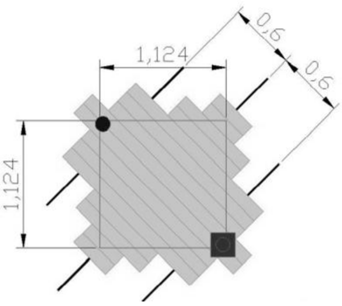

Figure 6 Geometry of "±45° plates"

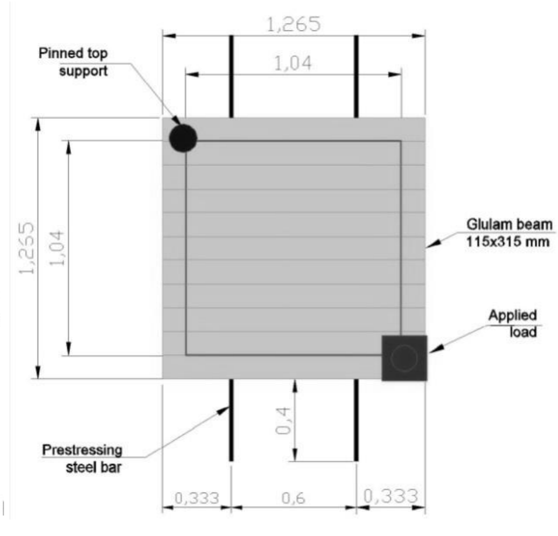

Figure 5 Geometry of "0° plate"

of 20mm, and characteristic yield strength of approximately 1100 MPa, see Figure 7.

The geometry of test specimens was chosen due to easy comparison with results from experiments performed in the development of Ritter's design guide (Oliva et al., 1990). Most design models for timber bridges are in some way based on Kirchhoff's theory of thin plates. Due to this fact, this theory was used for evaluation of experimental results even though the depth to length ratio could not be fulfilled. In order to reveal the effect of this ratio during testing the deflection of the loaded corner was limited to 1/20 of the thickness of the plate, instead of 1/10 suggested by Kirchhoff.

4.2 Setup for testing the decks

The three specimens were loaded at one corner with a hydraulic jack with a maximum capacity of 200 kN.

All four corners were equipped with load cells to record the applied load as well as the resulting reaction forces.

The load and reaction forces were distributed to the test specimens by a 200x200x25 mm³ steel plate. This was to avoid local deformations at the supports. The supports were free to rotate with steel balls between the load cell and the steel plate.

Figure 7 Test of "0° plate" with deflection measured in middle and in three corners.

The five different levels of prestressing were tested and these levels can be seen in Table 1. The prestressing bars were equipped with strain gauges monitoring the prestress.

The lateral deformations were recorded with linear variable differential transducers (LVDT) positioned in the middle of the plate, over the corners with supports on the bottom side and two of them in the loaded corner, see Figure 7.

5 Results

Static testing of the beams resulted in an average longitudinal MOE of 13.4 GPa. The dynamic measurements of the same material parameter gave a result of 14.0 GPa, which is a 4.5 % larger then the MOE obtained by static testing.

In Figure 8 the test results from the "0° plate" are shown. What can be noted in the figure is that the curves show a nearly bi-linear behaviour. For prestress levels PSL-3 and PSL-4 the test was stopped at a lower load level to prevent irreversible interlaminar slip. Prestress levels PSL-1, PSL-2 and PSL-5 resulted in irreversible slip.

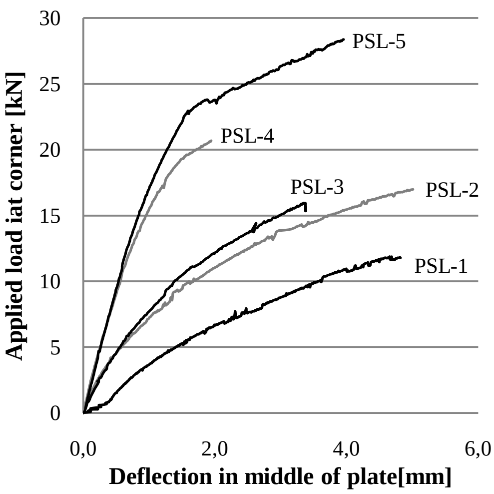

Figure 8 Load vs. deflection for different prestress levels (PSL), for "0° plate"

In Figure 9 the results for the “+45° plate” is shown and in Figure 10 the results for the ”-45° plate” is shown. Once again measurements for PSL-5 were recorded a bit longer than for the other PSL.

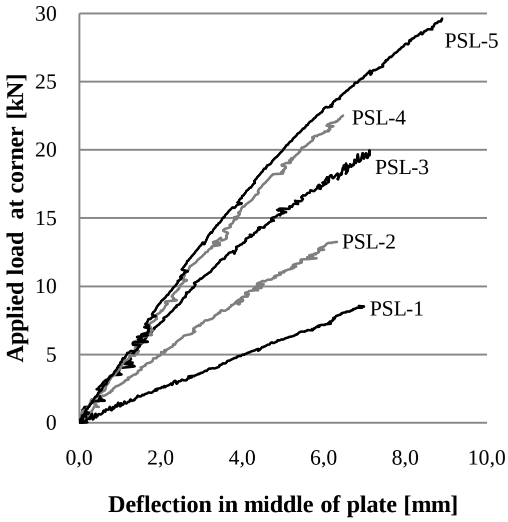

Figure 9 Load vs. deflection for different prestress levels (PSL), for ”+45° plate”

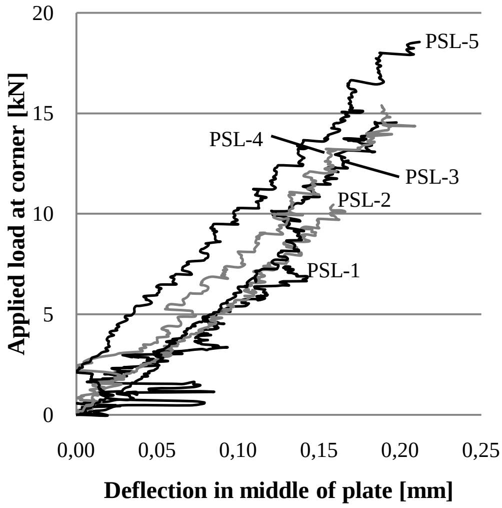

Figure 10 Load vs. deflection for different prestress levels (PSL), for ”-45° plate”

6 Analysis

In Figure 8, the rate of increase for the load decreases at different load levels. This is more evident at higher prestress levels. The explanation of this phenomenon can be that, at this load level, the shear stresses generated by the twisting moment are larger than the resisting shear stresses generated by compressive stresses due to prestress. Figure 11 illustrates how a rotating moment occurs between the laminates.

A prestress level of 0.91 MPa with a MC of 10% together with an assumed friction coefficient of 0.24-0.28 (Kalbitzer, 1999) gives interlaminar slip at a load level of F_A = 23.6 kN which is the point where the change of slope occurs, cf. PSL-5 in Figure 8.

Since the tests were deflection controlled, the deformation will keep increase while the stresses are being redistributed. The data of interest is the data up to interlaminar slip, which will act as the upper limit when evaluating the recorded data.

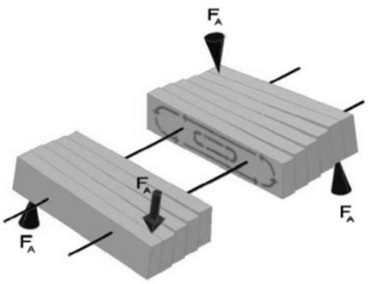

Figure 11 Rotating moment between laminates due to load and boundary conditions

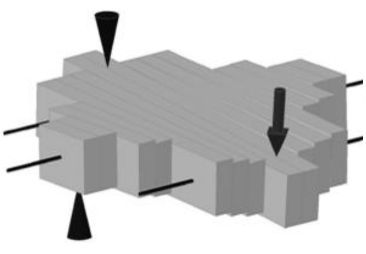

Figure 12 Exaggerated deformation shape for the ”+45° plate”

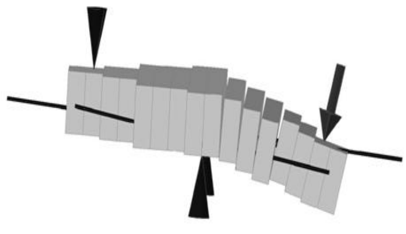

Figure 13 Exaggerated deformation shape for the ”-45° plate”

The result from the ”+45° plate” test (Figure 9) shows a nearly linear behaviour. The deformation of the plate is shown in Figure 12 with the stiff direction parallel to a line between the applied load and top support. This gives clear reading of the deflection in the middle of the plate. The data from this series is chosen in a similar way as for the ”0° plate”, where the resisting moment is calculated in the weakest shear plane.

Figure 10 shows that the deformations for the ”-45° plate” are very small. The LVDT used had a linear range of approximately 0.5% of 12.5 mm. This is the reason why the lines in Figure 10 fluctuate as they do. When load is applied, the plate will deform according to Figure 13, where the stiff direction of the plate is perpendicular to a line between the applied load and top boundary condition. This results in that the middle of the plate deforms little while the loaded corner is subjected to interlaminar shear stresses as well as transverse bending moment. The combined effect of shear stress and bending moment is hard to predict, so the chosen data is data between a load level of 4 and 8 kN. In that range the overall behaviour of all five prestress levels is nearly linear.

The results from the three tests where used in Equations 4, 5 and 6, together with the static value of E_x, to obtain values for E_y and G_{xy}. The obtained values are shown for each prestress level in Table 1.

Table 1 Results from twisting tests for different prestress levels

Notation of prestress levels (PSL)	Prestress level [MPa]	Results for *Gxy* [MPa]	*Gxy / Ex* [%]	Results for *Ey* [MPa]	*Ey / Ex* [%]
PSL-1	0.29	90	0.67	76	0.57
PSL-2	0.46	132	0.99	127	0.93
PSL-3	0.65	116	0.86	169	1.26
PSL-4	0.79	347	2.59	222	1.66
PSL-5	0.91	395	2.59	222	1.66

7 Discussion

7.1 Material parameters for orthotropic plate

Several studies have shown that influence of wood species, within softwood species, is not of great importance when determining material parameters for SLT-decks. When comparing European Pine with European Spruce there are close to no influence on the friction coefficient (Kalbitzer, 1999). It is also stated in a paper by Oliva et al. (1990) that the variation in results from three different softwood species was smaller than the variation in the results for one single species. Using a SLT-deck made up by glulam beams from Norway spruce should not significantly influence the test results.

One of the fundamental requirements for a SLT-deck to function as a plate is the ability to transfer stresses from one beam into neighbouring beams. This is depending on the friction between the laminates. A higher friction coefficient results in a better stress redistribution within the laminates. MC together with surface roughness has the largest influence on the friction coefficient up to a MC of about 19%. For MC above 19%, prestress has the largest influence.

The decks tested in this study had an approximate MC of 9% which is very low. Typical MC in glulam beams at time of assembly is 12-16%. According to Kalbitzer (1999) the friction coefficient would have been twice the value if the tested decks had a MC of about 14% instead of 9%. This would definitely influence both the values for E_y and G_{xy}. This is also considered in EN 1995-2:2004 where the friction coefficient for planed timber against planed timber is twice as high for a MC above 16% compared to a MC below 12%.

However, EN 1995-2:2004 does not take MC into account when determining the elastic properties E_y and G_{xy}.

According to Kollmann, F. P. & Côte, W. A. (1968) the longitudinal MOE is the least sensitive, out of all MOE's, to change in MC. The changes in MOE in both radial and tangential direction are significantly larger than the change in longitudinal direction when the MC is changing.

The large thickness of the tested plates may have caused that desired uniform deformation did not occur. The glulam beams where rather short in span compared to the height and this made the glulam beams very stiff.

A comparison is made for several international studies, see Table 2. Results from the experiments are presented at two different prestress levels to be able to make a clear comparison. The values for these two prestress levels are obtained with linear interpolation of the results.

Table 2 Comparison between different material parameters for SLT-decks

Source of origin / timber	E_y/E_x [%]	G_{xy}/E_x [%]	Reference prestress level [MPa]
Present study - glulam	1,4%	1,9%	0,70
Australian – sawn	1,5%	2,5%	0,70
Australian - planned	2,0%	3,0%	0,70
Oliva et al. (1990)	1,7%	1,7%	0,70
Davalos et al. (1996)	2,9%	4,6%	0,70
Dahl, K. (2006) - sawn	3.1%	4.2%	0,60
Present study - glulam	0,7%	0,6%	0,35
Ritter's Design Guide	1,3%	3,0%	0,35
EN 1995-2:2004 - sawn	1,5%	6,0%	0,35
EN 1995-2:2004 - planned	2,0%	6,0%	0,35
Oliva et al. (1990)	1,3%	1,3%	0,35
Davalos et al. (1996)	1,6%	3,3%	0,35
Canadian – high MOE	2,0%	3,5%	Unknown
Canadian – Low MOE	2,5%	5,5%	Unknown

7.2 Comparison of design models

Comparison of several design models and material parameters is performed by applying two concentrated forces of 50 kN each, representing a typical axle loading with a distance of 2 m, to a simply-supported rectangular plate with a span length of 10 m and plate width of 7 m. The load is positioned in the middle of the plate and 0.5 m from the edge of the plate. The concentrated force is distributed over an area of 200x200 mm². A value for E_x is assumed to be 13.5 GPa. The prestress is assumed to be at least 0.7 MPa. The plate is designed to fulfil the requirements of a deflection limitation of span/400. The orthotropic finite element analyses are made with 900 shell elements with orthotropic material parameters. Simplified analyses are performed for an effective width b_{eff} calculated according to respective simplified method.

Table 3 Comparison of three methods for simplified analysis to an orthotropic FE-model with two different material parameters input. Load is positioned either in the middle or close to the edge.

Notation of design method	Design method	Required deck thickness when loaded in middle [mm]	Percentage of DM-1 [%]	Required deck thickness when loaded at edge [mm]	Percentage of DM-1 [%]
DM-1	Orthotropic FEM, material parameters according to EN 1995-2:2004	240	100%	285	100%
DM-2	Orthotropic FEM, material parameters according to present study	250	104%	300	105%
DM-3	Simplified analysis according to EN 1995-2:2004	360	150%	360	126%
DM-4	Simplified analysis according to Ritter, M. (1990)	285	119%	285	100%
DM-5	Simplified analysis according to Crews, K. (2002)	280	117%	280	98%

The thickness of the plate will differ for the orthotropic plate model when the point load is placed close to the edge instead of in the middle. For the simplified analysis the thickness of the plate will remain the same independent of the load position.

There are several studies with comparisons between methods of simplified analysis that are indicating the same results, simplified analysis according to EN 1995-2:2004 is a very conservative method to use (Crews, 2006) (Dahl, 2006).

8 Conclusion

Material parameters for SLT-decks can be seen in Table 2 for different prestress levels. The test specimens were constructed out of glulam beams made from of Norway spruce with rather large dimensions. In EN 1995-2:2004, various MC in timber is considered for the coefficient of friction but not for material parameters for orthotropic plate theory. The influence of various MC requires more research to fully understand its influence on SLT-decks.

MC in the test specimens were about 9%, which affected the decks performance and influenced the capability of comparing with other studies. However, it might give an indication to behaviour of SLT bridges in extremely dry environments.

When comparing design methods, the influence of varying material parameters as input data to an orthotropic model only produced an approximate 5% difference between the high values suggested in EN 1995-2:2004 and low values obtained in this study. The difference between the simplified analysis suggested in EN 1995-2:2004 and design methods suggested by Ritter and Crews is approximately 25-35%.

The difference in required deck thickness between the two design-methods suggested in EN 1995-2:2004 is approximately 25-50%.

9 Acknowledgment

The experimental work was performed by the authors together with T. Kruglowa and G. Jónsson. For their work we are truly grateful.

This research work is a part of the research project 'Competitive Timber Bridges' which is financed by VINNOVA (Swedish institute for research and innovation for sustainable growth) together with representative from the glulam industries and some consultant companies in Sweden.

10 References

Comité Européen de Normalisation, CEN, (2004): *EN 1995-2:2004.* Eurocode 5 – Design of Timber Structures, Part 2 – Bridges, 2004.

Crews, K. (2002): *Behaviour and Critical Limit States of Transversely Laminated Timber Cellular Bridge Decks.* PhD Thesis, Faculty of Engineering, University of Technology, Sydney, Australia, 2002.

Crews, K. (2007): *Recommended procedures for determination of distribution widths in the design of stress laminated timber plate decks*. CIB – W18 Proceedings meeting thirty-nine, Florence, Italy, 2006

Dahl, K. (2002): *Tverrspente Dekker i Tre – Vurdering av aktuelle beregningsmetoder basert på fullkala forsøk* (Stress laminated timber decks – Evaluation of pressent calculation methods based on full scale testing, In Norwegian). Master's thesis, Norges Landbrukshøgskole, Trondheim, Norway, 2002.

Dahl, K., Bovim, N. I., Malo, K. A. (2006): *Evaluation of Stress Laminated Bridge Decks Based on Full Scale Tests*. 9th WCTE Timber Engineering Conference, Portland, Oregon, 2006.

Davalos, J., Sharma S., Shaki, S., Moody, R., Hernandez, R. (1996): *System Stiffness for Stress-Laminated Timber Bridge Decks.* International Wood Engineering Conference, Vol. 1, Sheraton New Orleans, Louisiana, 1996, pp. 213-220.

Jónsson, G. P., Kruglowa, T. (2009): *Determination of Design Values for Stress-Laminated Timber Decks.* Master's Thesis, Department of Structural Engineering, Chalmers University of Technology, Göteborg, Sweden, 2009.

Kalbitzer, T. (1999): *Experiments regarding the Coefficient of Friction between Laminations.* Master's Thesis, Technische Universität München, Munich, Germany, 1999.

Kollmann, F. P. & Côte, W. A. (1968): *Principles of Wood Science and Technology I: Solid Wood.* Springer-Verlag, Berlin Heidelberg, Germany, 1968.

Ohlsson, S., Perstorper, M. (1992): Elastic wood properties from dynamic tests and computer modelling. *Journal of Structural Engineering.* Vol.118, No. 10, 1992, pp. 2677-2690.

Oliva, M., Dimakis, A., Ritter, M., Tuomi, R. (1990): *Stress-laminated wood bridge decks: experimental and analytical evaluations.* United States Department of Agriculture, Forest Service, Forest Products Laboratory, FPL-RP-495, Madison, Wisconsin, 1990.

Ritter, M., (1990): *Timber Bridges – Design, Construction, Inspection and Maintenance.* United States Department of Agriculture, Forest Service, Washington DC, 1990.

Szilard, R. (2004): *Theory and Applications of Plate Analysis*. John Wiley & Sons, Hoboken, New Jersey, Canada, 2004.

Tsai, S. (1965): Experimental Determination of the Elastic Behavior of Orthotropic Plates. *Journal of Engineering for Industry*, Transactions of American Society of Mechanical Engineers, August 1965, pp. 315-318.

CIB-W18/42-15-1

INTERNATIONAL COUNCIL FOR RESEARCH AND INNOVATION
IN BUILDING AND CONSTRUCTION

WORKING COMMISSION W18 - TIMBER STRUCTURES

DESIGN ASPECTS ON ANCHORING THE BOTTOM RAIL IN PARTIALLY ANCHORED WOOD-FRAMED SHEAR WALLS

U A Girhammar
Department of TFE – Civil Engineering, Umeå University

B Källsner
School of Technology and Design, Växjö University
SP Wood Technology – Technical Research Institute of Sweden

SWEDEN

Presented by U A Girhammer

S. Aicher questioned from a practical point of view why a stiff steel plate was not used instead of washer as a cheap effective solution. U.A. Girhammar replied that the stiff steel plate is a safe option. S. Aicher asked why this was not calculated. U.A. Girhammar replied that an analytical study is underway and results will be available soon.
H.J. Larsen commented about the statement that design rules are needed and more research is also needed. He asked why you don't come up with design rules so that more research is not needed. U.A. Girhammar agreed that they will aim to achieve this.
B. Källsner stated that the use of a stiff steel plate is an economic question. S. Aicher stated that may be use of a small washer with a small stiff wood plate can also be done. B. Källsner said that this would not be common practice.
I. Smith commented that foundation is also important because the rigidity of the foundation will influence the performance such that a mechanistic based approach would be more difficult. U.A. Girhammar stated they have not yet addressed this issue.
B. Dujic stated that this failure mode is unrealistic because the influence of vertical stud acting as a restraint has been ignored. B. Källsner stated that in this situation the vertical stud will follow the sheathing material and there will be separation between the stud and the plate; therefore, its influence will be minimal.
B. Dujic and U.A. Girhammar also discussed the issue of the influence of the aspect ratio of the wall.
S. Winter commented that bolts are doweled to concrete with small edge distances; therefore, brittle failure mode in the concrete may occur. Also multi story building would need hold-downs to carry uplift and anchor bolts would carry racking forces. The subject of this paper is more suited for small simple building. B. Källsner said that concentrated forces can be more distributed without the hold-down devices which could be desirable.
H.J. Blass commented that we need a unified design method that can cover all cases and the plastic design is such a method.
C. Ni said that this issue has been identified in the Northridge Earthquake. In N. America we specify the use of large washer to achieve the desired safety. Minimum splitting strength is difficult to estimate and unreliable as annual ring orientation can come into play also. U.A. Girhammar agrees that annual ring orientation is important.
B.J. Yeh asked about the anchor bolt spacing as this is a two dimensional issue. In US no more than 40 mm o/c and washer size is 75 mm diameter minimum. U.A. Girhammar agrees and will study it.
S. Aicher stated that the spacing and diameter of nails are unrealistic. This will be problematic because it is not practical to convert results to reality. U.A. Girhammar stated that the experiment was designed to force the desire mode of failure so that we can measure the splitting strength.
B. Källsner provided a comment towards H.J. Larsen's question that a simple solution is not apparent because the situation is more complex.

Design aspects on anchoring the bottom rail in partially anchored wood-framed shear walls

Ulf Arne Girhammar
Department of TFE – Civil Engineering, Faculty of Science and Technology,
Umeå University, Sweden

Bo Källsner
School of Technology and Design, Växjö University, Sweden
SP Wood Technology – Technical Research Institute of Sweden

Abstract

A plastic design method capable of analyzing the load-bearing capacity of partially anchored wood-framed shear walls has been developed by the authors. In such walls the leading stud is not fully anchored against uplift and corresponding tying down forces are developed in the sheathing-to-framing joints along the bottom rail. These joint forces will introduce crosswise bending of the bottom rail with possible splitting failure along the bottom of the rail in line with the anchor bolts. If the bottom rail fails in a brittle manner, the applicability of the plastic method can be questioned. Therefore, design recommendations with respect to the bottom rail need to be given as prerequisites for using the plastic method.

This paper deals with the design of the anchor bolts needed to tie down the bottom rail properly and to eliminate any possible brittle failure modes. It describes the experimental results for sheathed bottom rails of different designs subjected to vertical uplift forces. The effect of different washer sizes and location of the anchor bolts in the width direction on the failure load due to splitting of the bottom rail is presented. The experimental results indicate that the decisive design parameter is the distance from the edge of the washer to the loaded edge of the bottom rail.

1 Introduction

1.1 Background

The authors have at previous CIB-W18 meetings presented a series of papers dealing with a new plastic analysis and design method for light-frame timber shear walls [1]. The method is capable of analyzing the load-bearing capacity of partially anchored shear walls. In a partially anchored shear wall the leading stud is not fully anchored against uplift and corresponding tying down forces are developed in the sheathing-to-framing joints along the bottom rail in the sheathing segments near the leading stud. These tying down forces in the joints will introduce crosswise bending of the bottom rail with possible splitting failure along the bottom of the rail. Also, other failure modes or serviceability problems may occur in the bottom rail.

If the bottom rail fails in a brittle manner, the applicability of the plastic method can be questioned. Therefore, design recommendations with respect to the bottom rail need to be given as prerequisites for using the plastic method. This paper deals with the requirements on and the design of the anchor bolts needed to tie down the bottom rail properly and to eliminate any possible brittle failure modes. It focuses on trying out the proper design of washers or clamping plates for the anchor bolts in the bottom rail in order to eliminate different kinds of splitting failures. This work was conducted in order to present design values in a Swedish handbook for the design of light-frame timber shear walls based on the plastic design method [12].

1.2 Objective and scope

The overall purpose of the research project is to develop a plastic method for the design of wood-framed shear walls in the ultimate limit state with different anchoring, loading and geometrical conditions and with different sheet and framing materials, and fasteners used. The aim is also to evaluate the bounds of applicability and determine the needed restrictions in order for the plastic method to work. For proper application of the plastic method it is necessary to ensure ductile behaviour of the sheathing-to-framing joints and to avoid brittle failure of the bottom rail in particular.

The objective of this paper is to present the experimental results for sheathed bottom rails in light-frame timber shear walls of different geometrical configurations with respect to the anchor bolts and, based on the evaluation of these test results, to present an empirical expression for the load-carrying capacity of these anchored bottom rails.

The strength of the bottom rail is studied by varying the size of the washers for the anchor bolts and the position of them along the width of the bottom rail. All washers used in this study are rigid (thick plates). Both specimens with double and single sided sheathing are tested.

2 Actions on the bottom rail

2.1 General

The difference between fully and partially anchored shear walls is illustrated in Figure 1. In the first case, the uplift of the shear wall is prevented fully by some kind of a tying down device at the leading stud resulting in a concentrated force at the end of the wall (Figure 1a). The notation fully anchored means that there is no uplift of the studs of the wall, especially of the leading stud. In the case of partially anchored shear walls, the sheathing-to-framing joints along the bottom rail will counteract the uplift of the wall (Figure 1b). In the latter case, there is some uplift of the studs of the wall. In general, the anchor bolts are always subjected to shear forces, and in the case of partially anchored shear walls, also to tensile forces.

It is important that no brittle failure of the bottom rail occurs in order to enable the development of the force distribution shown in Figure 1b. The load-carrying capacity of the shear wall needs to be attained before any failure of the bottom rail is initiated. Unfortunately, different kinds of failure modes may develop in the bottom rail under this type of anchoring.

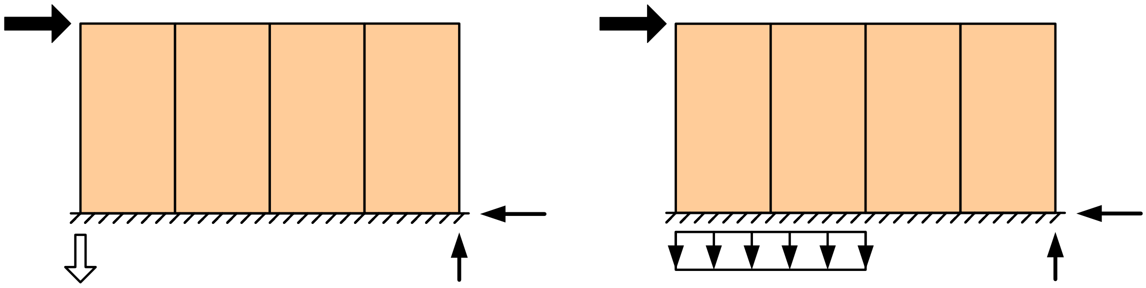

(a) (b)

Figure 1. Two principal ways to anchor wood-framed shear walls subjected to horizontal loading: (a) fully anchored shear wall – a concentrated anchoring of the leading stud; and (b) partially anchored shear wall – a distributed anchoring of the bottom rail.

2.2 Failure modes of the bottom rail

Due to the uplifting forces in the sheets at the sides of the bottom rail, the following failure modes for the rail are most critical:

(1) Splitting failure along the bottom of the rail due to crosswise or transverse bending and tension stresses perpendicular to the grain (cupping of the bottom rail), Figure 2. Note the increased tensile forces in the bolts due to prying action in case of one-sided sheathing.

(2) Splitting failure along the side of the bottom rail in line with the fasteners between the sheathing and the bottom rail due to vertical shear forces generated by the fasteners, Figure 3. This failure mode may occur when small distances between the fasteners are used.

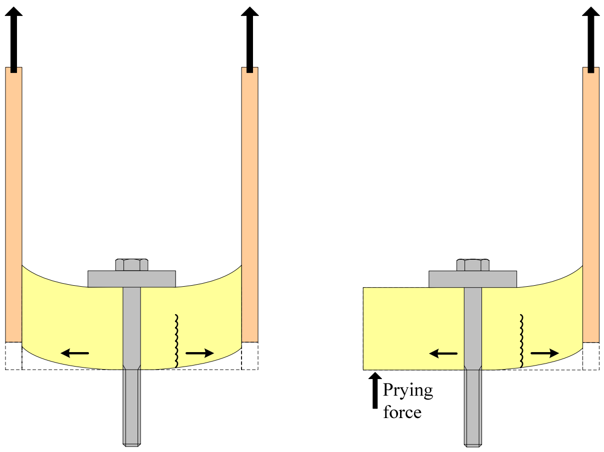

(a) (b)

Fig. 2. Crosswise bending of the bottom rail introducing tension perpendicular to grain and splitting failure along the bottom of the rail (cupping of the bottom rail): (a) two-sided sheathing and (b) one-sided sheathing including prying action (schematic figure).

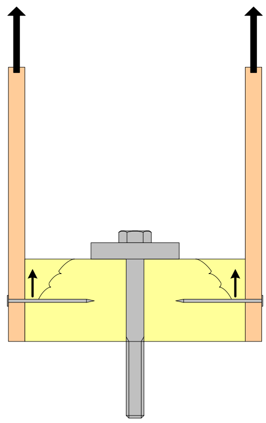

Fig. 3. Vertical shear forces causing splitting failure at the side of the bottom rail in line of the sheathing-to-framing fasteners (schematic figure).

Other failure modes or serviceability problems for the bottom rail that need to be addressed are:

(3) Large deformations with respect to punching or crushing of the bolt head or washer through or into the bottom rail due to the tensile forces in the bolts, Figure 4.

(4) Large deformations with respect to lengthwise bending of the bottom rail due to the uplifting forces in the sheathing-to-framing joints between the anchor bolts, Figure 5.

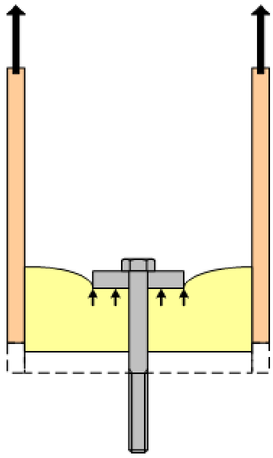

Fig. 4. Plastic compression of wood perpendicular to grain causing large deformations or, in exceptional cases, punching failure (schematic figure).

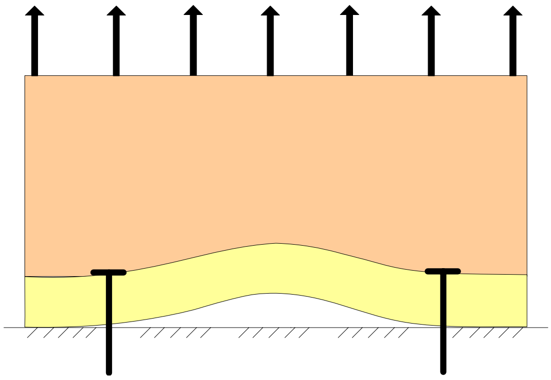

Fig. 5. Lengthwise bending of the bottom rail due to uplift at the end of the shear wall causing large deformations along the bottom rail (schematic figure).

The first two failure modes are the most severe ones. The last two modes will seldom lead to failure in the regular sense. The effect of plastic compression or punching according to Figure 4 and lengthwise bending according to Figure 5 will not be discussed in this paper.

The main parameters that are decisive for these failure modes are the size of the washers, the location of the anchor bolts in the width direction of the bottom rail, and the centre distances of the anchor bolts and sheathing-to-framing fasteners in the bottom rail.

3 Background on anchoring of bottom rail

3.1 General

Eurocode 5 gives two simplified calculation methods A and B to determine the load-carrying capacity of shear walls. As an alternative to these methods, testing according to the European Standard EN 594 [2] may be used to determine the racking resistance. This standard does not require that the leading stud should be tied down and, therefore, the shear wall tested will experience uplift at the loaded end. Thus, the bottom rail will be subjected to uplift and the design of the anchor bolts for the bottom rail will become important. This is also true for method B.

The EN 594 standard prescribes that the bottom rail may be fixed in a manner so that the bottom rail is restrained from sliding, rotating and cupping under uplift forces in order to provide an upper bound datum such that the maximum racking capacity of the panel and its components can be tested. Holding down bolts, two in each segment (distance between the first anchor bolt and the end of the wall, 150 mm; centre distance of anchor bolts, 600 mm), are normally used with large washers (50 mm diameter or equivalent is recommended for use with 90 mm wide framing timber) and shall be tightened until the washers start to penetrate the bottom rail. Other forms of fixing may also be used and where washers are not appropriate the fixings may be increased to provide equivalent resistance and spread across the width of the rail if necessary to reduce cupping forces. Where the maximum racking capacity of the panel is being tested the fixings should be the equivalent of those mentioned above. In the latter case there is a higher risk that the racking capacity may be restricted by the base fixings used.

3.2 Previous research

Prion and Lam [3] pointed out the fact that when designing shear walls, it is important to understand the differences between hold downs and anchor bolts. Anchor bolts provide horizontal shear continuity between the bottom rail and the foundation. They are not designed to transmit vertical forces to the foundation, although some capacity can be achieved, if necessary. In this case, the bottom row of nails transmits the vertical forces in the sheathing to the bottom rail (instead of the vertical end stud) where the anchor bolts will further transmit the forces into the foundation. Because of the eccentric load transfer, transverse bending is created in the bottom rail and splitting often occurs. To prevent such a brittle failure mode, large washers (preferably square or rectangular) need to be provided to affect the eccentric load transfer from the sheathing through the nails, into the bottom rail to the anchor and foundation. Hold downs, on the other hand, directly connect the vertical end stud to the foundation. Because of the large concentrated forces, these hold downs are substantially larger than anchor bolts. As failure of the hold downs often occurs in a brittle manner, capacity design principles need to be employed to ensure that the wall fails in shear along the its nail connectors before any of the hold downs connections fail. When no hold downs are provided, the vertical restraint is provided by the anchor bolts, by a transverse wall that is attached to the end stud, or by vertical loads on the wall from an upper storey or roof. In the case of anchor bolts providing uplift resistance, the vertical anchor forces are carried by a number of nails along the bottom rail, which are thus deemed ineffective for the transfer of horizontal shear forces. Such a shear wall will thus have a reduced shear capacity.

Ni and Karacabeyli [4] presented two methods – one empirical and one mechanics-based – to account for the partial uplift when no hold down connections are used. They point out that in most design codes, lateral load capacities for shear walls are given for walls which are fully restrained against overturning by means of hold-down (or tie-down) connections. Hold-down connections, on the other hand, are not always used in conventional wood-frame construction, particularly at the end of wall segments near openings. Dead loads and perpendicular walls or corner framing, for example, at the end of shear wall segments may help reduce uplift forces to be resisted by hold-down connectors. For an end stud in tension without hold-down connection, the force is resisted by the nail joints attaching the edge of the panel to the bottom rail. The force is then further transferred via the anchorage on the bottom rail to the supporting structure. In their tests, the bottom rails of the walls were attached to the foundation through 12.7 mm diameter anchor bolts spaced at 406 mm on centre. The distance between the centre of the first anchor bolt and the outer edge of the wall was 203 mm. They did not seem to experience any failure of the bottom rails during the experiments, indicating that their design of the anchorage of the bottom rail was sufficient.

Experimental work devoted to the specific question of anchoring the bottom rail with respect to both shear and tensile forces are very scarce. Hirai and Namura et al. [5-8] studied the lateral (shear) resistance of anchor-bolt joints between bottom rails and foundations. Leitch et al. [9] noted the importance of a robust bottom rail connection and its ability to offer secure anchorage. They discussed the need for the anchorage to be able to ensure that both applied lateral (shear) and overturning forces are transferred safely to the foundation, but they conducted tests only on the lateral resistance of timber-to-concrete dowel type connections used in timber platform frame.

Duchateau [10] studied the uplift resistance of bottom rails in wood shear walls without hold-downs. Field observations following extreme earthquake events and laboratory testing had identified a key area to improve upon in wood-frame shear walls as maintaining bottom rail structural integrity. Due to current load paths through the bottom rail when resisting overturning, coupled by construction misalignment, traditional bottom rail designs split along the line of anchor bolts and lose lateral resistance. She conducted an experimental study on a new type of bottom rail in wood shear walls (hollow core bottom rails made of durable wood thermoplastic composites).

Yeh and Williamson [11] presented an experimental study on the combined shear and uplift resistance of wood structural panel shear walls. These kinds of shear walls have been used to resist combined shear and wind uplift forces for many years in the U.S. Full-scale combined shear and uplift tests were conducted showing that the cross-grain bending of the bottom rail, which is a brittle failure mode, could be avoided by using 75 × 75 × 6 mm plate washers with anchor bolts (16 mm diameter anchor bolts spaced at 400 mm on centre; 38 × 88 mm bottom rail). These tests were conducted in lateral shear and tension (uplift) separately, and the effect of combined shear and uplift was evaluated based on an engineering analysis. However, full-scale combined shear and wind uplift tests were also conducted to gather more data on this subject. The test setup was capable of increasing the shear and wind uplift forces simultaneously until failure was reached by using a pulley system controlling the bi-axial forces in both lateral and vertical directions. Results of the study were used to support the development of engineering standards and changes to the national building code in the U.S. Also, tests were conducted using another combined shear and wind uplift test equipment that was capable of bi-axial loading in both lateral and vertical directions with independent but synchronized loading mechanisms. The vertical load can be applied as either an uplift force or a downward gravity load.

A major concern is the possible cross-grain bending of the bottom rail due to the non-concentric uplift forces acting on one face of the wall. This cross-grain bending can split the bottom rail, usually 38 × 88 mm timber, and the design value for this property is unavailable in the code. In one test series 16 mm anchor bolts and 75 × 75 × 3 mm or 75 × 75 × 6 mm plate washers at 400 mm on centre were used. For all tests 38 × 88 mm studs at 400 mm on centre, 11/12 mm OSB sheathing, and 3.3/3.8 × 64/76 mm common nails at 100/150 mm (300 mm on intermediate studs) on centre were used. Among all bi-axial tests, one failed as a result of cross-bending failure on the bottom rail of the wall due to the use thin 3 mm plate washers. When the thicker 6 mm plate washers were used, the plate washers did not bend and there was no cross-grain bending failure on the wall bottom rail.

4 Testing program

4.1 Specification of bottom rails tested

Tests on sheathed bottom rails subjected to vertical uplifting forces were conducted with different sizes of washers and locations of anchor bolts and with single or double sided load application. The testing arrangements are shown in Figure 6. Only 600 mm centre distance between the two anchor bolts was used in this study.

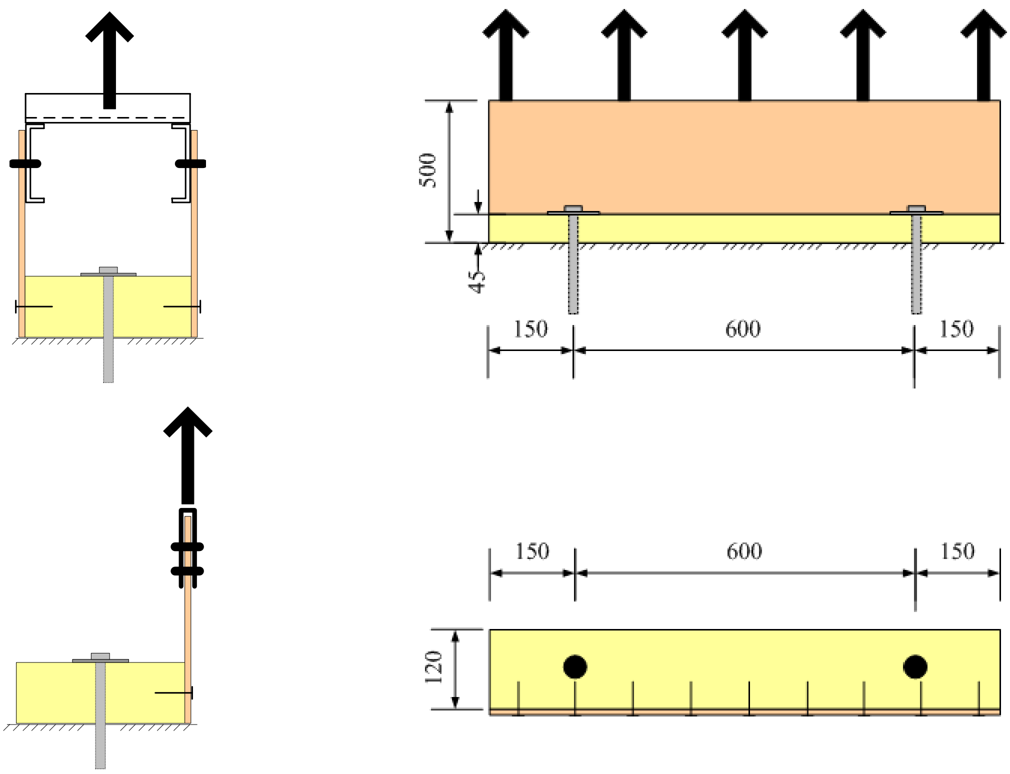

Figure 6. Testing of splitting of sheathed bottom rails subjected to single and double sided vertical uplift (schematic figures).

The different tests for series 1-4 are summarized in Table 1.

Table 1. Specifications of bottom rails tested. Only rigid (thick) washers were used. The clamping moment for the washers was 40 Nm.

Series	Configuration	Anchor bolt position	Size of washers [mm]	Number of tests
1	Double sheathing	Centre 60 mm from sheathing	# 40 × 15 # 60 × 15 80 × 70 × 15 100 × 70 × 15	10[1)]
2	Single sheathing	Centre 60 mm from sheathing	# 40 × 15 # 60 × 15 80 × 70 × 15 100 × 70 × 15	10[1)]
3	Single sheathing	3/8 point 45 mm from sheathing	# 40 × 15 # 60 × 15 80 × 70 × 15	10[1)]
4	Single sheathing	1/4 point 30 mm from sheathing	# 40 × 15 # 60 × 15	10[1)]

1) 8 specimens with the pith downwards and 2 specimens with the pith upwards. No distinction is made between the two cases in this study.

4.2 Test specimens and testing procedure

For all test specimens, the sheathing was fastened to the bottom rails with mechanical fasteners. Both single and double sided sheathing were tested. The details of the test specimens were as follows:

- Bottom rail: Pine (Pinus Silvestris), C24, 45×120 mm. As far as possible, pith-cut timber was used. In most test specimens the pith was oriented downwards against the supporting structure; in a few specimens of each series the pith was turned upwards.
- Sheathing: Hardboard, C40, 8 mm (wet process fibre board, HB.HLA2, Masonite AB).
- Sheathing-to-timber joints: Annular ringed shank nails, 50×2.1 mm (Duofast, Nordisk Kartro AB). The joints were hand-nailed and the holes were pre-drilled, 1.7 mm. Nail spacing was 25 mm or 50 mm. Edge distance was 22.5 mm along the bottom rails. The aim was to use over-strong joints.
- Anchor bolt: ϕ 12 (M12). The holes in the bottom rails were pre-drilled, 14 mm.

All tests were performed under displacement control with a constant rate of 2 mm/min. The vertical load was applied as a tension force along the sheathing. The bottom rails and sheathing of the specimens were not conditioned, but taken from the same respective batches.

For each test specimen, the density and moisture content of the bottom rail were determined.

5 Test results and evaluation

The results of the different test series are summarized in Table 2. A brittle type of failure by splitting of the bottom of the rail was the typical failure mode, see Figure 7a. In a few tests when large washers were used, splitting failure of the side of the bottom rail along the sheathing-to-framing fasteners took place, see Figure 7b.

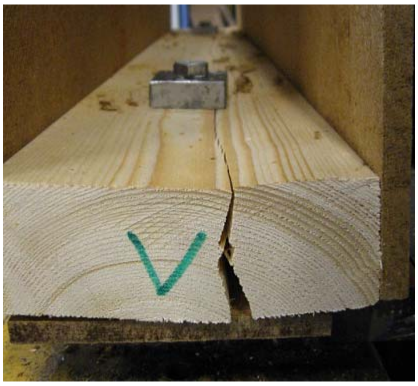
(a)


(b)

Figure 7. (a) Splitting failure along the bottom of the rail due to crosswise bending; (b) Splitting failure of the side of the rail along the sheathing-to-framing fasteners.

The test results in Table 2 are illustrated in Figures 8-11. The failure load versus the size of the washers is shown in Figure 8. The various test results for single and double sided sheathing and for the various locations of the anchor bolts are shown. Linear relationships between the failure load and the size of the washer are illustrated in the figure.

Table 2. Test results for bottom rails subjected to vertical uplift forces. The failure load F_{split} corresponds to the load at which splitting occurs due to crosswise bending (in most cases) or due to the sheathing-to-framing joints (for large washers). In the last three columns, the plus/minus standard deviation is given for the different test series.

Series	Size of washers [mm]	Distance from washer edge to loaded edge of bottom rail [mm]	F_{split} [kN]	Dry density [kg/m^3]	Moisture content [%]
1	40	40	22.1 ± 1.4	395 ± 28	13.1 ± 0.8
	60	30	28.4 ± 2.7	399 ± 08	11.8 ± 0.8
	80	20	36.2 ± 5.9	382 ± 55	12.4 ± 1.0
	100	10	39.7 ± 3.6	371 ± 31	13.3 ± 0.5
2	40	40	12.1 ± 1.6	413 ± 22	13.3 ± 0.8
	60	30	12.9 ± 2.4	370 ± 18	12.5 ± 0.7
	80	20	17.2 ± 2.4	377 ± 14	12.9 ± 0.2
	100	10	22.7 ± 4.2	398 ± 22	12.6 ± 0.8
3	40	25	16.9 ± 2.7	424 ± 27	13.1 ± 0.6
	60	15	19.9 ± 2.9	391 ± 26	12.6 ± 0.5
	80	5	25.8 ± 2.8	420 ± 08	13.4 ± 0.4
4	40	10	21.4 ± 3.0	344 ± 39	12.5 ± 0.7
	60	0	28.9 ± 1.9	419 ± 35	13.1 ± 0.7

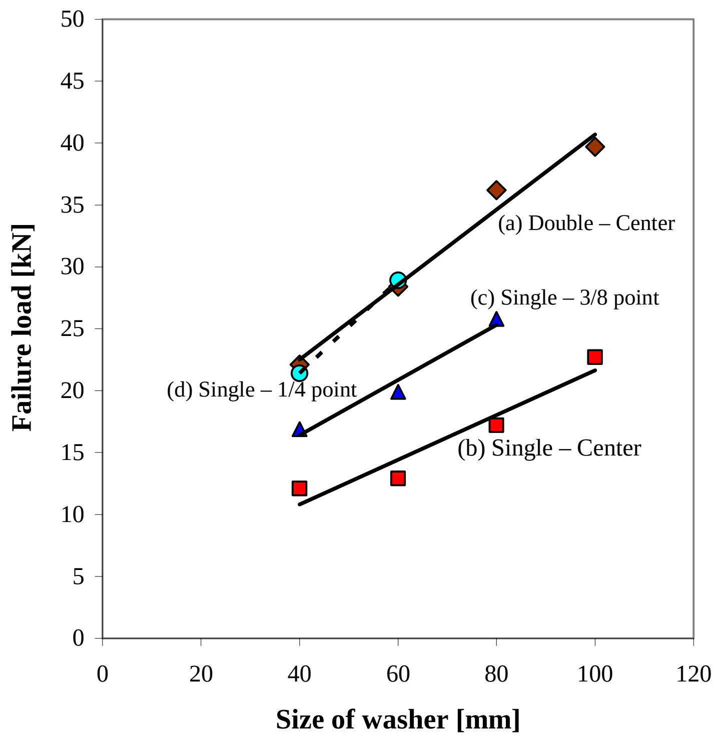

Figure 8. Failure load versus size of washers with respect to anchoring of bottom rails in shear walls with double sheathing and (a) centre location of anchor bolts; and with single sheathing and (b) centre location (60 mm from edge); (c) 3/8 point location (45 mm from edge); and (d) 1/4 point location (30 mm from edge) of the anchor bolts.

The mean values of the failure load versus the distance from the edge of the washer to the loaded edge of the bottom rail are shown in Figure 9. The test results for single sided sheathing with the three locations of the anchor bolts are given in the diagram. A corresponding diagram where all the test data are shown is given in Figure 10. In these figures, an exponential relationship between the failure load and the edge distance is illustrated.

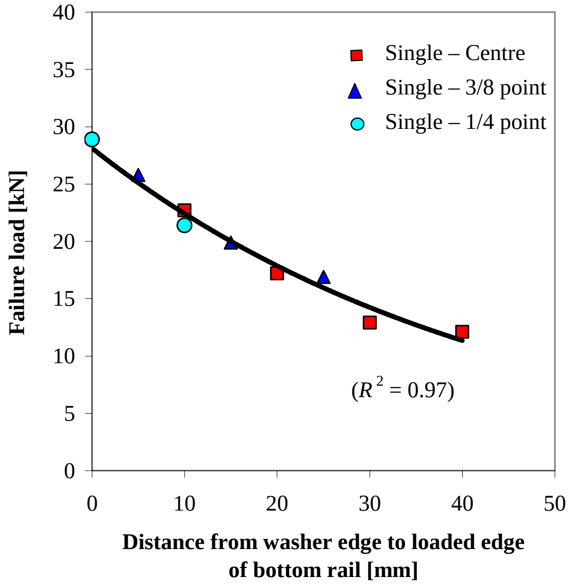

Fig. 9. *Mean values of the failure load versus distance from washer edge to loaded edge of bottom rail. For details, see Figure 8.*

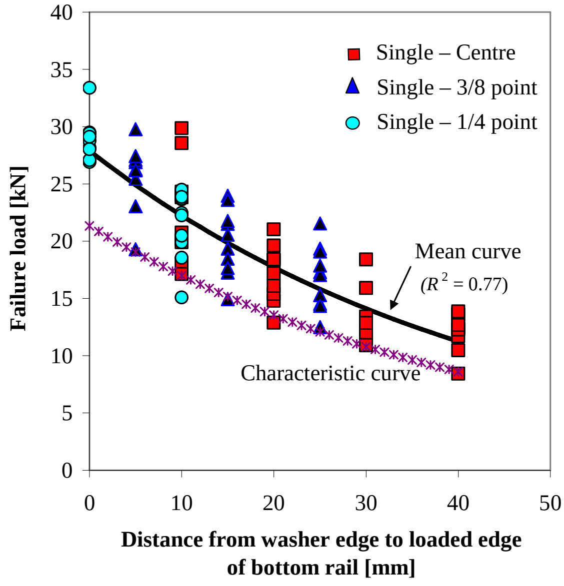

Fig. 10. *Individual test values for the failure load versus distance from washer edge to loaded edge of bottom rail. For details, see Figure 8.*

The empirical relationship for the mean value of the load-carrying capacity (F_{mean}) versus the distance from the washer edge to the loaded edge of the bottom rail (a_{edge}) in Figure 10 is given by

$$F_{\mathrm{mean}} \leq 27.9\,\mathrm{e}^{-0{,}0227 a_{\mathrm{edge}}} \quad [\mathrm{kN}] \tag{1}$$

According to Figure 2, for single sided sheathing the uplifting force is half of that for double sided sheathing, if the prying force is assumed to be located at the edge of the bottom rail. The relative failure load defined as

$$\text{Relative failure load} = \frac{F_{\mathrm{split}}(\text{Double sheathing - bolt located at centre})}{F_{\mathrm{split}}(\text{Single sheathing - bolt located at centre})} \tag{2}$$

is shown in Figure 11. It is evident that the relative failure load is approximately two, i.e. the force in the anchor bolts will be the same in both cases of single and double sided sheathing. This fact needs to be accounted for in the design of the anchor bolts. The tension stresses at the bottom of the rail will also approximately be the same in both cases.

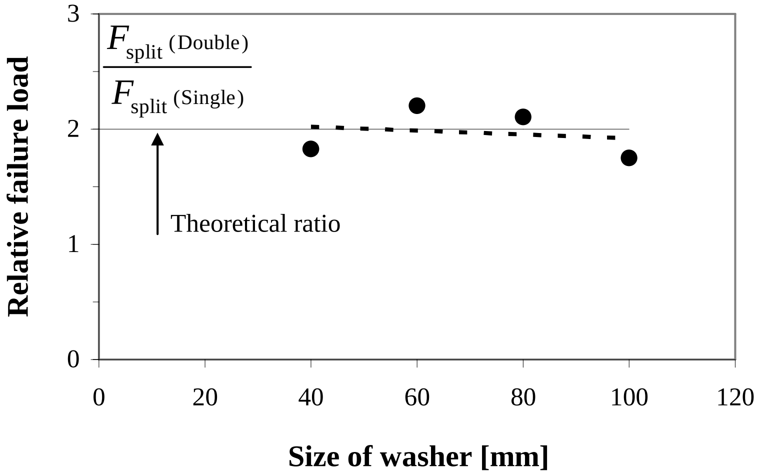

Figure 11. Relative failure load versus size of washer with respect to anchoring of bottom rails in shear walls. Relative failure load, see Equation (2); solid line denotes the theoretical ratio and dashed line the trend curve for the experimental results.

In a general case, the forces in each sheet are unequal and the anchor bolts are located eccentrically in the bottom rail according to Figure 12. In the figure and Equation (3), the uplifting forces are shown as characteristic (k) forces per unit length ($q_{i,\mathrm{k}}$) (distributed over the length 0.9 m according to Figure 6). Both uplifting forces must fulfil the condition according to Equation (3). If those distributed uplifting forces do not maintain equilibrium with respect to the anchor bolt, a prying compression force occurs between the bottom rail and the foundation that results in additional tension forces in the anchor bolt. If the prying force is assumed to act at the very edge of the bottom rail, the resulting tensile force in the anchor bolt ($F_{\mathrm{anchor,k}}$) is given by Equation (4), where s_{anchor} is the centre distance between the anchor bolts.

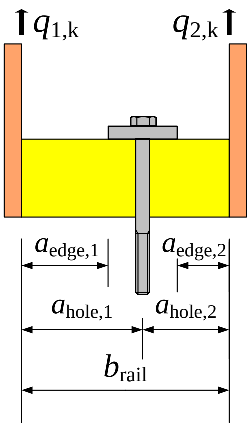

$$q_{i,\mathrm{k}} = 23.7\ \mathrm{e}^{-0{,}0227\, a_{\mathrm{edge},i}} \ \ [\mathrm{kN/m}] \tag{3}$$

$$F_{\mathrm{anchor,k}} = \begin{cases} \dfrac{b_{\mathrm{rail}}}{a_{\mathrm{hole,1}}} q_{2,\mathrm{k}} s_{\mathrm{anchor}} & \text{if } q_{2,\mathrm{k}} a_{\mathrm{hole,2}} \geq q_{1,\mathrm{k}} a_{\mathrm{hole,1}} \\ \dfrac{b_{\mathrm{rail}}}{a_{\mathrm{hole,2}}} q_{1,\mathrm{k}} s_{\mathrm{anchor}} & \text{if } q_{1,\mathrm{k}} a_{\mathrm{hole,1}} \geq q_{2,\mathrm{k}} a_{\mathrm{hole,2}} \end{cases} \tag{4}$$

Figure 12. An eccentrically anchored bottom rail subjected to distributed uplifting forces $q_{i,k}$. Various distances are defined. The centre distance between anchor bolts is s_{anchor}. The distributed forces $q_{i,k}$ are applied in line with the shear planes of the sheathing-to-framing joints.

Note that if the anchor bolt is centrically located in the bottom rail, the tensile force in the anchor bolt will become equal in both cases of single and double sided sheathing. In case of single sided sheathing, the tensile force can be decreased by locating the anchor bolt eccentrically in the bottom rail.

It should be pointed out that a more close evaluation of the test results are needed, especially with respect to the different failure modes, annual ring orientation, and possible initial cracking of the bottom rail when clamping it to the foundation due to initial cupping or twisting of the bottom rail. The influence of the width and thickness on the load-carrying capacity of the bottom rail also needs to be addressed for a more conclusive evaluation.

No theoretical models for determining the load-carrying capacity for the different failure modes are given here. A fracture mechanics study is underway.

6 Code implications

When partially anchored shear walls are used, it is necessary to specify the design of the anchoring of the bottom rail. Eurocode 5 does not give any recommendations concerning these things. The testing standard EN 594 recommends that washers of 50 mm diameter should be used for a 90 mm wide and 38 mm thick framing. For other widths and thicknesses of the timber framing, recommendations are needed in Eurocode 5.

This study shows the importance of establishing design rules with respect to splitting failure of the bottom rail. It indicates that there is a clear relationship between the failure load versus the distance from the edge of the washer to the loaded edge of the bottom rail. This distance seems to be the decisive design parameter for the determination of the minimum size of the washers in order to avoid splitting of the bottom rail.

7 Conclusions

The tests indicate that

- the failure load of the bottom rail increases with decreasing distance from the edge of the washer to the loaded edge of the bottom rail, regardless of the location of the anchor bolts in case of single sided sheathing; and
- the failure load of the bottom rail for double sided sheathing and centre location of the anchor bolts is twice that of single sided sheathing.

The present study needs to be extended to include theoretical modelling of the load-carrying capacity of the bottom rail and a parameter study of the influencing factors.

Acknowledgements

The authors express sincere appreciation to Henrik Juto, B.Sc., Umeå University, for conducting the experiments and to the Regional Council of Västerbotten, the County Administrative Board of Västerbotten and The European Union’s Structural Funds – The Regional Fund for their financial support.

References

[1] Källsner B., and Girhammar U.A. Plastic design of partially anchored wood-framed wall diaphragms with and without openings, Proceedings CIB-W18 Meeting, Karlsruhe, Germany, Paper 38-15-7, 2005.

[2] European Standard EN 594: Timber structures – Test methods – Racking strength and stiffness of timber frame wall panels. European Committee for Standardisation (CEN), CEN/TC 124, prEN 594:2006, Brussels, 2006.

[3] Prion, H.G.L. and Lam, F. Shear walls and diaphragms – Chapter 20, pp. 383-408. In: Timber Engineering. Edited by S. Thelandersson and H.J. Larsen, John Wiley & Sons Ltd, Chichester, England 2003.

[4] Ni, C. and Karacabeyli, E. Capacity of shear wall segments without hold-downs. Wood Design Focus, Vol. 12, No. 2, pp. 10-17, 2002.

[5] Hirai, T., Namura, K., Yanaga, K., Sasaki, Y., and Koizumi, A. Design lateral resistance of rows of anchor-bolt joints. Proceedings of the 8th World Conference on Timber Engineering, Vol. IIIa, pp. 251-254, Lahti, Finland 2004.

[6] Namura, K., Yanaga, K., Sasaki, Y., Koizumi, A., and Hirai, T. Lateral resistance of anchor-bolt joints between timber-sills and foundations – I. Single-shear tests of anchor-bolt joints of Japanese post and beam constructions. Mokuzai Gakkaishi, Vol. 51, No. 2, p. 110-117, 2005 (in Japanese).

[7] Hirai, T., Namura, K., Yanaga, K., Koizumi, A. and Tsujino, T. Lateral resistance of anchor-bolt joints between timber sills and foundations – II. Effective lateral resistance of multiple anchor-bolt joints. Journal of Wood Science, Vol. 52, No. 2, p. 1-6, 2006.

[8] Hirai, T., Namura, K., Kimura, T., Tsujino, T., and Koizumi, A. Lateral resistance of anchor-bolt joints between timber sills and foundations – III. numerical simulations of the effect of sill thickness on the effective lateral resistance of multiple anchor-bolt joints. Journal of Wood Science (2006) 52:295-301.

[9] Leitch, K., Hairstans, R., Abbott, D., Dodyk, R., and McAndrew, S. Experimental study of timber-to-concrete dowel type connections used in timber platform frame. Proceedings of the 10th World Conference on Timber Engineering, Miyazaki, Japan 2008.

[10] Duchateau, K.A. Structural design and performance of composite wall-foundation connector elements. Washington State University, Department of Civil and Environment Engineering, Master Thesis, 144 pp., 2005.

[11] Yeh, B. and Williamson, T.G. Combined shear and wind uplift resistance of wood structural panel shearwalls. Proceedings CIB-W18 Meeting, St. Andrews, Canada, Paper 41-15-6, 2008.

[12] Källsner B., and Girhammar U.A. Horizontal stabilization of timber frame buildings – Plastic design of timber wall panels. SP Technical Research Institute of Sweden, SP Report 2008:47, 81 pp., Stockholm 2009 (in Swedish).

INTERNATIONAL COUNCIL FOR RESEARCH AND INNOVATION IN BUILDING AND CONSTRUCTION

WORKING COMMISSION W18 - TIMBER STRUCTURES

NEW SEISMIC DESIGN PROVISIONS FOR SHEARWALLS AND DIAPHRAGMS IN THE CANADIAN STANDARD FOR ENGINEERING DESIGN IN WOOD

M Popovski
E Karacabeyli
Chun Ni
FPInnovations-Forintek
Vancouver, BC

P Lepper
G Doudak
Canadian Wood Council
Ottawa, Ontario

CANADA

Presented by M Popovski

A. Buchanan asked about the basis to come up with this process. M. Popovski answered that the work is a little bit of everything with past Nonlinear time step analysis, test results from the past and consultation with design community. A. Buchanan stated that he does not understand the concept of non-yielding diaphragm. M. Popovski said that it came from National Building Code of Canada provisions. I. Smith added reinforced concrete diaphragm is non-yielding and the NBCC committee is dominated by concrete experts. He also commented that there are many uncertainties on the load side. C. Ni said that this is an issue for hybrid construction with concrete or masonry walls and wood diaphragm.

R. Steiger discussed the over-strength factor of 1.2 to modify the load versus the resistance. M. Popovski said that there are plans to do this.

M. Fragiacomo stated that in EC5 there is no over-strength design factor and asked why this factor was applied to the 1st floor. M. Popovski explained that the provisions tried to address the issue of soft story failure in the 1st two stories.

A. Buchanan commented that one can't tell the building to have yielding at every point simultaneously. The key is to make sure we don't have yielding in undesirable places. You try to do this but it is not apparent that it has been achieved.

New Seismic Design Provisions for Shearwalls and Diaphragms in the Canadian Standard for Engineering Design in Wood

Marjan Popovski, Erol Karacabeyli, Chun Ni

FPInnovations-Forintek, Vancouver, BC, Canada

Peggy Lepper, Ghasan Doudak

Canadian Wood Council, Ottawa, Ontario, Canada

Abstract

This paper summarises the newly developed seismic design provisions for shearwalls and diaphragms that were introduced in the 2009 edition of the Canadian Standard for Engineering Design in Wood (CSA O86). The new provisions address seismic design loads for wood diaphragms, shearwalls, anchor bolts, hold-down connections, shearwall-to-diaphragm connections and similar load transfer elements. In addition, the provisions include clauses for wood-based diaphragms used in hybrid buildings with masonry, concrete, or steel vertical seismic force resisting systems (SFRSs). Two different design approaches are provided: a) cases when diaphragms may yield; and b) cases where diaphragms are stiff and are not expected to yield. The new design provisions have significantly improved the alignment of CSAO86 with the current 2005 edition of the National Building Code of Canada (NBCC), as well as with the upcoming 2010 edition of NBCC.

1 Introduction and Background

One of the main issues that got designers' and wood industry's attention in Canada after the 2005 edition of the NBCC came into effect in 2006 was the new approach for seismic design of diaphragms. The 2005 NBCC clause 4.1.8.15.1 requires that ″Diaphragms and their connections shall be designed so as not to yield″. The building code commentary to the Clause states that forces due to seismic loads applied to the diaphragm must be increased to reflect the actual lateral load capacity of the Seismic Force Resisting System (SFRS). The intention of the NBCC Clause is to ensure proper force transfer and prevent structural collapse by ensuring that the energy dissipation be confined to those elements that can behave inelastically during an earthquake, while all other elements (including diaphragms) are designed to be stronger to allow this mechanism to develop. Such requirements, based on the well known capacity-based design philosophy, have already been in place for many years in the seismic design of structures in other material standards in Canada and around the world. Such design philosophy did not exist in the 2005 supplement to the Canadian Standard for Engineering Design in Wood (CSAO86, 2005), and that created confusion within the design community especially regarding diaphragm design. The only design Code that currently has a capacity-based approach for wood structures in general is the Eurocode 8 (EN, 1998-1) where in its chapter eight, specific rules for seismic design of timber buildings are given.

Although well suited for concrete and to some degree to steel structures with stiff diaphragms, the NBCC clause has had large implications on the design of wood-frame structures that usually have flexible diaphragms that may yield. It also made the design of wood-hybrid buildings, structures that utilize masonry or concrete shearwalls and wood floor or roof diaphragms, to be very impractical, if not impossible to achieve. In the case of single storey hybrid buildings, such as sports arenas with wood roofs, for example, the wood roof diaphragm and connections connecting it to the walls had to be stronger than the capacity of the concrete or the masonry walls below, which would be difficult if not impossible to achieve.

The Lateral Load Design Task Group (LLDTG) of CSAO86, in collaboration with the Canadian Wood Council (CWC) staff, members of the Canadian National Committee on Earthquake Engineering (CANCEE), and input from the design community, developed new design provisions for shearwalls and diaphragms that will bring design of wood light frame structures in line with the philosophy of capacity-based design. Impact studies were also conducted using the proposed design procedures to investigate their impact on the design of various building throughout the country. Two design firms from Vancouver, BC and the CWC staff were involved in the impact studies. One of the impact studies focused on multi-storey platform-frame buildings; the other focused on single-storey hybrid buildings consisting of masonry walls and a wood roof. The final version of the proposal was accepted by the CSAO86 Technical Committee at the January 2009 meeting.

The new design requirements for shearwalls and diaphragms were developed in light of the capacity-based design philosophy, the current practices adopted by the design community, and the lessons learned from observed seismic performance of wood-frame structures during past earthquakes and from number of full-size shaking table tests. They were also developed considering prevention of the very few observed failures of wood frame buildings which were mainly related to the soft-story mechanism that developed at the first storey of multi-storey buildings during past earthquakes (Rainer and Karacabeyli, 1999).

2 The New CSAO86 Section for Design of Shearwalls and Diaphragms

In NBCC, like in many other model building codes throughout the world, the equivalent static force procedure states that the total seismic design shear force V for a building can be determined as the total elastic shear force V_E divided by the force modification factors. In NBCC two different force modification factors are included: R_o factor that accounts for the over-strength of the components of the SFRS, and R_d factor that accounts for the ductility of the SFRS.

The new seismic design provisions for shearwalls and diaphragms were implemented as a new Section 9.8 in the 2009 edition of CSAO86. The entire Section 9 was actually renamed “Lateral Load Resisting Systems” and has replaced the previous section named “Shearwalls and Diaphragms”. The new provisions state that the seismic design forces for diaphragms should be determined using the appropriate procedures and corresponding values for the force modification factors R_o (for over-strength) and R_d (for ductility) for each different SFRS provided in the NBCC. In Clause 9.8 of CSA O86, guidance is provided for design of structures in high and low seismic regions. Distinction between low and high seismic zones was made with aim to minimize the impact of changing the current design and construction practise in vast regions of the country where seismic loads are relatively low.

2.1 Structures in High Seismic Zones

The majority of the clauses in section 9.8 of CSA O86 apply to structures that are located in high seismic zones in Canada. These are zones where the value of the product $I_E F_a S_a(0.2)$ determined according to NBCC is equal to or greater than 0.35,

where:

I_E = Building Importance Factor (1.0 for normal buildings);

F_a = Acceleration-based site coefficient (1.0 for soil site class C);

$S_a(0.2)$ = 5% damped spectral response acceleration for period of 0.2 s expressed as ratio of gravity.

All other zones will be treated as low seismic zones.

2.1.1 The Over-capacity of wood-based SFRSs

In Clause 9.8.3 the provisions introduce an over-capacity coefficient, C_i, for storey 'i' of the building, and for each of the two orthogonal horizontal directions. This coefficient that is greater than or equal to 1.0, can be determined as:

$$C_i = \frac{V_{ri}}{V_{fi}} \qquad [1]$$

where:

V_{ri} = factored resistance of the wood-based SFRS in a given storey 'i';

V_{fi} = factored seismic load for storey 'i' obtained using R_d R_o coefficients for the wood-based SFRS according to NBCC.

The intention of the over-capacity coefficient is to determine how much additional resistance is available in the final design of the structure versus the actual demand. For example a perfect design of a wood-frame shearwall may require nail spacing around the wall perimeter to be 110 mm o.c., but the wall is designed and built with nail spacing of 100 mm (4 inches) o.c., creating reserve capacity in the wall.

For wood-frame structures that have three or more storeys, the vertical SFRSs is required to be designed so that the ratio of the over-capacity coefficient of the second storey C_2 and the over-capacity coefficient of the first storey C_1 is within the limits given below:

$$0.9 < \frac{C_2}{C_1} \le 1.2 \qquad [2]$$

The intent of limiting the ratio of the over-capacity coefficients for the first two stories according to equation [2] is to ensure that the desired ductile nail yielding mode is not entirely confined to the shearwalls on the first or second storey only, and thus try to prevent the formation of soft or weak storey failure mechanism in that storey. If C_2 is significantly greater than C_1, the second storey may not yield at all, and there could be a soft storey effect at the first storey. Similarly, if C_2 is significantly less than C_1, the second storey could start to yield first, without transferring the force to the first storey, leading to a soft storey on the second storey. Only the first two storeys were included in limiting the ratio of the over-capacity coefficients because the results from dynamic analyses on four storey platform frame buildings suggested that the first two storeys contribute the most to the seismic response and energy dissipation of the building, and thus are deemed to be most important. One can always check the remaining C_{i+1}/C_i ratios along the remaining storeys of the building by applying the same procedure.

2.1.2 Anchor bolts and hold-downs

Anchorages and hold-downs are important components for providing adequate seismic performance of the shearwalls and the building in general. For example, if the ultimate strength of any of these elements is lower than that corresponding ultimate capacity of the shearwall, the sheawall will not be able to fully develop its capacity and the much needed non-linear response for which it was designed. Based on the test data from quasi-static tests on shearwalls, as well as from the numerous shaking table tests around the world, the current design practice in terms of use of anchor bolts and hold-downs seems to give satisfactory wall performance with no failures in anchorages or hold-downs observed.

To further reduce the likelihood of failure, new provisions in Clause 9.8.2 of CSA O86 require that anchor bolts, inter-storey connections resisting seismic shear forces, and hold-downs resisting seismic uplift forces of a shearwall or a shearwall segment be designed for seismic loads that are at least 20% greater than the force that is being transferred.

2.1.3 Wood Diaphragms Supported on Wood Shearwalls

Although reported failures of wood diaphragms during past earthquakes have been rare, diaphragms can be a controlling factor in the overall seismic behaviour of the structure because the design of the elements of the vertical SFRS is dictated by the assumption on the in-plane stiffness of the diaphragm. Diaphragm flexibility can vary between the two boundary cases:

- Flexible diaphragms, that undergo significant deformations in their own plane, and transfer the horizontal loads to the elements of the vertical SFRS underneath according to their tributary areas;
- Rigid diaphragms that undergo insignificant deformations in their own plane and transfer the loads according to the stiffness of the elements of the supporting SFRS regardless of their tributary area. In this case, the torsional response of the structure must be evaluated.

Although most of the wood-based diaphragms in engineered structures are somewhere between the two boundary cases given above, at this point almost all wood-based diaphragms are assumed in the design to be flexible. This is especially the case in platform frame construction, which is the most prominent system used in residential applications in North America. In this system, the horizontal wood-frame diaphragms, collect and transfer the loads to the vertical SFRSs, the wood shearwalls.

Clause 9.8.4 of the new provisions covers the design loads for wood diaphragms supported on wood shearwalls. In this case, seismic design forces for diaphragms at each storey ‘i’, for each orthogonal horizontal direction, is to be calculated as:

$$V_{Di} = C_{Di} \cdot F_i \tag{3}$$

where:

V_{Di} = seismic design load on the diaphragm at storey ‘i’;

C_{Di} = diaphragm coefficient at storey ‘i’ for each horizontal direction defined as the lesser of C_i or 1.2;

F_i = factored seismic force at storey i calculated using $R_d \cdot R_o$ for the wood shearwalls.

The value of the coefficient C_{Di} was limited to 1.2 to reflect the fact that even using the current design practice without any increase on the diaphragm design force, no diaphragms failures had occurred in platform frame construction during the past earthquakes or during shaking table tests (Filiatrault et. al. 2002).

2.1.4 Wood Diaphragms in Buildings with SFRSs other than Wood Shearwalls

Clause 9.8.5 in the new provisions covers buildings that use reinforced concrete, masonry, steel, or wood-based structural systems other than wood shearwalls for the vertical SFRSs, and have wood diaphragms. Vertical SFRSs are to be designed according to the appropriate CSA material standards. The provisions address two cases: a) where diaphragms may yield, and b) where diaphragms are not expected to yield.

Diaphragms that are designed and detailed according to the existing clause 9.5 of CSAO86 and are sheathed with wood-based structural panels are expected to exhibit ductile behaviour. In cases where they will yield before the supporting SFRS, they are to be designed for seismic loads determined using the $R_d \cdot R_o$ factors for the vertical SFRS. To be consistent with the 2005 and 2010 NBCC a force limit was introduced stating that the seismic design load for such diaphragms could not be less than loads determined using $R_d \cdot R_o = 2.0$.

When diaphragms are not expected to yield before the supporting SFRS, and when the SFRS is a wood-based system other than wood shearwalls, they are to be designed to resist a seismic force V_{Di} determined as:

$$V_{Di} = 1.2 \cdot C_i \cdot F_i \qquad [4]$$

where:

V_{Di} = seismic design load on the diaphragm at storey ‘i’;

C_i = over-capacity coefficient at storey ‘i’ equal to the value of C_i determined according to equation [1]

F_i = factored seismic force at storey ‘i’ calculated using the R_d R_o for the SFRS.

In cases when the wood diaphragms are supported on non-wood SFRSs (hybrid structures) the seismic design load on the diaphragm at storey ‘i’ is to be calculated as:

$$V_{Di} = \gamma_i F_i \qquad [5]$$

where:

γi = the over-strength coefficient applied at level ‘i’ for the vertical SFRS determined on principles of capacity based design in accordance with the applicable CSA material standard.

Again, to be consistent with the requirements of the NBCC a force cut-off was introduced so that the seismic design load V_{Di}, need not exceed the value of load F_i determined using $R_d \cdot R_o = 1.3$.

2.1.5 Design of Force Transfer Elements

To ensure adequate performance of the structural system during an earthquake, the design loads on critical system components and force transfer elements were increased. Diaphragm chords, splice joints, structural members and connections of diaphragms around openings, as well as all other load-transfer elements, are to be designed for a seismic load that is at least 20% greater than the seismic design load on the diaphragm V_{Di}.

Similarly, connections and drag struts that transfer shear forces between the segments of the vertical SFRS and the diaphragm are to be designed for seismic loads that are at least 20% greater than the shear force that is being transferred. Parts of the diaphragm around wall offsets are to be designed for seismic loads that are at least 20% greater than the seismic design load of the offset SFRS.

To be consistent with the requirements the NBCC a force cut-off was introduced so that the seismic design forces used for the design of force transfer elements, need not exceed the forces determined using $R_d \cdot R_o = 1.3$. A summary of the proposed design philosophy for wood diaphragms according to 2009 CSAO86 and 2010 NBCC is shown in Figure 1.

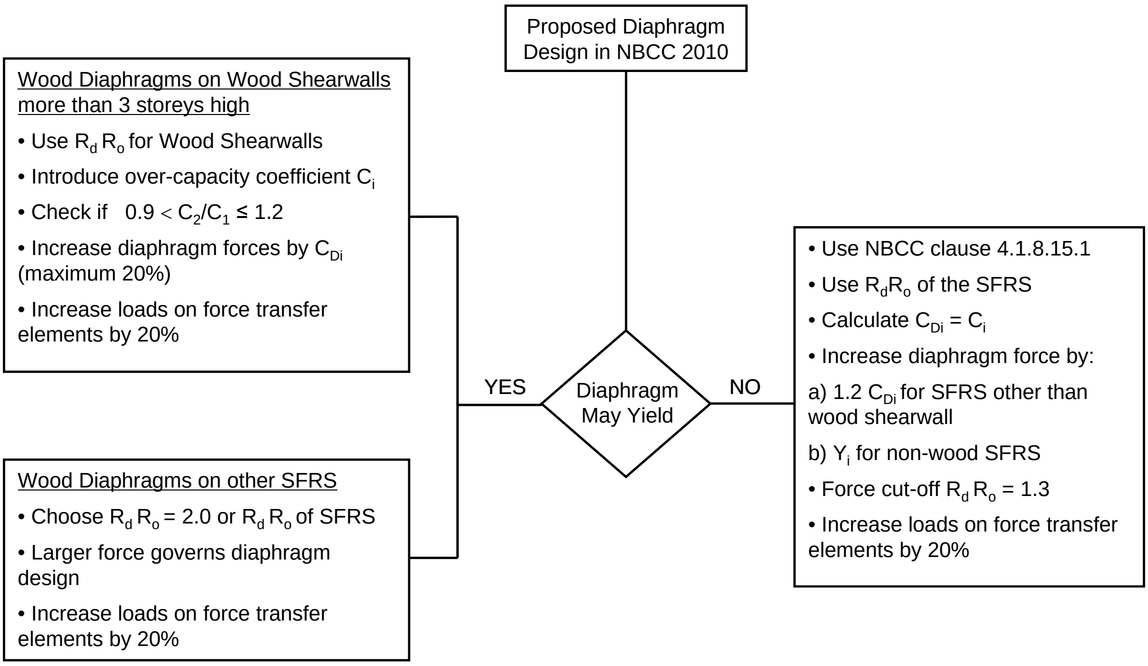

Figure 1. Proposed design philosophy for wood diaphragms according to 2009 CSAO86 and 2010 NBCC

2.2 Structures in Low Seismic Zones

Most of the requirements of the new Clause 9.8 do not apply to structures located in low-seismic zones, which are defined as regions of the country where the value of $I_EF_aS_a(0.2)$ according to NBCC is lower than 0.35. In such case no increase of seismic design loads on the diaphragms is proposed. In low seismic regions, seismic design forces for diaphragms are allowed to be determined in accordance with equation [3] with the over-capacity coefficient C_i taken as unity. Force transfer elements, however, are to be designed as in buildings in high seismic zones, which is according to rules given in Section 2.1.5 of this paper.

3 Proposed Procedure for Wood-Frame Buildings

The suggested process of determining the seismic shear forces on shearwalls and diaphragms for a structure with more than 3 storeys (Figure 2) can be summarised as follows:

1. Determine the seismic storey shear forces F_i according to Clause 4.1.8.11 and 4.1.8.15 of the NBCC. Only forces distributed according to first mode of vibration are shown in Figure 2. Attention should be paid as NBCC specified diaphragm forces may be governed by other distributions (e.g. V/n, where *n* is number of stories);
2. Obtain the cumulative factored seismic shear forces V_{fi} at each storey *i* as a sum of the factored seismic forces above that storey;
3. Design the shearwalls at each storey of the structure using the cumulative factored seismic loads;
4. Determine the actual factored shear resistance of each storey, V_{ri} , that is related to the existing number and length of shearwalls on that storey;
5. Calculate the over-capacity coefficient for each storey C_i as a ratio of V_{ri} and the factored load for that storey V_{fi};
6. Determine the over-capacity coefficients C_{Di} for diaphragms at each storey *i* as the lesser of C_i and 1.2;
7. Determine the seismic design loads for the diaphragms at each storey by multiplying the factored seismic shear load of each storey F_i by the seismic coefficient C_{Di};
8. Check the ratio of C_2/C_1 to be within the limits of: $0.9 < C_2/C_1 \leq 1.2$. If the ratio is not within the specified limits, either reduce or increase the actual resistance in one of the stories (i.e. V_{r1} or V_{r2}). The purpose of limiting the C_2/C_1 ratio within the specified limits is to ensure that non-linear behaviour begins to develop at the first storey, closely followed by the second storey, thereby ensuring that the response of the structure corresponds to first mode of vibration that is consistent with the design assumptions;
9. One could check the remaining C_{i+1}/C_i ratios along the remaining storeys of the building and apply the same procedure especially if the building has up to six storeys. Results from dynamic analyses on four storey platform frame buildings suggest that the first two storeys contribute the most to the seismic response and energy dissipation of the building.

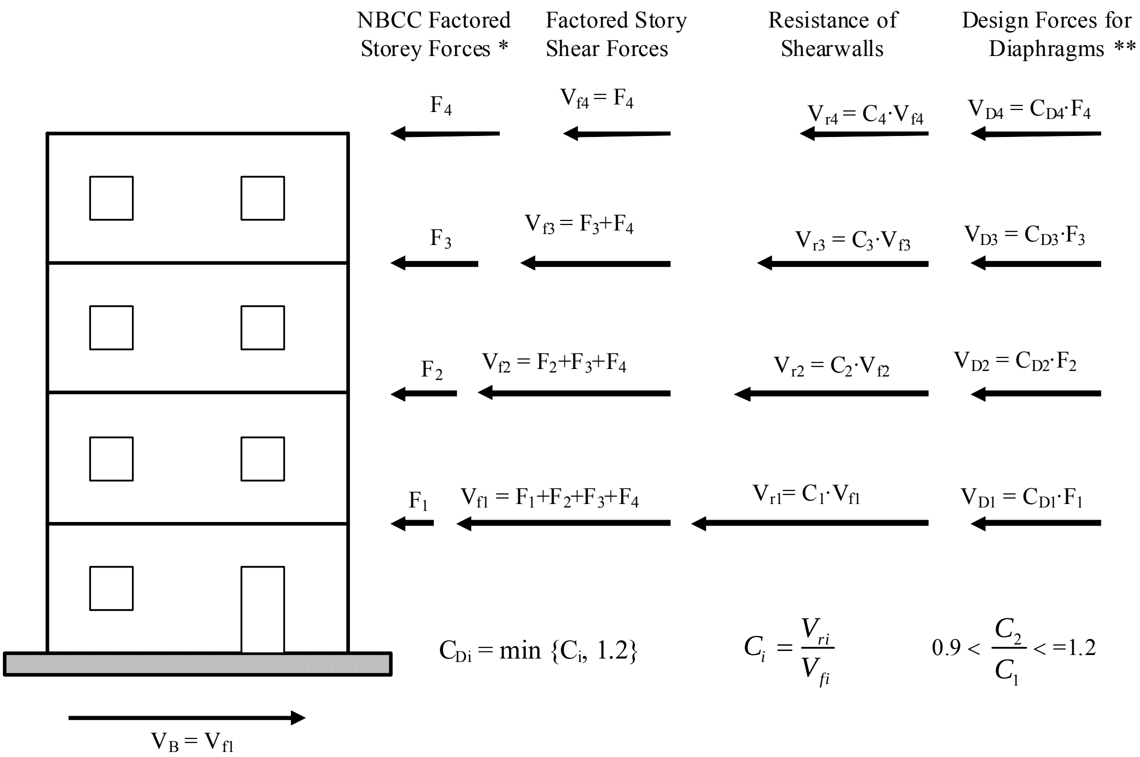

** Force distribution according to first mode of vibration is shown. ** There may be other distributions possible according to NBCC that would cover the V/n case for diaphragms.*

Figure 2. Distribution of the seismic design forces for a 4-storey wood-frame structure

4 Conclusion

The paper describes in detail the newly developed seismic design provisions for shearwalls and diaphragms that are included in the 2009 edition of the Canadian Standard for Engineering Design in Wood (CSAO86, 2009). The new design provisions have significantly improved the alignment of CSAO86 with respect to the current 2005 edition of the National Building Code of Canada (NBCC), as well as with the upcoming 2010 edition of NBCC.

5 References

CSAO86. 2005. Canadian Standards Association Standard O86 - Engineering Design in Wood. CSA, Toronto, Ontario, Canada.

CSAO86. 2009. Canadian Standards Association Standard O86 - Engineering Design in Wood. CSA, Toronto, Ontario, Canada.

EN 1998-1:2004 (E). Eurocode 8: Design of structures for earthquake resistance – Part 1: General rules seismic actions and rules for buildings. European Committee for Standardization. Brussels, Belgium.

Filiatrault, A., Fischer, D., Folz, B., Chia-Ming, U. 2002. Experimental parametric study on the plane stiffness of wood diaphragms. Canadian Journal of Civil engineering. 29:554-556.

NBCC. 2005. National Building Code of Canada. Canadian Commission on Building and Fire Codes, National Research Council of Canada, Ottawa, Ontario.

NBCC. 2010. National Building Code of Canada, Public Review Version. Canadian Commission on Building and Fire Codes, National Research Council of Canada, Ottawa, Ontario.

Rainer, H., Karacabeyli, E. 1999. Performance of Wood-frame Building Construction in Earthquakes. Special Publication 40. Forintek Canada Corp.

CIB-W18/42-15-3

**INTERNATIONAL COUNCIL FOR RESEARCH AND INNOVATION
IN BUILDING AND CONSTRUCTION**

WORKING COMMISSION W18 - TIMBER STRUCTURES

STABILITY CAPACITY AND LATERAL BRACING FORCE OF METAL PLATE CONNECTED WOOD TRUSS ASSEMBLIES

Xiaobin Song
F Lam

University of British Columbia

CANADA

Hao Huang
Minjuan He

Tongji University

CHINA, P. R.

Presented by F. Lam

H.J. Blass asked about the use of battens versus sheathing. F. Lam replied that testing is expensive therefore we used a combined testing/modeling approach and only addressed a limited number of cases to verify the model. With a verified model we can apply it to battens as well.
H.J. Blass asked why only one set of webs were tied to a support. F. Lam responded that it is intended to push and test the model as much as possible by introducing complication condition in the testing. H.J. Blass commented that in the 2D analogy bending moment will be introduced into the web when diagonal braces are not tied to the web nodal point. F. Lam agreed.
T. Poutanen asked about the load –deformation curve of the truss system as he suspects the load would not decrease much due to buckling. F. Lam said the load-deformation information would be available in Dr. Song's thesis. The load was sustained for a long time after buckling occurred. K. Crews asked whether loading was kept up after the failure. F. Lam replied no.
P. Quenneville asked what factor one would recommend instead of the 2% rule. F. Lam said that for the system studied the 2% rule is too conservative by a factor of 2 or more. Since only one system was studied, more work should be done with a variety of system and cases to come up with sound recommendation.
J. Köhler found the work interesting to tie probability of failure to system behaviour. He asked whether sensitivity analysis of model uncertainties were studied, F. Lam replied this was not yet done. The reliability work is a framework within which more study and analysis should be done and can be done.

Stability capacity and lateral bracing force of Metal Plate Connected Wood Truss Assemblies

Xiaobin Song[(1)], Frank Lam[(1)] Hao Huang[(2)] and Minjuan He[(2)]

[(1)] Department of Wood Science, University of British Columbia, Canada

[(2)] Department of Building Engineering, Tongji University, China, P. R.

Abstract

This paper presents the results of experimental and numerical studies on the critical buckling load and lateral bracing force of metal plate connected wood truss assemblies. Material property tests and full-scale tests of individual trusses and truss assemblies were conducted. The material properties test results were used as input parameters to finite element method based models, which were then verified based on the test results of individual trusses and truss assemblies. Good agreement was achieved. It was also found that the 2% design rule for the lateral bracing system overestimated the lateral bracing force in the tests. The generated database and the output of the models can be applied to more general structural configurations, and contribute to the improvement of the design methods for lateral bracing system.

1. Introduction

Metal plate connected (MPC) wood trusses are widely used in light frame residential and low-rise commercial buildings in North America. The truss members are typically made of 38 mm thick dimension lumber which, under compression loading, is susceptible to buckling due to insufficient lateral stiffness. Continuous lateral bracing (CLB) system is commonly used to reinforce these members.

Existing methods for evaluating the critical buckling load and lateral bracing force of such members (systems) are mostly based on beam-column theory using linear elastic material properties (Winter 1958, Plaut 1993, Plaut and Yang 1993, Munch-Andersen 2004). The 2% rule-of-thumb is commonly used by design engineers to estimate the lateral bracing force which is considered as 2% of the compression load carried by the member. This rule is based on the assumptions that the compression member is simply supported and out-of-plumb by 1% of its length (Throop 1947). This rule is questionable since it is merely strength-based and ignores the bracing stiffness (Waltz et al. 2000).

The stability capacity and lateral bracing force of MPC wood truss assemblies are influenced by many factors including system and load sharing effects, semi-rigid MPC connections, nonlinear behaviour of nail connections (used with lateral bracing members and roof sheathing material), and initial out-of-plane deformation of compression truss members. Out of these factors, the out-of-plane rotational stiffness of MPC connections has not been studied before; others were not studied from the perspective of stability of the systems (Wolfe et al. 1986, Wolfe and LaBissoniere 1991, Mayo 1982, Lam and Varoglu 1988, Gupta and Gebremedhin 1990, Foschi 1977, Waltz et al. 2000, Ellegaard 2002).

This paper presents the results of a study on the critical buckling load and lateral bracing force of MPC wood truss assemblies. Based on previous work on wood beam-columns (Song and Lam 2009), this study focused on full-scale tests of individual trusses and truss assemblies of which the test results were used as input parameters and verification for finite element method (FEM) based models of the individual trusses and truss assemblies. The adequacy of the 2% rule-of-thumb for the design of lateral bracing member (system) was also studied.

2. Material and Configurations of the Trusses and Truss Assemblies

The trusses were fabricated with Spruce Pine Fir (SPF) dimension lumber of 38×89 mm^2 and 38×139 mm^2 in cross-sectional sizes. The lumber was machine stress graded as MSR1650f-1.5E. Two types of truss plates (MT18HSTM and MT20TM, provided by Mitek Canada, Inc.) were used. Twenty-six sheets of four-ply plywood, 1219×2438 mm^2 in size and 11.9 mm in thickness, were used as sheathing material. 10d and 6d common nails were used for the lateral bracing members and plywood sheathing, respectively. The modulus of elasticity of the dimension lumber, the flexural stiffness of the plywood sheathing and the load-displacement relationship of the nail connections were tested (Song 2009). The properties of the metal truss plates were obtained from Liu’s work (2008).

Double Howe truss was designed for a (top chord) slope of 6:12 and a span of 12.19 m. All truss joints were fabricated with MT20TM plates except the tension splice joints of the bottom chords, which were fabricated with MT18HSTM plates to avoid connection failure during testing. All metal truss plates were slightly oversized for the same consideration. The individual truss design is shown in Fig. 1.

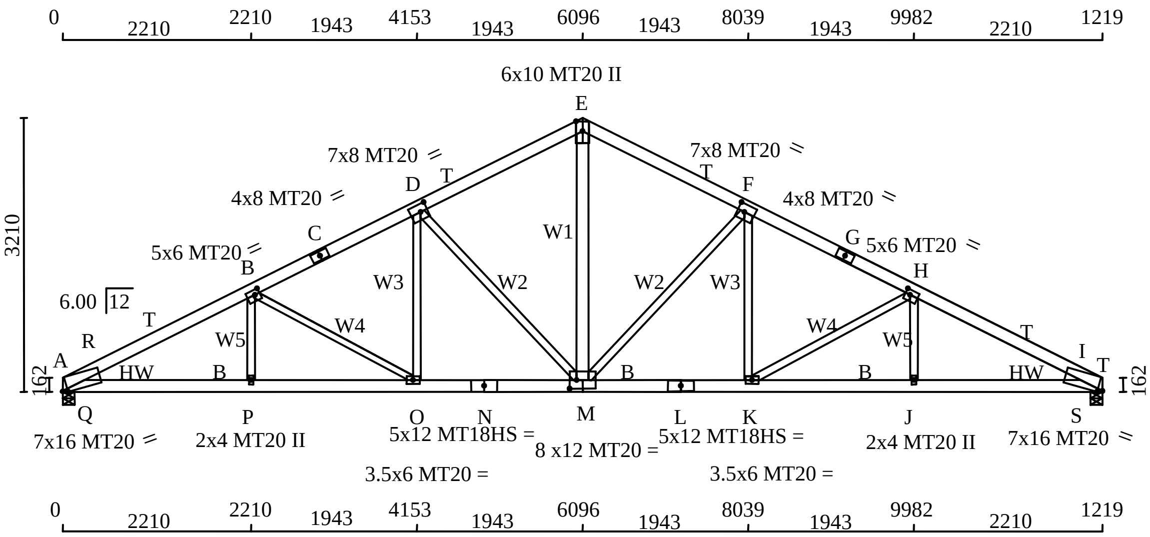

Fig. 1 Double Howe truss design (all dimensions in mm except plate dimensions are shown in inches with 1 inch = 25.4 mm)

Two truss assemblies were constructed; each with five trusses spaced 610 mm on centre and fastened to the bearing plates by screws. The trusses were sheathed by plywood panels which were connected to the top chords by 6d nails, spaced 152.4 mm on centre at the edges and 304.8 mm on centre at the interior area. The difference between the two truss assemblies lies in the provision of the bracing members, which are shown schematically in Fig. 2.

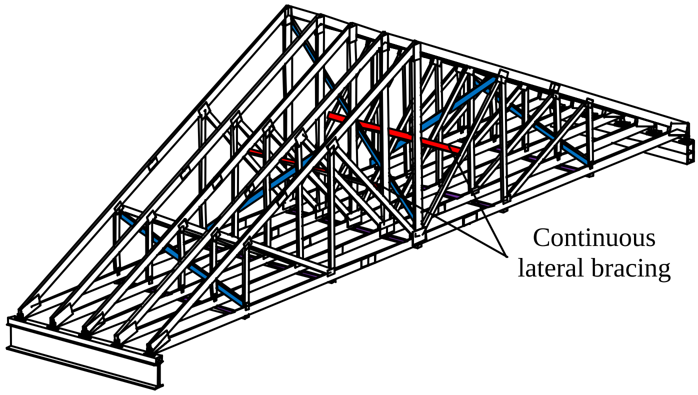

Fig. 2 Continuous lateral and auxiliary bracing systems of a five-bay truss assembly

Both truss assemblies were installed with an auxiliary bracing system, which consisted of five bottom chord ties and five diagonal web braces, as shown in Figure 2. The second truss assembly was also reinforced by an additional continuous lateral bracing (CLB) system (two lateral bracing members, as shown in Figure 2). Both the CLB and auxiliary bracing systems were installed by using two 10d nails in each brace to truss connection.

3. Test setup and procedures

3.1 Test setup

The individual trusses and truss assemblies were tested in the Timber Engineering and Applied Mechanics Laboratory of the University of B.C., Canada. The individual trusses were simply supported within the truss plane, having a clearance of 471 mm measured from the bottom chords. Steel columns and jigs were used to laterally support the trusses without interfering with their in-plane behavior. The truss assemblies were similarly supported with the truss located at the first bay connected to the steel columns and jigs. The test setup is shown in Fig. 3.

Fig. 3 Test setup for individual trusses and truss assemblies

3.2 Test procedures

The individual and assembly tests were conducted in six stages. In the first stage of testing, fifteen trusses were tested nondestructively to evaluate their stiffness property. Concentrated loads were applied onto nodes B, D, F, and H (see Fig. 1). The loading was continued up to roughly 25% of the critical buckling load.

The stiffness of the individual trusses was found to be similar. As a result, in the second stage, five trusses were randomly selected for the critical buckling load study. The loads were applied at the same positions as in the first stage.

In the third stage, the first truss assembly was tested to buckling failure. No CLB system was installed at this stage. Four concentrated loads were applied at nodes D and F of the second and fourth trusses. The W2 webs were observed to experience significant lateral deformation, after which the load was removed without having any member broken.

The assembly was retested in the fourth stage, after installation of a CLB system.

In the fifth stage, the second truss assembly was nondestructively tested to study its load distribution behavior. One truss of the assembly was loaded at a time, at nodes D and F up to 8.0 kN.

In the last stage, the second truss assembly was loaded in the same pattern as in third stage, with a CLB system. One of the two lateral bracing members (see Fig. 2) was fixed at one end to measure the lateral bracing force. The loading was continued until member breakage.

4. Test results and model verification

The FEM based models of individual truss and truss assemblies were developed by using an in-house computer program, SATA, with the nonlinear three-dimensional beam element, plate element, spring element and MPC connection elements. Details of the configuration of the FEM models and the formulation of the elements were presented by Song (2009).

The stiffness of the individually tested trusses was evaluated based on the relationship between the reaction force and the bottom chord deflections. The FEM based model of individual trusses was first calibrated based on the truss stiffness, which was evaluated using the bottom chord midspan deflections, to account for the variation of the material properties, truss plate placement and workmanship. The calibrated model was then verified by the truss stiffness evaluated using the deflections at the other bottom chord panel joints. The results are shown in Fig. 4.

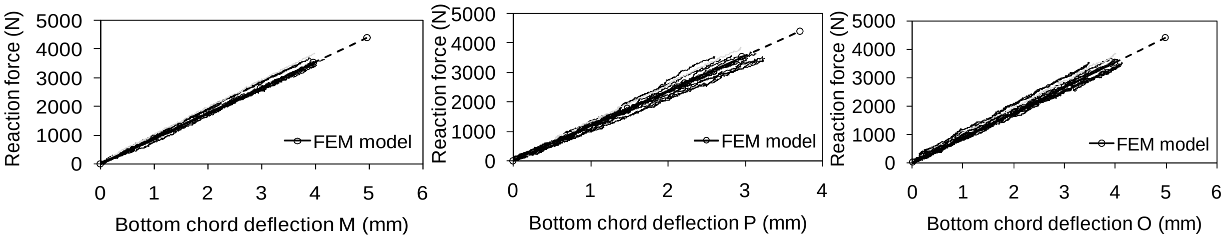

Fig. 4 Test results and model predictions of individual truss stiffness

It was found from the individual truss buckling tests (second stage) that the load carrying capacity of the individual trusses was dominated by the buckling failure of the W2 webs, of which the magnitude and direction were dependent on the initial out-of-plane deformation of the W2 webs. Close observation of the buckling deformation of the W2 webs (Fig. 5) indicated that the out-of-plane rotational stiffness of the MPC connections played an important role in the critical buckling load of the webs.

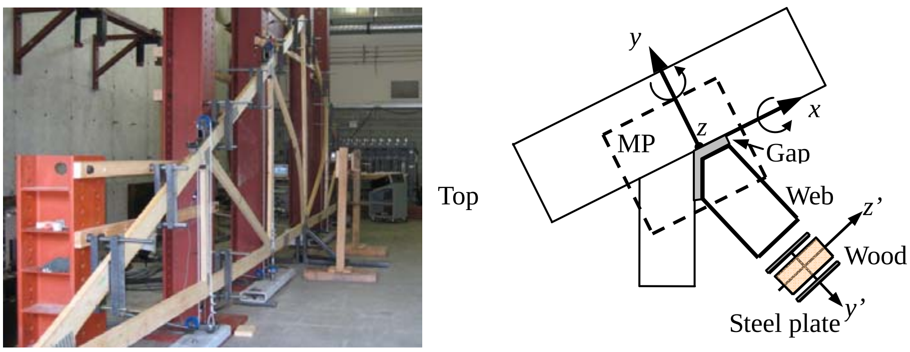

Fig. 5 Buckling and simplified model of out-of-plane rotational stiffness of MPC connection

A simplified model was developed to estimate the out-of-plane rotational stiffness of the MPC connections, as shown in Fig. 5. The obtained stiffness was further calibrated based on the load-lateral deformation relationship of the trusses. The results are shown in Fig. 6, in which, the model predictions were based on different values of the out-of-plane rotational stiffness, namely the stiffness from the pin-connection assumption (used in current design k=0), the model estimation (k=5.78x10^{9} N.mm) and the calibrated stiffness (k=3.5x10^{7} N.mm).

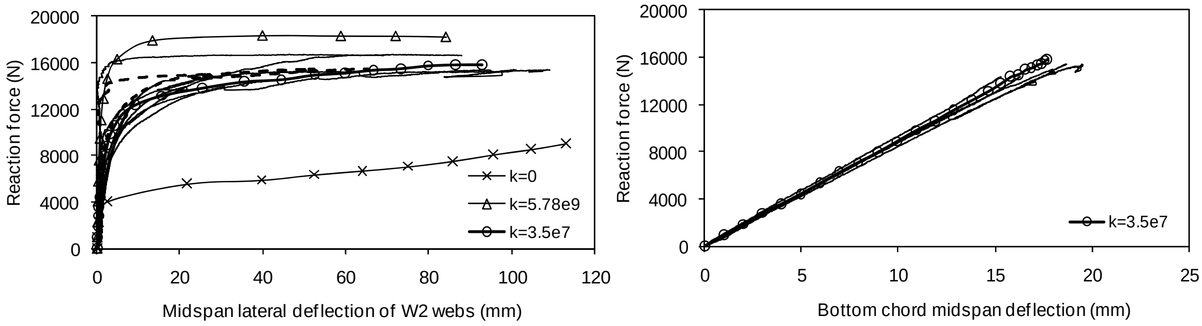

Fig. 6 Test results and model predictions of the applied load, lateral deflection of W2 webs and bottom chord midspan deflections

Short keeper nails were installed by the truss manufacturer to hold the truss plate in position during manufacturing. Such nails were not accounted for in the model. To evaluate the influence of the keeper nails, in one case some of the keeper nails were removed from the truss connections before testing. The dashed line in the left graph of Fig. 6 corresponds to the test results of one truss with less keeper nails on the MPC connections than the other four trusses. It can be seen that the influence of the keep nails on the critical buckling load and web lateral deflection of the truss is immaterial.

The results of the first truss assembly reinforced by a CLB system were presented in comparison with the second truss assembly, as shown in Fig. 7.

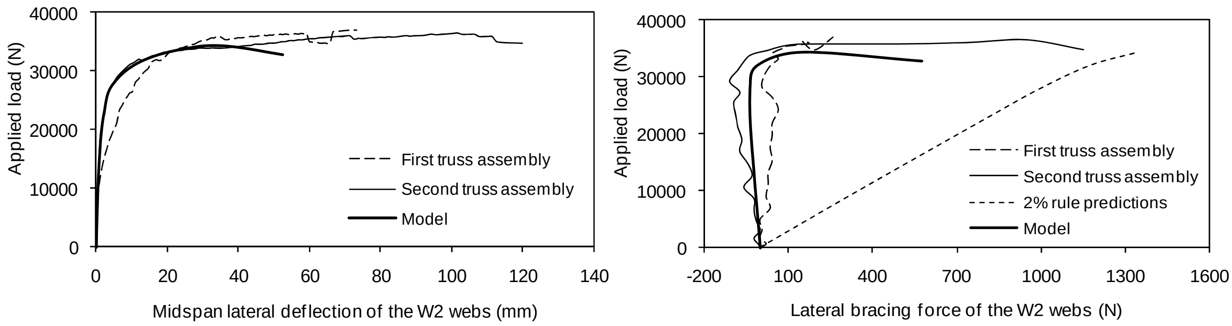

Fig. 7. Test results and model predictions of the applied load, lateral bracing force and midspan lateral deformation of W2 webs of the truss assemblies

The first part of Fig. 7 shows the relationship between the applied load and the midspan lateral deformation of the buckled webs (W2 webs). The dashed line corresponds to the results of the first truss assembly retested after installation of a CLB system. The difference between the test results of the two truss assemblies was mainly caused by the residual deformation (damage) on the MPC connections of the first truss assembly due to the loading in stage 3. It can be seen that this influence is small and the model predictions agreed very well with the test results, in terms of the maximum load and the lateral deformation.

The second part of Fig. 7 shows the relationship between the applied load and the lateral bracing force based on the test results, model predictions and 2% rule-of-thumb, respectively. It can be seen that the residual damage did not affect the lateral bracing force either. Again, the computer model predictions agreed very well with the test results; however, the 2% rule-of-thumb significantly overestimated the lateral bracing force. The reasons included the rigidity generated by the out-of-plane rotational stiffness and the randomness in the initial lateral deformation of the W2 webs were not considered in the 2% rule.

5. Conclusion

This paper presented the results of a study on the critical buckling load and lateral bracing force of MPC wood trusses and truss assemblies. Basic material property tests and full-scale tests of MPC wood trusses and assemblies were conducted, of which the results were used as input parameter and verification for FEM based models. The following conclusions were made based on the results.

The stiffness of individual trusses were similar despite the variation in material properties, truss plate placement and workmanship; however, the critical buckling loads of the trusses were influenced by the initial out-of-plane deformation and the out-of-plane rotational stiffness of the MPC connections of the compression members. It was also found the influence of the keeper nails on the test results of the individual trusses was immaterial.

The 2% rule-of-thumb was found to overestimate the lateral bracing force, due to the out-of-plane rotational stiffness of the MPC connections and the randomness in the initial out-of-plane deformation of the braced webs.

It should be kept in mind that these conclusions were based on the test results of the particular truss configurations and load situations used in this study; however, this work provides a framework about how to test and evaluate the critical buckling load and lateral bracing force of MPC wood truss assemblies.

Acknowledgement

The support received from Natural Sciences and Engineering Research Council of Canada (grants CRDP J 315282), Canadian Wood Council, Western Wood Truss Association, Jager Building Systems, Alpine Systems Corp, and Mitek is gratefully acknowledged.

Reference

Ellegaard, P. 2002. Analysis of timber joints with punched metal plate fasteners with focus on knee joints. Ph.D. thesis defended publicly at Aalborg University on February 5, 2002.

Foschi, R.O. 1977. Analysis of wood diaphragms and trusses, part II: Truss-plate connections. Canadian Journal of Civil Engineering, Vol. 4, pp. 353-363.

Gupta, R., and Gebremedhin, K.G. 1990. Destructive testing of metal-plate connected wood truss joints. J. Structural Engineering. 116(7), pp. 1971-1982.

Lam, F. and Varoglu, E. 1988. Reliability of trusses and roof systems. Research report, Forintek Canada Corporation, Vancouver, B.C., Canada.

Liu, X.Q. 2008. Ph.D thesis under preparation of the Department of Wood Science, University of British Columbia, Vancouver, Canada.

Mayo, A.P. 1982. Trussed rafter roofs—load distribution and lateral stability. Building Research Establishment Information Paper.

Munch-Andersen, J. 2004. Bracing of timber members in compression. International council for research and innovation in building and construction.” Working commission W18, CIM-218/37-15-5.

Plaut, R.H. 1993. Requirements for lateral bracing of columns with two spans. Journal of Structural Engineering. 119(10):2913-2931.

Plaut, R.H., and Yang, J.G. 1993. Lateral bracing forces in columns with two unequal spans. Journal of Structural Engineering. 119(10):2896-2912.

Song, X. B. and Lam, F., 2009. Stability analysis of laterally braced wood beam-columns subjected to biaxial eccentric loading. Accepted by Computers and Structures, Elsevier.

Song, X.B., 2009. Stability and reliability analysis of metal plate connected wood truss assemblies. Thesis submitted as partial fulfillment for the degree of Ph.D. Department of Wood Science, University of British Columbia, Vancouver, Canada

Throop, C.M. 1947. Suggestions for safe lateral bracing design. Engineering News Record, pp. 90-91.

Waltz, M.E., McLain, T.E., Miller, T.H., and Leichti, R.J. 2000. Discrete bracing analysis for light frame wood truss compression webs. Journal of structural engineering, 126(9), pp. 1086-1092

Winter, G. 1958. Lateral bracing of columns and beams. American society of civil engineers, transaction, paper No. 3044:807-826

Wolfe, R.W. and LaBissoniere, T., 1991. Structural Performance of Light-Frame Roof Assemblies II. Conventional Truss Assemblies. Res. Paper FPL-RP-499, US Forest Products Laboratory, 32 pp.

Wolfe, R.W., Percival, D. H. and Moody, R. C., 1986. Strength and stiffness of Light-Frame Sloped Trusses. Res. Paper FPL 471, US Forest Products Laboratory, 16 pp.

CIB-W18/42-15-4

INTERNATIONAL COUNCIL FOR RESEARCH AND INNOVATION
IN BUILDING AND CONSTRUCTION

WORKING COMMISSION W18 - TIMBER STRUCTURES

IMPROVED METHOD FOR DETERMINING BRACED WALL REQUIREMENTS FOR CONVENTIONAL WOOD-FRAME BUILDINGS

Chun Ni
FPInnovations Forintek Division

H Rainer
Rainer Dynamics Inc.

E Karacabeyli
FPInnovations Forintek Division

CANADA

Presented by C Ni

B.J. Yeh asked whether the analysis shown in Tables 1 and 2 take gypsum in to consideration. He asked in the case of baseline braced wall line how can one conclude that it is inadequate. C. Ni explained that there is no need for partition or interior wall because of the geometry in one direction and in the other direction gypsum wall board was considered as an interior wall with gypsum on both sides. B.J. Yeh commented that wind and seismic being different in US code. Gypsum is good in wind but not good in seismic. N. Chun said it makes a lot of sense to separate the two cases.
A. Ceccotti asked whether the Canadian prescriptive code requires buildings to be symmetrical. N. Chun responded yes it is a requirement in the Canadian prescriptive code. A. Ceccotti then asked how one would define symmetry as for example in cases of a garage.
S. Aicher received definition of braced wall panel and the bottom plate only anchored to foundation; no requirement of hold-down.
I. Smith commented that light frame construction can be susceptible to moisture so the case of wind with or without rain needs to be considered. T.G. Williamson responded that the buildings are assumed water tight so issue of rain and moisture does not come into play. In US there is a 100 plus page document prepared to explain the 10 page prescriptive code. H.J. Blass commented that it would be easier to just design shear wall and braced wall. C. Ni stated Part 9 of the Canadian code is a prescriptive code so we need this information. The philosophy is that these buildings tend to perform well so they don't need engineering design.

Improved method for determining braced wall requirements for conventional wood-frame buildings

Chun Ni
Wood Engineering Scientist
FPInnovations Forintek Division, Canada

Hans Rainer
Consultant
Rainer Dynamics Inc., Canada

Erol Karacabeyli
Manager, Building Systems Department
FPInnovations Forintek Division, Canada

Introduction

Wood-frame construction is by far the most common structural system in North America for single-family houses and low-rise multi-family dwellings, constituting over 80 % of all residential housing [4]. In North-America, wood-frame construction can be built either by following prescriptive codes or engineering design codes. Conventional wood-frame construction refers to buildings that are designed and built according to the prescriptive rules such as those in Part 9 of National Building Code of Canada (NBCC) or the US International Residential Code (IRC).

The prescriptive rules in the codes are largely developed based on historical practice for housing and small buildings as well as pre-engineered solutions. Although buildings designed and constructed with the prescriptive rules have performed well in past earthquakes and resulted in relatively few casualties, a very few wood-frame buildings have collapsed or suffered serious damage, particularly where lack of adequate bracing created a weak first storey [9].

In this paper, bracing requirements for conventional wood-frame construction in the current codes are discussed. An improved method to better rationalize the bracing requirements for conventional wood-frame construction is presented. The lateral load capacities of braced walls are also discussed.

Current seismic requirements for conventional wood-frame construction

The current 2005 National Building Code of Canada [6] does not have any specific seismic requirements for conventional wood-frame buildings. However, Appendix A-9.4.1.1.(3) of 2005 NBCC states:

> "In cases where lateral load design is required, the 'Engineering Guide for Wood Frame Construction' (CWC Guide) provides acceptable engineering solutions as an alternative to Part 4. The CWC Guide also contains alternative solutions and provides information on the applicability of the Part 9 prescriptive structural requirements to further assist designers and building officials to identify the appropriate design approach."

The 2004 CWC Guide [3] requires that where the spectral acceleration Sa (0.2) is greater than 0.74 g, the minimum length of braced wall panels in the first storey shall be: a) 25% of braced wall band for one and two storey buildings, and b) 40% of braced wall band for three storey buildings. The minimum length of braced wall panel is 1.2 m for interior walls with GWB sheathed on both sides, and 1.2 m for exterior walls with wood-based panels sheathed on one side and GWB on the other side. The distance from the end of the braced wall to the building corner shall not exceed 2.4 m, and the distance between braced wall segments shall not be greater than 6.4 m. Maximum building dimension in high seismic areas is 15.0 m.

Requirements on the spacing of braced wall bands are also provided. The spacing shall not be greater than 7.6 m for 0.99 g < Sa (0.2) ≤ 1.2 g, 10.6 m for 0.74 g < Sa (0.2) ≤ 0.99 g and 12.2 m for Sa (0.2) ≤ 0.74 g.

Bracing requirements to resist lateral loads due to high wind and earthquakes have been proposed in Part 9 of 2010 NBCC. The proposed lateral load provisions are an important step in addressing the safety of Part 9 buildings under wind and seismic loads. In the new NBCC 2010 bracing requirements are largely developed based on the US International Residential Code for 1 and 2 family dwellings.

The proposed NBCC bracing requirements are essentially the same as those in the 2004 CWC Guide except that instead of 1.2 m the minimum length of braced wall panel shall be 600 mm if the wall panel is located at the end of a braced wall band and connected to an intersecting braced wall, or 750 mm otherwise.

Evaluation of current seismic requirements for conventional wood-frame construction

As the seismic force on a building is a function of the mass of the building, the bracing requirements as a constant percentage of building lengths are not compatible with the physics of the phenomenon.

Two floor dimensions, 4.8 m × 15 m and 15 m × 15 m, that meet the minimum code bracing requirements were considered. For each floor dimension, buildings of one, two and three storeys were studied. The building length of 15 m represents the maximum building dimension allowed in Canadian codes for high seismic regions. The building length of 4.8 m represents the smallest building dimension which meets the requirements of minimum

25% of braced wall length and 1.2 m braced wall length. Plan views of the building layout are shown in Figures 1.

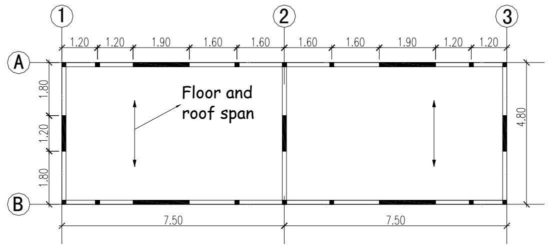

a) First storey floor layout of one- and two-storey 4.8 m × 15 m building

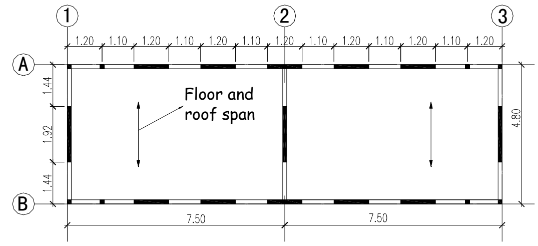

b) First storey floor layout of three-storey 4.8 m × 15 m building

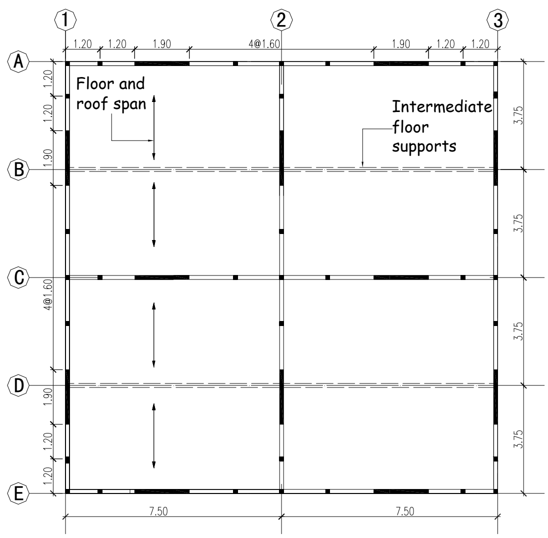

c) First storey floor layout of one- and two-storey 15 m × 15 m building

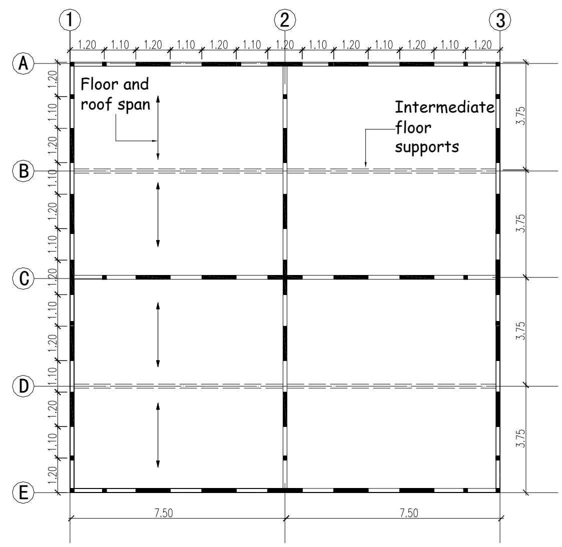

d) First storey floor layout of three-storey 15 m × 15 m building

Figure 1 Plan views of the first storey of one-, two- and three-storey buildings in accordance with the bracing requirements in Canadian codes

The lengths and locations of the braced wall panels were **chosen to represent** as much as possible **the most unfavourable case** for lateral load resistance. As a result, panels were located at or close to the maximum distance from the building corners and the distance between braced wall panels was 6.4 m, the maximum distance allowed by Canadian codes. It was assumed that for 4.8 m × 15 m building the roof trusses and floor joists span across the short direction. For 15 m × 15 m buildings the roof trusses were assumed to span from the exterior walls to the middle braced wall, whereas the floors span only half that distance to intermediate supports. The window and door openings were assumed to reach substantially the full storey height.

Although the sample buildings have less than optimum architectural and functional features, they nevertheless satisfy the minimum building code requirements and therefore could be built. One of the advantages of using extreme permissible configurations is that it will highlight characteristics of the code provisions that may be inadequate or unreasonable. In reality, wood-frame houses would generally contain more walls than the minimum wall lengths required by building codes, and thus would possess larger lateral resistance.

It is assumed that the building studied has storey height of 3.0 m. The roof area is 20% greater than the floor area. The unit weights of walls as well as roof and floor are:

• unit weight of roof (without concrete tile)	1.0 kPa (25% snow load included)
• unit weight of floor (without concrete topping)	0.5 kPa
• unit weight of exterior and interior wall	0.25 kPa

Exterior walls consist of SPF studs spaced at 400 mm on center and 9.5 mm wood-based panels sheathed on one side and 12.5 mm gypsum wallboard sheathed on the other side. The wood-based panels are fastened to wall framing with 8d common nails (3.3 mm in diameter) spaced at 150 mm on center at panel edges and 300 mm at intermediate studs. The gypsum wallboards are fastened to wall framing with drywall screws spaced at 200 mm on center everywhere.

Interior walls consist of SPF studs spaced at 400 mm on center and 12.5 mm gypsum wallboard on both sides. The gypsum wallboards are fastened to wall framing with drywall screws spaced at 200 mm on center at panel edges and intermediate studs.

Two methods were used to evaluate the lateral load capacities of the chosen buildings: a) wall panels partially restrained against uplift, and b) wall panels fully restrained against uplift. As was demonstrated in research [8], existing methods of analysis for walls partially restrained against uplift underestimate the lateral load capacity of the building, therefore representing a lower bound for estimating the lateral load capacity of the building. On the other hand, the maximum lateral load capacity of a wall is achieved when it is fully restrained against uplift (i.e. the use of hold-downs). The second method thus represents an upper bound for estimating the lateral load capacity of the building. The actual lateral load capacity of the building should therefore lie somewhere between the capacities of these two methods.

Summary of the base shear and lateral load capacities of the studied buildings are provided in Tables 1 and 2. The lateral load capacities of fully restrained walls sheathed with wood-based panels and GWB are determined in accordance with CSA O86 [2]. The base shear is determined in accordance with Part 4 of 2005 NBCC with ductility-related force modification factor R_d equal to 2.0. For wall panels partially restrained against uplift, the lateral load capacities are determined based on mechanics-based method in reference [8].

Buildings with floor dimension of 4.8 m × 15 m highlighted the potential inadequacy of having braced wall length as a constant percentage of building length. The results showed the imbalance between the required lengths of braced walls in short and long directions of a rectangular building. While the lateral load capacity in the long direction of the building is adequate for the two- and three-storey building and is in fact overly conservative for the one-storey building, the lateral load capacity in the short direction of the building may not be sufficient to resist the base shear forces.

For buildings with floor dimension of 15 m × 15 m, the lateral load capacity of fully restrained braced walls is adequate for the one-storey building at $S_a(0.2) = 0.75$ and 1.0 as well as the three-storey building at $S_a(0.2) = 0.75$.

Table 1 Base shear and lateral load capacity of 4.8 m × 15 m building

No. of storeys	$S_a(0.2)$ (g)	V_d[1] (kN)	Long direction (Loadbearing)				Short direction (Non-loadbearing)			
			R_1[2] (kN)	R_2[3] (kN)	V_d/R_1	V_d/R_2	R_1[2] (kN)	R_2[3] (kN)	V_d/R_1	V_d/R_2
1	0.75	14.6	29.5	41.6	0.50	0.35	8.4	15.5	1.74	0.94
	1.0	19.5	29.5	41.6	0.66	0.47	8.4	15.5	2.32	1.26
	1.2	23.4	29.5	41.6	0.79	0.56	8.4	15.5	2.78	1.51
2	0.75	22.4	34.7	41.6	0.65	0.54	9.9	15.5	2.27	1.44
	1.0	29.8	34.7	41.6	0.86	0.72	9.9	15.5	3.02	1.92
	1.2	35.8	34.7	41.6	1.03	0.86	9.9	15.5	3.63	2.31
3	0.75	32.6	53.6	65.8	0.61	0.50	18.9	24.8	1.72	1.31
	1.0	43.4	53.6	65.8	0.81	0.66	18.9	24.8	2.30	1.75
	1.2	52.1	53.6	65.8	0.97	0.79	18.9	24.8	2.75	2.10

Note:
1. V_d - base shear
2. R_1 - lateral load capacities of partially restrained walls
3. R_2 - lateral load capacities of fully restrained walls

Table 2 Base shear and lateral load capacity of 15 m × 15 m building

No. of storeys	$S_a(0.2)$, g	V_d[1] (kN)	Long direction (Loadbearing)				Short direction (Non-loadbearing)			
			R_1[2] (kN)	R_2[3] (kN)	V_d/R_1	V_d/R_2	R_1[2] (kN)	R_2[3] (kN)	V_d/R_1	V_d/R_2
1	0.75	43.0	35.5	49.1	1.21	0.88	29.8	49.1	1.44	0.88
	1.0	57.4	35.5	49.1	1.61	1.17	29.8	49.1	1.93	1.17
	1.2	68.8	35.5	49.1	1.94	1.40	29.8	49.1	2.31	1.40
2	0.75	64.5	40.1	49.1	1.61	1.31	33.9	49.1	1.90	1.31
	1.0	86.0	40.1	49.1	2.15	1.75	33.9	49.1	2.54	1.75
	1.2	103.2	40.1	49.1	2.58	2.10	33.9	49.1	3.04	2.10
3	0.75	91.0	61.7	77.5	1.48	1.17	51.0	77.5	1.78	1.17
	1.0	121.3	61.7	77.5	1.97	1.57	51.0	77.5	2.38	1.57
	1.2	145.6	61.7	77.5	2.36	1.88	51.0	77.5	2.86	1.88

Note: The same as in Table 1.

The results showed that the two-storey building has the largest discrepancies between the base shear and the lateral load capacity. This is because the required minimum lengths of braced wall panels are the same for one-storey and two-storey buildings in Canadian building codes. These results indicate that this requirement may be inadequate and more braced wall panels may be needed for two-storey buildings.

In Canadian codes, the same braced wall lengths are required for a building regardless the intensity of design spectral response acceleration $S_a(0.2)$. Although the codes tend to deal with this issue by requiring different maximum spacing between braced wall lines at different levels of $S_a(0.2)$, they also require that braced walls sheathed with wood-based panels on both sides shall not be spaced more than 15.0 m when $S_a(0.2)$ is greater than 0.75. As a result, a building meeting the minimum bracing requirements would have the same amount of braced walls, although different maximum spacing between braced wall lines is required at different levels of $S_a(0.2)$. Consequently, the same lateral load capacities are obtained for buildings regardless the intensity of $S_a(0.2)$. The results show that while bracing requirements are adequate for low design spectral response acceleration (i.e. $S_a(0.2) = 0.75$), they may be not adequate for high design spectral response acceleration such as $S_a(0.2) = 1.2$.

Improved formulations for seismic requirements of Part 9 buildings

As mentioned earlier, since the seismic force on a building is a function of the mass of the building, the specifications of the length of braced wall panels as a constant percentage of building lengths are not compatible with the physics of the phenomenon. It would make more sense if the lengths of braced wall panels were a function of the mass of the building, or the floor area of the building as an approximation, since the floor and the roof are the major contributors to the total mass. In the following, an area-based approach is investigated.

In the area-based approach, the seismic weight W which consists of weights of floors, roofs and walls is presented as a function of floor area. With seismic base shear V determined by the equivalent static force procedures in Part 4 of NBCC, the total length of braced wall panels required to resist the base shear in the main axis of a building is:

$$L_R = \frac{V}{v_R} = \frac{\frac{2}{3} I_E}{R_d R_o} \frac{w_r (1+\lambda_r) \frac{A_r}{A_f} + (n-1) w_f (1+\lambda_f)}{v_R} S_a(0.2) A_f = K_R S_a(0.2) A_f \qquad (1)$$

where

n	=	number of storeys
I_E	=	earthquake importance factor of the structure, $I_E = 1.0$
R_d	=	ductility-related force modification factor
R_o	=	overstrength-related force modification factor
w_r	=	unit weight of roof
A_r	=	roof area
λ_r	=	coefficient to account for half the total weight of the interior and exterior walls of the top storey to be added to roof
w_f	=	unit weight of floor
A_f	=	floor area
λ_f	=	coefficient to account for half the total weight of the interior and exterior walls above and below the floor to be added to the floor
L_R	=	required length of braced wall panels
v_R	=	the unit capacity of braced wall panels

The above equation was used to study the required lateral resistance of a Part 9 building. In this study, the unit weights for roof, floors and walls are the same as those used in the sample building. The coefficients λ_r and λ_f are also determined based on the sample buildings. Parameters for regular and heavy buildings are listed below:

Regular building

- unit weight of roof (without concrete tile) 1.0 kPa (25% snow load included)
- unit weight of floor (without concrete topping) 0.5 kPa
- unit weight of exterior and interior wall 0.25 kPa
- Coefficient λ_r 0.15
- Coefficient λ_f 0.60

Heavy building

- unit weight of roof (with concrete tile) 1.6 kPa (25% snow load included)
- unit weight of floor (with concrete topping) 1.3 kPa
- unit weight of exterior and interior wall 0.25 kPa
- Coefficient λ_r 0.09
- Coefficient λ_f 0.23

The lateral load capacities of exterior and interior walls are determined in accordance with CSA O86. For walls consiting of the same materials as those in the sample buildings, the lateral load capacities of exterior and interior walls that are fully restrained at the ends of the walls, v_R, are 5.48 kN/m and 1.96 kN/m, respectively. For exterior walls as the standard wall for resisting the lateral loads, the coefficient K_R is provided in Table 3. The minimum required total braced wall panels with different $S_a(0.2)$ are provided in Table 4.

Table 3 Coefficient K_R (%) for exterior walls

	Supporting roof only	Supporting roof plus one floor	Supporting roof plus two floors	Supporting roof plus three floors
Regular building	5	8	11	14
Heavy building	8	13	19	-

Table 4 Total required length of exterior braced wall panels as a percentage of storey floor area A_f

Building Type	$S_a(0.2)$	$K_R \times S_a(0.2)$, %			
		Supporting roof only	Supporting roof plus one floor	Supporting roof plus two floors	Supporting roof plus three floors
Regular building	0.75	4	6	8	10
	1.0	5	8	11	14
	1.2	6	10	13	17
Heavy building	0.75	6	10	14	-
	1.0	8	13	19	-
	1.2	9	16	23	-

For a building with both exterior walls and interior partition walls, the length of exterior walls plus 40% length of interior walls should be equal to or greater than the required length in Table 4. This is based on the fact that the capacity of the interior wall is approximately 40% that of the exterior walls.

For a rectangular building with building lengths L_1 and L_2, Equation 1 can also be expressed as a percentage of building length

$$\frac{L_{1,R}}{L_1} = K_R S_a(0.2)\frac{A_f}{L_1} = K_R S_a(0.2) L_2 \qquad (2)$$

and

$$\frac{L_{2,R}}{L_2} = K_R S_a(0.2)\frac{A_f}{L_2} = K_R S_a(0.2) L_1 \qquad (3)$$

In the 2004 CWC Guide and 2010 NBCC proposal, the required length of braced wall panels is a constant percentage of the building length parallel to the direction of loading. Based on Equations 2 and 3, the percentage of required length of braced wall panels should in fact be a function of the building length perpendicular to the direction of loading. This will address the imbalance between the required lengths of braced walls in short and long directions of a rectangular building.

Adjustment Factors for Required Length of Braced Walls

As noted, the required lengths of braced wall panels in Table 4 were developed based on the assumption that the braced wall panels are fully restrained and therefore have reached their full capacity. This assumption is not always true for a Part 9 building. In fact, the lateral load capacity of a braced wall is highly dependent on the boundary conditions of the wall. Depending on the amount of restraints, the lateral load capacity of a braced wall could vary from minimal capacity with no restraint to maximal capacity if uplift is fully prevented. As a result, the required lengths of braced walls in Table 4 need to be adjusted based on the boundary conditions of the wall. In this section, adjustment factors to lateral load capacity due to different boundary conditions will be discussed.

Many factors affect the lateral load capacity of a braced wall. For example, gravity load on the braced wall could greatly increase the lateral load capacity of a braced wall [7]. Where the gravity load is large enough to prevent uplift, the braced wall is then fully restrained and the full capacity can be reached. The floor and/or the storey above the braced wall also have a direct impact on the lateral load capacity of the braced wall [5]. A stiff floor and/or upper storey could provide significant restraint to counteract the uplift force and thus provide increased lateral resistance. In addition, transverse walls attached to the ends of the shear walls and sheathings above and below openings in the braced wall provide further resistance to the uplift at the ends of the full-height bracing panels [1].

Because of countless combinations of braced wall configurations and difficulty to fully quantify the contribution of above factors, it is decided that a conservative adjustment factor be developed based on a braced wall panel in the most unfavorable conditions in a Part 9 building. As a result, the test configuration for 1.22 m braced wall panels, as shown in Figure 2, was used as the basis for determining the adjustment factor. The test result indicates that the lateral load capacity of a braced wall is at least 50% of that of a fully restrained braced wall. This finding has been used in the previous evaluation of the bracing requirements in the 2004 CWC Guide and the proposed Part 9 of 2010 NBCC [8]. Since the sample buildings studied represent the most unfavorable buildings and boundary conditions for braced wall panels, the adjustment factors are developed from the ratios of the lateral load capacities of partially-restraint walls and fully-restraint walls in Tables 1 and 2. For heavy buildings, the increased dead load would help to prevent uplift, therefore increasing the lateral load capacity of braced walls. And as a result, the adjustment factors are increased accordingly. A summary of the recommended adjustment factors is provided in Table 5.

(a) wall test set-up

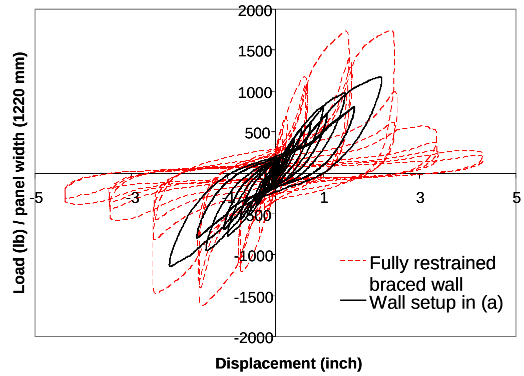

(b) load-displacement curves

Figure 2 Test configuration of braced wall in a Part 9 building

Table 5 Recommended adjustment factors for the required length of braced wall panels in Table 4

Building type		Supporting roof only	Supporting roof plus one floor	Supporting roof plus two floors	Supporting roof plus three floors
Regular building	Loadbearing	1.4	1.2	1.1	1.0
	Non-loadbearing	1.6	1.4	1.3	1.2
Heavy building	Loadbearing	1.2	1.0	1.0	-
	Non-loadbearing	1.4	1.2	1.1	

Summary and conclusions

The potential shortcomings of the bracing requirements for conventional wood-frame construction were analysed on selected building scenerios where the lengths and locations of the braced wall panels were **chosen to represent** as much as possible **the most unfavourable case** for lateral load resistance. The results showed the imbalance between the required lengths of braced walls in short and long directions of a rectangular building. While the lateral load capacity in the long direction of the building is adequate for the two- and three-storey buildings and is in fact overly conservative for the one-storey building, the lateral load capacity in the short direction of the building may not be sufficient to resist the base shear forces with the minimum bracing requirements in the codes. The results also showed that two-storey building has the largest discrepancies between the base shear and the lateral load capacity. This is because the required minimum lengths of braced wall panels are the same for one-storey and two-storey buildings in the codes.

A new method was proposed to better rationalize the bracing requirements for conventional wood-frame construction in Canadian and the US building codes. Instead of specifying the minimum length of braced wall panels as a constant percentage of the length of a building parallel to the direction of loading considered, the new method specifies the minimum length of braced wall panels as a function of floor area of the building. This will address the imbalance between the required lengths of braced walls in the short and long directions of a rectangular building.

Acknowledgements

Work on this project was suppoted by Canadian Forest Service of Natural Resources Canada and Canada Mortgage and Housing Corporation (CMHC) through its External Research Program. The assistance of Messrs Philip Eng and Paul Symons in carrying out shear wall tests, Dr. Kugbo Shim of Korean Forst Research Institute in analysing test data, and Ms Helen Guo in preparing the drawings is gratefully acknowledged.

References

[1] Cheng, H., Ni, C., Lu, X., and Karacabeyli, E. 2006. Effect of transverse walls and vertical load on the performance of shear walls, Proceedings of World Conference on Timber Engineering, Portland, Oragon, 2006.

[2] CSA, 2001. Engineering Design in Wood, Standard CSA O86-01, Canadian Standards Association, 178 Rexdale Boulevard, Etobicoke, Ont.

[3] CWC, 2004. Engineering Guide for Wood Frame Construction, Canadian Wood Council, Ottawa, ON.

[4] Fischer, D., Filiatrault, A., Folz, B., Uang, C-M., and Seible, F., 2001. Shake table tests of a two-story wood-frame house. Department of Structural Engineering, University of California, San Diego; CUREE publication No. W-06, Richmond, CA.

[5] Liu Y., Ni C., Rainer H., and Lu W.S., 2006. Effect of upper storey / floor on the performance of wood shear walls, Proceedings of World Conference on Timber Engineering, Portland, Oragon, 2006.

[6] NBCC 2005. National Building Code of Canada, National Research Council of Canada, Ottawa, ON.

[7] Ni, C. and Karacabeyli, E. 2002. Capacity of shear wall segments without hold-downs, Wood Design Focus, Summer 2002, p. 10 – 17.

[8] Ni, C., 2009. Wind and seismic design provisions for small wood buildings – Part A: Seismic, FPInnovations Forintek Division – Wastern Laboratory, Vancouver, BC, Prepared for Canadian Forest Service, Ottawa, ON, Mar 2009.

[9] Rainer, J. H, and Karacabeyli, E., 2000. Performance of wood-frame construction in past earthquakes, Proceedings of 12th World Conference on Earthquake Engineering, Auckland, New Zealand, 30 Jan. – 4 Feb, 2000.

CIB-W18/42-16-1

INTERNATIONAL COUNCIL FOR RESEARCH AND INNOVATION IN BUILDING AND CONSTRUCTION

WORKING COMMISSION W18 - TIMBER STRUCTURES

ADVANCED CALCULATION METHOD FOR THE FIRE RESISTANCE OF TIMBER FRAMED WALLS

S Winter
W Meyn

Technische Universität München

GERMANY

Presented by W Meyn

J. König stated his concern about the title of the paper as the paper deals with material properties and commented that one could verify the EC model with the calculations. S. Winter responded that the FEM based calculation model is intended to take into account the influence of cracks and find the phenomenon of the influence of mass transfer on fire performance including the heating effect due to the cracks. EC 5 is far on the safe side as shown in the experiments.

S. Aicher stated that there are no new cracks considered with existing cracks in the model. In reality new cracks can evolve between existing cracks. S. Winter replied that no new crack is an assumption.

A. Frangi commented on the differences between calculated and test results up to 20 minutes. The formation of cracks is very complex regarding material properties which can contribute to the added complication of these modeling processes. S. Winter responded that we have to start somewhere.

A. Buchanan received confirmation of how the thermal properties of the wall mass transfer are modeled and the specific heat capacity is calculated, not measured. A. Buchanan stated that moisture wave is an important issue. Lund University has done good work in this area with modeling.

Advanced Calculation Method for the Fire Resistance of Timber Framed Walls

Univ.-Prof. Dr.-Ing. Stefan Winter and Dr.-Ing. Wilhelm Meyn
Technische Universität München, Germany

1 Introduction

In the Meyn dissertation [1], a model was developed for determining two- and three-dimensional temperature distributions in the stud and cavity region of timber framed walls. The entire model is designed for calculation using an FEM program. Lone physical methods can also be used in a model based on manual calculation.

The model values, or the physical properties of the material defined in the model, were implemented in the ANSYS FEM program. The thermal verification of failure times is possible for any kind of wall construction by the use of solid wood, wood-based panels, gypsum plasterboard, fire protection gypsum plasterboard and mineral fibre insulation made of glass or rock wool. Materials, not listed here, for which thermal material data is still available, can also be included in the model. The ordering, thickness, density and moisture content of the materials are all freely definable. It is also possible to have a partially-insulated wall construction or one without any insulation.

To make the simulation of the thermal behaviour of timber framed walls as realistic as possible, crack formation in panel materials, opening of joints and changes to material properties caused by moisture transport was included in the complex model. These physical effects are triggered by specific temperatures in the FEM model. They are described in detail in the 3 chapters below.

2 Crack Formation in Panel Materials

To enable the simulation of cracks that develop due to material shrinkage (moisture loss) during a fire, a thermal crack model was developed based on practical knowledge.

An existing material stress, which varies according to the material temperature, is calculated and compared with the material strength, also temperature-dependent, in the model. Cracks begin to form when the existing thermal stress exceeds the material strength respectively when the temperature equilibrium of the two states is lost. Given a state of equilibrium in equation (1), the temperature as of which crack formation begins is known.

Sections 2.1 to 2.2.2 describe the equation (1) in detail and apply it to the example of fire protection gypsum plasterboard (Type F).

$$\text{exist. } \sigma_{fi(T)} = E_{fi(T)} \cdot \varepsilon_{fi(T)} = \frac{E_{fi(T)}}{E_{(20)}} \cdot E_{(20)} \cdot \frac{\Delta l}{l_0} \overset{!}{=} f_{k,fi(T)} = \frac{f_{fi(T)}}{f_{(20)}} \cdot f_{(20)} \tag{1}$$

2.1 Existing Material Stress

The existing material stress (left side of equation (1)) due to the thermal load comes from the theory of elasticity:

$$\text{exist. } \sigma_{fi(T)} = E_{fi(T)} \cdot \varepsilon_{fi(T)} = \frac{E_{fi(T)}}{E_{(20)}} \cdot E_{(20)} \cdot \frac{\Delta l}{l_0} \tag{2}$$

exist. $\sigma_{fi(T)}$: existing material stress in relation to temperature [N/mm²]

$E_{fi(T)}$: modulus of elasticity of the material in relation to temperature [N/mm²]

$\frac{E_{fi(T)}}{E_{(20)}}$: derived modulus of elasticity [-] (reduction in the modulus of elasticity under the effects of temperature in relation to the modulus of elasticity at room temperature)

$E_{(20)}$: modulus of elasticity at room temperature [N/mm²]

$\varepsilon_{fi(T)}$: material shrinkage due to moisture loss [-]

Δl: decrease in material length due to moisture loss [mm]

l_0: spacing between cracks [mm]

To help explain equation (2), the following sections look at the values and how they were derived for fire protection gypsum plasterboard (Type F).

2.1.1 Derived Modulus of Elasticity

The values in Figure 1 were calculated based on the test results from Walker et al. [2], Gonclaves et al. [3], the model concept of Young [4] and important benchmark data for the calcination of gypsum. Between 100 - 130°C, the reduction in the tensile strength and modulus of elasticity was chosen based on the calcination of the gypsum panels and hence also the reduction in density (see Figure 2).

A tendency towards a similar reduction in the density can also be seen from the findings from the various researchers in Figure 2. The gypsum panel loses the most mass between 20 and 130°C due to the evaporation of the free water and a large part of the bound water molecules. The mass of the gypsum panel then begins to fall again slowly up to 550 - 650°C. Between 130 and 650°C, the derived density, as used in the model, lies between the readings in Mehaffey [5] and Harmathy [6].

Figure 1:

Reduction of the modulus of elasticity (tensile) of fire protection gypsum plasterboard, relate to the modulus of elasticity at room temperature

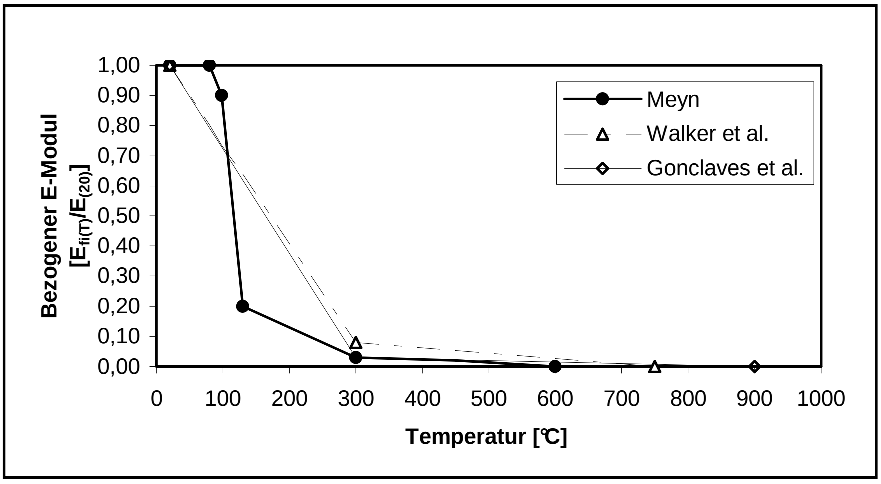

Between 650 and 700°C, an increased loss of mass is assumed in the model based on the work of Meyn [1], also found by Mehaffey [5] and Harmathy (quoted in [7]) The fire protection gypsum plasterboard lose approx. 10 % of their mass up to 1000°C.

Figure 2:

Reduction in the density of fire protection gypsum plasterboard versus temperature, relate to the size at room temperature

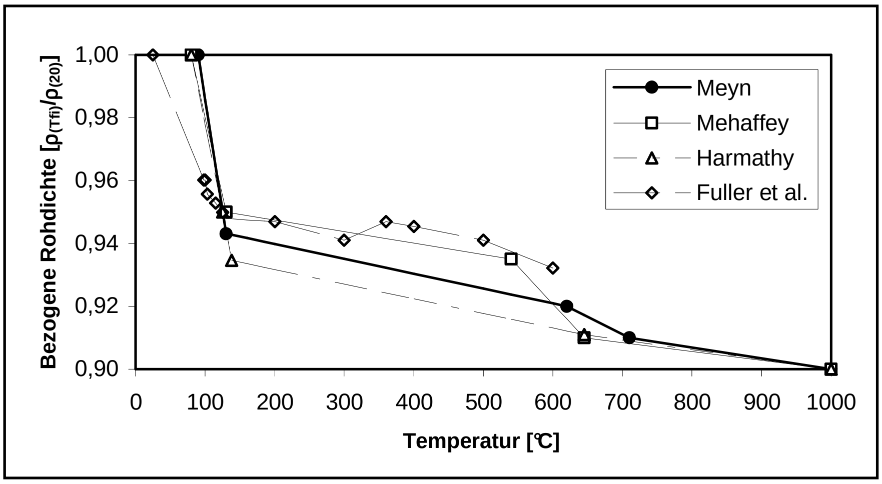

2.1.2 Decrease in Material Length due to Moisture Loss

The heat distribution in the timber frame wall is calculated in [1] with the aid of the ANSYS FEM program. To simulate crack formation, the parts were divided into a very fine FEM mesh (1 mm x 1 mm). In other words, cracks form in the model when the material length decreases by a millimetre.

2.1.3 Spacing between Cracks

In general, the average space between cracks was evaluated statistically in [1] based on the test findings (e.g. OSB, solid wood).

The fasteners were taken as fixed points on the plasterboards. The average space was 625 mm.

2.1.4 The modulus of Elasticity at Room Temperature

In the work of Meyn [1], the material values for room temperature were compiled from the literature. The basis for a study's inclusion was the material parameters and whether the testing apparatus was described. The model assumed a size of the modulus of elasticity for fire protection gypsum plasterboard of 3,291 N/mm² (see Table 1).

Table 1: Material attributes for panel materials (at room temperature)

	Tensile strength [N/mm²] Transverse direction of board	Compressive strength [N/mm²] Transverse direction of board	Elasticity modulus (tensile) [N/mm²] Transverse direction of board	Elasticity modulus (compressive) [N/mm²] Transverse direction of board
Panel materials				
Chipboard/OSB	-	-	2,340	-
Plywood board	38.8	-	3,640	-
Plasterboard (Type A)	1.09	5.46	3,534	457.5
Plasterboard (Type F)	1.14	5.96	**3,291**	475.5

2.2 Existing Material Strength (Tensile Strength)

The existing material strength ($f_{k,fi(T)} \mathrel{\hat{=}}$ tensile strength) due to the thermal load can be determined from the derived material strength for the temperature and the material strength at room temperature.

$$\mathbf{f_{k,fi(T)}}\mathbf{:}\ \frac{f_{fi(T)}}{f_{(20)}} \cdot f_{(20)} \tag{3}$$

$f_{k,fi(T)}$: characteristic strength according to temperature [N/mm²]

$\frac{f_{fi(T)}}{f_{(20)}}$: derived material strength [-] (reduction in strength due to temperature effects with respect to the material strength at room temperature)

$f_{(20)}$: tensile strength at room temperature [N/mm²]

To help explain equation (3), the next two sections look at values and how they are derived for fire protection gypsum plasterboard (Type F).

2.2.1 Material Strength at Room Temperature (Tensile Strength)

In [1], the material data at room temperature were compiled from the literature. A tensile strength of 1.14 N/mm² was assumed in the model for fire protection gypsum plasterboard (see Table 1).

2.2.2 Derived Strength (Tensile Strength)

The values in Figure 3 were determined based on the test results from Walker et al. [2], Gonclaves et al. [3], the model concept of Young [4] and important benchmark data for the calcination of gypsum.

Figure 3:

Reduction in the tensile strength of fire protection gypsum plasterboard, relative to the tensile strength at room temperature

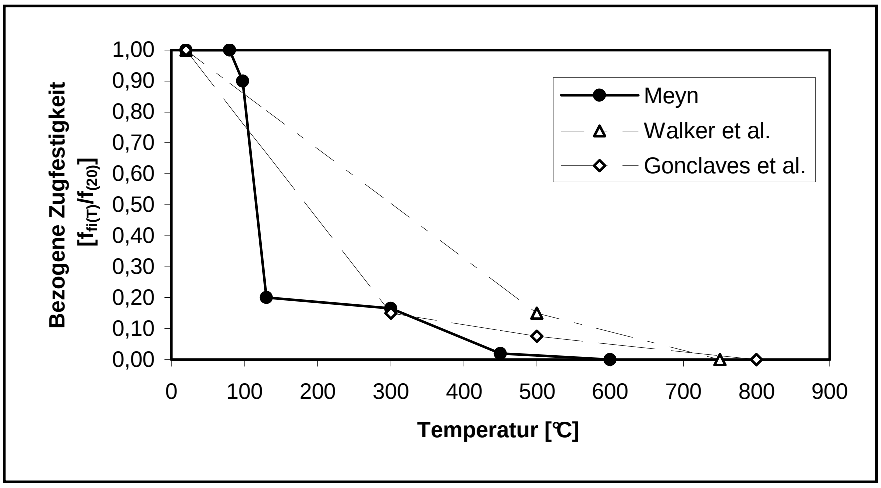

2.2.3 Sample Application: Crack Formation in Oriented Strand Boards (OSB)

Fig. 4 shows the temperature-dependent charring of an oriented strand board layer-by-layer at 5 minute intervals. The board with a width of 150 mm and a thickness of 18 mm was discretised into FEM elements 1 mm x 1 mm in size.

The charring and crack formation is considered by visual removing individual FEM elements (see Fig. 4). In the mathematical FEM model, the matrices for the “killed” elements were given a value close to zero and from this point on had only a negligible influence on the whole system. At the same time, the loss of elements activated thermal effects on the "new" surface of the part. The temperature load at this point then corresponds to the current standardised fire [10] in the combustion chamber.

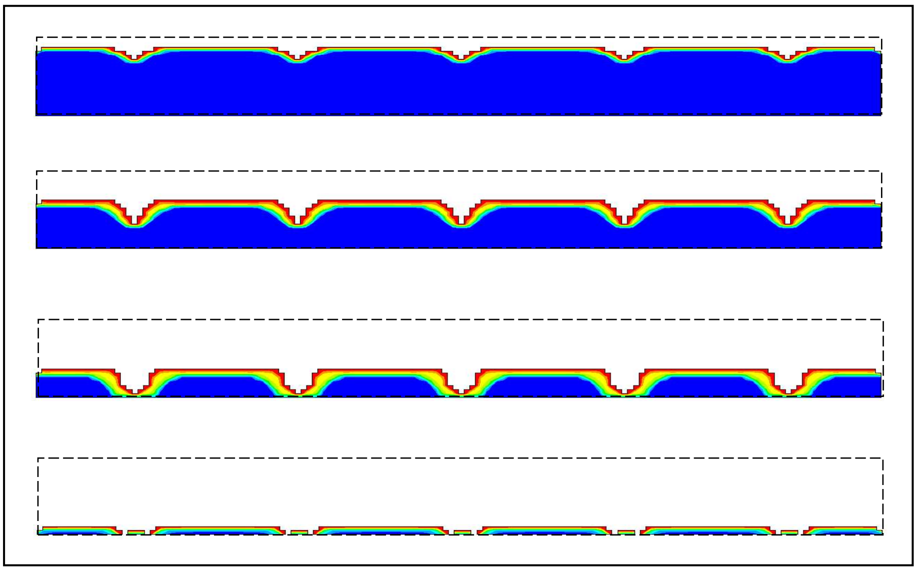

Figure 4: Charring of an 18 mm x 150 mm OSB-panel (after 5, 10, 15 and 20 minutes)

------ Initial edge of OSB

3 Crack and Joint Expansion

Cracks begin to form in the material after the equilibrium temperature (from Chapter 2) is exceeded due to the thermal load of the fire. These cracks expand as the temperature increases. The expansion is caused by the shrinkage of the material between the cracks. The shrinkage of this region is calculated using formula (4).

$$\mathbf{L_{k,fi(T)}} = \frac{L_{fi(T)}}{L_{(20)}} \cdot L_{r,fi(T)} \tag{4}$$

$\mathbf{L_{k,fi(T)}}$: characteristic length depending on temperature

$\frac{L_{fi(T)}}{L_{(20)}}$: derived length depending on temperature [-]

$L_{r,fi(T)}$: average space between two cracks [mm]

This change in length is considered in the model using a derived length. The change in length of fire protection gypsum plasterboard (Type F) was defined based on the observable changes to the gypsum during the calcination phases. The reduction data was based on the test results of Mehaffey [11] and Walker et al. [12].

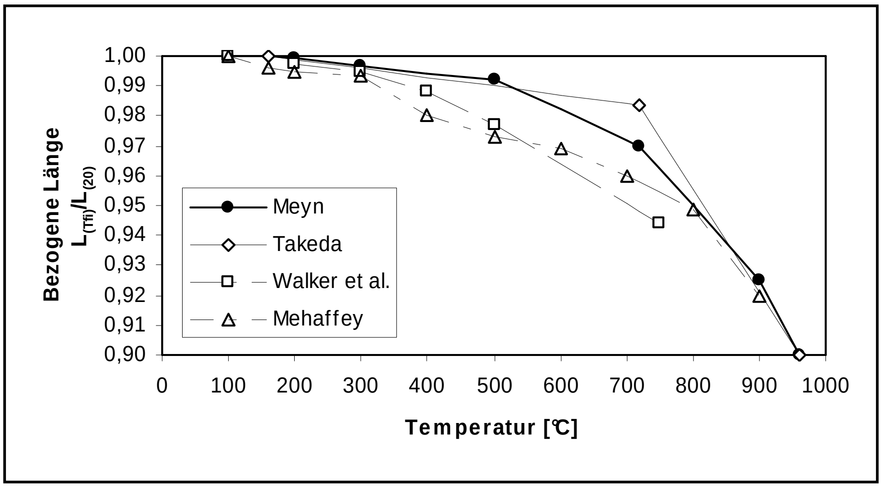

Figure 5: Reduction in the length of fire protection gypsum plasterboard, relative the length at room temperature

The widening of panel edges (joins) is simulated in the model according to the process described above.

4. Changes to Material Properties due to Moisture Transport

To calculate the heat distribution due to thermal conduction in solid materials (based on the Fourier equation), three temperature-dependent material parameters are required: the density, heat capacity and thermal conductivity. For the Meyn model [1], these values were taken from the literature.

To test the quality of the model, the calculated temperature curve was compared to the measured curve. To have comparison curves available for the test, Meyn [1] carried out his own fire tests with the thermal load based on the standard fire curve[10] on individual wall materials (pilot tests) and entire wall structures (full-scale tests). Temperatures were measured in the wall structures per layer with the aid of thermal elements.

After the thermal attributes for individual materials were secured by comparing them with the test data, this was used to calculate entire wall constructions. The result from the calculation of the fire resistance rating of a timber framed wall differed noticeably from the measured values. Following an in-depth examination of the temperature distribution in the wall, it was found that the heat storage capacity attribute for rock wool insulation was a significant reason for this difference. The following two sections take a detailed look at the factor responsible using the pilot and full-scale tests.

4.1 Pilot Test

A specific heat capacity of 0.23 Wh/(kg·K) ≙ 0.83 kJ/(kg·K) was taken from datasheet [8] for the rock wool insulation in timber framed walls. This value was assumed to be constant for all temperatures, as in König and Walleij [9].

Using the ANSYS FEM program, the measured temperature distribution at point A (see Fig. 6) was recalculated. In pilot test the rock wool insulation was directly exposed to the thermal energy of the combustion chamber. An initial value of 0.83 kJ/(kg·W) was chosen for the heat capacity. The curve for the calculated temperature almost covered the measured temperature curve completely. Due to the low intrinsic moisture of the insulation (0.80 %), there was no visible hold point in the temperature curve.

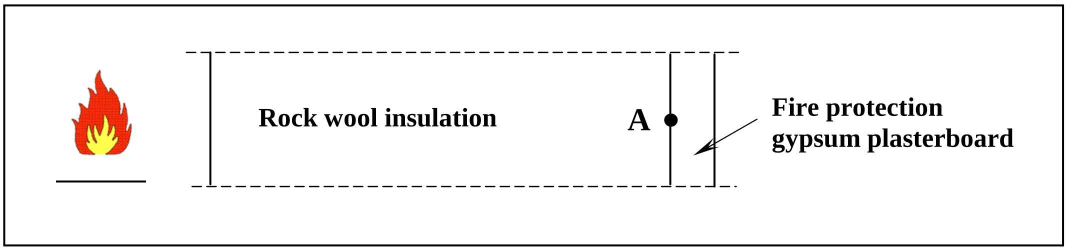

Fig. 6: Experimental set-up – Pilot

4.2 Full-scale Test

By recalculating the temperature curve for a full-scale test with the material attributes from the pilot, the calculated results were considerably different from the measured values. After calibrating the thermal attributes of the material for rock wool insulation, the result was a peak for the specific heat capacity that deviated markedly from that for the pilot study (see Fig. 7).

Since the peak for the specific heat capacity lies between 98 and 120°C, it is probably the case that a change of the aggregate state of water plays a part in the thermal process here (see Fig. 7). This spike cannot be explained by the insulation’s intrinsic moisture content. It is almost identical in the pilot and full-scale study (at 0.80 % and 1.29 % respectively). The moisture must have entered the insulation externally, from the side facing the fire.

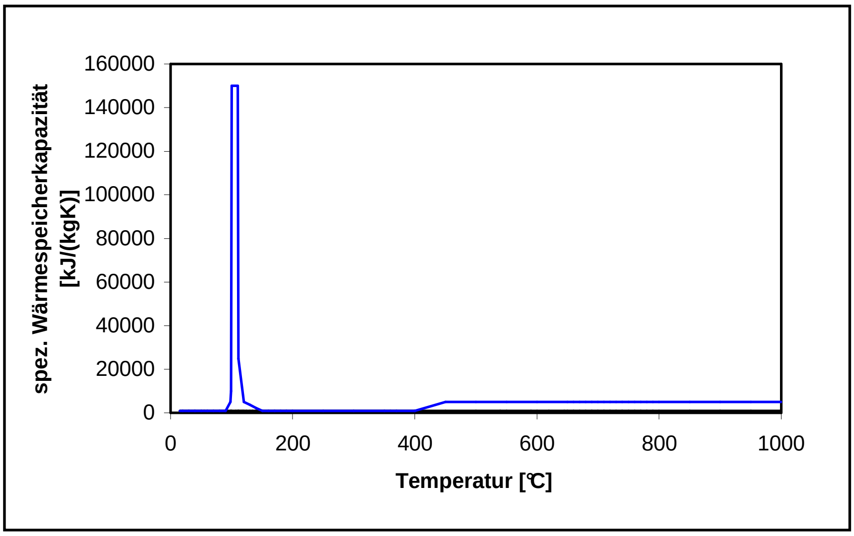

Figure 7:

Specific heat capacity versus the temperature of rock wool insulation (full-scale test)

On the side of the wall structure facing the fire, an oriented strand board (OSB) could be found as surface material between the combustion chamber and the rock wool insulation. When there is charring of wooden panels, a vapour pressure arises in the wooden cells of the panel material which arises due to the increase in temperature in the warming zone. Spatially, the pressure has an equal effect in all directions. For a stress-free expansion according to [13], water vapour needs approximately 1,700 times the original volume of water (1 l water ≙ approx. 1.7 m^3 water vapour). This increase in volume causes the wooden cells to burst open. The moisture which gets into the pyrolysis zone as a result of the vapour pressure, is transported outwards into the chamber as water vapour during the charring. The proportion of moisture forced inwards by the vapour pressure condenses in the cooler region of the profile and increases the wood moisture here.

Dorn and Egner [14] confirm this scenario with their findings. The external regions of the uncharred wood on the fire exposed side were completely desiccated, the wood moisture content increased by around 2 % inside the profile.
Janssens also describes in [15] that a part of the water vaporises on the surface subject to high thermal stresses and another part travels into the profile where it condenses at temperatures below 100°C.
In the tests of White and Schaffer [16] with a thermal load applied to one side, the moisture content of wood samples made from oak, pine and Douglas fir in the internal region of the profile increased by 10 % according to their measurements. The spikes in the moisture increase were found around the 100°C isotherm in each case. White und Schaffer explained the increase in moisture on account of a moisture wave which propagates at the speed of the charring within the profile due to the vapour pressure.
The calculations from both fire tests confirm the conclusions drawn by the researchers mentioned above.
Since the temperature in the panel profile is not homogenous during charring, but rather can be grouped into different zones, the water vapour can condense when reaching colder zones and is transformed back into water vapour again on account of the increasing temperature. This constantly repeating change in aggregate state requires considerable amounts of energy which does not contribute to an increase in the temperature of the material.

4.3 Procedure used to Determine the Peak Capacity

A model was developed in [1] to determine the size of the peak heat capacity at approx. 90 - 110 °C due to the moisture transport. The calculated data, $m_{w(1\text{-}mm)}$ (moisture content in kg for a 1.0 mm panel thickness per 1.0 m² of wall surface area) from the diagram in Fig. 8 can be used to derive the reference value for the maximum heat storage capacity, $C_{max,k}$. The κ_w factor was introduced to take into account the absolute mass of water between combustion chamber and mineral fibre insulation. Given a constant percentage of material moisture, the absolute water mass increases as the panel thickness increases. The correction value κ_w was defined as being non-linear since the wave of moisture in the charring area results in an increase of the moisture content in the condensation area. During determination of the κ_w factor, it has been assumed that a third of this material moisture escapes into the combustion chamber and two-thirds are compressed into the remaining profile due to water vapour pressure from where there is an increase in the amount of moisture - though this does not occur evenly as the water vapour condenses again in the cooler regions of the profile.

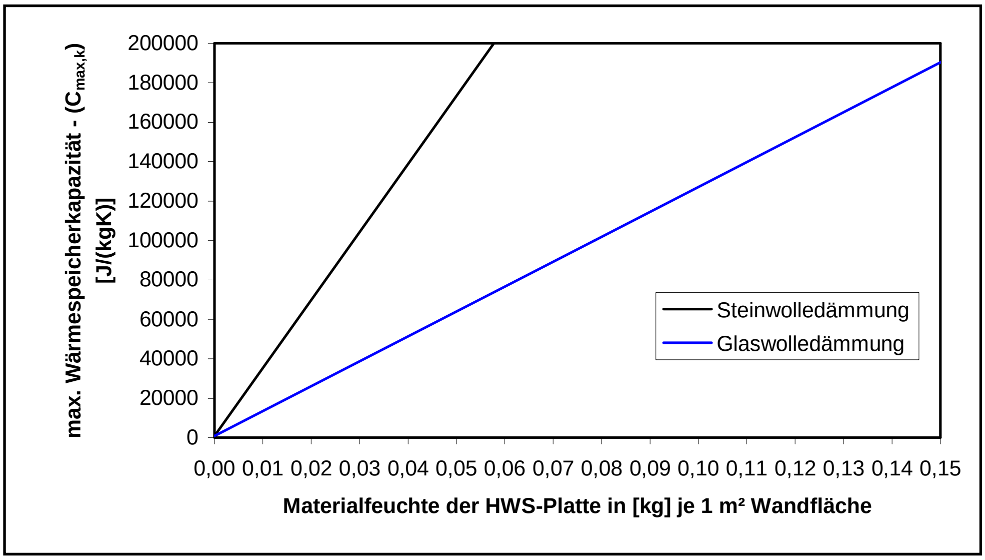

Fig. 8: Maximum heat storage capacity ($C_{max,k}$) of rock wool insulation (in the temperature range of approx. 90 – 120 °C) depending on the material moisture content per 1.0 mm panel thickness and a wall surface area of 1.0 m² for wood-based panels on the section facing the fire.

$$m_w = m_u - m_{dtr} \tag{5}$$

m_w:	mass of water (in kg – related to 1.0 m³)
m_u:	mass of moist wood-based panel (in kg – related to 1.0 m³)
m_{dtr}:	mass of kiln dry wood-based panel (in kg – related to 1.0 m³)

$$m_{w(1\text{-}mm)} = m_w/1000 \tag{5a}$$

m_w:	mass of water (in kg – related to 1.0 m)
$m_{w(1\text{-}mm)}$	mass of water (in kg – for 1 mm thickness and wall surface area of 1.0 m²)

$C_{max,d} = C_{max,k} \cdot \kappa_w$ (5b)

$C_{max,d}$: max. heat capacity (parameter)

$C_{max,k}$: max. heat capacity (reference value from Fig. 8)

κ_w: correction factor used to take panel thickness into account

κ_w (for d > 18 mm) = 1.0 + (3.212 · ln(d-18) + 4.067)/100

κ_w (for d = 18 mm) = 1.0

κ_w (for d < 18 mm) = 1.0 - (1.871 + 1.295 · d + 0.228 · d^2)/100

d = panel thickness [mm]

List of Literature

[1] Meyn, W.: Experimentelle und numerische Analyse des thermischen sowie Grundlagen des strukturmechanischen Verhaltens von Holzrahmenwänden bei thermischer instationärer Einwirkung unter Berücksichtigung des nicht linearen Materialverhaltens. Dissertation, Universität Leipzig, 2008 (ISBN 978-3-86624-435-1).

[2] Walker, D. und Lightfoot, M.: Mechanical Properties of Fire Rated Gypsum Board. Department of Civil and Building Engineering, Victoria University of Technology, Melbourne, 1995.

[3] Goncalves, T.; Clancy, P. und Poynter, W.: Mechanical Properties of Fire Rated Gypsum Board. Victoria University of Technology, Australia, 1996.

[4] Young, S. A.: Structural Modelling of Plasterboard-Clad, Light Timber-Framed Walls in Fire. Ph.D. Dissertation, Victoria University of Technology, Australia, 2000.

[5] Mehaffey, J. R.; Cuerrier, P. und Carisse, G.: A model for predicting heat transfer through gypsum board/wood-stud walls exposed to fire. In: Fire and Materials 18 (1994) 5, S. 297 – 305.

[6] Harmathy, T. Z.: DBR Paper No. 1080, National Research Council of Canada (NRCC), Ottawa, 1983.

[7] DiNenno, P. J. et al.: SFPE Handbook of Fire Protection Engineering. National Fire Protection Association Quincy, Massachusetts; Society of Fire Protection Engineers Bethesda, Maryland, 2002.

[8] Datenblatt: Novatherm Steinwolle

[9] König, J. und Walleij, J.: Timber frame assemblies exposed to standard parametric fires – Part 2: A design model for standard fire exposure. Swedish Institute for Wood Technology Research, Rapport I 0001001. Stockholm, 2000.

[10] DIN 4102-2:1977-09: Brandverhalten von Baustoffen und Bauteilen, Teil 2 – Bauteile, Begriffe, Anforderungen und Prüfungen.

[11] Mehaffey, J. R.: Development of Fire Endurance Models for Wood Stud Walls: Progress Report. Forintek Canada Corp., 1991.

[12] Walker, D. und Lightfoot, M.: Mechanical Properties of Fire Rated Gypsum Board. Department of Civil and Building Engineering, Victoria University of Technology, Melbourne, 1995.

[13] Cerbe, G. und Hoffmann, H.: Einführung in die Thermodynamik – Von den Grundlagen zur technischen Anwendung. 13. Aufl., Carl Hanser Verlag München, 2002.

[14] Dorn, H. und Egner, K.: Brandversuche an brettschichtverleimten Holzträgern unter Biegebeanspruchung, Sonderdruck aus: Holz als Roh- und Werkstoff 25 (1967), S. 308 – 320.

[15] Janssens, M. L.: Modelling of the thermal degradation of structural wood members exposed to fire. In: Fire and Materials 28 (2004) 2-4, S. 199 – 207.

[16] White, R. H. und Schaffer, E. L.: Transient moisture gradient in fire-exposed wood slab. In: Wood and Fiber 13 (1981) 1, S. 17 – 38.

CIB-W18/42-16-2

INTERNATIONAL COUNCIL FOR RESEARCH AND INNOVATION IN BUILDING AND CONSTRUCTION

WORKING COMMISSION W18 - TIMBER STRUCTURES

FIRE DESIGN MODEL FOR MULTIPLE SHEAR STEEL-TOTIMBER DOWELLED CONNECTIONS

C Erchinger

A Frangi

M Fontana

ETH Zurich, Institute of Structural Engineering

SWITZERLAND

Presented by A Frangi

H.J. Blass commented that in some dowels the edge distance after the fire duration is very low and asked if the model takes this into consideration. A. Frangi responded that the model considers this. H.J. Blass asked how the designer knows. A. Frangi replied the designer only needs charring depth and needs to respect minimum requirement according EC5.

R. Crocetti asked how manufacturing tolerance of the gap between steel plate and wood alter the results. A. Frangi replied the influence may not be too much.

A. Buchanan stated that the design method involves design at room temperature and allow for charring rate. The design method doesn't check the embedment strength of each dowel. Difference in the embedment strength for each dowel and along the length of the dowel would lead to more of a plastic deformation. He asked when FEM was done, was the dowel considered stationary or moving. A. Frangi replied that the dowel movement was not considered. He said there are two parameters (embedment strength and temperature) but one equation. Therefore one can make the adjustments to make it work.

T. Poutanen discussed rule of thumb to determine the volume of wood after charring.

S. Aicher asked in the 3D calculation was the temperature progression according to end grain face considered. A. Frangi replied yes.

S. Winter commented that the paper is excellent. Most discussions look for complicated issues however the final design proposal is actually very simple which is based on the cross section after charring.

Fire design model for multiple shear steel-to-timber dowelled connections

Carsten Erchinger, Andrea Frangi & Mario Fontana
ETH Zurich, Institute of Structural Engineering, 8093 Zurich, Switzerland

1 Introduction

Dowelled connections are made of circular cylindrical steel dowels, fitting tightly in pre-drilled holes and used for transferring loads perpendicular to the dowel axis. Multiple shear steel-to-timber connections with slotted-in steel plates and steel dowels (see Fig. 1) show a high load-carrying capacity and a ductile failure mode (plastic deformation of the dowels) at ambient temperature if minimum spacing and distance requirements of the dowels are respected, for example according to EN 1995-1-1 [1]. The load-carrying capacity of the connections primarily depends on the embedment strength of the timber members and the yield moment of the dowels. Due to the protection of the slotted-in steel plates against fire provided by the timber side members (see Fig. 1), a high fire resistance may be achieved. In order to accurately predict the structural performance in fire, knowledge on the temperature distribution in the cross-section as well as the influence of steel elements (slotted-in steel plates and steel dowels) on the charring of the timber members is required. This is challenging and complex due to the influence of several parameters like dowel diameter, geometry of the connection, different failure modes, different thermal properties of timber and steel as well as the thermal interaction between timber members and steel elements. Thus, only limited work has been carried out on the fire behaviour of steel-to-timber connections [2-4] and current standards do not contain consistent calculation models for the fire design of steel-to-timber connections taking into account the influences of the different parameters. The reduced load method given in EN 1995-1-2 [5] is only valid for laterally loaded symmetrical three-member connections (two shear planes, one steel plate in the middle) under ISO-fire exposure. The relative load-carrying capacity vs time given as a one-parameter exponential model is based on a still limited number of fire tests carried out on timber connections with bolts and nails [6-8]. For multiple shear steel-to-timber connections with two or three slotted-in steel plates no design models in the fire situation exist so far.

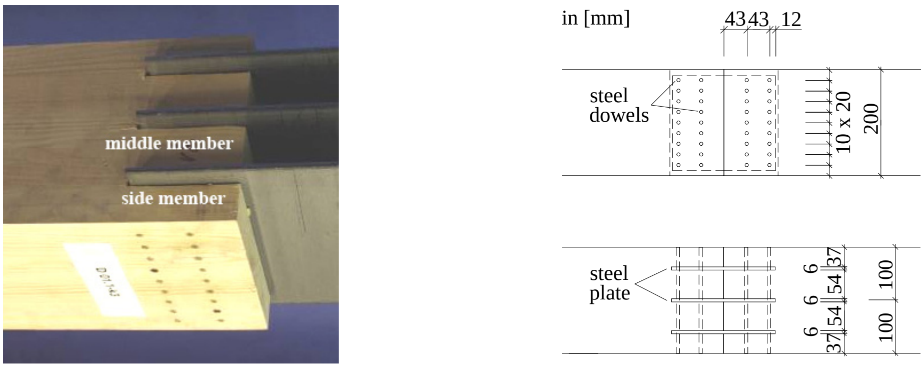

Figure 1 Typical multiple shear steel-to-timber connection with three steel plates (left) and example of the geometry of tested connection D1.1 (right)

A comprehensive research project on the fire behaviour of multiple shear steel-to-timber connections with two or three slotted-in steel plates and steel dowels has recently been performed at ETH Zurich [9]. The objective of the research project was the development of a fire design model for multiple shear steel-to-timber connections with slotted-in steel plates and steel dowels. In addition to 25 tensile tests at ambient temperature to determine the load-carrying capacity, the fire behaviour of the connections was experimentally analysed with 18 fire tests under constant tensile load [10]. All fire tests were performed under ISO-fire exposure on the horizontal furnace at the Swiss Federal Laboratories for Materials Testing and Research (EMPA) in Dubendorf. The paper first describes the main results of extensive experimental and numerical analyses on the fire behaviour of multiple shear steel-to-timber connections with slotted-in steel plates and steel dowels. Particular attention is given to the analysis of the influence of the steel elements on the charring of the timber members. Then, the design model for multiple shear steel-to-timber dowelled connections with slotted-in steel plates in fire is presented and compared to fire tests.

2 Fire behaviour of steel-to-timber dowelled connections

2.1 Fire tests

The test series consisted of 25 tensile tests performed at ambient temperature according to EN 26891 as well as 18 fire tests conducted under ISO-fire exposure. The timber cross-section was 200x200mm (strength class GL24h) with two or three slotted-in steel plates (thickness 5mm) and steel dowels. In the fire tests a constant tensile loading parallel to grain direction was applied with 30, 15 or 7.5% of the average measured load-carrying capacity F_u of 5 tensile tests performed at ambient temperature. As test parameters, the dowel diameter (6.3 and 12 mm), the number and configuration of the steel dowels, the thickness of the timber members (in order to reach a fire resistance of 60 minutes) and the load level (30, 15 and 7.5% of F_u) were varied. Table 1 gives an overview of the test programme and the main results. All details on the test specimens, test set-up and test results can be found in [9, 11].

Table 1 Overview of test programme on multiple shear steel-to-timber connections with slotted-in steel plates

Test name	Number of tests	Type of test	Tensile load [kN]	Fire resistance (mean value) [min]	Remarks
D1.1	5	ambient	until failure F_u	---	200x200mm (GL 24h), 3 steel
	2	ISO-fire	$0.3 \cdot F_u = 145$	33.0	plates, 2x9 steel dowels (6.3mm);
	2	ISO-fire	$0.15 \cdot F_u = 72$	36.0	(see Fig. 1 right)
	2	ISO-fire	$0.075 \cdot F_u = 36$	41.0	
D1.2	5	ambient	until failure F_u	---	280x280mm (GL 24h), 3 steel plates,
	2	ISO-fire	$0.3 \cdot F_u = 173$	73.0	2x9 steel dowels (6.3mm)
D1.3	2	ISO-fire	$0.3 \cdot F_u = 145$	64.5	Same as D1.1; protection by 3-layered timber boards (27mm)
D1.4	2	ISO-fire	$0.3 \cdot F_u = 145$	60.5	Same as D1.1; protection by gypsum plasterboards (15/18mm)
D2.1	5	ambient	until failure F_u	---	200x200mm (GL 36h), 3 steel plates,
	2	ISO-fire	$0.3 \cdot F_u = 188$	31.0	3x9 steel dowels (6.3mm)
D3.1	5	ambient	until failure F_u	---	200x200mm (GL 24h), 3 steel plates,
	2	ISO-fire	$0.3 \cdot F_u = 69$	32.5	3x3 steel dowels (6.3mm)
D4.1	5	ambient	until failure F_u	---	200x200mm (GL 24h), 2 steel plates,
	2	ISO-fire	$0.3 \cdot F_u = 124$	34.5	2x4 steel dowels (12mm)

All connections reached a fire resistance of more than 30 minutes. A reduction (connection D2.1) or increase (connection D3.1) of the number of dowels as well as the dowel diameter (connection D4.1) did not significantly increase the fire resistance. A reduction of the load level applied during the fire did not lead to a significant increase of the fire resistance. By increasing the thickness of the timber side members as well as the end distance of the dowels by 40 mm the connections reached a fire resistance of more than 70 minutes (connection D1.2). Connections protected by 27mm thick 3-layered cross-laminated timber boards made of spruce or gypsum plasterboards showed a fire resistance of around 60 minutes. Thus, from a fire design point of view these strategies were favourable in order to increase the fire resistance significantly.

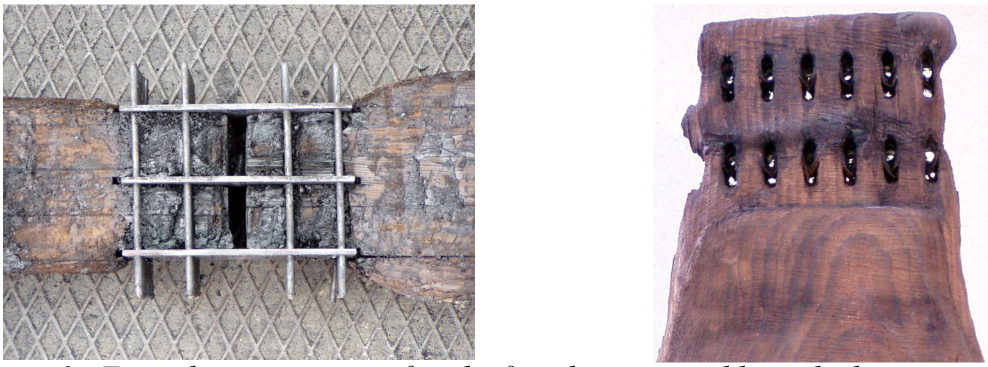

Figure 2 Typical test specimen after the fire characterized by embedment strength failure (failure mode I) with large ovalisation of the holes

Due to charring of the timber side members, the steel dowels were not able to form plastic hinges (see Fig. 2). Thus, the connections usually failed by embedment failure, known as failure mode I according to the Johansen yield model. Due to the heat flux from the steel dowels into the wood, the temperature close to the steel dowels was higher than in the inner part of the timber cross-section, leading to large ovalisations of the holes due to the temperature dependent reduction of the embedment strength of timber (see Fig. 2).

2.2 FE-thermal analysis

In addition to the fire tests an extensive thermal numerical study was performed using FEM (finite element method). The temperature development in the connection was calculated using three-dimensional finite element models implemented in ANSYS. The calculated temperatures were used for the mechanical analysis of the connection in fire. The heat transfer to the surface of the member was calculated using temperature-independent constant values according to EN 1991-1-2 for the resultant emissivity by radiation ε_{res} = 0.8 and the coefficient of heat transfer by convection α_c = 25 W/(m^2 K). Density, thermal conductivity and specific heat capacity of wood, charcoal and steel vary as a function of the temperature. The change of moisture, i.e. the evaporation of water at a temperature of about 100°C was implemented into the FE-simulation as latent heat. Mass transfer of moisture into or out of the wood was neglected. In the FE-thermal analysis, charring of wood (i.e. reduction of cross section) was taken into account by gradually changing the thermal properties of wood into those of charcoal with increasing temperature. For the FE-thermal analysis, an initial density of 450 kg/m^3 and an initial moisture content of 12% were considered (average values of test specimens). The temperature-dependent relationships for the density and specific heat of wood and charcoal were assumed according to EN 1995-1-2. Cracks in the charcoal increase the heat flux due to radiation and convection. Thus, the thermal conductivity values of the char layer used in FE-thermal analyses are ''effective'' values rather than ''real'' material properties in order to take into account the increased heat flux due to cracks above about 500°C and the degradation of the char layer at about 1000°C. For the FE-thermal analysis, the temperature-dependent relationship for the thermal conductivity of wood and charcoal was assumed according to EN 1995-1-2. For steel, the thermal properties were assumed according to EN 1993-1-2. If possible, the FE-thermal analysis was performed using symmetrical conditions in order to reduce the calculating time. A detailed description of the validation of the material properties used for the FE-thermal analysis can be found in [9].

The residual cross-section of connection D1.1 calculated numerically taking into account all areas with temperatures lower than 300°C as well as determined with the laser-scanning method after the fire test are shown in Fig. 3. A very good agreement was found between FE-thermal analysis and fire test. Further, it can be seen that the side members were completely charred and the steel dowels located close to the edge were embedded in charred wood. Corner roundings due to the superposition of heat flux from side and top/bottom as well as an increased charring close to the steel elements was calculated by the FE-thermal analysis. The middle slot did not show temperatures above 300°C so that no charring was expected there. All calculation results were confirmed by visual observation of the residual cross-sections after the fire tests.

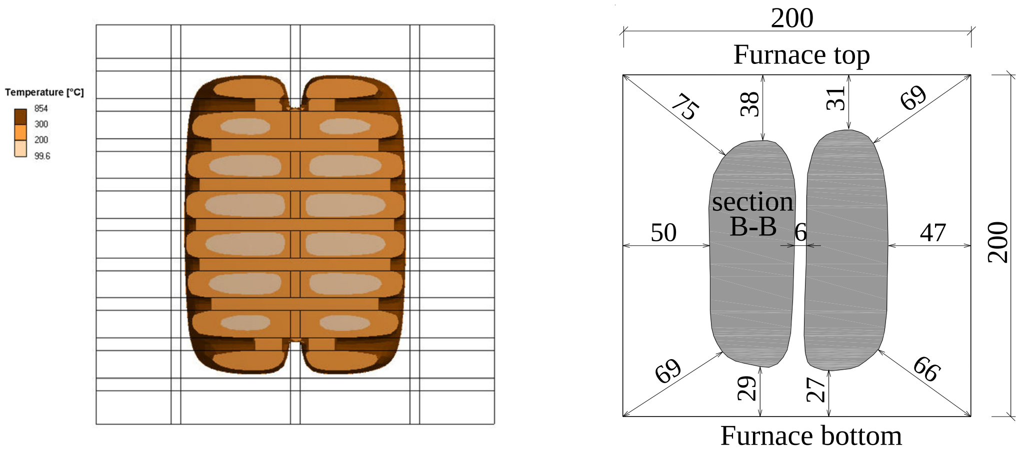

Figure 3 Residual-cross-section of the connection D1.1 at failure time of 33 minutes calculated numerically (left) as well as determined with the laser-scanning method

2.3 Calculation model

Because of charring of the timber side members, embedment failure (i.e. failure mode I according to the Johansen yield model) was observed during the fire tests (see Fig. 2). Thus, the fire resistance of the multiple shear steel-to-timber connections with slotted-in steel plates was calculated taking into account the temperature dependent reduction of the embedment strength of timber. The temperature of timber close to the dowels varied depending on the position of the dowel in the cross-section. Therefore, for the calculation of the load-carrying capacity of the connection in fire, for each dowel three-dimensional temperature fields were calculated using FE-thermal analysis as shown in Fig. 4. The three-dimensional temperature fields were divided into elements i with a width b_i of 10 mm and a length of half the spacing of the dowels (l = 3.5d) parallel to grain direction (i.e. load direction). The length of the element was divided into elements of 2 mm each (see Fig. 4).

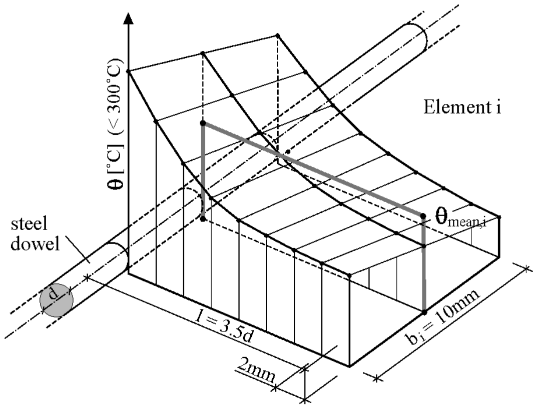

Figure 4 Element i of a three-dimensional temperature field between two fasteners within one row parallel to load direction in a multiple shear steel-to-timber connection with slotted-in steel plates and steel dowels

For the calculation of the load-carrying capacity of the connection in fire, the mean value of the temperature was calculated for each element i. Elements with a temperature higher than 300°C were not considered as the embedment strength of timber is assumed to decrease to zero for a temperature of 300°C (see Fig. 5 left). Then, the load-carrying capacity of the connection in fire was calculated according to Equation 1 by integration of all elements taking into account the temperature dependent reduction of embedment strength.

$$R_{fi} = n_{tot} \cdot \sum_{i=1}^{n} (f_{h,i(\theta_{mean,i})} \cdot b_i) \cdot d \tag{1}$$

where

R_{fi}	is the load-carrying capacity of the connection in fire [N]
n_{tot}	is the number of dowels in a connection [-]
$\theta_{mean,i}$	is the mean temperature of element i [°C]
$f_{h,i(\theta_{mean,i})}$	is the temperature-dependent embedment strength of element i [N/mm^2]
b_i	is the width of element i [mm]
d	is the diameter of the steel dowel [mm]

Unfortunately temperature-dependent properties of wood reported in the literature exhibit a large scatter and are partially in contradiction to each other. The main reason is that the test results are highly influenced by differences in the test methods used [12]. Few data is available on the influence of temperature on the embedment strength of timber. For simplicity, a bilinear relationship with break point at 100°C as shown in Fig. 5 left was assumed similar to the bilinear relationship for the temperature-dependent reduction of the compressive strength of timber given in EN 1995-1-2, which was derived from results of both small-scale and large-scale fire tests on loaded timber frame members in bending [13,14]. The assumed bilinear relationship for the temperature-dependent reduction of the embedment strength of timber shows a relative reduction to 50% of strength at 100°C and was calibrated to the results of the fire tests on multiple shear steel-to-timber connections with slotted-in steel plates and steel dowels performed during the research project at ETH Zurich (see Fig. 5 right).

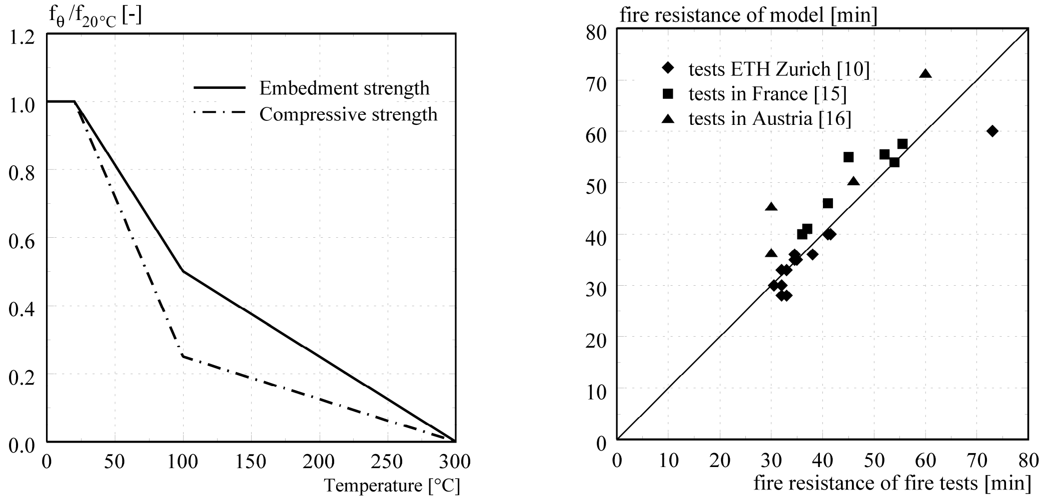

Figure 5 Left: temperature-dependent reduction of embedment strength assumed for the calculation model and compressive strength parallel to grain direction according to EN 1995-1-2; Right: comparison of fire resistance between calculation model and fire tests

Further, the model was used to calculate the load-carrying capacity of connections with only one steel plate in the middle tested under ISO-fire exposure in France [15] and Austria [16]. The calculation model slightly overestimated the fire resistance of the connections (see Fig. 5 right). A possible reason may be that connections with only one steel plate are more susceptible to stress concentration close to the dowels than connections with multiple steel plates. Further, the temperature fields in connections with only one steel plate are generally lower than the temperature fields in connections with two or three steel plates.

3 Design model

3.1 Introduction

An analytical design model for the calculation of the load-carrying capacity in fire of unprotected multiple shear steel-to-timber dowelled connections was developed in analogy with the reduced cross-section method according to EN 1995-1-2. The model is based on failure mode I according to the Johansen yield model (i.e. embedment failure) and takes into account the influence of the steel elements (i.e. steel plates and steel dowels) on the charring of the connection. The temperature dependent reduction of the strength of the steel dowels is not significant in comparison to the temperature dependent reduction of the embedment strength of timber and can be neglected. The model was developed for a fire resistance up to 60 minutes. The influence of thermal expansion of timber is small and was neglected [17].

For the relevant duration of the fire exposure it shall be verified that:

$$E_{d,fi} \leq R_{d,fi} \tag{2}$$

The design effects of actions in fire $E_{d,fi}$ is calculated according to EN 1990. For the calculation of the fire design resistance $R_{d,fi}$ the design strength values in fire $f_{d,fi}$ of timber are determined according to EN 1995-1-2 as follows:

$$f_{d,fi} = k_{mod,fi} \cdot \frac{k_{fi} \cdot f_k}{\gamma_{M,fi}} \tag{3}$$

where

$f_{d,fi}$: is the design strength in fire of timber
f_k: is the characteristic mechanical property (5% fractile) at ambient temperature
k_{fi}: is the modification factor for fire taking into account the 20% fractile
k_{fi} = 1.15 for connections and glued laminated timber
$k_{mod,fi}$: is the modification factor for fire taking into account the effects of temperature on the mechanical properties ($k_{mod,fi}$ = 1.0 for the Reduced cross-section method)
$\gamma_{M,fi}$: is the partial safety factor in fire ($\gamma_{M,fi}$ = 1.0 for accidental actions)

The effective cross-section is calculated by reducing the initial cross-section by the effective charring depth d_{ef} as shown in Fig. 6. For simplicity, the same value of d_{red} is used for charring on side (index s) and on top/bottom (index o).

$$d_{ef,s} = d_{char,s} + d_{red} \tag{4}$$

$$d_{ef,o} = d_{char,o} + d_{red} \tag{5}$$

The design value of the load-carrying capacity in fire $R_{d,fi}$ of the connection subjected to tension can be calculated as following:

$$R_{d,fi} = A_{ef} \cdot f_{t,0,k} \cdot k_{fi} \tag{6}$$

where

$R_{d,fi}$ is the design value of the load-carrying capacity in fire of the connection
A_{ef} is the effective cross-section
$f_{t,0,k}$ is the characteristic tensile strength parallel to the grain direction

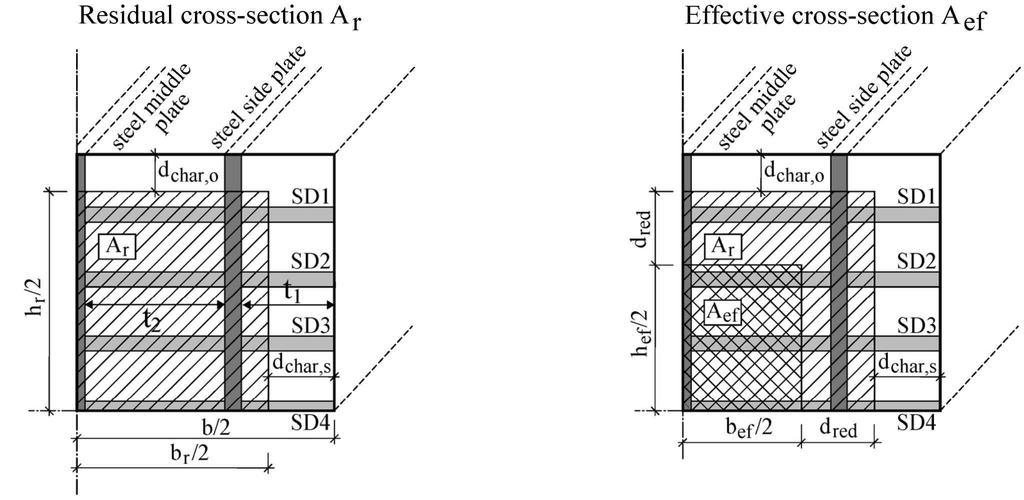

Figure 6 Residual (A_r) and effective cross-section (A_{ef}) for the determination of the load-carrying capacity of multiple shear steel-to-timber dowelled connections in fire, shown on the example of one quarter of cross-section of a connection with three slotted-in steel plates (SD = steel dowel)

The design model is based on the following assumptions:

- Unprotected multiple shear dowelled connections with two or three slotted-in steel plates. Spacings, edge and end distances of the dowels according to EN 1995-1-1 for ambient temperature design (except for the spacing between dowels parallel to grain direction: a_1 = 7d according to SIA 265 [18] instead of a_1 = 5d, where d is the diameter of the steel dowels). A comparative numerical analysis showed that the assumption of a spacing a_1 = 5d leads to a reduction of the load-carrying capacity $R_{d,fi}$ of the connection in the range of 10 to 15%.
- ISO-fire exposure on four sides.
- Glued laminated timber members with a minimum width of b ≥ 160 mm and a minimum thickness of the timber side member t_1 ≥ 35 mm (see Fig. 6). The thickness of the timber middle member t_2 (see Fig. 6) is 8d as normally required for the design at ambient temperature for failure mode III.
- For one (n=1) or two (n=2) dowels within one row parallel to the load direction at least strength class GL24h is required. In order to avoid net cross-section timber failure strength class GL36h should be used for connections with three dowels (n=3) within one row parallel to the load direction (see Fig. 7).

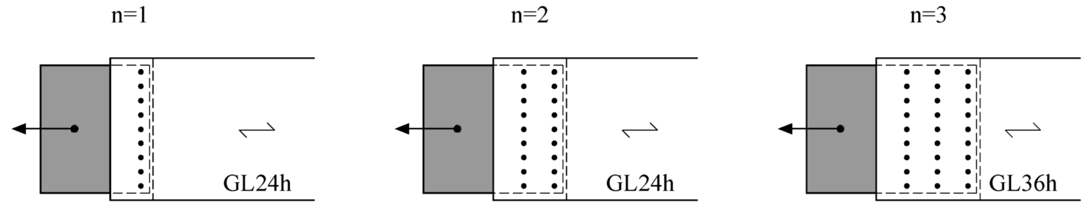

Figure 7 Minimal requirements on strength class of glued-laminated timber as a function of the number of dowels n within one row parallel to the load direction

In order to reach a fire resistance of 60 minutes the size of the timber members shall be increased by a thickness c (see Fig. 8). If the width b of the timber members is smaller than 200 mm, then a thickness of c = 45 mm is required; for b ≥ 200 mm a thickness of c = 40 mm is required. For a fire resistance between 30 and 60 minutes the thickness c can be linearly interpolated as follows:

$c = 1.5 \cdot t - 45$ for b < 200 mm and $30 \leq t \leq 60$ minutes (7)

$c = 4/3 \cdot t - 40$ for b ≥ 200 mm and $30 \leq t \leq 60$ minutes (8)

While the timber size is increased by a thickness c, the width of the steel plates should not be changed. Thus, an air gap is created leading to a better protection of the steel plates against heat due to the insulation effect of the air gap, particularly during the first phase of fire exposure (see Fig. 8).

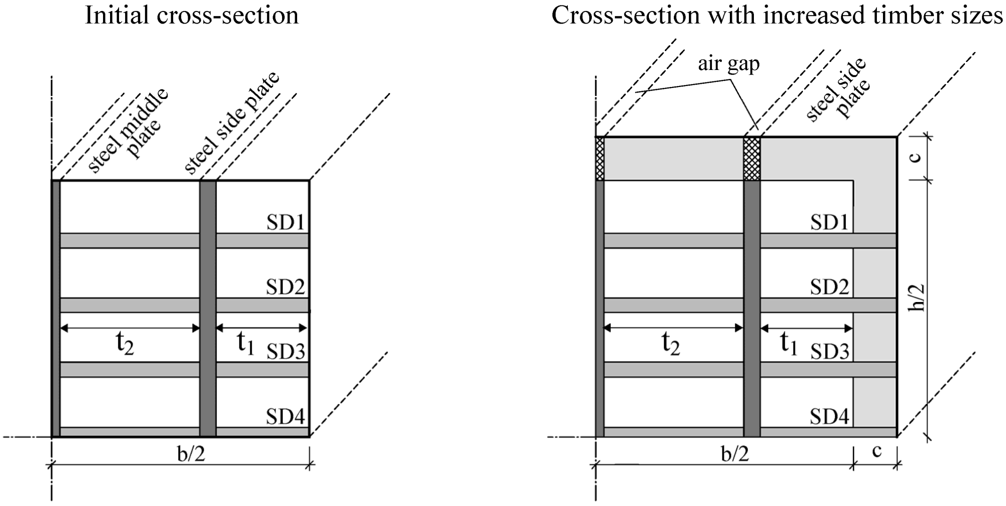

Figure 8 Definition of the timber size increased by a thickness c in order to reach a fire resistance of more than 30 minutes shown on the example of one quarter of cross-section of a connection with three slotted-in steel plates (SD = steel dowel)

3.2 Residual cross-section

An extensive FE-thermal analysis on a large number of geometries of multiple shear dowelled connections commonly used (see for example [19]) showed that the side charring $d_{char,s}$ is mainly influenced by the thickness of the timber side member t_1 (see Fig. 6). The required minimum thickness of the timber side member $t_1 \geq 35$ mm and the required increased size of the timber members by a thickness c for a fire resistance between 30 and 60 minutes allowed the development of the simplified charring model for the side charring as follows:

$d_{char,s} = \beta_0 \cdot t$ for $0 \leq t \leq 30$ minutes (9)

$d_{char,s} = \beta_0 \cdot 30 + 1.5 \cdot \beta_0 \cdot (t - 30)$ for $30 \leq t \leq 60$ minutes (10)

The charring model is based on the one-dimensional charring rate β_0 and is characterised by two charring phases. For simplicity linear relationships between charring depth and time are assumed for each phase. The influence of the steel plate on charring leads to an increased charring rate of $1.5 \cdot \beta_0$ during the second charring phase ($30 \leq t \leq 60$ minutes).

The extensive FE-thermal analysis on a large number of geometries of commonly used multiple shear dowelled connections allowed also the analysis of the top/bottom charring. The results of the extensive FE-thermal analysis showed that the top/bottom charring can be calculated assuming an increased charring rate of $1.1 \cdot \beta_0$ from beginning up to a fire duration of 60 minutes as follows:

$d_{char,o} = 1.1 \cdot \beta_0 \cdot t$ for $0 \leq t \leq 60$ minutes (11)

3.3 Effective cross-section

The depth d_{red} required for the calculation of the effective cross-section (see Fig. 6) was analysed by comparing the load-carrying capacity in fire of a large number of commonly used multiple shear dowelled connections calculated according to equation 1 and 6. The analysis showed that the depth d_{red} depends mainly on the following three parameters:

- the ratio between initial width b of the cross-section and width b_r of the residual cross-section
- the time of fire exposure t
- the number of dowels n within one row parallel to the load direction (see Fig. 7)

As the minimum thickness of the timber middle member t_2 required for the design at ambient temperature is 8d and timber cross-sections with a width greater than 300mm are unusual, connections with three slotted-in steel plates were analysed only for dowel diameters up to 10 mm (for 30 minutes fire resistance) as well as 8 mm (for 60 minutes fire resistance).

The depth d_{red} can be calculated according to equations 12 to 15 for a fire resistance of 30 minutes and equations 16 to 19 for a fire resistance 60 minutes. For a fire resistance between 30 and 60 minutes a linear interpolation can be carried out.

Fire resistance of 30 minutes

- Multiple shear steel-to-timber connection with two slotted-in steel plates:

n = 1: $d_{red} = -60(b/b_r) - 0.1d + 126.5$ [mm] with $8 \le d \le 16$ mm (12)

n = 2, 3: $d_{red} = -40(b/b_r) - n(0.5d - 2) + 94$ [mm] with $8 \le d \le 16$ mm (13)

- Multiple shear steel-to-timber connection with three slotted-in steel plates:

n = 1: $d_{red} = -60(b/b_r) - 0.4d + 133$ [mm] with $6 \le d \le 10$ mm (14)

n = 2, 3: $d_{red} = -40(b/b_r) - 0.4d(n+2) + 101$ [mm] with $6 \le d \le 10$ mm (15)

Fire resistance of 60 minutes

- Multiple shear steel-to-timber connection with two slotted-in steel plates:

n = 1: $d_{red} = -30(b/b_r) - 0.6d + 117$ [mm] with $8 \le d \le 12$ mm (16)

n = 2, 3: $d_{red} = -20(b/b_r) - d(0.2n + 1.4) + 101.5$ [mm] with $8 \le d \le 12$ mm (17)

- Multiple shear steel-to-timber connection with three slotted-in steel plates:

n = 1: $d_{red} = -30(b/b_r) + 115.5$ [mm] with $6 \le d \le 8$ mm (18)

n = 2, 3: $d_{red} = -20(b/b_r) - 4n + 94$ [mm] with $6 \le d \le 8$ mm (19)

The calculation of d_{red} is based on the strength class GL24h for connections with one or two dowels within one row parallel to the load direction, while for connections with three dowels within one row the strength class GL36h is assumed (see Fig. 7). For other strength classes the load-carrying capacity in fire $R_{d,fi}$ of connections with one or two dowels within one row can be increased with the conversion factors given in Table 2.

Table 2 Conversion factors for the calculation of the load-carrying capacity in fire $R_{d,fi}$ of multiple shear steel-to-timber connections taking into account different strength classes

Number of dowels within one row [-]	GL 24h	GL 28h	GL 32h	GL 36h
n = 1	1.00	1.08	1.13	1.18
n = 2	1.00	1.08	1.13	1.18
n = 3	---	---	---	1.00

Fig. 9 shows the comparison of numerically and analytically calculated values for the depth d_{red} and the load-carrying capacity in fire $R_{d,fi}$ for the example of multiple shear steel-to-timber dowelled connections with two or three slotted-in steel plates and two dowels within one row parallel to the load direction (n = 2) after 30 minutes ISO-fire exposure on four side. A good agreement can be observed between numerically and analytically calculated values. Further comparisons and details on the developed design model can be found in [9].

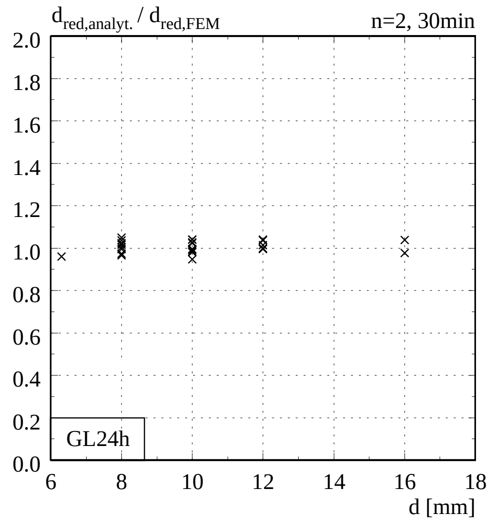

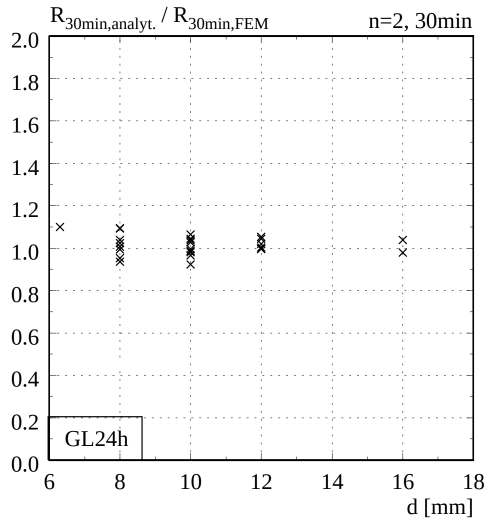

Figure 9 Comparison of numerically and analytically calculated values for the depth d_{red} (left) and the load-carrying capacity in fire (right) for the example of multiple shear steel-to-timber dowelled connections with two or three slotted-in steel plates and two dowels within one row parallel to the load direction (n = 2) after 30 minutes ISO-fire exposure on four sides

4 Conclusions

The load-carrying capacity of timber structures is often limited by the resistance of the connections. Thus, highly efficient connections as multiple shear steel-to-timber connections with slotted-in steel plates and steel dowels are needed for an efficient design. Connections with slotted-in steel plates achieve a high fire resistance because the steel plates are protected by the timber side members. The results of an extensive experimental analysis showed that shear steel-to-timber dowelled connections with two or three slotted-in steel plates designed for ambient temperature with a width of the timber members of 200mm reached a fire resistance of at least 30 minutes. A reduction of the load level from 30% to 15 or 7.5% of the average load-carrying capacity measured at ambient temperature did not lead to a significant increase of the fire resistance. By increasing the thickness of the side members as well as the end distance of the dowels by 40 mm the connections reached a fire resistance of more than 60 minutes. Connections protected by timber boards or gypsum plasterboards can reach a fire resistance of 60 minutes or more depending on the thickness and type of protection. Thus, from a fire design point of view the increase of the side member thickness or the protection by boards are efficient in order to increase the fire resistance significantly.

The load-carrying capacity of multiple shear steel-to-timber dowelled connections with slotted-in steel plates primarily depends on the charring of the timber members and the resulting temperature distribution in the residual cross-section. An extensive numerical analysis showed that slotted-in steel plates and steel dowels strongly influence the charring of the timber members and the temperature distribution in the residual cross-section. Based on the results of the experimental and numerical analyses, an analytical design model for the calculation of the load-carrying capacity of multiple shear steel-to-timber dowelled connections with slotted-in steel plates subjected to tension was developed. The design model is in analogy with the Reduced cross-section method according to EN 1995-1-2. The model takes into account the influence of the steel elements on charring and temperature distribution in the cross-section and allows accurate fire design of multiple shear steel-to-timber dowelled connections with slotted-in steel plates with different geometries for a fire resistance up to 60 minutes.

5 References

[1] EN 1995-1-1 (Eurocode 5). Design of timber structures, Part 1-1: General – Common rules and rules for buildings, CEN, Brussels, 2004.

[2] Lau P.H., Moss P.J., Buchanan A.H., Chuo T.C. Fire performance of connections in Laminated Veneer Lumber (LVL), Proceedings of 9th World Conference on Timber Engineering (WCTE), Portland, 2006.

[3] Fornather J. Brandverhalten von Holz unter besonderer Berücksichtigung stiftförmiger Verbindungsmittel – experimentelle und numerische Untersuchungen, PhD thesis, Institut für Konstruktiven Ingenieurbau, Universität für Bodenkultur Wien, Austria, 2003.

[4] Laplanche K, Dhima D, Racher P. Thermo-mechanical analysis of the timber connection under fire using 3D finite element model, Proceedings of 9th World Conference on Timber Engineering (WCTE), Portland, 2006.

[5] EN 1995-1-2 (Eurocode 5). Design of timber structures, Part 1-2: General – Structural fire design, CEN, Brussels, 2004.

[6] Norén J. Load-bearing capacity of nailed joints exposed to fire, Fire and Materials 1996; 20: 133-143.

[7] Dhima D. Vérification expérimentale de la résistance au feu d`assemblages d`elements en bois, CTICM, Réf. INC-99/399-DD/NB, France, 1999.

[8] Kruppa J, Lamadon T, Racher P. Fire resistance tests of timber connections, CTICM, Réf. INC-00/187-JK/NB, France, 2000.

[9] Erchinger C. Zum Verhalten von mehrschnittigen Stahl-Holz-Stabdübelverbindungen im Brandfall (PhD-thesis), IBK-Research report No. 314, Institute of Structural Engineering IBK, ETH Zurich, vdf Hochschulverlag AG, 2009

[10] Erchinger C, Fontana M, Mischler A, Frangi A. Versuche an mehrschnittigen Stahl-Holz-Stabdübelverbindungen und Rillennagelverbindungen bei Raumtemperatur und Normbrandbedingungen, IBK-Research report No. 293, Institute of Structural Engineering IBK, ETH Zurich, vdf Hochschulverlag AG, 2006,

[11] Frangi A, Erchinger C, Fontana M. Experimental analysis on the fire behaviour of steel-to-timber connections with slotted-in steel plates and nail connections, Fire and Materials, 2009. Paper in Press, DOI: 10.1002/fam.994.

[12] König J, Walleij L. Timber frame assemblies exposed to standard and parametric fires, Part 2: a design model for standard fire exposure, Swedish Institute for Wood Technology Research, Trätek Report I 0001001, Stockholm, 2000.

[13] König J, Norén J, Olesen FB, Hansen FT. Timber frame assemblies exposed to standard and parametric fires, Part 1: fire tests, Swedish Institute for Wood Technology Research, Trätek Report I 9702015, Stockholm, Sweden, 1997.

[14] König J. Fire resistance of timber joists and load bearing wall frames, Swedish Institute for Wood Technology Research, Trätek Report I 9412071, Stockholm, 1995.

[15] Ayme N, Joyeux D. Rapport du comportement au feu d`assemblages bois. Assemblages bois-métal en double cisaillement, Rapport SR2I-0.3/121-NA/PB, No CA 030156, CTICM, France, 2003.

[16] Fleischer H, Fornather J, Bergmeister K, Luggin W. Versuche an Holz-Stahlblech Verbindungen mit Stabdübeln, Grossbrandversuchsreihe 1 – GBV 1, Institut für Konstruktiven Ingenieurbau, Universität für Bodenkultur Wien, Austria, 2002.

[17] Frangi A, Fontana M. Thermal Expansion of Wood and Timber-Concrete Composite Members under ISO-Fire Exposure, Fire Safety Science 2003; 7, 1111–1122.

[18] SIA 265 (Swiss Standard), Timber Structures, Swiss Society of Engineers and Architects, Zurich, 2004.

[19] Holzbautabelle HBT1, Handbuch für die Bemessung, Lignum, Holzwirtschaft Schweiz, 1. Auflage, Zurich, 2005.

**INTERNATIONAL COUNCIL FOR RESEARCH AND INNOVATION
IN BUILDING AND CONSTRUCTION**

WORKING COMMISSION W18 - TIMBER STRUCTURES

COMPARISON BETWEEN THE CONDUCTIVE MODEL OF EUROCODE 5 AND THE TEMPERATURE DISTRIBUTION WITHIN A TIMBER CROSS-SECTION EXPOSED TO FIRE

M Fragiacomo

Dept. of Architecture and Planning, Univ. of Sassari

A Menis

Dept. of Structural Engineering, Univ. of Cagliari

ITALY

P Moss

A Buchanan

Dept. of Civil and Natural Resources Engineering, Univ. of Canterbury

NEW ZEALAND

I Clemente

Dept. of Civil and Environmental Engineering, Univ. of Trieste

ITALY

Presented by A Frangi

H.J. Blass commented that in some dowels the edge distance after the fire duration is very low and asked if the model takes this into consideration. A. Frangi responded that the model considers this. H.J. Blass asked how the designer knows. A. Frangi replied the designer only needs charring depth and needs to respect minimum requirement according EC5.

R. Crocetti asked how manufacturing tolerance of the gap between steel plate and wood alter the results. A. Frangi replied the influence may not be too much.

A. Buchanan stated that the design method involves design at room temperature and allow for charring rate. The design method doesn't check the embedment strength of each dowel. Difference in the embedment strength for each dowel and along the length of the dowel would lead to more of a plastic deformation. He asked when FEM was done, was the dowel considered stationary or moving. A. Frangi replied that the dowel movement was not considered. He said there are two parameters (embedment strength and temperature) but one equation. Therefore one can make the adjustments to make it work.

T. Poutanen discussed rule of thumb to determine the volume of wood after charring.

S. Aicher asked in the 3D calculation was the temperature progression according to end grain face considered. A. Frangi replied yes.

S. Winter commented that the paper is excellent. Most discussions look for complicated issues however the final design proposal is actually very simple which is based on the cross section after charring.

CIB-W18/42-16-3

**INTERNATIONAL COUNCIL FOR RESEARCH AND INNOVATION
IN BUILDING AND CONSTRUCTION**

WORKING COMMISSION W18 - TIMBER STRUCTURES

COMPARISON BETWEEN THE CONDUCTIVE MODEL OF EUROCODE 5 AND THE TEMPERATURE DISTRIBUTION WITHIN A TIMBER CROSS-SECTION EXPOSED TO FIRE

M Fragiacomo
Dept. of Architecture and Planning, Univ. of Sassari
A Menis
Dept. of Structural Engineering, Univ. of Cagliari
ITALY
P Moss
A Buchanan
Dept. of Civil and Natural Resources Engineering, Univ. of Canterbury
NEW ZEALAND
I Clemente
Dept. of Civil and Environmental Engineering, Univ. of Trieste
ITALY

MEETING FORTY TWO
DUEBENDORF
SWITZERLAND
AUGUST 2009

Comparison between the conductive model of Eurocode 5 and the temperature distribution within a timber cross-section exposed to fire

Massimo Fragiacomo(1), Agnese Menis(2), Peter Moss(3), Andy Buchanan(4), Isaia Clemente(5)

1 Dept. of Architecture and Planning, Univ. of Sassari, Italy
2 Dept. of Structural Engineering, Univ. of Cagliari, Italy
3,4 Dept. of Civil and Natural Resorces Engineering, Univ. of Canterbury, New Zealand
5 Dept. of Civil and Environmental Engineering, Univ. of Trieste, Italy

1 Introduction

Timber is a natural and sustainable resource which is being used more and more as structural material in buildings. Since timber is combustible, the fire design needs special attention. When a timber structural member is exposed to fire, physical, thermal and mechanical degradation phenomena occur in the material, leading to a very complex behaviour. Simplified design methods suggested by current codes of practice such as the Eurocode 5 Part 1-2 [1] assume strength capacity under fire to be dependent upon the residual cross-section, which is evaluated by computing the thickness of the charring layer lost from the original unburned section during the time of exposure to fire. In such a simplified design approaches, the charring rate is defined as the rate of movement of the 300ºC isotherm in the wood. Information on the temperature distribution within a timber cross-section during a fire is therefore crucial to compute the charring rate for different wood species and wood-based materials such as sawn timber, glue-laminated timber and laminated veneer lumber (LVL). The temperature distribution is also required for advanced numerical models where the structural fire resistance is calculated by taking into account the degradation of the mechanical properties (strength and modulus of elasticity) of timber with the temperature.

Analytical models based on experimental results for the temperature profiles of beams and slabs exposed to the standard ISO fire curve [2] or different fire conditions were proposed by Frangi and Fontana [3] and Janssens [4]. The temperature profiles can also be calculated using numerical models calibrated on experimental test results [5,6,7]. A rigorous modelling of the heat conduction process within timber members exposed to fire should consider all complex phenomena taking place in the material, including the mass transport of water vapour after evaporation, the charring of wood, the crack formation and the physical properties of the char layer. Due to the complexity of such rigorous models, reference to simplified conventional heat transfer models is usually made, where the phenomena listed above are implicitly accounted for in the thermal and physical properties of the material [6,8]. Until now, most of the numerical analyses were performed using thermal parameters derived by calibration of the models on experimental results. Different proposals can be found in literature for the variation of thermal and mechanical parameters with temperature, showing little agreement among them [1,6,9,10,11]. Such relationships are affected by several variables such as the shape of the fire curve, the wood species, the type of wood–based material, the conditions of the surrounding environment, etc. It is therefore important to perform further research into the thermal and physical parameters of timber when exposed to fire in order to improve the accuracy of the temperature prediction and, consequently, the accuracy of the fire resistance of timber members.

The paper investigates the temperature distribution in cross-sections made from spruce timber and radiata pine laminated veneer lumber (LVL) exposed to fire. Small (146×60 mm) and larger (300×105 mm and 360×133 mm) LVL members were tested in New Zealand under two-dimensional fire exposure at the University of Canterbury [12] and at BRANZ [13], respectively. Experimental results of 2D and 1D fire exposures were then compared with numerical values obtained by implementing a model of the thermal conduction process in the Abaqus FE code [14]. Different proposals among those found in literature for the variation of thermal and physical properties with temperature were compared. A new proposal is made in this paper which leads to a more accurate prediction of temperature distribution, particularly for larger sections subjected to 2D fire exposures.

2 Numerical model

Numerical analyses were carried out using a general purpose finite element code, Abaqus [14], rather than specific software such as Safir [7] for fire resistance of structural members. Exposure to fire was modelled by using the furnace temperature or ISO curve [2] as an input, and by imposing the boundary conditions of radiation and convection along the perimeter of the cross-section exposed to the fire. In the uncoupled heat transfer analyses, the material is described through the thermo-physical properties of density, specific heat and conductivity which govern the heat conduction process and depend upon the temperature. The two-dimensional meshes of the timber cross-sections were chosen so as to ensure accuracy of the results, and coincidence of the nodes with the location of the thermocouples in the experimental tests.

The uncertainty in the dependency of the thermo-physical properties of wood with temperature suggested the opportunity to carry out more numerical analyses, assuming the relationships proposed by different authors. Numerical results obtained according to the proposal by Moss et al. [10] highlighted a significant difference in the evaluation of the evaporation process in terms of specific heat with respect to Eurocode 5 [1]. Acceptable predictions of the temperature distributions of specimens exposed to fire were obtained using the relationships proposed by König and Walleij [6], Frangi [9] and by the Eurocode 5 [1]. By comparing the Eurocode 5 and Frangi's-proposals, it can be noted that they are conceptually similar for the specific heat, except for single values (Figure 1a). The diffusivity, which is the conductivity divided by the product of the density and the specific heat, is plotted in Figure 1d for all proposals. Since the curves are fairly close to each other, it is not surprising that both proposals led to overall similar numerical results, as will be shown in the following Sections. Since a slower rise in temperature in the deeper fibres than measured in the pilot furnace tests was predicted for larger sections subjected to 2D fire exposure (as shown later in the paper), a new proposal was made to improve the accuracy of the numerical modelling. This new proposal is based on the density and specific heat variations suggested by Eurocode 5. The conductivity values proposed by Frangi were assumed up to 550°C, and the Eurocode 5 values were considered for higher temperatures. Since there was still a delay in the numerical prediction of temperatures with respect to the experimental values, the conductivity was slightly increased (Figure 1c) in the range 550°C to 1200°C, so as to account for an increased thermal exchange in the charring layer due to convection and radiation through the cracks. The new proposal is summarized in Table 1.

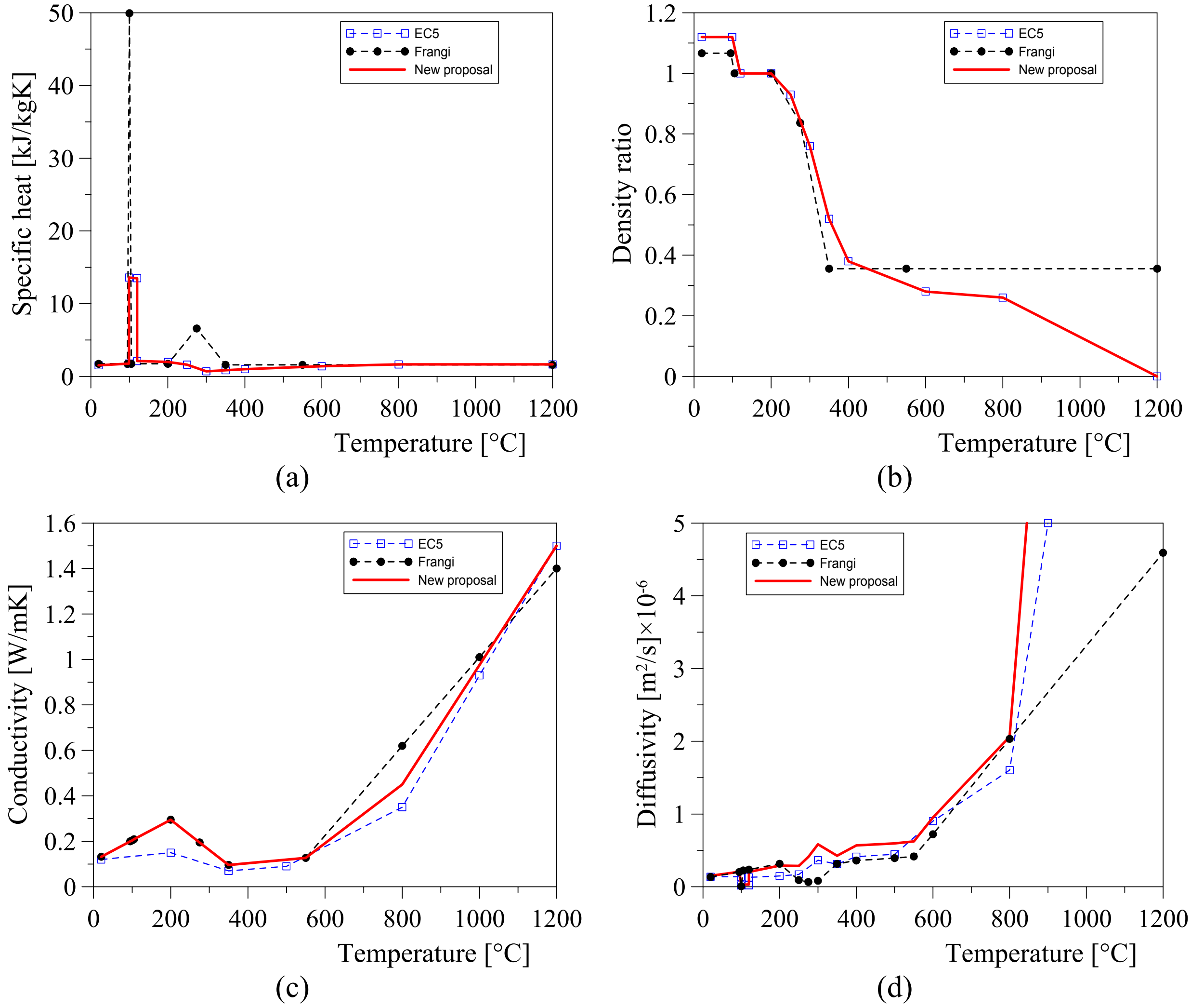

Figure 1: Different relationships adopted for the thermo-physical properties of wood: (a) specific heat, (b) density ratio, assuming an initial moisture content of 12% for EC5 and New Proposal, and 14% for Frangi's proposal, (c) conductivity, (d) diffusivity.

Table 1 Thermo-physical properties assumed in the new proposal (ω is the moisture content)

Temperature	°C	20	99	99	120	120	200	250
Conductivity	$W{\cdot}m^{-1}K^{-1}$	0.132	0.204	0.204	0.220	0.220	0.295	0.220
Specific heat	$kJ{\cdot}kg^{-1}K^{-1}$	1.53	1.77	13.60	13.50	2.12	2.00	1.62
Density ratio	-	1 + ω	1 + ω	1 + ω	1.00	1.00	1.00	0.93

Temperature	°C	300	350	400	550	600	800	1200
Conductivity	$W{\cdot}m^{-1}K^{-1}$	0.160	0.096	0.110	0.127	0.180	0.450	1.500
Specific heat	$kJ{\cdot}kg^{-1}K^{-1}$	0.71	0.85	1.00	1.30	1.40	1.65	1.65
Density ratio	-	0.76	0.52	0.38	0.305	0.28	0.26	0.00

3 Experimental-numerical comparisons

3.1 1D fire exposure of timber elements

Four unprotected timber members made from spruce were tested under ISO 834 standard fire in a small furnace at Trätek - Swedish Institute for Wood Technology Research. The specimens had 225×95 mm cross-section made from five 45×95 mm laminations and were subjected to one-dimensional exposure along the larger dimension so as to simulate the case of a 95 mm thick timber slab subjected to fire on the underside. The specimens were unloaded during the test and protected on three sides by fire resistant gypsum plaster boards. Six thermocouples were located at different depth (see Figure 2c). More information on test set-up, specimens, thermocouple location, and experimental results can be found in the report by König and Walleij [6]. The outcomes of the experimental tests and numerical analyses presented in the aforementioned report were used to validate the FE model proposed in this paper, and to investigate the influence of different thermo-physical properties on the temperature distribution.

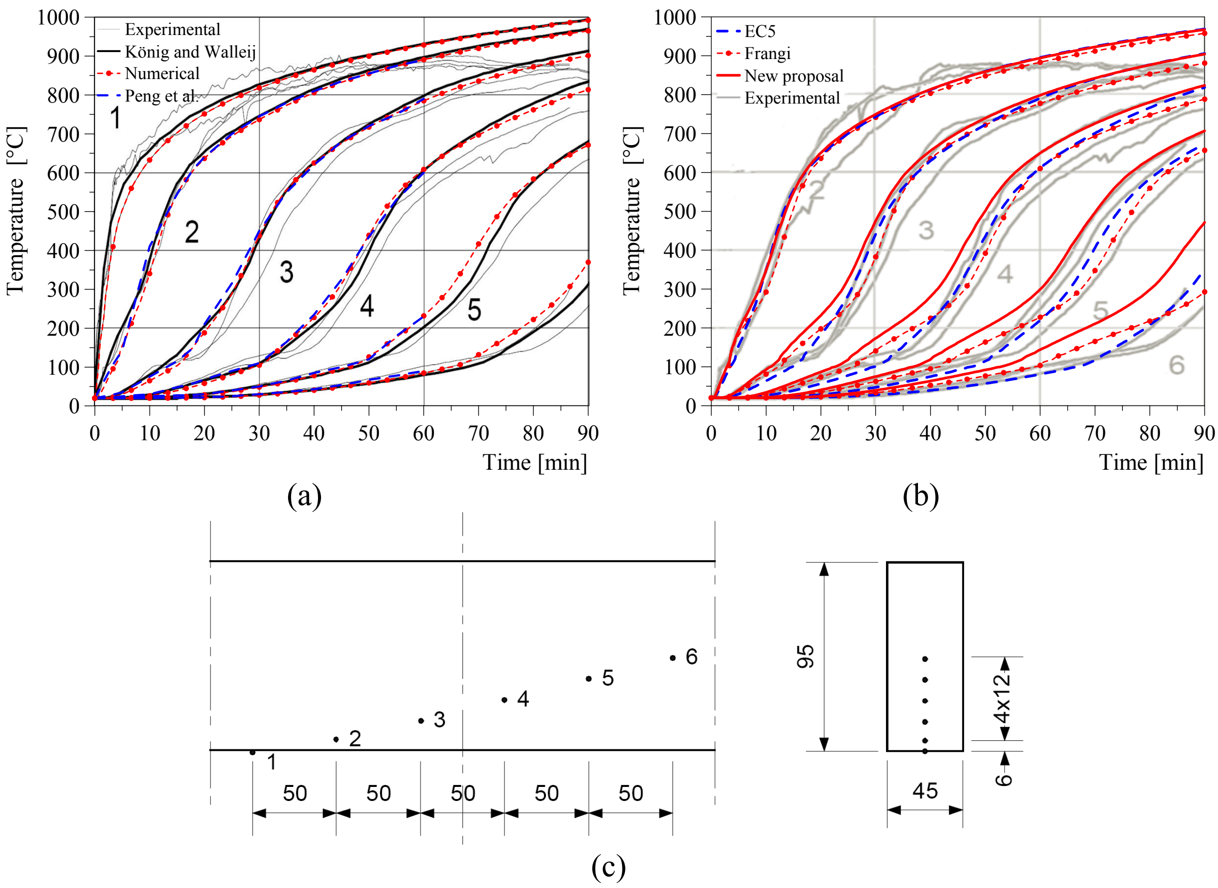

Figure 2: Comparison between experimental and numerical temperatures at different depths: (a) numerical results from different authors [5,6], (b) numerical results obtained with different thermo-physical properties, (c) thermocouple layout on elevation (left) and cross-section (right) of a specimen lamination (dimensions in mm) [6].

The 1D heat conduction process along the 95 mm depth of the timber was modelled using a 1.5×1.5 mm mesh, which was found to provide a stable and accurate numerical solution. The comparison with the experimental results, the numerical curves obtained by König and Walleij [6] using the computer program TempCalc [15], and the numerical curves obtained by Peng at al. [5] using Abaqus is displayed in Figure 2a for the temperature at different depths. The thermal properties suggested by König and Walleij were used in these analyses. A good correspondence between all the numerical and experimental curves can be noted at all thermocouple locations. Figure 2b compares the experimental curves with the numerical outcomes obtained using the proposed FE model with three different proposals for the thermo-physical properties, as discussed in the previous Section: the Eurocode 5 Part 1-2 [1], Frangi's [9], and the new proposal. The Eurocode 5 leads to an excellent approximation, with the numerical curves in close proximity to the experimental ones. The new proposal anticipates the heating process, particularly for the deeper fibres, however the approximation is still acceptable. The Frangi's proposal is slightly worse than the Eurocode 5 but better than the new proposal.

3.2 2D fire exposure of small LVL sections

Three similar fire tests on unloaded radiata pine LVL members were carried out at the University of Canterbury, New Zeland. The purpose was to investigate the temperature distribution within the cross-section exposed to fire on four sides. Since the tests were performed in a small custom-made furnace, the specimens had a cross-section of 146×600 mm and a length of 1000 mm. The layout of the 15 thermocouples inserted in each sample is displayed in Figures 3a and 3b, whilst Figure 3c shows a photo of a specimen during a fire test. Density and moisture content at ambient temperature were 570 kg/m^3 and 12%, respectively.

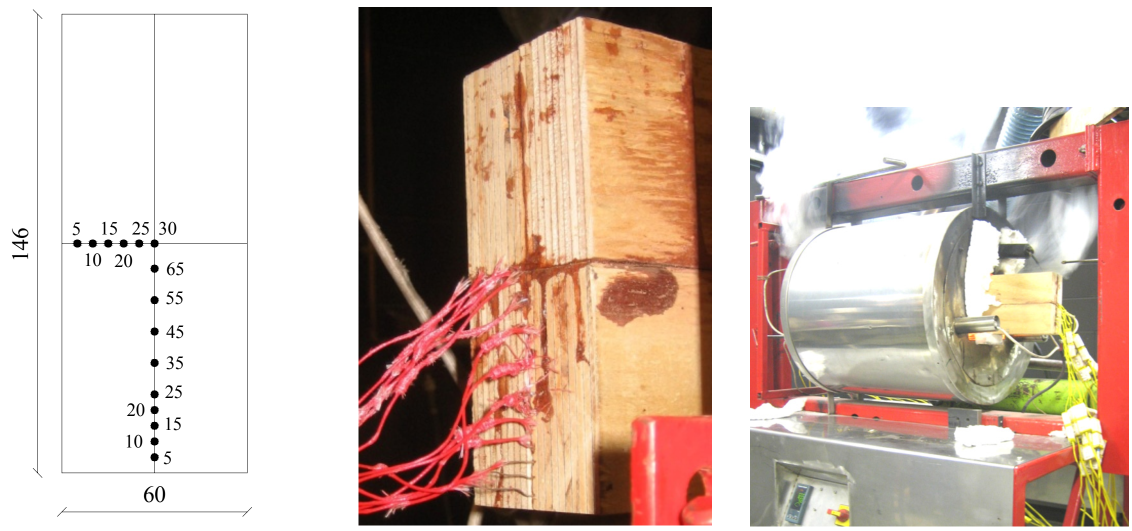

(a) (b) (c)

Figure 3: (a) Thermocouple layout (dimensions in mm), (b) instrumented specimen, (c) specimen in the custom-made furnace during a test [12].

Figure 4 displays the temperature in the furnace during the three fire tests. The experimental curves did not reach the higher values of the standard ISO 834 fire curve in order not to damage the furnace. The average temperature measured during the tests in the furnace was approximated with a piecewise-linear and used as an input in the numerical modelling. More information on the test setup and experimental outcomes can be found in the report by Menis [12] and in the paper by Fragiacomo et al. [16]. The 2D heat conduction process was modelled in Abaqus using a 2.5×2.5 mm mesh, which was found to provide a stable and accurate numerical solution.

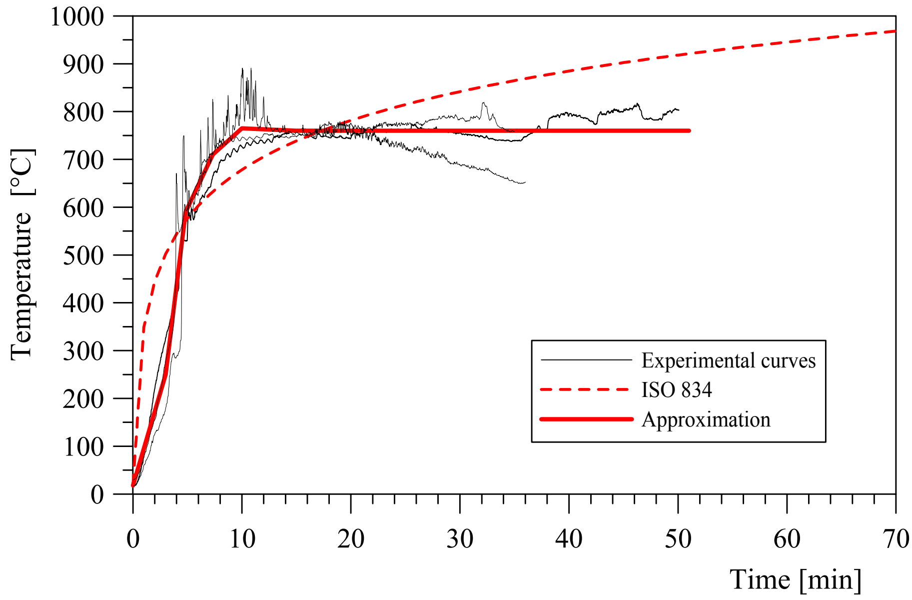

Figure 4: Temperature in the custom-made furnace during the fire tests.

Figure 5 displays both experimental and numerical results as temperature vs. time plots along the horizontal and vertical directions up to 20 mm depth. Such a value can be regarded as the depth of technical interest in structural fire design for the small cross-section tested in the custom-made furnace as it corresponds to one-third of the total breadth. By the time this depth has charred, the member has lost most of its strength capacity. It is therefore pointless to investigate the temperature distribution for larger depths. Numerical analyses were carried out by adopting different variations of density, specific heat and conductivity with temperature. Two proposals were initially considered: Eurocode 5 Part 1-2 [1] and Frangi [9]. As anticipated in the previous Section, both proposals lead to very similar curves. Both proposals slightly anticipate the heating up of the specimen along the vertical direction (long dimension), and show a delay in the heating up process along the horizontal direction (short dimension), particularly for the deeper fibres (Figure 5). The overall approximation, worse than for one-dimensional fire exposure as presented in the previous Section, is however acceptable in both directions given the significant scatter of the experimental curves. The new proposal leads to slightly better results in the horizontal direction and somewhat worse results in the vertical direction, with a worse approximation for deeper fibres.

3.3 2D fire exposure of larger LVL sections

Further fire tests were performed in the pilot furnace at BRANZ (Building Research Association of New Zealand). Three radiata pine LVL beams spanning 2.20 m were exposed to the standard ISO 834 fire on the lower and lateral sides. The beams were unloaded during the test and protected on the upper side by two gypsum boards rated 60 minutes fire resistance. Figure 6 shows the LVL beam in the pilot furnace during a fire test. Specimens 1 and 2 had a 300×105 mm cross-section whilst Specimen 3 had a slightly larger 360×133 mm cross-section. Every specimen had two cross-sections instrumented with 12 K-type thermocouples (Figure 7). The preparation of the specimens, experimental set-up, and the outcomes the fire tests are discussed at length in Lane's report [13].

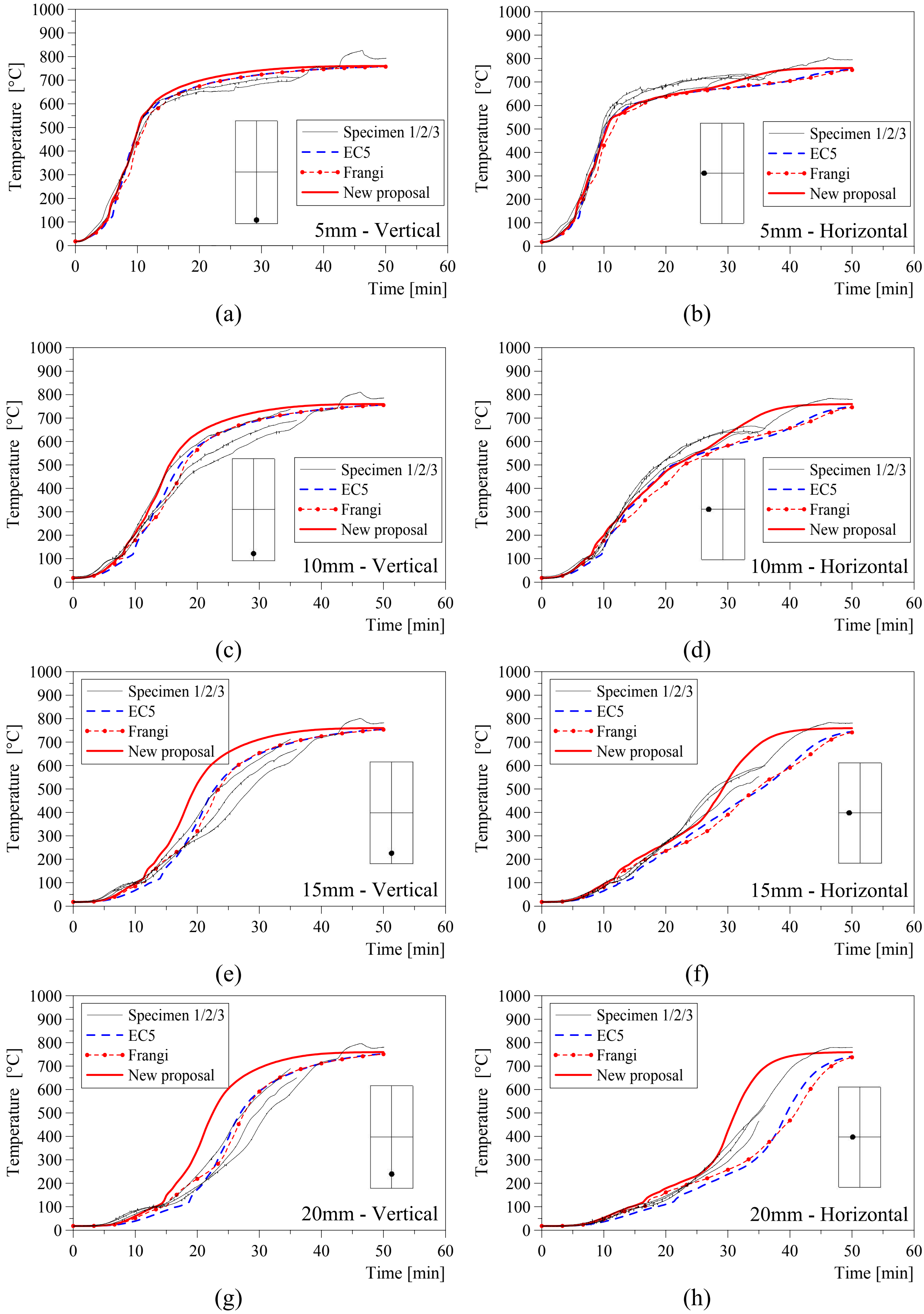

Figure 5: Comparison between experimental and numerical results at different depths and directions. (a) 5 mm-vertical, (b) 5 mm-horizontal, (c) 10 mm-vertical, (d) 10 mm-horizontal, (e) 15 mm-vertical, (f) 15 mm-horizontal, (g) 20 mm-vertical, (h) 20 mm-horizontal.

Figure 6: LVL beam in the pilot furnace during a test [13].

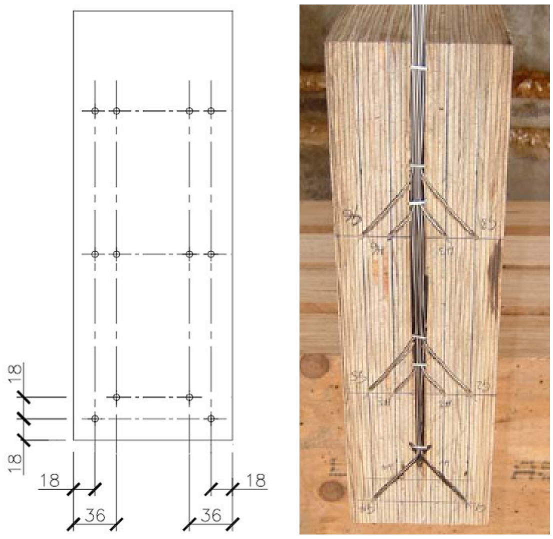

Figure 7: Layout of thermocouples in an instrumented beam section [13] (dimensions in mm).

Thermal analyses were carried out on the two different cross-sections, section 'A' (300×105 mm) and 'B' (360×133 mm), using the 2D Abaqus FE model. The standard ISO 834 fire curve was used as input. Figures 8 and 9 display the experimental-numerical comparisons for cross-sections 'A' and 'B', respectively. The temperature is plotted for the two different depths instrumented with thermocouples (18 and 36 mm), two different exposure conditions (close to the corner of the cross-section – double face exposure, and in the centre of the long dimension – single face exposure), and different proposals for the thermo-physical properties. Similar to the LVL sections tested in the custom-made furnace, both Frangi's [9] and Eurocode 5 [1] proposals lead to numerical curves close to each other. Both proposals, for both cross-sections, lead to fairly close agreement with the experimental results at the 18 mm depth under double face exposure (Figures 8a and 9a). The Eurocode 5 curve is, however, preferable as it is characterized by more uniform inclination closer to that of the experimental curves. At 36 mm depth, the heating process of LVL is predicted with a delay with respect to the experimental tests for both double and single face exposures and cross-sections (Figures 8c, 8d, 9c and 9d), particularly for the smallest one. A delay in the heating process can also be recognized for the numerical curves at 18 mm depth in the case of single face exposure (Figures 8b and 9b), where the numerical curves appear to be less inclined than the experimental ones. It should be highlighted, however, the notable scatter of the experimental values measured by the thermocouples. In some cases (e.g. Figures 8c and 8d), the charring of material (T=300°C) was reached with a 10 minutes delay between the first and the last thermocouple.

As mentioned in the introduction, an accurate prediction of the temperature distribution is meaningful in order to evaluate the fire resistance of a timber cross-section. In this respect, it is crucial to know the temperature vs. time curve at 36 mm depth until charring has occurred and, hence, the temperature of 300°C has been reached. When charring takes place at that depth, the total breadth has reduced down to less than half of the original size, leading to a small residual cross-section with little strength which is very likely to have reached failure conditions. For fibres closer to the surface, however, an accurate prediction of the temperature is critical at any temperature as it markedly affects the conduction process inside the cross-section. With the aim of improving the numerical prediction of the temperatures, some attempts were made to change the thermo-physical properties in order

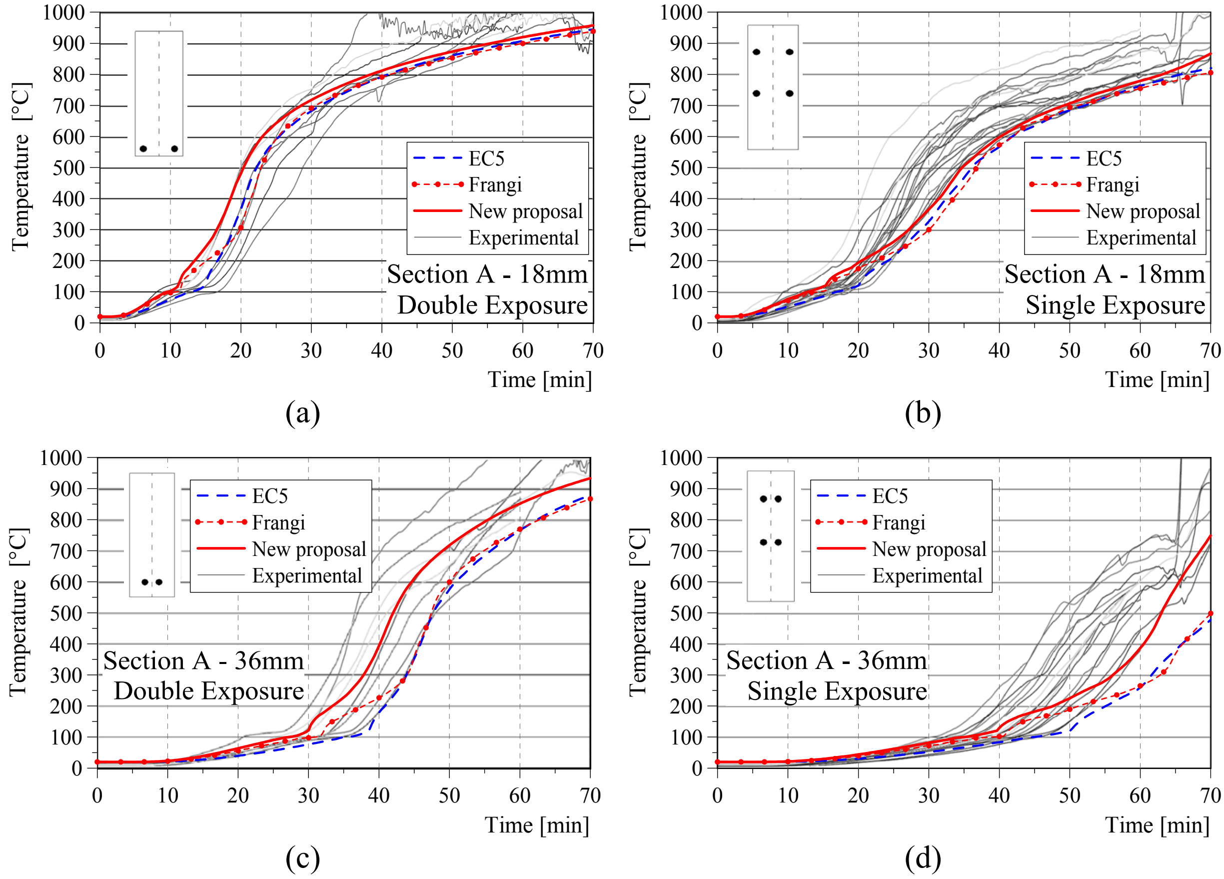

Figure 8: Comparison between experimental and numerical results at different depths for section 'A'.

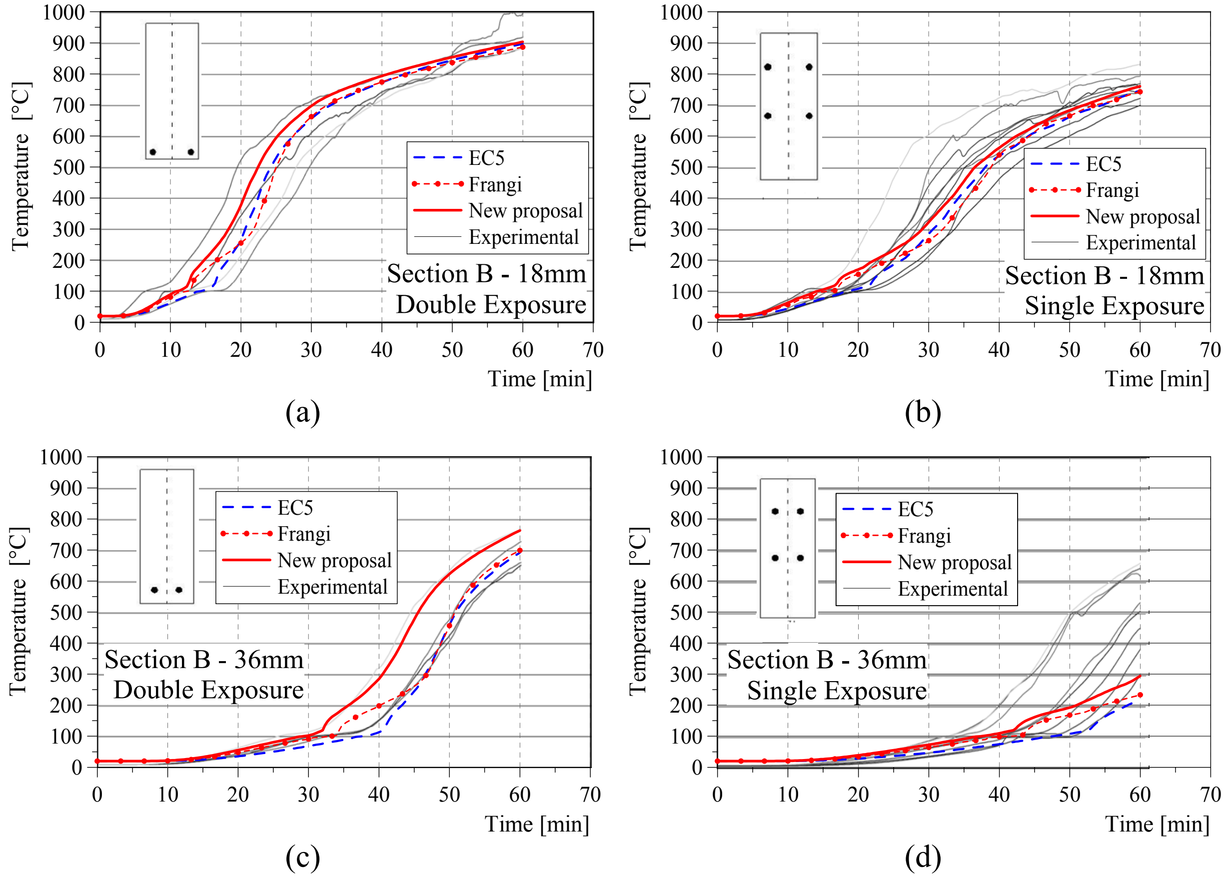

Figure 9: Comparison between experimental and numerical results at different depths for section 'B'.

to obtain closer agreement between experimental and numerical results for both cross-sections, types of exposure, and depths from the surface. Since the Eurocode 5 curves had a shape closer to the experimental ones, the variations of density and specific heat with temperature were assumed in accordance with such proposals. The conductivity, however, was varied as described in Section 2 and displayed in Figure 1c. The new proposal led to closer agreement with all the experimental curves for sections 'A' and 'B'.

4 Concluding remarks

This paper presents the outcomes of experimental tests conducted on small and larger laminated veneer lumber (LVL) cross-sections subjected to two-dimensional fire exposure. A 2D FE conductive model was implemented in Abaqus and validated on the experimental tests and numerical analyses carried out on timber sections subjected to one-dimensional fire exposure. Different proposals for the thermo-physical parameters were investigated. The Eurocode 5 proposal was found to predict the temperature distribution of small cross-sections subjected to 1D fire exposure with excellent accuracy. For small LVL cross-sections subjected to 2D fire exposure, however, the approximation was lower but still acceptable, whereas the 2D heating process of the larger cross-sections was predicted with a delayed temperature rise, particularly in the interior fibres. A new proposal for the conductive model was therefore made. This proposal assumes the same variations of density and specific heat as recommended in Eurocode 5 Part 1-2, but considers a variation of the conductivity according to Frangi up to 550°C, and then slightly increased values with respect to Eurocode 5 in the range 550°C to 1200°C. The new proposal leads to better predictions for the larger cross-sections and slightly worse, but still acceptable, predictions for the small LVL cross-section subjected to 2D fire exposure, and for the timber section subjected to 1D fire exposure, where the heating process of the inner fibres is slightly anticipated. It must be pointed out, however, that the small cross-section has less technical relevance than the other cross-sections as it is a narrow member with very low inherent fire resistance, probably needing additional passive protection if a given fire rating has to be achieved.

In order to generalize the new proposals, further experimental-numerical comparisons should be carried out on large members made from glulam or different wood-based materials. The numerical model will then be used for coupled thermal-stress analyses aimed at investigating the fire resistance of timber beams, timber-concrete composite structures, and connections.

5 References

1. European Committee for Standardisation (CEN). Eurocode 5. Design of timber structures. Part 1-2: General – Structural fire design; EN 1995-1-2. Brussels, Belgium, 2004.
2. International Organization for Standardization (ISO). Fire-resistance tests – Elements of building construction. Part 1: General Requirements. ISO 834-1. Geneva, Switzerland, 2003.
3. Frangi, A., Fontana, M. Charring rates and temperature profiles of wood sections. *Fire and Materials*, 2003; 27(2), 91-102.

4. Janssens, M.L. Modeling of the thermal degradation of structural wood members exposed to fire. *Fire and Materials*, 2004; 28(2-4), 199-207.

5. Peng, L., Hadjisophocleous, G., Mehaffey, J., Mohammad, M.A. Thermal investigation on heavy timber connections exposed to fire. *Proc. of the Canadian Society for Civil Engineering Annual Conference*, Québec, Canada, 2008.

6. König, J., Walleij, L. One-dimensional charring of timber exposed to standard and parametric fires in initially unprotected and post-protected situations. *Report I 9908029*, Swedish Institute for Wood Technology Research, Stockholm, Sweden, 1999.

7. Moss, P.J., Buchanan, A.H., Fragiacomo, M., Austruy, C. Experimental testing and analytical prediction of the behaviour of timber bolted connections subjected to fire. *Fire Technology*, Springer Science, DOI: 10.1007/s10694-009-0096-6, 2009.

8. König, J. Effective thermal actions and thermal properties of timber members in natural fires. *Fire and Materials*, 2006; 30(1), 51-63.

9. Frangi, A. Brandverhalten von Holz-Beton-Verbunddecken. *PhD Thesis*. Institute of Structural Engineering, ETH, Zurich, Switzerland, 2001 (in German).

10. Moss, P.J., Buchanan, A.H., Fragiacomo, M. Predicting the behaviour of timber connections subjected to fire. *Proc. of the 20th Australasian Conference on the Mechanics of Structures and Materials*, Toowoomba, Queensland, Australia, 2008, 857-863.

11. Cachim, P.B., Franssen, J-M. Comparison between the charring rate model and the conductive model of Eurocode 5. *Fire and Materials*, 2009, 33(3), 129-143.

12. Menis, A. Numerical and experimental investigations of LVL members exposed to fire. *Diploma Thesis*. University of Trieste, Italy, 2008 (in Italian).

13. Lane, W.P. Ignition, charring and structural performance of laminated veneer lumber. *Fire Engineering Research Report 05/3*. Dept. of Civil Engineering, University of Canterbury, Christchurch, New Zealand, 2005.

14. ABAQUS *User's Manual-Version 6.6 Hibbit*, Karlsson & Sorenson: Pawtucket, RI, U.S.A., 2006.

15. Fire Safety Design. *User's Manual for TCD 3.0 with TempCalc*. Lund, Sweden,1990.

16. Fragiacomo, M., Menis, A., Moss, P., Buchanan, A., Clemente, I. Numerical and experimental evaluation of the temperature distribution within a laminated veneer lumber (LVL) cross-section exposed to fire. Submitted to *Journal of Structural Fire Engineering*.